Biomimetics

Biomedical Science, Engineering, and Technology

The book series seeks to compile all the aspects of biomedical science, engineering and technology from fundamental principles to current advances in translational medicine. It covers a wide range of the most important topics including, but not limited to, biomedical materials, biodevices and biosystems, bioengineering, micro and nanotechnology, biotechnology, biomolecules, bioimaging, cell technology, stem cell engineering and biology, gene therapy, drug delivery, tissue engineering and regeneration, and clinical medicine.

Biomimetics

Advancing Nanobiomaterials and Tissue Engineering

Edited by

Murugan Ramalingam, Xiumei Wang, Guoping Chen, Peter Ma, and Fu-Zhai Cui

Scrivener
Publishing

WILEY

Contents

List of Contributors

Samad Ahadian received his PhD in materials science from Tohoku University, Japan in 2011. Since 2011, he has been working with Professor Ali Khademhosseini as a research associate at WPI-Advanced Institute for Materials Research, Japan. His research interests are tissue engineering, biomedical microdevices, and biomaterials. He is the author of more than 20 refereed journal papers that have been published in leading journals in the field, such as *Tissue Engineering*, *Lab on a Chip*, *Nano Letters*, and *Advanced Materials*.

Sheikh Rafi Ahmad was the founder and lead of the Centre of Applied Laser Spectroscopy at Cranfield University (Shrivenham) and has recently retired. He received his DPhil degree from the University of Oxford in 1972 on the topic of laser interaction with solid materials. The scope of his research field extended to include, among many diverse topics, laser ignition of energetic materials and laser-induced processing of natural and synthetic polymers for biomedical applications.

Mohamed A. Alkhodary is a lecturer of dentistry at Alexandria University in Egypt. In 2006 he earned his Masters on bone engineering and PhD on dental implant biomimetic laser grooving and protein coating in 2010.

Indu Bajpai is a PhD student in the Department of Materials Science and Engineering at the Indian Institute of Technology Kanpur, India. She has two recent publications in international journals and specialization is implants associated infection and treatment of bacterial infection by using external fields.

Bikramjit Basu is an associate professor at the Materials Research Center and Bio-Engineering Program, Indian Institute of Science, Bangalore, India. He earned his PhD in ceramics at Katholieke

Universiteit, Leuven, Belgium in 2001. He has authored/co-authored more than 200 peer-reviewed research papers. H-index of his publications is 28 and a total citation is more than 2000.

Qiang Cai is leading a research group in the Key Laboratory for Advanced Materials, Tsinghua University, China. His research interests are biomaterials and biomimetic synthesis of materials. He had received his PhD in 1998 from Jilin University.

Guoping Chen received his PhD from Kyoto University in 1997 and now is principal investigator and unit director of Tissue Regeneration Materials Unit, MANA, NIMS, Japan. His research interests include tissue engineering, polymeric porous scaffolds, biomimetic biomaterials, micro-patterning and surface modification. He has authored more than 200 publications with more than 2500 citations. He is an associate editor of *Journal of Materials Chemistry B*.

Fuzhai Cui is currently a full professor in the School of Materials Science and Engineering at Tsinghua University, China. He received his PhD degree in materials science from Tsinghua University in 1984. His research interests include biomineralization, bone tissue engineering, and surface modification of biomaterials. He has authored more than 300 SCI journal papers. He was honored with the "Somiya Award" from the International Union of Materials Research Societies in 2003, "State Natural Science Award 2011" and "State Technological Invention Award 2008" from the State Council of the P.R. China as the first achiever.

Timothy E.L. Douglas is a postdoctoral research fellow of the Research Foundation Flanders (FWO) at the Polymer Chemistry and Biomaterials (PBM) group at Ghent University, Belgium. He has published 32 peer-reviewed publications and 1 patent, mainly in the areas concerning enzymatic functionalization of hydrogel biomaterials, materials for bone regeneration and artificial extracellular matrices.

Rania M. Elbackly is a lecturer of endodontics and researcher at the tissue engineering labs, Faculty of Dentistry, Alexandria University, Egypt. She received her PhD in regenerative medicine and tissue engineering from the University of Genoa, Italy. Her main research focus is bone and dentin/pulp tissue regeneration. She is a member of TERMIS and has numerous publications and presentations at international congresses.

Ahmad M. Eweida is an assistant lecturer of Head and Neck Surgery, Faculty of Medicine; University of Alexandria. In 2012 he received his doctorate degree from the University of Erlangen-Nürnberg in Germany. His focus of research is bone regeneration and vascularization. Ahmad has a total of 17 publications and international presentations.

Syuji Fujii received his PhD from Kobe University in 2003, and is now an associate professor of Osaka Institute of Technology. He is the author of more than 140 publications and his research interests involve polymer particles, soft dispersed systems (emulsion, foam, liquid marble and dry liquid) and conducting polymers.

Tsutomu Furuzono received his PhD from Kagoshima University, Japan in 1996. He is now Professor and Department Chair of Dept. of Biomedical Engineering, School of Biology-Oriented Science and Technology at Kinki University. His research interests involve inorganic-organic biomaterials for artificial organs, medical devices and regenerative medicine.

Yoshihiro Ito is Chief Scientist and Director of Nano Medical Engineering Laboratory at RIKEN since 2004. He received his Dr. Eng. from Kyoto University in 1987. His research focus is on biomaterials science, combinatorial bioengineering for the creation of functional polymers, and soft nanotechnology.

Robert Kane received his PhD in bioengineering from the University of Notre Dame, USA, and is currently a postdoctoral researcher in the lab of Peter X Ma at the University of Michigan Dental School. His primary research focus is determining how to control cellular behavior through the physical properties of materials.

Naoki Kawazoe is a senior researcher at the National Institute for Materials Science in Japan. His research interest is in polymeric biomaterials for stem cell manipulation by using micropatterning. Since he received his PhD from Kyoto University in 1999, he has published more than 100 papers in the field of biomaterials.

Ali Khademhosseini is an internationally recognized bioengineer regarded for his contributions and research in the area of biomaterials and tissue engineering. Currently he is an associate professor at Harvard University and holds appointments at the Harvard-MIT

Division of Health Sciences Technology, Brigham & Women's Hospital and Tohoku University. He is also an associate faculty of the Wyss Institute and Harvard Stem Cell Institute. His research is based on developing micro and nanoscale technologies to control cellular behavior, developing microscale biomaterials and engineering systems for tissue engineering, drug discovery and cell-based biosensing.

Ferdous Khan graduated from Dhaka University, Bangladesh and then earned his PhD degree in polymer science in 1999 at Cranfield University. He was a research fellow at the University of Edinburgh, where he developed 100s of polymer-based biomaterials for tissue engineering applications such as polymer hydrogels for cartilage tissue regeneration, stem cells functioning and scaffolds for bone tissue engineering. He has authored more than 60 peer-reviewed journal articles. Currently, he is working as a Senior Polymer Chemist in Ocutec Limited, UK.

T. S. Sampath Kumar is a professor of metallurgical and materials engineering at the Indian Institute of Technology Madras, India. He is an internationally renowned materials scientist and has published numerous papers in the field. His research interests include bioceramics, functionally graded biomaterials, ceramic coatings and ceramic based drug delivery systems.

Sander Leeuwenburgh obtained his MSc degree in materials science at Delft University of Technology (2001) and his PhD degree at the Department of Biomaterials of Radboud University Medical Center in Nijmegen, The Netherlands (2006) where he was appointed as assistant professor in 2008.

Zhixu Liu received her master degree from Guangxi Normal University in 2013. She is currently a research assistance in the School of Materials Science and Engineering at Tsinghua University, China. Her research focuses on the calcium phosphate biomineralization on functional group surfaces.

Hongxu Lu obtained his PhD from the University of Tsukuba, Japan in 2009. He is currently a research associate at the University of New South Wales, Australia. His research involves developing ECM scaffolds for tissue engineering, drug delivery system and

construction of 3D tumor models. He has published 29 papers and received a Young Investigator Award from Japanese Society for Regenerative Medicine in 2012.

Peter X. Ma received his PhD in polymer science and engineering from Rutgers University. He then did his postdoctoral research at MIT and Harvard Medical School on biomaterials and tissue engineering. He is currently the Richard H. Kingery Endowed Collegiate Professor at the University of Michigan, Ann Arbor, MI, USA.

Mona K. Marei is a professor of prosthetic dentistry. She is the founder and the head of tissue engineering science and technology / laboratories, Alexandria University, Egypt. She is President of the African Materials Research Society. She is the principal investigator and team leader for a number of national and international projects and agreements in the field of biomaterials, biomedical engineering, regenerative medicine and tissue engineering. Dr. Marei has published numerous articles in the international scientific journals and received patent #23731 in July 2007 from the Ministry of scientific research, several awards, medals and certificates of recognition.

Naglaa Bahgat Nagy is an oral biology professor at the Faculty of Dentistry, Tanta University, Egypt. She got her PhD in anatomy and cell biology from the University of Illinois, Chicago, USA. Her research focuses on development, physiology and function of teeth and craniofacial structures. She has authored more than 20 publications. As a member of the Tissue Engineering Labs, Alexandria University, she is involved in all bone tissue engineering applications.

Masahiro Okada received his PhD from Kobe University in 2004, and is now an assistant professor of Osaka Dental University, Japan. He has been active in nano-biomedical research since 2004, focusing mainly on the synthesis and medical applications of nanostructured bioceramics such as hydroxyapatite nanocrystals.

Elzbieta Pamula works as a professor at the Department of Biomaterials at AGH University of Science and Technology in Krakow, Poland. She is the author of more than 200 publications (including 45 papers in SCI journals), mainly on the development of polymeric scaffolds for bone tissue engineering.

Ce Peng received his BSc (2011) in material sciences & engineering from Tsinghua University, China. He presently works as a master candidate under the supervision of Prof. Qiang Cai at School of Materials Science & Engineering. His research focuses on the controlled synthesis and biomedical applications of mesoporous silica.

Seeram Ramakrishna is the Director of HEM Labs at the National University of Singapore. He has authored five books and more than 400 four hundred international journal papers, which have attracted more than 14,000 citations.

Murugan Ramalingam is an associate professor and scientist at the Centre for Stem Cell Research, Christian Medical College and Hospital Campus, India. Concurrently he is an adjunct associate professor at the Tohoku University, Japan. He received his PhD in biomaterials from the University of Madras and has undergone training in ethical and policy issues on stem cells from Harvard University, USA. He is the author of more than 160 publications, including peer-reviewed journal papers, conference proceedings, book chapters, authored books, edited books, and patents relevant to biomaterials, stem cells, and tissue engineering. He is the Editor-in-Chief of the *Journal of Biomaterials and Tissue Engineering*, and the *Journal of Bionanoscience*. He is a recipient of several prestigious fellowships and awards, including CSIR Fellowship (India), SMF Fellowship (Singapore), NRC National Academies Fellowship (USA), Nationale Professeur des Universités (France) and Fellow of Royal Society of Chemistry (UK).

Mona S. Saad is an assistant lecturer of prosthodontics, Faculty of Dentistry, Alexandria University, Egypt. In 2011 her Masters centered on polymer nanocomposites preparation and characterization. She is now preparing for her PhD in bone engineering under supervision of Prof. Mona K. Marei.

Kaarunya Sampathkumar is a junior research fellow at the Centre for Stem Cell Research, Christian Medical College Campus, India. She received her MTech degree in medical nanotechnology from Sastra University. Her research interests include the development and characterization of nanobiomaterials for stem cell engineering, tissue regeneration, and smart drug delivery.

Azadeh Seidi is a biochemist at the Okinawa Institute of Science and Technology, Japan. Since earning her PhD from Tokyo Institute of Technology, she has focused her activities on biomedical researches, both on biochemical and engineering levels.

P. M. Sivakumar, has been a foreign postdoctoral researcher at of the Nano Medical Engineering Laboratory at Riken, Japan since 2012. He received his PhD biotechnology from IIT Madras, India. He has published more than 30 papers in peer-reviewed journals. His research interests include biofilm, bionanotechnology and biomaterials.

Tae Il Son is a professor in the Department of Biotechnology at Chung-Ang University in South Korea since 1990. He received his PhD in electronic chemistry from Tokyo Institute of Technology in 1989. His current research interests are in the areas of application of natural polymer (chitin/chitosan, gelatin, hyaluronic acid, starch, alginate etc.) derivatives for biomedical materials.

Alok Srivastava is a professor of medicine at the Christian Medical College, Vellore, India. He is the head of the Department of Haematology and the Center for Stem Cell Research which is unit of inStem, Bengaluru. He is involved with research in hemostasis, both clinical and genetic aspects and is currently coordinating the development of gene therapy for hemophilia in India.

Qi Wang is a bioengineering PhD student and research assistant working in Dr. Thomas J. Webster's Nanomedicine Lab at Northeastern University. He received his BS in chemical physics from the University of Science & Technology of China in 2010 and his MS in chemistry from Brown University in 2013. His research is focused on using nanostructured selenium as a novel coating material for preventing bacterial biofilm growth on various materials. He has published 4 literature articles and conference proceedings and gave 10 conference presentations concerning the use of nanoselenium as an antibacterial coating.

Xiumei Wang received her PhD degree in materials science and engineering from Tsinghua University, China in 2005. She is currently an associate professor on biomaterials, with major research interests on central nerve tissue engineering, angiogenesis,

self-assembling peptide, and biomineralization. She has authored more than 70 publications, including peer-reviewed journal papers, book chapters, authored books, and patents relevant to biomaterials. She was honored the "State Natural Science Award 2011" from the State Council of the P.R. China.

Thomas J. Webster is the chair and professor of the Department of Chemical Engineering at Northeastern University. He is also the founding chief editor for the *International Journal of Nanomedicine*. He received his PhD in chemical engineering from the Rensselaer Polytechnic Institute in 2000. Dr. Webster currently directs the Nanomedicine Laboratory which designs, synthesis, and evaluates nanomaterials for various implant applications. His lab group has produced at least 10 books, 35 book chapters, 335 literature articles and conference proceedings, and 15 provisional or full patents on the study of nanophase materials and implantable devices.

Samer H. **Zaky** is a research associate professor at Department of Oral Biology, University of Pittsburgh, USA. Samer was introduced to the tissue engineering field by Prof. Mona Marei. Awarded a Marie Curie Fellowship (FP6), he earned his PhD in regenerative medicine in 2009 from the University of Genoa, Italy. His research focuses on regenerating critical-size bone and bone/soft tissue interface defects together with the re-establishment of the stem cell niche.

Di Zhou is a foreign postdoctoral researcher of Nano Medical Engineering Laboratory at Riken, Japan since 2012. He received his PhD in polymer chemistry and physics from Soochow University, China in 2008. His current research interests are in the areas of polymer chemistry and biomaterials for tissue engineering.

Preface

Nature is the world's foremost amazing designer and manufacturer, creating unique materials with hierarchical structures and functions from the nanoscale to the macroscale. For centuries, humans have been trying to learn from nature and mimic its behaviors and processes in order to develop novel materials, structures, devices, and technologies, which are called biomimetics. One of the classic examples of a biomimetic process dates back more than five hundred years ago, when there was an effort made to create a "flying machine" that imitated the flight of birds. In addition to mimicking animals, people have already successfully replicated a wide range of colorful minerals, such as pearl, jade, and other gemstones. Nevertheless, the most substantial benefits of biomimetics will likely be for human medical applications, such as the development of bioprosthetics that mimic real limbs, and sensor-based biochips that interface with the human brain to assist in hearing and sight. It is evident that biomimetics is a field with endless possibilities.

Biomimetics today is a multidisciplinary subject, and it is the science of imitating or mimicking natural phenomena of a biological system in terms of its composition, structure and function as a model for design and engineering of new materials and systems suitable for all kinds of applications. Researchers have been seeking the principles and rules implemented by nature to inspire new ideas. From a materials point of view, it is called self-assembly, a bottom-up approach in which molecular structures are assembled with little or no external intervention to generate nano, micro and macro structures. Recent progress in biomimetic process and technology has led to a growing interest in the development of new materials and systems at different length scales, in particular at the nanoscale. Therefore, updating the recent progress on biomimetics is essential for advancing biomedical fields.

This book, entitled *Biomimetics: Advancing Nanobiomaterials and Tissue Engineering*, is an effort to compile all aspects of biomimetics

from fundamental principles to current technological advances, along with future trends in the development of nanoscale biomaterials and tissue engineering. Keeping these points in mind, the editors have undertaken the compilation of recent endeavors of biomimetically-designed materials and systems as a single reference for those who work in these areas. The scope of this book is principally confined to biologically inspired design of materials and systems for the development of next generation nanobiomaterials and tissue engineering. It is aimed at addressing state-of-the-art research progress in the applications of the principles, processes, and techniques of biomimetics for advancing key areas of biomedicine, such as nanobiomaterials and tissue engineering. The prospective outcomes of current advancements and challenges in biomimetic approaches are also presented.

This book is unique because it covers all important aspects dealing with the basic science of current technological innovations in key areas of biomaterials and tissue engineering. It is intended for a wide audience including students, researchers, professors, and industrial experts working in the fields of, but not limited to, material science and engineering, biomaterials, bioengineering, cell biology, biomedical sciences, tissue engineering, nanoscience, nanotechnology and nanomedicine. Overall, the book delivers new insights in the field of biomimetics to the readers.

<div align="right">

Murugan Ramalingam
Xiumei Wang
Guoping Chen
Peter Ma
Fu-Zhai Cui

</div>

Acknowledgements

1

Biomimetic Polysaccharides and Derivatives for Cartilage Tissue Regeneration

Ferdous Khan* and Sheikh Rafi Ahmad

School of Chemistry, The University of Edinburgh, UK

Abstract

Cartilage tissue engineering is an emerging technology for the regeneration of such tissues damaged by disease or trauma. Unlike other types of tissue, cartilage does not have a blood supply and, therefore, lacks regenerative capabilities. Hence, there is an urgent need to develop cartilage tissues in clinically translatable conditions for regeneration. This field of research involves the choice of the appropriate cells and biomaterials, devising signaling factors to the defect site for regeneration. The objective of this chapter is to provide a comprehensive synopsis of different approaches and recent advancements that have been taking place in this area, with an emphasis on various biomimetic polysaccharide-based biomaterials with integrated cell sources (e.g., chondrocytes, fibroblasts, and stem cells). Stem cells undergo chondrogenesis and deposit neocartilage in a variety of biomaterial-based scaffolds. However, there is still a limitation in recapitulating the properties of native tissues. Thus, the design of biomaterials that support the distribution of formed tissue is crucial for the optimization of cartilage formation. The state-of-the art of advances in biomaterials and knowledge of their interaction with cells are also evaluated in this chapter. Additionally, the importance of signaling factors on cellular behavior that promote the production of cartilage tissue, that, in turn, mimics native tissue properties, accelerates restoration of tissue function and is clinically translatable, has been addressed here. Finally, the challenges, limitation and future prospect of cartilage regeneration are discussed.

Keywords: Chitosan, hyaluronic acid, alginate, cellulose, biomimetic 3D scaffold, cartilage tissue engineering

---

*Corresponding author: ferdous.khan0@gmail.com

1.1   Introduction

Tissue engineering is a rapidly growing field of research which has the potential to provide permanent solutions to tissue damage and tissue loss to millions of people each year [1]. Many strategies have been developed for various tissues regeneration [2], most of which involve the use of cells, scaffolds, and growth factors independently or sometimes in combination of any of these.

Cartilage is a tough, flexible tissue found throughout the body, that acts as a shock absorber and covers the surface of joints allowing bones to slide over one another, reducing friction and preventing any damage. Cartilage, a predominantly avascular, aneural, and alymphatic tissue, is composed of sparsely distributed chondrocytes embedded within a dense extracellular matrix (ECM) [3]. This ECM is composed primarily of type II collagen and proteoglycans that provide the tissue with sufficient mechanical properties for function *in vivo*. The damaged cartilage has limited ability to self repair, unlike other tissues (such as skin or muscles), due to lack of blood supply.

The concept of cell-based therapies for cartilage regeneration and repair has been used clinically since 1987 to repair both craniofacial and articular cartilage defects via autologous chondrocyte transplantation (ACT), and have treated more than 12,000 patients worldwide in chondral defects [4]. This approach involves isolating chondrocytes from the donor biopsy cartilage tissue, expanding the cells *in vitro*, and delivering them to the cartilage defect site to produce new cartilage tissue. However, ACT has an inherent limitation due to insufficient cells obtained through the biopsy. With the advancement of research and development in the field of cartilage tissue engineering, new techniques are being examined and new cell sources and biomaterials are being studied that overcome these limitations and enhance and improve the quality of repair. Although research has been conducted extensively on cartilage tissue engineering over the last two decades [5, 6], limited products and treatments have moved from laboratory bench to patients' bedside, hence the need for more intensive research and development in this field.

Mesenchymal stem cells (MSCs) have been shown to undergo chondrogenesis and deposit neocartilage in a variety of TE scaffolds [7], however, there is still a limitation in recapitulating the properties of native tissues. For example, the diminished ability of MSCs to produce functional cartilage tissue is troubling, as the quality of tissue they produce determines their success as a viable cell source for cartilage repair and regeneration [8]. In addition to the amount and type of matrix produced, proper distribution of this matrix is essential for the optimization of tissue properties (e.g., mechanical). Thus, the design of biomaterials that support the distribution of formed tissue is crucial for the optimization of neocartilage formation by MSCs. Therefore, an overview of the emerging trends in cartilage tissue engineering, with an emphasis on the use of polymer matrices, is provided in this chapter. The material of choice in

the present analysis is polysaccharides-based polymer scaffold which is expected to encourage cellular growth and act as vehicles for cell delivery. Furthermore, the addition of growth factors with biomimetic polymer scaffolds will be discussed with respect to their effects on cellular behavior and cartilage tissue formation.

1.2   Strategies for Cartilage Tissue Engineering

There are several tissue engineering approaches for cartilage regeneration which are summarized in Figure 1.1. The cells explanted from an individual donor (Figure 1.1, A-1), may be cultivated *in vitro* to differentiate (A-2,3), and may be mixed with the hydrogel components prior to be reinfusion, preferentially in the same individual by injection (A-4). Cells can be encapsulated or seeded onto the hydrogel/scaffold (A-5) and implanted in the body to act as an artificial organ (A-6), or encapsulated and assembled in a bioreactor to serve as an external artificial organ (A-7,8). The growth factors can also be added in all types of *in vitro* cultivations prior to reinfusion of exposed cells in the body. The use of such growth factors in *in vitro* cell culture that are growing onto a scaffold requires a certain
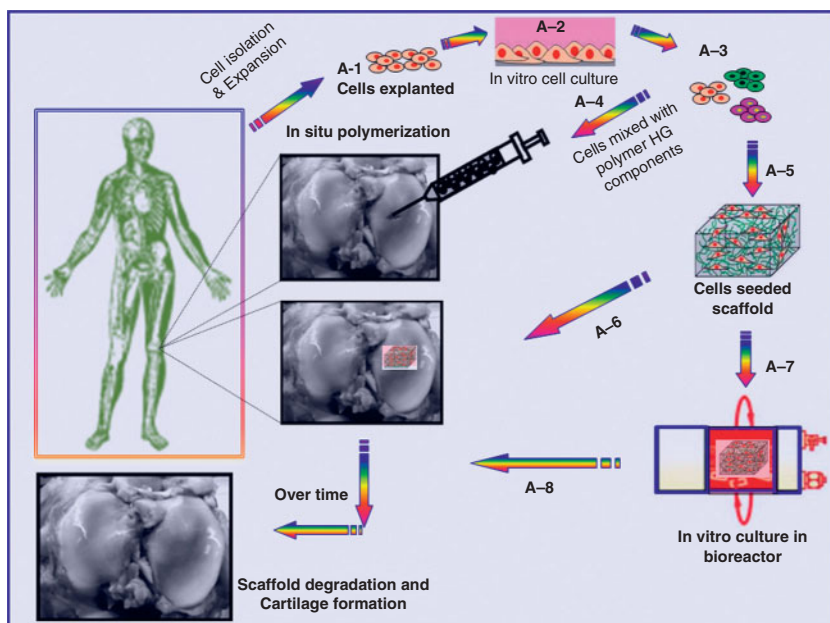
Figure 1.1 Scheme representing cartilage tissue engineering approaches showing injectable hydrogel systems to *in vitro* cell culture onto scaffold prior to implantation.

amount of time before implantation, allowing more time for the scaffold to degrade and cartilage to be formed (Figure 1.1).

1.3   Designing Scaffold for Cartilage Tissue Engineering

Scaffold should be designed to provide a 3D environment which is suitable for cartilaginous tissue production. In an ideal case the scaffold should have a number of essential characteristics which are as follows: (i) promote cells attachment, proliferation, viability and differentiation, and ECM production, (ii) allow diffusion of nutrients and waste products, (iii) adhere and integrate with the surrounding native cartilage, (iv) provide sufficient mechanical integrity depending on the defect location, and, finally, (v) controlled degradation.

Several researchers [9, 10] have found that the scaffolds degradation plays an important role in cartilage regeneration. Scaffold degradation can occur hydrolytically or enzymatically, and by controlling degradation temporally and spatially, scaffolds can accelerate and direct new tissue growth [9, 10]. Degradable scaffold has improved ECM distribution compared to completely non-degradable ones [9], and scaffolds with a slower degradation rate yielded cartilage of greater thickness in an osteochondral defect model as reported by Solchaga and coworkers [10].

Three different forms of polymeric scaffold, namely, hydrogels, sponges and fibrous meshes (Figure 1.2), have been fabricated and investigated
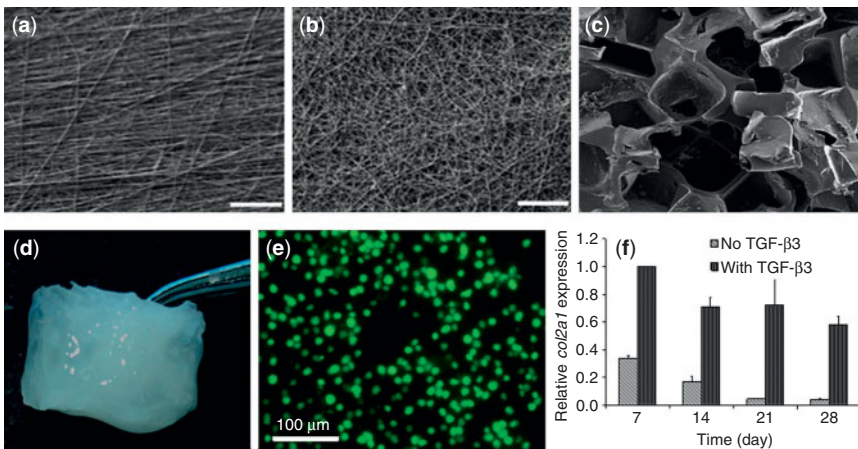
Figure 1.2 Representative examples of different forms of scaffolds utilized for cartilage tissue engineering. SEM images of (a, b) aligned and unaligned fibrous scaffolds, (c) sponge, (d) hydrogel scaffold, (e) skeletal cells growth (rounded cell morphology) within hydrogel, and (f) *col2a1* gene expression. Reprinted with permission from [6, 7, 12].

for use in tissue, engineered for effective cartilage repair. Such a physical form of scaffold mainly depends on the method of fabrication process, and chemical and physical properties of scaffold materials. For tissue regeneration the method of cell seeding and distribution within the scaffold play an important role and can dictate cell infiltration into the scaffold. The method of cell seeding selection, either static or dynamic, can also depend on the physical form of the scaffolds. The later cell seeding method (dynamic) can improve cellular distribution in the case of sponge and mesh types of scaffold [11], whereas hydrogel-based scaffolds typically support uniform cell distribution if cells are adequately suspended during gelation [12].

To date, a wide range of synthetic and natural polymers have been investigated to synthesize scaffold for cartilage regeneration. However, synthetic polymers do not have direct cell-scaffold interactions, and the degradation by-products may be toxic or elicit an inflammatory response. The natural polymers which have been investigated as possible bioactive scaffolding materials for cartilage engineering include: chitin and chitosan, hyaluronic acid (HA), alginate, starch, cellulose, agarose, fibrin, collagen, gelatin, and chondroitin sulphate (Table 1.1) [5–33]. These polymers can often interact with cells via cell surface receptors, and regulate or

Table 1.1 Types of natural polymers used as scaffolding materials for cartilage tissue engineering.

Natural Polymers	Advantages	Disadvantages	References
Agarose	Injectible and cells can be uniformly distributed within implant.	Foreign body giant cell reaction. Low resorbtion. Biochemical properties significantly inferior to native tissue.	[2, 7, 8]
Alginate	Easy to cross-linked to form gel under very mild conditions. Gel can be injected to avoid an open surgical procedure.	Lack of mechanical strength and handling properties, difficult to sterilize. Impurities affecting material properties.	[2, 7]

(Continued)

Table 1.1 (*Cont.*)

Natural Polymers	Advantages	Disadvantages	References
Chitin/ Chitosan	Hydrophilic surface promoting cell adhesion, proliferation and differentiation. Good biocompatibility and acceptable host response. Antibacterial activity.	Mechanical weakness and instability. Incapacity to maintain a predefined shape. Impurities affecting material properties.	[12–24]
Bacterial Cellulose	High purity, nanofibrous structure, high tensile strength and good biocompatibility.	Small pore size. Early stage of investigation as scaffold for TE, needs further investigations on *in vivo*.	[7, 110, 111, 114]
Collagen	Low antigenicity and good cell-binding properties.	Low biomechanical stiffness and rapid biodegradation. Toxicity of some of the crosslinking agents.	[7, 25, 26]
Chondroitin sulfate	Able to absorb and hold water, thereby giving cartilage its elasticity and fluidity	Highly water soluble and poor intrinsic gel formation properties. Low mechanical properties.	[19, 27, 37]
Fibrin glue	Improve histological Appearance. Can be used as carrier of growth factor.	Lack of mechanical properties. May evoke immune response. Does not permit host cell ingrowth.	[28, 29]

Table 1.1 (*Cont.*)

Natural Polymers	Advantages	Disadvantages	References
Gelatin	Highly biocompatible and biodegradable.	Animal derived product, highly expensive and batch-to-batch variation. Low mechanical strength.	[7, 30, 31]
Hyaluronic acid	No immunogenic properties, ease of chain size manipulation, Interactions with cell-surface receptors. Production through large-scale microbial fermentation.	Water solubility. Its anionic surface does not thermodynamically promote cell attachment and tissue formation.	[5, 6, 10, 68]
Silk fibroin	Long standing history of use in clinical applications. Slow degradability, versatility in processing, remarkable mechanical strength and thermal stability. Genetically tailorable composition and sequence.	Purification necessary. Contamination from residual sericin may cause biocompatibility problems.	[7, 32, 33]
Starch-based materials	Inexpensive, suitable for processing by diverse techniques and into diverse shapes.	*In vivo* degradation has not yet been fully assessed.	

direct cell function. Thus the following sections focus on several potential natural polysaccharides-based scaffolds for cartilage tissue engineering applications.

1.4   Natural Polysaccharides for Cartilage Tissue Engineering

Polysaccharides are a class of materials which are of rapidly growing interest to researchers in the field of biomaterial science. There are several factors which have specifically contributed to the importance of polysaccharide-based biomaterials such as: (i) Understanding of the critical role of saccharide moieties in cell signaling schemes and immune recognition. (ii) New and effective synthetic techniques to functionalize biologically active oligosaccharides, thereby allowing improvement in the properties of polysaccharide for functional performance. (iii) The significant increase of tissue engineering research pointing to the need for new materials with specific, controllable biological activity and biodegradability. Additionally, one of the most important properties of polysaccharides, in general, is their ability to form hydrogels either by hydrogen bonding or ionic interactions. Hydrogel formation can occur by a number of mechanisms and is strongly influenced by the types of monosaccharide involved, as well as the presence and nature of substituent groups. Hydrogels have potential application in tissue engineering, particularly in cartilage tissue regeneration. The following sections are focused on four different types of polysaccharides-based materials, namely chitin and chitosan, HA, alginate, starch and cellulose-based materials for potential cartilage tissue engineering applications.

1.4.1   Chitin and Chitosan (CS)-based Materials

CS is a partially de-acetylated derivative of chitin found in arthropod exoskeletons. Structurally, CS is a linear polysaccharide consisting of β (1, 4) linked D-glucosamine residues with a variable number of randomly located N-acetyl-glucosamine groups. It thus shares some characteristics with various glycosaminoglycans (GAGs) and hyaluronic acid present in articular cartilage. GAG analogy as components of a cartilage tissue scaffold appears to be a logical approach for enhancing chondrogenesis, and cartilage regeneration. Depending on the source and preparation procedure, the average molecular weight may vary in the range from 50 to 1000 kDa. The degree of deacetylation of commercially available CS varies from 50% to 90%. This is a semicrystalline polymer and the degree of crystallinity is a function of the degree of deacetylation. Minimum crystallinity is achieved at intermediate degrees of deacetylation. CS is normally insoluble

in aqueous solutions above pH 7, due to its stability and crystalline structure. However, in dilute acids, the free amino groups are protonated and the molecule becomes fully soluble below ~pH 5. Viscous solutions can be extruded and gelled in high pH solutions or in baths of non-solvents such as methanol. Such gel fibers can be subsequently drawn and dried to form high-strength fibers. This polymer has been extensively studied for industrial applications for film and fiber formation, and their preparation procedures and their mechanical properties have been reviewed extensively in the past [13, 14].

The most promising feature of CS is its excellent ability to be processed into porous structures for use in cell transplantation and tissue regeneration. Porous CS structures can be formed by freezing and lyophilizing of CS acetic acid solutions in suitable molds [12, 24]. During the freezing process, ice crystals nucleate from solution and grow along the lines of thermal gradients. Lyophilization generates a porous structure with controlled pore sizes through the variation of the freezing rate, i.e., the variation of ice crystal size. Pore orientation can also be directed by controlling the geometry of thermal gradients during freezing. The mechanical properties which are critically important for any tissue engineering applications and properties of CS scaffolds are mainly dependent on the pore sizes, pore orientations, and molecular weight of CS.

In order to improve physical, chemical, biological and mechanical properties of chitin and CS, a variety of techniques can be applied. For example, chemical derivatization of CS provides a powerful means to promote new biological activities and modify its mechanical properties. The primary amino groups on the molecule are reactive and provide a mechanism for side group attachment using a variety of mild reaction conditions. Generally, the addition of a side chain alters the structure of the material and often increases the solubility of the final compound, and allows for a wide range of scaffold processing opportunity. Of course, the precise nature of changes in chemical and biological properties depends on the nature of the side group. The variety of groups which can be attached to CS is almost unlimited, and side groups can be chosen to provide specific functionality, alter biological properties, or modify physical properties. Another example for modification of CS is the physical blending approach. CS has been combined with a variety of materials, such as poly(ethylenimine), poly(ε-caprolactone), poly(L-lactic acid) (PLLA), poly(2-Hydroxyethyle methacrylate) (PHEMA), poly(ethyelene oxide) (PEO) and poly(vinyl acetate) (PVAc) for potential application in orthopaedics and cell-based TE for cartilage regeneration [12, 34–36]. The blended CS form 3D hydrogel scaffold *via* hydrogen bonding interaction, and such a system provides an excellent environment for fetal skeletal cells growth and which is guided towards chondrogenic differentiation [12].

Structurally, CS consists of N-acetylglucosamine moiety, similar to cartilage specific ECM component, GAG, which play a critical role in regulating expression of the chondrocytic phenotype and in supporting chondrogenesis both *in vitro* and *in vivo* [2–5]. Since GAG properties include many specific interactions with growth factors, receptors and adhesion proteins, this suggests that the analogous structure in CS may also have related bioactivities. In fact, CS oligosaccharides have been shown to have a stimulatory effect on macrophages, and the effect has been linked to the acetylated residues [15]. Furthermore, both CS and chitin have been shown to exert chemo-attractive effects on neutrophils *in vitro* and *in vivo* [16, 17].

A number of researchers have examined the tissue response to various CS-based implants [18–24]. In general, these materials have been found to evoke a minimal foreign body reaction. In most cases, no major fibrous encapsulation has been observed. Formation of normal granulation tissue, often with accelerated angiogenesis, appears to be the typical course of healing. In the short term (less than 7 day), a significant accumulation of neutrophils in the vicinity of the implants can be seen, but this dissipates rapidly and a chronic inflammatory response does not develop. The stimulatory effects of CS and its fragments on the immune cells mentioned above may play a role in inducing local cell proliferation, and ultimately integration of the implanted material with the host tissue.

CS has been investigated as a scaffolding material in cartilage engineering [37, 38]. Chondrocytes cultured *in vitro* on CS substrates, maintained rounded morphology and preserved synthesis of cell-specific ECM molecules [38]. CS scaffolds seeded with chondrocytes showed partial repair of cartilage defects *in vivo*. CS was combined with other polymeric materials, like poly(lactic acid), hyaluronan and poly(ethylenimine), to improve chondrocyte attachment and the consequent cell adhesion, proliferation and biosynthetic activity [12, 39, 40]. When the human skeletal cells, derived from predominantly cartilaginous fetal femora, were cultured within the CS/PEI hydrogels, the cells maintained chondrocyte-like morphology (Figure 1.2e) [12], and the characteristic functional features were similar to those of normal cartilage.

Composites of CS–alginate–hyaluronan have been evaluated as scaffold for the development of cartilage regeneration, and *in vitro* experiments showed neocartilage formation, while implanted seeded scaffold led to partial repair of cartilage defect *in vivo* [41]. Recently, a thermosensitive CS–pluronic hydrogel has been designed and developed as an injectable cell delivery carrier for cartilage regeneration. *In vitro* cell culture using bovine chondrocytes showed a substantial increase in cell proliferation and GAGs synthesis during an incubation period of 28 days [42]. Furthermore, CS-based scaffolds have also been loaded with growth factors to promote cartilage regeneration: both CS and collagen/CS/GAGs

scaffolds loaded with TGF-1 were reported to promote cartilage regeneration [43, 44]. CS scaffolds loaded with epidermal growth factor resulted in the promotion of chondrogenesis [45]. The CS/(*N*,*N*-dicarboxymethyl) scaffolds, loaded with BMPs, have been reported to induce the healing of articular cartilage lesion in rabbit [46].

1.4.2   HA-based Materials

Hyaluronan (HA), a ubiquitous component of the extracellular matrix (ECM) of all connective tissues, is a non-sulfated glycosaminoglycan (GAG), consisting of repeating disaccharide units (*β*-1,4-D-glucuronic acid and *β*-1,3-*N*-acetyl-D-glucosamine) [47]. The ECM is a network composed of covalent and non-covalent interactions between GAGs and proteins. For example, chondroitin sulfate is covalently linked to proteoglycans which, in turn, have HA-binding modules that form multivalent high-affinity interactions with HA. These protein–ligand interactions stabilize and organize the ECM [48, 49], regulate cell adhesion and motility [50, 51], and mediate cell proliferation and differentiation [52]. As a consequence, HA and its derivatives have been widely investigated as materials for cell growth and tissue repair in biomedical applications [53–62].

HA has also been modified by the addition of functional group using crosslinking method to form a hydrogel [63]. This maintained chondrocyte viability and phenotype, and promoted the chondrogenic differentiation of MSCs when cultured in both *in vitro* and *in vivo* [63]. However, ECM distribution is limited without adequate space for diffusion due to slow degradability of this hydrogel. Ideally, scaffold degradation should match with ECM deposition and accumulation. Degradation can alter the diffusion of nutrients and waste, cell–scaffold interactions, and the distribution and retention of ECM proteins. Therefore, to control degradation of a scaffold, it is crucially important to select an appropriate approach: either chemical crosslinking and/or copolymerization of functional group on the backbone of HA. The MSCs encapsulated in HA functionalized hydrogels retained a rounded cell morphology [64], and the tuning of temporal scaffold properties can control neocartilage production by MSCs in this gel. The most important criterion of hydrogel must be the mechanical stability and control of degradation which can be done *via* crosslinking of methacrylate and aldehyde groups, ultimately leading to cartilage repair [65]. A careful balance of slow and fast degradable components and mechanical stability are the most important criteria for optimal growth of functional cartilage tissue.

HA is known to interact with chondrocytes *via* various surface receptors involved in sophisticated signaling pathways, which allow chondrocytes to maintain their original phenotype [66]. In addition, HA has been conjugated to alginate, CS and fibrin gel matrices to provide artificial ECM

environments [67]. However, the hydrophilic, polyanionic surfaces of HA biomaterials do not thermodynamically favor cell attachment and tissue formation [68]. Therefore, to enhance cell interactions, surfaces coated with ECM proteins such as type I collagen and fibronectin, have been developed by creating physically or covalently linked functional domains [69, 70]. Physical and biological characteristics of HA in its purified form, such as water solubility, rapid resorption, short residence time in the tissue, etc., limit its application as biomaterial [71]. Several attempts have been made to modify HA molecular structure and improve its properties. Covalent photo-induced crosslinking has been used to overcome these limitations and to provide long-term stability and increased mechanical strength [72]. For instance, porcine chondrocytes, encapsulated in photopolymerized HA hydrogels maintained viability and were able to produce neocartilage within the porous networks during 8 weeks in *in vitro* experiments [73]. The ethyl and the benzyl esters of hyaluronan named HYAFF®7 and HYAFF®11, respectively, are two of the most characterized hyaluronan derivative polymers. Both physicochemically and biologically they degrade at predictable rates through hydrolysis of the ester bonds (around 2 months for complete hydrolysis) [71]. Human chondrocytes, grown onto HYAFF®11 3D scaffolds, are able to re-express *in vitro* their differentiated phenotype [74], and to reduce the expression and production of molecules involved in cartilage degenerative diseases [75]. Histological evaluation of repaired tissue by HYAFF®11 scaffold, employed in chondrocyte transplantation *in vivo*, demonstrated a significant improvement of the quality of the healing in comparison to defects without grafted chondrocytes (Figure 1.3) [76].

1.4.3   Alginate-based Materials

Alginate is a naturally occurring linear polysaccharide, composed of (1–4)-linked β-D-mannuronic acid (M units) and α-L-guluronic acid (G units), with varying proportion and sequential distribution along the polymer chain. This polymer is known to be biocompatible [77] and forms hydrogels in the presence of multivalent cations (i.e., Ca^{2+}) by ionic interaction between the carboxylic acid groups, located on the backbone of this polymer and the chelating cation [78]. Researchers have developed calcium crosslinked alginate hydrogels for a variety of biomedical applications, including cell culture and transplantation, drug delivery and wound dressing [79–82]. Generally alginate is used in its physical form of hydrogels, which do not significantly enhance cell migration and proliferation, mainly due to their small pore sizes (nm scale). In order to achieve macroporous structure of scaffold, the lyophilization of alginate hydrogels was employed [83]. In a separate study, Eiselt *et al.* [83] developed a method for fabrication of macroporous alginate beads with high porosity (78%) and
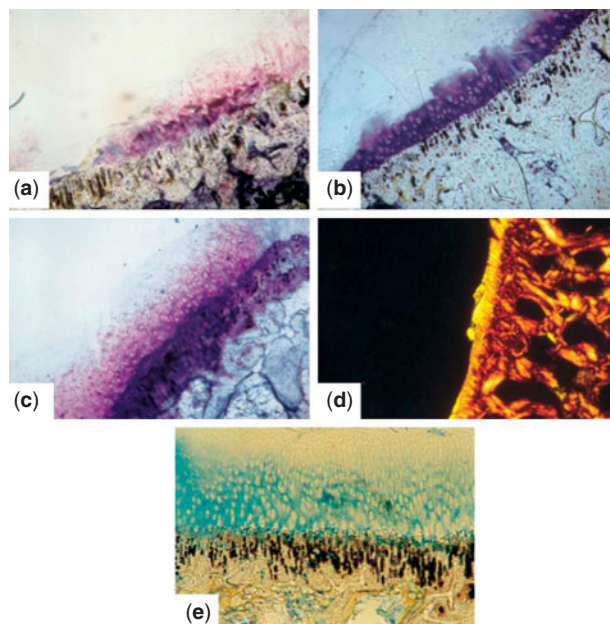
Figure 1.3 HA-based scaffold: (a) Histological evaluation of the defect implanted with chondrocyte-seeded Hyaff®-11 at 4 weeks after transplantation. The lesion is still present but some clusters of cartilagineous tissue shows on bone surface. (b) Histological evaluation of the defect implanted with chondrocyte-seeded Hyaff®-11 at 12 weeks after transplantation. Fibrous and hyaline-like cartilage populate the defect site. (c) Histological evaluation of the defect implanted with chondrocyte-seeded Hyaff®-11 at 24 weeks after transplantation. High prevalence of hyaline cartilage shows with an irregular surface. Toluidine blue staining (a-c). (d) Histological analysis of the defect implanted with chondrocyte-seeded Hyaff®-11 at 24 weeks after transplantation, columnar cartilage-like structure is visible and evidence of deposition of extracellular matrix. Safranin-O/fast green stain (polarized light microscopy). (e) Alcian blue staining of the defect implanted with chondrocyte-seeded Hyaff®-11 at 24 weeks after transplantation, evidence of proteoglycans production throughout the thickness of the newly formed cartilage. Reprinted with permission from [76].

interconnected pores, a suitable matrix for tissue growth as examined in *in vivo* implantation [84].

Alginate-based hydrogels have been widely studied for their potential application in cartilage tissue regeneration, both as scaffolds and as matrix for entrapment and delivery of biologically active molecules or cells [84–86]. In several studies, alginates have been combined with chondrocytes and either injected into the site of interest [87–89] or molded and then implanted [90]. Wang and coworkers [81] have reported on the development of a highly-organized three-dimensional alginate scaffold. They have

seeded them with porcine chondrocytes and then implanted them in the dorsal subcutaneous site of SCID mice and demonstrated the formation of cartilage-like structures 4 weeks after implantation. Chalain *et al.* [92] reported on a reconstruction of elastic cartilages using isolated chondrocytes harvested from human and porcine ears. Authors established an *in vitro* aggregation of isolated chondrocytes followed by the embedding of these aggregates in hydrogel synthesized by combination of alginate, collagen type I and k-elastin, and claimed the most efficient reconstruction of elastic cartilage after transplantation in athymic mice. Results of *in vivo* studies indicated that after four weeks of implantation the chondrocytes had produced ECM proteins consistent with cartilage [89–92].

1.4.4 Starch-based Materials

Starch is the major polysaccharide constituent of plant tissues. It is comprised of a mixture of a linear poly(1,4-*a*-D-glucopyranose) (amylose) and a branched poly(1,4-*a*-D-glucopyranose) with branches of (1,6-*a*-D-glucopyranose) (amylopectin) occurring nearly every 25 glucosidic moieties [93]. Starch is produced in the form of semicrystalline granules with different size and composition depending upon the source [93]. This polymer can easily be processed using a variety of techniques to give shape as required, for example, by 3D porous scaffolds, microparticles and gels. The starch-based products are totally biodegradable and cost-effective, and thus facilitate an enormous potential for a wide range of applications in the biomedical field [94, 95].

Starch-based polymeric systems are commonly blended with other polymers to provide good mechanical properties. Blends of starch with ethylene vinyl alcohol (SEVA-C), cellulose acetate (SCA), polycaprolactone (SPCL) and poly(lactic acid) (SPLA) have been proposed as potential alternative biodegradable materials for a wide range of biomedical applications [96]. The structure and functional properties of starch-based blended materials depend on blend components, material processing technique, incorporation and nature of additives, and reinforcement fillers [97–102].

Starch and polycaprolactone blend (SPCL) scaffolds had been fabricated by melt spinning, followed by fiber bonding. The processing technique involves fiber packing in an appropriate mold with posterior heating below the melting temperature (T_m) for a determined residence period that will allow the fibers to form a stable mesh structure. The material used was a 30/70 (wt.%) blend of corn starch with polycaprolactone (SPCL). These scaffolds were tested for cartilage tissue engineering. After 6 weeks of cell culture, bovine articular chondrocytes, seeded on the scaffolds under dynamic conditions, presented normal morphological features with an extensive presence of cells at the surface of the support structures, and

penetrating the scaffolds pores [103]. It was observed that the fiber mesh network for support of cell growth and development presents good inter-connectivity. The fiber network structure and an extensive porous area (approximately 75% as estimated by μCT) is an advantage with regard to the cells penetration into the bulk of the scaffold while at the same time enhancing nutrient diffusion and removal of metabolic wastes. Sa-Lima *et al.* [104] evaluated the starch-CS hydrogels induced chondrocytic differentiation and cartilage matrix accumulation and also the influence of starch in the chondrogenesis of encapsulated adipose derived stromal (ADSC) cells. The ADSC were found to be homogeneously encapsulated, viable, proliferating and maintaining the expression of typical chondrogenic markers genes, and depositing cartilage ECM molecules.

1.4.5   Cellulose-based Materials

Cellulose is the most abundant natural and renewable resource polysaccharide, available worldwide. This polymer exists in lignocellulosic material in forest and plants. Other sources are algae, bacteria biosynthesis, and chemosynthesis [105]. Among all celluloses, the bacterial cellulose (BC) has unique properties including high purity, a nanofibrous structure, high crystallinity, high tensile strength and good biocompatibility [106–110]. Thus, many researchers have focused on BC-based materials for various biomedical applications, including blood vessel engineering [111] and wound healing [112], which exhibited good *in vivo* biocompatibility after 12 weeks of subcutaneous implantation in rats, and were found to be well integrated into the host tissue without any chronic inflammatory responses [113]. Svensson *et al.* [114] have demonstrated that BC is a potential scaffolding material for cartilage regeneration, and investigated the native and chemically modified BC (by phosphorylation and sufation) materials using bovine chondrocytes. The results indicate that unmodified BC supports chondrocyte proliferation at levels of approximately 50% of the collagen type II substrate, while providing significant advantages in order to improve mechanical properties. Compared to tissue culture plastic and calcium alginate, unmodified BC showed significantly higher levels of chondrocyte growth. Even though chemically modified BC was able to mimic the glucosaminoglycans of native cartilage it did not significantly enhance chondrocyte growth. However, the porosity of the material was found to affect the chondrocyte viability.

For cartilage tissue engineering application, the delivery of cells by an injectable hydrogel scaffold as a noninvasive surgery procedure is a promising approach. In this application the desired cell-based construct must be retained at the repair site after being injected [115]. To achieve this requirement, researchers have focused on the development of a hydrophilic polymer able to exhibit self-reticulation properties [116]. An interesting
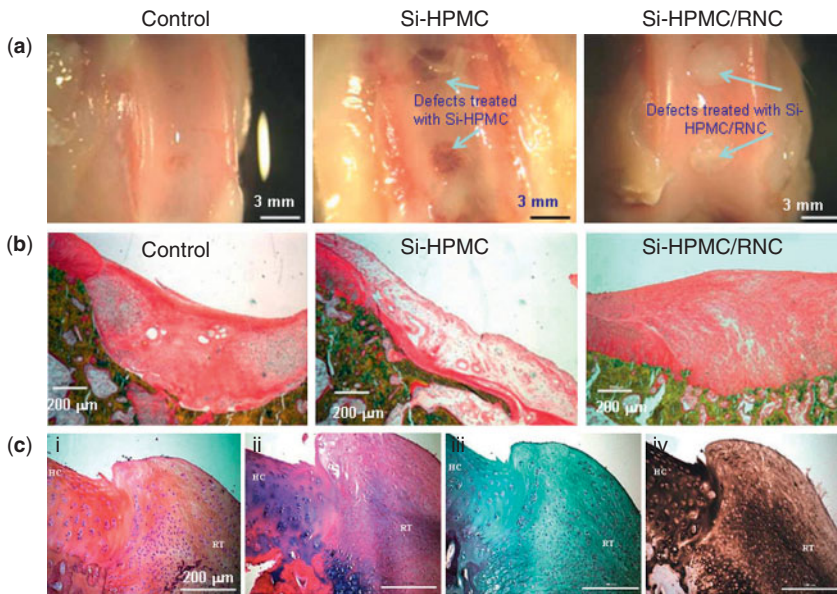
Figure 1.4 Cellulose-based scaffold for cartilage: (a) Macroscopic and (b) histological analysis of defects treated with Si-HPMC alone (Si-HPMC) or with Si-HPMC containing RNC (Si-HPMC/ RNC) 6 weeks after implantation and compared with defects left empty (as a control). (c) Immunohistological analysis of articular cartilage defects after 6 weeks implantation. Representative sections of defects filled with Si-HPMC containing autologous RNC were stained with hematoxylin/phloxin/safran (c-i), Alcian blue (c-ii), Masson's trichrome (c-iii), and immunostained for type II collagen (c-iv). HC: healthy cartilage. RT: repaired tissue. Reprinted with permission from [116].

self-setting, cellulose-based hydrogel has been developed by Vinatier *et al.* [116–118] which consists of silanized hydroxypropyl methylcellulose (Si-HPMC). The authors demonstrated that this Si-HPMC hydrogel was a suitable matrix for the *in vitro* three-dimensional culture of rabbit articular chondrocytes. The transplantation of Si-HPMC hydrogel containing autologous nasal chondrocytes led to the repair of an articular cartilage defect in a rabbit model (Figure 1.4). The transplantation of Si-HPMC hydrogel and cells constructed in an articular cartilage defect through percutaneous injection has paved the way for new therapeutic strategies for the treatment of cartilage defects in minimally invasive surgery. However, the density of hydrogel networks is critically important and need to be optimized for maintenance of the chondrocyte phenotype [119], and such parametric studies need major attention before implantation. Other research group [120] investigated the suitability of viscose cellulose sponges as a scaffold for cartilage tissue engineering. The sponges were also coated with recombinant human type II collagen and lyophilized, and then crosslinked with

glutaraldehyde. *In vitro* investigation showed that the cellulose and cellulose/recombinant type II collagen sponges supported the chondrocytes growth. These sponges provided a nontoxic environment for these cells and maintained chondrocyte morphology. Crosslinked type II collagen promoted a slight increase in scaffold stiffness, however, the constructs remained soft compared with normal articular cartilage, and is therefore a potential candidate material for cartilage tissue engineering.

1.5 Conclusions and Remarks on Prospects

Despite extensive research conducted on cartilage tissue engineering over the past four decades, a procedure for a successful repair of damaged cartilage still remains elusive. However, many new repair techniques have recently emerged which have demonstrated promising results in experimental animal models.

The current practice is the direct injection of autologous chondrocytes, whereas, the future cartilage therapies will most likely utilize complex tissue engineering strategies. For example, chondrocytes growth on fibrous or sponge 3D scaffolds with controlled pores, pore sizes and excellent mechanical properties have been demonstrated. They have been shown to have enhanced cell-cell communication and biological signaling pathways for promoting specific cartilage regeneration. The hydrogel-based system has been shown to have high potential for the delivery of chondrocyte to a localized area. However, for this system, the crosslinking density needs to be optimized prior to the cells encapsulation. To evaluate novel materials strategies an *in vitro* model needs to be developed to understand how materials and strategy influence the chondrocyte proliferation and maintain the chondrogenic genes' expression while providing a noncytotoxic microenvironment. This will provide valuable information that will allow for the design of *in vivo* animal study procedures. Designing an appropriate animal model is an important factor for monitoring cell fate, inflammatory response and long-term functional stability. While designing the experiment, it is also important to take into account the variation of cartilage thickness and different loading distribution in cartilage across species.

Over the past decade, there have been a growing number of investigations on the *in vivo* biocompatibility of these materials, with encouraging results in terms of host tissue response. However, there remains a lack of knowledge on the issue of the long-term *in vivo* studies as well as the tracking of biodegradation profile of these polysaccharide-based polymers. It is now our hope that with greater understanding of cartilage tissue engineering with a novel materials approach an effective solution to repair damaged cartilage will be available in the very near future.

References

1. R.S. Langer, J.P. Vacanti, *Scientific American*, Vol. 280, p. 86, 1999.
2. L. Danisovic, I. Varga, R. Zamborsky, D. Bohmer, *Experim. Biology Medicine*, Vol. 237, p. 10, 2012.
3. C. Goepfert, A. Slobodianski, A.F. Schilling, P. Adamietz, R. Portner, *Adv. Biochem. Engin. Biotechnol.*, Vol. 123, p. 163, 2010.
4. S. Marlovits, P. Zeller, P. Singer, C. Resinger, V. Vecsei, *European J. Radiology*, Vol. 57, p. 24, 2006.
5. M. Keeney, J.H. Lai, F. Yang, *Curr. Opinion Biotechnol.*, Vol. 22, p. 734, 2011.
6. I.L. Kim, R.L. Mauck, J.A. Burdick, *Biomaterials*, Vol. 32, p. 8771, 2011.
7. C. Chung, J.A. Burdick, *Adv. Drug Deliv. Rev.*, Vol. 60, p. 243, 2008.
8. R.L. Mauck, X. Yuan, R.S. Tuan, B. Chief, *Osteoarthritis Cartilage*, Vol. 14, p. 179, 2006.
9. S.J. Bryant, K.S. Anseth, *J. Biomed. Mater. Res. Part A*, Vol. 64A, p. 70, 2003.
10. L.A. Solchaga, J.S. Temenoff, J.Z. Gao, A.G. Mikos, A.I. Caplan, V.M. Goldberg, *Osteoarthritis and Cartilage*, Vol. 13, p. 297, 2005.
11. L.E. Freed, J.C. Marquis, G. Vunjaknovakovic, J. Emmanual, R. Langer, *Biotechnol Bioengin*, Vol. 43, p. 605, 1994.
12. F. Khan, R.S. Tare, R.O.C. Oreffo, M. Bradley, *Angew. Chem. Int. Ed.*, Vol. 48, p. 978, 2009.
13. S. Hirano, T. Midorikawa, *Biomaterials*, Vol. 19, p. 293, 1998.
14. Y. Qin, O.C. Agboh, *Med. Dev. Technol.*, Vol. 9, p. 24, 1998.
15. G. Peluso, O. Petillo, M. Ranieri, M. Santin, L. Ambrosio, D. Calabro, B. Avallone, G. Balsamo, *Biomaterials*, Vol. 15, p. 1215, 1994.
16. Y. Usami, Y. Okamoto, S. Minami, A. Matsuhashi, N.H. Kumazawa, S. Tanioka, Y. Shigemasa, *J. Vet. Med. Sci.*, Vol. 56, p. 761, 1994.
17. Y. Usami, Y. Okamoto, T. Takayama, Y. Shigemasa, S. Minami, *J. Biomed. Mater. Res.*, Vol. 42, p. 517, 1998.
18. T. Chandy, C. Sharma, *Biomater. Artif. Cell Artif. Organs*, Vol. 18, p. 1, 1990.
19. A. Denuziere, D. Ferrier, O. Damour, A. Domard, *Biomaterials*, Vol. 19, p. 1275, 1998.
20. H. Onishi, Y. Machida, *Biomaterials*, Vol. 20, p. 175, 1999.
21. R. Muzzarelli, V. Baldassarre, F. Conti, P. Ferrara, G. Biagini, G. Gazzanelli, V. Vasi, *Biomaterials*, Vol. 9, p. 247, 1988.
22. K. Nishimura, S. Nishimura, N. Nishi, I. Saiki, S. Tokura, I. Azuma, *Vaccine*, Vol. 2(1), p. 93, 1984.
23. T. Hamano, A. Teramoto, E. Iizuka, K. Abe, *J. Biomed. Mater. Res.*, Vol. 41, p. 270, 1998.
24. S.V. Madihally, H.W. Matthew, *Biomaterials*, Vol. 20, p. 1133, 1999.
25. L. De Franceschi, B. Grigolo, L. Roseti, A. Facchini, M. Fini, G. Giavaresi, M. Tschon, R.Giardino, *J. Biomed. Mater. Res. Part A*, Vol. 75A, p. 612, 2005.
26. T. Fujisato, T. Sajiki, Q. Liu, Y. Ikada, *Biomaterials*, Vol. 17, p. 155, 1996.
27. H.B. Fan, Y.Y. Hu, L. Qin, X.S. Li, H. Wu, R. Lv, *J. Biomed. Mater. Res. Part A*, Vol. 77A, p. 785, 2006.
28. D. Eyrich, F. Brandl, B. Appel, H. Wiese, G. Maier, M. Wenzel, R. Staudenmaier, A. Goepferich, T. Blunk, *Biomaterials*, Vol. 28, p. 55, 2007.

29. R.P. Silverman, D. Passaretti, W. Huang, M.A. Randolph, M.J. Yaremchuk, *Plastic and Reconstructive Surgery*, Vol. 103, p. 1809, 1999.
30. A. Hoshikawa, Y. Nakayama, T. Matsuda, H. Oda, K. Nakamura, K. Mabuchi, *Tissue Engineering*, Vol. 12, p. 2333, 2006.
31. W.Y. Xia, W. Liu, L. Cui, Y.C. Liu, W. Zhong, D.L. Liu, J.J. Wu, K.H. Chua, Y.L. Cao, *J. Biomed. Mater. Res. Part B-Applied Biomaterials*, Vol. 71B, p.373, 2004.
32. S. Hofmann, S. Knecht, R. Langer, D.L. Kaplan, G. Vunjak-Novakovic, H.P. Merkle, L. Meinel, *Tissue Engineering*, Vol. 12, p. 2729, 2006.
33. Y.Z. Wang, H.J. Kim, G. Vunjak-Novakovic, D.L. Kaplan, *Biomaterials*, Vol. 27, p. 6064, 2006.
34. F. Khan, J.O. Smith, J.M. Kanzcler, R.S. Tare, R.O.C. Oreffo, M. Bradley, *Advan. Fun. Mater.*, 2012, DOI: 10.1002/adfm.201202710 (Published on line).
35. F. Khan, S.R. Ahmad, *Macromol. Biosci.*, 2012, DOI: 10.1002/mabi.201200409.
36. F. Khan, R.S Tare, J.M. Kanczler, R.O.C. Oreffo, M. Bradley, *Biomaterials*, Vol. 31(8), p. 2216, 2010.
37. J.-K. F. Suh, H.W.T. Matthew, *Biomaterials*, Vol. 21, p. 2589, 2000.
38. A. Lahiji, A. Sohrabi, D.S. Hungerford, C.G. Frondoza, *J. Biomed. Mater. Res.*, Vol. 51(4), p. 586, 2000.
39. X.Z. Shu, Y. Liu, F. Palumbo, G.D. Prestwich, *Biomaterials*, Vol. 24, p. 3825, 2003.
40. A. Ramamurthi, I. Vesely, *J. Biomed. Mater. Res.*, Vol. 60, p. 195, 2002.
41. S. Hsu, S.W. Whu, S.-C. Hsieh, C.-L. Tsai, D. C. Chen, T.-S. Tan, *Artificial Organs*, Vol. 28(8), p. 693, 2004.
42. K.M. Park, S.Y. Lee, Y.K. Joung, J.S. Na, M.C. Lee, K.D. Park, *Acta Biomater,* Vol. 5(6), p. 1956, 2009.
43. S.E. Kim, J.H. Park, Y.W. Cho, H. Chung, S.Y. Jeong, E.B. Lee, I.C. Kwon, *J. Controlled Release*, Vol. 91(3), p. 365, 2003.
44. J.E. Lee, K.E. Kim, I.C. Kwon, H.J. Ahn, S.-H. Lee, H. Cho, H.J. Kim, S.C. Seong, M.C. Lee, *Biomaterials*, Vol. 25(18), p. 4163, 2004.
45. R.S. Tigli, M. Gumusderelioglu, *Int. J. Biological Macromol.*, Vol. 43(2), p. 121, 2008.
46. M. Mattioli-Belmonte, A. Gigante, R.A. Muzzarelli, R. Politano, A. De Benedittis, N. Specchia, A. Buffa, G. Biagini, F. Greco, *Med. Biol. Eng. Comp.*, Vol. 37, p. 130, 1999.
47. C.B. Knudson, W. Knudson, *Semin. Cell Dev. Biol.*, Vol. 12, p. 69, 2001.
48. J.R. Fraser, T.C. Laurent, U.B. Laurent, *J. Intern. Med.,* Vol. 242, p. 27, 1997.
49. G.P. Dowthwaite, J.C. Edwards, A.A. Pitsillides, *J. Histochem. Cytochem.*, Vol. 46, p. 641, 1998.
50. C. Hardwick, K. Hoare, R. Owens, H.P. Hohn, M. Hook, D. Moore, V. Cripps, L. Austen, D.M. Nance, E.A. Turley, *J. Cell Biol.*, Vol. 117, p. 1343, 1992.
51. W.F. Cheung, T.F. Crue, E.A. Turley, *Biochem. Soc. Trans.*, Vol. 27, p. 135, 1999.
52. J. Entwistle, C.L. Hall, E.A. Turley, *J. Cell Biochem.*, Vol. 61, p. 569, 1996.
53. P.A. Band, Hyaluronan derivatives: Chemistry and clinical applications, in T.C. Laurent, Ed., *The Chemistry, Biology and Medical Applications of Hyaluronan and Its Derivatives.* London, Portland Press, pp. 33–42, 1998.
54. P. Bulpitt, D. Aeschlimann, *J. Biomed. Mater. Res.*, Vol. 47, p. 152, 1999.

55. D. Campoccia, P. Doherty, M. Radice, P. Brun, G. Abatangelo, D. F. Williams, *Biomaterials*, Vol. 19, p. 2101, 1998.
56. Y. Luo, K.R. Kirker, G.D. Prestwich, *J. Control Release*, Vol. 69, p. 169, 2000.
57. K. Moriyama, T. Ooya, N. Yui, *J. Control Release*, Vol. 59, p. 77, 1999.
58. S. Ohya, Y. Nakayama, T. Matsuda, *Biomacromolecules,* Vol. 2, p. 856, 2001.
59. T. Pouyani, G.D. Prestwich, *Bioconjugate Chem.*, Vol. 5, p. 339, 1994.
60. G.D. Prestwich, K.P. Vercruysse, *Pharm. Sci. Technol. Today*, Vol. 1, p. 42, 1998.
61. G.D. Prestwich, Y. Luo, M.R. Ziebell, K.P. Vercruysse, K.R. Kirker, J.S. MacMaster, Chemically modified hyaluronan: New biomaterials and probes for cell biology, in G. Abatangelo, Ed., *New Frontiers in Medical Sciences: Redefining Hyaluronan,* London, Portland Press, pp. 181–194, 2000.
62. K.R. Kirker, Y. Luo, J.H. Nielson, J. Shelby, G.D. Prestwich, *Biomaterials*, Vol. 23, p. 3661, 2002.
63. C. Chung, J.A. Burdick, *Tissue Eng. Part A*, Vol. 15, p. 243, 2009.
64. C. Chung, M. Beecham, R.L. Mauck, J.A. Burdick. *Biomaterials*, Vol. 30, p. 4287, 2009.
65. Y.H. Jeon, J.H. Choi, J.K. Sung, T.K. Kim, B.C. Cho, H.Y. Chung, *J. Craniofac. Surg.,* Vol. 18, p. 1249, 2007.
66. G. Chow, C.B. Knudson, G. Homandberg, W. Knudson, *J. Biological Chemistry*, Vol. 270, p. 27734, 1995.
67. K. Lindenhayn, C. Perka, R.-S. Spitzer, H.-H. Heilmann, K. Pommerening, J. Mennicke, M. Sittinger, *J. Biomed. Mater. Res.*, Vol. 44, p. 149, 1999.
68. X.Z. Shu, Y. Liu, F. Palumbo, G.D. Prestwich, *Biomaterials*, Vol. 24, p. 3825, 2003.
69. A. Ramamurthi, I. Vesely, *J. Biomed. Mater. Res.*, Vol. 60, p. 195, 2002.
70. K. Ghosh, X.-D. Ren, X.Z. Shu, G.D. Prestwich R.A.F. Clark, *Tissue Eng.***,** Vol. 12, p. 601, 2006.
71. C. Eenschooten, F. Guillaumie, G.M. Kontogeorgis, E.H. Stenby, K. Schwach-Abdellaoui, *Carbohydr. Polym.*, Vol. 79 (3), p. 597, 2010.
72. J.L. Ifkovits, J.A. Burdick, *Tissue Eng.*, Vol. 13 (10), p. 2369, 2007.
73. J.A. Burdick, C. Chung, X. Jia, M.A. Randolph, R. Langer, *Biomacromolecules*, Vol. 6, p. 386, 2005.
74. B. Grigolo, G. Lisignoli, A. Piacentini, M. Fiorini, P. Gobbi, G. Mazzotti, M. Duca, A. Pavesio, A. Facchini, *Biomaterials***,** Vol. 23, p. 1187, 2002.
75. B. Grigolo, L. De Franceschi, L. Roseti, L. Cattini, A. Facchini, *Biomaterials*, Vol. 26, p. 5668, 2005.
76. B. Grigolo, L. Roseti, M. Fiorini, M. Fini, G. Giavaresi, N.N. Aldini, R. Giardino, A. Facchini, *Biomaterials,* Vol. 22, p. 2417, 2001.
77. G. KloKck, A. Pfefermann, C. Ryser, P. GroKhn, B. Kuttler, H. Hahn, U. Zimmermann, *Biomaterials*, Vol. 18(10), p. 707, 1997.
78. G.T. Grant, E.R. Morris, D.A. Rees, P.J.C. Smith, D. Thom, *FEBS Lett.*, Vol. 32, p. 195, 1973.
79. F.A. Peyton, in R.G. Craig, Ed., *Restorative Dental Materials*, 9th ed., St. Louis: Mosby, 1993.
80. I.R. Matthew, R.M. Browne, J.W. Frame, B.G. Millar, *Biomaterials*, Vol. 16(4), p. 275, 1995.
81. A. Atala, W. Kim, K.T. Paige, C.A. Vacanti, A.B. Retik, *J. Urol.*, Vol. 152, p. 641, 1994.

82. O. Smidsrod, G. Skjak-Braek, *Trends Biotechnol.*, Vol. 8(3), p. 71, 1990.

83. L. Shapiro, S. Cohen, *Biomaterials*, Vol. 18(8), p. 583, 1997.

84. P. Eiselt, J. Yeh, R.K. Latvala, L.D. Shea, D.J. Mooney, *Biomaterials*, Vol. 21, p. 1921, 2000.

85. C.-C. Wang, K.-C. Yang, K.-H. Lin, H.-C. Liu, F.-H. Lin, *Biomaterials,* Vol. 32, p. 7118, 2011.

86. S.-H. Hsu, T.-B. Huang, S.-J. Cheng, S.-Y. Weng, C.-L. Tsai, C.-S. Tseng. *Tissue Eng.: Part A*, Vol. 17, p. 1549, 2011.

87. A. Atala, W. Kim, K.T. Paige, C.A. Vacanti, A.B. Retik, *J. Urol.*, Vol. 152, p. 641. 1994.

88. K.T. Paige, L.G. Cima, M.J. Yaremchuk, J.P. Vacanti, C.A. Vacanti, *Plast. Reconst. Surg.*, Vol. 96, p. 1390, 1995.

89. Y.L. Cao, J. Pang, H.S. Zhan, Y.Y. Shi1, S.A. Abbah, W.W. Lu, X. Wang, S.C. Wang. *Scient. Res. Essays*, Vol. 6, p. 1364, 2011.

90. S.C.N. Chang, J.A. Rowley, G. Tobias, N.G. Genes, A.K. Roy, D.J. Mooney, C.A. Vacanti, L.J. Banassar, *J. Biomed. Mater. Res.*, Vol. 55, p. 503, 2001.

91. C.-C. Wang, K.-C. Yang, K.-H. Line, Y.-L. Liua, H.-C. Liuf, F.-H. Lina, *Biomaterials,* Vol. 33, p. 120, 2012.

92. T. de Chalain, J.H. Phillips, A. Hinek, *J. Biomed. Mater. Res.*, Vol. 44, p. 280, 1999.

93. R.F. Tester, J. Karkalas, Starch, in A. Steinbüchel, Ed., *Biopolymers,* Vol. 6. Weinheim, Wiley-VCH, pp. 381–438, 2002.

94. G.J.L. Griffin, Particulate starch based products, in G.J.L. Griffin, Ed., *Chemistry and Technology of Biodegradable Polymers,* Glasgow, Blackie Academic & Professional, pp.18–47, 1994.

95. G.A. Silva, O.P. Coutinho, P. Ducheyne, I.M. Shapiro, R.L. Reis, *Biomaterials*, Vol. 28, p. 326, 2007.

96. D. Puppi, F. Chiellini, A.M. Piras, E. Chiellini, *Prog. Polym. Sci.,* Vol. 35, p. 403, 2010.

97. M.E. Gomes, A.S. Ribeiro, P.B. Malafaya, R.L. Reis, A.M. Cunha, *Biomaterials*, Vol. 22, p. 883, 2001.

98. A.J. Salgado, M.E. Gomes, A. Chou, O.P. Coutinho, R.L. Reis, D.W. Hutmacher, *Mater. Sci. Eng. C*, Vol. 20, p. 27, 2002.

99. M.E. Gomes, J.S. Godinho, D. Tchalamov, A.M. Cunha, R.L. Reis, *Mater. Sci. Eng. C*, Vol. 20, p. 19, 2002.

100. G.A. Silva, A. Pedro, F.J. Costa, N.M. Neves, O.P. Coutinho, R.L. Reis, *Mater. Sci. Eng. C*, Vol. 25, p.237, 2005.

101. A.P. Marques, R.L. Reis, *Mater. Sci. Eng. C*, Vol. 25, p. 215, 2005.

102. N.M. Neves, A. Kouyumdzhiev, R.L. Reis, *Mater. Sci. Eng. C,* Vol. 25, p. 195, 2005

103. J.T. Oliveira, A. Crawford, J.M. Mundy, A.R. Moreira, M.E. Gomes, P.V. Hatton, R.L. Reis, *J. Mater. Sci. Mater. Med.*, Vol. 18, p. 295, 2007.

104. H. Sa-Lima, S.G. Caridade, J.F. Mano, R.L. Reis, *Soft Matter,* Vol. 6, p.5184, 2010.

105. D. Klemm, H.-P. Schmauder, T. Heinze, Cellulose, in A. Steinbüchel, Ed., *Biopolymers,* Vol. 6. Weinheim, Wiley-VCH, pp. 275–319, 2002.

106. S. Bae, M. Shoda, *Biotechnol. Prog.*, Vol. 20, p. 1366, 2004.

107. B. Fang, Y.-Z. Wan, T.-T. Tang, C. Gao, K.-R. Dai, *Tissue Eng. A*, Vol. 15, p. 1091, 2009.
108. S. Bielecki, A. Krystynowicz, M. Turkiewicz, H. Kalinowska, Bacterial cellulose, in A. Steinbüchel, Ed., *Biopolymers*, Vol. 5. Weinheim, Wiley-VCH, pp. 40–85, 2002.
109. R. Jonas, L.F. Farah, *Polym. Degrad. Stab.*, Vol. 59, p.101, 1998.
110. S. Yamanaka, J. Sugiyama, *Cellulose*, Vol. 7, p. 213, 2000.
111. D. Klemm, D. Schumann, U. Udhardt, S. Marsch, *Prog. Polym. Sci.*, Vol. 26, p. 1561, 2001.
112. W. Czaja, A. Krystynowicz, S. Bielecki, R.M. Brown Jr, *Biomaterials*, Vol. 27, p. 145, 2006
113. G. Helenius, H. Bäckdahl, A. Bodin, U. Nannmark, P. Gatenholm, B. Risberg, *J. Biomed. Mater. Res. A*, Vol. 76A, p. 431, 2006.
114. A. Svensson, E. Nicklasson, T. Harrah, B. Panilaitis, D.L. Kaplan, M. Brittberg, P. Gatenholm, *Biomaterials*, Vol. 26, p. 419, 2005.
115. M. Sittinger, D.W. Hutmacher, M.V. Risbud, *Curr. Opin. Biotechnol.*, Vol. 15(5), p. 411, 2004.
116. C. Vinatier, O. Gauthier, A. Fatimi, C. Merceron, M. Masson, A. Moreau, F. Moreau, B. Fellah, P. Weiss, J. Guicheux. *Biotechnol. Bioeng.*, Vol.102, p. 1259, 2009.
117. C. Vinatier, D. Magne, P. Weiss, C. Trojani, N. Rochet, G.F. Carle, C. Vignes-Colombeix, C. Chadjichristos, P. Galera, G. Daculsi, J. Guicheux, *Biomaterials*, Vol. 26, p. 6643, 2005.
118. C. Vinatier, D. Magne, A. Moreau, O. Gauthier, O. Malard, C. Vignes-Colombeix, G. Daculsi, P. Weiss, J. Guicheux, *J. Biomed. Mater. Res.*, Vol. 80A, p. 66, 2007.
119. R. Cancedda, B. Dozin, P. Giannoni, R. Quarto, *Matrix Biol.*, Vol. 22(1), p. 81, 2003.
120. H. Hertta Pulkkinen, V. Tiitu, E. Lammentausta, E.-R. Hämäläinen, I.I. Kiviranta, M. Lammi, *J. Bio.-Med. Mater. Eng.*, Vol. 16, p. S29, 2006.

Biomimetic Synthesis of Self-Assembled Mineralized Collagen-Based Composites for Bone Tissue Engineering

Xiumei Wang*, Zhixu Liu and Fuzhai Cui

School of Materials Science and Engineering, Tsinghua University, Beijing, China

Abstract

The self-assembled mineralized collagen fibrils are ubiquitous in most mammalian calcified tissues such as bone and dentine, which are hierarchically organized by collagen fibrils and hydroxyapatite (HA) crystallites giving these tissues unique hierarchical architectures and specialized functions. Therefore, many efforts have been concentrated on the thorough understanding of the collagen-medicated biomineralization processes and the biomimetic synthesis of the unique architectures for applications such as bone-defect repair and regeneration. In this chapter, we firstly highlight the current understanding of the self-assembling processes, microstructures and hierarchical organization of mineralized collagen fibrils in nature bone tissues, such as lamellar bones, woven bones, and zebrafish skeletal bones. And the biomimetic syntheses of self-assembled mineralized fibrils are then reviewed with emphases on mineralized collagen fibrils, although some other systems are also described. The biomimetric mineralized collagen fibrils, an organic/inorganic hybrid material that resembles the self-assembly of *in vivo* nanocomposites from nanoscale to micrometer scale, have been applied for the fabrication of biomimetic bone grafting materials showing great promise and success in clinical applications.

Keywords: Biomimetic, self-assembly, collagen, hydroxyapatite, bone tissue engineering, biomineralization

*Corresponding author: wxm@mail.tsinghua.edu.cn

2.1 Introduction

Hierarchical assembly of nanofibrils is ubiquitous in many biological tissues such as bone, muscle, and intestine, which plays important roles in enabling these tissues to perform specialized functions. Bone, for example, is made up of hierarchically assembled mineralized collagen fibrils with a precisely ordered organization of crystals of the mineral hydroxyapatite $(Ca_{10}(PO4)_6(OH)_2$, HA) in and around collagen matrix. The hierarchical assembly of natural bone has been thought to be due to its unique performances, including excellent intensity and toughness. Therefore, many efforts have concentrated on the thorough understanding of the processes and mechanisms involved in the formation of the unique architectures. These investigations have not just improved our understanding of collagen-mediated biomineralization in calcified tissues, but have also offered new ideas in the design and fabrication of new functional materials with biomimetic strategies.

Large bone defects, which are mostly caused by trauma, tumors or diseases, are quite common problems in a clinical setting with a high demand for bone substitutes. Current therapies of bone replacement include the use of autograft, allograft, or artificial bone material. Although autologous bone grafts are widely recognized as the "gold standard" for healing large bone defects, autologous transplantation in a clinical setting is limited because of the limited graft quantity, donor site morbidity and infection or pain to patients from secondary surgery [1, 2]. As for allografts, the main problem is the potential risk of transmitting diseases and the immunological response [3]. Therefore, it is quite necessary and crucial to develop a promising alternative to autografting and allografting. As we all know, many kinds of bone graft substitutes, such as HA, bioactive glass ceramics and poly(methyl methacrylate), have been developed and widely used for bone replacement and bone defect filling. However, these bone materials are not biodegradable or bioactive and do not match the requirements of bone regeneration and remodeling as permanent implantations. In recent years, bone tissue engineering has made great progress in large bone defects repair by creating novel artificial constructs to direct bone regeneration [4]. And the design and fabrication of synthetic biomaterials are the crucial elements of bone tissue engineering. According to biomimetic strategies, HA and collagen, as the main components of natural bone, have been consequentially applied for the synthesis of artificial bone materials [5–8]. In this sense, the most promising approach for bone regeneration is to realize a real bioactive artificial bone material mimicking the compositions, hierarchical organization, and biological functions of bone tissues.

In this chapter, we will highlight the current understanding of the microstructures and hierarchical organization of mineralized collagen fibrils in calcified tissues, as well as recent work involving biomimetic

synthesis of self-assembling mineralized collagen-based composites for bone tissue engineering.

2.2   Hierarchical Assembly of Mineralized Collagen Fibrils in Natural Bone

2.2.1   Panorama of Natural Bone

2.2.1.1   *Chemical Composition of Bone*

Bone is a type of specialized mineralized connective tissue with highly complex hierarchical structure composed primarily of 34% organic matrix, 65% inorganic minerals, and 1% water by weight [19]. It is a precisely organized natural hybrid nanomaterial with unique mechanical properties determined by its chemical composition and microstructure.

The organic matrix consists of around 90% type I collagen and 10% other so-called noncollagenous macromolecules, including acidic proteins, glycosaminoglycans, and proteoglycans. Collagen is a long, fibrous structural protein that provides flexibility of bone and structural templates for mineral deposition. The noncollagenous proteins contain over 200 different functional proteins, such as osteonectin, osteocalcin, bone morphogenetic proteins, bone proteoglycan, and bone sialoprotein [23]. And the inorganic part of bone is composed of nonstoichiometric carbonated HA with poor crystallinity [9]. The total carbonate content in HA is about 4–7% with replacing both PO_4^{3-} (B-type substitution) and OH^- (A-type substitution) in various lattice sites. The biological HA crystals are only 2–6 nm thick, 30–50 nm wide, and 60–100 nm long, which are directly related to the stiffness of bone. During the processes of HA biomineralization, several other calcium phosphate phases have been identified as intermediates [10–12]. There is evidence of the formation of an amorphous calcium phosphate (ACP) or Dicalcium Phosphate (DCPD) in the early stage of bone and cartilage mineralization, and then ACP transforms to octacalcium phosphate (OCP). OCP or DCPD will stabilize readily in the form of HA at last.

In bone tissues there are three types of bone cells, osteoblasts, osteocytes, and osteoclasts, entrapped in the homogeneous bone matrix, which are primarily responsible for bone formation, remodeling, and maintenance of osteoarchitecture. Osteoblasts are bone-forming cells and are generally considered to differentiate from preosteoblast, mesenchymal progenitor cells, which secrete bone matrix to form bone with further mineralization. Osteocytes are also bone-forming cells, which maintain bone as differentiated osteoblasts by secreting growth factors. Osteoclasts are bone-resorbing cells that are large with multinuclei. Osteoblasts and osteoclasts work simultaneously contributing to bone remodeling, which is the replacement of the old bone tissue by new bone tissue.

2.2.1.2 *Hierarchical Organization of Natural Human Bone*

The properties of bone are a list of apparent contradictions: strong but not brittle, lightweight but solid enough to support tissues, mechanically strong but porous, stable but capable of remodeling, and so on and so forth. Seven levels of hierarchical organization of human long bone from the molecular to the macroscopic scale were described by Weiner *et al.* [13, 14], shown in Figure 2.1. The basic building block of the bone materials is the mineralized collagen fibril (level 2), which is composed of very

Level 7: Whole bone

Level 6: Spongy vs Compact bone

Level 5: Cylindrical motifs: Osteons

Level 4: Fibril array patterns

Level 3: Fibril array

Level 2: Mineralized collagen fibril

Level 1: Major components
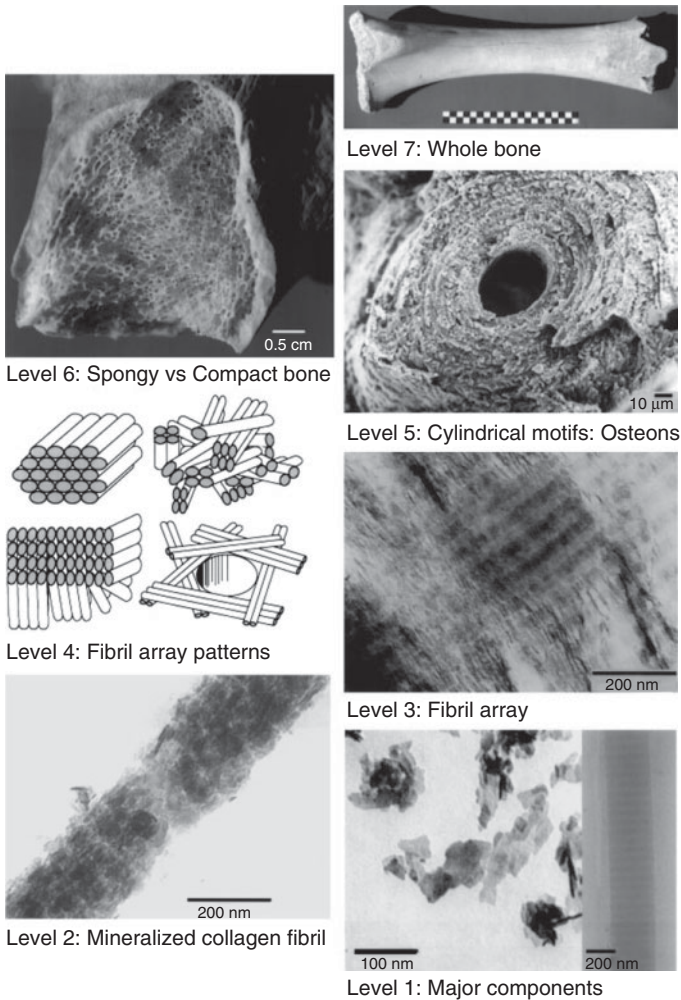
Figure 2.1 Schematic representation of the seven hierarchical levels of organization of human long bone. Reprinted with permission from [14].

hard material, the mineral and much softer material, the collagen fibrils (level 1). Mineralized collagen fibrils are always present in bundles or arrays aligned along their length (level 3). These fibril arrays organize into four common patterns: arrays of parallel fibrils, woven fiber structure, plywood-like structure, and radial fibril arrays (level 4). At a higher level of organization, the initially deposited primary bone undergoes internal remodeling and forms the secondary bone with a central canal for blood vessels and nerves, which is called "Haversian system" (level 5). The levels 6 and 7 refer to solid versus spongy bone and whole bones, respectively.

2.2.2 Self-Assembly of Mineralized Collagen Fibrils in Nature

2.2.2.1 *Collagen and Collagen Fibrils Array*

Collagen is the most abundant fibril-forming protein in mammalian tissues, accounting for up to one-third of all proteins. Collagen fibers are the main components of the extracellular matrix in various tissues [15, 16]. Variations in the amino acid sequence generate the different types of collagen: type I, II, III and so on. The main function of collagen is as an integrity and mechanical reinforcement of both soft and hard connective tissue [14, 17, 18]. Type I collagen molecule, as the major organic component of bone, is made up of three polypeptide strands called alpha peptides forming a triple helical assembly with approximately 300 nm long and 1.5 nm in diameter. A distinct feature of each alpha peptide chain of collagen is the repeated arrangement of amino acids Gly-X-Y, where X and Y can be any amino acid, but are frequently the amino acids proline and hydroxyproline, respectively [19]. The side chains of residues in X- and Y-positions point out of the helix, and play an important role in fibril formation through interactions between oppositely charged residues and through hydrophobic interactions between residues of different molecules. The three chains are arranged in parallel, and supercoiled along a common axis to form a right-handed triple helix [20].

The triple helical collagen molecules self-assemble with their long axes in parallel into a staggered arrangement in which each molecule is shifted with respect to its neighboring molecules forming characteristic D-periodic cross-striated pattern (where D = 67 nm, the characteristic axial periodicity of collagen) [21]. The successive molecules in same axial dimension are 40 nm apart, named "Hole" or "Gap" zone. The typical 67 nm period of cross-striation pattern of collagen assembly is widely observed by transmission electron microscope (TEM), atomic force microscope (AFM), and X-ray diffraction (XRD) investigation. The most widely accepted model for packing of collagen molecules is that five triple helices align hexagonally in cross section and longitudinally with approximately a quarter of the molecular length of staggered arrangement to form the five-stranded microfibrils. The diameter of the collagen fibrils in the five-stranded
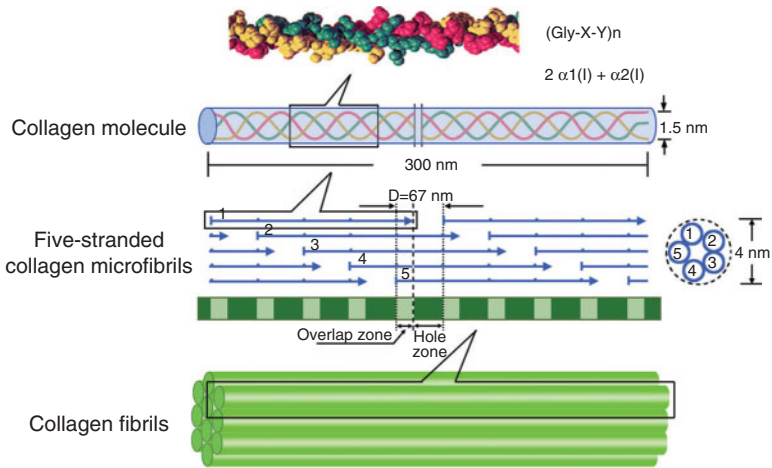
Figure 2.2 Structural assembly of collagen fibrils.

packing model should be about 3.6 nm according to 1.5 nm of diameter of single collagen molecule, which has been verified by TEM examination of native collagen fibrils. The collagen microfibrils are then assembled into collage fibrils in diameter from 35–500 nm that are further combined, oriented and laid up to form ordered structures with particular morphologies for tissues. The overwhelming consideration in the arrangement of collagen fibrils to form connective tissues is the resulting tissue function. The structural assembly of collagen fibrils is shown in Figure 2.2.

2.2.2.2 Structural Organization of Mineralized Collagen Fibrils

The basic building blocks of bone materials are mineralized collagen fibrils. The 67 nm periodic cross-striated pattern has been observed in both stained unmineralized collagen fibrils and mineralized collagen fibrils, which implies that the stain and minerals should deposit at the same location within the fibrils. The schematic diagram of the structural organization of mineralized collagen fibrils is shown in Figure 2.3. The first-formed minerals nucleate initially in the "hole" zones of assembled collagen fibrils with continuous growth, and then penetrate into the overlap regions of the fibrils. The tiny crystals, carbonated nano-HA with hexagonal crystal symmetry, are plate-shaped and array in parallel with preferred crystallographic orientation that is their c-axes co-align with the long axes direction of collagen fibrils.

The crystals are extremely small–in fact they are probably the smallest biologically formed crystals. In addition, the crystals may change in size and composition with age. Therefore, it is very difficult to determine the exact crystal dimensions in native occurring mineralized collagen fibrils. Although
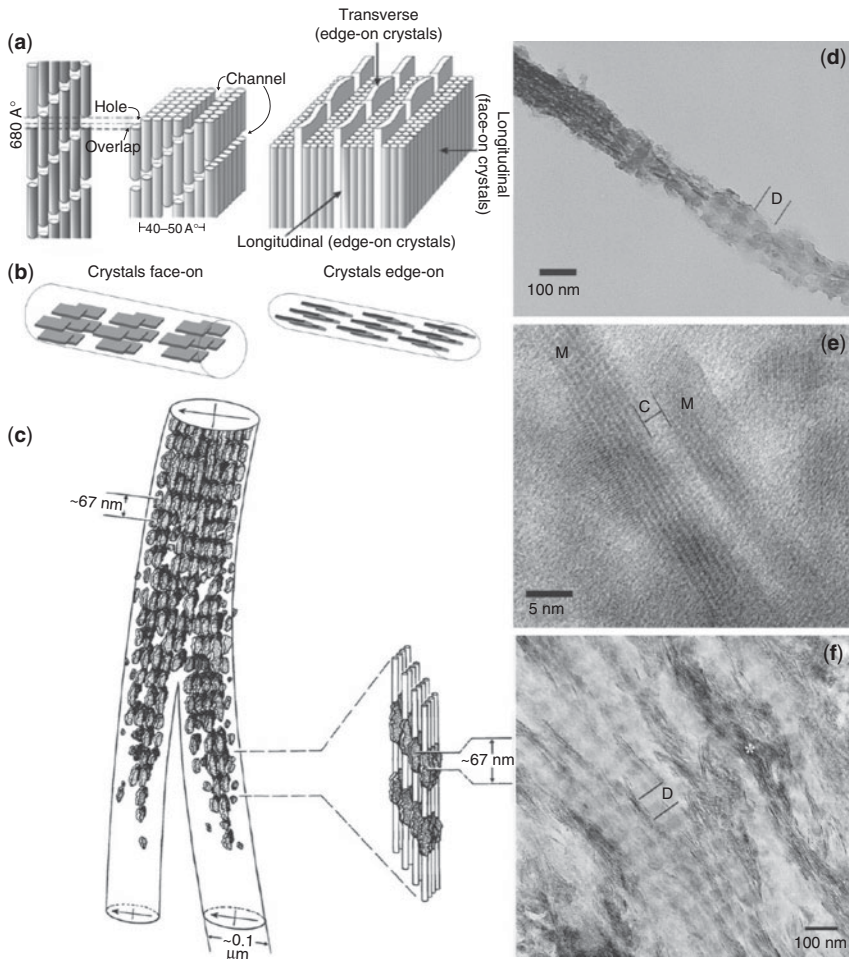
Figure 2.3 Structural organization of the mineralized collagen fibrils. (a) Model of mineralized collagen fibrils showing the arrays of the plate-like mineral crystals in the channels formed in staggered arranged collagen fibrils. (b) Face-on and edge-on projections of the crystals in the mineralized fibril. (c) The drawing of two mineralized collagen fibrils in avian tendon. (d) TEM micrograph of an isolated mineralized collagen fibril from human dentin. (e) HRTEM micrograph of two edge-on crystals in the mineralized collagen fibril. (f) TEM micrograph of an array of the mineralized fibrils from human dentin. Reprinted with permission from [34].

many methods including TEM, XRD, AFM, and Small angle X-ray scattering (SAXS) measurements have been used to analyze the HAp crystal size in mineralized collagen fibrils, it is clear that the values of crystal size from different measurements are not consistent. TEM examination is considered to be the most direct mean for visualizing these crystals. Robinson *et al.*, [22, 23]

reported that the dispersed human bone crystals are all plate-shaped with an average length of 40 nm and width of only slightly less. However, Fernandez-Moran *et al*. [24] reported the crystals are needle-shaped with 3–6 nm in diameter and 20 nm in length using the same examining technique, while the needle-shaped morphologies of the crystals were viewed as the edge-on projections of the plate-shaped crystals in the mineralized fibrils. Jackson *et al*. [25] used the TEM in the selected area dark field diffraction mode to measure the lengths of crystals in the c-axis direction, and obtained values of 32×16 nm for human bone. SAXS has also been used to estimate shape and smallest dimensions of the crystals. The results revealed needle-shaped crystals in bone and plate-shaped crystals in mineralized turkey tendon [24, 26–28]. Another approach for estimating bone crystal sizes is to measure X-ray reflection line widths for calculating. The resulting parameter is directly related to coherence length, which is the average distance between lattice dislocations in a given direction [29]. It can provide only an approximate estimate of crystal size, if it is assumed that the crystals are so small and perfect that their coherence lengths are similar to particle size dimensions [30]. Finean and Engstroml [31] firstly used this method to report human bone crystal lengths. Subsequently it has been widely used [25, 32, 33] to report the values obtained tend to be between 10 and 35 nm.

Although the mineral platelets are quite small, the dimensions and surface area are still much larger than the diameter of single collagen molecule. It is possible that collagen molecules interact with the minerals at the atomic and molecular levels forming ionic bonds between polar side-chain of collagen and calcium ions in the minerals.

Mineralized collagen fibrils from different type of bone tissues are always the same, but their higher level of organization varies significantly, which are primarily adapted to the variety of mechanical functions that bone fulfills. The mineralized collagen fibrils are always aggregated in bundles or arrays. The most common fibril array patterns are arrays of parallel fibrils, woven structure fibrils, plywood-like structure fibrils, and radial fibrils [14]. The parallel fibrils array is mostly found in mineralized turkey tendons and parallel fiber bone. The woven structure fibrils array found in woven bone is loosely packed with poorly oriented fibril bundles. Plywood-like structure fibrils array present in lamellar bone with successive layers of parallel fibrils. Radial fibrils array is the characteristic organization of dentin. The mineralized collagen fibrils are organized into layers that surround parallelly the plane of the pulp cavity wall.

2.2.2.3   *Examples of Mineralized Collagen Fibrils in Natural Tissues*

2.2.2.3.1   Lamellar Bones

Lamellar bone is the most abundant type of assembled structure of bone in many mammals, including human cortical and trabecular bone [13].

A basic structural motif of lamellar bone is the presence of arrays of parallel mineralized collagen fibrils, with successive arrays having different orientations to form a plywood-like structure. Weiner *et al.* investigated the organization of lamellar bones thoroughly and suggested that the lamellar bone could be viewed as a series of lamellar units. A lamellar unit is composed of five sublayers [35] containing successive arrays of aligned mineralized collagen fibrils, with their orientation to the lamellar boundary plane increasing in four increments of about 30°. The first sublayer of fibrils, adjacent to one side of the lamellar boundary, is aligned perpendicular to the long axis of the bone. Based on the fact that in vitrified transverse sections one layer is almost inevitably in the plane of the section, they proposed that this first sublayer should arbitrarily be assigned a value of 0° for the plywood angle. And the final array is oriented at 120° after four increments of 30° [13, 36]. The SEM micrographs have confirmed that the fifth sublayer is indeed oriented in a different direction from the other layers. The thicknesses of the five sublayers are roughly equal in some lamellar bone from different animals, while in some cases are not.

2.2.2.3.2   Woven Bones

It is known that woven bone differs from lamellar bone in the organization of mineralized collagen fibrils, cell populations, and its mechanical properties [37, 38]. Woven bone represents tissue in the early stages of bone mineralization, which is defined as having randomly distributed collagen fibrils and is deposited only during initial bone formation and fracture repair [39]. The collagen fibrils usually show some degree of preferential orientation parallel to the long axis of the bone, but do not lie parallel to one another. Especially, the collagen fibrils are interweaving and disperse in newly deposited bone [40].

In order to understand the differences between the morphology and distribution of collagen assembly in woven bone, Su *et al.* have examined mineralized collagen fibrils and isolated crystals from the mid-diaphyses of human fetal femurs. Despite the differences in the organization of collagen fibrils, the apatite crystals in woven bone are platelet-shaped, which are similar to mature crystals from lamellar bone [41–44]. These platelet-shaped apatite crystals of human woven bone deposited on the surfaces of collagen fibrils, within the intrafibrillar collagen spaces, and between collagen fibrils in their extrafibrillar regions [39]. The average crystal dimensions in woven bone are considerably smaller than those of mature crystals in lamellar bone because of a high rate of old bone resorption and new bone formation in woven material [38].

2.2.2.3.3   Zebrafish Skeletal Bone

Zebrafish have been originally accepted as a simple and powerful model animal to investigate the vertebrate biology, being well suited to both developmental and genetic analysis [45, 46]. Studies on bone mineralization

and bone diseases utilizing the zebrafish system were first proposed by Cui *et al.* from 1999 [47]. Investigations have shown that zebrafish have an endochondral ossification behavior similar to that of human bone [48]. Although there is no complete Haversian system in the zebrafish skeleton, it does have both the lamellar structure and the impressive hierarchical organization consistent with the description of human long bone. Together with its predominance in studies of systematic mutagenesis using recent advances in genetic techniques, zebrafish are thought to provide a potentially powerful and simple model system for the study of bone mineralization and bone diseases at the molecular level [49]. Therefore, it is of great importance to investigate the mineralization characteristics of collagen fibrils in zebrafish skeleton, which could have the potential to provide further but simplified insight in understanding the bone structure-function relations.

As illustrated in Figure 2.4, there are also seven-level hierarchical of organization in zebrafish skeletal bone with levels ranging in scale from micrometers to nanometers [14, 20, 49, 50]. In the zebrafish system, the basic building block of bone material is that of the mineralized collagen fibril (level 2), which itself is composed of a very hard material, the mineral, and a much softer material, the collagen fibrils (level 1). Mineralized collagen fibrils are always present in bundles or arrays aligned along their length (level 3). These fibril arrays are organized into two common patterns-arrays of parallel fibrils and a plywood-like structure (level 4). At a higher level of organization, the initially deposited bone undergoes internal remodeling to form the circular lamellar structure bone with a central canal for the notochord and two arches for the neural tube and blood vessels from the dorsal and ventral sides of the centra (level 5). Levels 6 refers to vertebrae and levels 7 refers to the whole skeletal bone.

The formation and organization of mineralized collagen fibrils in zebrafish bone are similar to those of human Haversian system. Cui *et al.*

Level 1 Major components   *Level 3* Fibril array   *Level 5* Lamellar structure   *Level 7* Skeleton bone

Level 2 Mineralized collagen fibril   *Level 4* Fibril array patterns   *Level 6* Vertebra
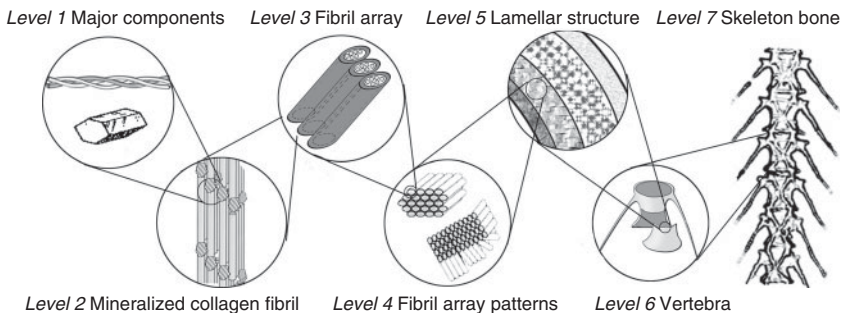
Figure 2.4 The seven hierarchical levels of organization of the zebrafish skeleton bone. Reprinted with permission from [50].
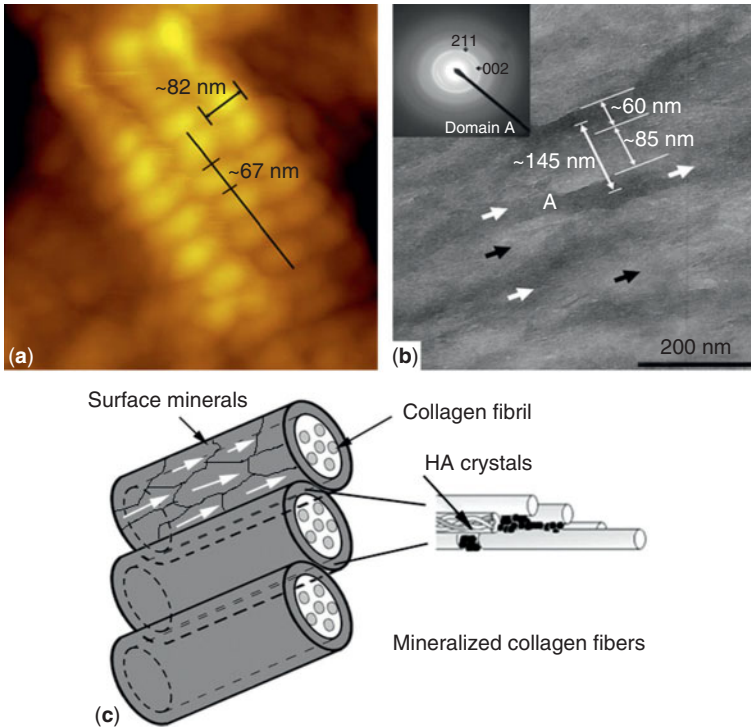
Figure 2.5 AFM and TEM micrographs of mineralized collagen fibril from zebrafish skeleton revealing the existence of mineralization both in the hole zone and on the surface of collagen. Reprinted with permission from [48].

has reported that the mineralized collagen fibrils became thicker and more ordered, with increased degree of mineralization and crosslinking from the outermost layer toward the center of the vertebra bone wall according to the AFM and TEM investigations. In association with the thicker and ordered fibrils, the nanomechanical properties as measured by nanoindentation significantly improve [66]. In addition, the AFM and TEM observations provide some new evidence for surface deposition of HA in the mineralized collagen fibrils. As shown in Figure 2.5, TEM observations of unstained zebrafish skeleton bone without decalcification treatments provide direct evidence for the deposition of the HA crystals on the surface of the fibrils making the mineralized fibrils compactly aligned, with the diameter increasing to more than 150 nm. Further supportive evidence was also supplied by the AFM observations, which indicated that the mineralized fibrils become thicker and more compactly aligned as the age of bone increases [48]. As a consequence of these processes, it is conjectured that as the mineralization becomes heavier, more minerals deposit on the surface, and therefore the fibrils become thicker.

2.3   Biomimetic Synthesis of Self-Assembled Mineralized Fibrils

2.3.1   *In Vitro* Self-Assembly of Mineralized Collagen Fibrils

Investigations of the mechanism on the formation and hierarchical assembly of mineralized collagen fibrils are of vital importance for not only understanding the processes of bone formation during development, but also offering novel ideas in the design and fabrication of new functional materials, such as tissue engineering scaffold materials and biomimetic engineering materials using biomimetic strategies [51]. The most important factor in the assembly of mineralized collagen fibrils is the elaborate alignment of HA crystals and collagen fibrils with proper chemical and structural interactions. Especially during the initial stage of collagen mineralization, how the collagen fibrils regulate HA crystals nucleation and deposition is still uncertain, although the previous hypothesis that the collagen/HA alignment is directed by the negatively charged carboxylate groups on the surface of collagen interacting with calcium ions in HA has been widely accepted. Direct and solid evidence are therefore quite necessary for confirming the previous theories.

Many research groups have attempted to mimic the collagen regulated biomineralization processes *in vitro* in order to achieve a better understanding of the structural organization in naturally occurring calcified tissues. Rhee *et al.* [52] investigated the nucleation of Ca-P crystals through chemical interaction with collagen by soaking a collagen membrane in a supersaturated simulated body fluid solution. Hartgerink *et al.* [53] combined the collagen fibrils and calcium phosphate together to obtain a homogeneously mineralized collagen gel in one process step, consisting of a three-dimensional network of collagen fibrils covered with calcium phosphate. Pederson and Ruberti [54] reported a strategy for exploiting temperature driven self-assembly of collagen and thermally triggered liposome mineralization to form a mineralized collagen composite.

Cui and colleagues [55] used different compositions of monomeric collagen and solutions containing calcium and phosphate ions, and then used either pH or temperature to induce the formation of hierarchically assembled mineralized collagen fibrils that resembles the structure in natural bone. The conventional and high-resolution TEM exanimations revealed the hierarchical organization of the mineralized collagen fibrils with tiny HA nanocrystals associating specifically with the surfaces of the collagen fibrils, which is the first evidence to support the previous hypothesis (Figure 2.6).

They investigated the nucleation sites and the conformation change of collagen during the initial stage of collagen mineralization, showing the interrelationship of collagen molecules and HA crystals. It was found that
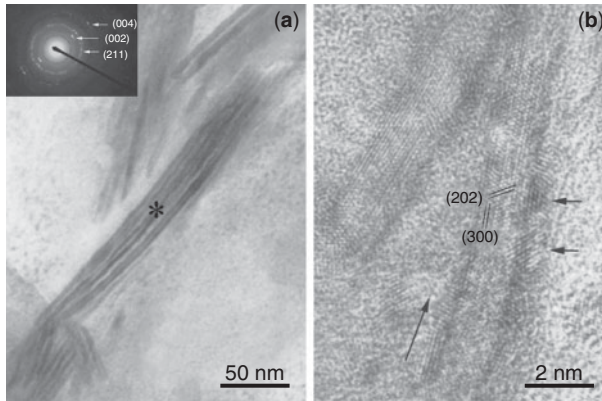
Figure 2.6 Conventional (a) and high-resolution TEM (b) micrographs of the hierarchical organization of the synthetic mineralized collagen fibrils TEM image of mineralized collagen fibrils. The two long arrows indicate the longitudinal direction of the collagen fibrils. The two short arrows indicate two HA crystals. Reprinted with permission from [55].

the collagen molecules combined with Ca^{2+} to direct the nucleation of HA by providing nucleation sites, while at the same time collagen molecules adopt marked conformations changes in response to the formation of calcium phosphate around them. Previous investigations of the nucleation sites of HA crystals on collagen fibers have suggested that the binding of calcium ions with the negatively charged carboxyl groups (-COOH) in the amino acid residues of collagen is one of the key factors for the first-step nucleation of HA crystals [56–59]. For the first time, the Cui group found that the carbonyl group (C=O) on collagen was another nucleation site besides the -COOH. They examined the chemical interactions of calcium ions and calcium phosphate crystals with collagen by using Fourier transform infrared spectroscopy (FTIR) [60]. They observed that the peak intensities of amides I, II, and III of collagen decreased significantly and the amide I peak underwent a red shift after mineralization, which indicated that the chemical interaction between carboxyl groups and Ca^{2+} ions formed in the mineralization and blocked the bond C=O stretch. The behavior of the nucleation sites exerts an important influence on the following crystal growth and the morphology of crystals. Beyond that, circular dichroism (CD) analysis was performed to investigate the conformation change of collagen during the initial process. An ultraviolet photometer was used for turbidity measurements of the mineralized system *in situ* to study the kinetic process of mineralization. According to the CD analysis results, they conjectured that the chelation between calcium ions and carbonyls of collagen shorten the distances between amino acid residues and increase the triple-helical propensity of the structure (Figure 2.7).
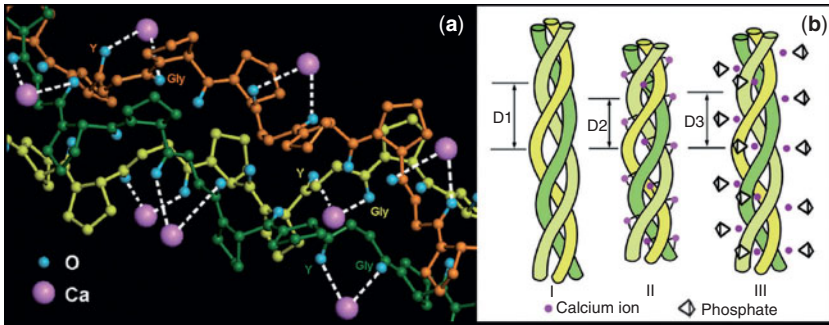
Figure 2.7 (a) The molecular model of collagen chelated with calcium ions. The Gly and Y carbonyls are always exposed to the aqueous environment and can combine with Ca2+. The chelate bonds are represented by dashed lines. (b) Sketch map of collagen conformation changes. I: collagen molecule in solution, II: collagen molecule combined with Ca2+, III: mineralized collagen after amorphous/crystalline conversion. Screw pitch D1 > D3 > D2. Reprinted with permission from [61].

When the phosphate ions were added into the calcium-containing collagen solution, calcium phosphate appeared and the combination of calcium ions and phosphate ions weakened the interaction between collagen and calcium ions. During the amorphous/crystalline conversion, the interactions between calcium ions and phosphate ions increased markedly. As a result, the chelation of calcium ions and collagen decreased rapidly. The subsequent crystal growth also influenced the collagen conformation and the partial structural recovery. It may be concluded by the process that the conformation of collagen changes rapidly during the amorphous/crystalline conversion and crystal ripening [61].

In the meantime, they built a molecular model to investigate the initial stage of the collagen-mineralization process [62]. Collagen was modeled as a collagen-like peptide $CH_3CO\text{-}(Gly\text{-}Pro\text{-}Pro)_{10}\text{-}NHCH_3$. Considering that the collagen-like peptide had a periodic structure, they specified seven C=O groups along the longitudinal axis of the collagen-like peptide whose structure has been optimized, as shown in detail in Figure 2.7a. Calcium ions were placed at a certain distance from specified C=O groups. Molecular mechanics simulations were then carried out to find the optimized structures. Calculation results showed that the calcium ions were attracted to an equilibrium position by the collagen-like peptide. The binding energies for the first, second, and third attracted calcium ion are 145.7 kCal/mol, 69.8 kCal/mol, and 47.1 kCal/mol, respectively. When more than one calcium ion was placed, the special spatial structure of the collagen-like peptide could arrange the attracted calcium ions. Simulation results for three calcium ions showed that the final structure was similar to that in HA crystal.
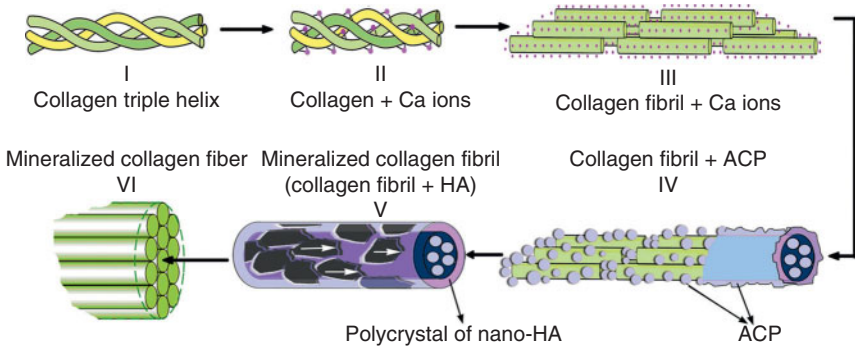
Figure 2.8 The hierarchical structure of a self-assembled HA-collagen composite. I: collagen triple helix molecule. II: collagen molecule combined with Ca2+. III: collagen fibril combined with Ca2+. IV: collagen fibrils with ACP. V: the organization of collagen fibrils with respect to HA crystals. VI: the organization of the mineralized collagen fiber.

According to the experimental results, they concluded the key mechanism behind how these mineralized collagen fibrils self-assembled. The hierarchical assembly of the specific mineralized fibers occurs in several stages, as shown in Figure 2.8. Firstly, triple-helical collagen molecules chelate Ca^{2+} through carboxyl and carbonyl groups and self-assemble into fibrils about 5 nm wide. In the second stage, ACP associated with the fibrils in their hole zones and the surface of collagen begin to form. And then amorphous/crystalline conversion happens forming HA crystals on the surface of collagen with their axes orienting along the long axes of the collagen fibrils. The diameters of the mineralized collagen fibrils are around 5.5–6.9 nm. Finally, the mineralized collagen fibrils organize parallelly to form mineralized collagen fibers with 77–192 nm wide.

These fundamental studies provide the basic theoretical support for the fabrication of HA/collagen composites and their application in bone regeneration [63, 64]. Moreover, the development of novel self-assembled structures should therefore improve our understanding of collagen-mediated mineralization in calcified tissues, and point the way to the development of new functional materials for biomimetic engineering.

2.3.2 *In Vitro* Self-Assembly of Mineralized Recombinant Collagen Fibrils

The recent development of recombinant protein expression technology provides a reliable, predictable and chemically defined source of purified human-like collagen polypeptide that is free of animal components. Recombinant human-like collagen (RHLC) has good prospects in tissue

engineering because of its innovative characteristics of non-virus dangers and mini-immunogenicity. Furthermore, the amino acid sequence of RHLC can be designed [65]. In 2005, RHLC were used to mediate mineralization *in vitro* for the first time [66, 67]. The assembly and morphology of the mineralized recombinant collagen fibrils, especially the crystal structures and chemical interactions between RHLC and calcium phosphate crystals were examined by SEM, TEM, Selected Area Electron Diffraction (SAED) and FTIR. TEM images and SAED exhibited that the RHLC fibers in the mineralized samples were surrounded by HA nanocrystals, which was similar with the mineralized native collagen fibrils. The FTIR spectra showed that the peak for amide I also shifted to a lower wavenumber because carbonyl groups of RHLC chelated with calcium ions. It revealed that the RHLC preferred to chelate calcium ions in solution and so can subsequently regulate the mineralization process forming self-assembled RHLC/HA composites. All these results indicate that the RHLC have the same function in the initial mineralization stage as natural collagen, although the content of various amino acids of them is not uniform.

2.3.3 *In Vitro* Self-Assembly of Mineralized Silk Fibroin Fibrils

Silks are generally defined as protein polymers that are spun into fibers by some Lepidoptera larvae such as silkworms, spiders, scorpions, mites and flies. Degummed silk fibers (i.e., fibroin) have been used as many kinds of biomaterials like drug delivery systems, artificial skin, and so on, for a long time [68]. Recently, fibroin was applied as a template for mimicking biomineralization.

Takeuchi *et al.* [69] had used silk sericin to induce the apatite deposition on its surface because sericin has more carboxyl groups to induce mineralization. However, it has been demonstrated that sericin protein, when used in biomaterials, would cause adverse problems for biocompatibility and hypersensitivity [70]. On the other hand, silk fibroin has been proven to be good biocompatible material and has been successfully used for various medical applications. Kong *et al.* [71] used soluble fibroin, which was obtained from *Bombyx mori* silk fibers after deguming sericin, as the organic template to regulate the mineralization of calcium phosphate. The calcium phosphate crystals precipitated in the aqueous solution of silk fibroin at pH 8 and room temperature. Fibroin protein could significantly promote the crystal growth forming carbonate-substituted HA crystals that were compounded with fibroin. The mineralized nanofibrils in the composites are rod like in shape with a diameter of about 2–3 nm. In addition, the concentration of fibroin solute affected the biomineralization of calcium phosphate [72]. Fibroin with a higher concentration had a more positive effect on the biomineralization process.

HA and silk fibroin are both excellent materials in biomaterials areas. HA has outstanding osteo-conductivity and bioactivity, and silk fibroin is also an extensively used biomaterial. The fibroin-HA nanocomposites have a good prospect to be explored as bone repair materials.

The structure, character and amino acid sequence of RHLC, silk fibroin and natural collagen are different [71]. The mineralization of RHLC and silk fibroin confirmed the proposed mechanism on the self-assembly of mineralized collagen fibrils introduced in Section 2.3.1. It is reasonable to speculate that most proteins could regulate calcium phosphate deposition during mineralization *in vitro*. As well as proteins, polypeptides also can be used in regulating mineralization [53]. With the help of gene technology, the recombinant proteins or polypeptides can be designed according to different demands, and therefore have various applications in bone tissue engineering.

2.3.4   *In Vitro* Self-Assembly of Mineralized Peptide-Amphiphilic Nanofibers

One of the great challenges for materials science is the creation of supramolecular materials in which the constituent units are highly regular molecular nanostructures. Fabrication of materials that resemble bone is very difficult because it involves two dissimilar organic and inorganic nanophases, each of which have a specific spatial relation with respect to each another. One way to accomplish this in an artificial system is to prepare an organic nanophase designed to exert control over crystal nucleation and growth of the inorganic component [53]. Studies on such template crystal growth methods have suggested that nucleation occurs on surfaces which expose repetitive patterns of anionic groups. These anionic groups tend to concentrate the inorganic cations creating a local supersaturation followed by oriented nucleation of the inorganic crystal phase. At present there is an increasing interest in the fabrication of HA/peptide composites using designed self-assembling systems.

Many groups have investigated the preparation of bone-like materials. Stupp *et al*. have reported several studies on the use of self-assembly and mineralization to prepare a nanostructured composite material that recreates the structural orientation between collagen and HA observed in bone [73–75]. The composite is prepared by self-assembly, covalent capture, and mineralization of a peptide-amphiphile (PA) which is synthesized by standard solid-phase chemistry ending with alkylation of the Nterminus of the peptide. Chemical structure of the peptide amphiphile molecule consists of five key structural features [53]. Region 1 is a long alkyl tail that conveys hydrophobic character to the molecule and, when combined with the peptide region, makes the molecule amphiphilic. Region 2 is composed of four consecutive cysteine residues that may form disulfide bonds with other

cysteines on neighboring PA peptides to polymerize the self-assembled structure. Region 3 is a flexible linker region of three glycine residues to provide the hydrophilic head group flexibility from the more rigid cross-linked region. Region 4 is a single phosphorylated serine residue that is designed to interact strongly with calcium ions and help direct mineralization of hydroxyapatite. Region 5 displays the cell adhesion ligand Arg-Gly-Asp (RGD). This peptide-amphiphile assembles into nanofibers, which are stable in alkaline solutions. Moreover, high-resolution TEM (HRTEM) observations have shown a donut-shaped pattern in the cross section of the fibers, indicating that the hydrophobic alkyl tails pack inside of the fiber micelle and leave the acidic moieties of the peptide exposed to the aqueous environment. The chemistry of the peptide region is thus repetitively displayed on the surface. HA are nucleated on the surfaces of the fibers. The orientation of the crystalline nuclei and the subsequent crystal growth are not random but are controlled by the micelles.

Molecular self-assembly is a powerful approach for the synthesis of novel supramolecular architectures. Zhang *et al.* have focused on the fabrication of several self-assembling peptides and proteins for a variety of studies of biomaterials [76]. Their studies have shown that a broad range of peptides and proteins have the ability to produce very stable nanofibers [77]. And these nanofibers are similar in scale to the extracellular matrices that are crucial in manufacturing artificial functional tissues.

2.4   Applications of Mineralized Collagen-based Composites for Bone Regeneration

2.4.1   Fabrication of Nano-HA/Collagen-based Composites

2.4.1.1   *Three-Dimensional Biomimetic Bone Scaffolds: Nano-HA/ Collagen/PLA Composite (nHAC/PLA)*

The gold standard for the treatment of large bone defects and nonunions is autologous bone grafting. However, the supply of autograft is limited and donor site morbidity is also a concern along with the required prolonged operation times [2]. The alternative of allogeneic bone has potential risks of disease transmission and infection [3]. In order to avoid the problems associated with either autologous or allogeneic bone grafts, there has been a continued interest in the use of synthetic bone graft materials during the past decades.

Bone tissue engineering is a promising method for the repair of large bone defects [78]. The ideal bone scaffold should promote early mineralization and support new bone formation, while at the same time allowing for replacement by new bone. Recently, a highly porous scaffold is

critical to control bone formation in three dimensions (3D) using the bone tissue engineering approach. The 3D scaffold materials were designed to mimic the bone-forming components of autograft, in order to facilitate the growth of vasculature into the material, and provide an ideal environment for bone formation [79–81]. Many researchers have fabricated HA and collagen composite by mixture or self-organization, followed by cross-linkage or uniaxial pressing to develop a large size material [82, 83].

Du *et al.* has developed a bone-like nano-hydroxyapatite/collagen (nHAC) composite by mineralizing the type I collagen sheet [64, 84]. This material is bioactive and biodegradable. However, its mechanical properties are too weak for practical application. In order to improve the mechanical strength and the forming ability of the material, a new bone tissue engineering scaffold material, nano-HA/collagen/poly(lactic acid) (nHAC/PLA) has been developed base on mineralized collagen fibrils [85, 86]. First, the collagen molecules and nano-HA are assembled into mineralized fibrils. Next, the mineralized collagen fibrils are assembled into parallel fibril bundles aligned along their longitudinal axis. The fibril array patterns also show the same pattern as seen in bone. The assembled mineralized collagen fibrils are found to distribute uniformly in the PLA matrix. The freeze-drying technique is used for keeping the nHAC component as initial status on the final in-patient use [86]. The material is similar to natural bone in main composition and hierarchical microstructure. On the histological level, interconnecting porous structure of the natural bone also can be found in the top hierarchical level of the nHAC/PLA scaffold composite. The suitable macroporous structure is important in order to obtain good implant incorporation through rapid vascularization, bone ingrowth and possible remodeling. In addition, the surface of composite gradually appeared smoother by biodegradation which is beneficial for the cells spreading out. This composite, combined with high compatibility and high strength, provides a promising scaffold in both traditional bone-defect repair and in bone tissue engineering.

2.4.1.2   *Injectable Bone Cement: Nano-HA/Collagen/Calcium Sulfate Hemihydrate (nHAC/CSH)*

The solid block is difficult to carve into the appropriate shape for irregular bone defects. Therefore, handling of this material in a clinical setting would be difficult, particularly when it is used in augmenting bony surfaces [87]. Mixture of calcium sulfate hemihydrates ($CaSO_4 \cdot 1/2H_2O$, CSH) and nHAC could form moldable cement that greatly enhance the handling characteristics. CSH itself has a long clinical history as a bone graft substitute, known as plaster or gypsum for its self-setting ability *in situ* after filling the defect, the lack of inflammatory response, or the promotion of bone healing [88–91].

The nHAC/CSH cement is fabricated by introducing CSH into nHAC. It is a new bone substitute with satisfactory biocompatibility, which can offer a satisfactory biological environment for growing new bone in the implants and to stimulate bone formation. The composite cement also may support the growth of blood vessels and osteogenic cells [92]. It can act not only as a void filler facilitating guided tissue regeneration, but also as an accelerator for the healing process [93]. Compared with others, nHAC/CSH is a promising material for bone tissue engineering in the clinical repair of large or irregular bony defects.

2.4.2   Functional Improvements of Mineralized Collagen-based Composites

New generation tissue-engineered scaffolds are bioactive and biodegradable simultaneously, and are capable of recruiting, programming and simulating host cells with specific cellular responses at the molecular level for *in situ* tissue regeneration. Bioactive molecules such as growth factors and cytokines have been loaded into biomaterial scaffolds to regulate cellular growth and related functions in a better way [94].

Growth factors can be effectively delivered to a bone defect through nanocomposites, and the *in vivo* efficacies of such methods should be evaluated exactly [86]. Bone morphogenetic protein-2 (BMP-2) is the most powerful member of BMP family in inducing bone formation [95, 96]. Recombinant human BMP-2 (rhBMP-2) has already been clinically applied to induce bone regeneration in both fracture healing and spinal fusion. The *in vivo* performance of the nanocomposite for bone repairing with rhBMP-2 has been proven better than that of the nanocomposite without rhBMP-2.

Platelet-rich plasma (PRP) has already been used for bone regeneration when combined with bone scaffolds. The rationale for the local application of PRP in bone tissue engineering is based on the autologous release of growth factors [97–99] (platelet-derived growth factor, transforming growth factor- , insulin-like growth factor, and vascular endothelial growth factor) present in the platelets without the risk of disease transmission or immunogenic reactions. PRP is absorbed into the scaffold material while under vacuum during fabrication by the collagen of nHAC/PLA. After implantation, platelets and their growth factors act in the earlier stage of the bone regenerative process due to the short life span of platelets. Therefore, the direct effects of growth factors only last 5–7 days if no controlled release material is involved [100]. After the initial burst of growth factors, the platelets synthesize and secrete additional growth factors for the remaining days of their life span to stimulate the proliferation and differentiation of stem cells at the defect site [101].

Rapid angiogenesis in tissue-engineered scaffolds has been thought to be a critical element determining the success of the transplantation,

especially for large-size defects. Inadequate vascularization developed in tissue-engineered materials has been a major obstacle for their clinical applications. Because the amount of oxygen required for cell survival is limited to a distance of approximately 200 μm from the supplying blood vessel, long-term survival and function of constructed tissue substitutes requires new blood vessels to provide nutrients and oxygen for the cells. Therefore, an adequate blood vessel supplied to the newly formed tissue and within the transplanted scaffold is thought to be essential in determining the success of new tissue regeneration. Promotion of angiogenesis in tissue engineering is always one of the major topics of tissue regeneration and tissue engineering. Vascular endothelial growth factor (VEGF) and its analogues has been applied in bone tissue engineering. Localized and sustained VEGF delivery improve mineralized tissue regeneration but does not substantially enhance the presence of the osteoid matrix as using a biomineral substrate alone does. This suggest that angiogenesis speeds the differentiation and/or maturation of both infiltrating osteoblasts and osteoblast precursor cells during neo-bone development, perhaps by providing a conduit for delivery of osteo-inductive soluble signals. It is noteworthy that the strategy to promote bone regeneration via inducing angiogenesis could be particularly important in large-sized defects, in which the presence of a vascular supply is perhaps more vital.

In both physiological and pathological processes, periosteum plays a determinant role in bone formation and fracture healing, in addition to the involvement of other important factors such as growth factors and mechanical loading [102, 103]. The periosteum is a highly vascularized tissue that contains osteogenic and chondrogenic progenitor cells as well as other related bioactive factors. Transplantation of autogenous or allogenous periosteum has been applied successfully in the repair of various-sized bone defects, especially in large bone defects. Bone healing induced by periosteum has natural advantages over the other methods, such as [16] healing with natural bone structure, optimal implant/host integrity, appropriate vascularization and minimal ectopic ossification through encasing of the defect site. Zhang *et al.* pointed out that periosteum engineering could assist in structural *de novo* bone formation and is therefore a promising method for bone defect restoration [104].

2.4.3   Examples of Animal Models and Clinical Applications

Rabbits and rats on which are created artificial bone defects are used to evaluate the *in vivo* performance of the nanocomposites. The results confirm that the composites have the excellent biocompatibility, osteocompatibility, and bioactivity with surrounding tissues, and the implants stimulate the formation of new bone growth. Moreover, compared to conventional biomaterials, the nanocomposites have been found to be

capable of enhancing the rate of bone-healing because of its nanostructural and compositional similarity to natural bone in main composition and hierarchical microstructure. Such kinds of composites can be readily incorporated into the bone metabolism, rather than remaining as a permanent implant [105].

Composites that are nHAC-based have now been successfully used for thousands of cases in clinical applications, including all the various types of hard tissue repair. Yu *et al.* have reported 64 cases of posterolateral fusion in patients from 46 to 79 years old. In all cases the wound healed and no abnormity was found in local and systematic examinations during long-term follow-up [106]. The safety of nHAC/PLA composites used in lumbar posterolateral fusion has already been proven. The study shows that using this composite combined with autologous bone leads to results similar to those found for autologous bone. The composites can thus be used as a supplement to autologous bone. Carefully controlled randomized clinical trials must nevertheless be carried out to verify the use of this biomimetic nHAC composite substitute for each spine application where it will be used. We can look forward to soon entering an exciting new era in the availability of biomimetic bone graft materials for the enhancement of lumbar spine fusion and for other orthopaedic surgery.

2.5   Concluding Remarks

Bone is a type of complex calcified tissue with hierarchical levels of organization. Although the hierarchical structures of many kinds of bone tissues, including human compact bone, long bone and woven bone, have been well described, there are still many open questions regarding the formation of the hierarchical nanostructure. For example, how do the related genes, biomacromolecules, matrix, and bone cells function synergically to direct the hierarchical assembly of collagen and inorganic ions forming such unique structures at the molecular level? What are the key regulators for the size, shape, and crystallography of Ca-P minerals? A deep-going understanding of the natural bone mineralization processes will provide sophisticated strategies for biomimetic fabrication of novel bone repair materials and other advanced technology engineering materials. The self-assembly of mineralized collagen fibrils in bone and its biomimetic synthesis have been reviewed in this article. The biomimetric mineralized collagen fibrils are organic/inorganic hybrid materials resembling the self-assembly of *in vivo* nanocomposites from nanoscale to micrometer scale, which have been successfully applied for the fabrication of biomimetic bone grafting materials. However, the clinical effects of the biomimetic bone grafting materials are close but not as good as the autologous bone grafts. It is believed that the main gap on repairing

between these two grafts is not the hierarchical structure but the bioactive components. Therefore, when it comes to the fabrication of composites mimicking natural bone for bone defect repair, functional biomimetics should be paid more attention along with the componental and structural biomimetics.

Besides, the unique assemblies of organic/inorganic hybrids are ubiquitous in many natural calcified tissues. Many features of biomineralization processes present in bone are also found in other systems. A better understanding of the structure, formation, and dissolution of such organic/minerals units in mineralized collagen will lead to improve the understanding on the formations of other calcified tissues. This knowledge will also be helpful in the treatment of widespread pathological calcifications, such as atherosclerosis, stone formation, or dental calculus. Further progress in the topic of mineralized collagen materials can be expected to come from modern genetics, where gene structures are now known to control the dynamic self-assembly of both cellular and protein processes.

References

1. C.J. Damien and J.R. Parsons, Bone graft and bone graft substitutes: A review of current technology and applications. *Journal of Applied Biomaterials*, 2(3): p. 187–208, 2004.
2. E.M. Younger and M.W. Chapman, Morbidity at bone graft donor sites. *J. Orthop. Trauma*, 3(3): p. 192–195, 1989.
3. T.W. Bauer and G.F. Muschler, Bone graft materials: An overview of the basic science. *Clinical orthopaedics and related research*, 371: p. 10–27, 2000.
4. P.X. Ma and J.H. Elisseeff, *Scaffolding in Tissue Engineering*. CRC Press, 2005.
5. R.E. Horch, *et al.*, Tissue engineering of cultured skin substitutes. *Journal of Cellular and Molecular Medicine*, 9(3): p. 592–608, 2007.
6. G.E. Amiel, *et al.*, Engineering of blood vessels from acellular collagen matrices coated with human endothelial cells. *Tissue Engineering*, 12(8): p. 2355–2365, 2006.
7. P.B. Saadeh, *et al.*, Repair of a critical size defect in the rat mandible using allogenic type I collagen. *Journal of Craniofacial Surgery*, 12(6): p. 573–579, 2001.
8. S.M. Vickers, L.S. Squitieri, and M. Spector, Effects of cross-linking type II collagen-GAG scaffolds on chondrogenesis *in vitro*: Dynamic pore reduction promotes cartilage formation. *Tissue Engineering*, 12(5): p. 1345–1355, 2006.
9. A. Nanci, *Ten Cate's Oral Histology-E-Book: Development, Structure, and Function*. Mosby, 2007.
10. T.G. Spiro, *Calcium in Biology*, Vol. 6. John Wiley & Sons, 1983.
11. J. Termine and E. Eanes, Comparative chemistry of amorphous and apatitic calcium phosphate preparations. *Calcified Tissue International*, 10(1): p. 171–197, 1972.
12. H. Zhang, *et al*. *Characterizing Hierarchical Structures of Natural Ivory*. Cambridge Univ Press, 1993.

13. S. Weiner, W. Traub, and H.D. Wagner, Lamellar bone: Structure–function relations. *Journal of Structural Biology*, 126(3): p. 241–255, 1999.
14. S. Weiner and H.D. Wagner, The material bone: Structure-mechanical function relations. *Annual Review of Materials Science*, 28(1): p. 271–298, 1998.
15. D. Shi, *Introduction to Biomaterials*. World Scientific, 2006.
16. W. Fan, Physiological investigation of periosteum structure and its application in periosteum tissue engineering. 2010.
17. G. Bilgen, *et al.*, Collagen content and electrophoretic analysis of type I collagen in breast skin of heterozygous naked neck and normally feathered commercial broilers. *Skin*, 9(1): p. 9, 1999.
18. D.J. Prockop and A. Fertala, The collagen fibril: The almost crystalline structure. *Journal of Structural Biology*, 122(1): p. 111–118, 1998.
19. K.E. Kadler, *et al.*, Collagen fibril formation. *Biochemical Journal*, 316(Pt 1): p. 1, 1996.
20. F.Z. Cui, Y. Li, and J. Ge, Self-assembly of mineralized collagen composites. *Materials Science and Engineering: R: Reports*, 57(1): p. 1–27, 2007.
21. A. Hodge and J. Petruska, Recent studies with the electron microscope on ordered aggregates of the tropocollagen molecule. *Aspects of Protein Structure*, p. 289–300, 1963.
22. R. Robinson and M. Watson, Collagen-crystal relationships in bone as seen in the electron microscope. *The Anatomical Record*, 114(3): p. 383–409, 1952.
23. R.A. Robinson, An electron-microscopic study of the crystalline inorganic component of bone and its relationship to the organic matrix. *The Journal of Bone & Joint Surgery*, 34(2): p. 389–476, 1952.
24. H. Fernandez-Moran and A. Engström, Electron microscopy and x-ray diffraction of bone. *Biochimica et Biophysica Acta*, 23: p. 260–264, 1957.
25. S. Jackson, A. Cartwright, and D. Lewis, The morphology of bone mineral crystals. *Calcified Tissue International*, 25(1): p. 217–222, 1978.
26. P. Fratzl, *et al.*, Nucleation and growth of mineral crystals in bone studied by small-angle X-ray scattering. *Calcified Tissue International*, 48(6): p. 407–413, 1991.
27. N. Matsushima, M. Akiyama, and Y. Terayama, Quantitative analysis of the orientation of mineral in bone from small-angle x-ray scattering patterns. *Jpn. J. Appl. Phys.*, 21(1): p. 186–189, 1982.
28. P. Fratzl, *et al.*, Mineral crystals in calcified tissues: A comparative study by SAXS. *Journal of Bone and Mineral Research*, 7(3): p. 329–334, 1992.
29. H.P. Klug and L.E. Alexander, X-ray diffraction procedures: For polycrystalline and amorphous materials, in *X-Ray Diffraction Procedures: For Polycrystalline and Amorphous Materials*, 2nd Edition, by H.P. Klug, L.E. Alexander, pp. 992. ISBN 0-471-49369-4. Wiley-VCH, May 1974., 1974. 1.
30. V. Ziv and S. Weiner, Bone crystal sizes: A comparison of transmission electron microscopic and X-ray diffraction line width broadening techniques. *Connective Tissue Research*, 30(3): p. 165–175, 1994.
31. J. Finean and A. Engstrom, Apatite crystallites in bone. *Biochimica et Biophysica Acta*, 23(1): p. 202, 1957.
32. L. Bonar, *et al.*, X-ray diffraction studies of the crystallinity of bone mineral in newly synthesized and density fractionated bone. *Calcified Tissue International*, 35(1): p. 202–209, 1983.

33. A. Boskey and S. Marks, Mineral and matrix alterations in the bones of incisors-absent (*ia/ia*) osteopetrotic rats. *Calcified Tissue International*, 37(3): p. 287–292, 1985.
34. E. Beniash, Biominerals—hierarchical nanocomposites: The example of bone. *Wiley Interdisciplinary Reviews: Nanomedicine and Nanobiotechnology*, 3(1): p. 47–69, 2011.
35. S. Weiner, *et al.*, Rotated plywood structure of primary lamellar bone in the rat: Orientations of the collagen fibril arrays. *Bone*, 20(6): p. 509–514, 1997.
36. S. Weiner, T. Arad, and W. Traub, Crystal organization in rat bone lamellae. *FEBS Letters*, 285(1): p. 49–54, 1991.
37. J. Smith, Collagen fibre patterns in mammalian bone. *Journal of Anatomy*, 94(Pt3): p. 329, 1960.
38. J. Buckwalter, *et al.*, Bone biology. *The Journal of Bone & Joint Surgery*, 77(8): p. 1276–1289, 1995.
39. X. Su, *et al.*, Organization of apatite crystals in human woven bone. *Bone*, 32(2): p. 150–162, 2003.
40. X. Su, *et al.*, Microstructure and micromechanical properties of the mid-diaphyses of human fetal femurs. *Connective Tissue Research*, 36(3): p. 271–286, 1997.
41. J.W. Moreau, R.I. Webb, and J.F. Banfield, Ultrastructure, aggregation-state, and crystal growth of biogenic nanocrystalline sphalerite and wurtzite. *American Mineralogist*, 89(7): p. 950–960, 2004.
42. H.M. Kim, C. Rey, and M.J. Glimcher, Isolation of calcium-phosphate crystals of bone by non-aqueous methods at low temperature. *Journal of Bone and Mineral Research*, 10(10): p. 1589–1601, 2009.
43. W. Landis, *et al.*, Mineral and organic matrix interaction in normally calcifying tendon visualized in three dimensions by high-voltage electron microscopic tomography and graphic image reconstruction. *Journal of Structural Biology*, 110(1): p. 39–54, 1993.
44. S. Weiner and P.A. Price, Disaggregation of bone into crystals. *Calcified Tissue International*, 39(6): p. 365–375, 1986.
45. M. Barinaga, Zebrafish: Swimming into the development mainstream. *Science*, 250(4977): p. 34–35, 1990.
46. M.C. Fishman, Zebrafish–the Canonical Vertebrate. *Science*, 294(5545): p. 1290–1291, 2001.
47. Y. Zhang, *et al.*, Mechanical properties of skeletal bone in gene-mutated *stöpsel* [dtl28d] and wild-type zebrafish (*Danio rerio*) measured by atomic force microscopy-based nanoindentation. *Bone*, 30(4): p. 541–546, 2002.
48. J. Ge, *et al.*, New evidence of surface mineralization of collagen fibrils in wild type zebrafish skeleton by AFM and TEM. *Materials Science and Engineering: C*, 27(1): p. 46–50, 2007.
49. X. Wang, *et al.*, Hierarchical structural comparisons of bones from wild-type and *liliput* [dtc232] gene-mutated zebrafish. *Journal of Structural Biology*, 145(3): p. 236–245, 2004.
50. F.Z. Cui and X.M. Wang, Mechanical and structural properties of skeletal bone in wild-type and mutant zebrafish (*Danio rerio*), in *Handbook of Biomineralization*, p. 381–396, 2007.
51. P. Yang, *et al.*, Hierarchically ordered oxides. *Science*, 282(5397): p. 2244–2246, 1998.

52. S.H. Rhee, J.D. Lee, and J. Tanaka, Nucleation of hydroxyapatite crystal through chemical interaction with collagen. *Journal of the American Ceramic Society*, 83(11): p. 2890–2892, 2000.

53. J.D. Hartgerink, E. Beniash, and S.I. Stupp, Self-assembly and mineralization of peptide-amphiphile nanofibers. *Science*, 294(5547): p. 1684–1688, 2001.

54. A.W. Pederson, J.W. Ruberti, and P.B. Messersmith, Thermal assembly of a biomimetic mineral/collagen composite. *Biomaterials*, 24(26): p. 4881–4890, 2003.

55. W. Zhang, S. Liao, and F. Cui, Hierarchical self-assembly of nano-fibrils in mineralized collagen. *Chemistry of Materials*, 15(16): p. 3221–3226, 2003.

56. S.H. Rhee and J. Tanaka, Effect of citric acid on the nucleation of hydroxyapatite in a simulated body fluid. *Biomaterials*, 20(22): p. 2155–2160, 1999.

57. M. Kikuchi, *et al.*, The biomimetic synthesis and biocompatibility of self-organized hydroxyapatite/collagen composites. *Bioceramics*12, p. 361–365, 1999.

58. S. Mann, *et al.*, Controlled crystallization of caco3 under stearic-acid mono-layers. *Nature*, 334(6184): p. 692–695, 1988.

59. S. Weiner, W. Traub, and S. Parker, Macromolecules in mollusk shells and their functions in biomineralization [and Discussion]. *Philosophical Transactions of the Royal Society of London. B, Biological Sciences*, 304(1121): p. 425–434, 1984.

60. W. Zhang, *et al.*, Nucleation sites of calcium phosphate crystals during collagen mineralization. *Journal of the American Ceramic Society*, 86(6): p. 1052–1054, 2003.

61. F. Cui, *et al.*, Conformation change of collagen during the initial stage of biomineralization of calcium phosphate. *J. Mater. Chem.*, 18(32): p. 3835–3840, 2008.

62. B. Yang and F. Cui, Molecular modeling and mechanics studies on the initial stage of the collagen-mineralization process. *Current Applied Physics*, 7: p. e2–e5, 2007.

63. C. Du, *et al.*, Tissue response to nano-hydroxyapatite/collagen composite implants in marrow cavity. *Journal of Biomedical Materials Research*, 42(4): p. 540–548, 1998.

64. C. Du, *et al.*, Three-dimensional nano-HAp/collagen matrix loading with osteogenic cells in organ culture. *Journal of Biomedical Materials Research*, 44(4): p. 407–415, 1999.

65. C. Yang, *et al.*, The application of recombinant human collagen in tissue engineering. *Biodrugs*, 18(2): p. 103–119, 2004.

66. Y. Wang, *et al.*, Investigations of the initial stage of recombinant human-like collagen mineralization. *Materials Science and Engineering: C*, 26(4): p. 635–638, 2006.

67. Y. Zhai, F. Cui, and Y. Wang, Formation of nano-hydroxyapatite on recombinant human-like collagen fibrils. *Current Applied Physics*, 5(5): p. 429–432, 2005.

68. H. Mori and M. Tsukada, New silk protein: Modification of silk protein by gene engineering for production of biomaterials. *Reviews in Molecular Biotechnology*, 74(2): p. 95–103, 2000.

69. A. Takeuchi, *et al.*, Apatite formation on silk fiber in a solution mimicking body fluid. *Key Engineering Materials*, 240: p. 31–34, 2002.

70. G.H. Altman, *et al.*, Silk-based biomaterials. *Biomaterials*, 24(3): p. 401–416, 2003.

71. X. Kong, *et al.*, Silk fibroin regulated mineralization of hydroxyapatite nanocrystals. *Journal of Crystal Growth*, 270(1): p. 197–202, 2004.

72. X. Kong, *et al.*, Effect of solute concentration on fibroin regulated biomineralization of calcium phosphate. *Materials Science and Engineering: C*, 26(4): p. 639–643, 2006.

73. G.M. Whitesides and B. Grzybowski, Self-assembly at all scales. *Science*, 295(5564): p. 2418–2421, 2002.

74. S.I. Stupp, *et al.*, Supramolecular materials: Self-organized nanostructures. *Science*, 276(5311): p. 384–389, 1997.

75. E.R. Zubarev, *et al.*, Conversion of supramolecular clusters to macromolecular objects. *Science*, 283(5401): p. 523–526, 1999.

76. S. Zhang, Fabrication of novel biomaterials through molecular self-assembly. *Nature Biotechnology*, 21(10): p. 1171–1178, 2003.

77. M. Fändrich, M.A. Fletcher, and C.M. Dobson, Amyloid fibrils from muscle myoglobin. *Nature*, 410(6825): p. 165–166, 2001.

78. U.A. Stock and J.P. Vacanti, Tissue engineering: Current state and prospects. *Annual Review of Medicine*, 52(1): p. 443–451, 2001.

79. R. Langer and J. Vacanti, *Tissue Eng. Sci.*, 260: 920–926, 1993.

80. H. Schliephake, C. Króly, and H. Wüstenfeld, Experimental study by fluorescence microscopy and microangiography of remodeling and regeneration of bone inside alloplastic contour augmentations. *International Journal of Oral and Maxillofacial Surgery*, 23(5): p. 300–305, 1994.

81. D. Tancred, B. McCormack, and A. Carr, A synthetic bone implant macroscopically identical to cancellous bone. *Biomaterials*, 19(24): p. 2303–2311, 1998.

82. M. Kikuchi, *et al.*, Self-organization mechanism in a bone-like hydroxyapatite/collagen nanocomposite synthesized *in vitro* and its biological reaction *in vivo*. *Biomaterials*, 22(13): p. 1705–1711, 2001.

83. M.C. Chang, *et al.*, Preparation of a porous hydroxyapatite/collagen nanocomposite using glutaraldehyde as a crosslinkage agent. *Journal of Materials Science Letters*, 20(13): p. 1199–1201, 2001.

84. C. Du, *et al.*, Formation of calcium phosphate/collagen composites through mineralization of collagen matrix. *Journal of Biomedical Materials Research*, 50(4): p. 518–527, 2000.

85. S. Liao, F. Cui, and Y. Zhu, Osteoblasts adherence and migration through three-dimensional porous mineralized collagen based composite: nHAC/PLA. *Journal of Bioactive and Compatible Polymers*, 19(2): p. 117–130, 2004.

86. S. Liao, *et al.*, Hierarchically biomimetic bone scaffold materials: Nano-HA/collagen/PLA composite. *Journal of Biomedical Materials Research Part B: Applied Biomaterials*, 69(2): p. 158–165, 2004.

87. X. Liu, *et al.*, Osteogenesis of mineralized collagen bone graft modified by PLA and calcium sulfate hemihydrate: *In vivo* study. *Journal of Biomaterials Applications*, 2012.

88. M. Vlad, *et al.*, Biphasic calcium sulfate dihydrate/iron-modified alpha-tricalcium phosphate bone cement for spinal applications: *In vitro* study. *Biomedical Materials*, 5(2): p. 025006, 2010.

89.   P. Wang, *et al.*, Calcium sulfate hemihydrate powders with a controlled morphology for use as bone cement. *Journal of the American Ceramic Society*, 91(6): p. 2039–2042, 2008.

90.   C. Grimsrud, *et al.*, The *in vitro* elution characteristics of antifungal-loaded PMMA bone cement and calcium sulfate bone substitute. *Orthopedics*, 34(8): p. 592, 2011.

91.   J.C. Liao, *et al.*, Transpedicular grafting after short-segment pedicle instrumentation for thoracolumbar burst fracture: Calcium sulfate cement versus autogenous iliac bone graft. *Spine*, 35(15): p. 1482–1488, 2010.

92.   H.Y. Liu, *et al.*, Improvement on the performance of bone regeneration of calcium sulfate hemihydrate by adding mineralized collagen. *Tissue Engineering Part A*, 16(6): p. 2075–2084, 2010.

93.   W. Walsh, *et al.*, Response of a calcium sulfate bone graft substitute in a confined cancellous defect. *Clinical Orthopaedics and Related Research*, 406(1): p. 228, 2003.

94.   X.B. Yang, *et al.*, Biomimetic collagen scaffolds for human bone cell growth and differentiation. *Tissue Engineering*, 10(7–8): p. 1148–1159, 2004.

95.   T. Sakou, Bone morphogenetic proteins: From basic studies to clinical approaches. *Bone*, 22(6): p. 591–603, 1998.

96.   E. Groeneveld and E. Burger, Bone morphogenetic proteins in human bone regeneration. *European Journal of Endocrinology*, 142(1): p. 9–21, 2000.

97.   J.V.D. Dolder, *et al.*, Platelet-rich plasma: quantification of growth factor levels and the effect on growth and differentiation of rat bone marrow cells. *Tissue Engineering*, 12(11): p. 3067–3073, 2006.

98.   G. Weibrich, *et al.*, Growth factor levels in platelet-rich plasma and correlations with donor age, sex, and platelet count. *Journal of Cranio-Maxillofacial Surgery*, 30(2): p. 97–102, 2002.

99.   H. Schliephake, Bone growth factors in maxillofacial skeletal reconstruction. *International Journal of Oral and Maxillofacial Surgery*, 31(5): p. 469–484, 2002.

100. H. Schoenfeld, *et al.*, Cryopreservation of platelets at the end of their conventional shelf life leads to severely impaired *in vitro* function. *Cardiovascular Journal of South Africa*, 17(3): p. 125, 2006.

101. A.J. García and C. Reyes, Bio-adhesive surfaces to promote osteoblast differentiation and bone formation. *Journal of Dental Research*, 84(5): p. 407–413, 2005.

102. K.N. Malizos and L.K. Papatheodorou, The healing potential of the periosteum: Molecular aspects. *Injury*, 36(3): p. S13-S19, 2005.

103. E. Seeman, Periosteal bone formation-a neglected determinant of bone strength. *New England Journal of Medicine*, 349(4): p. 320–323, 2003.

104. X. Zhang, *et al.*, A perspective: Engineering periosteum for structural bone graft healing. *Clinical Orthopaedics and Related Research*, 466(8): p. 1777–1787, 2008.

105. S. Liao, *et al.*, Lumbar spinal fusion with a mineralized collagen matrix and rhBMP-2 in a rabbit model. *Spine*, 28(17): p. 1954–1960, 2003.

106. X.L. Xu, *et al.*, Evaluation of different scaffolds for BMP-2 genetic orthopedic tissue engineering. *Journal of Biomedical Materials Research Part B: Applied Biomaterials*, 75(2): p. 289–303, 2005.

Biomimetic Mineralization of Hydrogel Biomaterials for Bone Tissue Engineering

Timothy E.L. Douglas[1],*, Elzbieta Pamula[2] and Sander C.G. Leeuwenburgh[3]

[1]Polymer Chemistry and Biomaterials (PBM) Group, Department of Organic Chemistry, Ghent University, Ghent, Belgium
[2]Department of Biomaterials, Faculty of Materials Science and Ceramics, AGH University of Science and Technology, Krakow, Poland
[3]Department of Biomaterials, Radboud University Nijmegen Medical Center, Nijmegen, The Netherlands

Abstract

Hydrogels, or three-dimensional polymer networks with entrapped water, are gaining interest as tissue engineering scaffolds due to advantages including injectability, exact fitting to the defect site and ease of incorporation of bioactive substances and cells. For bone regeneration, however, hydrogels lack the capacity to calcify which limits their suitability for hard tissue regeneration.

This chapter will review biomimetic approaches to mineralize synthetic and natural hydrogels for bone regeneration. Particular attention will be devoted to generation of extra nucleation sites by addition of ceramic nanoparticles, biomimetic mineralization in calcium- and/or phosphate-containing solutions, functionalization with calcium- and phosphate-binding species in the form of biomolecules and functional groups as well as enzymatically induced mineralization.

Keywords: Hydrogel mineralization, bone tissue engineering, alkaline phosphatase, calcium phosphate, nanoparticles, nanocomposite

3.1   Introduction

Hydrogels have been increasingly considered as candidate materials for tissue regeneration since these materials resemble the hydrated nature of the extracellular matrix. From a practical point of view, hydrogels can

---

*Corresponding author: Timothy.Douglas@UGent.be

be implanted using minimally invasive methods since hydrogel compo-
nents can be applied as a liquid that solidifies *in situ*. Hydrogels possess
a great versatility regarding the integration of various biomacromol-
ecules and functional groups that can aid in directing tissue regenera-
tion. Furthermore, hydrogels provide a three-dimensional environment
that facilitates controlled biochemical and biomechanical interaction with
encapsulated cells, while their high water content enables diffusion of
nutrients and removal of by-products of cell metabolism and hydrogel
degradation [1, 2]. Hydrogels have been mainly considered for applica-
tions in soft tissue engineering, but the versatility of hydrogels has resulted
in increased interest in potential application of hydrogels in regeneration
of bone and other hard tissues. The inertness – or lack of mineralizing
capacity – of hydrogels, however, is a major drawback that limits their
further use for hard tissue regeneration.

Mineralized, hard tissues in nature are formed via synthesis of an
organic matrix in an aqueous environment that acts as an organic tem-
plate for deposition of an insoluble, dispersed inorganic phase. In bone,
these inorganic components are calcium phosphates (CaPs), which are
first deposited in the form of nanocrystals, which act as nucleation sites
for further crystal growth until the apatitic CaP is the dominant compo-
nent phase. CaPs formation is aided by the presence of calcium-binding
moieties and enzyme-induced increases of the local concentration of free
phosphates.

In this chapter, the following approaches towards mineralization of
hydrogels will be disussed:

- Incorporation of inorganic calcium phosphate (CaP) nanopar-
  ticles into hydrogels as seeds for further mineralization
- Incubation of hydrogels in solutions containing calcium
  and/or phosphate ions
- Enzymatic mineralization
- Incorporation of mineralization-promoting biomacromolecules

Other approaches, outside the scope of this chapter, include growth
factor and cell encapsulation within hydrogels to promote cell-mediated
mineralization. Readers are referred to reviews on the subject by Salinas
and Anseth [3], Hunt and Grover [4], and Schmidt *et al.* [5].

3.2   Incorporation of Inorganic Calcium Phosphate Nanoparticles into Hydrogels

Mineralization of hydrogels by incorporation of apatitic crystals as
seeds for further calcification is the most obvious approach towards

mineralization of hydrogels for bone tissue regeneration, as the presence of apatitic minerals in bone-substituting implants generally improves their osteoconductivity (i.e., the guidance of bone tissue along implant surfaces). Furthermore, apatitic nanocrystals can serve as a substrate with high affinity for proteins such as growth factors that affect attachment, proliferation and differentiation of osteoblasts. Inorganic nanoparticles can control the stiffness of flexible hydrogels, similarly to their reinforcing function in bone tissue, which is important in view of the effect of matrix stiffness on differentiation of cells towards the osteoblastic phenotype [6]. In that respect, incorporation of inorganic particles such as calcium phosphate nanoparticles into the network of a hydrogel can enhance the bioactivity of the final construct and potentially modulate the mineralization process, thereby exerting strong effects on lineage specification and commitment of mesenchymal stem cells [7]. Degradation times and mechanical properties of organic-inorganic composite materials can be controlled to a large extent by the addition of inorganic phases. Moreover, the handling characteristics of such hydrogel composites can be greatly improved since brittle ceramic particles can be delivered in moldable or even injectable formulations. Finally, the addition of carbonated apatites in polymers can have a neutralizing effect on the acidic pH caused by the degradation by-products, thus minimizing excessive acidification and inflammation at the implantation site.

3.2.1 Inorganic Nanoparticles

There are many nano- and microstructured bioactive inorganic materials that can be used to render hydrogels mineralizable, such as bioglass [8, 9], but the most commonly used inorganic phase for reinforcement of hydrogels are apatitic CaPs since these ceramic nanoparticles strongly resemble the nanostructured mineral phase of bone. Apatitic nanoparticles are most frequently prepared using aqueous wet-chemical precipitation since this technique allows production of relatively large quantities of material at reasonable cost without the use of organic solvents. The properties of the resulting nanoparticles can be controlled by parameters such as the initial reactants, the preparation temperature, pH and the presence of additives during synthesis.

3.2.2 Hydrogel Composites Based on Natural Polymer Matrices

Advantages of natural hydrogels include their biocompatibility, biodegradability, commercial availability, and – in the case of proteins – presence of peptide sequences that modulate attachment of mesenchymal cells.

The most common natural polymers that have been mixed with calcium phosphate nanoparticles include collagen (and its denatured derivative gelatin), fibrin, alginate and chitosan.

Collagen (mostly collagen type I) is the main organic phase of bone tissue and therefore highly biocompatible, enzymatically degradable and processable into different forms such as sponges, fibers, tubes and sheets. An excellent review was dedicated to the use of collagen as a matrix phase for the incorporation of calcium phosphate nanocrystals [10]. The incorporation of hydroxyapatite nanocrystals in gelatin matrices has been studied in various forms such as sponges, films and microspheres [11–13]. Generally, the inclusion of hydroxyapatite nanocrystals was shown to reduce degradation and drug release rates whereas the calcification rates increased considerably. Moreover, the osteogenicity of cultured osteoblasts was shown to be increased by incorporation of hydroxyapatite nanoparticles [11].

Fibrin glue is a synthetic analogue of the blood coagulation process that creates a fibrin clot upon mixing of fibrinogen and thrombin, and it can be used as tissue adhesive in a wide variety of surgical applications due to its favorable biological performance. Le Nihouannen *et al.* [14] combined these beneficial properties of fibrin glue in terms of clinical handling and biocompatibility with the bioactive characteristics of an additional ceramic phase in order to develop a composite material for bone regeneration. Micro- and macroporous biphasic calcium phosphate granules (hydroxyapatite and *β*-tricalcium phosphate at a weight ratio of 60/40, respectively) were mixed with a fibrin glue matrix inducing extensive mineralization within the fibrin network.

Alginate has the unique capacity to form a gel in the presence of dissolved calcium ions, which is a very mild method to create crosslinks in an organic matrix. Various calcium phosphate phases have been included in alginate matrices such as gels or beads, either as microstructured granules or nanosized crystals [15–17]. Crosslinking of alginate matrices can be achieved by addition of soluble calcium sources such as calcium sulphate or calcium chloride. Another method to crosslink alginate gels involves release of soluble calcium ions from undissolved calcium-containing precursors such as calcium carbonate or calcium phosphate by adding acidifiers such as glucono-delta-lactone (GDL) that induce partial dissolution of these calcium-containing compounds due to local acidification [18].

Fedorovich *et al.* recently compared the efficacy of osteoinductive biphasic calcium phosphate microparticles *vs.* nanosized hydroxyapatite crystals upon embedding in Matrigel hydrogels. Histological and immunohistochemical analysis of the tissue response revealed that apatitic nanoparticles induced osteoclast activation but did not form bone, whereas biphasic nanoparticles were more effective in inducing ectopic bone formation [19].

3.2.3   Hydrogel Composites Based on Synthetic Polymer Matrices

Although naturally derived hydrogels exhibit beneficial desirable biological properties, these materials often display degradation profiles that are too fast to facilitate hard tissue regeneration. Moreover, chemical characteristics of natural hydrogels such as the molecular weight are usually characterized by a wide distribution, which limits the reproducibility and functionality of the materials. Synthetic hydrogels, on the contrary, can be prepared with tailored and highly reproducible chemical characteristics, thereby allowing for tight control over properties such as degradability.

The most common synthetic hydrogels that have been studied for application in bone tissue engineering include hydrogels based either on poly(ethylene glycol) (PEG), poly(2-hydroxyethyl methacrylate) (PHEMA) or poly(N-isopropylacrylamide) (PNIPAAm). For instance, PEG-based hydrogels were used as matrix for the addition of inorganic nanoparticles by Sarvestani et al. [20], who exploited the calcium-binding capacity of a glutamic acid peptide sequence (Glu$_6$) to increase the interaction strength between inorganic hydroxyapatite nanoparticles and poly (lactide-ethylene oxide-fumarate) (PLEOF). The peptide was functionalized with acrylate groups that enabled the formation of covalent bonds between the peptide and the organic polymer. In that way, the functionalized peptide acted as a linker between inorganic and organic composite phase. Hydroxyapatite nanocrystals have also been incorporated into hydrogels made of oligo(poly(ethylene glycol) fumarate) (OPF). The introduction of apatitic nanoparticles resulted in a pronounced increase of acellular calcification in simulated body fluid (SBF) as well as mineralized matrix production upon encapsulation of osteoblastic cells [21–23].

Patel et al. developed cyclic acetal hydrogels reinforced with hydroxyapatite nanocrystals for hard tissue engineering [24]. Incorporation of these nanoparticles into cyclic acetal hydrogels resulted in enhanced differentiation of bone marrow stromal cells by promotion of endogenous osteogenic signal expression. Elastomeric nanocomposites made of PHEMA with high mineral contents of about 37–50% were prepared by Song et al. [25] who exploited the high viscosity of ethylene glycol to facilitate dispersion and prevent sedimentation of the hydroxyapatite particles. The material supported osteoblastic differentiation and bone mineralization upon implantation in rats. Gaharwar et al. revealed similar elastomeric behavior of photopolymerizable PEG-based hydrogels that contain hydroxyapatite nanocrystals due to polymer nanoparticle interactions which interfered with the permanent crosslinking of PEG during photopolymerization [26]. In an alternative approach using self-assembling

peptide amphiphile nanofibrous scaffolds as a template for embedding of hydroxyapatite nanoparticles, Anderson *et al.* observed that the resulting composites possessed the capacity for bone healing using a critical size femoral defect rat model [27].

3.3   Biomimetic Mineralization in Calcium and/or Phosphate-Containing Solutions

Two main biomimetic approaches are proposed in the literature to create a mineral phase on the surface of and inside hydrogels by soaking/incubation in suitable mineralization solutions. The first approach is based on soaking of the hydrogel samples in mineralization solutions containing calcium and phosphate ions [28] in order to cause CaP nanocrystal formation after gel formation. The second approach involves *in situ* formation of CaP nanocrystals inside hydrogels during gel formation, which then serve as nucleation sites for further crystal growth upon incubation in a mineralization solution.

3.3.1   Soaking in Solutions Containing Calcium and Phosphate Ions

Baskar *et al.* showed hydroxyapatite formation on chitosan as a result of incubation in SBF [29]. Chesnutt *et al.* showed that degree of deacetylation of chitosan, concentration of SBF, and incubation time in SBF all influence the amount and composition of CaP formed [30]. Surface-mineralized chitosan hydrogels produced in this way were found to be suitable substrates for the distribution, attachment, migration and osteogenic diffrentiation of osteoblast-like cells [31].

SBF has been used to compare mineralizabilities of different hydrogel materials. Ichibouji *et al.* compared hydrogels consisting of pectin from different sources with different zeta potentials and detected differences in the amount of calcium bound and presence of mineral formed [32].

Skhilnyy *et al.* showed that poly(ethylene imine) (PEI) hydrogels mineralize with apatite and brushite after incubation in SBF, provided that crosslinking using poly(ethylene glycol) diglycidyl ether takes place beforehand [33]. The authors suggested that uncrosslinked PEI is more protonated, and thus can release more protons, leading to a decrease in pH and increasing solubility of CaP, hindering CaP precipitation.

Alternatives to soaking in the near-physiological solution SBF are (a) soaking in solutions with superphysiological concentrations of Ca^{2+} and PO_4^{3-} and (b) alternate soaking in Ca^{2+} and PO_4^{3-} solutions. Although these approaches are not suitable for mimicking mineralization behavior *in vivo*

after implantation, they permit faster mineral formation than incubation in SBF. Additionally, since simulation of *in vivo* conditions during mineralization is not the aim, there is more freedom to vary the experimental parameters, e.g., temperature, ion concentration, which allows more control over the type and amount of mineral formed.

Madhumathi *et al.* [34], induced hydroxyapatite mineralization in a chitosan hydrogel by alternate soaking in solutions of $CaCl_2$ and Na_2HPO_4, leading to formation of homogeneously dispersed hydroxyapatite deposits throughout the hydrogel after five soaking cycles. Du *et al.* [35] presoaked collagen matrices in PO_4^{3-} and immersed them in Ca^{2+} solutions. Under different experimental conditions, different crystal polymorphs were formed. Hutchens *et al.* [36] prepared composites of cellulose and calcium-deficient hydroxyapatite by alternate immersion of cellulose hydrogels in calcium and phosphate solutions. Similarly, Furuichi *et al.* [37] mineralized a polyacrylic acid hydrogel by crosslinking a polyacrylic acid polymer in the presence of $(NH_4)_2HPO_4$ solution with subsequent immersion in a Ca^{2+}-containing solution. Combination of presoaking in non-physiological solutions followed by incubation in physiological SBF solution is also possible. Hong *et al.* [38] used a cellulose hydrogel that was first presoaked in $CaCl_2$ solution and subsequently incubated in SBF, leading to uniform and dense biomimetic mineralization after 14 days.

It should be noted that mineralization by incubation in solutions of calcium and phosphate ions can be enhanced significantly by incorporation of biomacromolecules which stimulate mineralization (see Section 3.5.2), which has been reported for chitosan with added gelatin [39], or pectin [40].

3.3.2   *In Situ* Synthesis of Hydroxyapatite

The main drawback of soaking in SBF and/or non-physiological Ca^{2+} and PO_4^{3-} solutions, is the fact that minerals are deposited predominantly on the surface of the hydrogel samples but not in their bulk interior. The second approach, preforming of homogeneously distributed CaP nanoparticles throughout the entire volume of hydrogels during the hydrogel formation process, aims to improve homogeneity of mineralization.

Azami employed a double diffusion method whereby $CaCl_2$ and Na_2HPO_4 diffused into a gelatin gel from opposite sides to form amorphous CaP and brushite in the hydrogel's central region [41]. Subsequent incubation in SBF resulted in transformation of the mineral phase into hydroxyapatite. Chen *et al.* [42] created hydroxyapatite precipitates *in situ* within a chitosan hydrogel network by neutralizing acidic chitosan with tris-buffer solution containing $Ca(NO_3)_2$ and K_2HPO_4. Luo *et al.* [43] created chitosan/collagen hybrid gels with hydroxyapatite nanoparticles by neutralization of acidic chitosan/collagen solutions with $(NH_4)_2HPO_4$ and $Ca(NO_3)_2$ solutions.

3.4   Enzymatically-Induced Mineralization Using Alkaline Phosphatase (ALP)

The enzyme alkaline phosphatase (ALP) supports mineralization of bone *in vivo* by cleavage of phosphate from organic phosphate [44]. The enzyme acts as a catalyst for the hydrolysis of the organic phosphoesters, thereby increasing the local concentration of inorganic phosphate groups, which results in deposition of carbonated apatites. The use of ALP to induce homogeneous mineralization of hydrogels to increase their mechanical strength or render them more suitable for bone replacement applications is an alternative to incorporation of CaP particles, which tend to aggregate [22, 45].

ALP crosslinked to dentine-derived collagen sheets has induced mineralization *in vivo* [46–48]. Regarding applications as a biomaterial component to aid bone regeneration, ALP has been covalently linked to bioactive glass scaffolds by Verné *et al.* to increase bioactivity *in vitro* [49]. Osasthanon *et al.* covalently grafted ALP to a porous fibrin scaffold to induce mineral deposition *in vitro* and promote bone formation *in vivo* in a mouse calvarial defect [50]. ALP has also been electosprayed to form a coating on titanium implants [51, 52].

Mineralization of hydrogel materials has been achieved by incorporation of ALP followed by soaking in a solution containing calcium ions and glycerophosphate as a substrate for ALP, which cleaves off phosphate which is then free to react with calcium to form insoluble CaP within the gel. ALP-mediated mineralization has induced formation of calcium phosphate phases including apatite [47, 53, 54].

Studies on ALP incorporation into hydrogels to induce mineralization can be divided into two categories. In the first category, ALP-induced mineralization is an analytical tool to aid fundamental research into bone cell behavior, principles of biomineralization, and mineralizability of hydrogel materials. In the second category, ALP-induced mineralization is intended to improve hydrogels' suitability as scaffold materials for bone regeneration.

3.4.1   ALP-Induced Hydrogel Mineralization for Fundamental Research

In the first category, Filmon *et al.* cultivated osteoblasts on PHEMA hydrogels containing ALP, as a result of which the hydrogel surface was covered by CaP calcospherites found in natural bone [55]. Cells anchored to these calcospherites showed an increased spreading area. The calcospherites also promoted adsorption of the matrix proteins fibronectin and bone sialoprotein (BSP). In other work by the same group, the ability of different biphosphonates to inhibit ALP-induced mineralization of such hydrogels was compared [56, 57].

ALP has also been applied in fundamental research to test the mineralizability of hydrogel materials. Spoerke *et al.* added ALP to artificial self-assembling peptide amphiphile gels to cause mineralization under physiological conditions, with the aim of elucidating the role that ALP itself plays in directing mineral formation [58]. Gungormus *et al.* used ALP to compare mineral formation in three different artificial self-assembling peptide hydrogels, showing that ALP can aid in the screening of gels for mineralizability [59].

3.4.2   Enyzmatic Mineralization for Bone Regeneration Applications

In the second category, Douglas *et al.* succeeded in mineralizing membranes of Platelet-Rich Fibrin (PRF), a blood-derived hydrogel material widely applied in oral and maxillofacial surgery, which led to enhanced osteoblast spreading [53]. The same group also compared the mineralizability of three different hydrogels of interest for bone tissue engineering, namely catechol-poly(ethylene glycol) (cPEG), collagen type I and OPF [60]. Collagen type I displayed the highest mineralizability in terms of mineral:polymer ratio after mineralization, while mineral formation in cPEG was far superior to that in OPF, presumably thanks to the presence of catechol groups, which are known to have an affinity for hydroxyapatite [61]. Coatings of polydopamine, which contain many free catechol groups, were shown by Ryu *et al.* to be not only cytocompatible, but also able to promote hydroxyapatite formation on a wide range of polymeric and metallic biomaterials [62]. Such coatings are formed by substrate immersion in dopamine solution at pH 8.5 [63]. Hydrogels of gellan gum, a polysaccharide crosslinked ionically by calcium ions, have been used in cartilage tissue engineering [64]. Functionalization with polydopamine by immersion in dopamine solution led to enhanced mineralization, which in turn promoted osteoblast adhesion and proliferation [65]. Douglas *et al.* also incorporated ALP into thermogelling chitosan/*β*-glycerophosphate hydrogels, which resulted not only in mineralization, but also acceleration of gelation, which is desirable from a clinical point of view [66]. The exact mechanism by which ALP accelerated gelation is yet to be elucidated. ALP may split *β*-glycerophosphate into phosphate ions and glycerol, which may promote ionic and hydrophobic interactions between chitosan chains, in turn promoting gel formation. Another example of a system where ALP's action causes gelation was described by Thornton *et al.* [67], where dephosphorylation of the hydrogel precursor fluoren-9-ylmethoxycarbonyl resulted in reduction of electrostatic repulsion between monomers, permitting formation of fibrils by hydrophilic and hydrophobic interactions, which in turn led to gelation.

3.4.3 ALP Entrapment

In the aforementioned studies, ALP was incorporated by addition before gel formation and entrapped during formation of the polymer network during gelation. This strategy of ALP entrapment during gelation is universally applicable to all hydrogels and avoids the use of potentially toxic crosslinking agents that may also alter enzyme activity during chemical immobilization of the enzyme in the gel. Avoidance of toxic crosslinkers is also advantageous from a biomaterial application point of view. ALP's molecular weight has been reported to be 185 kD [68], which makes it a a larger molecule than many other bioactive molecules such as growth factors. For comparison, commonly used growth factors such as platelet-derived growth factor (PDGF), vascular endothelial growth factor (VEGF) and transforming growth factor beta 1 (TGF-β1) [69], have molecular weights of 32 kD [70], 46 kD [71] and 25 kD [72], respectively. The larger molecular weight of ALP hinders its release by diffusion, facilitating physical entrapment. In the aformentioned studies where ALP release was studied, it was shown that ALP is retained in hydrogels to a large extent. Filmon *et al.* showed that less than 40% of total ALP was released over 6 days from PHEMA gels containing ALP at an initial concentration of 6 mg/ml, and that release had dropped to almost zero after 6 days [56]. Douglas *et al.* incorporated ALP into cPEG (50 mg polymer/ml gel), collagen (3 mg/ml) and OPF (225 mg/ml) gels at a concentration of 2.5 mg ALP/ml gel and found that ALP release from OPF and cPEG was negligible, while 30% was released from collagen [60].

3.5 Enhancement of Hydrogel Mineralization Using Biomacromolecules

A wide range of naturally occurring biomacromolecules has shown affinity for calcium phosphate, such as proteoglycans, glycosaminoglycans [73], serum albumin [74] and lactoferrin [75]. Hence, numerous studies have been performed on the addition of biomacromolecules to hydrogels to promote their mineralization. Such studies fall into two categories, namely those dealing with fundamental research into the ability of a particular biomacromolecule to cause mineralization, and those involving biomacromolecule-enhanced mineralization for bone regeneration applications.

3.5.1 Systems to Test Mineralization-Inducing Potential of Biomacromolecules

In studies in the first category the hydrogel serves as an artificial extracellular matrix whose function is to immobilize the biomacromolecules and act

as a template for mineral formation. Different hydrogels have been used, including agarose, acrylamide and gelatin (for a review, see Silverman *et al.* [76]). One of the most promising biomacromolecules identified by these analytical test systems is bone sialoprotein (BSP), which was shown to promote mineralization of agarose [77] and gelatin [78] hydrogels. Potentiation of the mineralization-promoting effect of biomacromolecules by the hydrogel has been observed: BSP has promoted mineral formation more effectively in collagen hydrogels than in agarose [79] and gelatin [80]. From a fundamental research point of view, this suggests that hydrogel-biomacromolecule interactions should be taken into account when designing test systems. From the point of view of practical applications, this shows that the mineralization-promoting effect of biomacromolecules may be enhanced if they are combined with a suitable hydrogel. In another test system, Chirila *et al.* covalently immobilized artificially synthesized proteins containing nacrein motifs onto the surface of PHEMA hydrogels, which resulted in enhanced calcium uptake and CaP formation after incubation in a mineralization medium containing $CaCl_2$ and Na_3PO_4 [81].

3.5.2   Biomacromolecule-Enhanced Mineralization for Bone Regeneration Applications

While biomacromolecules examined in studies in the first category have generally originated from mammalian bone or hard tissue extracellular matrix, those in the second, application-orientated category are mainly of non-ECM origin. In general, these biomacromolecules have already shown affinity for calcium ions in non-biomaterial-related systems.

Dragusin *et al.* incorporated casein, a phosphoprotein found in milk and known to be a delivery vehicle for calcium, into PHEMA hydrogels to induce mineralization under physiological conditions [82]. After incubation in SBF, CaP formation occurred on regions rich in casein.

Fibroin, a protein created by silkworms in the production of silk, has regulated the formation of hydroxyapatite [83]. Zaharia *et al.* created hybrid hydrogels consisting of interpenetrating networks of silk fibroin and polyacrylamide [84]. Increasing the silk fibroin:polyacrylamide ratio led to increased formation of mineral deposits when hydrogels were incubated in SBF. Marelli *et al.* non-covalently incorporated different silk fibroin-derived polypeptide fragments into dense collagen hydrogels to compare their ability to promote mineralization during incubation in SBF [85]. Hydrophobic crystalline polypeptides proved effective in inducing apatite formation, in contrast to hydrophilic electronegative polypeptides, which did not promote mineralization.

The polysaccharide alginate, which possesses a high affinity for calcium ions due to its high negative charge density, has been added to hydrogels to promote mineralization. Stancu *et al.* added sodium alginate

to gelatin hydrogels and found that increasing alginate:gelatin ratio led to increased formation of apatite-like mineral deposits [86]. Cha *et al.* used photocrosslinking to covalently incorporate methacrylic alginate (MA) into hybrid microporous and nanoporous hydrogels of poly(ethylene glycol) monomethacrylate (PEGmM) and poly(propylene glycol) mono-methacrylate (PPGmM) [87]. By varying the mass fractions of MA and PPGmM, charge density and hydrophobicity could be tailored, respectively. After subsequent mineralization in a solution similar to SBF, increasing the mass fractions of MA and PPGmM promoted apatite formation in microporous gels but calcium carbonate formation in nanoporous gels. This demonstrated that not only charge density but also hydrophobicity and diffusive effects have a considerable influence in directing mineral formation.

3.6   Conclusions

This chapter gives an indication of the considerable promise of the bio-mimetic approaches to mineralize natural and synthetic hydrogels for bone tissue engineering and regeneration. The incorporation of inorganic calcium phosphate nanoparticles as mineralization nuclei into hydrogel matrices is the most obvious strategy towards hydrogel mineralization, but challenges still remain such as, e.g., the inhomogeneous mineral distributions that are observed for these gels due to nanoparticle aggregation and subsequent sedimentation.

Therefore, alternative approaches have been developed recently, including i) *in situ* synthesis of hydroxyapatite inside hydrogel matrices by nucleation and growth of nanohydroxyapatite crystals on organic templates (e.g., collagen, chitosan, fibroin) ii) enzymatically-induced mineralization of hydrogels, and iii) introduction of biomacromolecules which stimulate nucleation and precipitation of calcium phosphate nanocrystals. These three strategies have been found to be particularly useful to direct the amount, size, crystal structure, shape and distribution of the minerals created within hydrogel matrices. However, more fundamental understanding of these processes and further studies are required to exactly determine the mineral formation phenomena, taking into account both kinetics and thermodynamics, i.e., sequential creation of different types of calcium phosphates under various conditions.

From the point of view of biomedical applications, hydrogel mineralization appears to be a versatile strategy to enhance the response of osteoblastic and osteoprogenitor cells, but more *in vivo* studies followed by clinical tests are necessary to verify the bone formation and remodelling capacity of such inorganic/organic composites. Nevertheless, existing scientific reports demonstrate the great potential of mineralized hydrogels in the treatment of different bone tissue malfunctions.

References

1. D.S. Benoit, S.D. Collins, and K.S. Anseth, Multifunctional hydrogels that promote osteogenic hMSC differentiation through stimulation and sequestering of BMP2. *Adv. Funct. Mater.*, 17(13): p. 2085–2093, 2007.

2. M.M. Stevens, Biomaterials for bone tissue engineering. *Materials Today*, 11(5): p. 18–25, 2008.

3. C.N. Salinas and K.S. Anseth, Mesenchymal stem cells for craniofacial tissue regeneration: designing hydrogel delivery vehicles. *J. Dent. Res.*, 88(8): p. 681–92, 2009.

4. N.C. Hunt, and L.M. Grover, Cell encapsulation using biopolymer gels for regenerative medicine. *Biotechnol. Lett.*, 2010. 32(6): p. 733–42, 2010.

5. J.J. Schmidt, J. Rowley, and H.J. Kong, Hydrogels used for cell-based drug delivery. *J. Biomed. Mater. Res. A*, 87(4): p. 1113–22, 2008.

6. A.S. Rowlands, P.A. George, and J.J. Cooper-White, Directing osteogenic and myogenic differentiation of MSCs: Interplay of stiffness and adhesive ligand presentation. *Am. J. Physiol. Cell Physiol.*, 295(4): p. C1037–44, 2008.

7. A.J. Engler, *et al.*, Matrix elasticity directs stem cell lineage specification. *Cell*, 126(4): p. 677–89, 2006.

8. B. Marelli, *et al.*, Three-dimensional mineralization of dense nanofibrillar collagen-bioglass hybrid scaffolds. *Biomacromolecules*, 11(6): p. 1470–9, 2010.

9. B. Marelli, *et al.*, Accelerated mineralization of dense collagen-nano bioactive glass hybrid gels increases scaffold stiffness and regulates osteoblastic function. *Biomaterials*, 32(34): p. 8915–26, 2011.

10. D.A. Wahl and J.T. Czernuszka, Collagen-hydroxyapatite composites for hard tissue repair. *Eur. Cell Mater.*, 11: p. 43–56, 2006.

11. H.W. Kim, H.E. Kim, and V. Salih, Stimulation of osteoblast responses to biomimetic nanocomposites of gelatin-hydroxyapatite for tissue engineering scaffolds. *Biomaterials*, 26(25): p. 5221–30, 2005.

12. S.C. Leeuwenburgh, *et al.*, Mineralization, biodegradation, and drug release behavior of gelatin/apatite composite microspheres for bone regeneration. *Biomacromolecules*, 11(10): p. 2653–9, 2011.

13. A.T. Neffe, *et al.*, Gelatin functionalization with tyrosine derived moieties to increase the interaction with hydroxyapatite fillers. *Acta Biomater.*, 7(4): p. 1693–701, 2011.

14. D. Le Nihouannen, *et al.*, Micro-architecture of calcium phosphate granules and fibrin glue composites for bone tissue engineering. *Biomaterials*, 27(13): p. 2716–22, 2006.

15. N. Shiraishi, *et al.*, Preparation and characterization of porous alginate scaffolds containing various amounts of octacalcium phosphate (OCP) crystals. *J. Mater. Sci. Mater. Med.*, 21(3): p. 907–14, 2010.

16. R. Tan, *et al.*, Preparation and characterization of an injectable composite. *J. Mater. Sci. Mater. Med.*, 20(6): p. 1245–53, 2009.

17. G. Turco, *et al.*, Alginate/Hydroxyapatite biocomposite for bone ingrowth: A trabecular structure with high and isotropic connectivity. *Biomacromolecules*, 10(6): p. 1575–83, 2009.

18. C.K. Kuo and P.X. Ma, Ionically crosslinked alginate hydrogels as scaffolds for tissue engineering: Part 1. Structure, gelation rate and mechanical properties. *Biomaterials*, 22(6): p. 511–21, 2001.

19. N.E. Fedorovich, *et al.*, The osteoinductive potential of printable, cell-laden hydrogel-ceramic composites. *J. Biomed. Mater. Res. A*, 100(9): p. 2412–20, 2012.

20. A.S. Sarvestani, X. He, and E. Jabbari, Effect of osteonectin-derived peptide on the viscoelasticity of hydrogel/apatite nanocomposite scaffolds. *Biopolymers*, 85(4): p. 370–8, 2007.

21. M. Bongio, *et al.*, Biomimetic modification of synthetic hydrogels by incorporation of adhesive peptides and calcium phosphate nanoparticles: *In vitro* evaluation of cell behavior. *Eur. Cell Mater.*, 22: p. 359–76, 2011.

22. S.C. Leeuwenburgh, J.A. Jansen, and A.G. Mikos, Functionalization of oligo(poly(ethylene glycol)fumarate) hydrogels with finely dispersed calcium phosphate nanocrystals for bone-substituting purposes. *J. Biomater. Sci. Polym. Ed.*, 18(12): p. 1547–64, 2007.

23. M.R. Nejadnik, *et al.*, Facilitating the mineralization of oligo(poly(ethylene glycol)fumarate) hydrogel by incorporation of hydroxyapatite nanoparticles. *J. Biomed. Mater. Res. A*, 100(5): p. 1316–23, 2012.

24. M. Patel, *et al.*, Characterization of cyclic acetal hydroxyapatite nanocomposites for craniofacial tissue engineering. *J. Biomed. Mater. Res. A*, 94(2): p. 408–18, 2010.

25. J. Song, *et al.*, Elastomeric high-mineral content hydrogel-hydroxyapatite composites for orthopedic applications. *J. Biomed. Mater. Res. A*, 89(4): p. 1098–107, 2009.

26. A.K. Gaharwar, *et al.*, Highly extensible, tough, and elastomeric nanocomposite hydrogels from poly(ethylene glycol) and hydroxyapatite nanoparticles. *Biomacromolecules*, 12(5): p. 1641–50, 2011.

27. J.M. Anderson, *et al.*, Biphasic peptide amphiphile nanomatrix embedded with hydroxyapatite nanoparticles for stimulated osteoinductive response. *ACS Nano*, 5(12): p. 9463–79, 2011.

28. T. Kokubo and H. Takadama, How useful is SBF in predicting *in vivo* bone bioactivity? *Biomaterials*, 27(15): p. 2907–15, 2006.

29. D. Baskar, R. Balu, and T.S. Kumar, Mineralization of pristine chitosan film through biomimetic process. *Int. J. Biol. Macromol.*, 49(3): p. 385–9, 2011.

30. B.M. Chesnutt, *et al.*, Characterization of biomimetic calcium phosphate on phosphorylated chitosan films. *J. Biomed. Mater. Res. A*, 82(2): p. 343–53, 2007.

31. I. Manjubala, *et al.*, Growth of osteoblast-like cells on biomimetic apatite-coated chitosan scaffolds. *J. Biomed. Mater. Res. B Appl. Biomater.*, 84(1): p. 7–16, 2008.

32. T. Ichibouji, *et al.*, Apatite mineralization abilities and mechanical properties of covalently cross-linked pectin hydrogels. *Materials Science and Engineering C*, 29: p. 1765–1769, 2009.

33. A. Shkilnyy, *et al.*, Unprecedented, low cytotoxicity of spongelike calcium phosphate/poly(ethylene imine) hydrogel composites. *Macromol. Biosci.*, 9(2): p. 179–86, 2009.

34. K. Madhumathi, *et al.*, Wet chemical synthesis of chitosan hydrogel-hydroxyapatite composite membranes for tissue engineering applications. *Int. J. Biol. Macromol.*, 45(1): p. 12–5, 2009.

35. C. Du, *et al.*, Formation of calcium phosphate/collagen composites through mineralization of collagen matrix. *J. Biomed. Mater. Res.*, 50(4): p. 518–27, 2000.

36. S.A. Hutchens, *et al.*, Biomimetic synthesis of calcium-deficient hydroxyapatite in a natural hydrogel. *Biomaterials*, 27(26): p. 4661–70, 2006.
37. K. Furuichi, *et al.*, Preparation of hierarchically organized calcium phosphate-organic polymer composites by calcification of hydrogel. *Sci. Technol. Adv. Mater.*, 7: p. 219, 2006.
38. C.W. Kim, *et al.*, Fabrication of hybrid composites based on biomineralization of phosphorylated poly(ethylene glycol) hydrogels. *J. Mater. Res.*, 24: p. 50, 2009.
39. J. Li, *et al.*, Surface characterization and biocompatibility of micro- and nano-hydroxyapatite/chitosan-gelatin network films. *Materials Science and Engineering C*, 29: p. 1207–1215, 2009.
40. J. Li, *et al.*, Biomimetic multicomponent polysaccharide/nano-hydroxyapatite composites for bone tissue engineering. *Carbohydrate Polymers*, 85 p. 885–894, 2011.
41. M. Azami, *et al.*, Preparation of a biomimetic nanocomposite scaffold for bone tissue engineering via mineralization of gelatin hydrogel and study of mineral transformation in simulated body fluid. *J. Biomed. Mater. Res. A*, 100(5): p. 1347–55, 2012.
42. J. Chen, *et al.*, Characterization and biocompatibility of nanohybrid scaffold prepared via *in situ* crystallization of hydroxyapatite in chitosan matrix. *Colloids Surf. B Biointerfaces*, 81(2): p. 640–7, 2010.
43. D. Luo, *et al.*, Low temperature, pH-triggered synthesis of collagen–chitosan–hydroxyapatite nanocomposites as potential bone grafting substitutes. *Materials Letters*, 65: p. 2395–2397, 2011.
44. H. Orimo, The mechanism of mineralization and the role of alkaline phosphatase in health and disease. *J. Nippon. Med. Sch.*, 77(1): p. 4–12, 2010.
45. S.C. Leeuwenburgh, I.D. Ana, and J.A. Jansen, Sodium citrate as an effective dispersant for the synthesis of inorganic-organic composites with a nanodispersed mineral phase. *Acta Biomater.*, 6(3): p. 836–44, 2010.
46. W. Beertsen and T. van den Bos, Alkaline phosphatase induces the mineralization of sheets of collagen implanted subcutaneously in the rat. *J. Clin. Invest.*, 89(6): p. 1974–80, 1992.
47. Y. Doi, *et al.*, Formation of apatite-collagen complexes. *Journal of Biomedical Materials Research*, 31: p. 43–49, 1996.
48. T. van den Bos, *et al.*, Mineralization of alkaline phosphatase-complexed collagen implants in the rat in relation to serum inorganic phosphate. *J. Bone Miner. Res.*, 10(4): p. 616–24, 1995.
49. E. Verne, *et al.*, Alkaline phosphatase grafting on bioactive glasses and glass ceramics. *Acta Biomater.*, 6(1): p. 229–40, 2010.
50. T. Osathanon, C.M. Giachelli, and M.J. Somerman, Immobilization of alkaline phosphatase on microporous nanofibrous fibrin scaffolds for bone tissue engineering. *Biomaterials*, 30(27): p. 4513–21, 2009.
51. L.T. de Jonge, *et al.*, *In vitro* responses to electrosprayed alkaline phosphatase/calcium phosphate composite coatings. *Acta Biomater.*, 5(7): p. 2773–82, 2009.
52. C. Schouten, *et al.*, The effect of alkaline phosphatase coated onto titanium alloys on bone responses in rats. *Biomaterials*, 30(32): p. 6407–17, 2009.
53. T.E. Douglas, *et al.*, Enzymatically induced mineralization of platelet-rich fibrin. *J. Biomed. Mater. Res. A*, 100(5): p. 1335–46, 2012.

54. K. Yamauchi, *et al.*, Preparation of collagen/calcium phosphate multilayer sheet using enzymatic mineralization. *Biomaterials*, 25(24): p. 5481–9, 2004.

55. R. Filmon, *et al.*, Adherence of osteoblast-like cells on calcospherites developed on a biomaterial combining poly(2-hydroxyethyl) methacrylate and alkaline phosphatase. *Bone*, 30(1): p. 152–8, 2002.

56. R. Filmon, *et al.*, Poly(2-hydroxy ethyl methacrylate)-alkaline phosphatase: A composite biomaterial allowing *in vitro* studies of bisphosphonates on the mineralization process. *J. Biomater. Sci. Polym. Ed.*, 11(8): p. 849–68, 2000.

57. R. Filmon, *et al.*, *In vitro* study of the effect of bisphosphonates on mineralization induced by a composite material: Poly 2(hydroxyethyl) methacrylate coupled with alkaline phosphatase. *Morphologie*, 84(264): p. 23–33, 2000.

58. E.D. Spoerke, S.G. Anthony, and S.I. Stupp, Enzyme directed templating of artificial bone mineral. *Adv. Mater.*, 21: p. 425–430, 2009.

59. M. Gungormus, *et al.*, Self assembled bi-functional peptide hydrogels with biomineralization-directing peptides. *Biomaterials*, 31(28): p. 7266–74, 2010.

60. T.E. Douglas, *et al.*, Enzymatic mineralization of hydrogels for bone tissue engineering by incorporation of alkaline phosphatase. *Macromol. Biosci.*, 12(8): p. 1077–89, 2012.

61. W.M. Chirdon, W.J. O'Brien, and R.E. Robertson, Adsorption of catechol and comparative solutes on hydroxyapatite. *J. Biomed. Mater. Res. B Appl. Biomater.*, 66(2): p. 532–8, 2003.

62. J. Ryu, *et al.*, Mussel-inspired polydopamine coating as a universal route to hydroxyapatite crystallization. *Adv. Funct. Mater.*, 20: p. 2132–2139, 2010.

63. H. Lee, *et al.*, Mussel-inspired surface chemistry for multifunctional coatings. *Science*, 318(5849): p. 426–30, 2007.

64. J.T. Oliveira, *et al.*, Gellan gum: A new biomaterial for cartilage tissue engineering applications. J. Biomed. Mater. Res. A, 93(3): p. 852–63, 2010.

65. T. Douglas, *et al.*, Enzymatic mineralization of gellan gum hydrogel for bone tissue-engineering applications and its enhancement by polydopamine. *J. Tissue Eng. Regen. Med.*, 2012.

66. T.E.L. Douglas, *et al.*, Chitosan-based gels containing enzyme alkaline phosphatase. Patent application no. P6036192EP priority date 27.7.2011.

67. K. Thornton, *et al.*, Controlling stiffness in nanostructured hydrogels produced by enzymatic dephosphorylation. *Biochem. Soc. Trans.*, 37(Pt 4): p. 660–4, 2009.

68. S.P. Bruder and A.I. Caplan, A monoclonal antibody against the surface of osteoblasts recognizes alkaline phosphatase isoenzymes in bone, liver, kidney, and intestine. *Bone*, 11(2): p. 133–9, 1990.

69. Y.H. Kang, *et al.*, Platelet-rich fibrin is a bioscaffold and reservoir of growth factors for tissue regeneration. *Tissue Eng. Part A*, 17(3–4): p. 349–59, 2010.

70. H.N. Antoniades, Human platelet-derived growth factor (PDGF): purification of PDGF-I and PDGF-II and separation of their reduced subunits. *Proc. Natl. Acad. Sci. U.S.A.*, 78(12): p. 7314–7, 1981.

71. E. Tischer, *et al.*, Vascular endothelial growth factor: a new member of the platelet-derived growth factor gene family. *Biochem. Biophys. Res. Commun.*, 165(3): p. 1198–206, 1989.

72. J. Pfeilschifter, L. Bonewald, and G.R. Mundy, Characterization of the latent transforming growth factor beta complex in bone. *J. Bone Miner. Res.*, 5(1): p. 49–58, 1990.

73. G. Embery, *et al.*, Calcium- and hydroxyapatite-binding properties of glucuronic acid-rich and iduronic acid-rich glycosaminoglycans and proteoglycans. *Eur. J. Oral Sci.*, 106 Suppl 1: p. 267–73, 1998.

74. J. Watanabe and M. Akashi, Integration approach for developing a high-performance biointerface: Sequential formation of hydroxyapatite and calcium carbonate by an improved alternate soaking process. *Applied Surface Science*, 255: p. 344–349, 2008.

75. M. Iafisco, *et al.*, Adsorption and spectroscopic characterization of lactoferrin on hydroxyapatite nanocrystals. *Dalton Trans.*, 40(4): p. 820–7, 2012.

76. L. Silverman and A.L. Boskey, Diffusion systems for evaluation of biomineralization. *Calcif. Tissue Int.*, 75(6): p. 494–501, 2004.

77. G.K. Hunter, *et al.*, Nucleation and inhibition of hydroxyapatite formation by mineralized tissue proteins. *Biochem. J.*, 317 (Pt 1): p. 59–64, 1996.

78. A.L. Boskey, Osteopontin and related phosphorylated sialoproteins: Effects on mineralization. *Ann. N.Y. Acad. Sci.*, 760: p. 249–56, 1995.

79. G.S. Baht, G.K. Hunter, and H.A. Goldberg, Bone sialoprotein-collagen interaction promotes hydroxyapatite nucleation. *Matrix Biol.*, 27(7): p. 600–8, 2008.

80. L. Xu, *et al.*, Role of fibrillar structure of collagenous carrier in bone sialoprotein-mediated matrix mineralization and osteoblast differentiation. *Biomaterials*, 28(4): p. 750–61, 2007.

81. T.V. Chirila, *et al.*, Effect of motif-programmed artificial proteins on the calcium uptake in a synthetic hydrogel. Macromol. Biosci., 9(10): p. 959–67, 2009.

82. D.M. Dragusin, *et al.*, Caesin – PHema: *In vitro* formation of nanometric Ca-P nuclei. *Digest Journal of Nanomaterials and Biostructures*, 6(4): p. 1909–1918, 2011.

83. X.D. Kong, *et al.*, Silk fibroin regulated mineralization of hydroxyapatite nanocrystals. *Journal of Crystal Growth*, 270: p. 197–202, 2004.

84. C. Zaharia, *et al.*, Characterization and deposition behavior of silk hydrogels soaked in simulated body fluid. *Materials Science and Engineering C*, 32: p. 945–952, 2012.

85. B. Marelli, *et al.*, Silk fibroin derived polypeptide-induced biomineralization of collagen. *Biomaterials*, 33(1): p. 102–8, 2012.

86. I.C. Stancu, *et al.*, Porous calcium alginate-gelatin interpenetrated matrix and its biomineralization potential. *J. Mater. Sci. Mater. Med.*, 22(3): p. 451–60, 2011.

87. C. Cha, *et al.*, Integrative design of a poly(ethylene glycol)-poly(propylene glycol)-alginate hydrogel to control three dimensional biomineralization. *Biomaterials*, 32(11): p. 2695–703, 2011.

Biomimetic Nanofibrous Scaffolds for Bone Tissue Engineering Applications

Robert J. Kane[1] and Peter X. Ma[2,*]

[1]*Department of Biologic and Materials Sciences, University of Michigan, Ann Arbor, Michigan, USA*
[2]*Richard H. Kingery Endowed Collegiate Professor, Department of Biologic and Materials Sciences, University of Michigan, Ann Arbor, Michigan, USA*

Abstract

Numerous scaffold designs for bone tissue engineering have been developed, but to date there is no tissue scaffold available that meets all the requirements of an ideal scaffold material. Recent advances in materials processing and design have led to the development of several types of tissue engineering scaffolds with nanometer scale fibers exposed on the scaffold surface, which may improve the biological properties of these materials. The major methods of fabricating nanofibrous scaffolds are described, and the potential utility for bone tissue engineering applications is discussed. In general nanofibrous scaffolds induce more natural cellular behavior, and there is data that suggests they lead to more rapid healing compared to smooth-walled scaffold designs of the same material. Further refinements in processing techniques to better control pore size, interconnection, and fiber diameter and orientation should lead to even more effective scaffold designs.

Keywords: Biomimetic, nanofibrous, peptide amphiphile, electrospinning, thermally induced phase separation, tissue engineering, bone, scaffold

4.1 Bone Tissue Engineering and Scaffold Design

The ultimate goal of tissue engineering is the regeneration of poorly functioning, diseased, or otherwise missing tissue. A tissue engineering (TE) system is composed of one or more of the following elements—a scaffold providing three-dimensional support and spatial guidance, a population

---

Corresponding author: mapx@umich.edu

of cells to build the newly forming tissue, and signaling molecules such as growth factors (GFs), which direct cellular behavior. Since the tissue engineering concept was developed [1, 2], a huge variety of the above three components have been tried, with varying degrees of success. In the case of bone tissue engineering, easily harvested autogenous cell populations and osteoinductive signaling molecules (bone morphogenic proteins or BMPs) have been identified and characterized. However an optimal scaffold that accelerates healing while also being able to be produced at a clinically useful volume remains elusive [3–6]. A bone tissue engineering scaffold generally possesses the following attributes:

1. Sufficient mechanical integrity to survive implantation into the wound site and maintain shape during the tissue formation process.
2. High porosity and pore accessibility to allow for cellular infiltration, nutrient and waste diffusion, vascularization of the wound site, and formation of healthy native tissue. The scaffold should degrade as healing progresses, allowing tissue to completely fill the wound site.
3. Direct cellular behavior towards rapidly producing the target tissue, or at a minimum, do not impede healing or allow scar tissue formation.

While many scaffold designs satisfy one or two of these requirements, most are lacking in one or more properties that prevent their use as a general purpose bone tissue engineering scaffold. Bioactive materials sufficiently strong to be used directly as a bone graft replacement lack the porosity or degradability necessary for effective tissue regeneration [6–10]. Scaffolds with high porosity and excellent biological activity such as collagen sponges are too weak mechanically to be utilized in typical bone grafting applications [11]. However, when combined with BMPs they are effective at inducing bone growth in fully enclosed spaces, such as spinal fusion cages [12, 13], or as BMP-delivering adjuncts to traditional autografts [14].

A tissue's native extracellular matrix (ECM) by definition meets most of the requirements of a tissue engineering scaffold, especially bioactivity. Hence a common approach to scaffold design is to mimic the materials and structures naturally found in the target tissue [5, 15]. This approach is termed *biomimetic*—mimicking biological structures in the hope that their desirable properties will be replicated in an artificially constructed scaffold. This approach is not as straightforward as replicating the native ECM–the properties needed to support and maintain healthy tissue are not necessarily those required for regeneration of that same tissue. For example, prior to vascularization of the scaffold, a higher porosity is desired to allow for cell migration and nutrient diffusion than would otherwise be required if

the tissue was already vascularized. Furthermore, the ultimate goal of a TE approach is to encourage healing faster than would occur naturally, which may not be achievable in a structure that exactly emulates ECM properties. Nevertheless, biologically inspired scaffolds show great promise, especially for bone tissue engineering, where scaffold designs based on bone ECM and architecture are among the most effective developed to date.

4.1.1   Biomimetic Bone Tissue Engineering Scaffolds

The extracellular matrix (ECM) of bone tissue is composed of collagen fibrils 50–500 nm in diameter and several microns long, aligned parallel to one another in a ropelike configuration. Plate-shaped calcium phosphate nanocrystals similar to the synthetic mineral hydroxyapatite (HA) reinforce this collagen matrix and produce a resilient, stiff composite material [16]. Collagen and various forms of calcium phosphate minerals have a long history as biomaterials used in both degradable and permanent implants, are available commercially, and have been combined in a variety of ways to produce composite scaffolds [6, 9, 17]. The biological properties of these materials are generally excellent, with almost any combination of collagen and HA being osteoconductive, allowing for the growth of bone onto and into the material [18–20]. Hydroxyapatite also exhibits limited osteoinductive behavior in some animal models, being capable of inducing ectopic bone formation without growth factors [21, 22]. However scaffolds containing collagen or other biologically derived materials present issues of availability, potential immune response, and pathogen transmission. Non-biological materials such as pure calcium phosphate ceramics, polymers, or metals, are either nondegradable, mechanically incompatible with bone tissue, or do not offer the same level of bioactivity as scaffolds fabricated from natural materials. If the chemical or morphological properties that are inherent in biological materials can be replicated in more controllable synthetic materials, scaffold design would become considerably easier.

Scaffold morphology is also an important parameter for bone TE scaffold design. The ideal pore size appears to be 250–400 μm in diameter for bone tissue engineering applications, with as high interconnectivity and porosity as possible [23]. Individual pore accessibility to the exterior of the scaffold and scaffold permeability are strong predictors of where bone will grow within the scaffold, as well as whether a graft will integrate into the adjacent bone tissue [24]. Hence a suitable scaffold morphology consisting of highly interconnected macro-pores can be considered a minimum requirement for any bone TE scaffold design. It has proven difficult to fabricate a collagen or collagen-HA composite, or indeed any biologically derived material, with this pore structure while not becoming too fragile or brittle.

While natural materials offer excellent bioactivity, techniques for fabricating them into a suitable scaffold structure have often proven elusive. An alternate way is the biomimetic approach, i.e., utilizing a non-natural material that exhibits similar cellular interactions as biological materials, which may also overcome potential immune rejection and pathogen transmission concerns associated with naturally-derived biomaterials from cadaver or animal sources. Initial developments in this area focused on attaching small peptide sequences to synthetic materials in an attempt to provide more natural cell attachment sites [25, 26]. As an example, one can attach integrin-binding peptide sequences such as the RGD binding motif to artificial polymers and metals, which result in increased cell adhesion and osteogenic activity [27]. This approach separates the scaffold morphology and chemical activity–allowing for each to be optimized independently. For more detailed information on peptide functionalization of surfaces, see a review of the subject by Hersel *et al*. [27]. By similar reasoning, incorporating hydroxyapatite mineral coatings or particles on non-natural materials appears to enhance osteoconduction in metals and polymers that would not normally interact with bone tissue [28, 29]. These methods are not without drawbacks—surface modification with ligand binding sites on complex surfaces could be impractical for large-scale fabrication and coatings will eventually degrade *in vivo*, leaving bare synthetic surfaces.

More recent developments have tried to replicate not just the chemical features of a biological surface, but the morphology as well. Many ECM proteins self assemble into ropelike fibers a few nanometers in diameter and several microns in length. It was hypothesized that by mimicking this structure, more natural cellular behavior could be achieved [30]. In general terms, micron scale features control cellular shape and spreading direction, and nanoscale roughness controls cellular adhesion and chemical interaction with the surface [31–34]. These behaviors are intertwined—cell shape affects differentiation, and surface adhesion affects cell migration speed, among others, and untangling each cause and effect relationship has proven difficult. Note that it is not just the scale of the features, but their organization. An experiment using fibrinogen binding islands at various spacings and alignments demonstrated that stem cell differentiation into osteogenic or adipogenic phenotypes was controlled not just by the density or size of adhesion points, but also by their arrangement [35]. Much work remains to be done in this area as each study utilizes differing material surfaces, means of texturing, and cell types, making general guidelines difficult to formulate. While studies of 2D patterned surfaces are useful for determining basic relationships between surface topography and cellular behavior, it is not practical to use them to pattern the surface of a 3D scaffold, and until recently there were no suitable techniques for producing a three-dimensional scaffold with micro- or nanoscale topography.

Recently techniques for producing nanofibrous surface features on the order of 1–1000 nm in 3D constructs have been shown to induce similar cellular behavior to that seen on natural surfaces, without any special material treatment or coating, such as RGD ligand attachment. Three primary methods of fabricating 3D scaffolds with a nanofibrous structure exist: self-assembly, electrospinning, and thermally induced phase separation (TIPS). The advantages and biological properties of each will be addressed in turn.

4.2   Self-Assembled Nanofiber Scaffolds

4.2.1   Fabrication and Physical Properties

Self-assembly is the process by which simple components spontaneously form complex structures as a consequence of their intrinsic properties [36]. The concept originated from observation of biological molecules such as phospholipids, which spontaneously form lipid membranes and spheres [37], and of structural proteins such as collagen, which assemble into rope-like fibrils [38]. Initial attempts at synthesizing self-assembling molecules attempted to emulate the behavior of collagen proteins which self-assemble into fibrils, or of phospholipids which create micelles or membranes [39, 40]. These molecules formed spheres or membranes in aqueous solutions similar to biologically derived phospholipids whose structure they closely emulate. More complex molecules incorporating a hydrophobic fatty acid region, cysteine residues to induce disulfide crosslinking between monomers, and attachment of functional groups such as growth factor fragments or calcium chelators to induce mineralization were soon developed [41]. These molecules are typically called peptide amphiphiles (PA), to indicate they include both hydrophilic peptide and hydrophobic lipid domains. PAs can be assembled into a variety of forms including micelles and sheets, but their most common use in tissue engineering is to produce a nanofibrous gel, with fibers on the order of 1μm in length and ~10 nm in diameter [41, 42] (Figure 4.1). A unique advantage of PA gels is the ability to self-assemble in physiological conditions, allowing for the encapsulation of live cells into a gel, or for an injectable liquid to be inserted into the wound site, which then gels *in vivo*. While other types of self-assembling molecules exist [42], the vast majority of interest for TE applications has been with peptide amphiphile scaffolds due to their demonstrated capability to form a nanofibrous gel and their excellent biocompatibility.

The primary drawback of self-assembling systems is the inability to control scaffold microstructure as well as poor mechanical properties. PAs form gels with nanometer-sized pore spaces between individual nanofibers, and no techniques for creating PA scaffolds with macropores more
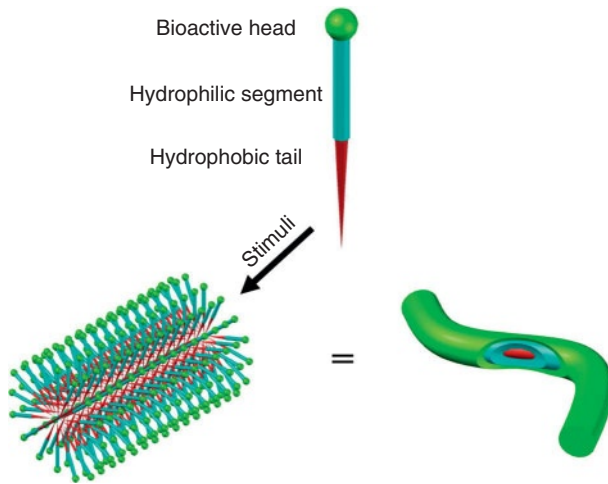
Figure 4.1 Schematic of peptide amphiphile molecule showing hydrophobic and hydrophilic segments, and a biologically active head (i.e., binding site or growth factor). The linear peptide amphiphiles self assemble into fibrillar micelle structures, which in turn form thicker fibers in a gel-like network. Adapted from Zhang *et al.*, 2012 [117], Copyright © 2012 Elsevier Inc., permission obtained from Elsevier Inc.

suitable for bone ingrowth have been reported. The hydrogel nature of the scaffolds renders PA-based materials extremely weak mechanically, unable to support any physiological loading. More complicated scaffolds incorporating peptide amphiphiles together with collagen and poly(glycolic-acid) fibers to obtain better mechanical properties and scaffold morphology have recently been developed, but the advantages of incorporating PAs into a collagen-based material have not been fully investigated [43]. Peptide-amphiphile-based self-assembly systems are by far the most common, but other self-assembling materials such as self-complementary collagen-like molecules [44], or peptides which form *β*-sheet structures [45] have also been produced and may ultimately offer improved control over scaffold morphology, but have only recently been developed and their potential is largely unknown.

4.2.2   Biological Properties of PA Scaffolds

For bone tissue engineering applications, the ultimate utility of PA or other self-assembled scaffolds is largely unknown. PA scaffolds with a phosphorylated serine residue, which binds strongly to calcium ions, have been shown to mineralize in a manner similar to natural collagen fibers [41], and MC3T3 murine pre-osteoblasts survive and proliferate while embedded in PA scaffolds for up to 3 weeks with no signs of toxicity

[46]. Interestingly, the embedded cells appeared to ingest the nanofibers. No attempts have been made to control or quantify the degradation rate of PA scaffolds *in vivo*, an important parameter of any TE scaffolding system. Few studies have investigated the potential of PA scaffolds to support bone growth *in vivo*, although they appear to be quite promising as cartilage tissue scaffolds [47]. One recent study found ectopic bone formation in rats when injected subcutaneously with PAs and free BMP-2, indicating that PAs have some potential as bone TE scaffolds [48], or at a minimum as BMP delivery agents. Much more work remains—including determining PA scaffold efficacy in a realistic fracture-healing model, before any conclusions on their utility can be made as bone tissue engineering scaffolds.

More recently the focus has shifted to covalently immobilizing growth factors or other drugs on the PA molecules, with the goal of spatially controlling growth factor distribution and preventing diffusion of the bioactive molecules out of the targeted wound site. Human mesenchymal stem cells showed increased SMAD expression, a component of the BMP activated signaling cascade, on PA sheets incorporating the active domain of BMP-2 when cultured *in vitro* [49]. PAs functionalized with a fragment of vascular endothelial growth factor (VEGF) were shown to be an effective treatment of ischemia in a mouse model [50]. Non-protein bioactive molecules can also be bound to peptide amphiphiles, such as the steroid dexamethasone [51]. This is particularly interesting for bone TE applications as dexamethasone could be used to simultaneously reduce wound site inflammation as well as promote osteogenic differentiation of invading mesenchymal stem cells.

4.2.3   Conclusions

Given the limitations in controlling scaffold morphology, and their hydrogel-like structure, current self-assembling systems should be seen more as easily tailorable, injectable drug or growth factor delivery systems at the moment, rather than as bone scaffolding materials *per se*. In spite of the difficulties in fabricating a suitable scaffold structure, PAs have demonstrated the capability to support mineralization and MSC differentiation *in vitro*. More studies are needed, especially in realistic injury models where the mechanical drawbacks of PA-based scaffolds are minimized, such as in spinal fusion procedures.

4.3   Electrospun Scaffolds

4.3.1   Fabrication and Physical Properties

The technique of electrospinning was developed nearly 100 years ago, but until recently was used primarily for the production of particulate filters

and synthetic non-woven textiles. Interest in the technique increased dramatically in the mid-1990s when it was reported that the technique could be refined to produce fibers as thin as 10 nm in diameter out of a wide variety of materials [52, 53]. Subsequent investigation has explored a range of fiber compositions, techniques for orienting the fibers, and for varying the pore size of the fiber mats.

The basic electrospinning apparatus is relatively simple (Figure 4.2a). A dissolved polymer in a volatile solvent is ejected from an electrically charged needle towards a collector target. The difference in electrical
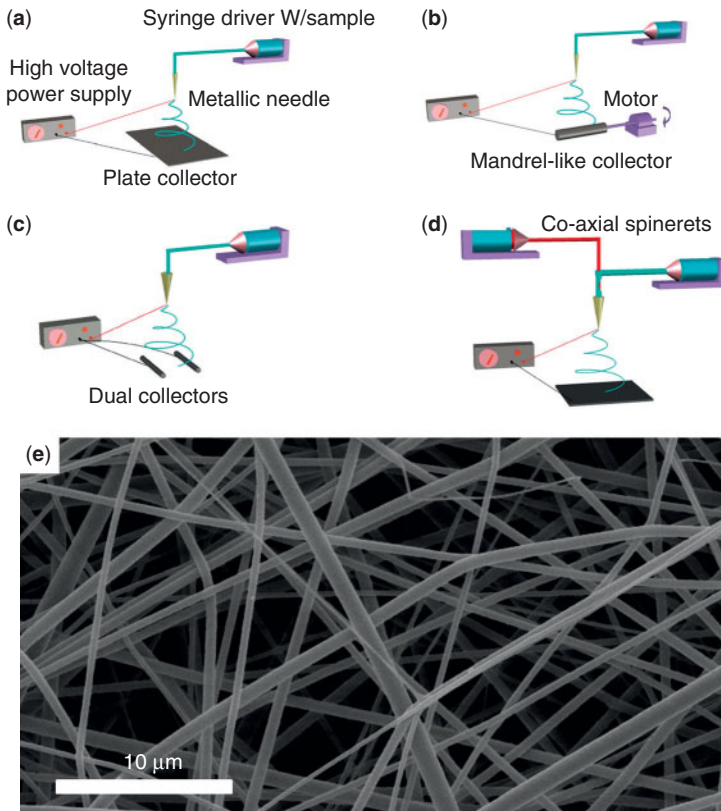
Figure 4.2 A basic electrospinning apparatus (a) consists of an electrically charged needle ejecting a polymer-solvent solution towards a collector plate. This basic design can be modified to produce aligned fibers though changes in the collector geometry (b, c), or used to fabricate composite nanofibers though co-axial needle designs (d). A SEM micrograph of typical PLA electrospun fibers shows a highly porous mat of fibers ~1 micron in diameter (e). Adapted from Zhang *et al.*, 2012 [117], Copyright © 2012 Elsevier Inc.

potential (typically 5–30 kV) between the needle and target draws a thin stream of the polymer solution towards the target located 5–30 cm away. Electrostatic repulsion in the polymer stream overcomes any surface tension and draws the stream into an extremely thin filament, which impacts the collector. The result is a mat of fibers 10 nm to several microns in diameter (Figure 4.2b) with high porosity. The final fiber diameter is affected by the type of polymer used, the choice of solvent, and parameters such as the strength of the electrical field, polymer solution flow rate, and distance to the collector [53, 54].

A variety of both natural and synthetic materials, mostly polymers, have been successfully used to fabricate nanofibrous electrospun materials. These include the biological materials collagen [55], chitosan [56], silk fibrin [57], cellulose [58], dextran [59], fibrinogen [60], and DNA [61]. Synthetic materials have included degradable polymers such as PLA [62], PGA [63], Poly (e-caprolactone) (PCL) [64], and nondegradable biocompatible materials such as nylon [65], and polyurethane [66], among others. Reinforced composites have been investigated, primarily hydroxyapatite-reinforced polymers [67–70]. Polymer-polymer blends such as collagen with PEO (Poly-ethelene oxide), chitosan with PCL, or even fibers reinforced with aligned rod-shaped viruses [71] or carbon nanotubes [69] are possible. A recently developed technique allows for the creation beds of metallic TiO nanofibers by mineralizing polyvinyl-pyrrolidone (PVP) electrospun nanofibers [72] through precipitation followed by burning off the polymer template—a technique that should work effectively with calcium phosphate minerals as well. By utilizing multiple needles [73], or needles inside of other needles (coaxial electrospinning) [74], composite scaffolds can be produced of two differing fiber compositions, giving even more control to the properties of the final nanofibrous mats. For a more complete listing of the various types of materials capable of being used, see the reviews by Huang *et al.* [54], and Li *et al.* [75].

In a typical electrospinning setup, a random mat of fibers is deposited onto a surface with a resulting porosity of 85–90%. By modifications to the orientation of the collector electrode, or the use of additional electrically charged rings or plates to "focus" the polymer filament, greater control can be achieved, although precise control of where the filament impacts the target has not been demonstrated. A simple and effective technique to produce highly aligned nanofibers scaffolds is to collect the fibers on the edge of a rotating disk, ensuring that nearly all fibers aligned parallel to the direction of rotation [76]. This technique is interesting in particular for neural tissue engineering, as aligned scaffold fabricated in this manner appear capable of directing the growth of neurons along a single axis [77, 78]. Another technique deposits a bed of fibers onto a rotating cylinder, creating a seamless tube for potential use as a vascular graft material. For

a discussion of various modifications to the electrospinning apparatus, see Teo and Ramakrishna [79].

More recently attempts have been made to increase the porosity of the fiber mats through either the use of sacrificial fibers [73], or a leachable porogen such as sodium chloride [80]. Such techniques succeed in increasing porosity, which presumably will lead to better cellular infiltration, but only limited studies have been conducted on these methods. An additional promising technique is referred to as wet spinning—depositing the spun fibers into a water bath instead of on a target which creates a loose, tangled web of fibers reminiscent of unspun cotton [81]. While lacking in mechanical properties, this material shows promise in applications such as cartilage defect repair or other applications where the wound site is completely enclosed and not subjected to load [82].

4.3.2 Biological Behavior of Electrospun Scaffolds

As with self-assembling scaffold designs, few studies have been conducted to determine the biological performance of electrospun scaffolds in bone TE applications, and even fewer have utilized *in vivo* testing, with no studies utilizing a fracture healing model. In general, electrospun scaffolds enhanced cellular proliferation and attachment compared to smooth surfaces [83]. This is likely due to the increased surface area of the fiber mats, allowing for increased protein adsorption onto the surface, and hence increased cell adhesion capability. One study looked at scaffolds made of the same PLGA polymer but varied the fiber diameter from 140–3600 nm and saw decreased cellular proliferation on small diameter fibers, and a similar experiment using PGLA fibers 250 or 2500 nm in diameter saw a similar effect, an effect attributed to increased cell adhesion [62]. At larger fiber diameters, cells treat each scaffold fiber as a flat surface, and cellular behavior is indistinct from a flat surface [62, 84].

Of particular concern to bone tissue engineering is the ability of the scaffolds to support differentiation into an osteoblast phenotype and for mineralized tissue formation. The data here is somewhat contradictory, with most studies finding that electrospun scaffolds of various diameters and materials are able to support differentiation and ECM deposition [85], but in one instance MC3T3 murine pre-osteoblasts appeared to have lower alkaline phosphatase (ALP) activity on PCL electrospun scaffolds than on flat surfaces [62]. A similar study using mineralized PLLA electrospun scaffolds reported increased ALP activity, possibly indicating that through better selection of scaffold composition, improvements in cellular behavior can be obtained [86].

An *in vitro* experiment from the Vacanti lab utilized electrospun PCL scaffolds seeded with MSCs for 4 weeks and then implanted in an ectopic site in a rat model [87]. The scaffolds maintained their shape over 4 weeks

of implantation, and mineralized collagen was seen upon retrieval. At a minimum, this indicates that electrospun nanofibrous scaffolds allow for the production of mineralized tissue within them, without the need for growth factors or other treatments. However the study did not compare the electrospun scaffolds with a solid-walled control scaffold, or vary any properties of the electrospun scaffolds, making it difficult to determine if the electrospun scaffold was more effective than traditional scaffold designs. In another study, addition of hydroxyapatite reinforcement to an electrospun PLLA scaffold led to ectopic bone tissue formation, but an apatite-free PLLA scaffold performed poorly, producing only scar tissue [88].

A major unaddressed concern with the use of electrospun scaffolds is their permeability to cellular infiltration. As bone typically heals by itself if the gap is less than ~1.5 cm [89], relatively thick scaffolds will need to be manufactured for any practical use. Nearly all electrospun scaffold studies utilize thin (< 1mm) sheets of fibers and even such studies show only limited cellular infiltration. A single *in vitro* study has shown suitable cellular infiltration into thin sheets of fibers, but this is attributed in most part to degradation of the scaffold itself [64]. Scaffolds with sacrificial fibers exhibited higher levels of MSCs in the center of the scaffolds after 3 weeks of culture [73] but the majority of cells were still on the surface. A thick scaffold fabricated with leached porogen channels through the scaffold showed over 4 mm of cellular infiltration by CFK2 chondrocytes within the scaffold by three weeks, but only adjacent to the channels [80]. An alternative approach takes advantage of electrospun scaffold impermeability by using it as a space-maintaining membrane for guided tissue regeneration. In this instance the goal is to direct osteoprogenitor cells from nearby periosteum on intact bone to the graft site while at the same time keeping out unwanted fibroblasts which would generate scar-like tissue in place of bone [90]. Here an impermeable membrane is actually desirable as it is able to better guide cell movement to the injury site. Studies have indicated that electrospun scaffolds are effective materials for this purpose [91] and may be able to enhance the healing rate of other types of scaffold designs when used together with them.

4.3.3   Conclusions

Electrospinning is an effective and controllable method for producing nanofibrous scaffolds using a wide variety of materials, but does suffer from a difficulty in producing scaffolds with sufficient pore sizes and cellular permeability. Nanometer-sized pores might be desirable on the surface of a scaffold, but are too small to allow for effective cellular and tissue infiltration into a thick scaffold material. Several groups have experimented with the incorporation of dissolvable fibers or particles to increase the pore volume, but the resulting materials are extremely

fragile mechanically. Consequently most electrospinning applications are restricted to where a highly aligned flat surface is desired, as the case of many neural TE applications, or where a thin, strong tube is required, as for vascular TE or guided tissue membrane applications.

4.4   Thermally Induced Phase Separation (TIPS) Scaffolds

4.4.1   Fabrication and Physical Properties

Phase separation is a phenomenon in which a homogeneous multicomponent system separates into two or more phases. A decrease in solubility of components of the mixture leads to distinct phases separating out of a single solution in order to reduce free energy in the system, such as resulting from temperature reduction [92]. This behavior can be used to separate a polymer solution (i.e., a solvent-polymer mixture) into regions of solvent-rich and polymer-rich composition. The solvent is then removed, and spaces formerly occupied by the solvent phase become empty pores. For tissue engineering purposes, phase separation can be utilized to produce highly porous open-celled foams with micro- or nanoscale structures whose properties can be tailored through varying the composition and processing parameters of the polymer solution.

The structure of the polymer foam is governed both by the polymer type and solubility in the chosen solvent as well as process parameters such as rate of cooling and final temperature [93]. While the relationships between these factors are complex, most effects can be thought of in terms of affecting the rate of the liquid-liquid phase separation, the size of subsequently generated polymer-rich liquid regions, and the ability of a given polymer chemistry to self assemble into a nanoscale fibrous architecture [30].

Our lab has pioneered a technique for creating highly porous (90%+) nanofibrous matrices from polymers, such as poly(L-lactic acid) (PLLA), though a thermally induced phase separation process (Figure 4.3) [30]. A variety of solvents and freezing temperatures have been investigated and material surface topographies range from nearly flat to nanofibrous, depending on polymer and processing conditions. By incorporating a second polymer in the polymer solution, for example poly(D,L-lactide) (PDLLA), a material with a partially nanofibrous, partially solid architecture can be produced [93]. Biological polymers such as gelatin can also be utilized to create surfaces with nanofibrous architecture [94]. Copolymers of PLA have been shown to produce a nanofibrous surface architecture as well, opening the possibility of further customization of chemical properties and degradation rates [95].
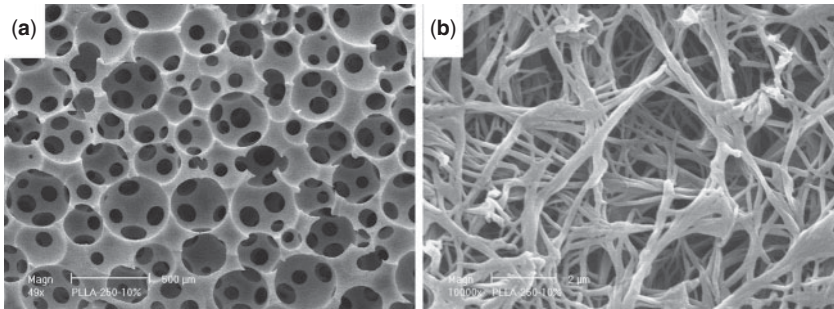
Figure 4.3 Phase-separated nanofibrous PLLA scaffold with macropores produced by a sacrificial porogen. At the microscale a highly interconnected open cell foam with uniform surface texture is visible (a), a magnified view of the same scaffold shows a interconnected web of PLLA nanofibers (b). Adapted from Wei & Ma, 2006 [98], Copyright © 2006 John Wiley and Sons.

By itself, the TIPS method suffers from the same drawbacks of other means of fabricating materials with nanoscale features, namely extremely small pore spaces that do not allow for cellular infiltration and tissue regeneration within the material. However the starting polymer solution is easily cast into a mold before phase separation, and through a sacrificial porogen approach it is possible to produce a scaffold with highly interconnected macropores that still exhibits a nanofibrous texture [96, 97] (Figure 4.3a). This method has several advantages—the size of the pores can be controlled precisely, and the level of interconnection can be controlled by partially melting the porogen particles prior to casting. In a PLLA-THF/Dioxane system, both paraffin [97] and fructose [98] microspheres have been successfully utilized to produce interconnected pore spaces, and other materials are likely compatible provided their solubility in the chosen solvent is not high. Solid freeform fabrication techniques (SFF) can be utilized to fabricate the sacrificial porogen mold [99], allowing for the design of scaffolds for specific anatomical sites in individual patients, or allowing for complex spatial variation in pore size and interconnectivity across a scaffold.

The compressive modulus of nanofibrous materials with 2–10% PLLA by mass ranges from 3–20 MPa, and scaffolds with included micropores can achieve a modulus of 300 kPA [100]. While not comparable to native bone tissue, a stiffness of 300 kPa is far higher then the expected moduli for macroporous electrospun materials, or of peptide amphiphile gels (1–10 kPa) [101].

4.4.2   Biological Behavior of TIPS Scaffolds

When soaked in bovine serum, nanofibrous PLLA scaffolds absorb over 4X more protein than comparable solid-walled scaffolds. Western blot

revealed the increase in adsorption of proteins known to mediate cell-surface interactions including fibronectin, vitronectin, and laminin [102]. Later investigation with partially nanofibrous scaffolds revealed total serum protein adsorption is directly proportional to the surface area of the scaffolds, which was 1000X greater in nanofibrous scaffolds compared to solid-walled scaffolds [93]. MC3T3 murine pre-osteoblasts cultured on scaffolds for 24 h exhibited a 1.7-fold increase in cell attachment compared to smooth-walled scaffolds, suggesting that cells more easily attached to nanofibrous matrices, likely due to increased protein adhesion in the initial stages of cellular colonization [102].

More interesting is the capability of NF scaffolds to induce osteoblastic behavior in progenitor cells. MC3T3 cells proliferated faster in smooth scaffolds, but on nanofibrous scaffolds with the addition of ascorbic acid to induce osteogenesis, exhibited significantly higher alkaline phosphatase activity as well as expression of bone sialoprotein (BSP), both markers of osteogenesis. Similar results have been obtained in murine and human embryonic stem cells [103, 104], human mesenchymal stem cells [105], and murine osteoblasts [106]. Finally, in a calvarial defect model, nanofibrous scaffolds resulted in significantly increased bone production at 8 weeks compared to smooth-walled scaffolds [107]. Most promising were islands of bone production in the center of the scaffold, separate from bone ingrowth in the periphery of the scaffold (Figure 4.4). This suggests that NF scaffolds possess some osteoinductive properties *in vivo*, and further tuning of scaffold properties may allow for even faster bone tissue nucleation and growth throughout the scaffold.
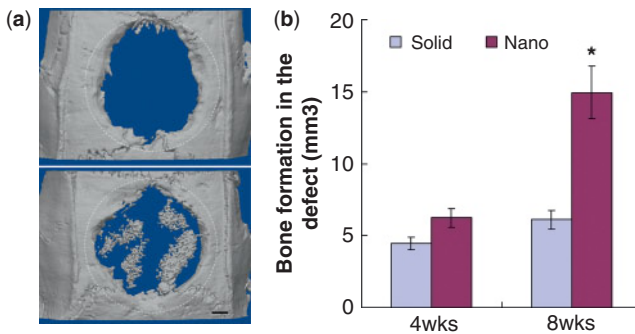
Figure 4.4 Micro-computerized tomography showing bone regeneration in a rat calvarial defect (dotted line), when using a nanofibrous PLLA scaffold (a, bottom), compared to a smooth-walled scaffold with identical pore microstructure (a, top). By 8 weeks a significant increase in bone volume is seen in the defect when using a nanofibrous scaffold compared to a smooth-walled scaffold with otherwise identical microstructure (b). Adapted from Woo *et al.*, 2009 [107], Copyright © 2009 Mary Ann Liebert Inc.

A finding from one of the above experiments suggested that cells are capable of binding directly to the scaffold nanofibers. Adding dehydroproline, an inhibitor of type I collagen fibril formation, to the culture reduced by 90% the expression of the $\alpha2$ integrin subunit on smooth-walled scaffolds, but showed little change in $\alpha2$ expression on the nanofibrous scaffolds [108]. Expression of BSP and OCN, late markers of bone formation, were likewise affected—nearly eliminated in smooth-walled scaffolds, but continued to be expressed, albeit at a lower level, on nanofibrous scaffolds. In essence it appeared that the nanofibrous scaffolds were emulating a collagenous surface to the degree that cells were expressing collagen-specific integrins while cell-secreted collagen fiber assembly was blocked. It was hypothesized that the $\alpha2\beta1$ integrin was somehow attaching directly to the scaffold nanofibers, possibly due to the helical structure of PLLA crystals which are similar in dimension and shape to the helical structure of collagen.

Techniques for increasing the bioactivity of TIPS nanofibrous scaffolds include addition of bioactive materials and the inclusion of growth factors or other drugs. Gelatin microspheres can be used as the sacrificial porogen, and during processing gelatin is transferred to the polymer matrix, obviating the need for an additional coating step. Cells cultured for 24 h on the gelatin-coated scaffolds exhibited a more spread morphology, and the amount of ECM deposited after 2 weeks culture was increased compared to uncoated scaffolds [109]. Hydroxyapatite also can be either incorporated into the polymer solution before scaffold fabrication, or precipitated onto the scaffold post-fabrication [110, 111]. HA containing nanofibrous scaffolds demonstrated increased bioactivity and osteogenic behavior *in vitro*.

Both solid-walled scaffolds [112], and nanofibrous scaffolds can be used to deliver growth factors or other drugs [113, 114]. A common approach to controlling drug elution out of scaffolds is the incorporation of micro- or nanospheres containing the drug molecule. Techniques have been developed to both embed nanospheres in PLLA matrix during fabrication as well as attaching them to the exposed surfaces of an already fabricated nanofibrous scaffold [114, 115]. While embedding the nanospheres directly is simpler, the surrounding polymer matrix affects sphere erosion and drug elution, and it is more difficult to precisely tailor the rate of drug delivery. Attaching nanospheres to a scaffold pore surface is more promising as it allows for precise control of drug elution kinetics independent of any scaffold properties. Other bioactive molecules have also been successfully incorporated into nanosphere-loaded TIPS scaffolds [113, 116].

4.4.3   Conclusions

Overall thermally inducible phase separation is a very useful and straightforward means of fabricating nanofibrous polymeric materials.

Macropores can be introduced through the incorporation of a leachable porogen, and the resulting scaffolds exhibit excellent mechanical properties compared to other candidate scaffold materials. Nanofibrous scaffolds exhibit higher bioactivity, and are capable of increasing osteogenic activity compared to smooth-walled scaffolds.

4.5   Overall Trends in Biomimetic Scaffold Design

Tissue engineering scaffolds have made great strides over the past two decades. Initially seem as a passive support that at best would not impede healing, scaffolds are now seen as a key means of controlling cellular behavior and accelerating the healing process. While the primary use of scaffolds is still for providing physical support and controlled drug or growth factor delivery, scaffold morphology and surface texture using various synthetic nanofibrous materials has been demonstrated to induce cellular behaviors that previously required growth factors or the use of biologically-sourced materials. Three major methods for production of these new types of scaffolds are self-assembly, electrospinning, and thermally induced phase separation.

The incorporation of nanofibrous materials as scaffolding systems for use in bone tissue engineering applications is still in its infancy, but initial results are very promising. In general, a nanofibrous surface, made from a wide variety of materials, allows for increased protein interaction with the surface, and hence increased cellular interaction and adhesion. Through unknown means this induces and accelerates osteogenic behavior, even leading to ectopic bone formation in an acellular porous poly(lactic acid) scaffold used to repair a mouse calvarial defect. It appears that this enhanced cellular attachment mimics what a cell senses on a biological surface, and responds more naturally than when on a traditional synthetic material. Further studies are needed to better understand this relationship between surface binding and cellular differentiation, osteogenesis, and the overall healing process.

Current nanofibrous scaffold fabrication techniques still possess important limitations in their mechanical and structural properties. Self-assembling scaffolds remain gel-like rather than a consolidated material, limiting cellular infiltration and mechanical properties. Electrospun scaffolds are easily customized in terms of nanofiber size and alignment, but suffer from very small pore sizes (on the same scale as the nano- or microfibers themselves), which again limit cellular infiltration. Electrospinning tends to form mats or sheets of fibers as well, rather than a bulk material more suitable for large bone-grafting applications. Thermally induced phase separation techniques can provide excellent control over pore size and connectivity and more suitable mechanical integrity, but limitations

in polymers capable of forming nanofibers and control over exact fiber diameter and orientation remains a challenge. Overall, the processing challenges associated with each appear surmountable, and refinements to fabrication technique should reduce or eliminate many of these concerns.

The potential to increase the efficacy of tissue engineering scaffolds by incorporating nanofibrous surface features appears vast. In nearly every instance, any type of nanofibrous scaffold has been shown to be equal or superior to similar scaffolds without nanoscale surface features, even though few studies have attempted to optimize nanofiber properties to achieve a specific cellular behavior. Further investigation in the form of a systematic look at the effects of nanofiber size, orientation, and composition on cellular behavior, and a better understanding of the cellular mechanisms that respond to nanofibrous surfaces should allow the creation of scaffolds far more effective at controlling and accelerating cellular behavior.

References

1. R. Langer and J.P. Vacanti, *Science*, Vol. 260, p. 920–6, 1993.
2. N. Peppas and R. Langer, *Science*, Vol. 263, p. 1715–20, 1994.
3. U. Kneser, D.J. Schaefer, E. Polykandriotis, and R.E. Horch, *Journal of Cellular and Molecular Medicine,* Vol. 10, p. 7–19, 2006.
4. P. Janicki, G. Schmidmaier, *Injury*, Vol. 42 Suppl 2, p. S77–81, 2011.
5. T. Cordonnier, J. Sohier, P. Rosset, and P. Layrolle, *Advanced Engineering Materials,* Vol. 13, p. 135–150, 2011.
6. P.V. Giannoudis, H. Dinopoulos, and E. Tsiridis, *Injury,* Vol. 36 Suppl 3, p. S20–7, 2005.
7. G.L. Converse, W. Yue, and R.K. Roeder, *Biomaterials,* Vol. 28, p. 927–35, 2007.
8. S. Bose, M. Roy, and A. Bandyopadhyay, *Trends in Biotechnology,* Vol. 30, p. 546–54, 2012.
9. W.R. Moore, S.E. Graves, and G.I. Bain, *ANZ Journal of Surgery,* Vol. 71, p. 354–61, 2001.
10. C.J. Damien and J.R. Parsons, *Journal of Applied Biomaterials,* Vol. 2, p. 187–208, 1991.
11. R.J. Kane and R.K. Roeder, *Journal of the Mechanical Behavior of Biomedical Materials,* Vol. 7, p. 41–9, 2012.
12. J.K. Burkus, E.E. Transfeldt, S.H. Kitchel, R.G. Watkins, and R.A. Balderston, *Spine*, Vol. 27, p. 2396–408, 2002.
13. W.F. McKay, S.M. Peckham, and J.M. Badura, *International Orthopaedics,* Vol. 31, p. 729–34, 2007.
14. L. Jones, *et al.*, *The Journal of Bone & Joint Surgery,* Vol. 88, p. 1431–41, 2006.
15. H. Shin, S. Jo, and A.G. Mikos, *Biomaterials,* Vol. 24, p. 4353–4364, 2003.
16. J.Y. Rho, L. Kuhn-Spearing, and P. Zioupos, *Medical Engineering & Physics,* Vol. 20, p. 92–102, 1998.
17. D.A. Wahl and J.T. Czernuszka, *European Cells & Materials,* Vol. 11, p. 43–56, 2006.

18. Al-Munajjed, *et al.*, *Journal of Biomedical Materials Research. Part B, Applied Biomaterials,* Vol. 90, p. 584–91, 2009.
19. W.J. Landis, F.H. Silver, and J.W. Freeman, *Journal of Materials Chemistry,* Vol. 16, p. 1495–1503, 2006.
20. M. Gelinsky, P.B. Welzel, P. Simon, A. Bernhardt, and U. König, *Chemical Engineering Journal,* Vol. 137, p. 84–96, 2008.
21. U. Ripamonti, *Biomaterials,* Vol. 17, p. 31–5, 1996.
22. H. Yuan, *et al.*, *Biomaterials,* Vol. 20, p, 1799–1806, 1999.
23. V. Karageorgiou and D. Kaplan, *Biomaterials,* Vol. 26, p. 5474–91, 2005.
24. C. Jones, C.H. Arns, D.W. Hutmacher, B.K. Milthrope, A.P. Sheppard, and M.A. Kanckstedt, *Biomaterials,* Vol. 30, p. 1440–51, 2009.
25. S.P. Massia and J.A Hubbell, *Journal of Biomedical Materials Research,* Vol. 25, p. 223–42, 1991.
26. M.D. Pierschbacher and E. Ruoslahti, *Nature,* Vol. 309, p. 30–33, 2003.
27. U. Hersel, C. Dahmen, and H. Kessler, *Biomaterials*, Vol. 24, p. 4385–4415, 2003.
28. J.L. Ong and D.C. Chan, *Critical Reviews in Biomedical Engineering,* Vol. 28, p. 667–707, 2000.
29. L. Sun, C.C. Berndt, K.A. Gross, and A. Kucuk, *Journal of Biomedical Materials Research,* Vol. 58, p. 570–92, 2001.
30. P.X. Ma and R. Zhang, *Journal of Biomedical Materials Research,* Vol. 46, p. 60–72, 1999.
31. K. Anselme, M. Bigerelle, B. Noel, E. Dufresne, A. Iost, and P. Hardouin, *Journal of Biomedical Materials Research,* Vol. 49, p. 155–66, 2000.
32. E.A. Cavalcanti-Adam, T. Volberg, A. Micoulet, H. Kessler, B. Geiger, and J.P. Spatz, *Biophysical Journal,* Vol. 92, p. 2964–74, 2007.
33. D.M. Brunette, B. Chehroudi, *Journal of Biomechanical Engineering,* Vol. 122, p. 49–57, 1999.
34. J. Park, S. Bauer, K.A. Schlegel, F.W. Neukam, K. von der Mark, and P. Schmuki, *Small,* Vol. 5, p. 666–71, 2009.
35. M.J. Dalby, *et al.*, *Nature Materials,* Vol. 6, p. 997–1003, 2007.
36. G.M. Whitesides and B. Grzybowski, *Science,* Vol. 295, p. 2418–21, 2002.
37. J.M. Schnur, *Science,* Vol. 262, p. 1669–76, 1993.
38. F.H. Silver, J.W. Freeman, and G.P. Seehra, *Journal of Biomechanics,* Vol. 36, p. 1529–1553, 2003.
39. Y.C. Yu, V. Roontga, V.A. Daragan, K.H. Mayo, M. Tirrell, and G.B. Fields, *Biochemistry,* Vol. 38, p. 1659–68, 1999.
40. W. Petka, J.L. Harden, K.P. McGrath, D. Wirtz, and D. Tirrell, *Science,* Vol. 281, p. 389–92, 1998.
41. J.D. Hartgerink, E. Beniash, and S.I. Stupp, *Science,* Vol. 294, p. 1684–8, 2001.
42. S. Zhang, *Nature Biotechnology,* Vol. 21, p. 1171–8, 2003.
43. H. Hosseinkhani, M. Hosseinkhani, F. Tian, H. Kobayashi, and Y. Tabata, *Tissue Engineering,* Vol. 13, p. 11–9, 2007.
44. T. Koide, D.L. Homma, S. Asada, and K. Kitagawa, *Bioorganic & Medicinal Chemistry Letters*, Vol. 15, p. 5230–3, 2005.
45. S. Zhang, T. Holmes, C. Lockshin, A Rich, *Proceedings of the National Academy of Sciences of the United States of America,* Vol. 90, p. 3334–8, 1993.

46. E. Beniash, J.D. Hartgerink, H. Storrie, J.C. Stendahl, and S.I. Stupp, *Acta Biomaterialia*, Vol. 1, p. 387–97, 2005.
47. R.N. Shah, *et al.*, *Proceedings of the National Academy of Sciences of the United States of America*, Vol. 107, p. 3293–8, 2010.
48. H. Hosseinkhani, M. Hosseinkhani, A. Khademhosseini, H. Kobayashi, *Journal of Controlled Release*, Vol. 117, p. 380–6, 2007.
49. J.-Y. Lee, *et al.*, *Biomaterials*, Vol. 30, p. 3532–41, 2009.
50. M.J. Webber, *et al.*, *Proceedings of the National Academy of Sciences of the United States of America*, Vol. 108, p. 13438–43, 2011.
51. M.J. Webber, J.B. Matson, V.K. Tamboli, and S.I. Stupp, *Biomaterials*, Vol. 33, p. 6823–32 (2012).
52. J. Doshi and D. Reneker, *Journal of Electrostatics*, Vol. 35, p. 151–60, 1995.
53. D. H. Reneker and I. Chun, *Nanotechnology*, Vol. 7, p. 216–23, 1996.
54. Z.-M. Huang, Y.-Z. Zhang, M. Kotaki, and S. Ramakrishna, *Composites Science and Technology*, Vol. 63, p. 2223–53, 2003.
55. J. Matthews, G.E. Wnek, D.G. Simpson, and G.L. Bowlin, *Biomacromolecules*, Vol. 3, p. 232–8, 2002.
56. F. Chen, *et al.*, *Journal of Biomaterials Science: Polymer Edition*, Vol. 19, p. 677–91, 2008.
57. B.-M. Min, *et al.*, *Biomaterials*, Vol. 25, p. 1289–97, 2004.
58. W.K. Son, J.H. Youk, and W.H. Park, *Biomacromolecules*, Vol. 5, p. 197–201, 2004.
59. H. Jiang, D. Fang, B.S. Hsiao, B. Chu, and W. Chen, *Biomacromolecules*, Vol. 5, p. 326–33, 2004.
60. G. Wnek, M. Carr, D. Simpson, and G. Bowlin, *Nano Letters*, Vol. 3, p. 213–16, 2003.
61. X. Fang and D.H. Reneker, *Journal of Macromolecular Science, Part B*, Vol. 36, p. 169–73, 1997.
62. S. Badami, M.R. Kreke, M.S. Thompson, J.S. Riffle, and A.S. Goldstein, *Biomaterials*, Vol. 27, p. 596–606, 2006.
63. E.D. Boland, T.A. Telemeco, D.G. Simpson, G.E. Wnek, and G.L. Bowlin, *Journal of Biomedical Materials Research*, Vol. 71B, p. 144–52, 2004.
64. H. Yoshimoto, Y.M. Shin, H. Terai, and J.P. Vacanti, *Biomaterials*, Vol. 24, 2077–82, 2003.
65. H. Fong, W. Liu, C. Wang, and R.A. Vaia, *Polymer*, Vol. 43, p. 775–80, 2002.
66. M.-S. Khil, D.-I. Cha, H.-Y. Kim, I.-S. Kim, and N. Bhattarai, *Journal of Biomedical Materials Research*, Vol. 67B, p. 675–679, 2003.
67. Y. Ito, *et al.*, *Journal of Bioscience and Bioengineering*, Vol. 100, p. 43–9, 2005.
68. W. Ji, *et al.*, *Biomaterials*, Vol. 33, p. 6604–14, 2012.
69. F. Mei, *et al.*, *Biomacromolecules*, Vol. 8, p. 3729–35, 2007.
70. X. Xu, X. Chen, A. Liu, Z. Hong, and X. Jing, *European Polymer Journal*, Vol. 43, p. 3187–96, 2007.
71. S.-W. Lee and A.M. Belcher, *Nano Letters*, Vol. 4, p. 387–90, 2004.
72. L.-H. Kao, H.-K. Lin, F.-J. Chuang, and W.-T. Hsu, *Materials Letters*, Vol. 82, p. 64–66, 2012.
73. B.M. Baker, *et al.*, *Biomaterials*, Vol. 29, p. 2348–58, 2008.
74. H. Jiang, *et al.*, *Journal of Controlled Release*, Vol. 108, p. 237–43, 2005.
75. D. Li and Y. Xia, *Advanced Materials*, Vol. 16, p. 1151–70, 2004.

76. Theron, E. Zussman, and A. Yarin, *Nanotechnology,* Vol. 6, p. 384–390, 2001.
77. X. Jiang, *et al.*, *Acta biomaterialia,* Vol. 8, p. 1290–302, 2012.
78. F. Yang, R. Murugan, S. Wang, and S. Ramakrishna, *Biomaterials,* Vol. 26, p. 2603–10, 2005.
79. W.E. Teo and S. Ramakrishna, *Nanotechnology,* Vol. 17, p. R89–R106, 2006.
80. J. Nam, Y. Huang, S. Agarwal, and J. Lannutti, *Tissue Engineering,* Vol. 13, p. 2249–57, 2007.
81. Y. Yokoyama, *et al.*, *Materials Letters,* Vol. 63, p. 754–56, 2009.
82. J. Coburn, M. Gibson, S. Monagle, Z. Patterson, and J.H. Elisseeff, *Proceedings of the National Academny of Sciences,* Vol. 109, p. 10012–17, 2012.
83. W.-J. Li, C.T. Laurencin, E.J. Caterson, R.S. Tuan, and F.K. Ko, *Journal of Biomedical Materials Research,* Vol. 60, p. 613–21, 2002.
84. C. Bashur, L. Dahlgren, A.S. Goldstein, *Biomaterials,* Vol. 27, p. 5681–8, 2006.
85. X. Xin, M. Hussain, and J.J. Mao, *Biomaterials,* Vol. 28, p. 316–25, 2007.
86. B.M. Whited, J.R. Whitney, M.C. Hofmann, Y. Xu, and M.N. Rylander, *Biomaterials,* Vol. 32, p. 2294–304, 2011.
87. M. Shin, H. Yoshimoto, and J.P. Vacanti, *Tissue engineering,* Vol. 10, p. 33–41, 2004.
88. E. Seyedjafari, M. Soleimani, N. Ghaemi, and I. Shabani, *Biomacromolecules,* Vol. 11, p. 3118–25, 2010.
89. J.P. Schmitz and J.O. Hollinger, *Clinical orthopaedics and related research,* p. 299–308, 1986.
90. C. Dahlin, A. Linde, J. Gottlow, and S. Nyman, *Plastic and Reconstructive Surgery,* Vol. 81, p. 672–6, 1988.
91. K.-H. Kim, *et al.*, *Journal of Biotechnology,* Vol. 120, p. 327–39, 2005.
92. P.X. Ma, in *Encyclopedia of Polymer Science and Technology*, J.I. Kroshwitz, Ed., John Wiley & Sons, Hoboken, NJ, 2005, p. 261–291.
93. G. Wei and P.X. Ma, *Biomaterials,* Vol. 30, p. 6426–34, 2009.
94. X. Liu and P.X. Ma, *Biomaterials* Vol. 30, p. 4094–103, 2009.
95. X. Liu and P.X. Ma, *Biomaterials,* Vol. 31, p. 259–69, 2010.
96. R. Zhang and P.X. Ma, *Journal of Biomedical Materials Research,* Vol. 52, p. 430–8, 2000.
97. P.X. Ma and J.W. Choi, *Tissue engineering,* Vol. 7, p. 23–33, 2001.
98. G. Wei and P.X. Ma, *Journal of biomedical materials research. Part A,* Vol. 78A, p. 306–15, 2006.
99. V.J. Chen, L. Smith, and P.X. Ma, *Biomaterials,* Vol. 27, 3973–9, 2006.
100. V.J. Chen and P.X. Ma, *Biomaterials,* Vol. 25, p. 2065–73, 2004.
101. M. Greenfield, J.R. Hoffman, M.O. de la Cruz, and S.I. Stupp, *Langmuir,* Vol. 26, p. 3641–7, 2010.
102. K.M. Woo, V.J. Chen, and P.X. Ma, *Journal of Biomedical Materials Research. Part A,* Vol. 67A, p. 531–7, 2003.
103. L. Smith, X. Liu, J. Hu, P. Wang, and P.X. Ma, *Tissue Engineering. Part A,* Vol. 15A, p. 1855–64, 2009.
104. L. Smith, X. Liu, J. Hu, and P.X. Ma, *Biomaterials,* Vol. 31, p. 5526–35, 2010.
105. J. Hu, K. Feng, X. Liu, and P.X. Ma, *Biomaterials,* Vol. 30, p. 5061–7, 2009.
106. K.M. Woo, *et al.*, Nano-fibrous scaffolding promotes osteoblast differentiation and biomineralization, *Biomaterials,* Vol. 28, p. 335–43, 2007.
107. K.M. Woo, *et al.*, *Tissue Engineering. Part A,* Vol. 15, p. 2155–62, 2009.

108. J. Hu, X. Liu, and P. X. Ma, *Biomaterials,* Vol. 29, p. 3815–21, 2008.
109. X. Liu, Y. Won, and P. X. Ma, *Biomaterials,* Vol. 27, p. 3980–7, 2006.
110. R. Zhang, and P. X. Ma, *Journal of Biomedical Materials Research,* Vol. 44, p. 446–55, 1999.
111. G. Wei, and P.X. Ma, *Journal of Biomedical Materials Research Part A,* Vol. 78A, p. 306–315, 2006.
112. H. Kim, H.W. Kim, and H. Suh, *Biomaterials,* Vol. 24, p. 4671–9, 2003.
113. K. Feng, *et al.*, *Journal of Controlled Release,* Vol. 146, p. 363–9, 2010.
114. G. Wei, Q. Jin, W.V Giannobile, and P.X. Ma, *Biomaterials,* Vol. 28, p. 2087–96, 2007.
115. P.X. Ma, *Advanced Drug Delivery Reviews,* Vol. 60, p. 184–98, 2008.
116. G. Wei, Q. Jin, W.V Giannobile, and P.X. Ma, *Journal of Controlled Release,* Vol. 112, p. 103–10, 2006.
117. Z. Zheng, J. Hu, and P.X. Ma, *Advanced Drug Delivery Reviews,* Vol. 64, p. 1129–41, 2012.

Bioactive Polymers and Nanobiomaterials Composites for Bone Tissue Engineering

Ferdous Khan* and Sheikh Rafi Ahmad

School of Chemistry, University of Edinburgh, UK

Abstract

The need for replacing or restoring the function of traumatized, diseased or lost bone has caused the rapid advancement of bioactive polymers and bionanomaterials in recent years. This has lead to the development of new strategies for regeneration and reconstruction of bone tissue. The idea is to combine progenitor or mature cells with biocompatible materials or scaffolds, with or without appropriate growth factors, to initiate repair and regeneration. Despite many developments and some breakthroughs in this very important field of applied research and development, challenges remain that need to be addressed in order to achieve functional and mechanically competent bone growth. To achieve this goal, an appropriate design of biocompatible materials and fabrication of scaffolds with structural integrity are needed as a temporary support for the regeneration of living constructs in bone tissue engineering. The polymeric biomaterials, in comparison to metallic and ceramic ones, offer many advantages. These include ease of processing with complex shapes, and the prospect of fabricating materials with a wide range of physical and mechanical properties. Amongst other advances, ceramics and phosphate-based glasses as bionanomaterials have been found to be an attractive strategy for bone implants. The incorporation of bionanomaterials into the polymer matrices also provides the added advantage of faster bone regeneration. This chapter focuses on advancements in bioactive polymers, bionanomaterials and their composites as scaffold materials for bone regeneration. Additionally, concepts, challenges, limitations and the potential of effective and efficient bone regeneration are addressed.

Keywords: Bioactive polymers, nanomaterials, polymer-nanocomposites, biomimetic 3D scaffold, bone tissue engineering

*Corresponding author: ferdous.khan0@gmail.com

5.1   Introduction

To restore functionality of bones or repair any defects caused by trauma, tumors, infections or congenital deficiencies, or damaged by accident is a most desired but clinically challenging procedure. Traditionally, autograft and allograft procedures are used for repairing bone defects, both of these have serious limitations [1, 2]. Although autografts are still considered as the gold standard in bone transplantation, their inherent problems, such as limited availability, donor site morbidity and risk of disease transmission from donor to recipient and immune rejection, have limited their clinical application [3, 4]. Allograft procedures are now considered attractive alternatives to autografts, and there have been a spate of research activities in finding and developing alternative procedures for tissue engineering both in academia and industry.

Tissue engineering has many complementary facets and research in this field is multidisciplinary with the aim of developing a new therapeutic philosophy encompassing aspects of replacement, restoration, maintenance and enhancement of tissue and organ functions. Research in this field started in the 1990s and since then significant progress has been made. Currently, tissue engineering is one of the most influential domains within new strategies for the treatment of diseased tissues and organs. Bone tissue engineering, however, is a new and emerging area of research with clinical applications in orthopaedic defects, bone tumors, repairing spinal injuries, maxillofacial, craniofacial, neck and head surgery. In recent years, a variety of biomaterials, derived from biological or synthetic materials, have been designed to provide extracellular matrix (ECM) scaffolds for new bone formation [5]. Such scaffolds are three-dimensional (3D) constructions that are implanted into the human body, leading to host integration without immune rejection.

In bone tissue engineering, the design and fabrication of 3D architecture scaffolds are a key requirement, because scaffolds can mimic the structure and function of the extracellular matrix (ECM) and support cell adhesion, proliferation and differentiation [6]. There are various fabrication techniques for constructing scaffolds, including conventional chemical engineering methods as well as advanced manufacturing technologies [7–10]. In recent years much attention has been given to advanced techniques in the tissue engineering field because they can control the external and internal structure of tissue engineering scaffolds and overcome some inherent limitations of conventional methods, such as manual intervention, inconsistent and inflexible processing procedures, and shape limitations [9, 10].

A variety of synthetic materials such as polymers and nanomaterials have been investigated for bone regeneration. These were derived from ceramics, glasses and other inorganic materials, nanotubes, and their composites, and were studied with or without cells and growth factors. In an ideal scenario, the synthetic biomaterials should have excellent biocompatibility, the ability

to restore with time, provide structural support while enhancing bone tissue formation, and be easy to use clinically and cost-effective [11]. Additionally, the materials should be shapeable, or polymerizable *in situ* to ensure good integration in the defective area [2]. Tissue engineering scaffolds should facilitate the colonization of cells and possess properties and characteristics that enhance cell attachment, proliferation, migration and expression of native phenotypes. The physical properties of scaffold such as porosity, the surface-area-to-volume ratio, pore size, pore interconnectivity, mechanical strength and overall geometry are all critically important factors in the design and fabrication of materials for bone tissue engineering [10, 12].

The search for innovative biomaterials is an iterative process for the development of a new therapeutic concept and now encompasses nanomaterials and their composites, particularly, polymers and nanocomposites. Because of high surface area, the nanomaterials have a high level of interaction with the lowest hierarchical levels, thereby enhancing their bioactivity. Such nanocomposites comprising a polymer matrix and bioactive micro/nanofillers constitute specific biomaterials for internal bone implants with biological and mechanical properties tailored for a given medical use.

This chapter focuses on the recent advancement in bioactive polymers and nanobiomaterial composites, the fabrication of 3D biomimetic scaffolds for bone tissue engineering, particularly in the study of polymer and non-metallic-based nanocomposites, both in *in vitro* and *in vivo* bone tissue regeneration. Additionally, this chapter discusses the structure and properties of the polymer-nanocomposites scaffolds.

5.2   Design and Fabrication of Biomimetic 3D Polymer-Nanocomposites Scaffolds

A variety of designs and processing and fabrication methods of 3D bone tissue engineering based on polymer-nanocompsites scaffolds have been developed. Each method has its advantages and disadvantages. The strategies of incorporation of bionanomaterials into polymer matrices to enhance structural, mechanical and biological properties are presented in Figure 5.1. The structure of the scaffold should act as a template for 3D tissue growth, which should ideally consist of a highly porous interconnected network with interconnected pores > 50 μm in diameter and pore diameters > 100 μm [13, 14]. High porosity, normally between 60% and 80% is required to accommodate osteoblasts or osteoprogenitor cells, which, in turn, allows cell proliferation and differentiation to enhance bone tissue formation. High interconnectivities between pores are also desirable for uniform cell seeding and distribution to facilitate the diffusion of nutrients into and diffusion of metabolites out of cell or scaffold constructs. The scaffold should have adequate mechanical stability to provide a suitable environment for
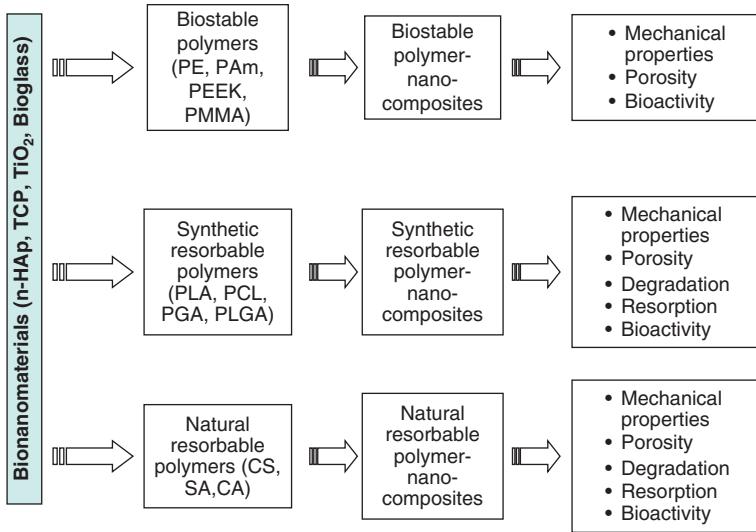
Figure 5.1 Strategies of polymer nanocomposites preparation to achieve mechanical, physical and biological properties of the composites for bone tissue engineering application. Hydroxyapatite (HAp), Tricalcium phosphate (TCP) and Titanium dioxide (TiO$_2$).

new bone tissue formation, as well as appropriate surface structure for adhesion and functioning of skeletal cells [15]. The development of 3D polymer-nanocomposites scaffold is based on the above criteria. Techniques considered here for scaffold manufacturing polymer nanocomposites are: solvent casting and particulate leaching, melt molding, gas foaming, electrospinning, microsphere sintering and more advanced rapid prototyping.

5.2.1   Solvent Casting and Particulate Leaching

This is a very simple method for fabricating tissue engineering scaffolds. With an appropriate thermal treatment, porous structure of scaffolds can be prepared with specific porosity, surface to volume ratio, pore size and pores interconnectivity. This method involves mixing water-soluble salt particles (e.g., sodium chloride, sodium citrate) into a polymer-nanocomposite solution. The mixture is then cast into a mold of desired shape. After the solvent is removed by evaporation or lyophilization, the salt particles are leached out to obtain a porous structure [16].

5.2.2   Melt Molding

Melt molding is an alternative method of 3D polymer-nanocomposites scaffolds fabrication. It has many advantages thanks to modern processing technologies, such as reproducibility, shapeability, homogeneous

distribution of filler and low cost. In melt molding, the optimization of the processing parameters such as compounding, compression and injection molding and extrusion, composition and shape are important [17]. The technique gives uniform particle distribution [18], particularly when twin-screw extrusion is used in the processing of polymer and nanocomposites.

5.2.3   Gas-Foaming Processes

Gas foaming has been developed as a method for producing porous 3D polymer scaffolds without the use of organic solvents. This happens to be very cost effective and environmentally friendly. This is desirable, as the residual solvent can have toxic effects *in vitro* and elicit an inflammatory response *in vivo*. In this method the molded samples are exposed to high pressure CO_2 to saturate the material. Subsequent reduction in pressure causes the nucleation and formation of pores in the composites of PLA and ceramic nanoparticles (HAp or β-TCP) from the CO_2 gas [19]. The main disadvantage of this method is that it yields a nonporous surface and closed-pore structure, with only 10–30% of interconnected pores. In order to improve porosity and interconnectivity of the pores, a method combining particulate leaching with the gas-foaming process has been developed (Figure 5.2a), albeit not being able to completely eliminate closed pores [20].
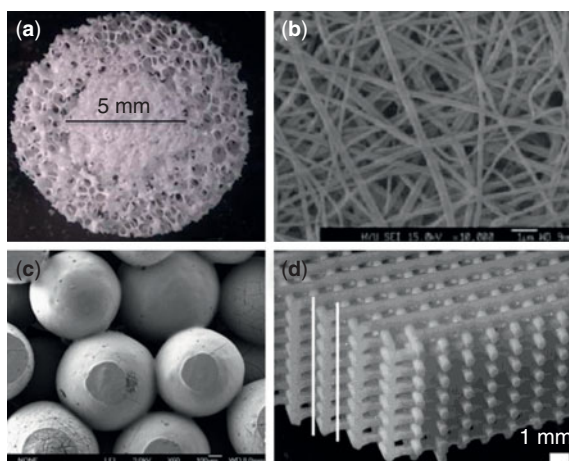
Figure 5.2 Representative examples of the structure of 3D scaffolds fabricated using various methods. (a) Stereomicroscope image of PLA-HA scaffold fabricated by gas foaming. (b) SEM image of PLA/HAp fibrous scaffold fabricated by electrospinning method. (c) SEM image of PLGA/n-HAp composite scaffold fabricated by microsphere sintering method. (d) A 3D periodic structure with a tetragonal symmetry of a scaffold fabricated using rapid prototyping method. Reprinted with permission from [20–23].

5.2.4   Electrostatic Spinning

Electrospinning is an interesting method which enables the production of fibrous scaffolds with fiber diameters within the range of submicron to nanometer (Figure 5.2b). In this process, a continuous filament is drawn from polymer-composite solution or melts by high electrostatic forces and is deposited on a grounded conductive collector [21]. This method is increasingly being used to produce fibers for tissue engineering scaffolds, which exhibit two important advantages. First, the interconnectivity of voids available for tissue in growth is suitable, and secondly, ultrathin fibers, produced by this method, offer high surface-to-volume ratio within the tissue scaffolds.

5.2.5   Microsphere Sintering

In this method, microspheres of polymer nanocomposites are synthesized using emulsion and solvent technique. Followed by sintering 3D porous microsphere scaffolds were achieved [22] (Figure 5.2c). It has been demonstrated that PLGA-nano-HA composites microspheres [21] exhibited osteoblastic phenotype expression and differentiation of mesenchymal stem cells (MSCs) toward the osteogenic linage.
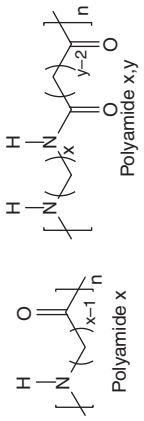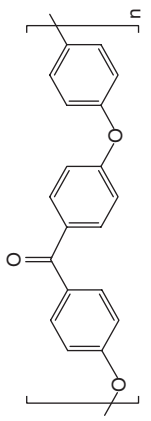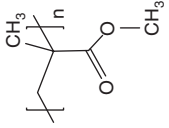
5.2.6   Rapid Prototyping

This is a group of technologies involving computer-aided design, materials science and engineering, which can build physical 3D biomimetic scaffolds using layer-by-layer deposition and laser sintering [23]. This offers new opportunities for 3D complex structure of materials at finer length scales, which rely on the quality of the filament of the ink material which is continuously extruded from a nozzle and deposited onto a substrate to yield complex structures in a layer-by-layer build sequence (Figure 5.2d). The process requires the optimization of viscosity and viscoelasticity of the ink and the hardening of the ink after extrusion from the nozzle. High resolution of complex 3D scaffold structures is achievable with feature sizes from a few hundred microns to submicron scale. By controlling ink rheology, a complex 3D scaffold consisting of continuous solid, high porosity and high pores interconnectivity has been constructed [23].

5.3   Nonbiodegradable Polymer and Nanocomposites

Nondegradable polymers have good mechanical properties and chemical stability and therefore are widely used in bone tissue engineering. The representative examples of nonbiodegradable polymers utilized as polymer matrices for nanocomposites preparation for bone tissue engineering are presented in Table 5.1. The most important synthetic nondegradable

Table 5.1 A list of non-bioresorbable polymers used as matrices for the composites preparation for bone tissue engineering applications.

Polymers	Structure of polymers	Polymer Nanocomposites	Comments
Polyethylene (PE) (HDPE, UHMWPE)		HDPE/HAp, HDPE/β-TCP [29–32]. TCP/HDPE [41] and TCP/HDPE/ UHMWPE [42].	*In vitro, in vivo* bone tissue modelling and orthopedic implants.
Polyamides (PAm)	Polyamide x, Polyamide x,y	PAm/HAp [44].	Load bearing bone repair.
Poly(ether ether ketone) (PEEK)		PEEK/HAp [47–49]. PEEK/ TCP [50–53].	Load bearing bone repair.
Poly(methyl methacrylate) (PMMA)		PMMA/HAp [62, 63], PMMA/TCP/BaSO$_4$ [64, 65], PMMA/TCP [68].	Bone cement.

polymers in bone tissue engineering include polyethylene (PE), polyamides (PAs), poly(methyl methacrylate) (PMMA), poly(ether ether ketone) (PEEK), polypropylene (PP), and selected polyurethanes (PUs). These polymers are also known to be biostable in the human body and employed in a wide range of biomedical applications. For example, ultra-high-molecular-weight polyethylene (UHMWPE) for acetabular cups [24–26]. However, it is to be noted that each polymer material has its own characteristic advantages and disadvantages. Composites and nanocomposites can offer a suitable set of properties which often show an excellent balance between strength and toughness, and usually possess improved characteristics compared to their individual components. The desired advances are primarily related to improving their biocompatibility and performance, both of which are already remarkable in terms of actual clinical applications. Since natural bone is an organic/inorganic hybrid material, made of collagen and apatite, composites consisting of a polymer matrix and apatite-based nanoparticles seem to be suitable candidates for bone tissue engineering applications.

5.3.1   Polyethylene Nanocomposites

Polyethylenes (PE), particularly in its high-density (HDPE) or UHMWPE (ultra-high-molecular-weight) form are used as polymer matrices for the preparation of nanocomposites with HAp. UHMWPEs are linear chains with very high molecular weight in the range of between $(2–10) \times 10^6$ Da. These have very high wear resistance, chemical resistance and low coefficient of friction, and are self-lubricating, and can be processed by either sintering, compression molding or by extrusion [27]. However, the shorter lifetime of UHMWPE is one of the major drawbacks which limit its application for total hip replacement. Numerous attempts have been made to improve UHMWPE-based devices' life-time, as well as incorporation of ceramic nanoparticles for improvements in other parameters such as reinforcements, high-temperature recrystallization and crosslinking [28]. PE allows large amounts of bioceramic particles to be incorporated into the matrix via melt-processing using current technologies. Particulate HAp-reinforced HDPE composites have been developed since the early 1980s [29] for bone replacement and commercialized (HAPEX) by Smith & Nephew. They were the first bioactive ceramic/polymer composites designed for mimicking the structure and properties of bone, and have supported research and development of other bioactive composites using the same rationale [24]. The close elastic modulus matching of HDPE/HAp composite to bone shows promise in solving the problem of bone resorption that has been encountered with the use of implants made up of conventional materials, such as metals and ceramics, which possess much higher modulus values than human cortical bone [30].

In another approach, synthetic HAp whiskers were utilized as reinforcement for orthopaedic biomaterials [31]. High-density polyethylene

(HDPE) was reinforced with either the synthesized HAp whiskers or a commercially available spherical HAp powder using a novel powder processing technique that facilitated uniform dispersion of the additive in the matrix prior to compression molding. An increase of the volume fraction of either of the two reinforcement types by more than 0–50 vol% resulted in increased elastic modulus, a maximum in ultimate tensile stress and decreased work-to-failure rate. Due to alignment of the whiskers in the matrix during processing, composites containing HAp whiskers were anisotropic and had higher elastic modulus, maximum tensile strength and work-to-failure rate relative to composites reinforced with spherical HAp.

Other researchers [32] studied the effect of partially stabilized zirconia (PSZ) on the biological properties of the HDPE/HAp composites by investigating the simultaneous effect of HAp and PSZ volume fractions on the *in vitro* response of human osteoblast cells. It was found that the volume fraction of HAp has a significant effect on the bioactivity of the composites. The composites provided a favorable site for cell attachment, with cells frequently found to be anchoring to the HAp particles. Interestingly, the results show that the addition of PSZ into the HDPE/HAp composites does not adversely affect the biological properties of these composites and, in some cases, composites with PSZ showed better biological results than HDPE/HAp systems [32].

Tricalcium phosphate [TCP; $Ca_3(PO4)_2$] is another class of ceramic-based effective candidate material for bone tissue engineering, which showed excellent osteoconductivity and bioactivity [33–35]. Although there are several types of TCP such as, β-TCP, α- TCP, α' TCP, and γ-TCP [36], only β -TCP is widely used for bone tissue engineering due to its simple and defined fabrication process. It has been reported [37–39] in several studies that nanoparticle β-TCP composites could enhance the cellular proliferation and bioactivity of osteoblast cells. However, the lack of tensile strength of β-TCP alone limited the application of this biomaterial in load-bearing clinical applications [40]. Therefore, the combination of low grain-sized β-TCP particles with flexible polymer matrices, e.g., polyethylene (PE), could improve its mechanical properties for a wide range of applications such as artificial hip joints. Homaeigohar and coworkers [41] investigated the skeletal cell lines proliferation using β-TCP/HDPE blends as matrix and confirmed significant improvement. Therefore, β-TCP nanoparticles blended with HDPE or UHMWPE as scaffolds can be used for bone tissue remodeling of effective matrices (Table 5.1) [42].

5.3.2   Polyamides Nanocomposites

Polyamides (PAs) are semicrystalline engineering polymers with a wide range of suitable properties. There are a number of different PAs, but PA-6,6 has good mechanical properties, exhibits good biocompatibility

with the human body and is considered to be a useful polymer for bio-medical applications. PA-6,6 displays some structural similarity to collagen, and the depolymerization products (hexamethylenediamine and hexanedioic acid) act *in vivo* as antibacterial agents [43]. However PA-6,6 lacks the ability for specific interactions with bone tissue. Therefore, it is compensated by preparation of PA-composites with HAp nanoparticles additives to enhance bioactivity [43] with the prospect of being an effective bone replacement material. It has been reported in a separate study, that polyamide (PA 8063) and nanoHAp can be used to prepare bone-like composites with high HAp content and with good homogeneity and chemical interface bonding [44]. Additionally, it can be comparable with natural bone; the synthetic nanocomposites had been found to give bone-like structure almost similar to that of human. The nanoHAp provides the bioactivity for the composite through interactions with natural bone, and PA is responsible for mechanical strength and toughness. Therefore, PA/HAp nanocomposites could be one of the better groups of bioactive materials for load-bearing bone repair or substitution [44]. The solution method can be used to prepare PA-6/nanoapatite (NA) biocomposites [45] with uniform distribution in the PA-6 matrix. Authors also reported that a molecular level of interactions exists between nanoparticles and PA-6, which eventually improves the mechanical properties of the composites. This will be similar to natural bone architecture with interconnected porous network having porosity of 80% and mean pore size of ~ 300 μm, and at the same time providing good biocompatibility. The composite prepared with 65% NA content with 35% PA showed high mechanical strength close to the natural bone [45]. The scaffolds were fabricated by the "injecting foam method" with interconnected pores having ~ 80% porosity and mean pore size of ~ 300 μm. When implanted into cortical bone, the composite combined directly with the natural bone without fibrous capsule tissue between implant and host bone.

5.3.3   Poly(ether ether ketone) (PEEK) Nanocomposites

PEEK is a polyaromatic, semicrystalline, rigid, thermoplastic polymer with high mechanical properties, and resistence to chemicals, radiation and temperature. It also offers ease of processing. Besides, PEEK is non-cytotoxic and can be repeatedly sterilized using conventional steam, γ-irradiation and ethylene oxide treatment without deterioration of its mechanical properties. All these benefits have rendered particulate-reinforced PEEK attractive for structural support material for orthopaedic implants [46]. PEEK is a bioinert polymer, and the addition of ceramic-based nanoparticles such as HAp in the PEEK matrix enhance biocompatibility and natural bone formation and mechanical properties in the region of cortical bone, making it a potential candidate for use in load-bearing applications [47].

HAp particulates have been incorporated into PEEK matrix using a variety of processing techniques, i.e., melt compounding, granulating and injection molding [48]. Authors have demonstrated the feasibility of fabricating PEEK/HAp biocomposites with high HAp loading of up to 40 vol% [49], which was achieved through appropriate selection of the processing parameters.

Tricalcium phosphate has been used to prepare PEEK/TCP composites using a variety of methods, for example, compounding and injection molding [50] and selective laser sintering (SLS) [51–53]. The latter method can also be used to produce macroporous scaffolds with a network structure similar to that of bones.

Cell attachment on bioactive PEEK composites has been demonstrated using fibroblasts [54], human osteoblasts [43, 50], and human fetal osteoblasts [53]. Osteoblast proliferation and spreading were reported to be greatest for bioglass (45S5)-reinforced PEEK, followed by PEEK and then β-TCP-reinforced PEEK [50, 51, 53]. However, another study reported no differences in osteoblast proliferation and alkaline phosphatase activity (differentiation) for PEEK, HA-reinforced PEEK, and Sr-HA-reinforced PEEK [55]. HA alone is known to suppress cell proliferation but enhance differentiation [56]. Systematic investigations for the effects of the bioactive reinforcement composition, content, size, and morphology on cellular behavior are needed in the future. Recently, research results on carbon nanotubes (CNTs)/PEEK composites have been reported [57, 58]. The authors undertook studies on their physical and mechanical properties. However, it was indicated that further studies on CNT-based PEEK composites need to be conducted to understand cellular behavior and the mechanism of bone tissue formation.

5.3.4   Poly(methyl methacrylate) (PMMA) Nanocomposites

PMMA and its derivatives are the polymers most commonly used as bone cements for fixation in orthopaedic surgeries. PMMA is an amorphous thermoplastic polymer and is still the current standard for cement-held prostheses. It is an inert material for fibroblastic cells observed at the bone–cement interface. It forms a strong bond with the implant, but the bond between the cement and the bone is considered to be weak, with fibroblastic cells observed at the implant site. Incorporation of HAp increases the biological response to the cement from tissue around the implant site, thus giving increased bone apposition. Research revealed that the addition of up to 40 wt% of HAp to PMMA cement has been shown to increase the fracture toughness, and that the addition of up to 15 wt% of HAp led to an increase in flexural modulus, while the tensile and compressive strengths remained unchanged [59]. Dalby and coworkers [60] used an *in vitro* tissue culture model to evaluate the biological response of conventional PMMA and

PMMA/HAp composites. An increase in biological activity of bone cements in response to increasing HAp content was observed. The authors suggested that loading of HAp into cements could be the way forward in producing active materials with the the biological properties that benefit the patient.

Kwon and coworkers conducted studies [61] that showed that a PMMA/HAp composite (30 wt% of HAp) increased the interfacial shear strength at the bone–implant interface 6 weeks after implantation in rabbits. Several other studies also found that the addition of HAp can enhance the mechanical properties of bone cements, although the extent of improvement varied, depending on the type of bone cement [62]. The response of osteoblasts to PMMA/HAp materials was also investigated by Moursi *et al.* [63], and found that osteoblasts proliferation was improved when PMMA/HAp was used when compared to those of traditional materials (titanium and PMMA).

The PMMA-based nanocomposites with various forms of TCP were also investigated by several other research groups [64–68]. The preparation of PMMA-based composites were enriched with β-TCP and $BaSO_4$ to improve the inherent porosity of cement, thus increasing the amount of absorbed antibiotic. These properties and their *in vitro* and *in vivo* performance have also been studied [64, 65]. Yasuda *et al.* [67] reported the a-TCP dissolved in the body faster than both HAp and β-TCP. Thus, the biocompatibility of HAp/a-TCP and HAp/β-TCP composites is expected to be different from each other. Authors demonstrated the method of preparation of dense HAp/a-TCP composites by a colloidal process. The colloidal process suppresses agglomeration due to electrostatic, steric or electrostatic repulsive force by polymer dispersant. An addition of the appropriate amount of dispersant leads to a good dispersion of particles, resulting in better mechanical properties. The composite of HAp/a-TCP was dispersed in PMMA matrix and was found to form porous structure containing 100 µm-sized pores to incorporate cells needed for bone regeneration and to allow bone ingrowth. The biological properties of PMMA/a-TCP composite was tested by means of *in vitro* and *in vivo* investigations and the results were compared with those for controlled PMMA. Osteoblast cultures (MG63) demonstrated that composites significantly improved osteoblast viability [68], and the implant of PMMA/a-TCP composite successfully osteointegrated in trabecular and cortical tissue within 12 weeks. Recently, other types of nanomaterials, namely carbon nanotubes [69] and wollastonites [70], have been incorporated into the PMMA matrix, and their physical and mechanical properties have been investigated [69].

5.4   Biodegradable Polymer and Nanocomposites

Over the last two decades there has been an increasing demand for biodegradable and bioresobable materials for tissue engineering and

therapeutic systems in order to replace the nonbiodegradable materials. This evolution is aimed at helping injured tissues or repairing diseased tissues with delivery of pharmaceutical and bioactive molecules to enhance tissue regeneration [71]. Both synthetic- and naturally-derived biodegradable polymeric materials have been investigated as biomaterials for bone tissue regeneration and reconstruction. The most common degradable polymeric materials used as matrices for polymer nanocomposites preparation (Table 5.2) for bone tissue engineering application is described in the following sections.
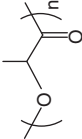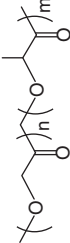
5.4.1   Synthetic Biodegradable Polymers and Nanocomposites
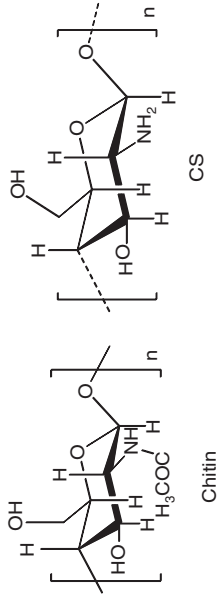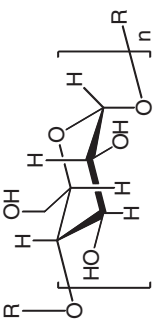
Synthetic biodegradable polymers are attractive candidate materials for biomedical applications such as drug delivery devices, orthopaedic fixation devices and different types of tissue engineering scaffolds [72, 73]. The materials include poly(lactic acid) (PLA), poly(glycolic acid) (PGA), poly(dioxanone) and poly(caprolactone) (PCL), and their copolymers have been accepted worldwide for use as medical devices [72]. The other important synthetic biodegradable polymers which are currently used in biomedical applications are polyphosphazenes, polyanhydrites, and poly(amino acids). However, the polyester-based materials have shown significant prospects and, therefore, the next section will focus on the preparation of polymer nanocomposites using PLA, PCL, PGA and their copolymer as matrix materials. Synthetic biomaterials are generally biologically inert and have more predictable properties than natural polymers. For applications like bone tissue regeneration, the material should have a certain level of biological activity, therefore strategies have been developed to incorporate biological motifs such as HAp and TCP nanoparticles into the polymer matrix.

5.4.1.1   Poly(Lactic Acid) Nanocomposites

The poly(L-lactide) (PLLA) is a semicrystalline and bioresorbable polymer, and the resorption kinetics of PLLA is different from that of poly(D,L-lactide) (PDLLA). It requires more than 2 years to be completely resorbed [73]. PLLA exhibits a wide range of suitable properties including high mechanical strength, low elongation, and high values of the following: modulus, stiffness, chemical and impact resistance, good wear and friction. All these properties make PLLA a better candidate material than amorphous polymers for load-bearing orthopaedic applications [73–76]. Many researchers have reported that the bioactivity of PLA-based materials for bone fracture repair can be enhanced by incorporation of HAp nanoparticles into the matrix. The reports provided details of sample preparation protocols, mechanical properties, interface structure, biocompatibility and biodegradability of the PLA-HAp nanocomposites [74–82].

Table 5.2 Typical examples of synthetic and natural biodegradable polymers used as matrices for nanocomposites preparation and their applications in bone tissue engineering.

Polymers	Structure	Polymer-Nanocomposites	Comments
Poly((L)-lactic acid) (PLLA)		PLLA/HAp [74–77]	Bone tissue engineering (e.g., rods, miniscrews, miniplates).
Polycaprolactone (PCL)		PCL/HAp [86–88]	*In vitro* cellular growth for bone repair.
Poly(lactide-co-glycolide) (PLGA)		PLGA/HAp [95]	*in vivo* submaxilla bone formation (rabbit model).
Poly(propylene fumarate) (PPF)		PPF/TCP [96].	*In vitro* osteoblast differentiation.

Polymers	Structure	Polymer-Nanocomposites	Comments
Chitin and Chitosan	Chitin CS	Chitin/HAp [103], CS-Gel/HAp [105]. CS/TCP [107].	*In vitro* cellular cellular compatibility and osteoblast differentiation, and *in vivo* bone formation in rabit model [103]. *In vitro* cells proliferation and osteogenic differentiation [105]. Injectable bone graft substitute cytocompatible [107].
Starch		Starch-EVA/HAp [18].	*In vitro* and *in vivo* models, the SEVA-C-based materials was biocompatible in addition to their bone-matching mechanical properties makes them promising materials for bone replacement/ fixation [18].
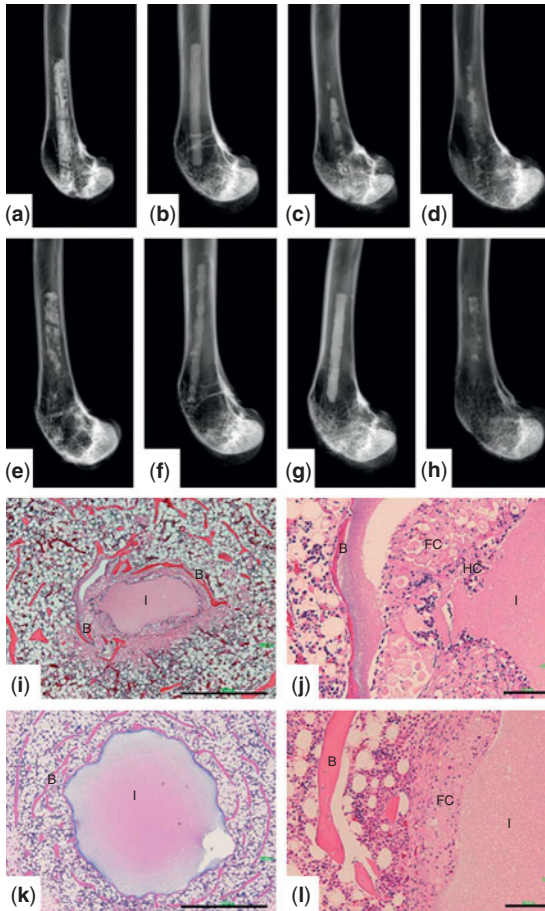
Figure 5.3 Lateral radiographs of the distal femurs implanted with uncalcified-HAp/PLLA (u-HAp/PLLA) and calcified HAp/PLLA (c-HAp/PLLA) composites rods. (a) u-HA40/PLLA at 66 months after implantation, (b) u-HA40/PLLA at 76 months after implantation, (c) u-HAp40/PLLA at 79 months after implantation, (d) u-HAp30/PLLA at 88 months after implantation, (e) c-HAp40/PLLA at 66 months after implantation, (f) c-HAp40/PLLA at 76 months after implantation, (g) c-HAp40/PLLA at 79 months after implantation, (h) c-HAp30/PLLA at 88 months after implantation.

Histochemical analysis with Hematoxylin–eosin staining of decalcified sections of the distal femurs. (i, j) u-HAp30 at 88 months after implantation, (k) c-HAp40 at 79 months after implantation, (l) c-HAp40 at 76 months after implantation. Although there were limited numbers of samples, histology of the u-HAp was similar to c-HAp. Remodelled trabecular bone encircled the residual material. The rod had been infiltrated by a few histiocytes. The rods had been phagocytosed by histiocytes transformed to foam cells. No infection or inflammatory reaction were seen in the follow-up period. B = bone; I = implant; HC = histiocyte; FC = foam cell (original magnification; (i, j) $\times$ 20, bar = 1000 μm, high magnification; (k, l) $\times$ 100, bar = 100 μm). Reprinted with permission from [75].

HAp-containing bioactive composites are suitable as bone-filling materials without any side effects, which has been demonstrated by implantation in an animal model *in vivo* for bone tissue regeneration (Figure 5.3) [75, 76]. The complete process of bioresorption and concurrent bone replacement of rods made of forged composites of PLLA and raw HAp particles implanted in the femoral medullar cavities of rabbits has been described [77]. The results of this procedure in terms of bioresorption, osteoconductive bioactivity and bone replacement in three implantation sites were compared (Figure 5.3).

Recently, researchers have demonstrated [78, 82] that PLLA can be functionalized by chemical grafting onto the hydroxyl groups in the surface of nanoHAp particles by ring-opening polymerization. These PLLA-grafted HAp materials had better mechanical and bending strength with improved cellular compatibility [82] which are required for bone tissue regeneration as compare to that of non-grafted composites. The composites of poly(D,L-lactide) (PDLLA) and HAp have been developed which possess biodegradation, biocompatibility and shape memory properties [83]. Such shape memory effect may have a certain advantage for some bone implant applications to mimic the exact shape of the bone. Other researchers [85] have reported that titanium dioxide (TiO_2) nanoparticles can be used as a promising filler material for use in designing bone tissue engineered constructs based on PLA matrices.

5.4.1.2 *Poly(ε-caprolactone) (PCL) Nanocomposites*

PCL is a linear polyester and a semicrystalline polymer with a degree of crystallinity (50%) and a glass transition temperature of about −60°C and melting temperature of about 65°C. Currently, PCL is regarded as a candidate polymer for tissue engineering, as it shows suitable mechanical properties to serve as a scaffold in applications where a highly resilient material is required, e.g., bone substitution, where the physical properties of the scaffold have to be maintained for at least 6 months [86]. The PCL/HAp composite scaffolds fabricated using PCL as matrix and HAp nanoparticles as a filler material, prepared by phase inversion and solution casting techniques, have been found to give [86] better mechanical strength and osteoblast growth (in comparison to pure PCL). The topic has been the subject for a spate of research activities by many research groups around the world [87, 88]. Some authors have reported [87] that the mechanical properties of the composites, particularly the values of elastic modulus, is within the same range of that for human cortical bone, following addition of 20% HAp into the polymer matrix. Furthermore, PCL/HAp scaffolds have been used for *in vitro* cell culture studies using primary human osteoblasts. Observation of a high proliferation rate and a moderate increase of alkaline phosphatase activity indicated osteogenic

differentiation was taking place. It was, therefore, concluded that the structure of a scaffold along with its surface physicochemical characteristics affect cellular behavior and functions. Additionally improved mechanical parameters achieved by using such scaffold are crucial for implant performance.

In a separate investigation, Azevedo *et al.* [88] reported on the preparation of PCL/HAp composite scaffolds by two different procedures. The first consisted of a conventional blending of the polymer and reinforcement material in an extruder. The second method encompassed grafting of PCL onto the surface of HAp particles. This was a ring-opening polymerization of caprolactone in the presence of HAp. Although an increase in the modulus occurred for the composites obtained by both the methods, the method of grafting of the HAp particles was found to be a more promising route for obtaining composites with more suitable properties for use in orthopaedics.

5.4.1.3   *Polyglycolide and Poly(lactide-co-glycolide) Nanocomposites*

Polyglycolide (PGA) is the simplest linear aliphatic polyester, characterized by a high degree of crystallinity (45–55%) with high melting temperature (220–225°C), and a glass transition temperature of 35–40°C [89, 90]. PGA alone has high stiffness, which limits the scope for its application. Therefore, the copolymers of glycolide with L-lactide and D,L-lactide have been developed for orthopaedic and drug delivery applications [89, 91]. However, foams produced from PLGA were found to have insufficient compressive strength to be used in any load-bearing tissue application [91]. The use of PLGA/HAp composite materials to assist in the bone healing process, by either stabilizing the defect site or improving the osteoconductivity of existing biomaterials, has been studied [92], with controlled porosities that have minimal compressive yield strength and can be seeded with cells. The ability to control porosity, however, is an important factor as it plays a critical role for the cellular functionality. In a separate investigation, PLGA fibers with HAp particles have been processed by solution spinning [93].They reported that the presence of HAp particles in the PLGA composites fiber accelerated deposition of calcium phosphate from simulated body fluid (SBF) solution, thereby enhancing *in vitro* and *in vivo* bone formation [93–95].

The influence of bioactive additives, such as short carbon fibers (CF), HAp nanoparticles and bioglass, on the thermal and mechanical properties of PLGA composite has been examined under *in vitro* conditions. It was reported that the presence of bioactive particles affects the process of apatite growth on composite surface in which a chemical bond between the implant and the bone tissue is formed. Despite the deterioration of mechanical properties after incubation under *in vitro* conditions, the

PLGA/HAp composites still showed advantageous biological behavior [93]. Further work has reported on the resorption process of PLGA/HAp nanocomposites implanted into rabbit submaxilla bones [95]. The resorption of composite occurred simultaneously with the formation of new bone tissue, and authors found that after 3 weeks following the implantation the bone–implant interface becomes rough, which indicated resorption of polymer with bone tissue ingrowth.

5.4.2   Natural Polysaccharide Nanocomposites

The natural polysaccharides have attracted a significant interest in scientific and industrial communities for biomedical applications. This is due to their attractive properties such as good biodegradability, low toxicity, low manufacturing cost, low disposal cost, environmental friendly production and disposal and renewability prospect [97]. A large variety of natural materials have been studied and proposed for biotechnological applications. Some of these offer additional advantages for tissue engineering applications such as biological signaling, cell adhesion, cell responsive degradation, re-modeling, etc. However, the down side of using natural polymers is that these may rapidly degrade with the possible loss of biological properties during formulation and storage, often compromising their use as unique scaffold materials. Despite the minor downside, the current research has been focused on the use of natural polymers which include chitin and chitosan, starch and cellulose-based polymer composites, for the fabrication of scaffolds for bone tissue regeneration.

5.4.2.1   *Chitin and Chitosan and Their Nanocomposites*

Chitin, poly (*β*-(1–4)-N-acetyl-D-glucosamine), is a natural polysaccharide of major importance, synthesized by an enormous number of living organisms (e.g., in the shells of crabs and shrimp, the cuticles of insects, and the cell walls of fungi and yeast) [97, 98], and it is the most abundant polymer after cellulose. Chitosan, is the most important (an N-deacetylated) derivative of chitin containing varying fractions of the two residues [98] randomly distributed *β*-(1–4)-linked D-glucosamine (deacetylated unit) and N-acetyl-D-glucosamine (acetylated unit). It is obtained by (partial) deacetylation of chitin in the solid state under alkaline conditions or by enzymatic hydrolysis.

Chitin and CS-based nanocomposite materials enhance bone formation both *in vitro* and *in vivo* (Table 5.2) [99, 100], but its mechanical weakness and instability, together with its incapacity to maintain a predefined shape, limits the scope of its applicability. Therefore, researchers combined CS with a variety of materials including HAp, calcium phosphate

for potential application in orthopaedics and cell-based tissue engineering applications [101–109]. By incorporating calcium phosphate into CS scaffold both the compressive modulus and yield strength are significantly improved and a reinforced microstructure has been achieved [106]. The loading of natural coralline into CS microporous scaffolds was also found to cause an increase in compressive modulus, and to have a positive impact on the adhesion of MSCs [107]. The composites of CS/HAp have been found to promote the formation of bone-like apatite on their surfaces after soaking in SBF, and to enhance the attachment, proliferation and differentiation of osteoblast-like cells [108].

Wan *et al.* have investigated the interactions of chitin with calcium species [99]. In one strategy, HAp was dispersed in chitin to produce intimately blended material. Preliminary mechanical tests revealed a reduction in strength for the more highly filled composites, but they also revealed retention of the plastic properties of the polymer that may be favorable for bone substitute applications [99]. Chitin/HAp composites were also investigated by Ge *et al.* [103]. HAp in 25%, 50%, and 75% (w/w) fractions was incorporated into chitin solutions and processed into air- and freeze-dried methods. These materials were then exposed to cell cultures and implanted into the intramusculature of a rat model, and they proved to be non-cytotoxic and degradable *in vivo*. The presence of the HAp filler enhanced calcification as well as accelerated degradation of the chitin matrix. Composites with various CS/HAp ratios were obtained by Yamaguchi and coworkers [104] using the co-precipitation method. In these composites, calcium phosphate formed crystalline HAp when acetic acid and lactic acid were used in the preparation solvents for CS. The calcium phosphate was found to be amorphous when organic acids having more than two carboxyl groups were applied. Biodegradable CS/Gel/HAp composites were prepared by Zhao [105], and obtained a structure similar to that of normal human bone as 3D biomimetic scaffolds by phase separation. By changing the solid content and the compositional variables, the authors controlled the porosities and densities of the scaffolds. Histological and immunohistochemical staining and SEM observations indicated that the osteoblasts attached to and proliferated on the scaffolds. The presence of HAp in the CS/Gel composite promoted initial adhesion of human mesenchymal stem cells (hMSC) and supported long-term growth in 3D porous CS/Gel/HAp scaffolds [106]. Kong *et al.* [108] have investigated CS/nanoHAp scaffolds for bone tissue regeneration, and studied the bioactivity of the composite scaffolds by examining the apatite formed on the scaffolds incubated in SBF. The authors suggested that compared with pure CS, the composite with nanoHAp could form apatite more readily during the biomimetic process. It is an important finding because cells presented better proliferation on the apatite-coated scaffolds than on CS scaffolds.

5.4.2.2   Starch Nanocomposites

The starch molecule has two important functional groups, the –OH groups that are susceptible to substitution reactions, and the C–O–C groups where chain breakage starts. By reaction of its –OH groups, chemical modification of starch can be performed, leading to materials with various properties, and can be used as scaffolds for hard tissue engineering [17, 109, 110]. Biodegradable starch-based polymers have recently been proposed as having great potential for several applications in the biomedical field, such as bone replacement implants, bone cements, drug delivery systems, and tissue engineering scaffolds [111]. The development of new processing techniques and the reinforcement with various (nano) fillers has resulted in materials with mechanical properties matching those of bone [110]. Mendes and coworkers [18] described an extensive biocompatibility evaluation (*in vitro* and *in vivo*) of biodegradable starch-based materials aimed at orthopaedic applications as temporary bone replacement/fixation implants. For that purpose, they studied a polymer starch/ethylene vinyl alcohol blend (SEVA) and a composite of SEVA reinforced with HAp particles (Table 5.2). As a result of their investigation it was found that SEVA and SEVA/HAp materials did not show relevant toxicity in both short- and long-term *in vitro* testing. Furthermore, when implanted, these materials induced a satisfactory tissue response.

The biocompatibility of two different blends of corn-starch, SEVA and starch/ cellulose acetate (SCA), and their respective composites with HAp, was studied by Marques *et al.* [110]. Authors found that both types of starch-based polymers exhibit a cytocompatibility that might allow for their use as biomaterials. Furthermore, SEVA blends were found to be less cytotoxic for the tested cell line, although cells adhere better to SCA surface. Considering the overall behavior of SEVA, SCA and their composites with HAp, it can be expected that their cytocompatibility will allow their use, in the near future, in bone replacement/fixation and/or tissue engineering scaffolding applications.

5.4.2.3   Cellulose Nanocomposites

Cellulose is another type of polysaccharide produced from plants, biosynthesized by different types of microorganisms, enzymatic *in vitro* synthesis, and chemosynthesis from glucose derivatives. Cellulose is a very high molecular weight polymer with very highly crystalline and is infusible and insoluble in all but the most aggressive, hydrogen-bond-breaking solvents such as N-methylmorpholine-N-oxide.

Bacterial cellulose (BC)/HAp nanocomposites were examined by Wan *et al.* [111]. The most striking features of BC are its high mechanical strength and modulus, as well as its biodegradability. Compared with other natural biodegradable polymers, BC presents much better mechanical properties,

which are required in most cases when used as scaffold in tissue engineering. Compared with animal derived polymers, BC is free of any occurrence of cross-infection that can be associated with collagen. The authors found that there are different interactions between unphosphorylated and phosphorylated BC fibers and HAp. It was found that phosphorylated BC could act as potential substrate for apatite nucleation. The observed 3D porous network structure and interconnected pores, whose parameters can be adjusted over a wide range, make the BC/HAp composites promising materials in tissue engineering. In addition, it is expected that the advantageous mechanical properties of BC will allow the design of a wide range of BC/HAp composites with mechanical properties ranging from those analogous to soft tissues to those similar to hard tissues, by controlling the ratio of HAp to BC and their 3D structure.

Jiang and coworkers [112] developed a new type of bone-replacing material composed of different weight ratios of nanoHAp and a CS-carboxymethylcellulose network. NanoHAp was uniformly dispersed in the composite in the form of nanometer-grade short crystals, which ensured that the composite had high compressive strength. For the composite with 40 wt% NanoHAp, the compressive strength reached nearly 120 MPa, which can meet the requirement of initial mechanical properties for bone repair material. Moreover, its weight loss was up to 56.44% after soaking in SBF for 8 weeks, which indicates a degradable composite. Next, apatite particles aggregated to form a bioactive apatite layer deposited on the surface.

5.5   Conclusions and Future Remarks

Therapeutic repair of damaged bone tissue and its regeneration engineering protocols have generated significant interest in the scientific and medical communities research, and developments in these fields, particularly in preclinical animal models and in clinical pilot studies have, so far, been very promising. Recent progress in the design and incorporation of bionanomaterials into the biocompatible polymer matrices, and processing technologies able to produce porous structure with high porosity with tailored mechanical and biological properties, provided some unique protocols for the development of polymer nanocomposites scaffolds. Recent studies indicate that designing scaffolds construct with the combination of ceramic nanoparticles (e.g., HAp, TCP) into the polymer matrix, have great potential for optimal bone tissue regeneration. In particular, biodegradable polymer–nanoHAp composites display controllable bioresorption kinetics and the sufficient mechanical strength needed for applications in bone tissue engineering. The high surface area nanostructured HAp allows the interactions with the lowest hierarchical levels of bone structure, although

the mechanisms of polymer/nanomaterials with bone tissue remain unknown. As for the technological development, the challenge is to design and manufacture a biodegradable nanocomposite scaffold possessing a tailored porosity and pore structure which is able to withstand *in vivo* load and sustain its properties for a sufficiently extended time.

Various scaffold production techniques for the processing of a variety of polymeric nanocomposite materials are currently employed. Each presents some advantages over others along with its characteristic shortcoming, such as, the lack in control of scaffold porosity, pore size and distribution, and the presence of residual toxic solvent into the scaffold. The problems of controlling accuracy and reproducibility for manufactured scaffolds at an industrial scale and in a cost effective manner still remain unresolved and have to be addressed in future R&D in this field.

References

1. B.L. Seal, T.C. Otero, A. Panitch, *Mater Sci Eng,* Vol. 34, p. 147, 2001.
2. C. Laurencin, Y. Khan, S.F. El-Amin, *Expert Rev Med Devices,* Vol. 3, p. 49, 2006.
3. B. Hall, *Bones and Cartilage: Developmental Skeletal Biology*, San Diego, Academic Press, 2005.
4. W.G. De Long, M. Mckee, W. Smith , R. Sanders, *et al.*, *J. Bone Joint Surg. Am.,* Vol. 89A, p. 649, 2007.
5. C.V.M. Rodrigues, P. Serricella, A.B.R. Linhares, *et al.*, *Biomaterials,* Vol. 24, p. 4987, 2003.
6. K. Seunarine, N. Gadegaard, M. Tormen, D.O. Meredith, M.O. Riehle, C.D.W. Wilkinson, *Nanomedicine,* Vol. 1, p. 281, 2006.
7. K.F. Leong, C.K. Chua, K.F. Leong, *et al.*, *Biomaterials,* Vol. 24, p. 2363, 2003.
8. A.J. Salgado, O.P. Coutinho, R.L. Reis, *Macromol. Biosci.*, Vol. 4, p. 743, 2004.
9. B. Duan, M. Wang, W.Y. Zhou, W.L. Cheung, Z.Y. Li, W.W. Lu. *Acta Biomater.,* Vol. 6, p. 4495, 2010.
10. K.H. Tan, C.K. Chua, K.F. Leong, *et al.*, *Biomaterials*, Vol. 24, p. 3115, 2003.
11. S.N. Parikh, *Orthopedics,* Vol. 25, p. 1301, 2002.
12. S.H. Teoh, *Engineering Materials for Biomedical Applications,* World Scientific, Singapore, 2004.
13. (a) F. Khan, J. O. Smith, J. M. Kanzcler, R. S. Tare, R.O.C. Oreffo, M. Bradley, *Advan. Fun. Mater.,* 2012, DOI: 10.1002/adfm.201202710.
14. (b) F. Khan, S.R. Ahmad, *Macromol. Biosci.,* 2012, DOI: 10.1002/mabi.201200409.
15. X. Liu, P.X. Ma, *Ann. Biomedical Engineering*, Vol. 32, p. 477, 2004.
16. L. Fang, L.Y. Leng, P. Gao, *Biomaterials*, Vol. 27, p. 3701, 2006.
17. M.E. Gomes, A.S. Ribeiro, P.B. Malafaya, *et al.*, *Biomaterials,* Vol. 22, p. 883, 2001.
18. S.C. Mendes, R.L. Reis, Y.P. Bovell, A.M. Cunha, C.A. van Blitterswijk, J.D. de Bruijn, *Biomaterials,* Vol. 22, p. 2057, 2001.
19. L.M. Mathieu, T.L. Mueller, P.B. Bourban, *et al.*, *Biomaterials*, Vol. 27, p. 905, 2006.

20. J.-S. Son, S.-G. Kim, J.-S. Oh, M. Appleford, S. Oh, J.L. Ong, K.-B. Lee, *J. Biomed. Mater. Res. Part A*, Vol. 99A, p. 638, 2011.
21. S.I. Jeong, E.K. Ko, J. Yum, C.H. Jung, Y.M. Lee, H. Shin, *Macromol. Biosci.,* Vol. 8, p. 328, 2008.
22. Q. Lv, L. Nair, C.T. Laurencin, *J. Biomed. Mater. Res.,* Vol. 91A, p. 679, 2009.
23. F. Khan, S.R. Ahmad, Fabrication of 3D scafffolds and organ printing for tissue regeneration, in M. Ramalingam, S. Ramakrishna, and S. Best, Eds., *Biomaterials and Stem Cells in Regenerative Medicine*, CRC Press, p. 101–121. 2012.
24. M. Wang, *Biomaterials*, Vol. 24, p. 2133, 2003.
25. J.F. Mano, R.A. Sousa, L.F. Boesel, *et al.*, *Compos. Sci. Techn.,* Vol. 64, p. 789, 2004.
26. S. Blazewicz, Non-metalic multifunctional composites in biomaterials engineering, in A.J. Nadolny, Ed., *Biomaterials in Regenerative Medicine*, Polish Academy of Sciences, Warszawa, 2006.
27. H.F. Mark, in *Encyclopedia of Polymer Science and Technology*, Wiley, New York, 2004.
28. L. Eschbach, *Int. J. Care Injured,* Vol. 31, p. S-D22, 2000.
29. W. Bonfield, M.D. Grynpas, A.E. Tully, *et al.*, *Biomaterials,* Vol. 2, p. 185, 1981.
30. M. Wang, W. Bonfield, *Biomaterials,* Vol. 22, p. 1311, 2001.
31. R.K. Roeder, M.M. Sproul, C.H. Turner, *J. Biomed. Mater. Res.*, Vol. 67A, p. 801, 2003.
32. A.Y. Sadi, M.A. Shokrgozar, S. Homaeigohar, *et al.*, *J. Mater. Sci. Mater. Med.*, Vol. 17, p. 407, 2006.
33. H.M. Elgendy, M.E. Norman, A.R. Keaton, C.T. Laurencin, *Biomaterials,* Vol. 14, p. 263, 1993.
34. J.E. Devin, M.A. Attawia, C.T. Laurencin. *J. Biomater. Sci. Polym. Ed.,* Vol. 7, p. 661, 1996.
35. T. Arinzeh, T. Tran, J. Mcalary, G. Daculsi, *Biomaterials,* Vol. 26, p. 3631, 2005.
36. K. Sugiyama, M. Tokonami, *Phys. Chem. Miner.*, Vol. 15, p. 125, 1987.
37. C. Zou, W. Weng, K. Cheng, P. Du, G. Shen, G. Han, B. Guan, W. Yan, *J. Biomed. Mater. Res. A,* Vol. 87, p. 38, 2008.
38. C. Ergun, H. Liu, T.J. Webster, E. Olcay, S. Yilmaz, F.C. Sahin, *J. Biomed. Mater. Res. A,* Vol. 85, p. 236, 2008.
39. C. Ergun, H. Liu, J.W. Halloran, T.J. Webster, *J. Biomed. Mater. Re. A*, Vol. 80, p. 990, 2007.
40. M.J. Yaszemski, R.G. Payne, W.C. Hayes, R. Lander, A.G. Mikos, *Biomaterials,* Vol. 17, p. 175–185. 1996.
41. S.Sh. Homaeigohar, M.A. Shokrgozar, J. Javadpour, A. Khavandi, A.Y. Sadi, *J. Biomed. Mater. Res. A*, Vol. 78, p. 129, 2006.
42. M.B.H. Abadi, I. Ghasemi, A. Khavandi, M.A. Shokrgozar, M. Farokhi, S.Sh. Homaeigohar, A. Eslamifar. *Polym. Compos.*, 31: p. 1745–1753, 2010.
43. M. Huang, J.J. Feng, J. Wang, X. Zhang, Y. Li, Y. Yan, *J. Mater. Sci. Mater. Med.*, Vol. 14, p. 655, 2003.
44. W. Jie, L. Yubao, C. Weiqun, Z. Yi, *J. Mater. Sci.,* Vol. 38, p. 3303, 2003.
45. J. Wei, Y. Li, K.-T. Lau. *Composites Part B,* Vol. 38, p. 301, 2007.
46. M.S.A. Bakar, M.H.W. Cheng, S.M. Tang, S.C. Yu, K. Liao, C.T. Tan, K.A. Khor, P. Cheang, *Biomaterials,* Vol. 24, p. 2245, 2003.

47. S. Yu, K.P. Hariram, R. Kumar, P. Cheang, K.K. Aik, *Biomaterials*, Vol. 26 p. 2343, 2005.
48. M.S.A. Bakar, P. Cheang, K.A. Khor, *Composites Science and Technology*, Vol. 63, p. 421, 2003.
49. M.S.A. Bakar, P. Cheang, K.A. Khor, *Materials Science & Engineering, A: Structural Materials: Properties, Microstructure and Processing*, Vol. A345(1–2), p. 55, 2003.
50. L. Petrovic, D. Pohle, H. Munstedt, T. Rechtenwald, K.A. Schlegel, S. Rupprecht, *J. Biomed. Sci.*, Vol. 13, p. 41, 2006.
51. D. Pohle, S. Ponader, T. Rechtenwald, *et al.*, *Macromol. Sympos.*, Vol. 253, p. 65, 2007.
52. C. von Wilmowsky, R. Lutz, U. Meisel, S. Srour, *et al.*, *J. Bioact. Compatible. Polym.*, Vol. 24, p. 169, 2009.
53. C. von Wilmowsky, E. Vairaktaris, D. Pohle, *et al.*, *J. Biomed. Mater. Res.*, Vol. 87A, p. 896, 2008.
54. K.H. Tan, C.K. Chua, K.F. Leong, M.W. Naing, C.M. Cheah, *J. Engineer Medicine Part H,* Vol. 219, p. 183, 2005.
55. K.L. Wong, C.T. Wong, W.C. Liu, *et al.*, *Biomaterials,* Vol. 30, p. 3810, 2009.
56. R. Shu, R. McMullen, M.J. Baumann, L.R. McCabe, *J.Biomedical Mater. Res.*, Vol. 67A p. 1196, 2003.
57. A.M. Díez-Pascual, M. Naffakh, C. Marco, G. Ellis, *J. Phys. Chem. B*, Vol. 116, p. 7959, 2012.
58. A.M. Díez-Pascual, J. Guan, B. Simard, M.A. Gómez-Fatou, *Composites: Part A,* Vol. 43, p. 997, 2012.
59. C.I. Vallo, P.E. Montemartini, M.A. Fanovich, J.M. Porto López, T.R. Cuadrado, *J. Biomed. Mater. Res.*, Vol. 48, p. 150, 1999.
60. M.J. Dalby, L.D. Silvio, E.J. Harper, W. Bonfield, *Biomaterials,* Vol. 23, p. 569, 2002.
61. S.Y. Kwon, Y.S. Kim, Y.K. Woo, S.S. Kim, J.B. Park, *Bio-Medical Mater. Eng.,* Vol. 7, p. 129, 1997.
62. E.J. Harper, J.C. Behiri, W. Bonfield, *J. Mater. Sci. Mater. Med.,* Vol. 6, p. 799, 1995.
63. A.M. Moursi, A.V. Winnard, P.L. Winnard, J.J. Lannutti, R.R. Seghi, *Biomaterials,* Vol. 23, p. 133, 2002.
64. G. Giavaresi, E.B. Minelli, M. Sartori, *et al.*, *J. Mater. Sci.: Mater. Med.,* Vol. 23, p. 1247, 2012.
65. G. Giavaresi, M. Sartori, A. Benini, T. Della Bora, *et al.*, *J. Orthopaedic Res.,* Vol. 30, p. 348, 2012.
66. K.A. Bhat, P. Rajangam, S. Dharmalingam, *J. Mater. Sci.,* Vol. 47, p. 1038, 2012.
67. H.Y. Yasuda, S. Mahara, N. Terashita, Y. Umakoshi, *Materials Transactions,* Vol. 43, p. 1332, 2002.
68. M. Fini, G. Giavaresi, N.N. Aldini, *et al.*, *Biomaterials,* Vol. 23, p. 4523, 2002.
69. R. Ormsby, T. McNally, C. Mitchell, P. Halley, D. Martin, T. Nicholson, N. Dunne, *Carbon*, Vol. 49, p. 2893, 2011.
70. E. Bernardo, P.C.I. Cacciotti, A. Bianco, R. Bedini, R. Pecci, K. Pardun, L. Treccani, K. Rezwan, *J. Europ. Ceram. Soc.,* Vol. 32, p. 399, 2012.
71. M. Vert, *Prog. Polym. Sci.,* Vol. 32, p. 755, 2007.

72. P. Gunatillake, R. Mayadunne, R. Adhikari, *Biotechnol. Ann. Rev.,* Vol. 12, p. 301, 2006.

73. J.E. Bergsma, W.C. de Bruijn, F.R. Rozema, R.R.M. Bos, G. Boering, *Biomaterials*, Vol. 16, p. 25, 1995.

74. T. Furukawa, Y. Matsusue, T. Yasunaga, Y. Shikinami, M. Okuno, T. Nakamura, *Biomaterials,* Vol. 21, p 889, 2000.

75. S. Hasegawa, S. Ishii, J. Tamura, T. Furukawa, M. Neo, Y. Matsusue, Y. Shikinami, M. Okuno, T. Nakamura, *Biomaterials*, Vol. 27, p. 1327, 2006.

76. Y. Shikinami, M. Okuno, *Biomaterials*, Vol. 22, p. 3197, 2001.

77. Y. Shikinami, Y. Matsusue, T. Nakamura, *Biomaterials*, Vol. 26, p. 5542, 2005.

78. Z. Hong, P. Zhang, C. He, X. Qiu, A. Liu, L. Chen, *et al.*, *Biomaterials*, Vol. 26, p. 6296, 2005.

79. L.M. Mathieu, T.L. Mueller, P.-E. Bourban, D.P. Pioletti, R. Muller, J.-A.E. Manson. *Biomaterials*, Vol 27, p. 905, 2006.

80. J.-S. Son, S.-G. Kim, J.-S. Oh, M. Appleford, S. Oh, J.L. Ong, K.-B. Lee, *J. Biomed. Mater. Res. Part A,* Vol. 99A, p. 638, 2011.

81. H. Diao, Y. Si, A. Zhu, L.Ji , H. Shi, *Mater. Sci. Eng. C,* 32, p. 1796, 2012.

82. Z. Hong, X. Qiu, J. Sun, M. Deng, X. Chen, X. Jing, *Polymer,* Vol. 45, p. 6699, 2004.

83. X. Zheng, S. Zhou, X. Li, J. Weng, *Biomaterials*, Vol. 27, p. 4288–4295, 2006.

84. Q. Lv, L. Nair, C.T. Laurencin, *J. Biomed. Mater. Res.,* Vol. 91A, p. 679, 2009.

85. L.-C. Gerhardt, G.M. R. Jell, A.R. Boccaccini, *J. Mater. Sci.: Mater. Med.,* Vol. 18, p. 1287, 2007.

86. G. Ciapetti, L. Ambrosio, L. Savarino, D. Granchi, E. Cenni, N. Baldini, S. Pagani, *et al.*, *Biomaterials*, Vol. 24, p. 3815, 2003.

87. F. Causa, P.A. Netti, L. Ambrosio, G. Ciapetti, N. Baldini, S. Pagani, D. Martini, A. Giunti, *J. Biomed. Mater. Res.,* Vol. 76A, p. 151, 2006.

88. M.C. Azevedo, R.L. Reis, M.B. Claase, D.W. Grijpma, J. Feijem, *J. Mater. Sci. Mater. Med.,* Vol. 14, p. 103, 2003.

89. J.M. Middleton, A.J. Tipton, *Biomaterials*, Vol. 21, p. 2335, 2000.

90. O.G. Lewis, W. Fabisial, Sutures, in *Kirk-Othmer Encyclopedia of Chemical Technology,* 4th ed. Wiley, New York, 1997.

91. R.C. Thomson, M.J. Yaszemski, J.M. Powers, *et al.*, *J. Biomater. Sci. Polym. Ed.*, Vol. 7, p. 23, 1995.

92. R. Thomson, *Biomaterials*, Vol. 19, p. 1935, 1998.

93. J. Buczynska, E. Pamula, S. Blazewicz, *et al.*, *Eng. Biomater.,* Vol. 58–60, p. 85, 2006.

94. P. Rosol, J. Chlopek, K. Pielichowska, *et al.*, *Eng. Biomater.,* Vol. 47–53, p. 88, 2005.

95. J. Chlopek, A. Morawska-Chochol, P. Rosol, *Eng. Biomater.,* Vol. 58–60, p. 98, 2006.

96. S.J. Peter, L. Lu, D.J. Kim, *et al.*, *Biomaterials*, Vol. 21, p. 1207, 2000.

97. M. Rinaudo, *Prog. Polym. Sci.,* Vol. 31, p. 603, 2006.

98. E. Khor, L.Y. Lim, *Biomaterials*, Vol. 24, p. 2339, 2003.

99. I.Y. Kim, S.J. Seo, H.S. Moon, *et al.*, *Biotechn. Adv.,* Vol. 26, p. 1, 2008.

100. A. Di Martino, M. Sittinger, M.V. Risbud, *Biomaterials,* Vol. 26, p. 5983, 2005.

101. A.C.A. Wan, E. Khor, G.W. Hastings, *J. Biomed. Mater. Res.*, Vol. 38, p. 235, 1997.

102. A.C.A. Wan, E. Khor, G.W. Hastings, *J. Biomed. Mater. Res.*, Vol. 41, p. 541, 1998.
103. Z. Ge, S. Baguenard, L.Y. Lim, *et al.*, *Biomaterials*, Vol. 25, p. 1049, 2004.
104. I. Yamaguchi, K. Tokuchi, H. Fukuzaki, *et al.*, *J. Biomed. Mater. Res.,* Vol. 55, p.20, 2001.
105. F. Zhao, Y. Yin, W.W. Lu, *et al.*, *Biomaterials*, Vol. 23, p. 3227, 2002.
106. F. Zhao, W.L. Grayson, T. Ma, *et al.*, *Biomaterials*, Vol. 27, p. 1859, 2006.
107. H. Liu, H. Li, W. Cheng, *et al.*, *Acta Biomater.,* Vol. 2, p. 557, 2006.
108. L. Kong, Y. Gao, G. Lu, *et al.*, *Eur. Polym. J.,* Vol. 42, p. 3171, 2006.
109. R. Chandra, R. Rustgi, *Prog. Polym. Sci.,* Vol. 23, p. 1273, 1998.
110. A.P. Marques, R.L. Reis, J.A. Hunt, *Biomaterials*, Vol. 23, p. 1471, 2002.
111. Y.Z. Wan, Y. Huang, C.D. Yuan, *et al.*, *Mater. Sci. Eng. C*, Vol. 27, p. 855, 2007.
112. L.Y. Jiang, Y.B. Li, L. Zhang, *et al.*, *Mater. Sci. Eng. C*, Vol. 29, p.193, 2009.

Strategy for a Biomimetic Paradigm in Dental and Craniofacial Tissue Engineering

Mona K. Marei[1,*], Naglaa B. Nagy[2], Mona S. Saad[3], Samer H. Zaky[4], Rania M. Elbackly[5], Ahmad M. Eweida[6] and Mohamed A. Alkhodary[7]

[1]Professor, Department of Prosthodontics; head of Tissue Engineering Laboratories, Faculty of Dentistry, Alexandria University, Egypt

[2]Professor, Oral Biology Department, Faculty of Dentistry, Tanta University and Tissue Engineering Laboratories, Faculty of Dentistry, Alexandria University, Egypt

[3]Assistant lecturer, Department of Prosthodontics; researcher at the Tissue Engineering Laboratories, Faculty of Dentistry, Alexandria University, Egypt

[4]Postdoctoral associate, Center of Craniofacial Regeneration, McGowan Institute of Regenerative Medicine, University of Pittsburgh, USA; researcher at the Tissue Engineering Laboratories, Faculty of Dentistry, Alexandria University, Egypt

[5]Lecturer, Department of Conservative Dentistry; researcher at the Tissue Engineering Laboratories, Faculty of Dentistry, Alexandria University, Egypt

[6]Assistant lecturer, Faculty of Medicine, Department of Head and Neck and Endocrine Surgery; researcher at the Tissue Engineering Laboratories, Faculty of Dentistry, Alexandria University, Egypt

[7]Lecturer, Department of Prosthodontics; researcher at the Tissue Engineering Laboratories, Faculty of Dentistry, Alexandria University, Egypt

Abstract

Biomimetics deals with the realization of processes and construction, as well as the development of principles of nature in technological applications and devices, i.e., there is a transfer (of knowledge) from biology to technology. It is worth noting that identical copies from nature to technology are not feasible in biomimetics. Instead, biomimetics encompasses a creative conversion into technology that is often based

*Corresponding author: mona.marei@gmail.com

on various steps of abstractions and modifications, i.e., an independent successive construction that is a "new invention" rather than a blueprint of nature. It has been argued that we now need a new generation of 3D culture systems that would offer a middle ground between the bare bones approach of a standard petri dish and a live organism model, such as a rat, or mouse. The new strategy of tissue engineering and regenerative medicine at large, is to construct biomimetic matrices to mimic nature's hierarchical structural assemblages and mechanisms of simplicity and elegance that are conserved throughout genera and species.

The current generation of tissue engineering is a true integration of biology and engineering that makes it possible to design "biomimetic" environments that subject the cell to the combinations of factors known to guide tissue development and regeneration *in vivo*. The implications of this collaborative approach are likely to extend beyond the current goal of answering complex biological questions using new bioengineering tools, to the derivation of entirely new concepts that will shape future advances in regenerative medicine.

In this perspective chapter, we will focus on the development and use of biomimetic platforms that provide the interface between biological questions and engineering tools in the field of dental and craniofacial tissue engineering.

6.1   Introduction

Tissue engineering is an emerging multidisciplinary dynamic field in which the collective knowledge of medicine, biology, engineering, micro and nanotechnologies and understanding of the interactions of materials with the physiological environment are brought together and applied synergistically toward the design of new materials, devices, and techniques in regenerative medicine (Figure 6.1).

During the last couple of decades, great efforts have been directed toward creating systems that could resemble the native environment of tissues. In fact, important areas of tissue engineering have already taken advantage of such structures to understand the phenomena occurring at the interface of biomaterial-biological entities, applying the concepts into a tissue engineering strategy [1]. Hence, tissue engineering has evolved from being a tissue replacement strategy to one that aims to recapitulate developmental pathways to boost the body's own intrinsic healing capacity. As a result, a new generation of tissue engineering and regenerative medicine that integrates biology and engineering has emerged making it possible to design biomimetic environments that will guide tissue development and regeneration *in vivo*. An example of a biomimetic concept for bone regeneration is one where the trophic and immunomodulatory effects of mesenchymal stem cells MSCs, scaffolds resembling the natural extracellular matrix, and approaches to deliver multiple growth factors are combined in a delicate synchronized fashion which has changed our perception of the field today [2].
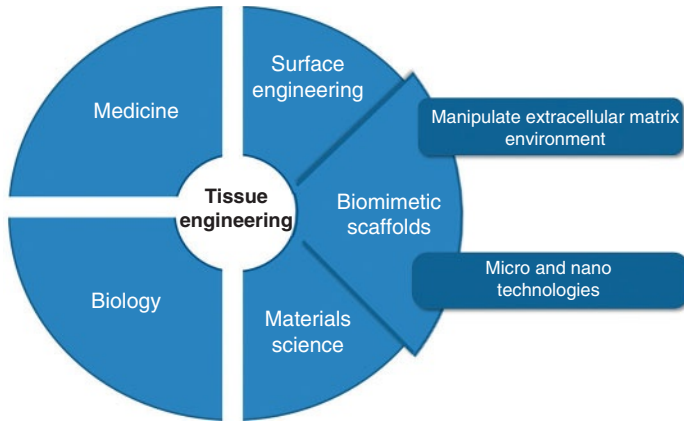
Figure 6.1 Schematic illustration of the different fields involved in the current tissue engineering strategy highlighting the inputs brought to biomimetics.

6.2 Biomimetics: Definition and Historical Background

6.2.1 Definition

Biomimetics is the field of scientific endeavor, which attempts to design systems and synthesize materials through biomimicry. Bio meaning life and mimesis meaning imitation are originally derived from Greek [3]. In the 1950s, Otto Schmitt coined the term "Biomimetics" for the transfer of ideas and analogues from biology to technology. He attempted to produce a physical device that explicitly mimicked the electrical action of a nerve. By 1957, he had come to perceive what he would later label biomimetics [4]. Then came the term bionics which was coined by Jack Steele of the US Air Force in 1960. He defined it as the science of systems which have some function copied from nature, or which represent characteristics of natural systems or their analogues [4].

In 1969, Schmitt used the word biomimetics in the title of a paper and the word made its first public appearance in Webster's Dictionary in 1974, accompanied by the following definition: The study of the formation, structure, or function of biologically produced substances and materials (as enzymes or silk) and biological mechanisms and processes (as protein synthesis or photosynthesis) especially for the purpose of synthesizing similar products by artificial mechanisms which mimic natural ones [5].

Recently, biomimetics has been defined as "A relatively young study embracing the practical use of mechanisms and functions of biological science in engineering, design, chemistry, electronics, and so on" [6]. In the

1970s, "biomimetic chemistry" came along aiming at molecular-level modeling of enzymes and biomembranes [6].

The emergence of biomimetic materials into tissue engineering came after sequential stages of material development. While "first generation" materials were intended to be bioinert, they were required to achieve a suitable combination of physical properties to match those of the replaced tissue with a minimal toxic response in the host [7, 8]. In "second generation" materials this concept evolved into one where materials were bioactive and resorbable and elicited a controlled reaction with physiological environment.

As characterization tools and techniques continued to advance, the understanding of how tissues work and form improved. Developments in the creation of engineered surfaces and bulk architecture of scaffold materials showed that the design of biomimetic materials is basic messages learnt from studies of cell behavior in the extracellular matrix. Indeed, "third generation" materials were produced to be an extension of the second generation but designed and tailored to stimulate specific cellular responses at the molecular level and to elicit specific interactions with cell surface receptors that direct cell differentiation, proliferation and extracellular matrix production and organization [9]. A key concept is that biomimetic materials can imitate the extracellular matrix chemically and structurally to stimulate tissue formation in a manner analogous to cell-cell communication.

6.2.2   Concept of Duplicating Nature

One important aspect of tissue engineering is the development of new biomaterials to facilitate cell–material interactions, which can be achieved by mimicking certain advantageous features of natural extracellular matrix (ECM) [10]. Since the concept of tissue engineering emerged two decades ago, scientific advances in biomaterials, biology, and medicine have created unique opportunities to fabricate tissues in the laboratory by combining scaffolds (artificial extracellular matrices), cells, and biologically active molecules. In an ideal situation, scaffolds would incorporate the functions of natural extracellular matrix (ECM), specifically, they would provide support for cell attachment and proliferation, deliver and retain biochemical factors, enable diffusion of nutrients for cells, and exert suitable mechanical and other stimuli for cell function. For these reasons, scaffolds should mimic the natural ECM in order to provide the optimal physiological environment for cells to guide tissue development and regeneration [11, 12].

6.2.3   Strategies to Achieve Biomimetic Engineering

Initial approaches aimed at improving the adhesiveness of biomaterial surfaces to increase the bioactivity of biomaterials by coating them with

ECM macromolecules, such as fibronectin, elastin, laminin, and collagens, or their integrin-binding epitopes including RGD. Recently, the development of nanotechnology has led to the construction of biomimetic surfaces with a defined nanopattern, eliciting tissue-specific cellular responses by stimulating integrin clustering so that they comply with the nanoscale features of the natural microenvironment of cells.

The goal is to provide environmental instructive cues and matrix conditions to stimulate and trigger proteins and cells in their recognition to biomaterials and to take subsequent biological actions. For these reasons the materials produced by such strategies are called "smart materials." In order to develop biomimetic scaffolds for tissue engineering, there are three important parameters [13, 14] (Figure 6.2):

a) Physical properties
b) Specific chemical signals from peptide epitopes contained in a wide variety of extracelluar matrix molecules
c) The hierarchal nanoscale topography of microenvironmental adhesive sites
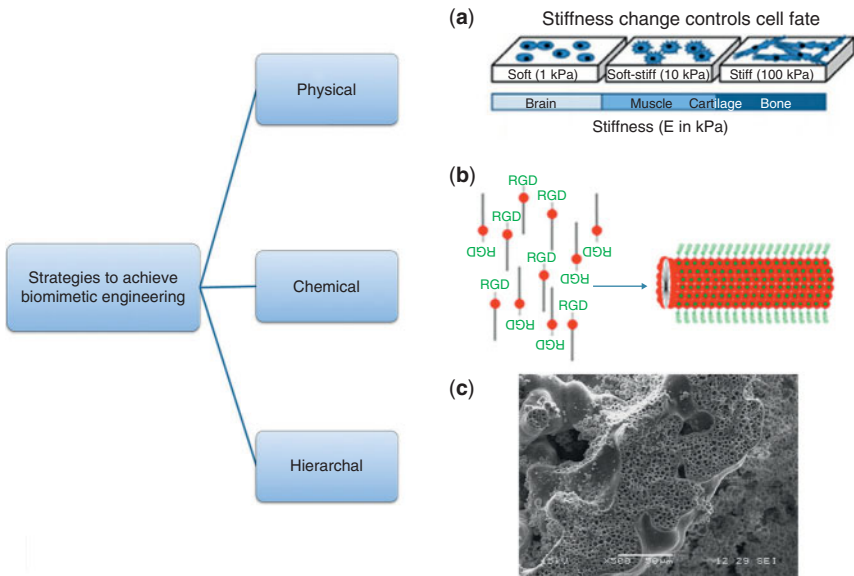

Figure 6.2 Schematic illustration of the different strategies to achieve biomimetic engineering traits that are mimetic to native tissue. This can be achieved by (a) physical mimicking of the stiffness of the native tissues, (b) chemical mimicking of cell-integrins-extracellular matrix activity through biomimetic surface tailoring with extracellular molecules, including RGD peptide, and (c) hierarchal mimicking of the architecture of the native tissues (ex:mesoporous bioactive glass). (a) and (b) reprinted with permission from [12].

6.2.3.1 Physical Properties

These refer to the elasticity, stiffness, and resilience of the cellular environment. Recently it has been shown that not only cell surface interactions, but also the resilience and local stiffness of biomaterials contributes significantly to cell behavior and cell differentiation [15, 16].

Depending on the physical stiffness of the biomaterial substrate, *in vitro* cellular responses are modulated. This is directly related to the term mechanotransduction, which can be defined as the process by which cells convert their mechanical stimuli into biochemical responses [13, 17]. Anchorage-dependent cells attach to the substrate through the transmembrane proteins (e.g., integrins). Shortly after this attachment, structural and signaling proteins are recruited at the intracellular space, forming a focal adhesion complex. Subsequently the harmonized action of the proteins provides a signal transduced through the actin–myosin complexes that are found in the cytoskeleton, which ultimately leads to a certain form and level of mechanical reaction of the cells [17]. While neural cells have generally been shown to favor a much softer substrate [18], with bone-associated cells, biomaterial substrates with stiffness over 100 kPa, which is close to the stiffness of natural bone, usually favorably dictate cellular responses, including initial cell adhesion and osteogenesis [13, 19, 20].

This concept of physical elasticity as a determinantof cellular behavior should be borne in mind when developing smart biomaterials for regenerative purposes and in the understanding of the cellular phenomena occurring on the biomaterials, aside from chemical or biochemical cues [13].

6.2.3.2 Specific Chemical Signals from Peptide Epitopes Contained in a Wide Variety of Extracelluar Matrix Molecules

Besides aiming to reproduce the ECM structure, biomimetics also aims to reproduce the ECM chemistry. Since an implant first contacts its host environment, proteins are the first biological entities to interact with the surface of the biomaterial [21, 22]. In fact, the surface of the material gets covered by a layer of proteins, just a few seconds after implantation in a competitive process. Proteins are the key elements creating a bridge between the non-biological surface of materials and cells [23]. Indeed, the proteic layer adsorbed onto the material's surface will interact with the cell receptors at the cell membrane surface [22]. Thus, the presence of specific molecules is mandatory for suitable attachment and proliferation of cells onto the surface of a given substrate [24].

A more elegant tailoring of the internal chemistry of biomaterials that further echoes native ECM organization and structure has become

possible by means of nanotechnology. An example of smart composite biomaterials are self-assembled biomaterials with cell-instructive cues. Self-assembly is the spontaneous formation of ordered structures which may be utilized for spatially orienting peptides with nanoscale precision [25]. Studies demonstrate that ECM-mimetic peptide constructs which reproduce the *in vivo* structure of their adhesive and modulatory domains on a nanoscale can greatly enhance the outcome for tissue engineering applications,in particular, self-assembled peptides have been utilized as biomaterials. The ECM contains within its structure certain molecules that are recognized by cells and that promote adhesion, proliferation, and differentiation. One example is the Arg-Gly-Asp (RGD) peptide, the most common epitope sequence well known for encouraging cell adhesion [26, 27]. Several studies have utilized self-assembled molecules incorporating the RGD sequence and have also nanopatterned RGD to enhance the osteogenic differentiation of cells *in vitro* [25].

Not only the nanostructure but also nanospacing between the self assembled molecules affects the cellular activity via mimicking the nanoscale spacings and orientations of cell binding sequences within ECM. For example: the full-length fibronectin (FN) molecule contains both an RGD adhesion site and a Pro–His–Ser–Arg–Asn (PHSRN) synergy site spaced approximately 3.2 nm apart from each other [28] (Figure 6.3) [29].

6.2.3.3   The Hierarchal Nanoscale Topography of Microenvironmental Adhesive Sites

Early scaffold design only incorporated macropores at the micron scale to allow tissue ingrowth, blood vessel formation, and nutrient delivery to the newly formed tissue [30–35]. Now, it is speculated that alloplastic
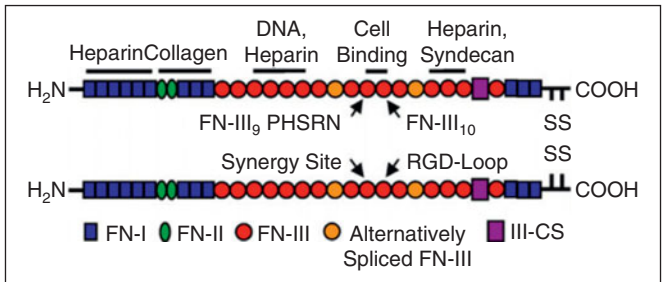

Figure 6.3 Structure of plasma fibronectin and location of major binding sites. Reprinted from [25].

nanosurfaces possess topographic elements truly scaled to naturally occurring substrates [28].

Nanoscale modification of material surfaces could contribute to the mimicry of cellular environments to favor the process of rapid bone accrual. Since the surface roughness of bone is approximately 32 nm, making it within the nanoscale range, current nanotechnology advances have granted great advantages in the field of dental implant treatment [36–39].

Nanotopography alters protein/surface interactions, which are believed to control osteoblast adhesion [40]. This is a critical aspect of the osseointegration process. Additionally, focal adhesion is affected by the nanotopography, especially nanopattern spacing. Cells are remarkable in their ability to sense nanostructure (Figure 6.4). Nanofeatures of a surface affect both cell adhesion and cell motility. It has been suggested that 70–100 nm features of an implant surface are scaled to function directly with the focal adhesion of cells [28].
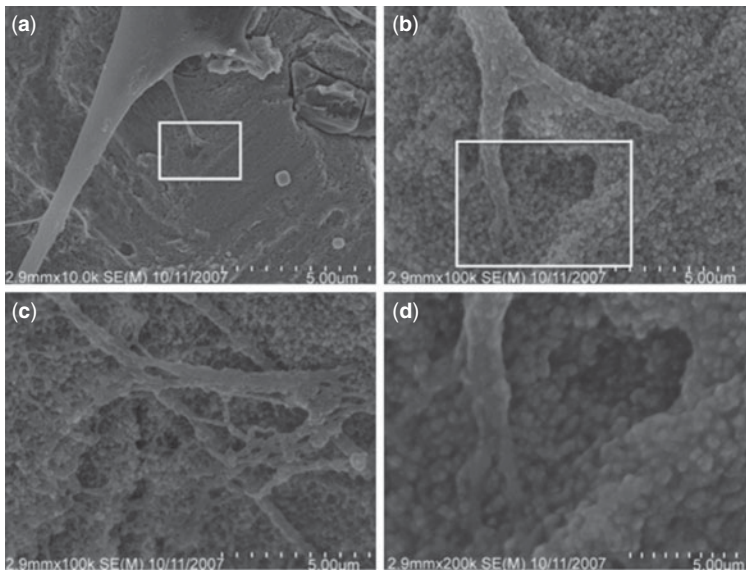

Figure 6.4 Nanoscale topography-cell interactions. There is apparent affinity of cells for nanoscale features. 20–40 nm are interactive points for lamellipodia of spreading cells. The cause and effect relationship is a current point of investigation. (a) 10,000_ image of adherent cell, (b) and (c) represent 100,000_ images of the same adherent cell and (d) 200,000_ magnification of the cell with nanofeatures. (b) Higher magnification of the rectangle in (a). (d) Higher magnification of the rectangle in (b). Reprinted with permission from [28].

6.3   Developmental Biology in Dental and Craniofacial Tissue Engineering: Biomimetics in Development and Growth (e.g. model of wound healing)

An understanding of the complex interfaces that exist between proteins, minerals, cells and their environment in biological systems is critically important in craniofacial development because reactions and interactions occurring at these interfaces govern their properties and functionalities. A new strategy of tissue engineering is to mimic the hierarchical structural assemblages and mechanisms of simplicity and elegance that are conserved throughout generations and species.

The craniofacial region is the most developmentally and anatomically sophisticated part in vertebrates. Its development and growth is a complex, strictly controlled continuous biological process that involves an interrelationship between its various components developmentally, structurally and functionally. It could be broadly divided into three overlapping stages. The first stage is the soft tissue stage during which the framework of the craniofacial region is formed. During the second stage, the chondrocranium together with the cartilaginous facial skeleton are formed, Meckel's cartilage in the lower jaw and nasal capsule in the naso-maxillary complex. The third stage (consolidation stage) is characterized by formation of skeletal and muscular elements.

The first stage of human craniofacial development begins at the end of the second week of prenatal life by formation of the prochordal plate in bilaminar embryonic disc. Formation of the prochordal plate establishes the antro-posterior axis of the embryo and determines the future position of the buccopharyngeal membrane. On the third week, primitive streak mesoderm or embryonic mesoderm emerges to form the trilaminar embryonic disc (Gastrulation). Later on that week, the neural plate, folds and forms a tube together with formation of a distinctive type of ecto-mesenchymal cells or the neural crest cells. Induction of neural crest cells requires contact mediated interactions between surface ectoderm and neuroepithelium [41]. Interestingly, BMP signaling seems to play a critical role in positioning the border of the neural plate as well as induction and migration of neural crest cells, since BMP4 and BMP7 could substitute for non-neural ectoderm in neural crest cell induction [42].

Concomitant with their induction along the dorsolateral edge of the neural plate, neural crest cells undergo complete or partial epithelial-mesenchymal transition that is marked by changes in cell adhesion and cytoarchitecture. This delamination of neural crest cells depends on regulated cadherin expression since overexpression of neuroepithelial cadherins prevents neural crest emigration [43]. Following delamination from

the neural tube, neural crest cells undergo well-orchestrated directed migration along specific pathways to their precise final destinations. The majority of cranial neural crest cells that are derived from the hindbrain migrate ventrolaterally from the neural tube in three distinct sub-ectodermal streams adjacent to the even-numbered rhombomeres (rhombomere-2, 4 & 6). In keeping with their craino-caudal axial origins, the three streams of neural crest cells precisely populate the first, second and third pharyngeal arches, respectively [44].

During migration, neural crest cells are exposed to a wide variety of signals controlling their polarity, directionality and possibly their commitment. Surprisingly, when the first arch (mandibular) neural crest cells were grafted posteriorly in place of second (hyoid) or third (visceral) arch, the transplanted neural crest cells formed duplicate first arch skeletal and muscular elements [45]. These observations led to the proposal of the neural crest pre-programming model [46]. Upon reaching their final destinations, neural crest cells proliferate and eventually differentiate into definite cell types, though multi-potent neural crest stem cells with high plasticity continue to exist and preferentially localize in a niche-like structure in various types of tissues [47].

When the human embryo is about 3.5 weeks old (3 mm CR stage) the primitive oro-nasal cavity is a narrow slit-like space lined by ectoderm, bounded above by the under surface of the brain capsule and below by the upper surface of the developing heart (Figure 6.5). This close approximation to the developing nervous and cardiovascular system ensures close integration and coordination.
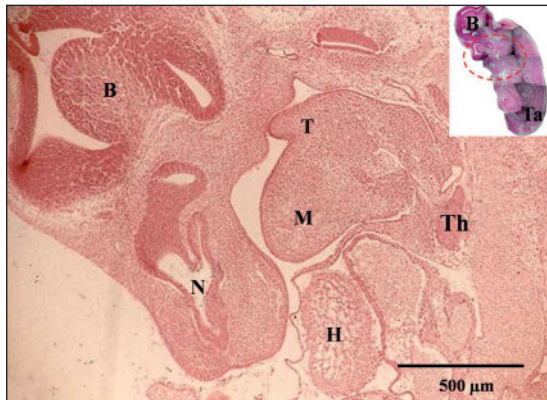

Figure 6.5 Histological para-sagittal section of developing mouse head 13 days pre-natal showing primitive stomatodeum between the developing brain above and the developing heart below. Inset shows the section of the entire embryo at lower magnification. (B), developing brain; (Ta) tail; (N), nasal cavity; (T), developing tongue (Th), thyroid; (H), developing heart; (M), mandibular arch.

Simultaneously, with neural crest cell migration, there is sequential appearance of 5–6 pharyngeal arches; each arch having its own nerve, blood supply and cartilaginous rod. The first arch, the mandibular arch forms the lower boundary of the developing stomatodeum together with giving rise to the maxillary process, from its upper and back part (Figure 6.6). The bilateral maxillary processes make the roof and the posterior partition between the oral and the nasal cavities through its septal and palatine processes, respectively. Derivatives of branchial arches also form an essential component in the craniofacial region. Branchial arches undergo bilateral symmetrical fusion in the midline to form the mandible, the lower lip and the tongue. This fusion which requires several different morphologic and molecular events, implies disappearance of the covering epithelium which could undergo migration, apoptosis and epithelial-mesenchymal transition [48]. Interestingly, molecular investigation revealed that p53 coordinates cranial neural crest cell growth, delamination and epithelial mesenchymal transition by affecting gene expression at discrete developmental stages, and that disruption of these processes could lead to craniofacial defects [49].

It is worth noting that appearance of the cartilaginous elements of the pharyngeal arches together with their differentiation marks the beginning of the second stage of craniofacial development (from about the 6th to 9th weeks prenatal). During this stage, the cartilaginous cranial base or the chondrocranium is formed. It provides the platform upon which the brain grows and around which the face grows. Interestingly, the anterior and posterior cranial bases, which grow independently, are derived from two distinct embryologic origins, the neural crest and paraxial mesoderm, respectively [50].

Meckel's cartilage develops within the mandibular arch and extends from the developing cranial base, in the region of the otic capsule, to the

Figure 6.6 SEM of developing mice head at the age of 13 days prenatal. The mandibular arch forms the lower boundary/floor of the developing oronasal cavity. 1, medial nasal process; 2, lateral nasal process; 3, maxillary process; 4, mandibular process; T, tail region; H, developing heart; arrow, stomatodeum.

middle line where it meets the cartilage of the opposite side [51]. Thus, beside its articulation with the vertebral column, it seems obvious that the chondrocranium is directly and indirectly attached to the maxillary and mandibular facial skeleton, respectively. Therefore, its growth could morphologically set up the structural foundation of many aspects of the craniofacial architecture [52].

Formation of the primary and secondary palates also takes place during this stage. The primary palate joins the secondary (lateral) palatine process, after their elevation. Then, the anterior part undergoes ossification, which extends from pre-maxillary, maxillary and palatine centers, to form the hard palate, whereas muscles develop posteriorly to form the soft palate. These developmental processes are strictly controlled by a complex genetic cascade that involves a number of critical developmental genes [53].

The third stage of craniofacial development seems to coincide with the beginning of human fetal life at the beginning of the 9th week. It is characterized by formation of osseous and muscular tissues. The skeleton of human skull consists of two parts; the viscerocranium, which forms the facial bones, and the neurocranium that lodges the brain and compromises membranous neurocranium that forms the vault of the skull and the cartilaginous neurocranium that forms the cranial base. The latter serves as a growth plate that undergoes endochondral bone ossification; in an orderly postro-anterior pattern [54]. It is only after skeletal muscle formation that secondary cartilage appears in the developing mandible. Interestingly, in relation to the condylar head of the ramus, the definitive tempromandibular joint (TMJ) replaces the primitive jaw joint that was initially developed between the incus and malleus [55]. Also, after formation of the basal parts of the maxilla and mandible, their alveolar processes begin their development in relation to the developing tooth germs.

Regarding tooth development, it is yet another highly coordinated and complex process. It relies upon cell-cell interactions that result in tooth initiation and morphogenesis, both of which are regulated by sequential and reciprocal interactions between the epithelium and the underlying neural crest derived mesenchyme [56]. These signaling pathways include the TGFß, BMP, Wnt, FGF, Hedgehog and Eda (Ectodysplasin, a TNF signal) which are used reiteratively during advancing tooth development [57].

It is noteworthy that the primary transient inductive role of epithelium was shown in mice recombination studies which confirmed that prior to the bud stage of development the potential to induce tooth morphogenesis resides in the epithelium. Only epithelium of the first branchial arch could instruct tooth formation when cultured with neural crest derived cells from second arch mesenchyme or with premigratory trunk neural crest [58]. After the bud stage, this instructive capacity for tooth formation

shifts from oral epithelium to the underlying mesenchyme which could instruct tooth development when combined with non-dental epithelium [59]. Interestingly, mesenchymal dental papilla maintains the capacity to regenerate differentiated dental tissues including dentin, cementum and periodontal ligament [60].

Morphologically, tooth formation starts by mapping the shape of the crown. Then, specialized cells of dentin and enamel begin secretion of their characteristic matrices, respectively. The size and shape of the crown are regulated by the enamel knots that adjust growth and determine the sites of epithelial folds which correspond directly to the cusp pattern of the mature tooth [61]. After crown formation, the Hertwig's epithelial sheath (HERS) maps the shape of the root. Then, secretions of radicular dentin and cementum matrices commence together with HERS fragmentation. This fenestrated network of epithelial cells known as epithelial cell rests of Malassez (ERM) is the only dental epithelium that remains after tooth eruption (Figure 6.7). Interestingly, ERM cells were isolated and induced to proliferate, thus offering a possible source for dental epithelium stem cell [62]. In addition, mesenchymal stem cells have been identified in dental pulp of human deciduous and permanent teeth as well as in the dental follicle [63–65] . These stem cells could be cultured *in vitro* and differentiated *in vivo* into odontoblasts, cementoblasts and periodontal ligament cells, though there is no evidence that they have the capacity to participate in tooth morphogenesis.

In conclusion, craniofacial development as well as tooth generation are induced by the appropriate cells that form tissue through their
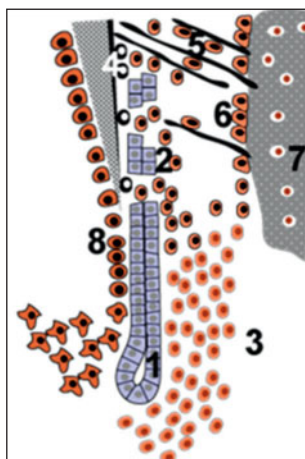

Figure 6.7 (1) The HERS, (2) epithelial rests of Malassez, (3) dental follicle, (4) cementoblasts, (5) periodontal ligament, (6) alveolar cells, (7) bone, and (8) odontoblasts.

proliferation and secretion of suitable matrix. The proliferated cells communicate and specialize to form different types of cells, each for specific function, using their secreted matrix to help in their function and communication. In wound healing, the body tries to mimic what happens during normal development. It attempts to replace the damaged tissues taking advantage of the temporary extracellular matrix consisting of fibrin–fibronectin meshwork which is formed during the first hemorrhagic phase. This matrix facilitates migration of different cell types that proliferate to regenerate or repair the defect. The initial inflammatory reaction helps in the healing process through its mediators which attract appropriate cells that perceive and correctly respond to the matrix signals.

6.4 The Paradigm Shift in Tissue Engineering: Biomimetic Approaches to Stimulate Endogenous Repair and Regeneration

6.4.1 Harnessing Endogenous Repair via Mesenchymal Stem Cells

Mesenchymal stem cells have long been defined by their self-renewal and multipotential differentiation properties. The growing consensus is that mesenchymal stem cells and pericytes sharing a panel of common markers are actually one and the same [66]. The present theory is that pericytes are released from broken or inflamed blood vessels at the site of tissue damage to become mesenchymal stem cells (MSC). The latter are then activated by the injury releasing a myriad of bioactive molecules which first modulate the immune response and then secrete trophic factors thereby creating a regenerative microenvironment [67].

In light of recent evidence from MSC therapy studies for cardiovascular disease it seems unlikely that they directly contribute to replenishing differentiated cell populations. Indeed, MSC engraftment in the heart has been shown to be quite low as is their transdifferentiation post-transplantation into cardiomyocytes [68]. This has led to the belief that the positive role of MSC is rather via immunomodulatory and remodeling effects. Bone marrow-derived MSC can secrete trophic factors that induce activation and proliferation of cardiac progenitor cells thus mediating cardiovascular regeneration. This will probably lead to next generation MSC-based therapeutics that exploit the MSC secretome. Analysis of the *in vitro* secreting profile of MSC has since shown that they secrete a variety of cytokines that are anti-apoptotic, immunosuppressive, proliferation enhancing, and angiogenesis modulating [69].

Bone marrow derived stromal cells (BMC) have also been shown to stimulate arteriogenesis through paracrine mechanisms [70]. Evidence shows

that BMC do not promote vascular growth by incorporating into vessel walls but rather by acting as cytokine factories. The injected cells could not be co-localized with endothelial or smooth muscle cell markers but strongly accumulated around growing collateral arteries and expressed several growth factors and cytokines. Indeed, MSC subjected to hypoxia show increased expression of a panel of genes encoding cytokines related to arteriogenesis such as VEGF-, MCP-1, bFGF, IL-6, PLGF, etc.

Thus the MSC secretome is a combination of growth factors, cytokines and chemokines that is further modulated by physiological, pharmacological, cytokine or growth factor pre-conditioning and /or genetic manipulation. Taking advantage of the MSC secretome provides an approach to mimic their effects *in vivo* in the injury microenvironment. If a cell-free therapy based on the use of the MSC secretome is to be devised, a clear understanding of how the lesion microenvironment can affect secretome profile is a must [68]. Adult stem cells respond to specific cues by their surroundings thus producing different factors to respond to the dynamic microenvironment of the lesion [71]. It is also important to note that different progenitor and stem cell sub-populations have different proteomic profiles and so secrete different factors. It has been established that serum-deprived MSC are highly angiogenic. They up-regulate the secretion of prosurvival and angiogenic factors in their conditioned media such as IGF-1, VEGF-A, angiopoietins, and HGF in addition to IL-6, IL-8, and CXCL1 [68]. These act both in an autocrine and paracrine fashion [72].

Hypoxia has also been shown to affect angiogenic and osteogenic properties of MSC. MSC subjected to temporary hypoxia (48 hrs) expressed more bFGF, VEGF, IL-8, and osteopontin [73] while showing less effective osteogenic differentiation. This behavior is of utmost clinical relevance since physiological oxygen tension falls to 1% in the fracture hematoma. This creates an initial hostile environment for implanted MSC-seeded tissue engineering constructs. MSC appear to react to this environment by secreting more angiogenic factors and modulating angiogenic processes to promote vascular invasion of the constructs. The increased secretion of osteopontin may point to their enhancing macrophage infiltration which also interacts with bone formation.

Being a dynamic organ itself, bone is constantly subjected to remodeling. Osteoblasts are derived from MSC and during osteogenesis the secretory profile of MSC largely changes [74]. It has also been shown that mouse BMSC implanted in ceramic scaffolds into syngenic mice gave rise to bone of host origin [75, 76]. It was proposed that the exogenous BMSC release numerous factors in the immediate implant vicinity thus creating a likable microenvironment to support recruitment of host cells. This fact combined with newly formed vascular networks can facilitate the cellular cross-talk between the implant milieu and the host circulation system facilitating the recruitment process. Future bone regeneration studies

should aim at harnessing the full potential of implanted MSC to enhance their *in situ* survival not only to improve their engraftment and transdifferentiation, but rather to enhance their autocrine and paracrine effects to trigger host endogenous regeneration cascades [67] (Figure 6.8).

Using state-of-the-art bioengineered materials will allow enhanced control of cells and presentation of the MSC secretome after transplantation. MSC can be primed to modify their secretome by internalizing 1–2 micron-sized biodegradable particles containing differentiation particles [77]. Enhancing MSC homing to the injury site to enhance their autocrine and paracrine effects has also been approached by engineering the surface of MSC using adhesion ligands to enhance cell rolling which is a crucial step in cell homing [78]. Furthermore, delivering the cytokines on their own by a controlled release device may partially mimic cellular effects or alternatively enhance endogenous cell ability to respond to injury signals and direct tissue repair in the absence of transplanted cells [71].

6.4.2 Inflammation, Angiogenesis and Tissue Repair

It is the injury microenvironment that dictates how the healing process will proceed. Particularly the inflammatory phase of the wound healing cascade that further modulates angiogenesis and tissue formation and that unduly affects the performance of transplanted MSC.
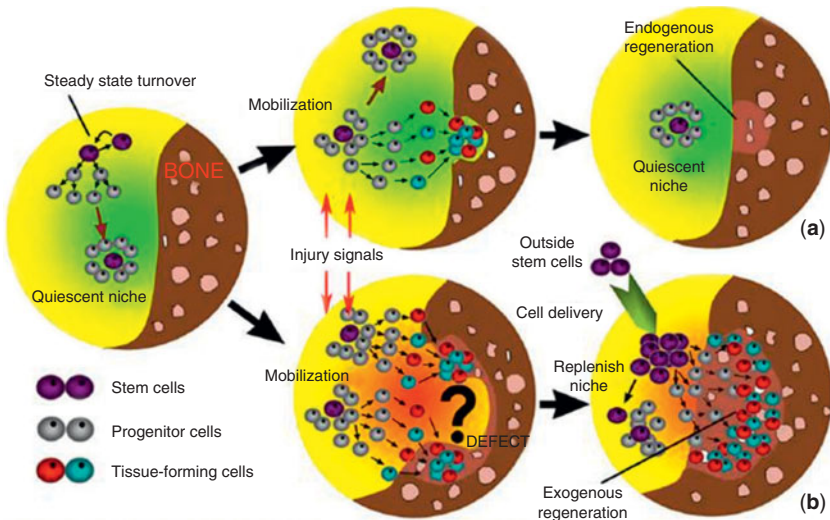

Figure 6.8 Schematic illustration of tissue regeneration via (a) endogenous regenerative approaches, and (b) exogenous cell delivery technologies. Reprinted with permission from [2].

Recently, mechanisms of vascular remodeling of tissue engineered vascular grafts have shown it to be a process largely dependent on an inflammatory response to the implanted construct [79]. Although seeded bone-marrow-derived cells were no longer found 1 week after implantation, they were found to secrete high levels of MCP-1 which is a potent monocyte chemokine resulting in a strong recruitment of monocytes to the tissue engineered graft. The recruited host monocytes in turn secreted cytokines, growth factors, and proteases necessary to trigger migration/proliferation of endothelial cells which eventually led to remodeling of the graft. Therefore, inflammatory responses to implanted materials may not necessarily be detrimental and together with the paracrine effects of implanted cells may cooperate to bring about vascular remodeling.

Some authors suggest that local inflammation initiates bone regeneration by stimulating the migration of MSC, fibroblasts, endothelial and immune cells, such as macrophages, that drive the formation of the soft callus during fracture repair [80]. The earliest phase of fracture healing is in fact characterized by local tissue hypoxia and an inflammatory response. Hypoxia and hypoxia inducible factor (HIF) reestablish the disturbed oxygen supply by promoting angiogenesis via increased secretion of VEGF, IL-6, and IL-8. IL-6 and -8 are strong pro-inflammatory factors that are up-regulated during hypoxia and increase the migration of leukocytes [80].

Moreover, a common feature in both normal bone remodeling and fracture repair is the requirement for vascularization. During fracture repair this is tightly linked to the inflammatory phase of healing. Inflammatory cytokines such as IL-1β have been shown to potentiate endothelial cell responses increasing their proliferation and augmenting their ability to form tube-like structures *in vitro* [81]. Transplanted MSC also appear to react to the inflammatory environment by secreting MCP-1 and GCP-2 which then lead to increased VEGF presence at the site of injury [82]. Manipulating the local inflammatory environment by providing the right signals may stimulate endogenous repair responses. Insight from stem cell-based bone repair studies have shown the limited contribution of the cells to newly formed bone, and confirm the evolving hypothesis that they may act principally through secreted trophic factors which are mostly proangiogenic. When further coupled with the local inflammatory environment they can lead to vascular ingrowth and host progenitor cell recruitment [83].

6.4.3   Biomimetic Model of Nature's Response to Injury?

Concurrent with this new concept is another old idea being revisited; that of circulating progenitor cells which can be mobilized in response to injury and contribute to the healing process. It has been shown that fracture may

induce mobilization of endothelial progenitor cells from the bone marrow to peripheral blood and that these cells themselves can promote both neovascularization and osteogenesis in damaged bone tissue [84]. Peripheral blood of fracture patients showed an increase in the number of circulating CD133+ and CD34+ cells 48 hrs after fracture indicating their possible role in initiating the healing process. Circulating osteoprogenitor cells have also been identified in fracture calluses of mice. These cells may home to sites of injury by virtue of the inflammatory milieu containing high levels of chemoattractants such as SDF-1 and BMPs. Activation of the SDF-1/CXCR4 axis by hypoxia, angiogenic peptides, and inflammatory cytokines may play a significant role. It has been speculated that owing to the intimate relationship between vasculature and bone, these circulating cells indeed find their way to the injury site via blood vessels [85].

However, it is important to note that although it appears that circulating osteogenic cells are major contributors to bone formation, late stage osteoblastic cells and osteocytes expressing collagen type I and osteocalcin do not circulate. It appears that the primary role of these cells is not bone forming but that the latter is an adaptive response to injury or abnormal cytokine signaling [85]. Levels of circulating cells fall to normal within a few days after fracture or BMP-2 implantation, meaning that their response is transient provoked by the injury and the inflammatory nature of that site [86, 87]. The presence of these circulating osteogenic cells holds great clinical promise. Strategies could be developed to enhance the migration of these cells thereby promoting natural endogenous repair mechanisms. By increasing their mobilization they could be easily isolated from peripheral blood and utilized for cell-based therapies.

6.5 Extracellular Matrix Nano-Biomimetics for Craniofacial Tissue Engineering

Within the paradigm of tissue regeneration, knowledge has lately unfolded about a whole new world of dwarfs, or *nanos*, where the actual molecular events that orchestrate cellular behavior, function and fate take place. In the frame of the progressively acquired knowledge, nanotechnology is being applied for tissue regeneration by deliberately fine tuning molecular particles in a microenvironment where the cells, the regeneration key players, would recognize and "feel" their native home to attach, migrate, proliferate, differentiate and secrete tissue-specific matrix.

Although no less challenging from any other application, nanotechnology is of particular relevance in the regeneration of the craniofacial complex. Craniofacial tissues harbor highly specialized and functional structures residing within a small volume demanding minimally invasive interventions for aesthetic considerations. As for the uniqueness of the

craniofacial area, nanotechnology has to deal with the specific require-ments of mechanical strength of the structures bearing the occlusal stress and strain—mostly provided by the large muscles of mastication [88, 89], the high vascularization need and the regeneration against microbial assault in the oral cavity [90].

For regeneration of craniofacial structures, the advancing tissue engi-neering approach, mainly employing a substrate or scaffold, cells and growth factor delivery [1], has already accomplished tremendous strides, yet with some confronting hurdles toward the clinical translation [91–93]. The insufficiency of harvested cells, their immunogenicity in allogenic set-ting and their *ex-vivo* manipulation are high on the list of challenges [93]. For a tissue-specific scaffold, the controlled resorption rate, the desirable mechanical properties, the constant growth factors availability, the steady mass transfer into the core and the hierarchical vascular growth are chal-lenges nanotechnology aims high to deal with [90, 94].

6.5.1   Nanotechnology for Biomimetic Substrates

A pivotal aspect of a scaffold to support cellular components, is how far do the latter recognize their substrate to accomplish a certain desired function. As a biomimetic approach, nanotechnology is directed to con-trol the cellular microenvironment by tailoring biomaterials' architecture and properties to emulate the complexity and functionality of extracel-lular matrix (ECM), a substrate that cells would acknowledge as native (Figure 6.9).

ECM is a nanoarchitecture of interweaving hierarchically organized nanofibers (10 to several 100s of nanometers) that store, activate and release a wide range of biological factors together with providing cell support and directing cell behavior through cell-cell and cell-soluble fac-tor interactions [95, 96]. Prevalent views support that, nanoscopically, surface topography has a more profound effect on single cell adhesion, morphogenesis, migration, alignment and differentiation than pore size and geometry microscopically [97–100]. In analogy to a fluid reversing the law of gravity on a capillarity level, these biomaterials exhibit unique surface properties on the nanoscale. Compared to conventional micron-structured materials, nanotopographic materials have higher surface area that increases their surface energy and wettability generating anisotropic stresses and affecting the cell-surface/protein interface [101–103].

6.5.2   From Macro to Nano: Dentin-Pulp Organ Perspective

Extracellular matrix provides key physical (topographical and bio-chemical) information transmitted to the cell that can recognize, feel, or
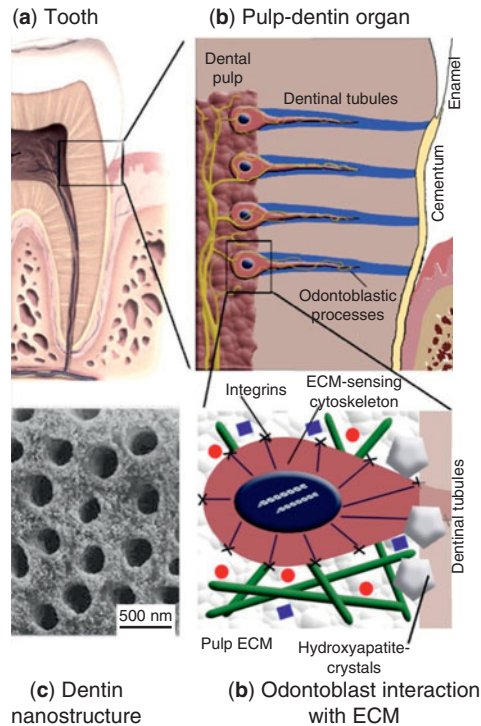
(a) Tooth **(b)** Pulp-dentin organ

Dental pulp

Dentinal tubules

Enamel

Cementum

Odontoblastic processes

Integrins

ECM-sensing cytoskeleton

Dentinal tubules

Pulp ECM

Hydroxyapatite-crystals

500 nm

(c) Dentin nanostructure

(b) Odontoblast interaction with ECM

Figure 6.9 Macro-nano structure: Dentin/pulp organ. (a) Illustration of tooth at organ level (macro level). (b) Odontoblast cell position in the pulp/dentin (micro level). (c) Enlarged illustration of the odontoblast interaction with pulpal non-mineralized and mineralized extracellular matrix (nano level). (d) Dentin micro/nano structure may help in the reconstruction of pulp-dentin organ scaffold.

"Braille-read" its bed through the environment-sensing cytoskeleton and integrin receptors (Figure 6.9). The information carried from ECM by actin-myosin forces propagates to the cytoskeleton-caged nucleus initiating intracellular signaling cascades that ultimately alters genes expression to direct the cellular tissue-specific spatiotemporal behavior (adhesion, contraction, migration, proliferation, differentiation, self-renewal and apoptosis) [104]. Macroscopically, dentin is a calcified tissue forming the stress-bearing body of the tooth and bearing odontoblastic processes. However the properties and mechanics of the environment around the odontoblast cell might be very different from the macroscopic properties of the tissue they weave. An odontoblast in contact with the dental pulp soft matrix and the dentin hard surface provides an example of a hierarchically structured microenvironment where mechanically and biologically different matrices impact the cellular behavior.

Recent advances in nanotechnology have enabled the design and fabrication of nanoscale ECM-analog materials [105, 106]. To maintain tissue-specific architecture and function, the ECMs of various tissues in the craniofacial complex differ in their chemical composition and spatial organization of the collagens, elastins, proteoglycans and adhesion molecules, and in their mechano-physical properties that engage micro-environmental sensing or mechanotransduction of the cells. Mechanotransduction is the regulation of cellular function by environmental mechanical cues. Mechanical stress and strain *in vivo* are the key regulatory mechanical cues that guide cell morphogenesis and affect the healthy maintenance of tissues [107]. To design tissue-specific scaffolds, the recapitulation of the surface chemical and mechanical properties on the nanoscale is a crucial factor that functional tissue engineering cannot afford to overlook.

6.5.3   Nanotechnology for Engineering Craniofacial Mineralized Collagenous Structures

Bone is a complex structure of mineralized collagen fibrils forming the basic building blocks of mineralized hard tissues. The regulation of the intrafibrillar mineralization process takes place through interactions between the collagen matrix, the noncollagenous extracellular proteins and the hard inorganic components composed of nanocrystalline hydroxyapatite (HA) (20–80nm long and 2–5nm thick) [108]. During bone regeneration, the HA serves as a chelating agent for mineralization of osteoblasts while the collagen provides mechanical support, promoting adhesion and proliferation [94]. It is such a peculiar structure that, when mirrored on the nanolevel, would achieve the desirable osteoconductivity and mechanical properties that ought to characterize a bone engineering scaffold.

At present, nanotechnology has been fine-tuning the emulation of the collagenous organic and/or the HA mineral phases of bone to achieve the osteoconductivity and mechanical properties [109, 110]. The synthesis of scaffolds with a pattern of highly mineralized collagen fibrils identical to those of natural bone, with nanoapatite crystallites preferentially aligned along the collagen fibril axes, have already demonstrated a boost in bone regeneration [109]. The HA nanoparticles incorporated within a bone engineering scaffold have demonstrated enhancement in compressive mechanical properties and stiffness as well as improvement of the *in vitro* bioactivity of the construct [111], while the apatite nanostructure on the surface of HA particles can be designed as a biomimetic surface to promote osteogenic differentiation [112].

To deal with the limitations of calcium phosphate and polymeric scaffolds, nanoparticles-based bone TE technologies have been introduced. For instance, the introduction of nanoparticle-composite scaffolds demonstrated increase in mechanical strength for bone grafts, the development

of novel delivery and targeting systems of genetic material encoding osteogenic growth factors, and the fabrication of nanofibrous scaffolds to support cell growth and differentiation through morphologically-favored architectures [113]. Polymeric nanofiber matrices have been explored to be biologically similar to the native bone extracellular matrix architecture and, when incorporated onto biodegradable microscopically porous polymeric 3D scaffolds, have the potential to be used as bone biomimetic regeneration substrates. Their nanoscale topography enhances cellular adhesion and MSCs stimulation to produce bone mineral, while the scaffold's open geometry and porosity promotes cell penetration and nutrient transport [114].

Carbon nanotubes have recently attracted attention in bone regeneration materials due to their excellent mechanical strength, their promotion to cell attachment and proliferation and their pro-osteogenic properties showing support to osteoblastic growth and modulation of the osteoblastic phenotype. Besides, they can be readily incorporated as reinforcing agents into the 3D architectures of a polymeric scaffold [115–117] that would not otherwise perform as efficiently [118].

On the other hand, nanoscale strategies are being developed to include in the scaffold functional motif sequences of complex biomimetic materials or short peptides that promote cellular adherence and osteogenic differentiation and maturation [119–121]. Modifications of polymer surface with BMP-related peptide [122, 123], full length BMP [124] or osteocalcin crosslinked to nano-HA [125, 126] have been employed to mimic extracellular matrix signaling and have been shown to enhance osteoblastic cell attachment and bone matrix synthesis. As compared to conventional polymers, the adsorption and conformation of proteins that regulate osteoblasts adhesion and functions (such as fibronectin and vitronectin) were enhanced on nanophase surfaces [127]. Regarding a yet limited application for dental tissue, scaffold coating with RGD integrins recognition sequence resulted in more mineralized osteodentin-like tissue [128]. Being similarly mineralized collagenous tissues, such nanoengineering approaches could be applied for dentin and cementum, however, potential avenues and directions have yet to be fully exploited [110].

In conclusion, nanoscale technologies offer compelling benefits in terms of controlling scaffold architecture, biomechanics, growth factor delivery, vascularity, cellular spatial orientation and temporal signaling.

6.6 Biomimetic Surfaces, Implications for Dental and Craniofacial Regeneration; Biomaterial as Instructive Microenvironments

When a surface of an implant material comes in contact with biological systems, initial events are dominated by protein adsorption, blood

platelets, and inflammatory cell adhesion. These events constitute what is regarded as the native response to the material and do not represent the optimal behavior between a material and host tissue. The goal of several current strategies is to provide enhanced osseous stability through nano- and/or micro-surface mediated events acting as instructive micro- and nanoenvironments that can improve the quality of the tissues regenerated at the scaffold tissue interface. These strategies can be divided into those that attempt to enhance the integration of new bone through changes in surface topography, and strategies to use the implant as a vehicle for local delivery of a bioactive coating that may achieve osteoinduction of new bone differentiation along the bone/implant interface [129, 130].

Commercially pure titanium grade 4 and its alloys in the form of the currently used titanium-aluminum-vanadium, or the future promising titanium tin tantlum are used for the manufacturing of dental implants to restore lost teeth and in the form of parts of the cranium to restore bone lost as a result of tumor or trauma. Cranial implants can be custom made using the titanium casting machines, ready made in the form of plates and screws, and recently, precisely custom made using rapid prototyping technology.

6.6.1   Biology of Osseointegration

Bone healing around implants is normally an inflammatory reaction elicited by the surgical trauma and modified by the presence of the implant. Various cell types, growth factors and cytokines are involved; a hematoma is formed at the bone-implant interface and may play a role as a scaffold for peri-implant bone healing.

The blood cells entrapped at the implant interface are activated and release cytokines and other soluble, growth and differentiation factors. The formed fibrin matrix acts as a scaffold (osteoconduction) for the migration of osteogenic cells and eventual differentiation (osteoinduction) of these cells in the healing compartment. Osteoblasts and mesenchymal cells seem to migrate and attach to the implant surface from day one after implantation, depositing bone-related proteins and creating a noncollagenous matrix layer on the implant surface that regulates cell adhesion and binding of minerals. This matrix is a calcified afibrillar layer on the implant surface, involving poorly mineralized osteoid similar to the bone cement line that is rich in calcium, phosphorus, osteopontin and bone sialoprotein.

A few days after implantation, osteoblasts in direct contact with the implant surface begin to deposit collagen matrix directly on the early formed cement line on the implant surface. Being completely enveloped by the mineralizing front of calcifying matrix; osteoblasts became clustered as osteocytes in bone lacunae. The early deposition of newly

calcified matrix on the implant surface is followed by the arrangement of the woven bone and bone trabeculae. This suggested that the implant surface is positively recognizable from the osteogenic cells as a biomimetic scaffold which may favor early peri-implant osteogenesis [129–135].

6.6.2 Implant Surface Modification: Laser Micromachining and Biomimetic Coating

The surface of an implantable material may be modified so that the biology of the surface is better served to interact with the surrounding environment (Figure 6.10). This is generally done by laser micro-machining and micro-texturing and the feature size is on the order of a cell diameter (10μm). Cells interact with grooves or micro-textured patterns at the micron-scale (Figure 6.11). At the sub-micron scale, the interactions between cell constituents and the underlying substructure result in biochemical adhesion, while at the nanoscale, the biochemical interactions between protein molecules and synthetic surfaces promote the self organization of protein molecules and cell attachment [136]. Indeed, *in vitro* experimental studies [137, 138] have demonstrated that well-developed filopodia directly entered nanometer-sized pores for the initial attachment of osteoblastic cells.

Biomimetic coatings created by the precipitation of calcium phosphate apatite crystals onto the titanium surface from simulated body fluids (SBF) have been shown to be more soluble in physiological fluids and
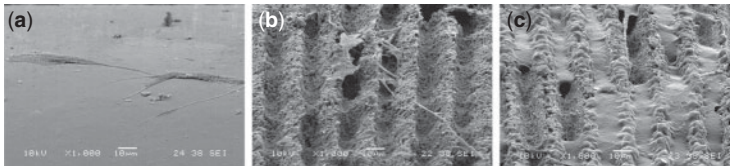

| Control | Laser grooved | Laser/RGD |
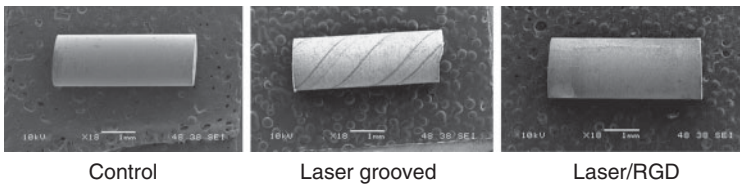
Figure 6.10 SEM of titanium surface.

Bone marrow mesenchymal stem cell culture, 1 day

Figure 6.11 Surface laser microgrooves as instructive topography affecting cellular orientation. (a) Flat surface encourages random cell orientations. (b,c) Micro-grooves help align the cells through a process called *contact guidance*.

resorbable by osteoclastic cells like dentin materials thus avoiding draw-backs of plasma-sprayed HA coatings [139–148].

The surface of titanium dental implants may be coated with bone-stimulating agents such as growth factor members of the transforming growth factor (TGF) family, in particular bone morphogenetic proteins (BMPs), platelet-derived growth factor (PDGF) and insulin-like growth factors (IGF-1 and 2) [149–154]. Other candidates are molecules controlling the bone remodeling process such as antiresorptive drugs, e.g., biphos-phonates [155–158]. Chemical treatment of titanium dental implants with fluoride is yet another approach to enhance osseointegration [159–161].

A more sophisticated approach mentioned above involves coating the implant with RGD (arginine-glycine-aspartic acid). RGD is a cell adhesion receptor molecule that interacts with membrane-bound talin and vinculin proteins to promote the cellular surface adhesion process. In other words, RGD's role is to accelerate the process of tissue binding to the implant surface. This has been empirically demonstrated, with up to a two-fold increase in cellular adhesion strength after 12 hours of cell culture time [162, 163].

6.7 Angiogenesis, Vasculogenesis, and Inosculation for Life-Sustained Regenerative Therapy; The Platform for Biomimicry in Dental and Craniofacial Tissue Engineering

One of the most particular features of any normally functioning tissue is its ability to interact with the surrounding tissues to ensure homeostasis. Active incorporation within the vascular network of the organism would help this interaction take place effectively. Adequate vascularization of any tissue, or tissue construct, is then a prerequisite for its sustainability and integration or simply for its "biomimicry." On the other hand, cre-ating such a vascularized tissue, or tissue construct, will have to follow some bio-inspired strategies mimicking the physiological healing and vas-cularization processes.

6.7.1 Vascularization to Reach Biomimicry; A Prerequisite for Life Sustained Regeneration

To engineer a three dimensional (3D) tissue construct suitable for trans-plantation, a vascular supply to the developing tissue is necessary for survival. Simple diffusion normally limits oxygen and nutrition supply to cells to a maximum range of 200 μm into a given matrix [164], so sub-optimal initial vascularization after grafting will definitely limit survival

of cells in the center of large, cell-loaded constructs. While issues of vascularization are of utmost importance for critical-size defect regeneration all over the body, some features are particularly important for craniofacial defects [165].

Within the craniofacial bones, the vascular supply is more consistent with that of the cancellous bone where the blood, in contrast to compact bone, reaches its anatomical destinations more directly without significant branching. It is to be noted that most of the mid-facial bones are covered by mucosa over large areas of their surfaces. Thus, every part of these bones retains its periosteal blood supply. The blood supply of the mandible, however, is a mixture of that of the compact and cancellous bones and is therefore more susceptible to compromise [166, 167]. Although the craniofacial region has this abundant blood supply, it is commonly compromised after treatment with radiotherapy following cancer surgery [165].

Bone regeneration is principally a part of the fracture healing process. The majority of fractures heal well under standard conservative or surgical therapy. However, extended bone defects following trauma or cancer resection require more sophisticated treatment, as spontaneous bone healing is unexpected. In a similar way, bone regeneration at the central region of large constructs usually fails due to the absence of adequate vascularization [164]. Although blood vessel ingrowth is often noted in implanted tissue constructs over time, the vascularization is too slow or too limited to provide adequate nutrient and oxygen transport to the transplanted cells [168].

6.7.2   Patterns of Construct Vascularization

Neovascularization of grafted tissues or constructs occurs either by sprouting of microvessels from pre-existing vasculature, a process termed angiogenesis [169], or by *in situ* capillary plexus formation from endothelial precursor cells (EPCs), a process termed vasculogenesis [170] (Figure 6.12). A third pattern, namely "inosculation" refers to the development of direct connections between the already existing capillaries of a tissue graft or construct and angiogenic recipient-site vasculature [171] (Figure 6.12).

6.7.2.1   Angiogenesis

The predominant mechanism of microvascular formation is that of angiogenesis through migration, proliferation, and cooption of the existing endothelium [172]. Sprouting angiogenesis commences mainly with proteolytic degradation of the basement membrane around endothelial cells (ECs) of a pre-existing capillary or venule [173].
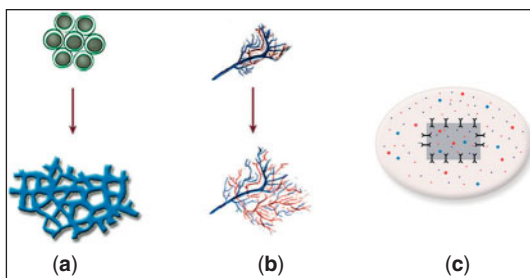
Figure 6.12 Patterns of vascularization. (a) Capillary plexus formation from endothelial precursor cells (vasculogenesis), (b) sprouting of microvessels from pre-existing vasculature (angiogenesis), (c) direct connections between the already existing capillaries of a tissue construct and angiogenic recipient-site vasculature (inosculation).

The majority of currently applied approaches for construct vascularization rely on the so-called *extrinsic mode of angiogenesis* of constructs. In this case the neovascular bed invades the scaffold from the periphery [174]. Although extrinsic vascularization techniques have been relatively successful, there is a delay in recipient blood vessel growth into the scaffold, resulting in limited blood perfusion and oxygen supply to implanted tissues. Thus, the method is suitable for tissue thicknesses of just 2 to 3 mm and unsuitable for vascularization of thick constructs [175].

An intrinsic mode of angiogenesis, however, is based on a concept that a definite artery or vein can serve as a source of new blood vessels for prefabrication of tissue for transplantation. Prefabrication is a technique of re-vascularization of a tissue graft by implanting an arterio-venous loop (AVL) or a vascular pedicle underneath or within a tissue graft, resulting in spontaneous angiogenic development from the loop or pedicle and subsequent revascularization of the tissue graft [176]. This technique was recently introduced for craniofacial regeneration in animal models [177, 178].

6.7.2.2 *Vasculogenesis*

A network of newly developed microvessels may be engineered *in vitro* by seeding scaffolds with endothelial cells [179]. After implantation of those tissue constructs, the endothelial cells should develop interconnections to the blood vessels of the surrounding tissue, resulting in an adequate perfusion of the prefabricated microvascular network in a couple of days.

However, there are a considerable number of unsolved problems to upgrade this approach to a clinical level. Although different seeding methods for 3D polymeric scaffolds have been established, it is unclear whether they can guarantee a homogeneous distribution of endothelial

cells throughout a large tissue construct. Moreover, the seeding of a scaffold with endothelial cells does not necessarily result in the development of new blood vessels *in vitro*, because this process depends on the coordinated release of a variety of signaling factors such as vascular endothelial growth factor (VEGF) and platelet-derived growth factor (PDGF) and involves other cell types, including smooth muscle cells and pericytes, which are normally found under *in vivo* conditions but not necessarily *in vitro* [180]. Recent biomimetic technologies have improved cell culture and seeding techniques for the development of tissue constructs, which bear their own intrinsic vascular system before implantation and engraftment.

6.7.2.3   Inosculation

Inosculation is characterized by a coordinated interaction between the implanted preformed microvascular network and the microvasculature of the host site. It was previously suggested that the vessels within skin grafts merely provide a conduit for ingrowing wound bed vessels, what is known as "internal inosculation," where the host vasculature is playing the active role and inosculation takes place inside the prevascularized graft [181].

In contrast to this mechanism of internal inosculation, recent studies provide evidence that the preformed microvascular network actively contributes to the process of graft revascularization leading to "external inosculation" [182].

It should be mentioned here that inosculation will not only change micro hemodynamics and oxygen distribution within a prevascularized tissue construct, but will also open the door for infiltrating leukocytes and other inflammatory cell types. This recruitment of circulating leukocytes into the grafted tissue will depend on their interaction with the microvascular endothelium [183].

It is of importance in this context to point out that any implanted tissue (natural or engineered) will be remodeled on implantation. The microvascular network that is implanted may be completely different or absent after remodeling *in vivo* [173]. Vascular remodeling, and even vascular regression, are crucial for maturation and integration after construct implantation, yet premature vessel remodeling and regression within a construct could become a major obstacle to maintaining *in vivo* developed microvascular networks within a construct [184].

From the postulated vascularization strategies an acceptable protocol for construct vascularization would benefit from extrinsic angiogenesis for small constructs (2–3mm thick), intrinsic angiogenesis for larger constructs wherever local vascular axes are available, and from vasculogenesis for large cell-loaded constructs.

6.7.3 Biomimicry to Reach Vascularization; Simulating a Vascularizing Milieu

It is now clear that the process of vascularization that occurs in nature is a multifactorial process where every cellular, molecular, architectural, and mechanical factor has its is own role. Because these tasks are not yet precisely and quantitatively defined, normal physiological healing process remains the best strategy for adequate vascularization. Recent research is trying to incorporate all these factors together in order to mimic this strategy.

6.7.3.1 Scaffold Properties

In their way of mimicking the biological tissues, synthetically derived polymer scaffolds should not only be biocompatible and biodegradable, but should also ensure an optimal interaction with endothelial cells to promote angiogenesis. To develop scaffolds that fulfill these properties, it is of great importance to investigate how different biomaterials modulate endothelial cell function [185, 186].

In addition to the cellular interaction with biomaterials, the architecture of the scaffold itself seems to play an important role in adequate vascularization. The 3D structure of a scaffold by itself could change the angiogenic activity of incorporated cells [187]. In addition, the pore size of the scaffolds has been shown to be a critical determinant of blood vessel ingrowth, which is significantly faster in larger pores (160–270 µm) [188]. Pore interconnectivity has also been shown to be equally if not superiorly important [189]. Apart from the architecture of the scaffold, the degradation products that are formed during the incorporation process of the implant might influence the ingrowth of blood vessels into scaffolds [180].

The desire to improve the interaction between cells and synthetic scaffolds has resulted in a development of hybrid scaffolds in which biological matrix components such as laminin, fibronectin fragments or RGD sequence, were directly incorporated into synthetic scaffolds. These scaffolds are likely to improve microvascular network migration and growth because the cells can now easily recognize the scaffold surfaces as biological components and are therefore likely to result in better cell interaction with the scaffold, cell migration, spreading, and subsequent vessel infiltration into the scaffold; processes otherwise controlled by the ECM [190].

6.7.3.2 Growth Factor Incorporation

As vascularization is a multifactor process driven by numerous growth factors (GFs) released at a precise time and concentration, a variety of angiogenic factors have been tested aiming to further promote vascularization of tissue engineering constructs.

VEGF, the most widely used, and its receptors are involved in branching and remodeling of the vasculature and are, therefore, key regulators of angiogenesis. They are involved in endothelial cells (EC) migration and in the maturation process of the nascent vessels [191]. Moreover, VEGF and its receptors function as vascular permeability factors [192]. Additional angiogenic factors include the fibroblast growth factors (FGF), platelet-derived growth factors (PDGF), angiopoietins, and the transforming growth factors (TGF) [193].

6.7.3.3   Coculture Techniques

Coculture of endothelial cells with target tissue cells and fibroblasts has shown improved induction and stabilization of angiogenesis. Endothelialized human tissue-engineered skin consisting of capillary network was introduced by coculturing keratinocytes, dermal fibroblasts, and human umbilical vein endothelial cells (HUVEC) on 3D porous chitosan/collagen. Capillary tubes were clearly observed in the coculture system while were absent in the monoculture of each cell type. The vascularized engineered skin was then implanted in mice, and the mouse blood was detected in the *in vitro* generated vasculature after 4 days [194]. In another model, cocultured neural progenitor cells and brain-derived immortalized microvascular EC on macroporous hydrogel showed significantly higher blood vessel density after 6 weeks *in vivo*; this is in opposition to the separately cultured cells [195].

Yet, coculturing for promoting angiogenesis was demonstrated to be an uneasy task, as cocultivation of EC together with fibroblasts, pericytes, or vascular smooth muscle cells in fibrin gel did not lead to capillary networks, while younger or embryonic fibroblasts were able to support such endothelial organization in other gel systems [196].

Several studies have recently reported the successful creation of tissue-engineered vascular grafts with good long-term function by seeding different grafts with bone marrow cells and endothelial progenitor cells. In culture, these cells have been shown to give rise to 3 blood vessel cell components, namely endothelial cells, pericytes, and vascular smooth muscle cells [197–200].

6.7.3.4   Creating Vascular Patterns

Biomimetic approaches aiming for construct vasculogenesis should not only target the biological and cellular aspects of vasculogenesis but should also mimic the 3D hierarchal structure of natural capillary networks. Fabrication of channels mimicking the vascular networks lead to the development of constructs with a preformed capillary "pattern." The quest to create such microcirculatory network within the scaffolds *in vitro*

has led to the evolution of highly sophisticated approaches of microvascular engineering, such as soft photolithographic techniques [201], and the development of computational simulation models of vascular assembly and remodeling, such as cellular automata computer models [202].

6.7.3.5 Back to Nature

Because so much effort is required for mimicking nature, development of methods for reuse of natural structures is an evolving approach. These naturally occurring scaffolds can be processed so that they retain growth factors, glycosaminoglycans, and structural elements such as fibronectin, elastin, and collagen. These components were proved to be important regulators of angiogenesis. For example, elastic fibers of extracellular matrix scaffolds were shown to act as "microguides" for endothelial cell and pericyte migration during capillary sprouting [203].

A whole-heart scaffold with intact 3D geometry and vasculature was created by decellularizing cadaveric hearts using detergents for coronary perfusion [204]. Porcine jejunal segments were decellularized in a similar technique, and seeded with porcine microvascular endothelial cells [205].

Naturally occurring scaffolds, however, have got their own disadvantages including rapid degradation, potential to harbor infection, and the immunologic response of the host to such implants. It seems that the ideal scaffold, which promotes angiogenesis of engineered tissue sufficiently, has not yet been determined.

6.8 Conclusion

Being unique in structure and function, as well as in their developmental origins, dental and craniofacial tissues pose significant challenges to tissue engineering. Indeed, the field of dental and craniofacial tissue engineering is now changing from a tissue replacement strategy to one that aims to mimic the body's own natural developmental pathways to stimulate endogenous regeneration. Biomimetic strategies are slowly yet steadily leading the path to a new generation of tissue-engineered constructs that have gained insight from multidisplinary areas such as developmental biology, proteomics, genomics, nanotechnology, biomimetic surface modification, stem cell biology, biomaterial science, and many others. Through the application of biomimetic strategies to regenerate tissue, the hurdles of the past two decades may be overcome paving the way to a new era where tissue engineering and regenerative medicine applications become a standard of treatment rather than just translational research.

Acknowledgements

References

1. R. Langer and J.P. Vacanti, Tissue engineering, *Science,* Vol. 260, pp. 920–6, May 14 1993.
2. F.M. Chen, H.H. Sun, H. Lu, and Q. Yu, Stem cell-delivery therapeutics for periodontal tissue regeneration, *Biomaterials,* Vol. 33, pp. 6320–44, Sep 2012.
3. K. von der Mark, J. Park, S. Bauer, and P. Schmuki, Nanoscale engineering of biomimetic surfaces: Cues from the extracellular matrix, *Cell Tissue Res.,* Vol. 339, pp. 131–53, Jan 2010.
4. J.M. Harkness, A life time of connection: Otto Herbert Schmitt, 1913–1998, *Phys. Perspect.,* Vol. 4, pp. 456–90, 2002.
5. O.H. Schmitt, Some interesting and useful biomimetic transforms, in *Third International Biophysics Congress,* Boston, 1969.
6. J.F. Vincent, O.A. Bogatyreva, N.R. Bogatyrev, A. Bowyer, and A.K. Pahl, Biomimetics: Its practice and theory, *J. R. Soc. Interface,* Vol. 3, pp. 471–82, Aug 22 2006.
7. L.L. Hench, Biomaterials, *Science,* Vol. 208, pp. 826–31, May 23 1980.
8. L.L. Hench and J.M. Polak, Third-generation biomedical materials, *Science,* Vol. 295, pp. 1014–7, Feb 8 2002.
9. J.M. Anderson, The future of biomedical materials, *J. Mater. Sci. Mater. Med.,* Vol. 17, pp. 1025–8, Nov 2006.
10. L.R. Rui, *Current Opinion in Solid State and Materials Science,* Vol. 7, p. 263, 2003.
11. X. Liu and P.X. Ma, Polymeric scaffolds for bone tissue engineering, *Ann. Biomed. Eng.,* Vol. 32, pp. 477–86, Mar 2004.
12. P.X. Ma, Biomimetic materials for tissue engineering, *Adv. Drug Deliv. Rev.,* Vol. 60, pp. 184–98, Jan 14 2008.
13. W.J.E. Pérez R.A., J.C. Knowles and H.W. Kim, vol. doi:10.1016/j. addr.2012.03.009,, 2012.
14. S. Wang, M.M. Falk, A. Rashad, M.M. Saad, A.C. Marques, R.M. Almeida, M.K. Marei, and H. Jain, Evaluation of 3D nano-macro porous bioactive glass scaffold for hard tissue engineering, *J. Mater. Sci. Mater. Med.,* Vol. 22, pp. 1195–203, May 2011.
15. A.J. Engler, S. Sen, H.L. Sweeney, and D.E. Discher, Matrix elasticity directs stem cell lineage specification, *Cell,* Vol. 126, pp. 677–89, Aug 25 2006.
16. A.J. Engler, H.L. Sweeney, D.E. Discher, and J.E. Schwarzbauer, Extracellular matrix elasticity directs stem cell differentiation, *J. Musculoskelet. Neuronal. Interact.,* Vol. 7, p. 335, Oct-Dec 2007.
17. D.E. Ingber, Cellular mechanotransduction: Putting all the pieces together again, *FASEB J.,* Vol. 20, pp. 811–27, May 2006.

18. N.D. Leipzig and M.S. Shoichet, The effect of substrate stiffness on adult neural stem cell behavior, *Biomaterials,* Vol. 30, pp. 6867–78, Dec 2009.
19. C.B. Khatiwala, S.R. Peyton, M. Metzke, and A.J. Putnam, The regulation of osteogenesis by ECM rigidity in MC3T3-E1 cells requires MAPK activation, *J. Cell Physiol.,* Vol. 211, pp. 661–72, Jun 2007.
20. H.J.P. Kong, T.R. Polte, E. Alsberg, and D.J. Mooney, *Cell Biol.,* Vol. 102, p. 4300, 2011.
21. R. Barbucci and A. Magnani, Conformation of human plasma proteins at polymer surfaces: The effectiveness of surface heparinization, *Biomaterials,* Vol. 15, pp. 955–62, Oct 1994.
22. M. Malmsten, Formation of adsorbed protein layers, *J. Colloid. Interface Sci.,* Vol. 207, pp. 186–199, Nov 15 1998.
23. D.G. Castner and B.D. Ratner, *Surf. Sci.,* Vol. 500, p. 28, 2002.
24. C.R. Jenney and J.M. Anderson, Adsorbed serum proteins responsible for surface dependent human macrophage behavior, *J. Biomed. Mater. Res.,* Vol. 49, pp. 435–47, Mar 15 2000.
25. A. Shekaran and A.J. Garcia, Nanoscale engineering of extracellular matrix-mimetic bioadhesive surfaces and implants for tissue engineering, *Biochim. Biophys. Acta,* Vol. 1810, pp. 350–60, Mar 2011.
26. H. Cui, M.J. Webber, and S.I. Stupp, Self-assembly of peptide amphiphiles: From molecules to nanostructures to biomaterials, *Biopolymers,* Vol. 94, pp. 1–18, 2010.
27. H. Hosseinkhani, M. Hosseinkhani, and H. Kobayashi, *J. Bioact. Compat. Polym.,* Vol. 21, p. 277, 2006.
28. G. Mendonca, D.B. Mendonca, F.J. Aragao, and L. F. Cooper, Advancing dental implant surface technology--from micron- to nanotopography, *Biomaterials,* Vol. 29, pp. 3822–35, Oct 2008.
29. A. Krammer, D. Craig, W.E. Thomas, K. Schulten, and V. Vogel, A structural model for force regulated integrin binding to fibronectin's RGD-synergy site, *Matrix Biol.,* Vol. 21, pp. 139–47, Mar 2002.
30. L.G. Griffith, *Emerging Design Principles in Biomaterials and Scaffolds for Tissue Engineering,* Annals of the New York Academy of Sciences, 2002.
31. T.M.Y. Freyman, I.V. Yannas and L.J. Gibson, *Prog. Mater. Sci.,* Vol. 46, p. 273, 2001.
32. J.R. Jones, P.D. Lee, and L.L. Hench, Hierarchical porous materials for tissue engineering, *Philos. Transact. A Math. Phys. Eng. Sci.,* Vol. 364, pp. 263–81, Jan 15 2006.
33. V. Karageorgiou and D. Kaplan, Porosity of 3D biomaterial scaffolds and osteogenesis, *Biomaterials,* Vol. 26, pp. 5474–91, Sep 2005.
34. D.W. Hutmacher, Scaffolds in tissue engineering bone and cartilage, *Biomaterials,* Vol. 21, pp. 2529–43, Dec 2000.
35. K. Rezwan, Q.Z. Chen, J.J. Blaker, and A.R. Boccaccini, Biodegradable and bioactive porous polymer/inorganic composite scaffolds for bone tissue engineering, *Biomaterials,* Vol. 27, pp. 3413–31, Jun 2006.
36. J.C. Hansen, J.Y. Lim, L.C. Xu, C.A. Siedlecki, D.T. Mauger, and H.J. Donahue, Effect of surface nanoscale topography on elastic modulus of individual osteoblastic cells as determined by atomic force microscopy, *J. Biomech.,* Vol. 40, pp. 2865–71, 2007.

37. J.Y. Lim, A.D. Dreiss, Z. Zhou, J.C. Hansen, C.A. Siedlecki, R.W. Hengstebeck, J. Cheng, N. Winograd, and H.J. Donahue, The regulation of integrin-mediated osteoblast focal adhesion and focal adhesion kinase expression by nanoscale topography, *Biomaterials,* Vol. 28, pp. 1787–97, Apr 2007.

38. J.Y. Lim, J.C. Hansen, C.A. Siedlecki, J. Runt, and H.J. Donahue, Human foetal osteoblastic cell response to polymer-demixed nanotopographic interfaces, *J. R. Soc. Interface,* Vol. 2, pp. 97–108, Mar 22 2005.

39. E.L. Palin, H. Liu and, T.J. Webster, *Nanotechnology,* Vol. 16, p. 1828, 2002.

40. G. Balasundaram, M. Sato, and T.J. Webster, Using hydroxyapatite nanoparticles and decreased crystallinity to promote osteoblast adhesion similar to functionalizing with RGD, *Biomaterials,* Vol. 27, pp. 2798–805, May 2006.

41. M.A. Selleck and M. Bronner-Fraser, Origins of the avian neural crest: The role of neural plate-epidermal interactions, *Development,* Vol. 121, pp. 525–38, Feb 1995.

42. K.F. Liem Jr., G. Tremml, H. Roelink, and T.M. Jessell, Dorsal differentiation of neural plate cells induced by BMP-mediated signals from epidermal ecto-derm, *Cell,* Vol. 82, pp. 969–79, Sep 22 1995.

43. S. Nakagawa and M. Takeichi, Neural crest emigration from the neu-ral tube depends on regulated cadherin expression, *Development,* Vol. 125, pp. 2963–71, Aug 1998.

44. A. Lumsden, N. Sprawson, and A. Graham, Segmental origin and migration of neural crest cells in the hindbrain region of the chick embryo, *Development,* Vol. 113, pp. 1281–91, Dec 1991.

45. P. Hunt, J. Whiting, I. Muchamore, H. Marshall, and R. Krumlauf, Homeobox genes and models for patterning the hindbrain and branchial arches, *Dev. Suppl.,* Vol. 1, pp. 187–96, 1991.

46. E. Theveneau and R. Mayor, Neural crest delamination and migration: From epithelium-to-mesenchyme transition to collective cell migration, *Dev. Biol.,* Vol. 366, pp. 34–54, Jun 1 2012.

47. P. Kang and K.K. Svoboda, Epithelial-mesenchymal transformation during craniofacial development, *J. Dent. Res.,* Vol. 84, pp. 678–90, Aug 2005.

48. A. Rinon, A. Molchadsky, E. Nathan, G. Yovel, V. Rotter, R. Sarig, and E. Tzahor, p53 coordinates cranial neural crest cell growth and epithelial-mesenchymal transition/delamination processes, *Development,* Vol. 138, pp. 1827–38, May 2011.

49. X. Nie, Cranial base in craniofacial development: developmental features, influence on facial growth, anomaly, and molecular basis, *Acta Odontol. Scand.,* Vol. 63, pp. 127–35, Jun 2005.

50. J.H. Scott, N.B.B. Symons, *Introduction to Dental Anatomy*. Edinburgh, London: Churchill Livingstone, 1974.

51. N.B. Nagy, The relationships between palatal shelf elevation and histogene-sis of nasomaxillary complex: A proposed mechanism for palatal shelf eleva-tion in mice, *Cairo Dental Journal,* Vol. 14, p. 7, 1998.

52. M.L. Moss and R.W. Young, A functional approach to craniology, *Am. J. Phys. Anthropol.,* Vol. 18, pp. 281–92, Dec 1960.

53. T.W. Cendekiawan, R.W.K. and A.B.M. Rabie, *The Open Anatomy Journal*, Vol. 2, p. 67, 2010.

54. S.B. Milam, Pathophysiology and epidemiology of TMJ, *J. Musculoskelet. Neuronal. Interact.,* Vol. 3, pp. 382–90; discussion 406–7, Dec 2003.

55. M. Mina and E.J. Kollar, The induction of odontogenesis in non-dental mesenchyme combined with early murine mandibular arch epithelium, *Arch. Oral Biol.,* Vol. 32, pp. 123–7, 1987.

56. A.G.S. Lumsden, *Development,* vol.Vol. 103, p. 155, 1988.

57. I. Thesleff, Epithelial-mesenchymal signalling regulating tooth morphogenesis, *J. Cell Sci.,* Vol. 116, pp. 1647–8, May 1 2003.

58. E.J. Kollar and G.R. Baird, *Embryol. Exp. Morphol,* Vol. 24, p. 173, 1970.

59. S. Gronthos, M. Mankani, J. Brahim, P.G. Robey, and S. Shi, Postnatal human dental pulp stem cells (DPSCs) in vitro and in vivo, *Proc. Natl. Acad. Sci. U.S.A.,* Vol. 97, pp. 13625–30, Dec 5 2000.

60. J. Jernvall and I. Thesleff, Reiterative signaling and patterning during mammalian tooth morphogenesis, *Mech. Dev.,* Vol. 92, pp. 19–29, Mar 15 2000.

61. Y. Shinmura, S. Tsuchiya, K. Hata, and M.J. Honda, Quiescent epithelial cell rests of Malassez can differentiate into ameloblast-like cells, *J. Cell Physiol.,* Vol. 217, pp. 728–38, Dec 2008.

62. B.M. Seo, M. Miura, S. Gronthos, P.M. Bartold, S. Batouli, J. Brahim, M. Young, P.G. Robey, C.Y. Wang, and S. Shi, Investigation of multipotent postnatal stem cells from human periodontal ligament, *Lancet,* Vol. 364, pp. 149–55, Jul 10–16 2004.

63. I. Thesleff and M. Tummers, Tooth organogenesis and regeneration, in *StemBook,* Cambridge (MA), 2008.

64. P.A. Trainor, D. Sobieszczuk, D. Wilkinson, and R. Krumlauf, Signalling between the hindbrain and paraxial tissues dictates neural crest migration pathways, *Development,* Vol. 129, pp. 433–42, Jan 2002.

65. S. Yasser, N. Nagy, and M.K. Marei, *Maced. J. Med. Sci.,* Vol. http://dx.doi.org/10.3889/MJMS.1857- 5773.2012.0249, 2012.

66. A.I. Caplan and D. Correa, The MSC: An injury drugstore, *Cell Stem Cell,* Vol. 9, pp. 11–5, Jul 8 2011.

67. R.M. El Backly and R. Cancedda, Bone marrow stem cells in clinical application: harnessing paracrine roles and niche mechanisms, *Adv. Biochem. Eng. Biotechnol.,* Vol. 123, pp. 265–92, 2010.

68. S.H. Ranganath, O. Levy, M.S. Inamdar, and J.M. Karp, Harnessing the mesenchymal stem cell secretome for the treatment of cardiovascular disease, *Cell Stem Cell,* Vol. 10, pp. 244–58, Mar 2 2012.

69. T. Schinkothe, W. Bloch, and A. Schmidt, In vitro secreting profile of human mesenchymal stem cells, *Stem Cells Dev.,* Vol. 17, pp. 199–206, Feb 2008.

70. M. Heil, T. Ziegelhoeffer, B. Mees, and W. Schaper, A different outlook on the role of bone marrow stem cells in vascular growth: Bone marrow delivers software not hardware, *Circ. Res.,* Vol. 94, pp. 573–4, Mar 19 2004.

71. S. Roche, G. D'Ippolito, L.A. Gomez, T. Bouckenooghe, S. Lehmann, C.N. Montero-Menei, and P.C. Schiller, Comparative analysis of protein expression of three stem cell populations: Models of cytokine delivery system in vivo, *Int. J. Pharm.,* Jan 20 2012.

72. A. Oskowitz, H. McFerrin, M. Gutschow, M.L. Carter, and R. Pochampally, Serum-deprived human multipotent mesenchymal stromal cells (MSCs) are highly angiogenic, *Stem Cell Res.,* Vol. 6, pp. 215–25, May 2011.

73. E. Potier, E. Ferreira, R. Andriamanalijaona, J.P. Pujol, K. Oudina, D. Logeart-Avramoglou, and H. Petite, Hypoxia affects mesenchymal stromal cell

osteogenic differentiation and angiogenic factor expression, *Bone,* Vol. 40, pp. 1078–87, Apr 2007.

74. J.M. Kim, J. Kim, Y.H. Kim, K.T. Kim, S.H. Ryu, T.G. Lee, and P.G. Suh, Comparative secretome analysis of human bone marrow-derived mesenchymal stem cells during osteogenesis, *J. Cell. Physiol.,* Jun 1 2012.

75. R. Tasso, A. Augello, S. Boccardo, S. Salvi, M. Carida, F. Postiglione, F. Fais, M. Truini, R. Cancedda, and G. Pennesi, Recruitment of a host's osteoprogenitor cells using exogenous mesenchymal stem cells seeded on porous ceramic, *Tissue Eng. Part A,* Vol. 15, pp. 2203–12, Aug 2009.

76. R. Tasso, F. Fais, D. Reverberi, F. Tortelli, and R. Cancedda, The recruitment of two consecutive and different waves of host stem/progenitor cells during the development of tissue-engineered bone in a murine model, *Biomaterials,* Vol. 31, pp. 2121–9, Mar 2010.

77. D. Sarkar, J.A. Ankrum, G.S. Teo, C.V. Carman, and J.M. Karp, Cellular and extracellular programming of cell fate through engineered intracrine-, paracrine-, and endocrine-like mechanisms, *Biomaterials,* Vol. 32, pp. 3053–61, Apr 2011.

78. D. Sarkar, J.A. Spencer, J.A. Phillips, W. Zhao, S. Schafer, D.P. Spelke, L.J. Mortensen, J.P. Ruiz, P.K. Vemula, R. Sridharan, S. Kumar, R. Karnik, C.P. Lin, and J.M. Karp, Engineered cell homing, *Blood,* Vol. 118, pp. e184–91, Dec 15 2011.

79. J.D. Roh, R. Sawh-Martinez, M.P. Brennan, S.M. Jay, L. Devine, D.A. Rao, T. Yi, T.L. Mirensky, A. Nalbandian, B. Udelsman, N. Hibino, T. Shinoka, W.M. Saltzman, E. Snyder, T.R. Kyriakides, J.S. Pober, and C.K. Breuer, Tissue-engineered vascular grafts transform into mature blood vessels via an inflammation-mediated process of vascular remodeling, *Proc. Natl. Acad. Sci. U.S.A.,* Vol. 107, pp. 4669–74, Mar 9 2010.

80. P. Kolar, T. Gaber, C. Perka, G.N. Duda, and F. Buttgereit, Human early fracture hematoma is characterized by inflammation and hypoxia, *Clin. Orthop. Relat. Res.,* Vol. 469, pp. 3118–26, Nov 2011.

81. A. Rosell, K. Arai, J. Lok, T. He, S. Guo, M. Navarro, J. Montaner, Z.S. Katusic, and E.H. Lo, Interleukin-1beta augments angiogenic responses of murine endothelial progenitor cells in vitro, *J. Cereb. Blood Flow Metab.,* Vol. 29, pp. 933–43, May 2009.

82. H.H. Cho, Y.J. Kim, J.T. Kim, J.S. Song, K.K. Shin, Y.C. Bae, and J.S. Jung, The role of chemokines in proangiogenic action induced by human adipose tissue-derived mesenchymal stem cells in the murine model of hindlimb ischemia, *Cell Physiol. Biochem.,* Vol. 24, pp. 511–8, 2009.

83. S. Khosla, J.J. Westendorf, and U.I. Modder, Concise review: Insights from normal bone remodeling and stem cell-based therapies for bone repair, *Stem Cells,* Vol. 28, pp. 2124–8, Dec 2010.

84. X.L. Ma, X.L. Sun, C.Y. Wan, J.X. Ma, and P. Tian, Significance of circulating endothelial progenitor cells in patients with fracture healing process, *J. Orthop. Res.,* Vol. 30, pp. 1860–6, Nov 2012.

85. R.J. Pignolo and M. Kassem, Circulating osteogenic cells: implications for injury, repair, and regeneration, *J. Bone Miner. Res.,* Vol. 26, pp. 1685–93, Aug 2011.

86. X.L. Ma, X.L. Sun, C.Y. Wan, J.X. Ma, and P. Tian, Significance of circulating endothelial progenitor cells in patients with fracture healing process, *J. Orthop. Res.,* Apr 23 2012.

87. S. Otsuru, K. Tamai, T. Yamazaki, H. Yoshikawa, and Y. Kaneda, Circulating bone marrow-derived osteoblast progenitor cells are recruited to the bone-forming site by the CXCR4/stromal cell-derived factor-1 pathway, *Stem Cells,* Vol. 26, pp. 223–34, Jan 2008.

88. S.W. Herring and P. Ochareon, Bone--special problems of the craniofacial region, *Orthod. Craniofac. Res.,* Vol. 8, pp. 174–82, Aug 2005.

89. W.L. Hylander and K.R. Johnson, In vivo bone strain patterns in the zygomatic arch of macaques and the significance of these patterns for functional interpretations of craniofacial form, *Am. J. Phys. Anthropol.,* Vol. 102, pp. 203–32, Feb 1997.

90. J. Yuan, Y. Cao, and W. Liu, Biomimetic scaffolds: Implications for craniofacial regeneration, *J. Craniofac. Surg.,* Vol. 23, pp. 294–7, Jan 2012.

91. B.J. Costello, G. Shah, P. Kumta, and C.S. Sfeir, Regenerative medicine for craniomaxillofacial surgery, *Oral Maxillofac. Surg. Clin. North Am.,* Vol. 22, pp. 33–42, Feb 2010.

92. J.J. Mao, W.V. Giannobile, J.A. Helms, S.J. Hollister, P.H. Krebsbach, M.T. Longaker, and S. Shi, Craniofacial tissue engineering by stem cells, *J. Dent. Res.,* Vol. 85, pp. 966–79, Nov 2006.

93. S.H. Zaky and R. Cancedda, Engineering craniofacial structures: Facing the challenge, *J. Dent. Res.,* Vol. 88, pp. 1077–91, Dec 2009.

94. T. Dvir, B.P. Timko, D.S. Kohane, and R. Langer, Nanotechnological strategies for engineering complex tissues, *Nat. Nanotechnol.,* Vol. 6, pp. 13–22, Jan 2010.

95. M.M. Stevens and J.H. George, Exploring and engineering the cell surface interface, *Science,* Vol. 310, pp. 1135–8, Nov 18 2005.

96. J. Taipale and J. Keski-Oja, Growth factors in the extracellular matrix, *FASEB J.,* Vol. 11, pp. 51–9, Jan 1997.

97. S.A. Hacking, E. Harvey, P. Roughley, M. Tanzer, and J. Bobyn, The response of mineralizing culture systems to microtextured and polished titanium surfaces, *J. Orthop. Res.,* Vol. 26, pp. 1347–54, Oct 2008.

98. A. Curtis and C. Wilkinson, New depths in cell behaviour: Reactions of cells to nanotopography, *Biochem. Soc. Symp.,* Vol. 65, pp. 15–26, 1999.

99. T.J. Webster, C. Ergun, R.H. Doremus, R.W. Siegel, and R. Bizios, Specific proteins mediate enhanced osteoblast adhesion on nanophase ceramics, *J. Biomed. Mater. Res.,* Vol. 51, pp. 475–83, Sep 5 2000.

100. G. Colon, B.C. Ward, and T.J. Webster, Increased osteoblast and decreased Staphylococcus epidermidis functions on nanophase ZnO and TiO2, *J. Biomed. Mater. Res. A,* Vol. 78, pp. 595–604, Sep 1 2006.

101. L. Zhang and T.J. Webster, Nanotechnology and nanomaterials: Promises for improved tissue regeneration, *Nano Today,* pp. 66–80, 2009.

102. N. Tran and T.J. Webster, Nanotechnology for bone materials, *Wiley Interdiscip. Rev. Nanomed. Nanobiotechnol.,* Vol. 1, pp. 336–51, May-Jun 2009.

103. C.J. Bettinger, R. Langer, and J.T. Borenstein, Engineering substrate topography at the micro- and nanoscale to control cell function, *Angew Chem. Int. Ed. Engl.,* Vol. 48, pp. 5406–15, 2009.

104. A. Buxboim, I.L. Ivanovska, and D.E. Discher, Matrix elasticity, cytoskeletal forces and physics of the nucleus: How deeply do cells 'feel' outside and in?, *J. Cell Sci.,* Vol. 123, pp. 297–308, Feb 1 2010.

105. M. Goldberg, R. Langer, and X. Jia, Nanostructured materials for applications in drug delivery and tissue engineering, *J. Biomater. Sci. Polym. Ed.*, Vol. 18, pp. 241–68, 2007.

106. J. Shi, A.R. Votruba, O.C. Farokhzad, and R. Langer, Nanotechnology in drug delivery and tissue engineering: From discovery to applications, *Nano Lett.*, Vol. 10, pp. 3223–30, Sep 8 2010.

107. D.B. Burr, A.G. Robling, and C.H. Turner, Effects of biomechanical stress on bones in animals, *Bone*, Vol. 30, pp. 781–6, May 2002.

108. A.L. Boskey, Biomineralization: An overview, *Connect Tissue Res.*, Vol. 44 Suppl 1, pp. 5–9, 2003.

109. Y.K. Kim, L.S. Gu, T.E. Bryan, J.R. Kim, L. Chen, Y. Liu, J.C. Yoon, L. Breschi, D.H. Pashley, and F.R. Tay, Mineralisation of reconstituted collagen using polyvinylphosphonic acid/polyacrylic acid templating matrix protein analogues in the presence of calcium, phosphate and hydroxyl ions, *Biomaterials*, Vol. 31, pp. 6618–27, Sep 2010.

110. E. Sachlos, D. Gotora, and J.T. Czernuszka, Collagen scaffolds reinforced with biomimetic composite nano-sized carbonate-substituted hydroxyapatite crystals and shaped by rapid prototyping to contain internal microchannels, *Tissue Eng.*, Vol. 12, pp. 2479–87, Sep 2006.

111. K.S. Jack, S. Velayudhan, P. Luckman, M. Trau, L. Grondahl, and J. Cooper-White, The fabrication and characterization of biodegradable HA/PHBV nanoparticle-polymer composite scaffolds, *Acta Biomater.*, Vol. 5, pp. 2657–67, Sep 2009.

112. G. Wang, L. Zheng, H. Zhao, J. Miao, C. Sun, N. Ren, J. Wang, H. Liu, and X. Tao, In vitro assessment of the differentiation potential of bone marrow-derived mesenchymal stem cells on genipin-chitosan conjugation scaffold with surface hydroxyapatite nanostructure for bone tissue engineering, *Tissue Eng. Part A*, Vol. 17, pp. 1341–9, May 2011.

113. K. Kim and J.P. Fisher, Nanoparticle technology in bone tissue engineering, *J. Drug Target.*, Vol. 15, pp. 241–52, May 2007.

114. M.J. Dalby, N. Gadegaard, R. Tare, A. Andar, M.O. Riehle, P. Herzyk, C.D. Wilkinson, and R.O. Oreffo, The control of human mesenchymal cell differentiation using nanoscale symmetry and disorder, *Nat. Mater.*, Vol. 6, pp. 997–1003, Dec 2007.

115. S.L. Edwards, J.A. Werkmeister, and J.A. Ramshaw, Carbon nanotubes in scaffolds for tissue engineering, *Expert Rev. Med. Devices*, Vol. 6, pp. 499–505, Sep 2009.

116. L.P. Zanello, B. Zhao, H. Hu, and R.C. Haddon, Bone cell proliferation on carbon nanotubes, *Nano Lett.*, Vol. 6, pp. 562–7, Mar 2006.

117. X. Shi, B. Sitharaman, Q.P. Pham, F. Liang, K. Wu, W.E. Billups, L.J. Wilson, and A.G. Mikos, Fabrication of porous ultra-short single-walled carbon nanotube nanocomposite scaffolds for bone tissue engineering, *Biomaterials*, Vol. 28, pp. 4078–90, Oct 2007.

118. B. Sitharaman, X. Shi, X.F. Walboomers, H. Liao, V. Cuijpers, L.J. Wilson, A.G. Mikos, and J.A. Jansen, In vivo biocompatibility of ultra-short single-walled carbon nanotube/biodegradable polymer nanocomposites for bone tissue engineering, *Bone*, Vol. 43, pp. 362–70, Aug 2008.

119. F. Gelain, D. Bottai, A. Vescovi, and S. Zhang, Designer self-assembling peptide nanofiber scaffolds for adult mouse neural stem cell 3-dimensional cultures, *PLoS One*, Vol. 1, p. e119, 2006.

120. J. Xu, X. Zhou, H. Ge, H. Xu, J. He, Z. Hao, and X. Jiang, Endothelial cells anchoring by functionalized yeast polypeptide, *J. Biomed. Mater. Res. A,* Vol. 87, pp. 819–24, Dec 1 2008.

121. E.L. Rexeisen, W. Fan, T.O. Pangburn, R.R. Taribagil, F.S. Bates, T.P. Lodge, M. Tsapatsis, and E. Kokkoli, Self-assembly of fibronectin mimetic peptide-amphiphile nanofibers, *Langmuir,* Vol. 26, pp. 1953–9, Feb 2 2009.

122. H.H. Xu, M.D. Weir, and C.G. Simon, Injectable and strong nano-apatite scaffolds for cell/growth factor delivery and bone regeneration, *Dent. Mater.,* Vol. 24, pp. 1212–22, Sep 2008.

123. Z.Y. Lin, Z.X. Duan, X.D. Guo, J.F. Li, H.W. Lu, Q.X. Zheng, D.P. Quan, and S.H. Yang, Bone induction by biomimetic PLGA-(PEG-ASP)n copolymer loaded with a novel synthetic BMP-2-related peptide in vitro and in vivo, *J. Control. Release,* Vol. 144, pp. 190–5, Jun 1 2010.

124. W.D. Chan, H. Perinpanayagam, H.A. Goldberg, G.K. Hunter, S.J. Dixon, G.C. Santos, Jr., and A.S. Rizkalla, Tissue engineering scaffolds for the regeneration of craniofacial bone, *J. Can. Dent. Assoc.,* Vol. 75, pp. 373–7, Jun 2009.

125. A.S. Sarvestani, X. He, and E. Jabbari, Effect of osteonectin-derived peptide on the viscoelasticity of hydrogel/apatite nanocomposite scaffolds, *Biopolymers,* Vol. 85, pp. 370–8, Mar 2007.

126. A.S. Sarvestani, X. He, and E. Jabbari, Osteonectin-derived peptide increases the modulus of a bone-mimetic nanocomposite, *Eur. Biophys. J.,* Vol. 37, pp. 229–34, Feb 2008.

127. T.J. Webster, L.S. Schadler, R.W. Siegel, and R. Bizios, Mechanisms of enhanced osteoblast adhesion on nanophase alumina involve vitronectin, *Tissue Eng.,* Vol. 7, pp. 291–301, Jun 2001.

128. W.P. Xu, W. Zhang, R. Asrican, H.J. Kim, D.L. Kaplan, and P.C. Yelick, Accurately shaped tooth bud cell-derived mineralized tissue formation on silk scaffolds, *Tissue Eng. Part A,* Vol. 14, pp. 549–57, Apr 2008.

129. R. Dimitriou and G.C. Babis, Biomaterial osseointegration enhancement with biophysical stimulation, *J. Musculoskelet. Neuronal. Interact.,* Vol. 7, pp. 253–65, Jul-Sep 2007.

130. A.F. Mavrogenis, R. Dimitriou, J. Parvizi, and G.C. Babis, Biology of implant osseointegration, *J. Musculoskelet. Neuronal. Interact.,* Vol. 9, pp. 61–71, Apr-Jun 2009.

131. U. Joos, H.P. Wiesmann, T. Szuwart, and U. Meyer, Mineralization at the interface of implants, *Int. J. Oral Maxillofac. Surg.,* Vol. 35, pp. 783–90, Sep 2006.

132. G. Kirmizidis and M.A. Birch, Microfabricated grooved substrates influence cell-cell communication and osteoblast differentiation in vitro, *Tissue Eng. Part A,* Vol. 15, pp. 1427–36, Jun 2009.

133. L. Le Guehennec, A. Soueidan, P. Layrolle, and Y. Amouriq, Surface treatments of titanium dental implants for rapid osseointegration, *Dent. Mater.,* Vol. 23, pp. 844–54, Jul 2007.

134. S. Makihira, Y. Mine, E. Kosaka, and H. Nikawa, Titanium surface roughness accelerates RANKL-dependent differentiation in the osteoclast precursor cell line, RAW264.7, *Dent. Mater. J.,* Vol. 26, pp. 739–45, Sep 2007.

135. J.L. Ricci, J. Charvet, S.R. Frenkel, R. Chang, P. Nadkarni, J. Turner, and H. Alexander, Bone engineering, in *Bone Response to Laser Microtextured Surfaces*, J.E. Davies, Ed., Toronto, Canada: Em2 Inc., 2000.

136. K. Anselme, M. Bigerelle, B. Noel, A. Iost, and P. Hardouin, Effect of grooved titanium substratum on human osteoblastic cell growth, *J. Biomed. Mater. Res.,* Vol. 60, pp. 529–40, Jun 15 2002.

137. M. Bigerelle, K. Anselme, B. Noel, I. Ruderman, P. Hardouin, and A. Iost, Improvement in the morphology of Ti-based surfaces: A new process to increase in vitro human osteoblast response, *Biomaterials,* Vol. 23, pp. 1563–77, Apr 2002.

138. X. Zhu, J. Chen, L. Scheideler, T. Altebaeumer, J. Geis-Gerstorfer, and D. Kern, Cellular reactions of osteoblasts to micron- and submicron-scale porous structures of titanium surfaces, *Cells Tissues Organs,* Vol. 178, pp. 13–22, 2004.

139. L. Agata De Sena, M. Calixto De Andrade, A. Malta Rossi, and G. de Almeida Soares, Hydroxyapatite deposition by electrophoresis on titanium sheets with different surface finishing, *J. Biomed. Mater. Res.,* Vol. 60, pp. 1–7, Apr 2002.

140. F. Barrere, M.M. Snel, C.A. van Blitterswijk, K. de Groot, and P. Layrolle, Nano-scale study of the nucleation and growth of calcium phosphate coating on titanium implants, *Biomaterials,* Vol. 25, pp. 2901–10, Jun 2004.

141. F. Barrere, C.M. van der Valk, R.A. Dalmeijer, C.A. van Blitterswijk, K. de Groot, and P. Layrolle, In vitro and in vivo degradation of biomimetic octacalcium phosphate and carbonate apatite coatings on titanium implants, *J. Biomed. Mater. Res. A,* Vol. 64, pp. 378–87, Feb 1 2003.

142. P. Habibovic, J. Li, C.M. van der Valk, G. Meijer, P. Layrolle, C.A. van Blitterswijk, and K. de Groot, Biological performance of uncoated and octacalcium phosphate-coated Ti6Al4V, *Biomaterials,* Vol. 26, pp. 23–36, Jan 2005.

143. P. Habibovic, C.A. van Blitterswijk, K. de Groot, and P. Layrolle, *J. Am. Ceram. Soc.,* Vol. 85, p. 517, 2002.

144. S. Leeuwenburgh, P. Layrolle, F. Barrere, J. de Bruijn, J. Schoonman, C.A. van Blitterswijk, and K. de Groot, Osteoclastic resorption of biomimetic calcium phosphate coatings in vitro, *J. Biomed. Mater. Res.,* Vol. 56, pp. 208–15, Aug 2001.

145. J. Wang, J. de Boer, and K. de Groot, Preparation and characterization of electrodeposited calcium phosphate/chitosan coating on Ti6Al4V plates, *J. Dent. Res.,* Vol. 83, pp. 296–301, Apr 2004.

146. X.X. Wang, W. Yan, S. Hayakawa, K. Tsuru, and A. Osaka, Apatite deposition on thermally and anodically oxidized titanium surfaces in a simulated body fluid, *Biomaterials,* Vol. 24, pp. 4631–7, Nov 2003.

147. U.M. Wikesjo, R.G. Sorensen, A. Kinoshita, and J.M. Wozney, RhBMP-2/alphaBSM induces significant vertical alveolar ridge augmentation and dental implant osseointegration, *Clin. Implant Dent. Relat. Res.,* Vol. 4, pp. 174–82, 2002.

148. B. Yang, M. Uchida, H.M. Kim, X. Zhang, and T. Kokubo, Preparation of bioactive titanium metal via anodic oxidation treatment, *Biomaterials,* Vol. 25, pp. 1003–10, Mar 2004.

149. P. Boyne and S.D. Jones, Demonstration of the osseoinductive effect of bone morphogenetic protein within endosseous dental implants, *Implant Dent.,* Vol. 13, pp. 180–4, Jun 2004.

150. Y.C. Huang, C. Simmons, D. Kaigler, K.G. Rice, and D.J. Mooney, Bone regeneration in a rat cranial defect with delivery of PEI-condensed plasmid DNA encoding for bone morphogenetic protein-4 (BMP-4), *Gene Ther.,* Vol. 12, pp. 418–26, Mar 2005.

151. S. Josse, C. Faucheux, A. Soueidan, G. Grimandi, D. Massiot, B. Alonso, P. Janvier, S. Laib, P. Pilet, O. Gauthier, G. Daculsi, J. J. Guicheux, B. Bujoli, and J.M. Bouler, Novel biomaterials for bisphosphonate delivery, *Biomaterials,* Vol. 26, pp. 2073–80, May 2005.

152. Y. Liu, K. de Groot, and E.B. Hunziker, BMP-2 liberated from biomimetic implant coatings induces and sustains direct ossification in an ectopic rat model, *Bone,* Vol. 36, pp. 745–57, May 2005.

153. V.F. Stenport, A.M. Roos-Jansaker, S. Renvert, Y. Kuboki, C. Irwin, T. Albrektsson, and N. Claffey, Failure to induce supracrestal bone growth between and around partially inserted titanium implants using bone morphogenetic protein (BMP): An experimental study in dogs, *Clin. Oral Implants Res.,* Vol. 14, pp. 219–25, Apr 2003.

154. D.N. Tatakis, A. Koh, L. Jin, J.M. Wozney, M.D. Rohrer, and U.M. Wikesjo, Peri-implant bone regeneration using recombinant human bone morphogenetic protein-2 in a canine model: A dose-response study, *J. Periodontal Res.,* Vol. 37, pp. 93–100, Apr 2002.

155. H. Kajiwara, T. Yamaza, M. Yoshinari, T. Goto, S. Iyama, I. Atsuta, M.A. Kido, and T. Tanaka, The bisphosphonate pamidronate on the surface of titanium stimulates bone formation around tibial implants in rats, *Biomaterials,* Vol. 26, pp. 581–7, Feb 2005.

156. S.J. Meraw, C.M. Reeve, and P.C. Wollan, Use of alendronate in peri-implant defect regeneration, *J. Periodontol.,* Vol. 70, pp. 151–8, Feb 1999.

157. B. Peter, D.P. Pioletti, S. Laib, B. Bujoli, P. Pilet, P. Janvier, J. Guicheux, P.Y. Zambelli, J.M. Bouler, and O. Gauthier, Calcium phosphate drug delivery system: Influence of local zoledronate release on bone implant osteointegration, *Bone,* Vol. 36, pp. 52–60, Jan 2005.

158. M. Yoshinari, Y. Oda, H. Ueki, and S. Yokose, Immobilization of bisphosphonates on surface modified titanium, *Biomaterials,* Vol. 22, pp. 709–15, Apr 2001.

159. L.F. Cooper, Y. Zhou, J. Takebe, J. Guo, A. Abron, A. Holmen, and J.E. Ellingsen, Fluoride modification effects on osteoblast behavior and bone formation at TiO2 grit-blasted c.p. titanium endosseous implants, *Biomaterials,* Vol. 27, pp. 926–36, Feb 2006.

160. J.E. Ellingsen, C.B. Johansson, A. Wennerberg, and A. Holmen, Improved retention and bone-tolmplant contact with fluoride-modified titanium implants, *Int. J. Oral Maxillofac. Implants,* Vol. 19, pp. 659–66, Sep-Oct 2004.

161. K. Yokoyama, T. Ichikawa, H. Murakami, Y. Miyamoto, and K. Asaoka, Fracture mechanisms of retrieved titanium screw thread in dental implant, *Biomaterials,* Vol. 23, pp. 2459–65, Jun 2002.

162. J. Benesch, J.F. Mano, and R.L. Reis, Proteins and their peptide motifs in acellular apatite mineralization of scaffolds for tissue engineering, *Tissue Eng. Part B Rev.,* Vol. 14, pp. 433–45, Dec 2008.

163. M.J. Avaltroni, J. Schwartz, M.P. Danahy, B.M. Silverman, E.L. Hanson, J.E. Schwarzbauer, K.S. Midwood, and E.S. Gawalt, *Materials Science and Engineering,* Vol. 23, p. 395, 2003.

164. A.S. Goldstein, T.M. Juarez, C.D. Helmke, M.C. Gustin, and A.G. Mikos, Effect of convection on osteoblastic cell growth and function in biodegradable polymer foam scaffolds, *Biomaterials,* Vol. 22, pp. 1279–88, Jun 2001.

165. W.W. Hu, B.B. Ward, Z. Wang, and P.H. Krebsbach, Bone regeneration in defects compromised by radiotherapy, *J. Dent. Res.,* Vol. 89, pp. 77–81, Jan 2010.

166. C.D. Friedman, Trauma: Basic principles of craniofacial bone healing and repair, in *Facial Plastic and Reconstructive Surgery*, I.D. Papel, Ed., New York: Thieme Medical Publishers, 2009, p. 920.

167. M.K. Marei, M.A. Alkhodary, R.M. Elbackly, S.H. Zaky, A.M. Eweida, M.A. Gad, N. Abdel-Wahed, and Y.M. Kadah, Principles, applications, and technology of craniofacial bone engineering, in *Integrated Biomaterials in Tissue Engineering*, M. Ramalingam, Z. Haidar, S. Ramakrishna, H. Kobayashi, and Y. Haikel, Eds., UK: Wiley-Scrivener, 2012.

168. E. Polykandriotis, A. Arkudas, R.E. Horch, M. Sturzl, and U. Kneser, Autonomously vascularized cellular constructs in tissue engineering: Opening a new perspective for biomedical science, *J. Cell Mol. Med.,* Vol. 11, pp. 6–20, Jan-Feb 2007.

169. P. Carmeliet, Angiogenesis in life, disease and medicine, *Nature,* Vol. 438, pp. 932–6, Dec 15 2005.

170. T. Asahara, T. Murohara, A. Sullivan, M. Silver, R. van der Zee, T. Li, B. Witzenbichler, G. Schatteman, and J.M. Isner, Isolation of putative progenitor endothelial cells for angiogenesis, *Science,* Vol. 275, pp. 964–7, Feb 14 1997.

171. J.M. Converse, J. Smahel, D.L. Ballantyne, Jr., and A.D. Harper, Inosculation of vessels of skin graft and host bed: A fortuitous encounter, *Br. J. Plast. Surg.,* Vol. 28, pp. 274–82, Oct 1975.

172. L.L. Nguyen and P.A. D'Amore, Cellular interactions in vascular growth and differentiation, *Int. Rev. Cytol.,* Vol. 204, pp. 1–48, 2001.

173. Z. Lokmic and G.M. Mitchell, Engineering the microcirculation, *Tissue Eng. Part B Rev.,* Vol. 14, pp. 87–103, Mar 2008.

174. U. Kneser, E. Polykandriotis, J. Ohnolz, K. Heidner, L. Grabinger, S. Euler, K.U. Amann, A. Hess, K. Brune, P. Greil, M. Sturzl, and R.E. Horch, Engineering of vascularized transplantable bone tissues: Induction of axial vascularization in an osteoconductive matrix using an arteriovenous loop, *Tissue Eng.,* Vol. 12, pp. 1721–31, Jul 2006.

175. O.C. Cassell, S.O. Hofer, W.A. Morrison, and K.R. Knight, Vascularisation of tissue-engineered grafts: The regulation of angiogenesis in reconstructive surgery and in disease states, *Br. J. Plast. Surg.,* Vol. 55, pp. 603–10, Dec 2002.

176. U. Kneser, D.J. Schaefer, E. Polykandriotis, and R.E. Horch, Tissue engineering of bone: The reconstructive surgeon's point of view, *J. Cell Mol. Med.,* Vol. 10, pp. 7–19, Jan-Mar 2006.

177. A.M. Eweida, A.S. Nabawi, H.A. Elhammady, M.K. Marei, M.R. Khalil, M.S. Shawky, A. Arkudas, J.P. Beier, F. Unglaub, U. Kneser, and R.E. Horch, Axially vascularized bone substitutes: A systematic review of literature and presentation of a novel model, *Arch. Orthop. Trauma Surg.,* Vol. 132, pp. 1353–62, Sep 2012.

178. A.M. Eweida, A.S. Nabawi, M.K. Marei, M.R. Khalil, and H.A. Elhammady, Mandibular reconstruction using an axially vascularized tissue-engineered construct, *Ann. Surg. Innov. Res.,* Vol. 5, p. 2, 2011.

179. D.J. Mooney and A.G. Mikos, Growing new organs, *Sci. Am.,* Vol. 280, pp. 60–5, Apr 1999.
180. M.W. Laschke, Y. Harder, M. Amon, I. Martin, J. Farhadi, A. Ring, N. Torio-Padron, R. Schramm, M. Rucker, D. Junker, J.M. Haufel, C. Carvalho, M. Heberer, G. Germann, B. Vollmar, and M.D. Menger, Angiogenesis in tissue engineering: breathing life into constructed tissue substitutes, *Tissue Eng.,* Vol. 12, pp. 2093–104, Aug 2006.
181. H.A. Zarem, B.W. Zweifach, and J.M. McGehee, Development of microcirculation in full thickness autogenous skin grafts in mice, *Am. J. Physiol.,* Vol. 212, pp. 1081–5, May 1967.
182. M.W. Laschke, M. Rucker, G. Jensen, C. Carvalho, R. Mulhaupt, N.C. Gellrich, and M.D. Menger, Improvement of vascularization of PLGA scaffolds by inosculation of in situ-preformed functional blood vessels with the host microvasculature, *Ann. Surg.,* Vol. 248, pp. 939–48, Dec 2008.
183. E.C. Butcher, Leukocyte-endothelial cell recognition: Three (or more) steps to specificity and diversity, *Cell,* Vol. 67, pp. 1033–6, Dec 20 1991.
184. Z. Lokmic, F. Stillaert, W.A. Morrison, E.W. Thompson, and G.M. Mitchell, An arteriovenous loop in a protected space generates a permanent, highly vascular, tissue-engineered construct, *FASEB J.,* Vol. 21, pp. 511–22, Feb 2007.
185. C.J. Kirkpatrick, R.E. Unger, V. Krump-Konvalinkova, K. Peters, H. Schmidt, and G. Kamp, Experimental approaches to study vascularization in tissue engineering and biomaterial applications, *J. Mater. Sci. Mater. Med.,* Vol. 14, pp. 677–81, Aug 2003.
186. K. Peters, H. Schmidt, R.E. Unger, M. Otto, G. Kamp, and C.J. Kirkpatrick, Software-supported image quantification of angiogenesis in an in vitro culture system: application to studies of biocompatibility, *Biomaterials,* Vol. 23, pp. 3413–9, Aug 2002.
187. E. Pinney, K. Liu, B. Sheeman, and J. Mansbridge, Human three-dimensional fibroblast cultures express angiogenic activity, *J. Cell Physiol.,* Vol. 183, pp. 74–82, Apr 2000.
188. A. Artel, H. Mehdizadeh, Y.C. Chiu, E.M. Brey, and A. Cinar, An agent-based model for the investigation of neovascularization within porous scaffolds, *Tissue Eng. Part A,* Vol. 17, pp. 2133–41, Sep 2011.
189. F. Bai, Z. Wang, J. Lu, J. Liu, G. Chen, R. Lv, J. Wang, K. Lin, J. Zhang, and X. Huang, The correlation between the internal structure and vascularization of controllable porous bioceramic materials in vivo: A quantitative study, *Tissue Eng. Part A,* Vol. 16, pp. 3791–803, Dec 2010.
190. T.A. Petrie, J.R. Capadona, C.D. Reyes, and A.J. Garcia, Integrin specificity and enhanced cellular activities associated with surfaces presenting a recombinant fibronectin fragment compared to RGD supports, *Biomaterials,* Vol. 27, pp. 5459–70, Nov 2006.
191. R.K. Jain, Molecular regulation of vessel maturation, *Nat. Med.,* Vol. 9, pp. 685–93, Jun 2003.
192. N. Ferrara, H.P. Gerber, and J. LeCouter, The biology of VEGF and its receptors, *Nat. Med.,* Vol. 9, pp. 669–76, Jun 2003.
193. T. Kaully, K. Kaufman-Francis, A. Lesman, and S. Levenberg, Vascularization-the conduit to viable engineered tissues, *Tissue Eng. Part B Rev.,* Vol. 15, pp. 159–69, Jun 2009.

194. P.L. Tremblay, V. Hudon, F. Berthod, L. Germain, and F.A. Auger, Inosculation of tissue-engineered capillaries with the host's vasculature in a reconstructed skin transplanted on mice, *Am. J. Transplant.*, Vol. 5, pp. 1002–10, May 2005.

195. M.C. Ford, J.P. Bertram, S.R. Hynes, M. Michaud, Q. Li, M. Young, S.S. Segal, J.A. Madri, and E.B. Lavik, A macroporous hydrogel for the coculture of neural progenitor and endothelial cells to form functional vascular networks in vivo, *Proc. Natl. Acad. Sci. U.S.A.*, Vol. 103, pp. 2512–7, Feb 21 2006.

196. V. Nehls, E. Schuchardt, and D. Drenckhahn, The effect of fibroblasts, vascular smooth muscle cells, and pericytes on sprout formation of endothelial cells in a fibrin gel angiogenesis system, *Microvasc. Res.*, Vol. 48, pp. 349–63, Nov 1994.

197. S.W. Cho, S.H. Lim, I.K. Kim, Y.S. Hong, S.S. Kim, K.J. Yoo, H.Y. Park, Y. Jang, B.C. Chang, C.Y. Choi, K.C. Hwang, and B.S. Kim, Small-diameter blood vessels engineered with bone marrow-derived cells, *Ann. Surg.*, Vol. 241, pp. 506–15, Mar 2005.

198. N. Hibino, T. Shin'oka, G. Matsumura, Y. Ikada, and H. Kurosawa, The tissue-engineered vascular graft using bone marrow without culture, *J. Thorac. Cardiovasc. Surg.*, Vol. 129, pp. 1064–70, May 2005.

199. S. Kaushal, G.E. Amiel, K.J. Guleserian, O.M. Shapira, T. Perry, F.W. Sutherland, E. Rabkin, A.M. Moran, F.J. Schoen, A. Atala, S. Soker, J. Bischoff, and J.E. Mayer, Jr., Functional small-diameter neovessels created using endothelial progenitor cells expanded ex vivo, *Nat. Med.*, Vol. 7, pp. 1035–40, Sep 2001.

200. J. Yamashita, H. Itoh, M. Hirashima, M. Ogawa, S. Nishikawa, T. Yurugi, M. Naito, K. Nakao, and S. Nishikawa, Flk1-positive cells derived from embryonic stem cells serve as vascular progenitors, *Nature*, Vol. 408, pp. 92–6, Nov 2 2000.

201. S. Kaihara, J. Borenstein, R. Koka, S. Lalan, E.R. Ochoa, M. Ravens, H. Pien, B. Cunningham, and J.P. Vacanti, Silicon micromachining to tissue engineer branched vascular channels for liver fabrication, *Tissue Eng.*, Vol. 6, pp. 105–17, Apr 2000.

202. S.M. Peirce, E.J. Van Gieson, and T.C. Skalak, Multicellular simulation predicts microvascular patterning and in silico tissue assembly, *FASEB J.*, Vol. 18, pp. 731–3, Apr 2004.

203. C.R. Anderson, A.M. Ponce, and R.J. Price, Immunohistochemical identification of an extracellular matrix scaffold that microguides capillary sprouting in vivo, *J. Histochem. Cytochem.*, Vol. 52, pp. 1063–72, Aug 2004.

204. H.C. Ott, T.S. Matthiesen, S.K. Goh, L.D. Black, S.M. Kren, T.I. Netoff, and D.A. Taylor, Perfusion-decellularized matrix: Using nature's platform to engineer a bioartificial heart, *Nat. Med.*, Vol. 14, pp. 213–21, Feb 2008.

205. K. Linke, J. Schanz, J. Hansmann, T. Walles, H. Brunner, and H. Mertsching, Engineered liver-like tissue on a capillarized matrix for applied research, *Tissue Eng.*, Vol. 13, pp. 2699–707, Nov 2007.

206. D. Kaigler, G. Pagni, C.H. Park, S.A. Tarle, R.L. Bartel, and W.V. Giannobile, Angiogenic and osteogenic potential of bone repair cells for craniofacial regeneration, *Tissue Eng. Part A*, Vol. 16, pp. 2809–20, Sep 2010.

Strategies to Prevent Bacterial Adhesion on Biomaterials

Indu Bajpai[1] and Bikramjit Basu[2,*]

[1]Department of Materials Science and Engineering, Laboratory for Biomaterials, Indian Institute of Technology Kanpur, Kanpur, India
[2]Laboratory for Biomaterials, Materials Research Centre, Indian Institute of Science, Bangalore, India

Abstract

Implants causing infection is a very serious concern in the biomedical field. A variety of disease–causing bacteria, *Enterococcus*, *Staphylococcus*, *Streptococcus* and coagulase negative *Staphylococci*, are antibiotic resistant and cause a serious threat to public health worldwide. Prosthetic infection can be reduced either by modifying the biomaterial surface with antibacterial agents, like Ag, ZnO and iron oxide, or by application of external electric and magnetic fields. The chapter starts with an introduction to the molecular biological structure of bacterial cells, their growth behavior, mechanism of bacterial adhesion, and biofilm formation on biomaterial surface. This introductory section is followed by a discussion of bacterial adhesion on biomaterial surface via physicochemical interactions, and molecular and cellular interactions between bacteria and surfaces. Emphasis is placed on how the bacterial adhesion on biomaterial surface becomes firmer by the selective–bridging function of the capsules, fimbriae and slime. A part of this chapter discusses various factors that influence bacterial adhesion such as (i) presence of serum proteins or antibiotics, (ii) bacterial hydrophobicity, (iii) bacterial surface charge, (iv) tissue proteins (serum) such as albumin, fibrinogen, thrombin, platelets, and (v) material surface characteristics such as surface chemical composition, surface roughness, surface configuration. An important aspect of this chapter is the discussion on the recent development of synthetic biomaterials, such as glass ceramics, HA–Ag and HA–ZnO composites, with good antimicrobial properties. How the addition of Ag/ZnO needs to be tailored to have a compromise between the cytotoxicity and antimicrobial properties is illustrated. The recent efforts towards the development of iron oxide–containing biocomposites are also discussed in view of the fact that iron oxide nanoparticles are toxic for bacteria cells, whereas they are safe

Corresponding author: bikram@iitk.ac.in

for eukaryotic cells via generating reactive oxygen species (ROS) and have synergistically–inducing magnetic properties for potential use as controls for cell fate processes. Although implants with magnetic properties have been shown to be successful for treatment of bone defect, the cure of malignant bone tissue and the restoration of large bone defects still provide major clinical challenges. A number of magnetic biomaterials such as magnetic Ca/P–based materials, bioactive glass ceramics and ferrimagnetic calcium phosphate glass–ceramics are reported prospective materials for malignant bone tumors in hyperthermia therapy. After discussing these aspects, this chapter concludes with a discussion on the effect of electric and magnetic field on bacterial adhesion and growth behavior *in vitro*.

Keywords: Magnetic field, electric field, hydroxyapatite, ZnO, Ag, iron oxide

7.1 Introduction

Biomaterials are very important from a healthcare prospective because they are used to replace lost tissues and treat many diseases. Optimally designed biomaterials provide temporary scaffolding to facilitate new tissue growth [1]. In order to cure the bone defects, a variety of synthetic biomaterials have been anticipated as bone fillers. Among these biomaterials, bioglass and calcium–phosphate ceramics represent bioactive materials having the aptitude to achieve direct biological bond with bone [2]. The biomaterials must show good mechanical responses as well as bone–mimicking properties in physical terms and must be biocompatible in order to prevent biological rejection, which hampers device performance. It is therefore highly preferable that synthetic biomaterial be "inert" and not toxic towards the host organism [3]. Its host response should be good in order to minimize the chances of aspect loosening, which may lead to revision surgery. A good biomaterial should have natural bone–like properties [4]. The issues associated with synthetic biomaterials are summarized in Figure 7.1.

It has been reported that more than 2,00,000 primary hip and 2,00,000 primary knee arthroplasties are performed each year in the USA [5]. Also, 0.5% and 2.5% of them are reported to experience prosthetic infection within 10 years [5, 6]. A variety of disease–causing bacteria have become antibiotic resistant and this has been a serious threat to public health worldwide [7]. Among these pathogenic microorganisms, *Enterococcus*, *Staphylococcus*, *Streptococcus* and coagulase negative *Staphylococci* are common species that are responsible for a wide variety of infections and diseases [8].

The nosocomial infections have an effect on approximately 10% of all inpatients, leading to a delay in discharge by an average of 11 days, or directly causing 5000 deaths/year in the UK [9]. These bacterial strains are becoming a major cause for hospital–acquired infections [10]. Total joint replacement affected by sepsis can have catastrophic results in the form
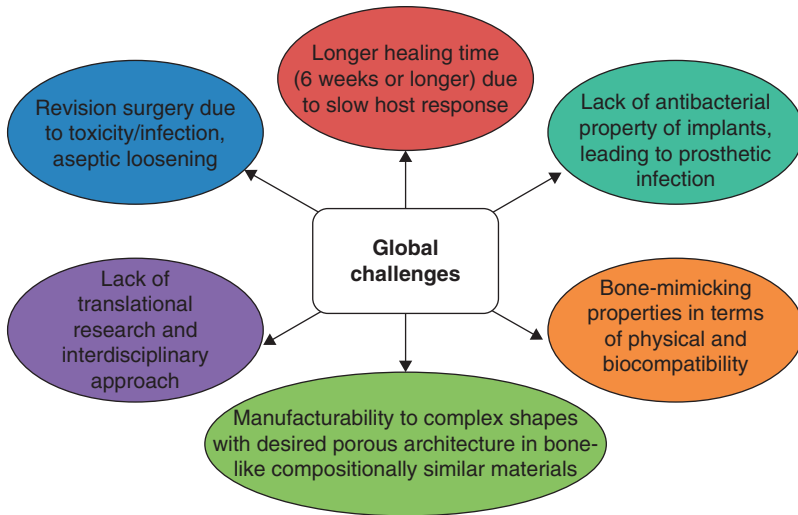
Figure 7.1 Summary of some of the major challenges driving the research on biomaterial, illustrating the need to develop material with bone–mimicking and antibacterial properties (adapted from ref.[4]).

of impant failure and can cause prolonged hospitalization or even sometimes death. It is therefore concluded that infections restrict the long–term use of implanted devices [11]. No fully effective treatment technique is available to cure such infection, therefore, the infected implanted device is surgically removed [9].

Staphylococcus aureus and *S. epidermidis*, highly resistant towards antibiotics, cause local infections such as wounds, as well as prosthetic infection [12, 13]. Some main sources of bacterial infections in patients are hospital environment, surgical devices, contaminated disinfectants and already present distant local infections [14]. Therefore, innovative strategies are needed to develop the drugs, scaffolds or external treatment techniques that can be directly applied to the site of infections with minimal side effects, along with protecting the patient from bacterial infection. Prosthetic infection can be reduced either by modifying the biomaterial surface with antibacterial agents like Ag and ZnO, and/or by application of external fields as shown in Figure 7.2.

The current research has become fascinated by the use of inorganic antimicrobial agents for the control of microbial infection. Antimicrobial properties have been confirmed for metallic nanoparticles and metal oxide powders [15]. The inorganic materials can be used in different forms, such as powders coated on cellulose fibers, or as a part of organic/inorganic composite [16, 17]. The potential application of inorganic antimicrobial agents are leading the way because of their safety and stability,
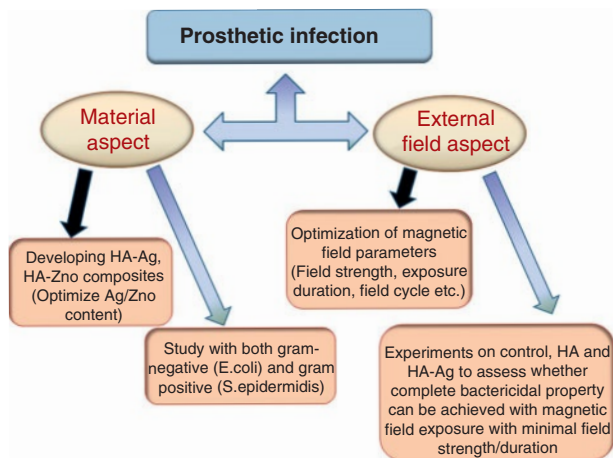
Figure 7.2 Different aspects for preventing prosthetic infection, illustrating two development approaches: the development of new biomaterial and the application of external field.

as compared to organic antimicrobial agents [18, 19]. At present, most reported antibacterial inorganic materials are ZnO, TiO_2, CuO, MgO, CaO, Fe_3O_4 and Ag_2O, as well as metals like Ag and Cu [20]. However, few studies have shown quantitative evaluation of the antibacterial activity of these materials [18, 21].

This chapter starts with characteristics of bacteria, including structure of cell wall, different types of proteins, growth and adhesion behavior, interaction with biomaterial surface and factors influencing its adhesion. After the detailed description on bacteria cells, the chapter addresses the synthetic biomaterials with microbial property, such as glass ceramic, HA–Ag/HA–ZnO composites and magnetic biocomposites, etc. After discussing the material aspect to preventing prosthetic infection, the chapter focuses on the influence of external field on bacterial adhesion and biofilm formation, where the effect of both electric as well as magnetic fields was reported. The chapter closes with some comments on the work regarding prosthetic infections.

7.2 Characteristics of Prokaryotic Cells

Bacteria are a group of unicellular microorganisms of procaryotic cells with typical diameter size of 1–2 µm [22]. In the procaryotic cells, all the intera-cellular material like genetic material (DNA) is not bound by membrane and spreads anywhere in the cytoplasm of cells. No nuclear membrane

exists in prokaryotic cells like in eukaryotic cells [23]. Characteristically, procaryotic cells consist of three main regions, a) flagella and pili (made up of surface proteins); b) cell wall and plasma membrane; and c) cytoplasm [24]. A typical structure of bacteria is shown in Figure 7.3 [25].

Flagella are found on the bacterial cell surface and consist of filamentous protein, and such flagellum is attached to rotating motor apparatus connected to the plasma membrane [24]. Bacteria swim in the fluid with the movement of flagella motorized through chemiosmotic potential [26].

Pili are composed of proteins and are very thin and shorter in length compared to flagella, so they appear like hairs on the cell surfaces. The key role of these pili (fimbriae) is to help in adhesion on the substrate surfaces [27]. On the basis of cell shape, bacteria are grouped in almost three categories: rod (*bacillus*), sphere (*coccus*), or spiral (*spirilla* and *spirochetes*), although rod shaped bacteria, which are curved, are called *vibrios* (Figure 7.4) [24].
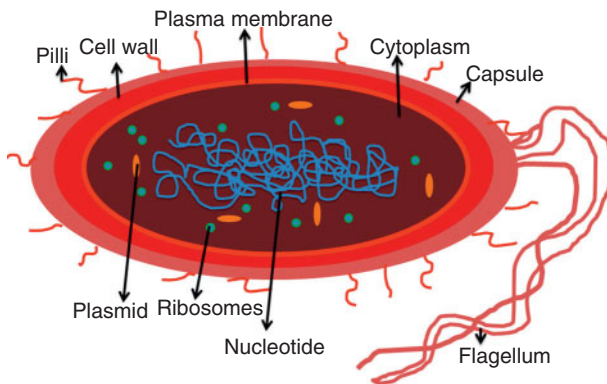
Figure 7.3 A typical structure of prokariotic cell (adapted from ref. [25]).
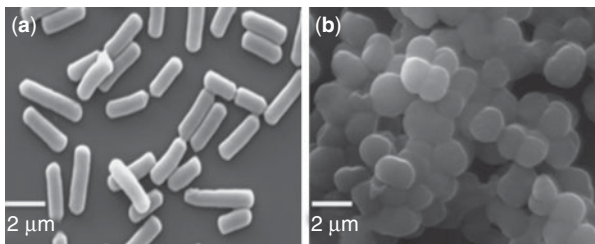
Figure 7.4 The morphology of different types of bacteria: (a) *Escherichia coli* (unpublished image), (b) *S. aureus* (unpublished image).

7.2.1   Architecture of Bacterial Cell

Prokaryotic cells have several distinct surface layers that are briefly mentioned below.

Capsules: If the high molecular weight polysaccharides film deposits strongly on the cell wall, it is called a capsule, and otherwise, it is known as an extracellular material slime. The main function of these layers is to avoid phagocytosis [28].

Cell wall: Gram staining classifies bacteria on the basis of different cell wall structures. A class of bacteria that are stained by gram stain are named as gram positive bacteria and the rest are known as gram negative bacteria. The gram strain reacts with the peptidoglycane layer of bacteria and produces a crystal violet color [29]. The peptidoglycane layer is comparatively thick and peripheral to the cell wall in gram–positive bacteria. Whereas, this layer is very thin in gram–negative bacteria and is located inbetween the inner membrane and outer membrane [30, 31]. The difference in cell wall of both gram positive and gram negative bacteria is shown in Figure 7.5. Other important constituents of the cell wall include the following:

Peptidoglycan: Peptidoglycane is a long strand of alternating polymer of N–acetylmuramic acid (NAM) and N–acetylglucosamine (NAG) [32]. Highly–thick and crosslinked peptidoglycan layer is present in gram–positive cells, while it is very thin in gram–negative cells. The peptidoglycan layer is the main target of antimicrobial activity [33].
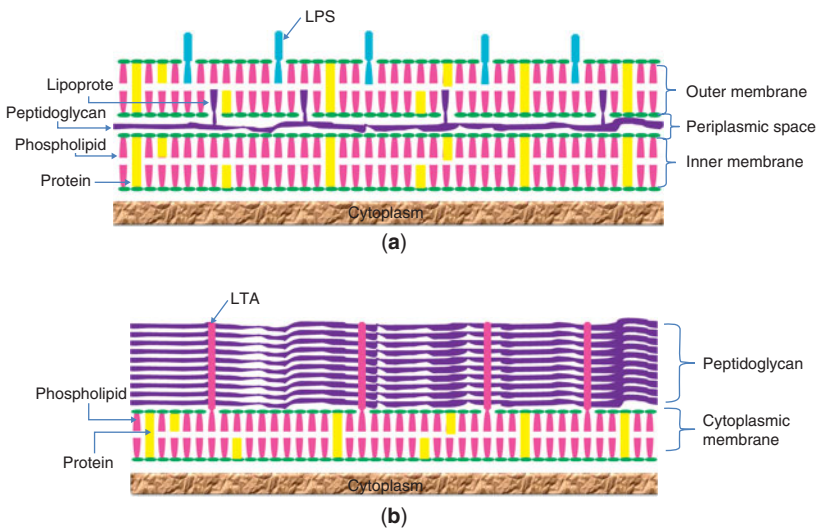
Figure 7.5 Cell wall structure of (a) gram–negative, and (b) gram–positive bacteria (adapted from ref. [23]).

Lipoteichoic acids: In lipoteichoic acids (LTA), polysaccharides lengthen through the peptidoglycan layer and come out on the cell surface [34]. Only gram–positive bacteria have these LTA structures which work like antigenic determinants [35].

Lipopolysaccharides: The lipopolysaccharides (LPS) are present on the cell surface of the gram–negative bacteria and are connected to the outer membrane of the bacteria by lipid molecules [36].

Bacterial growth: Bacteria growth is similar to eukaryotic growth in which a single cell divides into two daughter cells; this process is known as binary fission of the cells (Figure 7.6). During the division process chromosomal DNA duplicates, followed by inward growth of the bacterial membrane and cell wall, and finally a mother cell divides into two daughter cells [7]. Bacteria have their usual habit to form a colony on the substrate. The colony of *E.coli* bacteria is shown in Figure 7.7, where the substrate is the gelatine–coated glass control.

Bacteria just after division

Bacteria in division state

2 μm
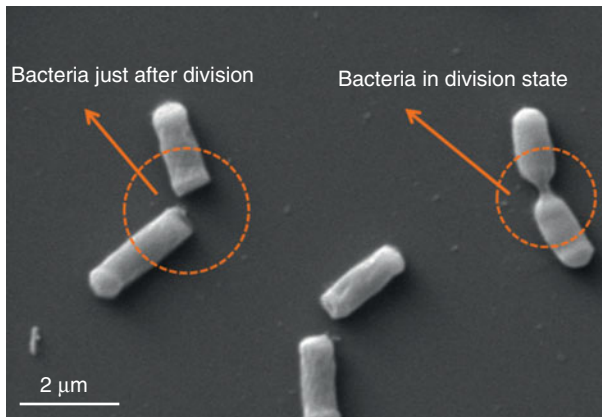
Figure 7.6 SEM image revealing binary fission of *E.coli* bacteria after growing on a tissue culture glass control surface (unpublished image).

20 μm

10 μm
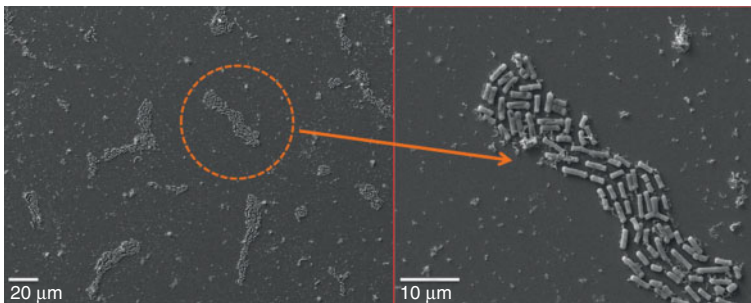
Figure 7.7 SEM images to illustrate colony formation of *E.coli* on glass substrate (unpublished image).

One of the important characteristics of bacteria is their *generation time (G),* the doubling time for a prokaryotic population. In general, G is different for different types of microbials and most of the bacteria have the generation time of approximately 30 minutes to three hours [37]. Certain bacteria, for example, *Escherichia coli,* have very short generation times of 20 mins under optimal conditions. The bacterial population follow the exponential growth curve. The generation time of the cells can be calculated by the following formula:

$$G = t/2.3\log(b/B) \tag{7.1}$$

Where G is generation time, t is culture time, B is number of cells at the beginning of culture and b is number of cells at the end of culture [23].

7.2.2   Bacterial Growth Behavior *In Vitro*

The bacterial growth curve is comprised of four phases known as lag phase, log phase, stationary phase and, finally, death phase [23]. The characteristic growth curve is shown in Figure 7.8, where logarithms of the actual numbers in the population are plotted along the Y– axis and the incubation time is plotted along the X–axis.

In the **lag phase**, the population remains constant and no cell division occurs [24]. When cells are transferred into the new culture medium they take some time in physiological adaptation rather than directly going into the division phase. After the lag phase of growth curve, cells come into the **log phase** during which binary fission occurs, and this corresponds to the exponential growth of bacteria up to the optimal level. During the next phase, i.e., the **stationary phase**, cells stop division, but do not start dying, and the number of cells remains constant. The last phase is the
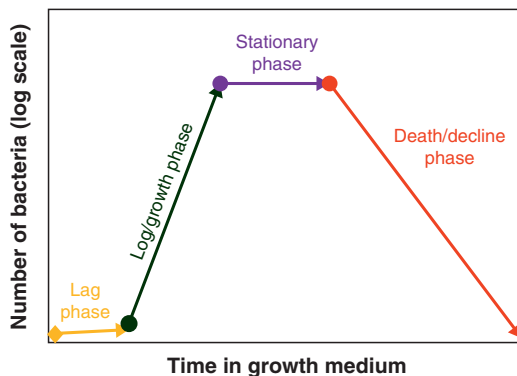
Figure 7.8 Typical illustration of growth behavior of bacteria in growth medium in vitro (adapted from ref. [24]).

death phase which arises because of accretion of waste near the cell, the dearth of nutrients in the growth medium, and the detrimental environmental conditions which results in the rapid death of cells [7].

7.2.3   Bacterial Adhesion and Biofilm Formation

The prokaryotic cells also have a tendency to adhere on biomaterial substrate [29]. After adhesion they proliferate to form cell clusters on the material surface, as shown in Figure 7.9. A mass of bacterial cells along with their extracellular material (slime) is called biofilm [38]. Only a limited number of bacteria can be accumulated in a established biofilm, other excess adherent bacterial cells get away from the slime layer and form new colony on another place of the substrate material [39]. In a study it was reported that some bacterial strains that do not generate slime are found comparatively less adherent and therefore less harmful for humans [32]. Slim layers work as a shield for bacteria *viz.* protection against phagocytosis, antibiotic effects and high flow conditions [40]. The immune system can easily kill the bacteria that are less susceptible to the adhesion on surface. Many slime–generating bacteria developed antibiotics resistance after adhering to the biomaterial surface [41]. Prosthetic infection occurs when a bacterial population defeats the local host defense system [42].
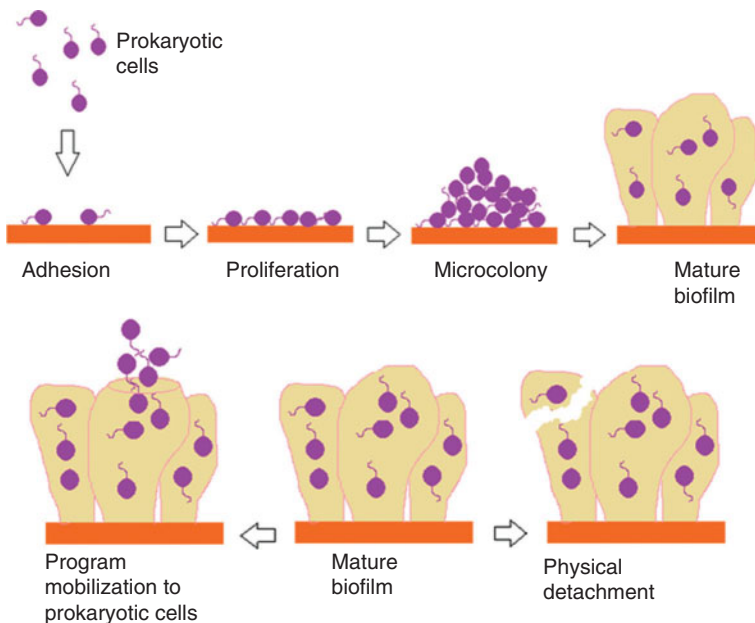
Figure 7.9 Schematic illustration of various stages in bacterium biofilm formation (adapted from ref. [43]).

7.2.4   Physicochemical Interactions between Bacteria and Surfaces

Adsorption and attachment are the primary steps for bacterial adhesion to surfaces [44]. Generally, bacterial cells choose solid surfaces on which to proliferate instead of surrounding growth liquid medium. Bacteria initially adhered to the biomaterial surface through physical interactions like long–range interaction (nonspecific, distances > 50 nm) and were further attached by the short range (distances < 5 nm) [45]. After this initial attachment, bacteria makes chemical bonds with the surface proteins [46].

After the physicochemical interactions between bacteria and biomaterial surfaces, molecular–specific reactions become predominant for adhesion. The bacterial adhesion on biomaterial surface becomes stronger by the selective–bridging function of the capsules, fimbriae and slime [47]. Bacteria has polysaccharide strands that mediate in the attachment to various biomaterial surfaces [48]. Also, bacteria have different types of surface proteins (for example, *S. aureus* with fibronectin) [49]. The interaction between bacteria and biomaterial is illustrated in Figure 7.10.

7.2.4.1   Factors Influencing Bacterial Adhesion

Bacterial adhesion is an extremely complicated process that is affected by many factors including the culture environment, surface chemical composition, surface roughness and bacterial characteristics, etc. These factors are briefly explained below.

7.2.4.1.1   Culture Environment

Environmental factors that affect the bacterial adhesions are temperature, bacterial population in growth medium, duration of culture, antibiotics concentration in growth medium and associated flow conditions [9]. Flow conditions highly affect the attached bacterial population as well as the biofilm arrangement and performance [50]. Higher shear rates are
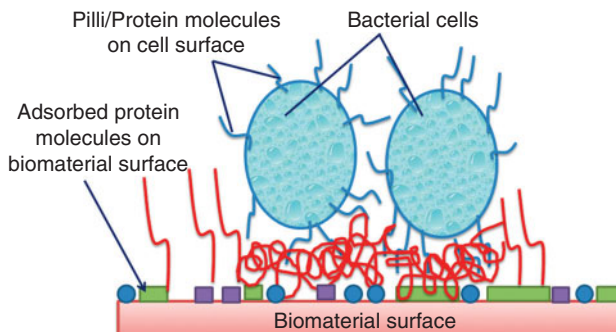
Figure 7.10 Illustration of the interaction of bacterial cells on biomaterial (adapted from ref. [9]).

considered to be responsible for reducing the bacterial attachment on the surface [51].

The bacterial adhesion depends on shear stresses [52]. In a study, it is reported that shear stress of 0.5 pN mm^{-2} increases *E. coli* accumulation and a lack of shear might cause bacterial detachment [53]. Bacterial adhesion is also very sensitive to the antibiotics and, hence, the bacterial susceptibility and antibiotic concentration will influence the adhesion [54]. In most of the studies, it is reported that the antibiotic treatment is less effective for adhered bacterial cells than nonadherent cells, because bacterial cells alter their metabolism and formulate resistance towards unfavorable conditions [55].

7.2.4.1.2   Surface Chemical Composition

The surface chemical composition plays a very important role in the bacterial adhesion and proliferation process. Surface charge of the biomaterial depends on the functional group. And this generated charge influences hydrophobicity of materials. Therefore, chemical bonds affect the bacterial adhesion on substrate surface. Surface modification with different types of materials, like ZnO and Ag, reduces the bacterial adhesion, and surface modification with bioactive material, like hydroxyapatite, enhances the bacterial adhesion [56].

7.2.4.1.3   Surface Roughness

Bacteria prefer to adhere and proliferate on irregular biomaterial surfaces rather than ultra–smooth surface. More surface area on the roughened surfaces may attract the cells for colonization. For example, polymethylmethaacrylate amplify bacterial adhesion when surface roughness is slightly increased [57].

7.2.4.1.4   Surface Configuration

Bacterial infection is reported to be more prominent in porous implants than in dense scaffold. Therefore it can be concluded that porous surface promotes bacteria adhesion. Pores have higher surface area than the flat surface, and bacteria prefer to enlarge their contact with surface. Moreover, bacteria move towards grooves and adhere to increase their contact area with surface, but if pore sizes are much bigger than the cell size the bacteria may drift toward flat surface rather than irregular surface [58].

7.2.4.1.5   Bacterial Characteristics

Bacterial adhesion not only depends on substrate characteristics and environmental conditions, but is greatly influenced by their own physicochemical characteristics. Some important bacterial characteristics are discussed below.

Bacterial hydrophobicity: It is well known that bacteria with hydrophobic surface characteristics prefer to adhere on hydrophobic material surfaces. Shear stress greatly influences the bacterial adhesion on surface [9].

The shear stresses in the range of 0–8 dyn/cm² showed more adhesion of *S. epidermidis* with higher hydrophobicity. This effect on adhesion with different hydrophobicity was found to be less prominent when the shear stresses increase. The bacterial surface hydrophobicity was found to be ineffective for adhesion at the shear stress of more than 15 dyn/cm² [59].

Bacterial surface charge: Cells acquire charge on their surface. Some bacterial species contain positive charge and some contain negatively–charged surfaces because different types of bacteria have different surface chemical structure. Cell surface charge may alter according to the age of bacteria. Cells may alter their surface charge in growth medium corresponding to pH and charged ions of the culture medium [9]. Cell surface charges play a dominant role in adhesion on biomaterial surface [60].

7.2.4.1.6 Tissue Proteins (Serum)

Bacterial adhesion vastly depends on serum proteins. The effect of some important proteins, like albumin, fibrinogen and thrombin, is discussed below. Generally, serum proteins are attached to the cell surface through the specific receptor–ligand interactions [9].

Albumin: In most of the studies, polymer, ceramic and metallic biomaterial surfaces coated with albumin are reported to inhibit bacterial adhesion on surface. The cause of this inhibitory effect of albumin was suggested to enhance hydrophilicity of albumin–coated surfaces [9].

Fibrinogen: It is one of the important factors for the adhesion of bacteria. *Staphylococci* adhesion is found to be higher on fibrinogen absorbed surfaces [61].

Platelets: In a study, it was found that the contact–activated platelets mediate *bacterial* adhesion to the polyethylene substrate instead of absorbed plasma proteins, because the adhesive coefficient to the protein–adsorbed polyethylene surface was notably lower as a minimum one order of magnitude than to the platelets [62]. In another study, the adhesion of *S. aureus* was found to be around 30–fold higher for platelets compared to albumin–PMMA [63].

7.2.5 Synthetic Biomaterials with Microbial Resistance Property

Hydroxyapatite $(Ca_{10}(PO_4)_6(OH)_2)$ is one of the extensively used hard tissue replacement material because of compositional similarity with natural bone, good biocompatibility and its ability to facilitate strong biological bond with bone [64]. On the other hand, poor mechanical properties of monolithic HA like low fracture toughness (< 1 MPa m$^{-1/2}$) do not enable it to endure the normal operating loads of bones or joints [65]. Importantly, hydroxyapatite (HA) lacks antibacterial property. Implant–associated infections are serious and widespread

complications in orthopedic surgery, and the problem usually leads to removal of the implant [66]. The artificial implants in the body obstruct the host defence mechanism and win over the dose of antibiotics [66– 68]. Therefore, a high dose of antibiotics is crucial to avoid such prosthetic infections, but higher concentration of antibiotics enhances side effects in body [66]. Hence, it is preferable that the implant itself have antibacterial properties to reduce the chances of infections.

7.2.5.1   Glass–Ceramics

Many studies have reported the response of interaction of bioactive ceramics with microorganisms [69]. The studies showed that microbial–induced degradation occurred *in vitro* and the presence of bacteria increases the levels of calcium in the growth media [66]. Infection is harmful for the host as well as for the implant itself [63]. Proteins of the growth medium are easily absorbed on the HA surface, resulting in a suitable environment for bacterial adsorption and proliferation [70]. The silver particles with HA coating were also found to exhibit admirable antimicrobial property. Silver is a ductile metal, so when it is reinforced in brittle HA matrix, it stops the crack propagation by crack–bridging mechanism. Silver reinforcement shows the elastoplastic stretching along the crack wake, thereby increasing the toughness and strength of composites [69]. Therefore, metallic (Ag/Ti, etc.) or ceramic (Al_2O_3, ZrO_2, mullite, etc.) particulates are commonly incorporated in HA matrix. In addition to the potential for improvement in mechanical properties, silver provides advantageous biochemical inertness and an antibacterial effect [69, 71].

It is found that a specific glass ceramic composition exhibits good antimicrobial property for both gram positive and gram negative bacteria. Kalmodia *et al.* reported the *in vitro* cellular and antimicrobial response of SiO_2–MgO–Al_2O_3–K_2O–B_2O_3–F glass ceramics (GC) having fluorophlogopite crystalline phase as a major constituent. Fluorine and boron content in base glass affects the cytocompatibility and antibacterial property. The cellular morphology of mouse fibroblast L929 cells shown in Figure 7.11 exhibit cytocompatibility of GC substrate. In this work it is also reported that lower fluorin content in GC enhances the osteoconduction and viability of eukaryotic cells [72]. The mechanical properties obtained with SiO_2–MgO–Al_2O_3–K_2O–B_2O_3–F glass ceramic are summarized in Table 7.1.

It is found that a specific glass ceramic composition exhibits good antimicrobial property for both gram positive and gram negative bacteria. Also, the glass ceramic, with higher fluorine content has less quantified antimicrobial property (84% CFU/ml in M3 vs 77% CFU/ml in M2). It appears that a higher amount of SiO_2 in glass ceramic suppresses the beneficial effect of F⁻ as far as bactericidal effect is concerned, as fewer numbers of bacteria appear to adhere on glass ceramic with higher florin content (see Figure 7.12) [72].
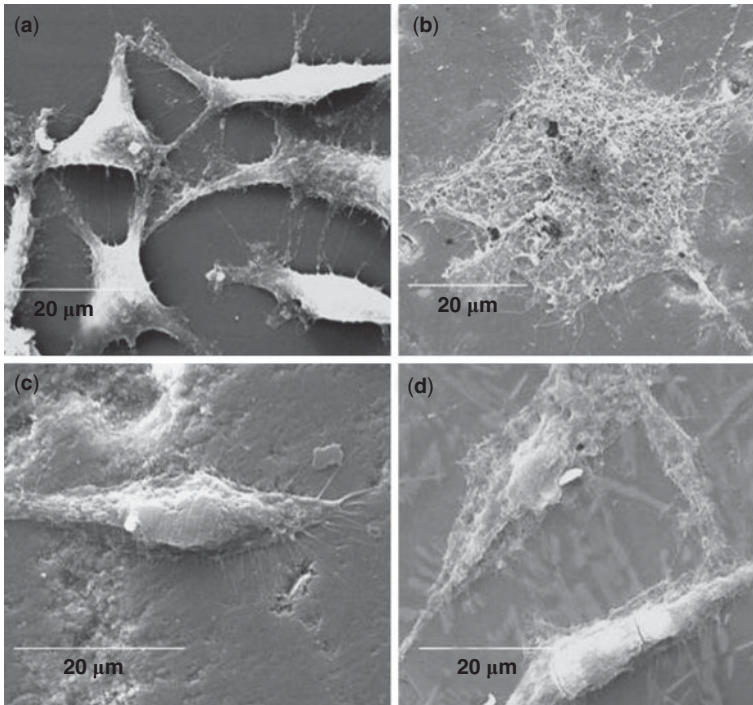
Figure 7.11 Scanning electron micrographs of L929 mouse fibroblast cells grown on (a) Control, (b) M1, (c) M2 and (d) M3 glass ceramic samples. The microspikes and filipodium are formed on the M1 surface, whereas M2 and M3 show lamellipodia. Table 7.1 mentions the glass ceramic composition [72]. (With permission from Springer Science+Business Media)

Table 7.1 Compositions of base glass (in wt%) [72, 73].

Starting Materials	Precursor Constituent	M1	M2	M3
Quartz Powder	SiO_2	47.98%	48.94%	42.57%
White Tabular Alumina	Al_2O_3	17.62%	16.29%	17.81%
MgO powder	MgO	19.36%	17.45%	18.80%
K_2CO_3	K_2O	8.25%	7.15%	7.81%
Boric Acid (H_3BO_3)	B_2O_3	5.17%	5.25%	10.02%

Table 7.1 (Cont.)

Starting Materials	Precursor Constituent	M1	M2	M3
NH_4F/MgF_2	F^-	1.08%	3.85%	2.53%
Hardness, GPa		8.2 ± 1.5	6.4 ± 1.2	4.9
Flexural Strength (three point)		94.9 ± 14.0 3	80.6 ± 7.7	
E–modulus, GPa		57.6 ± 2.8	69.7 ± 2.9	
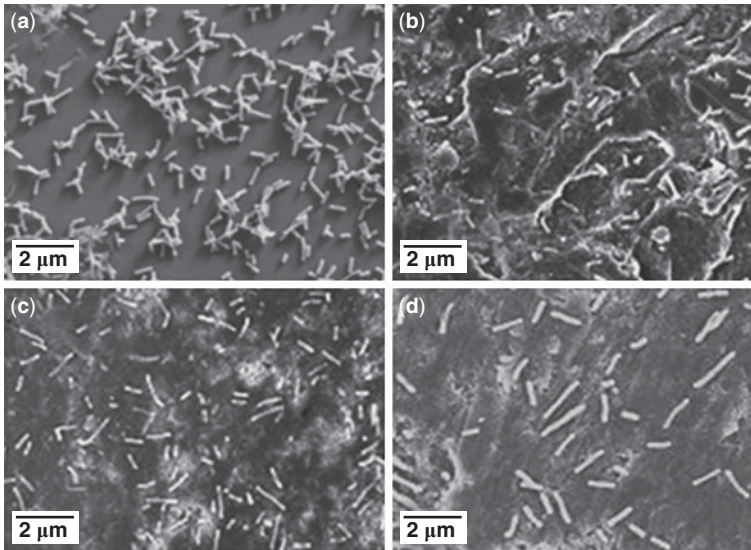
Figure 7.12 SEM images of the *Escherichia coli* bacteria after 4 h of incubation on (a) Control, (b) M1, (c) M2 and (d) M3 glass ceramic samples [72]. (With permission from Springer Science+Business Media)

7.2.5.2   HA–based Biocomposites with Bactericidal Property

Nath *et al*. reported the mechanical and antimicrobial property of mechanically mixed HA–10 wt% Ag composite, sintered at 1200°C in pressureless sintering. The overall cell attachment, cellular bridge formation and cell proliferation behavior of L929 mouse fibroblast cells on HA–10 wt% Ag does not cause any significant difference in reference to pure HA. The combined result of alkaline phosphatase activity and osteocalcin expression

indicates that HA–10 wt% Ag composites reveal comparable/better bone cell differentiation and better bone mineralization property than single phase HA. This HA–10 wt% Ag composite provides excellent bactericidal property against *E.coli* bacteria without compromising the *in vitro* cytocompatibility property of HA (Figure 7.13) [74]. In another study, silver–doped hydroxyapatites $Ca_{10-x}Ag_x(PO_4)_6(OH)_2$ ($0.0 \leq x \leq 0.5$), sintered at 1200°C for 2 hours shows good antibacterial property, but MTT results of L929 fibroblast cells cultured for 3 and 5 days show the cytotoxicity, when $x > 0.3$ [75].

Among metal oxide powders, ZnO has already been studied extensively and it demonstrates significant growth inhibition of a broad spectrum of bacteria. It is suggested that ZnO generates reactive oxygen species (ROS) in presence of water and oxygen. This ROS reacts with bacterial cells and kills the bacteria by damaging their cell membrane (Figure 7.14). The production of H_2O_2 is explained by the following set of equations [76].

$$ZnO + hv \rightarrow e^- + h^+$$
$$h^+ + H_2O \rightarrow {}^\bullet OH + H^+$$
$$e^- + O_2 \rightarrow {}^\bullet O_2^-$$
$${}^\bullet O_2 + H^+ \rightarrow HO_2^\bullet$$
$$HO_2^\bullet + H^+ + e^- \rightarrow H_2O_2 \tag{7.2}$$
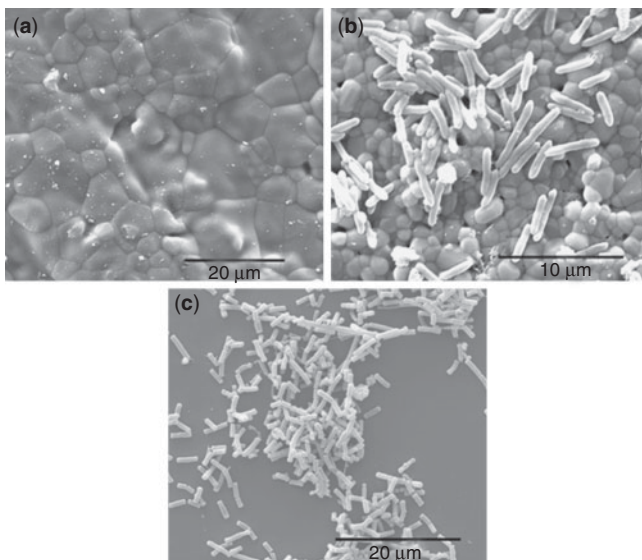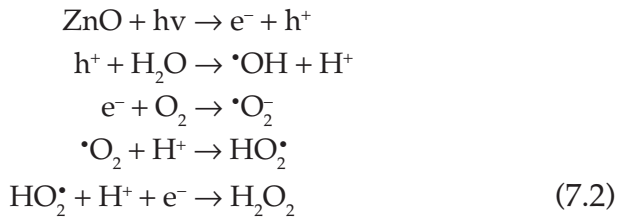
Figure 7.13 SEM images revealing *E.coli* bacterial cell adhesion on substrate: (a) HA–10 wt% Ag composite (sintered at 1200°C), (b) pure HA (sintered at 1200°C) and (c) negative control polymer disc after 4 hours of inoculation [74]. (With permission from Springer Science+Business Media)

Water enters inside   Bacterial cell is destroyed
the bacterial cell
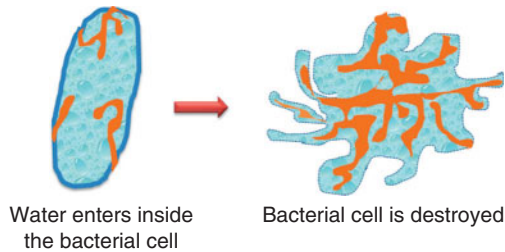
Figure 7.14 Schematic illustrating the cell membrane damage through ROS [75].

The generated negatively–charged ions touch the cell surface, therefore, hydroxyl ions and superoxides cannot enter into the cell membrane to generate any toxicity. However, H_2O_2 can go through the cell membrane and cause toxicity [20]. In view of the fact that the radical formation takes place on the surface of particles, antibacterial activity will be higher for particles with greater surface area. Therefore, smaller–sized ZnO particles reveal enhanced antimicrobial property [78, 79]. Available literature suggests that ZnO is cytocompatible up to a certain concentration. According to Atsuo *et al.*, MC3T3–E1 cells cultured on Zn–TCP/HA composite proliferated without any cytotoxic effect up to a zinc content of 1.20 wt%, while releasing zinc up to a concentration of 3.53 mg/L. Also, Zn^{2+} stimulates the alkaline phosphate activity and bone protein synthesis [80]. Bandopadhyay *et al.* synthesized the HA–ZnO and TCP–ZnO composites with a varying concentration of ZnO from 0.5 to 3.5 wt%, and reported cytotoxic response to OPC1 human osteoblast cells over 1.5 wt% ZnO concentration. Both TCP and HA samples showed good cell attachment after 5 days in culture for up to 1.5% ZnO doping [81].

Saha *et al.* prepared different composites of HA and ZnO with varing content of ZnO (5–30 wt%), and they optimized the composition showing good antimicrobial property along with good cytocompatibility. In order to investigate the antibacterial property of different HA–ZnO composites, *E. coli* and *S. aureus* were cultured for 4 hours on these composites. In order to assess the cytotoxity of HA–ZnO composites, human osteoblast–like SaOS2 cells and mouse fibroblast L929 cells were cultured. The results show that the antibacterial property increases with the increased content of ZnO in the HA–ZnO composites (Figure 7.15). It was concluded that HA with lower than 10 wt% ZnO is cytocompatible with good bactericidal property. Figure 7.16 shows the antibacterial and cytotoxic effect of HA–20ZnO for *E.coli/S.aureus* and human osteoblast–like SaOS2 cells, respectively. Florescence microscopy images in Figure 7.17 show the cytocompatibility of human osteoblast–like SaOS2 cells on different HA–ZnO composites [82, 83]. After comparing the antibacterial and cytotoxic effect of different HA–ZnO composites, it is concluded that HA
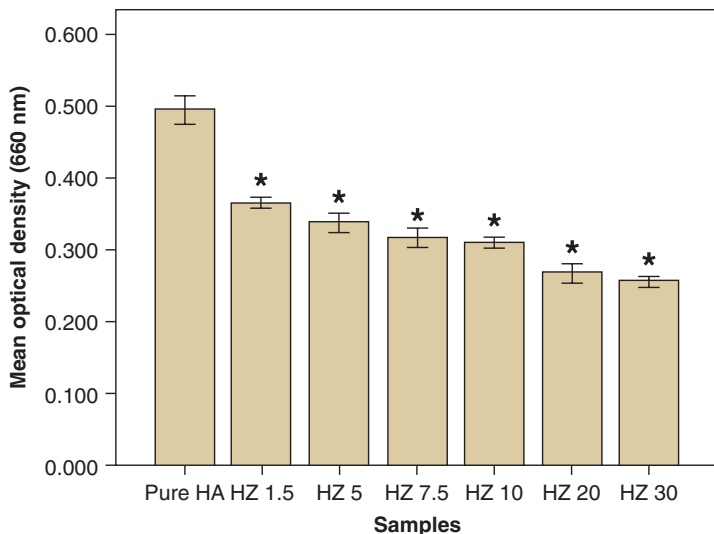
Figure 7.15 Mean optical density data after 4 h of incubation of *E. coli* bacterial on Pure HA, HZ 1.5, HZ 5, HZ 7.5, HZ 10, HZ 20, and HZ 30 powder samples. * Represents significant difference at $p < 0.05$ with respect to pure HA and error bars correspond to ±1.00 SE [82]. (With permission from John Wiley and Sons)

with lower than 10 wt% ZnO is cytocompatible with good bactericidal property.

7.2.5.3 *Nanoparticles Treatment to Reduce Bacterial Infection*

Iron oxide (IO) have attracted the interest of researchers because of its biocompatibility as well as magnetic properties [84]. It is hypothesized that iron oxide nanoparticles could kill bacteria without showing any cytotoxicity in eukaryotic cells via reactive oxygen species (ROS) [85]. It is reported that 4.25 mg/mL concentration of iron oxide nanoparticles show better osteoblast cell density than the cells cultured in iron oxide–free growth medium [86]. Taylor *et al.* reported the concentration dependent bactericidal effects of magnetic IO nanoparticles on *S. epidermidis*. The CFU of *S. epidermidis* was found to gradually decrease after 12, 24, and 48 hours incubated with 100 µg/mL, 1 mg/mL, and 2 mg/mL concentration of IO nanoparticles, respectively [87]. It is suggested that ROS can cause damage to proteins and DNA in bacteria [88]. The generated H_2O_2 consequently reacts with ferrous irons through the Fenton reaction and produces hydroxyl radicals, which are recognized to damage biological macromolecules [85]. Tran *et al.* reported the dose–dependent antibacterial effect of polyvinyl alcohol (PVA)–coated iron oxide nanoparticles for *S.aureus* via live/dead assay. The inhibitoriest effect of iron oxide for *S.aureus* is observed at highest concentration (3 mg/mL) [12]. Ferrofluids have good colloidal stability and
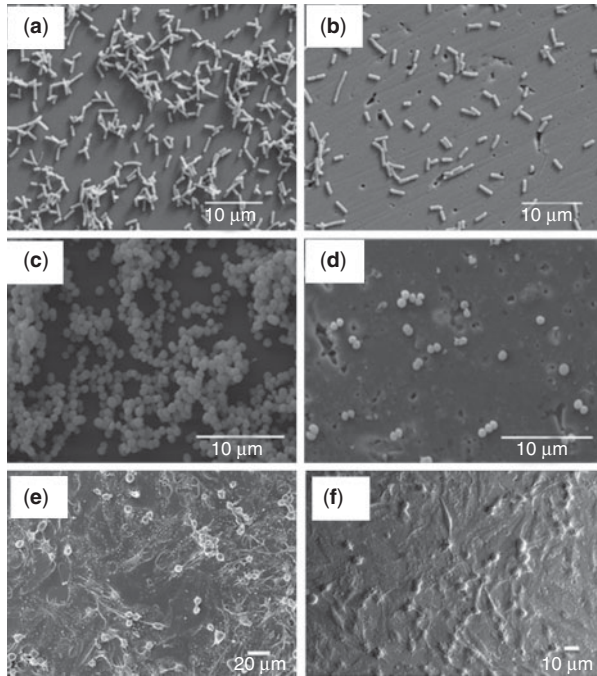
Figure 7.16 SEM images of *E.coli* bacteria adhered on (a) control (b) HA–20 wt% ZnO, *S. aureus* bacteria adhehered on (c) Control (d) HA–20 wt% ZnO and Human Osteoblast–like cells SaOS2 on (e) control, and (f) HA–20wt% ZnO samples [82, 83]. (With permission from John Wiley and Sons)
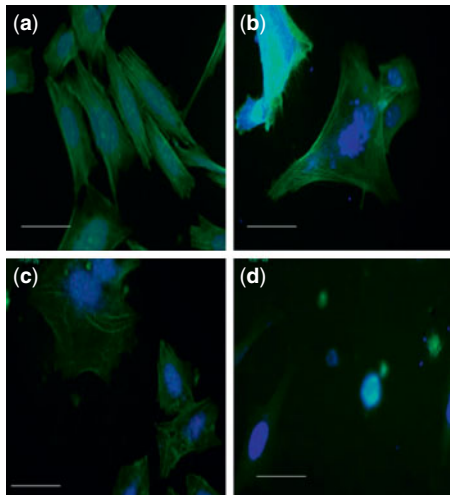
Figure 7.17 Fluorescence microscopic images of SaOS2 human osteoblast–like cells adhered on (a) Control (b) pure HA (c) HZ10 (d) HZ20, after 72 hrs of culture (micron bar = 50 μm) [83]. (With permission from John Wiley and Sons)

may be stored for long periods of time as an aqueous suspension lacking agglomeration, yet, they do not reveal significant antibacterial properties [89]. It is reported that iron oxide particles work as Fenton's reagent (Fe^{2+}/Fe^{3+} in solutions), where iron oxide particles react with hydrogen peroxide and turn out hydroxyls as well as peroxide radicals [90].

Gupta *et al.* reported the reduction of cytotoxicity and improved cellular uptake of superparamagnetic iron oxide nanoparticles (SPION) of average size (13.6 nm) by surface modification with pullulan (Pn). The average particle size of Pn modified SPIONS was found around 42 ± 2.5 nm. Cell culture was carried out with infinity telomerase–immortalized primary human fibroblast cells (hTERT–BJ1). Figure 7.18 shows a dose–dependent toxicity of SPION–treated cells incubated for 24 h. Cell viability was reduced up to 80% of control at the 0.05 mg/ml concentration of SPION, and such reductions increase at higher concentrations. Pn–SPION exhibited ~ 92% cell viability even at highest concentration (2.0 mg/ml). The results of cell culture experiments have indicated that cellular uptake of SPIONs can be enhanced by its surface modification with pullulan, which is noncytotoxic. In particular, pullulan was internalized by cells via a different route than the SPION endocytosis. Pullulan modified iron oxide nanoparticles are therefore suggested for imaging of target imaging [91].

Dalai *et al.* reported the influence of light (UV–illuminated) on the toxicity of TiO_2 nanoparticles (50–200 nm) at concentration of 0.05 µg/mL to 1µg/mL for *Bacillus licheniformis* bacteria. The dose–dependent decrease in the bacterial cell viability was found by standard plate count and MTT assays; such a decrease was found unaffected in the presence of light for low concentration and 2 h exposure. Intracellular ROS generation, an important cause of cell death, was found to be significantly increased when bacteria were incubated with TiO_2 nanoparticles under the light.
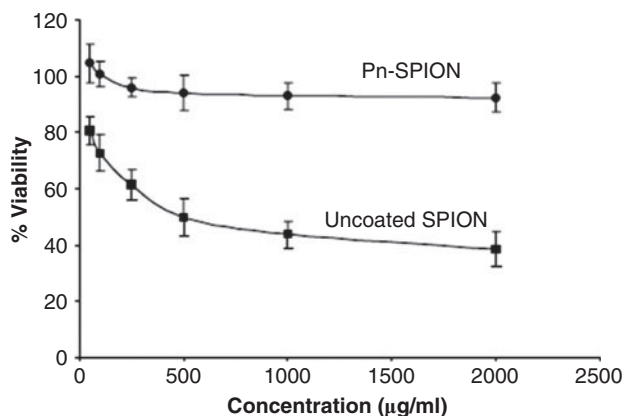
Figure 7.18 Cytotoxicity profile of SPION and Pn–SPION when incubated with human fibroblast as determined by MTT assay [91]. (Copyright (2013), with permission from Elsevier)
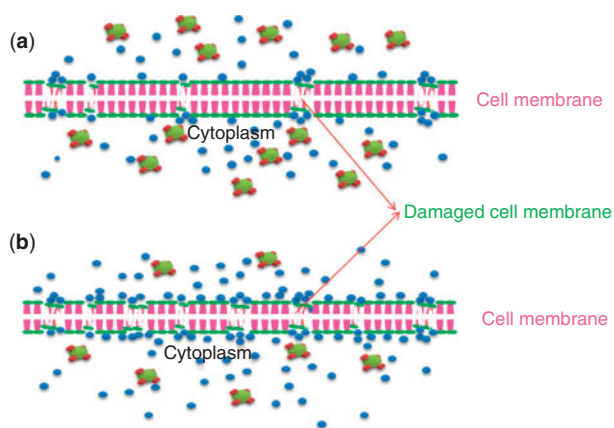
Figure 7.19 Schematic illustration of proposed TiO_2 nanoparticle–induced toxicity mechanisms in *Bacillus licheniformis* bacteria under (a) light and (b) dark conditions, ● represents TiO_2 nanoparticles and 🌟 represents generated ROS (adapted from ref. [92]).

The attachment of nanoparticles on cell wall is also responsible for membrane damage, and a significantly higher concentration of nanoparticles were attached on bacteria under dark condition, causing higher membrane damage. The toxicity was found to be treatment dose and duration–dependent. The difference in the mechanism of nanoparticle interaction with bacterial in presence of light and in dark condition is schematically represented in Figure 7.19 [92].

7.2.5.4   HA–based Magnetic Biocomposites

Hyperthermia therapy for cancer treatment with the use of magnetic biomaterials can be a prospective treatment alternative. For the treatment of bone tumor, the diseased tissue is surgically removed, and thus, bone graft material is implanted in created bone defect region for treatment [93]. It is reported that heat, produced by magnetic biomaterial, can be utilized for treatment of cancer because magnetic scaffold will generate localized heating inside the tumor when exposed to magnetic field [90]. Cancer cells are reportedly killed in the temperature range of 43–46°C, whereas normal cells remain unaffected at these temperatures [94]. Although implants with magnetic properties have been shown successful in treatment of the bone defect, the cure of malignant bone tissue and the restoration of large bone defects still present major clinical challenges [95]. A number of magnetic biomaterials, such as magnetic Ca/P–based materials, bioactive glass ceramics, ferrimagnetic calcium phosphate glass–ceramics, are reported [95–100].

Ajeesh *et al*. reported the cytocompatibility and enhanced radiopacity of different composites of magnetic iron oxide and HA. Here, the results were compared between the HA–based composites containing Fe_3O_4 with that

containing Fe_2O_3. All prepared samples were found to retain high X–ray opacity. The results of *in vitro* biomineralization studies and MTT assay depict a better bioactivity of hematite phase compared to the magnetite phase of iron oxide. The cytotoxicity study also reveals that up to 40 wt% iron oxide (hematite) in HA is not detrimental to the osteoblast cell activity [101].

Eniu *et al.* reported the magnetic properties of $CaO–P_2O_5–SiO_2–Fe_2O_3$ glass–ceramics sintered at 1500°C. These glass samples exhibited the ferromagnetic behavior with saturation magnetization ~ 8 Gscm^3/g after heat treatment at 1100°C. The main contributors to magnetization are found to be iron ions from magnetite Fe_3O_4, along with an additional contribution from $\gamma–Fe_2O_3$ (maghemite). Also, the EPR studies indicated the presence of low–sized magnetic domain of iron ions in glass samples [102].

Wu *et al.* developed a multifunctional mesoporous bioactive glass (MBG) scaffold that is suggested for both hyperthermic as well as local drug delivery applications [95]. They prepared three MBG–Fe (MBG, MBG–5Fe and MBG–10Fe) scaffolds with a highly porous structure of large pore size (300–500 μm) and fingerprint–like mesopores (4.5 nm), as shown in Figure 7.20.

The MBG scaffolds enclose a well–organized mesoporous structures with straight channels (pore size about 5 nm), while MBG–5Fe and MBG–10Fe scaffolds contain built–in curved channels with fingerprint–like mesopores of size around 4.5 nm. Mechanical properties were not found to be influenced by the addition of Fe into the prepared MBG scaffolds. The MBG, MBG–5Fe and MBG–10Fe scaffolds revealed the compressive strengths 50 ± 4.7, 48 ± 2.5 and 46 ± 5.4 kPa, respectively. In contrast, the MBG–10Fe scaffolds had a well–developed hysteresis loop compared to
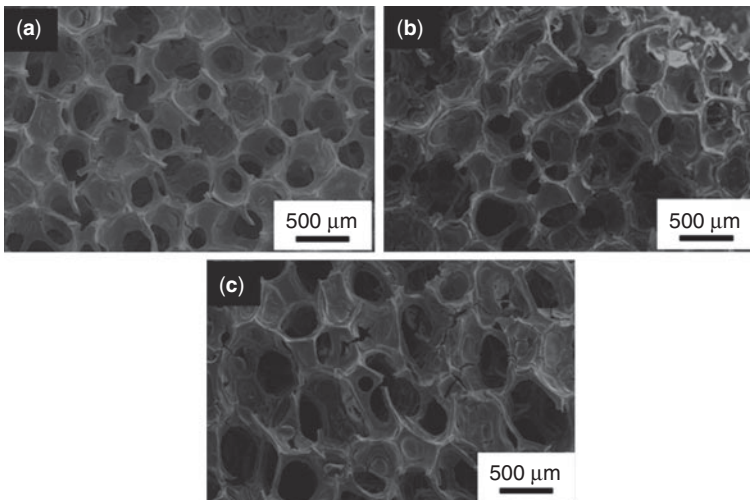
Figure 7.20 SEM analysis for the MBG scaffolds with different Fe contents. (a) MBG; (b) MBG–5Fe; (c) MBG–10Fe [95]. (Copyright (2013), with permission from Elsevier)
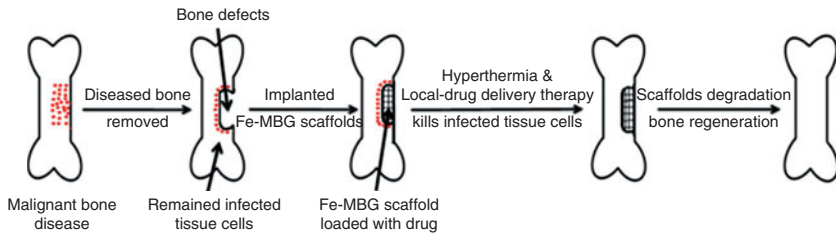
Figure 7.21 Illustration for the potential applications of Fe–MBG scaffolds with multifunctional properties for the treatment of bone disease and the regeneration of bone defects [95]. (Copyright (2013), with permission from Elsevier)

the other two scaffolds, indicating the increased magnetic strength with increased Fe content. Release of SiO_4^{-4} in simulated body fluid is not found to be affected by the presence of Fe in MBG scaffold constituted by 80% SiO_2. These developed MBG–Fe scaffolds were found to be magnetic, bioactive and biodegradable, and simultaneously maintained sustained drug delivery. Therefore, they can be prospective materials for hyperthermia therapy as well as local drug delivery applications [95]. A schematic of treatment of bone disease and regereration is shown in Figure 7.21.

Lu *et al.* prepared the HA/MWCNTs composite with ferromagnetic properties via an *in situ* process, where MWCNTs with mean diameter of 40–60 nm were used. It was reported that addition of CNTs to HA resulted in weak ferromagnetic properties with the saturation magnetization, remanent magnetization and coercivity values of 0.13 emu/g, 0.02 emu and 354.55 Oe, respectively, at room temperature [103].

Bretcanu *et al.* synthesized glass ceramic with composition $24.7SiO_2$, $13.5 Na_2O$, $13.5 CaO$, $3.3 P_2O_5$, $14 FeO$ and $31Fe_2O_3$ (wt%) by traditional melting at 1400, 1450, 1500 and 1550°C. The sum of the iron oxides is 45 wt%. The melting of the above glass ceramic composite at higher temperature (1550°C) showed the formation of magnetite. The saturation magnetization varies from 18.6 to 31.5 emu/g, while the coercive field varies from 35 to 180 Oe [104]. Ebisawa *et al.* reported the bioactivity of 36 wt% Fe_3O_4 incorporated in $CaO–SiO_2$– based glass ceramic. Bone–like apatite crystal formation in simulated body fluid showed the *in vitro* bioactivity of these ferromagnetic glass ceramics [105].

7.2.6   Influence of External Field on Bacterial Adhesion and Biofilm Growth

It has now been widely recognized that an immuno–incompetent, fibro–inflammatory zone is created after any device implantation in the body, providing a favorable environment for bacterial proliferation which results in biomaterial–associated infection [106]. With the use of external field, this problem of infection can be solved to some extent as shown below.

7.2.6.1   Electric Field

Biofilm formation and microbial adhesion have been extensively studied and are generally believed to depend on the factors explained in Section 7.2.4. In a study, it was reported that application of 100 µA direct current (DC) showed 78% bacterial detachment, whereas 100 µA block current stimulated only 31% of initially–adhered *staphylococci* to detach from surgical stainless steel [107].

In another study on electric field with block currents of 15, 60 and 100 µA of different frequencies (0.1–2 Hz) and varying duty cycles (5–50%), significant bacterial detachment from stainless steel is reported. Figure 7.22 depicts that 100 µA block current show *staphylococci* detachment of ~ 76 % from stainless steel substrate, but the duty cycle 5% was reported insufficient to cause bacterial detachment [106]. However, the direct currents have a disadvantage over alternating current, by generating an excess of ions on the steel that results in terms of negative osteogenesis and fixation [108]. It is reported that the applied alternating field direct the hydrated ions to go along the fields as well as dragging water along with them. As a result of such fluid flow, cells experience an additional force, that motivate bacterial detachment [109].

7.2.6.2   Magnetic Field

The available literature regarding magnetic effect on bacterial cells provides the evidence that magnetic field kills bacteria [110]. The effect of magnetic field on the bacterial cell depends on the exposure duration as well as strength of magnetic induction [111]. The effects of magnetic fields are not necessarily to be bacteriostatic, as some studies report that the bacterial
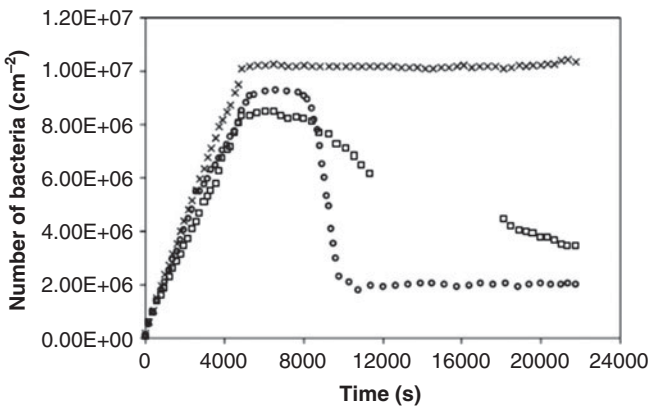
Figure 7.22 Three examples of times series involving adhesion and electric current–induced detachment of *S. epidermidis* from stainless steel. Here o: 2 Hz, 50%, 100µA; □: 0.5 Hz, 50% , 100 µA; ×: 2 Hz, 5%, 100µA [106]. (Copyright (2013), with permission from Elsevier)

population increases during exposure of the growing culture to the magnetic fields [112]. However, a majority of the experiments till now show a negative effect of magnetic field on bacteria, and the effects were more pronounced with increasing strength of magnetic fields, time of exposure and temperature [113]. As far as the frequency is concerned, inhomogeneous fields were found to be more effective in reducing the cell number than the homogeneous ones [114]. In addition, it has also been shown that the intermediate frequency magnetic field has no effect on the morphology of the bacteria, irrespective of the exposure time [115]. Further, it has also been shown that extremely low frequency and low magnitude magnetic fields have no effect on the viability of bacteria [116]. When the magnitude of field strength is considerably increased, the static magnetic fields have been shown to cause cell surface damage [113]. But even ultra–strong magnetic fields, applied after different types of costressing factors, were not able to cause inactivation in bacteria [117]. On the other hand, very low strength magnetic fields have been shown to have no effect on viability of the bacteria. Moderate intensity static magnetic field of 100 mT was found to inhibit the adhesion of *E. coli* bacteria and *S. epidermidis* bacteria on control as well as sintered HA substrate as the magnetic field exposure duration is increased from 30 min to 120 min (Figure 7.23) [110].

Table 7.2 provides a summary of experiments and results of several magnetic field experiments to assess the efficiency in causing antibacterial property along with explanations. The antibacterial efficiency is

Control (0 min)   HA surface (0 min)

Control (60 min)   HA surface (120 min)
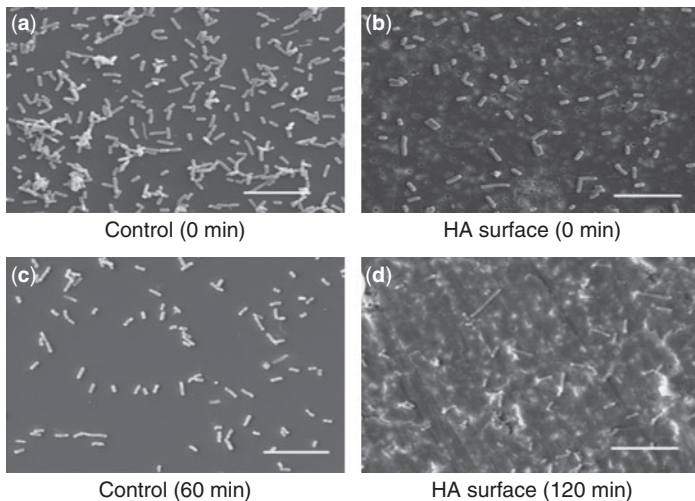
Figure 7.23 Magnetic field exposed *E.coli* bacteria on (a) Control (MF exposure duration = 0 min), (b) Control (MF exposure duration = 60 min), (c) HA (MF exposure duration = 0 min), and (d) HA, MF exposure duration = 0 min. (bar = 10 μm, magnetic field strength =100 mT) [110]. (With permission from John Wiley and Sons)

Table 7.2 Effects of magnetic field on bacterial growth and viability.

Magnetic Field Strength	Type of Bacteria and Exposure Time	Biological Effects	Comments
$B_m = 2.7$–10 mT at 50 Hz	*E. coli* (0–12 min.)	Ability to form colonies decreased with– • increasing mag. field • time of exposure	Possible effect of electro-magnetic field on the permeability of the ionic channels in the membrane or formation of free radicals due to magnetic field [111].
Clinical electromag-netic bone stimulator ($B_m = 1.5$ mT)	*E. coli* (40 min.) *P. aeruginosa* (50 min.) *B. magaterium* (90 min.) *S. aureus* (90 min.)	No obvious differences were found between test and control with any of the four bacterial species	The Magnetic fields of a bone stimulator have hardly any effect on bacteria [120].
2.7–10 mT	*E. coli* *L. adecarboxylata* *S. aureus* (12 min. all)	• Exponential decrease with mag. field • Number of CFU decreases with time of exposure	• *E. coli* is much more susceptible to mag. field compared to *S. aureus* • The decrease of the CFU starts immediately after the magnetic field was switched on [121].

Magnetic Field Strength	Type of Bacteria and Exposure Time	Biological Effects	Comments
450 mT Static Magnetic Field (SMF)	*E. coli* (8 hours)	The relative number of CFU of tested strain decreased with– • longer exposure time • Higher treatment temperature.	Cell surface damage occurred when bacteria were exposed to SMF, authors support free radicals theory that the damage might be caused by some oxygen free radicals which were produced by SMFs treatment [113].
Applied ultrasound, then high hydrostatic pressure, then pulsed electric field, then 18 T pulsed magnetic field 10–15 kHz	*E. coli* Culture time is not given (Possibly immediate effects were checked)	A pulsed magnetic field of 18T is not capable of causing inactivation of *Escherichia coli* when applied even after mild treatments used as stressing factors	• EDTA was used to remove Ca^{2+} and Mg^{2+} ions from the cell wall. • The loss of these ions increases the permeability of the cell wall and allows anti–microbial agents to act on the cytoplasmic membrane [117].
91 mT at 2 kHz, 1.1 mT at 20 kHz and 0.11 mT at 60 kHz	*Salmonella typhimurium* *E. coli* (48 hours)	IFMFs(Intermediate frequency Magnetic fields) given did not have detectable	The Intermediate frequency magnetic fields would not affect the process of drug metabolism,

(Continued)

Table 7.2 (*Cont.*)

Magnetic Field Strength	Type of Bacteria and Exposure Time	Biological Effects	Comments
		mutagenicity in the bacterial mutation using the given bacteria	radical reactions or the repair process of DNA in either prokaryotic or eukaryotic cells [115].
30, 60, 80 and 100 mT (Magnetic fields were applied in aerobic and anaerobic conditions).	*Streptococcus mutans, Staphylococcus aureus and Escherichia coli* (24 hours)	Findings suggested that– • Oxygen related to growth the cases of *S. mutans, S. aureus.* • No growth effects were detected on *E. coli* culture	• Magnetic fields may induce active oxygen formation. • Radical reactions with these paramagnetic ions of oxygen are effected by magnetic fields. • Mechanism of effect of magnetic field may be different in gram positive and gram negative bacteria [119].
10 mT at 50 Hz	*E.coli, P.denitrificans* (1hour)	No change in bacterial morphology was observed in both type of bacteria	Using the scanning near field optical microscopy could provide other interesting information for these biological objects [122].

Magnetic Field Strength	Type of Bacteria and Exposure Time	Biological Effects	Comments
100 mT Static Magnetic Field	E.coli, S.epidermidis (4 hours)	Reduction in CFU and bacterial membrane was ruptured	Bactericidal effect of SMF was higher for gram positive and it was observed to increase with increasing exposure duration [110].
1–10 mT at 2–50 Hz	E. coli and Proteus vulgaris Photobacterium (7 to 16 hours)	The results support the concept that bacteria are quite resistant to electromagnetic fields, probably because of compensation and self regulation.	• The experiments suggest the inability of ELF (extremely low frequency) magnetic fields on the viability of bacteria. • E. coli may be able to tolerate even higher temperatures without a change in protein pattern [116].
10 T	Secondary structures of protein in E. coli and Staphylococcus aureus (5,10,20,30,40,50 and 60 min.)	The ultra strong static magnetic field has a great impact on the secondary structures of protein in E. coli and has little impact on those of protein in S. aureus.	The reason might be related to the shape and wall structure of the protein cell, the E coli has a very thin wall thickness of 10 nm the magnetic field force is therefore easy to penetrate the cell wall [118].
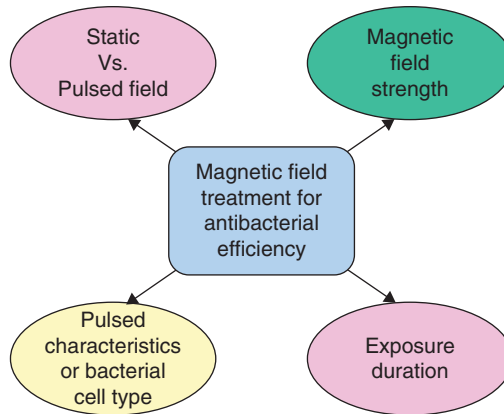
Figure 7.24 Schematic of characteristics of magnetic field influencing antibacterial efficiency.

found to vary according to type of field (static or pulsed field), strength of applied field and exposure duration. Different types of bacteria respond differently under the same type of external field, as shown in Figure 7.24.

Two reasons are being proposed: (a) the effect of electromagnetic fields on the permeability of the ionic membrane, and (b) formation of free radicals due to magnetic field [111]. It has been suggested that oxygen–free radicals are produced due to magnetic field, which react with the ions in growth medium [113]. It has also been proposed that the bactericidal might be related to the shape and wall structure of the protein cell. The *E. coli* bacterium has a very thin wall thickness of 10 nm, and the magnetic field force can therefore easily penetrate the cell wall as shown in Figure 7.25 [118]. Further, it has been proposed that the effect of magnetic field may be different on gram–positive and gram–negative bacteria [119]. As far as the strength of magnetic field is concerned, most of the experiments are reported to be carried out at field strength of less than 100 mT, while some researchers found positive response of magnetic field for bacterial infection, but such response is reported to be dependent on exposure duration. In some of the work, low magnetic field was found to cause bactericidal property in a specific bacterial strain, however, was found inefficient for other types of bacterial cells. Such observations indicate that the magnetic field response is also cell type dependent. Very few studies are carried out at field strength of more than 100 mT, where similar types of effects as described above were reported. Schematic of a external static magnetic field setup used in a study is shown in Figure 7.26 [113].
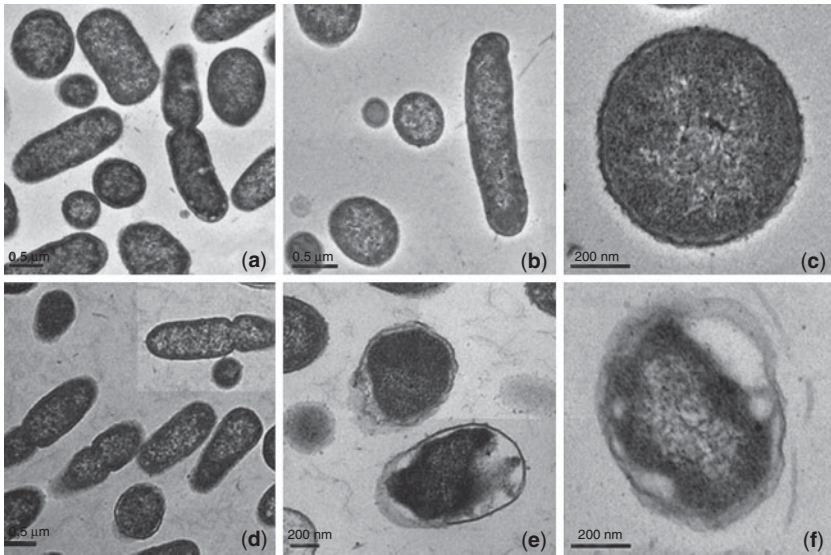
Figure 7.25 TEM of SMFs–treated and untreated *E. coli* cells. (a–c) Images of untreated cells; (d–f) images of SMFs–treated cells. The cell walls of untreated samples were complete while the cell walls of SMFs–treated samples were obviously damaged [113]. (Copyright (2013), with permission from Elsevier)
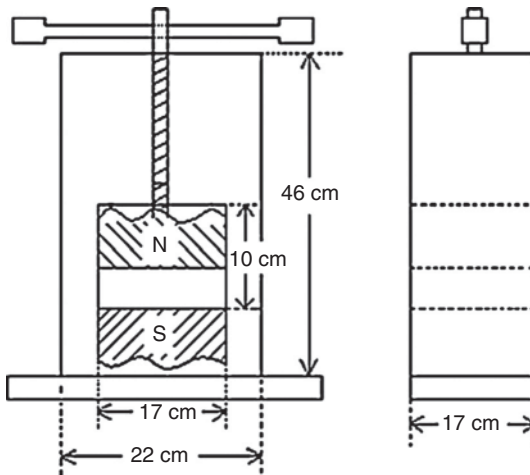
Figure 7.26 YT–QCLTY permanent magnet (produced by Yitian magnetic material Corp Ltd., Shenzhen, China). The magnetic field induction ranges from 450 mT to 3500 mT. The space for exposure was 17 cm × 17 cm × 10 cm (utmost) [113]. (Copyright (2013), with permission from Elsevier)

7.3   Summary

This chapter discussed some strategies associated with prosthetic infection. Based on the discussion in this review, four different ways to reduce prosthetic infection can be summarized. One is the delivery of nanoparticles at the infection site and the second is biomaterial modification, e.g., reinforcement of HA with Ag/ZnO/Iron oxide. The third approach is the treatment of the infected site by the use of external electric field, and the fourth and last option is the application of external magnetic field on the bacterial infection. All four approaches are illustrated in Figure 7.27.

A considerable part of this review discussed the development of HA–based biomaterials with antibacterial properties. It has been categorically emphasized that the addition of Ag/ZnO to HA needs to be a tailored compromise between antibacterial and cell viability property. In other words, the addition of the second phase is to be such that it is enough to kill bacteria, but not the mammalian cells.

In order to introduce the antibacterial property, oxide nanoparticles like ZnO, TiO_2, etc., can be delivered at the optimal dosage, and experimental evidence points toward the fact that such nanoparticles generate ROS and kill the infectious cells. As far as magnetic nanoparticles are concerned, Fe_3O_4 are used as antibacterial agent as well as drugs for hyperthermia therapy to kill the cancerous cells. The development of magnetic biocomposites/glass ceramics based on HA–Fe_2O_3 and MBG–Fe, etc., are suggested as potential material for cancer treatment.

As far as the external field application is concerned, the electric field is found to stimulate the bacterial detachment. Both direct current and block current of 100 µA are capable of detaching the adhered bacteria up to a reasonable amount (~ 75%).

Contradictory results were found with the use of external magnetic field on bacterial viability. However, some *in vitro* experiments suggest the
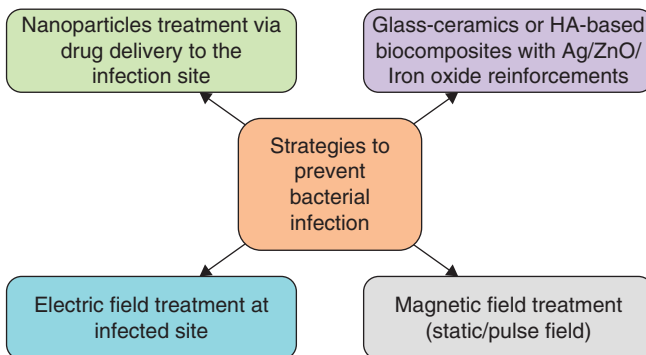
Figure 7.27 Summary of strategies to address prosthetic infection.

effectiveness of the external magnetic field to kill the bacterial cells. The antibacterial response of magnetic field is observed to be dependent on many parameters *viz.* strength of applied field, exposure duration, bacterial cell type and type of magnetic field used. Overall, the influence of the external electric/magnetic fields on mammalian cells is yet to be investigated, and requires careful experimentation to independently probe the influence of such fields on prokaryotic and eukaryotic cells.

Acknowledgement

References

1. M.M. Stevens, Biomaterials for bone tissue engineering. *Materials Today,* 11:18–25, 2008.
2. J.M. Sautier, J.R. Nefussi, N. Forest, Surface reactive biomatemials in osteoblast culture: An ultrastructural study, *Biomaterials,* 13:400–402, 1992.
3. N. Huebsch, D.J. Mooney, Inspiration and application in the evolution of biomaterials, *Nature,* 462:426–432, 2009.
4. B. Basu, D. Katti, A. Kumar, *Advanced Biomaterials: Fundamentals, Processing and Applications*, John Wiley & Sons, 2009.
5. Y.H. An, R.J. Friedman. Laboratory methods for studies of bacterial adhesion, *Journal of Microbiological Methods*, 30:141–152, 1997.
6. W.Y. Matar, S.M. Jafari, C. Restrepo, M. Austin, J.J. Purtill, J. Parvizi, Preventing infection in total joint arthroplasty, *J. Bone Joint Surg. Am.,* 92:36–46, 2010.
7. J. Carlet, V. Jarlier, S. Harbarth, A. Voss, H. Goossens, D. Pittet, Ready for a world without antibiotics? The Pensières antibiotic resistance call to action. *Antimicrobial Resistance and Infection Control,* 11:1–13, 2012.
8. N. Jones, B. Ray, K.T. Ranjit, A.C. Manna, Antibacterial activityof ZnOnanoparticle suspensions on a broad spectrum of microorganisms. *FEMS Microbiol. Lett.,* 279:71–76, 2008.
9. M. Katsikogianni, Y.F. Missirlis. Concise review of mechanisms of bacterial adhesion to biomaterials and of techniques used in estimating bacteria material interactions, *European Cells and Materials*, 8:37–57, 2004.
10. C.v. Eiff, G. Peters, C. Heilmann, Pathogenesis of infections due to coagulase–negative staphylococci, 11:677–685, 2002.
11. Y.H. An and R.J. Friedman, Prevention of sepsis in total joint arthroplasty, *Journal of Hospital Infection,* 33:93–108, 1996.
12. N. Tran, A. Mir, D. Mallik, A. Sinha, S. Nayar, T.J. Webster, Bactericidal effect of iron oxide nanoparticles on Staphylococcus aureus, *International Journal of Nanomedicine,* 5 277–283, 2010.

13. M.E. Rupp, G.L. Archer, Coagulase–negative staphylococci: Pathogens associated with medical progress, *Clinical Infection Diseases*, 19:231–245, 1994.

14. Randomized clinical trial of prevention of central venous catheter–related bloodstream infection by use of an antiseptic–impregnated catheter. *Annals of Internal Medicine*, 127:257–266, 1997.

15. G.S. El–Housseiny, M.M. Aboulwafa, N.A. Hassouna, Adherence, Invasion and cytotoxicity of some bacterial pathogens, *Journal of American Science*, 6:260–268, 2010.

16. A. Lipovsky, Y. Nitzan, A. Gedanken, R. Lubart, Antifungal activity of ZnO nanoparticles—the role of ROS mediated cell injury, *Nanotechnology*, 22 105101–105106, 2011.

17. J. Fabrega, S.R. Fawcett, J. Renshaw, J.R. Lead, Silver nanoparticle impact on bacterial growth: Effect of pH, concentration, and organic matter, *Environ. Sci. Technol.*, 43:7285–7290, 2009.

18. J. Sawai, Quantitative evaluation of antibacterial activities of metallic oxide powders (ZnO, MgO and CaO) by conductimetric assay, *Journal of Microbiological Methods*, 54:177–182, 2003.

19. X.W. Guo, C.A. Min, Z. Qiang, Preparation of TiO_2 thin film and its antibacterial activity, *Journal of Wuhan University of Technology – Mater. Sci. Ed.*, 19:16–18, 2004.

20. M. Fang, J.–H. Chen, X.–L. Xu, P.–H. Yang, H.F. Hildebrand, Antibacterial activities of inorganic agents on six bacteria associated with oral infections by two susceptibility tests, *International Journal of Antimicrobial Agents*, 27:513–517, 2006.

21. M. Heinlaan, A. Ivask, I. Blinova, H.–C. Dubourguier, A. Kahru, Toxicity of nanosized and bulk ZnO, CuO and TiO2 to bacteria Vibrio fischeri and crustaceans Daphnia magna and Thamnocephalus platyurus, *Chemosphere*, 71:1308–1316, 2008.

22. S.–H. Kim, H.–S. Lee, D.–S. Ryu, S.–J. Choi, D.–S. Lee, Antibacterial activity of silver–nanoparticles against Staphylococcus aureus and Escherichia coli, *Korean J. Microbiol. Biotechnol.*, 39:77, 2011.

23. http://www.immunologyschools.com/Free_Course/genmicr.htm.

24. K. Todar. Chapter overview of bacteriology, *Todar's Online Textbook of Bacteriology*, 2012:1–6.

25. http://micro.magnet.fsu.edu/cells/bacteriacell.html.

26. H.C. Berg, The rotary motor of bacterial flegella, *Annu. Rev. Biochem.*, 72:19–54, 2003.

27. J. Swanson, Studies on gonococcus infection IV. Pili: Their role in attachment of gonococci to tissue culture cells, *The Journal of Experimenta Medicine*, 137:571–589, 1973.

28. D. Scholl, S. Adhya, C. Merril, Escherichia coli K1's capsule is a barrier to bacteriophage T7, *Applied and Environmental Microbiology*, 71:4872–4874, 2005.

29. one MaiP, *Fundamentals of Microbiology*, Pearson Education Inc. 2008:86.

30. W.W. Navarre, O. Schneewind, Surface proteins of gram–positive bacteria and mechanisms of their targeting to the cell wall envelope, *Microbiology and Molecular Biology Reviews*, 63:174–229, 1999.

31. T. Mosmann, Rapid colorimetric assay for cellular growth and survival: Application to proliferation and cytotoxicity assays, *J. Immunol. Methods*, 65:55–63, 1983.

32. J.F. Fisher, S. Mobashery, 2007 Astellas USA foundation award: Host–guest chemistry of the peptidoglycan, *J. Med. Chem.*, 53(13):4813–4829, 2010.

33. R. Schwandner, R. Dziarski, H. Wesche, M. Rothe, C.J. Kirschning, Peptidoglycan– and lipoteichoic acid–induced cell activation is mediated by toll–like receptor, *The Journal of Biological Chemistry*, 274:17406–17409, 1999.

34. T.J. Silhavy, D. Kahne, S. Walker, The bacterial cell envelope, *Cold Spring Harb. Perspect. Biol.*, 2010.

35. I. Ginsburg, Role of lipoteichoic acid in infection and inflammation, *Lancet Infectious Diseases*, 2:171–79, 2002.

36. C. Alexander, E.T. Rietschel, Bacterial lipopolysaccharides and innate immunity, *Innate Immunity*, 7:167–202, June 2001.

37. H. Tagai, H. Aoki, *Preparation of Synthetic Hydroxyapatite and Sintering of Apatite Ceramics*, Wiley, Chichester 1980.

38. G. O'Toole, H.B. Kaplan, R. Kolter. Biofilm formation as microbial development, *Ann. Rev. Microbiol.*, 54:49–79, 2000.

39. N. Karamanos, H. Panagiotopoulou, A. Syrokou, C. Frangides, A. Hjerpe, G. Dimitrakopoulos, E. Anastassiou, Identity of macromolecules present in the extracellular slime layer of Staphylococcus epidermidis, *Biochimie*, 77:217–224, 1995.

40. J. Costerton, Introduction to biofilm, *Intern. J. Antimicrob. Agents.*, 11:217–221, 1999.

41. I.G. Duguid, E. Evans, M.R.W. Brown, P. Gilbert, Effect of biofilm culture upon the susceptibility of Staphylococcus epidermidis to tobramycin, *J. Antimicrob. Chemother.*, 30:803–810, 1992.

42. R. Donlan and J. Costerton, Biofilms: Survival mechanisms of clinically relevant microorganisms, *Clin. Microb. Reviews*, 15:167–193, 2002.

43. J.W. Costerton, P.S. Stewart, E.P. Greenberg, Bacterial biofilms: A common cause of persistent infections, *Science*, 284:1318–1322, 1999.

44. H.H.M. Rijnaarts, W. Norbe, E.J. Bouwer, J. Lyklema, A.J.B. Zehnder, Reversibility and mechanism of bacterial adhesion, *Col. Surf. B: Bioint.*, 4:5–22, 1995.

45. B. Gottenbos, H.J. Busscher, H.C.V.D. Mei, P. Nieuwenhuis, Pathogenesis and prevention of biomaterial centered infection, *J. Mat. Sci.: Mat. In. Med.*, 13:717–722, 2002.

46. C. Mayer, R. Moritz, C. Kirschner, W. Borchard, R. Maibaum, J. Wingender, H.–C. Flemming, The role of intermolecular interactions: Studies on model systems for bacterial biofilms, *International Journal of Biological Macromolecules*, 26:3–16, 1999.

47. D. Mack, Molecular mechanisms of Staphylococcus epidermidis biofilm formation, *J. Hosp. Inf.*, 43:S113–S125, 1999.

48. X. Wang, J.F. Preston, T. Romeo, The pgaABCD locus of Escherichia coli promotes the synthesis of a polysaccharide adhesin required for biofilm formation, *Journal of Bacteriology*, 186:2724–02734, 2004.

49. F. Götz, Staphylococcus and biofilms, *Molecular Microbiology*, 43(6):1367–1378, 2002.

50. J.E. Duddridge, C.A. Kent, J.F. Laws, Effect of surface shear stress on the attachment of Pseudomonas fluorescens to stainless steel under defined flow conditions, *Biotechnol. Bioeng.* 24:153–164, 1982.

51. H.T. Chang, B.E. Rittmann, D. Amar, R. Heim, O. Ehrlinger, Y. Lesty, Biofilm detachment mechanisms in a liquid fluidised bed, *Biotechnol. Bioeng.*, 38:499–506, 1991.

52. M.S. Shive, S.M. Hasan, J.M. Anderson, Shear stress effects on bacterial adhesion, leukocyte adhesion, and leukocyte oxidative capacity on a polyetherurethane, *J. Biomed. Mater. Res.,* 46:511–519, 1999.

53. W.E. Thomas, L.M. Nilsson, M. Forero, E.V. Sokurenko, V. Vogel, Shear–dependent 'stick–and–roll' adhesion of type 1 fimbriated Escherichia coli, *Molecular Microbiology,* 53:1545–1557, 2004.

54. W. Kohnen, C. Kolbenschlag, S. Teske–Keiser, B. Jansen, Development of a long–lasting ventricular catheter impregnated with a combination of antibiotics, *Biomaterials,* 24 4865–4869, 2003.

55. C.R. Arciola, D. Campoccia, L. Montanaro, Effects on antibiotic resistance of Staphylococcus epidermidis following adhesion to polymethylmethacrylate and to silicone surfaces, *Biomaterials,* 23:1495–1502, 2002.

56. V.A. Tegoulia, S.L. Cooper, Staphylococcusaureus adhesion to self–assembled monolayers: Effect of surface chemistry and fibrinogen presence. *Colloids and Surfaces B: Biointerfaces,* 24:217–228, 2002.

57. R.D. Boyd, J. Verran, Use of atomic force microscope to determine the effect of substratum surface topography on bacterial adhesion, *Langmuir,* 18:2343–2346, 2002.

58. K.J. Edwards and A.D. Rutenberg, Microbial response to surface microtopography: The role of metabolism in localized mineral dissolution, *Chemical Geology,* 180:19–32, 2001.

59. K. Vacheethasanee, J.S. Temenoff, J.M. Higashi, A. Gary, J.M. Anderson, R. Bayston, R.E. Marchant, Bacterial surface properties of clinically isolated Staphylococcus epidermidis strains determine adhesion on polyethylene. *Inc. J. Biomed. Mater. Res.,* 42:425–432, 1998.

60. Y.–L. Ong, A. Razatos, G. Georgiou, M.M. Sharma, Adhesion forces between E. coli bacteria and biomaterial surfaces, *Langmuir,* 15:2719–2725, 1999.

61. R.B. Dickinson, J.A. Nagel, D. Mcdevitt, T.J. Foster, R.A. Proctor, S.L. Cooper, Quantitative comparison of clumping factor– and coagulase–mediated Staphylococcus aureus adhesion to surface–bound fibrinogen under flow, *Infection and Immunity,* 63:3143–3150, 1995.

62. I.–W. Wang, J.M. Anderson, R.E. Marchant, Staphylococcus epidermidis adhesion to hydrophobic biomedical polymer is mediated by platelets, *J. Infect. Dis.,* 167:329–336, 1993.

63. M. Herrmann, Q.J. Lai, R.M. Albrecht, D.F. Mosher, R.A. Proctor, Adhesion of Staphylococcus aureus to surface–bound platelets: Role of fibrinogen/fibrin and platelet integrins, *J. Infect. Dis.,* 167:312–322, 1993.

64. H. Oguchi, K. Ishikawa, K. Mizoue, K. Seto and G. Eguchi, Long-term histological evaluation of hydroxyapatite ceramics in humans, *Biomaterials* 16:33–38, 1995.

65. J-W. Choi, Y-M. Kong, and H-E. Kim, Reinforcement of Hydroxyapatite Bioceramic by Addition of Ni3Al and Al_2O_3, *J. Am. Ceram. Soc.,* 81:1743–48, 1998.

66. Q. L. Feng, T. N. Kim, J. Wua, E. S. Park, J. O. Kim, D. Y. Lim, F. Z. Cui, Antibacterial effects of Ag-HAp thin films on alumina substrates, *Thin Solid Films*, 335:214–219, 1998.

67. W. Zimmerli and P. Sendi, Pathogenesis of implant-associated infection: the role of the host, *Semin Immunopathol* 33:295–306, 2011.

68. D. N. Rushton, G. S. Brindley, C. E. Polkey, G. V. Browning, Implant infections and antibiotic-impregnated silicone rubber coating, *Journal of Neurology, Neurosurgery, and Psychiatry* 52:223–229, 1989.

69. S.M.F. Asmus, S. Sakakura, G. Pezzotti, Hydroxyapatite toughened by silver inclusions, *Journal of Composite Materials,* 37:2117–2129, 2003.

70. N. Rameshbabu, T.S.S. Kumar, T.G. Prabhakar, V.S. Sastry, K.V.G.K. Murty, K.P. Rao, Antibacterial nanosized silver substituted hydroxyapatite: Synthesis and characterization, *J. Biomed. Mater. Res. Appl. Biomater.,* 80A:581–591, 2007.

71. T.K. Chaki and P.E. Wang, Densification and strengthening of silver–reinforced hydroxyapatite–matrix composite prepared by sintering, *J. Mat. Sci.: Mat. Med.,* 5:533–542, 1994.

72. S. Kalmodia, A.R. Molla, B. Basu, In vitro cellular adhesion and antimicrobial property of SiO_2–MgO–Al_2O_3–K_2O–B_2O_3–F glass ceramic, *J. Mater. Sci.: Mater. Med.,* 21:1297–1309, 2010.

73. A.R. Molla, B. Basu, Microstructure, mechanical, and in vitro properties of mica glass–ceramics with varying fluorine content, *J. Mater. Sci.: Mater. Med.*, 20:869–882, 2009.

74. S. Nath, S. Kalmodia, B. Basu, Densification, phase stability and in vitro biocompatibility property of hydroxyapatite–10 wt% silver composites, J. Mater. Sci.: Mater. Med., 21:1273–1287, 2010.

75. B. Singh, A.K. Dubey, S. Kumar, N. Saha, B. Basu, R. Gupt, In vitro biocompatibility and antimicrobial activity of wet chemically prepared Ca_{10}–$xAgx(PO_4)_6(OH)_2$ (0.0 x 0.5) hydroxyapatites, *Materials Science and Engineering,* 31:1320–1329, 2011.

76. N. Padmavathy and R. Vijayaraghavan, Enhanced bioactivity of ZnO nanoparticles—an antimicrobial study, *Sci. Technol. Adv. Mater.,* 9:35004–35010, 2008.

77. http://www.bio2usa.com/oxygenkillspathogens.html.

78. O. Yamamoto, Influence of particle size on the antibacterial activity of zinc oxide, *International Journal of Inorganic Materials,* 3 643–646, 2001.

79. J.–H. Yuan, Y. Chen, H.–X. Zha, L.–J. Song, C.–Y. Li, J.–Q. Li, X.–H. Xia, Determination, characterization and cytotoxicity on HELF cells of ZnO nanoparticles, *Colloids and Surfaces B: Biointerfaces,* 76:145–150, 2010.

80. A. Ito, K. Ojima, H. Naito, N. Ichinose, T. Tateishi, Preparation, solubility, and cytocompatibility of zinc–releasing calcium phosphate ceramics, *J. Biomed. Mater. Res.,* 50:178–183, 2000.

81. A. Bandyopadhyay, E.A. Withey, J. Moore, S. Bose, Influence of ZnO doping in calcium phosphate ceramics, *Materials Science and Engineering C,* 27:14–17, 2007.

82. N. Saha, K. Keskinbora, E. Suvaci, B. Basu, Sintering, microstructure, mechanical, and antimicrobial properties of HAp–ZnO biocomposites, *J. Biomed. Mater. Res. Part B,* 95B:430–440, 2010.

83. N. Saha, A.K. Dubey, B. Basu, Cellular proliferation, cellular viability, and bio-compatibility of HA–ZnO composites, *J. Biomed. Mater. Res. Part B,* 100B:256–264, 2011.

84. A. Gupta and M. Gupta, Synthesis and surface engineering of iron oxide nanoparticles for biomedical applications, *Biomaterials,* 26:3995–4021, 2005.

85. D1 Touati, Iron and oxidative stress in bacteria, Archives of Biochemistry and Biophysics, 373:1–6, 2000.

86. R.A. Pareta, E. Taylor, T.J. Webster, Increased osteoblast density in the presence of novel calcium phosphate coated magnetic nanoparticles, Nanotechnology, 19:265101–265106, 2008.

87. E.N. Taylor, T.J. Webster, The use of superparamagnetic nanoparticles for prosthetic biofilm prevention, *International Journal of Nanomedicine,* 4:145–152, 2009.

88. H. Sies, Oxidative stress: Oxidants and antioxidants, *Experimental Physiology,* 82:291–295, 1997.

89. S. Laurent, D. Forge, M. Port, A. Roch, C. Robic, L. Vander Elst, R.N. Muller, Magnetic iron oxide nanoparticles: Synthesis, stabilization, vectorization, physicochemical characterizations, and biological applications, *Chem. Rev.,* 108:2064–2110, 2008.

90. D. Arcos, R.P.D. Real, M. Vallet–Regi, A novel bioactive and magnetic biphasic material, *Biomaterials,* 23 2151–2158, 2002.

91. A.K. Gupta and M. Gupta, Cytotoxicity suppression and cellular uptake enhancement of surface modified magnetic nanoparticles, *Biomaterials,* 26 1565–1573, 2005.

92. S. Dalai, S. Pakrashi, R.S.S. Kumar, N. Chandrasekaran, A. Mukherjee, A comparative cytotoxicity study of TiO_2 nanoparticles under light and dark conditions at low exposure concentrations, *Toxicology Research,* 1:116–130, 2012.

93. E. Andronescu, M. Ficai, G. Voicu, D. Ficai, M. Maganu, A. Ficai, Synthesis and characterization of collagen/hydroxyapatite: Magnetite composite material for bone cancer treatment, *J. Mater. Sci.: Mater. Med.,* 21:2237–2242, 2010.

94. T.–W. Wang, H.–C. Wu, W.–R. Wang, F.–H. Lin, P.–J. Lou, M.–J. Shieh, T.–H. Young, The development of magnetic degradable DP–Bioglass for hyperthermia cancer therapy, *J. Biomed. Mater. Res.,* 83A:828–837, 2007.

95. C. Wu, W. Fan, Y. Zhu, M. Gelinsky, J. Chang, G. Cuniberti, V. Albrecht, T. Friis, Y. Xiao, Multifunctional magnetic mesoporous bioactive glass scaffolds with a hierarchical pore structure, *Acta Materialia,* 7:3563–3572, 2011.

96. C.–H. Hou, S.–M. Hou, Y.–S. Hsueh, J. Lin, H.–C. Wu, F.–H. Lin, The in vivo performance of biomagnetic hydroxyapatite nanoparticles in cancer hyperthermia therapy, *Biomaterials,* 30:3956–3960, 2009.

97. G.D. Li, D.L. Zhou, Y. Lin, T.H. Pan, G.S. Chen, Q.D. Yin, Synthesis and characterization of magnetic bioactive glass–ceramics containing Mg ferrite for hyperthermia, *Materials Science and Engineering C,* 30:148–153, 2010.

98. Y.–K. Lee, S.–Y. Choi, Crystallization and properties of Fe_2O_3–CaO–SiO_2 glasses, *J. Am. Ceram. Soc.,* 79:992–996, 1996.

99. N. Bock, A. Riminucci, C. Dionigi, A. Russo, A. Tampieri, E. Landi, V.A. Goranov, M. Marcacci, V. Dediu, A novel route in bone tissue engineering: Magnetic biomimetic scaffolds, *Acta Biomaterialia,* 6:786–796, 2010.

100. I. Bajpai, K. Balani and B. Basu, Spark plasma sintered HA-Fe$_3$O$_4$ based multifunctional magnetic biocomposites, *Journal of the American Ceramic Society*, (in press, 2013).

101. M. Ajeesh, B.F. Francis, J. Annie, P.R.H. Varma, Nano iron oxide–hydroxyapatite composite ceramics with enhanced radiopacity, *J. Mater. Sci.: Mater. Med.,* 21:1427–1434, 2010.

102. D. Eniu, D. Cacaina, M. Coldea, M. Valeanu, S. Simon, Structural and magnetic properties of CaO–P$_2$O$_5$–SiO$_2$–Fe$_2$O$_3$ glass–ceramics for hyperthermia, *Journal of Magnetism and Magnetic Materials,* 293 310–313, 2005.

103. X.Y. Lu, N.Y. Zhang, L. Wei, J.W. Wei, Q.Y. Deng, X. Lu, K. Duan, J. Weng, Fabrication of carbon nanotubes/hydroxyapatite nanocomposites via an in situ process, *Applied Surface Science,* 2012:Article in press.

104. O. Bretcanu, E. Verne, M. Coisson, P. Tiberto, P. Allia, Magnetic properties of the ferrimagnetic glass–ceramics for hyperthermia, *Journal of Magnetism and Magnetic Materials,* 305:529–533, 2006.

105. Y. Ebisawa, F. Miyaii, T. Kokubo, K. Ohura, T. Nakamura, Bioactivity of ferrimagnetic glassceramics in the system FeO–Fe$_2$0$_3$–CaO–Si0$_2$, Biomoterials, 18:1277–1284, 1997.

106. A.J. van der Borden, H.C. van der Mei, H.J. Busscher, Electric block current induced detachment from surgical stainless steel and decreased viability of Staphylococcus epidermidis, *Biomaterials,* 26:6731–6735, 2005.

107. A.J. van der Borden, H.C. van der Mei, H.J. Busscher, Electric–current–induced detachment of Staphylococcus epidermidis strains from surgical stainless steel, *J. Biomed. Mater. Res. Part B: Appl. Biomater.,* 68B:160–164, 2004.

108. A.E. Clark, L.L. Hench, H.A. Paschall, The influence of surface chemistry on implant interface histology: A theoretical basis for implant materials selection, *J. Biomed. Mater. Res.,* 10:161–174, 1976.

109. A.J. van der Borden, H. van der Werf, H.C. van der Mei, H.J. Busscher, Electric current–induced detachment of Staphylococcus epidermidis biofilms from surgical stainless steel, *Applied and Environmental Microbiology,* 70:6871–6874, 2004.

110. I. Bajpai, N. Saha, B. Basu, Moderate intensity static magnetic field has bactericidal effect on E. coli and S. epidermidis on sintered hydroxyapatite, *Journal of Biomedical Materials Research Part B: Applied Biomaterials,* 100B:1206–1217, 2012.

111. L. Strašák, V. Vetterl, J. Smarda, Effects of low–frequency magnetic fields on bacteria Escherichia coli, *Bioelectrochemistry,* 55:161–164, 2002.

112. D.C. Ramon, J.T. Martin, M.R. Powell, Low–level, magnetic–field–induced growth modification of Bacillus subtilis, Bioelectromagnetics, 8:275–282, 1987.

113. W. Ji, H. Huang, A. Deng, C. Pan, Effects of static magnetic fields on Escherichia coli, *Micron,* 40:894–898, 2009.

114. K. Tsuchiya, K. Nakamura, K. Okuno, T. Ano, M. Shoda, Effect of homogeneous and inhomogeneous high magnetic fields on the growth of Escherichia coli, *Journal of Fermentation and Bioengineering,* 81:343–346, 1996.

115. S. Nakasono, M. Ikehata, M. Dateki, S. Yoshie, T. Shigemitsu, T. Negishi, Intermediate frequency magnetic fields do not have mutagenic, co–mutagenic

or gene conversion potentials in microbial genotoxicity tests, *Mutation Research,* 649:187–200, 2008.

116. R. Mittenzwey, R. Susmuth, W. Mei, Effects of extremely low–frequency electromagnetic fields on bacteria the question of a co–stressing factor, *Bioelectrochemistry and Bioenergetics,* 40:21–27, 1996.

117. M.F. San Martin, F. Harte, H. Lelieveld, G.V. Barbosa–Cánovas, B.G. Swanson, Inactivation effect of an 18–T pulsed magnetic field combined with other technologies on Escherichia coli, *Innovative Food Science & Emerging Technologies,* 2:273–277, 2001.

118. Z. She, X. Hu, X. Zhao, Z. Ren, G. Ding, FTIR investigation of the effects of ultra–strong static magnetic field on the secondary structures of protein in bacteria, *Infrared Physics & Technology,* 52:138–142, 2009.

119. M. Kohno, M. Yamazaki, I. Kimura, M. Wada, Effect of static magnetic fields on bacteria: Streptococcus mutans, Staphylococcus aureus, and Escherichia coli, *Pathophysiology,* 7:143–148, 2000.

120. P.J. White, A.T. Barker, I.S. Foulds, Insensitivity of several bacteria and fungi to the magnetic field generated by a bone stimulator, *European Journal of Clinical Microbiology,* 1:255–256, 1982.

121. L. Fojt, L. Strašák, V. Vetterl, J. Smarda, Comparison of the low–frequency magnetic field effects on bacteria Escherichia coli, Leclercia adecarboxylata and Staphylococcus aureus, *Bioelectrochemistry,* 63:337–341, 2004.

122. L. Fojt, P. Klapetek, L. Strašák, V. Vetterl, 50 Hz magnetic field effect on the morphology of bacteria, *Micron,* 40:918–922, 2009.

Nanostructured Selenium – A Novel Biologically-Inspired Material for Antibacterial Medical Device Applications

Qi Wang[1] and Thomas J. Webster[1,2,*]

[1]Bioengineering Program, College of Engineering, Northeastern University, Boston, Massachusetts, USA
[2]Department of Chemical Engineering, College of Engineering, Northeastern University, Boston, Massachusetts, USA

Abstract

Biofilms are a common cause of persistent infections on medical devices as they are easy to form but hard to treat. The polymeric matrix structure in biofilms increases the resistance of bacteria to conventional treatment methods such as antibiotics. Nanostructured selenium is considered to be a novel material for antibacterial applications. Unlike other metal-based antibacterial materials used in the healthcare industry (like silver), selenium is a naturally occurring micro-nutrient needed for a healthy lifestyle, and is recommended at a daily intake of 55 μg-70 μg by the FDA. In human beings, nutrition from selenium is achieved from 25 selenoproteins or enzymes with selenocysteine at their active center. Such proteins are fundamental for our antioxidant defense systems and other processes. This chapter will discuss studies which have coated nanostructured selenium on various materials from medical devices (for example, implants, catheters, prostheses and so on) to introduce antibacterial properties to the surface, thus preventing biofilm formation on those materials. This method is considered as a potential safe and effective way to reduce bacteria functions leading to medical device infections without relying on antibiotics. After discussion of such promising research, this chapter will provide thoughts on the future use of such novel biomimetic selenium materials in medicine.

Keywords: Selenium nanoparticles, bacterial infections, antibacterial properties, implant materials

---

Corresponding author: th.webster@neu.edu

8.1   Bacterial Biofilm Infections on Implant Materials

A biofilm is an aggregate of bacteria in which bacterial cells adhere to each other on a wet or moist surface. Biofilms may form on living or non-living surfaces and can be prevalent in natural, industrial and hospital settings [1, 2]. The formation of a biofilm (as shown in Figure 8.1) begins with the attachment of free-floating bacterial cells to the surface. As the bacterial cells propagate quickly, the biofilm structure develops becoming more complicated. At the last stage, the bacterial cells release into the environment and contaminate other surfaces.

Biofilms are considered easy to form but hard to treat, which can cause wide-spread infections [4] in the human body, for example, through catheter infections, infections on the inert surfaces of artificial implants [5] and the formation of dental plaques [6] (Figure 8.2). Statistics show that biofilms are involved in an estimated 80% of all infections [7]. These biofilm infections can be serious and hard to treat because the development of the biofilm structure may allow for bacteria to be increasingly antibiotic resistant, because the bacteria in the biofilm are held together and protected by a matrix of EPS (extracellular polymeric substance or exopolysaccharide). This matrix protects bacteria cells within it and facilitates communication among them through biochemical signals, resulting in their increased resistance to detergents and antibiotics. In some cases the effect of antibiotic resistance can be increased a thousand-fold [8]. Thus, bacteria in biofilms are frequently related with persistent infections [9] in the body.

An implanted medical device provides a surface for bacteria to attach to and multiply in a patient's body, resulting in the formation of a biofilm. Bacterial biofilm infection is a problem for all implants. For example, infection is one of the most common causes for failure of a hip implant, responsible for 14% of the total number of revision surgeries [11]. Another example
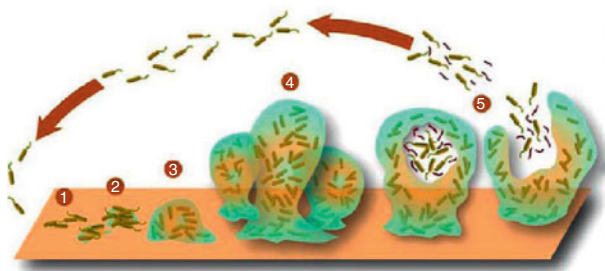
Figure 8.1   The biofilm life cycle [3]. 1: individual cells populate the surface. 2: EPS (exopolysaccharide) is produced and attachment becomes irreversible. 3 & 4: biofilm architecture develops and matures. 5: single cells are released from the biofilm.
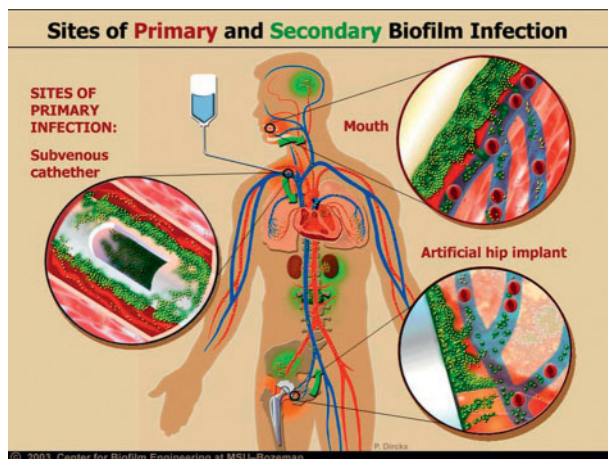
Figure 8.2 Common sites of biofilm infection [10]. Once bacteria enter the circulatory system, they can spread to any moist surface of the human body.

of implant infection relates to catheters, which is the most common and complicated problem associated with catheter usage. Infections are the most serious complication of tunneled dialysis catheters, resulting in serious systemic infections, including endocarditis, osteomyelitis, epidural abscess, septic arthritis, and even death [12]. Infections lead to implant failure, extended hospital stay, and additional treatment/surgeries. Bacteria infect up to 54% of all catheters [13] and cause many serious complications including patient death. For example, catheter infection is associated with a mortality rate of 12% to 25% among critically ill patients [14]. Catheter-associated urinary tract infection (CAUTI) is the most common type (accounting for 40%) of hospital-acquired infection resulting in serious complications such as bloodstream infection, and even death [15]. Each year, in US acute-care hospitals and extended-care facilities, CAUTI affects approximately 1 million patients who then will have increased institutional death rates [16]. The cost incurred by infections in the US is nearly $11 billion annually [17].

Implant associated infections are difficult to treat because of biofilm formation. Bacteria in a biofilm can escape from the film and enter the blood, lungs, etc., causing serious problems. Biofilms tenaciously bind to surfaces. More importantly, bacteria in biofilms are extremely resistant to antibiotic treatment due to the slow transport of antibiotic molecules through the polymeric-like biofilm substance, altered micro-environment within the biofilm and higher number of "persister" cells (cells that are resistant to many types of stress) within the biofilm compared to planktonic cells [18].

Among the most common pathogens found on infected implants, *Staphylococcus aureus* is responsible for 20% of catheter infections and 35% of orthopedic implant infections [19–21]. *Staphylococcus aureus* is one of the

bacterium commonly found in numerous infections. These infections can be serious when they occur on surgical wounds, in the bloodstream, or in the lungs. Each year, there are 11 million outpatient/emergency room visits and 464,000 hospital admissions in the US alone due to *Staphylococcus aureus* infections [22]. *Staphylococcus aureus* have been found on a wide range of medical devices including prosthetic heart valves, central venous catheters, urinary catheters, orthopedic prostheses, penile prostheses, contact lenses, endocarditis, otitis media, osteomyelitis, and sinusitis [23]. Therefore, it is significant to develop a method to prevent bacteria from attaching on the surface of today's medical devices. The use of antibiotics is not a strategy that is working, nor is it a natural biomimetic approach towards decreasing bacteria function.

8.2 Nanomaterials for Antibacterial Implant Applications

A common method to treat implant infection is though systemic antibiotic therapy. However, this method has not shown satisfactory results to date. For example, systemic antibiotic (vancomycin and gentamicin) administration alone without catheter removal is only 22 to 37% effective in treating blood infection associated with using long-term (more than 2 weeks) central venous catheters. In addition, this mode of antibiotic administration has the disadvantage of causing side effects and creating a pool of antibiotic-resistant bacteria. Another treatment method is the local delivery of antibiotics. In this method, antibiotic molecules are incorporated (for example, by adsorption or impregnation) onto the surface or into the coatings on implants so that they will slowly release locally over an extended period of time after implantation. Because of the use of antibiotics, this method also has significant drawbacks including ineffectiveness against antibiotic-resistant bacteria (such as methicillin-resistant *Staphylococcus aureus* or MRSA, important bacterium that infects all implants). An emerging approach to prevent implant infection is engineering raw implant surfaces to resist bacterial attachment and colonization. Since the implant surface itself is an important source of infection and bacterial adhesion to the implant surface and is important in the pathogenesis of infection, the most promising and straightforward strategy towards decreasing infection is to fabricate implant materials that resist bacteria attachment [24]. However, currently materials used as implants have been shown to be ineffective in resisting bacterial infection [25–27].

In recent years, nanomaterials have drawn increasing attention from many researchers because these materials exhibit special properties stemming from their biologically-inspired nanoscale dimensions, which are different compared with conventional or bulk materials. An important

feature of nanomaterials or nanoparticles is the vastly increased ratio of surface area to volume, which allows for potentially increased interactions between nanomaterials and biological targets, such as mammalian cells and bacteria [28]. As a result, nanomaterials will likely exert a stronger interaction with bacterial cells which may affect their growth and propagation. Thus, various nanomaterials were developed and studied for their potential antibacterial applications.

One of the most widely investigated antibacterial materials are silver nanoparticles and silver-based materials [29]. Silver nanoparticles interact with and kill bacteria through two possible mechanisms [30]. As shown in Figure 8.3, one mechanism is that silver nanoparticles bind to the bacterial cell wall and cell membrane and interact with thiol group compounds found in the respiratory enzymes of bacterial cells, thus inhibiting the respiration process [31]. Silver forms stable S-Ag bonds with thiol group compounds or participate in catalytic oxidation reactions resulting in the formation of disulfide bonds (R-S-S-R). In the other mechanism, the silver nanoparticles penetrate inside the bacterial cell and interact with DNA molecules because of releasing reactive oxygen species (ROS) and silver ions. DNA molecules turn into a condensed form (only when DNA molecules are in a relaxed state, do they replicate effectively) and lose their replication ability leading to cell death [33]. Besides silver nanoparticles, copper containing materials [34, 35], ZnO nanoparticles [36], polymer films [37] and so on have also been studied for antibacterial purposes. But how these materials interact
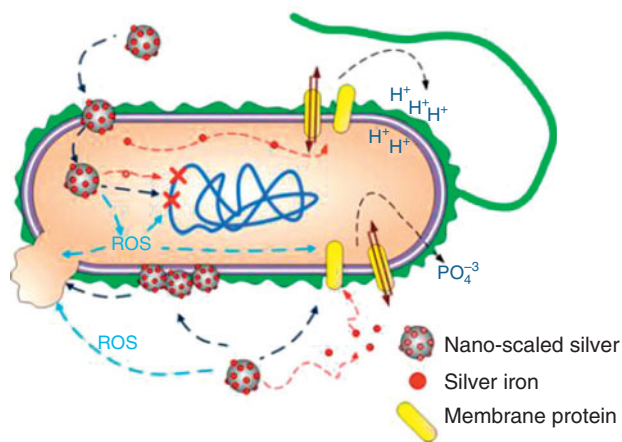
Figure 8.3 Diagram summarizing nanoscaled silver interactions with bacteria [32]. Nanoscaled silver may (1) release silver ions and generate reactive oxygen species (ROS); (2) interact with membrane proteins affecting their correct function; (3) accumulate in the cell membrane affecting membrane permeability; and (4) enter into the cell where it can generate ROS, release silver ions, and affect DNA.

with bacteria remains largely unknown and there is not a material that is well established and widely accepted for antibacterial purposes.

8.3   Selenium and Nanostructured Selenium

Selenium belongs to the group of metalloids from the chalcogen family in the periodic table of elements. It exists in a range of oxidation states from +6 to −2. Selenium has various allotropic forms, such as the red amorphous form, black vitreous form, three (α, β, γ) of red crystalline monoclinic forms and the gray/black crystalline hexagonal form [38–41]. Commercially, selenium is produced as a byproduct of copper refining. It is used in electronics, glass, ceramics, steel and pigment manufacturing [42]. Selenium is naturally found in humans and animals as a part of selenoproteins, which play an important role in antioxidant defense systems, thyroid hormone metabolism and redox control of cell reactions [43].

Previously, selenium and its compounds were studied for reducing or preventing cancers. It has been shown that high levels of selenium in the blood (~154 µg/ml) correlate with reduced numbers of cancers including pancreatic, gastric, lung, nasopharyngeal, breast, uterine, respiratory, digestive and gynecological cancer [44]. Moreover, people living in areas of low soil selenium (lower than 0.05 ppm) and people with decreased plasma selenium levels (below 128 ng/ml) have higher cancer incidence and/or cancer mortality [45, 46]. Many *in vitro* studies also demonstrated the inhibitory effects of selenium on the growth of many cancerous cell lines [47–49]. However, the mechanisms of selenium-related chemoprevention are complex and remain largely unknown [50].

Recently, as the organic forms of selenium have been studied for their biological effects, the elemental selenium nanoparticles have also drawn some attention in many studies [51]. Various methods of synthesizing selenium nanoparticles have been reported [52–56]. In a easy and quick precipitation method, selenium nanoparticles were synthesized by reducing sodium selenite with glutathione [57, 58]. The hypothesized mechanism below was based on several reactions involving sulfur, because selenium and sulfur are in the same group in the periodic table.

(a) $4\,GSH + Na_2SeO^3 \rightarrow GSSeSG + GSSG + 2NaOH$

(b)

$$Se{-}S + OH^- \rightarrow GSOH + GSSe^-$$

(c) $GSSe^- \rightarrow GS^- + Se$
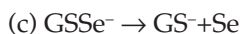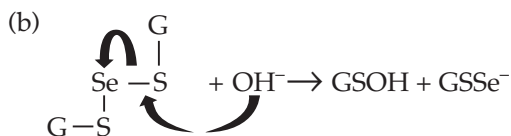
(d) $GS^- + GSOG \rightarrow GSSG + OH^-$ (8.1)

In this mechanism, selenodiglutathione (GSSeSG) is considered as an intermediate, which releases element selenium at alkaline pH. Similar to the alkaline hydrolysis of disulfide bonds (RSSR) that gives a sulfenic acid (RSOH) and a thiolate (RS$^-$) [59], the hydroxide anion is believed to cleave the selenotrisulphide bond in GSSeSG (step b). This step is favored at alkaline pH [59], so we need to add NaOH into the solution, and more NaOH results in the faster reaction. In step c, the release of selenium from the intermediate selenopersulfide anion (GSSe$^-$) is similar to what has been reported for hydrodisulphide anion (RSS$^-$) [60]. In fact, the evidence of the occurrence of selenopersulfide (GSSe$^-$) as the initial reaction product has been reported [61].

Because of the small size and higher ratio of surface area to volume compared to conventional selenium materials, selenium nanoparticles were believed to have different possible mechanisms against bacterial growth and biofilm formation, such as the change in hydrophobicity of the surface preventing bacteria from attachment [62]. It certainly represents a more natural and biomimetic manner to decrease bacteria attachment.

In a possible mechanism towards inhibiting bacteria, nanostructured selenium may serve as a catalyst, oxidizing thiol groups, and reducing oxygen to superoxide [63]. As thiol is an essential substance for bacteria function, selenium can inhibit bacteria by depleting their thiol levels. This intracellular thiol depletion mechanism is significant because healthy cells are more resilient to this effect than bacteria cells. Moreover, the nano features of the selenium coating and the change in hydrophobicity that may have resulted from coating polycarbonate with selenium nanoparticles [62] may also serve as an important role in inhibiting biofilm formation. However, the mechanism of selenium inhibited bacteria growth in biofilms is likely complicated and further studies are certainly required.

8.4 Selenium Nanoparticles for Antibacterial Applications

8.4.1 Antibacterial Properties of Selenium Compounds

In several studies, researchers provided the evidence of the antibacterial properties of many selenium compounds. For example, selenium-enriched probiotics have been shown to strongly inhibit the growth of pathogenic *Escherichia coli in vivo* and *in vitro* [64]. *Escherichia coli* was cocultured *in vitro* with each of four probiotic strains individually. A cell-free culture supernatant (CFCS) of each probiotic strain and the four-strain mix were examined for their antibacterial activity, using the cylinder plate method. *In vitro* results demonstrated that cocultures with probiotics significantly reduced the number of *Escherichia coli*. The different sizes of inhibition zones made by each CFCS proved that *Escherichia coli* was inhibited by the metabolites

of the probiotics. In the *in vivo* studies, Kunming mice were allocated to different groups supplemented with selenium-enriched and other probiotics. After 28 days, the mice were inoculated with pathogenic *Escherichia coli* so that we could compare mortality rates and inspect other indexes of each treatment. It was found that the mortality of the group with selenium-enriched probiotics was the lowest. Thus, selenium-enriched probiotics can strongly antagonize pathogenic *Escherichia coli in vitro* and *in vivo*.

What is more, a synthesized organoselenium compound was shown to be as effective as penicillin in inhibiting *Pseudomonas aeruginosa* and *Staphylococcus aureus* growth in solution *in vitro* [65]. Specifically, organoselenium molecules (N-substituted benzisoselenazol-3(2H)-ones, analogues of ebselen, whose name was unrevealed for proprietary reasons) covalently bonded to silicone hydrogel contact lenses to transform the lenses into antibacterial materials. The contact lenses were coated with the organo-selenium molecules and tested against colonization of *Pseudomonas aeruginosa* and *Staphylococcus aureus*. The results showed little or no bacterial biofilm formation on the coated lenses after 4 days of incubating the lenses in bacteria solutions. In contrast, uncoated lenses showed extensive bacterial biofilm formation. The safety of the organo-selenium coated lenses was also tested by placing them into the eyes of New Zealand albino rabbits for up to 2 months. There was no sign of toxicity for the eyes wearing the coated lenses as well as the eyes wearing uncoated lenses.

8.4.2 Selenium Nanoparticles Inhibit *Staphylococcus Aureus* Growth

A previous study [66] tested the growth of *Staphylococcus aureus* in the presence of selenium nanoparticles. Selenium nanoparticles were synthesized by the reduction of sodium selenite by glutathione and stabilized by bovine serum albumin. Transmission electron microscopy (TEM) images of selenium nanoparticles showed that the particles were spherical and approximately 40–60 nm in diameter (Figure 8.4). Further investigation of the size distribution of the selenium nanoparticles by Dynamic light scattering (DLS) revealed that most of the particles had hydrodynamic diameters around 100 nm. The sizes observed by DLS were larger than those determined by TEM images because BSA molecules bound to the surface of the selenium nanoparticles created a layer that made the particles appear larger [67, 68]. Nanoscale sizes of the synthesized selenium nanoparticles promoted a desirable large surface area important for increasing interactions with bacteria.

Importantly, the bacterial assays in this study clearly showed a slow, inhibited growth profile of *Staphylococcus aureus* in the presence of selenium nanoparticles. Bacterial growth was inhibited approximately 20 times (compared with controls) after 3 hours, 50 times after 4 hours, and 60 times after 5 hours (Figure 8.5). It was the first time it was shown
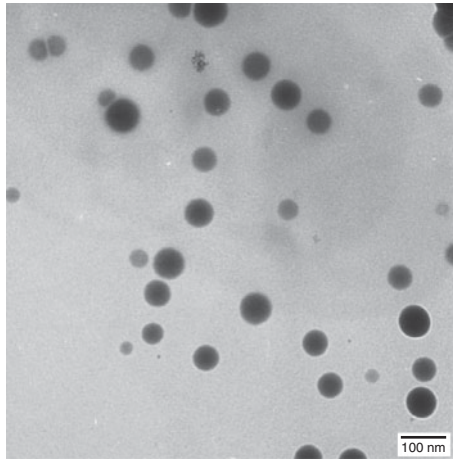
Figure 8.4 Transmission electron microscopy image of selenium nanoparticles stabilized in bovine serum albumin and dispersed in water [66].
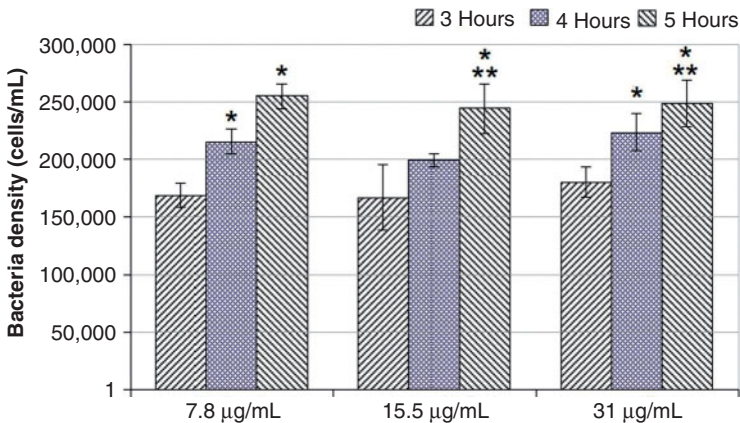
Figure 8.5 Growth profiles of bacteria in the presence of selenium nanoparticles. Data = Mean ± standard deviation by mean, n = 3. *P < 0.05 compared with 3 hours (compared with the same selenium nanoparticle concentration group); **P < 0.05 compared with 4 hours (compared with the same selenium nanoparticle concentration group). There was no significant difference in bacterial densities between different selenium nanoparticle concentrations at each time point tested. (Bacteria densities for control groups were 4,083,480, 11,662,534, and 15,315,887 cells/mL at 3, 4, and 5 hours, respectively). See [66] for more details.

that the selenium nanoparticles synthesized by a simple colloidal method strongly inhibited the growth of *Staphylococcus aureus* in solution compared with no treatment. As mentioned before, bacterial biofilms such as those that form on implants, were considered even more difficult to be

treated compared with planktonic bacteria in the solution. Thus, a further study particularly targeting bacterial biofilms, as shown in the following section, needs to implemented to achieve more efficient solutions to fight implant infections.

8.4.3   Selenium Nanoparticles for Preventing Biofilm Formation on Polycarbonate Medical Devices

Unlike many metal-based antibacterial materials used in the healthcare industry, selenium is a naturally occurring micronutrient needed for a healthy lifestyle and is recommended for daily intake by the FDA. In human beings, nutrition from selenium is achieved from 25 selenoproteins or enzymes with selenocysteine at their active center [69], which are fundamental for a human's antioxidant defense system and other processes. Importantly, a low selenium intake (less than 40 g per day) has been associated with an increased risk of mortality, poor immune function, and cognitive decline [70]. Clearly, thus, using nanoparticles of selenium is a much more natural way to kill bacteria than synthetic antibodies.

Polycarbonate medical devices have been coated with nano-selenium [71]. Two difference coating conditions were used in order to achieve various sizes of selenium nanoparticles. Most of the selenium nanoparticles were approximately 50–100 nm in diameter and they were well-distributed on the polycarbonate surface (Figure 8.6). The concentration of selenium nanoparticles on the polycarbonate surfaces were around 20 g/m^2 as assessed by atomic absorption spectroscopy (AAS). Besides using an ASTM (American Society for Testing and Materials) adhesion test, it was demonstrated that larger nanoparticles had less adhesion strength to the underlying polycarbonate substrate than smaller selenium nanoparticles.

Most significantly, *in vitro* studies on selenium-coated polycarbonate showed that the selenium coatings on polycarbonate significantly inhibited *Staphylococcus aureus* growth 8.9% and 27% compared with an uncoated polycarbonate surface after 24 and 72 hours, respectively (Figure 8.7). Importantly, this was accomplished without using antibiotics but rather with an element (selenium) that is natural to the human body. Thus, this study suggests that coating polymers (particularly, polycarbonate) with nanostructured selenium is a fast and effective way to reduce bacteria functions that lead to medical device infections. As polycarbonate samples coated under different conditions had different abilities to inhibit bacterial growth, the concentration, size, and coverage of selenium on polycarbonate needs to be optimized.

8.4.4   Preventing Bacterial Growth on Paper Towels

Lastly, in the hospital environment, hand washing has been identified as the most significant manner of preventing the spread of microbial
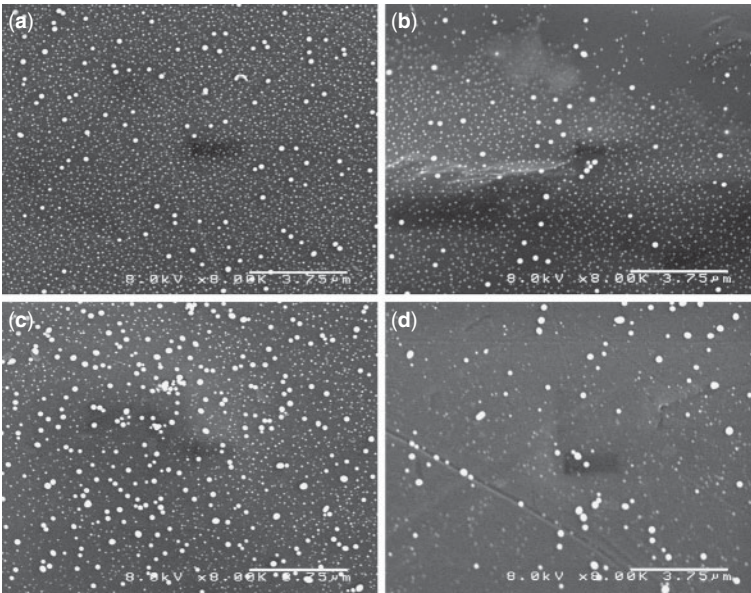
Figure 8.6 SEM images of selenium-coated polycarbonate samples before and after a tape test. (a) 0.5M NaOH, coating for 30 seconds and before a tape test. (b) 0.5M NaOH, coating for 30 seconds and after a tape test. (c) 1.0M NaOH, coating for 60 seconds and before a tape test. (d) 1.0M NaOH, coating for 60 seconds and after a tape test. The coverage of selenium nanoparticles on the surface for image (a), (b), (c), (d) was 11.74%, 6.94%, 11.38%, 5.88% respectively. See [71] for more details.
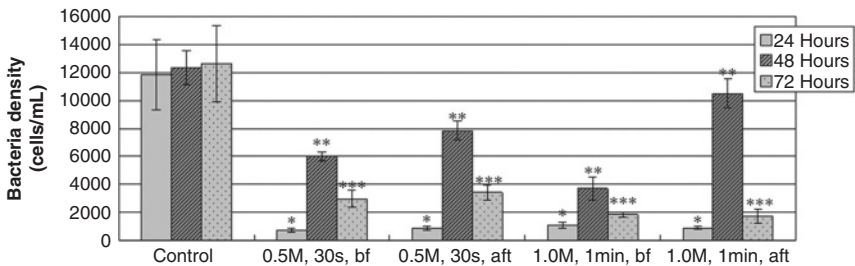
Figure 8.7 Bacteria (*Staphylococcus aureus*) growth on the surface of polycarbonate. Polycarbonate samples were treated with bacteria (*Staphylococcus aureus*) in 0.03% TSB (Tryptic Soy Broth) and were incubated for 24, 48 or 72 hours. The media was changed with 0.03% TSB every 24 hours for those samples incubated for 48 or 72 hours. The control group is uncoated polycarbonate. bf = before tape test; aft = after tape test. Data=Mean ± standard deviation by mean, n=3; See [71] for more details.

infections [72, 73], with hand drying as the critical last stage of the hand washing process. Among the three frequently used methods to dry hands (hot air dryers, cloth towels and paper towels), paper towels have been recognized as the most hygienic method of hand drying [74, 75]. However, in some circumstances, such as for paper towels hanging in sink splash zones or those used to clean surfaces, they have been considered as potential sources of bacteria contamination [76]. Besides paper towels that are used for hand drying, there are concerns for many other paper products in terms of bacteria contamination or infections, for example, food wrapping in the food industry [77], wallpaper in a doctor's suite, filter paper in water purifying system [78] and so on. All of these materials are prone to bacteria growth and, thus, are sources for continual contamination.

One of the most promising approaches towards preventing infection is coating paper products with antimicrobial materials. For example, Wenbing Hu and his colleagues introduced antibacterial properties to filter paper by coating the paper with graphene oxide, which showed about a 70% inhibition to *Escherichia coli* growth after 2 hours. However, the graphene-based paper had mild cytotoxicity resulting in 20% of healthy mammalian A945 cell death after 2 hours [79]. Chule *et al.* studied the antibacterial activities of ZnO nanoparticle-coated paper [80] and results showed a significant decrease in bacteria counts after 24 hours. Besides ZnO nanoparticles, silver nanoparticles have also been loaded on filter paper for antibacterial purposes, processing strong antibacterial properties.

But one major problem for ZnO and silver nanoparticles and other metal-based materials is their toxicity to healthy cells due to the generation of reactive oxygen species [81, 82]. Those materials may result in severe health problems when they are used as coatings on paper products such as for food wrapping or clinical applications.

Therefore, selenium nanoparticles were coated on normal paper towel surfaces, introducing significant effectiveness towards preventing *Staphylococcus aureus* growth on the paper surfaces [83]. As shown in Figure 8.8a, selenium nanoparticles were well distributed and completely covered the surface. Some of the selenium nanoparticles were also observed in the fiber structure on the top surface. Diameters for most of the selenium particles were around 50 nm. According to AAS results, the concentration of the selenium nanoparticles on the coated paper towel surface was 69.00 g/m². There were no particles observed for the uncoated paper towel (Figure 8.8b).

Based on the bacterial assays, the selenium-coated paper towel samples significantly inhibited *Staphylococcus aureus* biofilm formation compared with uncoated paper towel samples. As seen in Figure 8.9, the selenium-coated paper towels had 88.6%, 88.9% and 88.8% less bacteria attached than the uncoated paper towels after 24, 48 and 72 hours, respectively. Moreover, from the 24 hour culture time to the 48 hour culture time, there was an increase in bacteria numbers on the uncoated paper towel
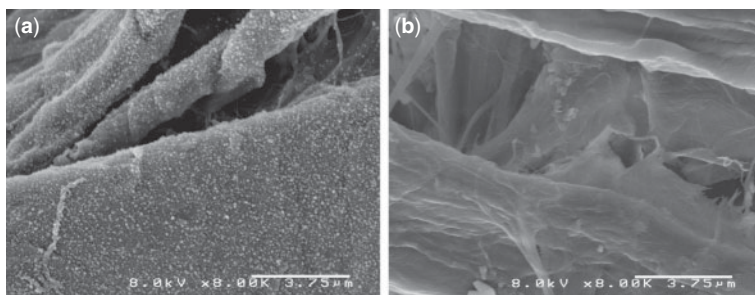
Figure 8.8 SEM images of selenium-coated (image a) and uncoated paper (image b) towel samples. The coating condition for image (a) was 0.5M NaOH for 30 seconds. The concentration of selenium on the paper towel as measured by AAS was 69.00 g/m^2 for the selenium-coated paper towels and 0 g/m^2 for the uncoated paper towels. See [83] for more details.
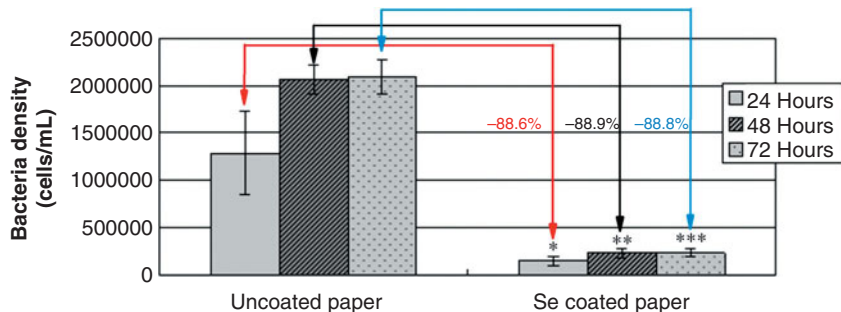
Figure 8.9 Bacteria (*Staphylococcus aureus*) growth on the surface of uncoated and selenium-coated paper towels. Paper towel samples were treated with bacteria (*Staphylococcus aureus*) in 0.03% TSB (Tryptic Soy Broth) and were incubated for 24, 48 or 72 hours. The control group is the uncoated paper towels. Data=Mean ± standard deviation, n=3. See [83] for more details.

samples, but was constant after the 72 hours culture time, implying that the uncoated paper towel was saturated by bacteria after just 48 hours of treatment. In contrast, the bacteria numbers on the selenium-coated paper towels remained at a low level, not increasing from 24 to 48 to 72 hours, indicating successful inhibition of bacterial growth. Overall, the bacteria growth and biofilm formation on paper towels were successfully inhibited after coated with selenium nanoparticles, again representing a natural biomimicking approach towards fighting bacteria.

8.5   Summary and Outlook

In summary, this chapter presented and demonstrated the potential applications of biologically-inspired nanostructured selenium as an antibacterial

surface coating. Specifically, the selenium coatings significantly decreased bacterial growth, thus, inhibiting biofilm formation on both various polymer and paper towels. All of these antibacterial effects were achieved without using antibiotics. However, several aspects and more in-depth studies need to be further explored to achieve a better understanding of the antibacterial properties of nanostructured selenium and to expand the applications of nanostructured selenium as an antibacterial coating material. Particularly, the antibacterial properties should be further tested on different bacteria species because compared with *Staphyloccocus aureus* in most studies, other different bacterial species, such as *Staphylococcus epidermidis*, *Pseudomonas aeruginosa* and *Escherichia coli*, may have various sizes, surface proteins, cell membranes and other features, which may reveal different interactions with nanostructured selenium coatings. Last but not least, *in vivo* studies in animals and humans should be implemented to further investigate the antibacterial properties and safety concentrations of nanostructured selenium as a novel biomaterial. Only until these studies are conducted will we know the true value of the use of biologically-inspired nano-selenium in a wide range of medical applications.

References

1. L. Hall-Stoodley, J.W. Costerton, P. Stoodley, Bacterial biofilms: From the natural environment to infectious diseases, *Nat. Rev. Microbiol.*, 2(2):95–108, Feb 2004.
2. G. Lear and G.D. Lewis, Eds., *Microbial Biofilms: Current Research and Applications*, Wymondham NR18 0JA: Caister Academic Press, 2012.
3. A.B. Cunningham, J.E. Lennox, and R.J. Ross, Eds., *Biofilm Hypertextbook*, Montana State University Center for Biofilm Engineering, 2011.
4. J.W. Costerton, Introduction to biofilm, *Int. J. Antimicrob. Ag.*, 11(3–4):217–221, May 1999.
5. M.E. Auler, D. Morreira, F.F.O. Rodrigues, *et al.*, Biofilm formation on intrauterine devices in patients with recurrent vulvovaginal candidiasis, *Med. Mycol.*, 48(1):211–216, Feb 2010.
6. A.H. Rogers, *Molecular Oral Microbiology*, Wymondham NR18 0JA: Caister Academic Press, 2008.
7. Research on microbial biofilms (PA-03–047): NIH, National Heart, Lung, and Blood Institute, 2002.
8. P.S. Stewart, J.W. Costerton, Antibiotic resistance of bacteria in biofilms, *Lancet*, 358(9276):135–138, Jul 14 2001.
9. J.P. Nataro, M.J. Blaser, and S. Cunningham-Rundles, Eds., *Persistent Bacterial Infections*, Washington DC: ASM Press, 2000.
10. P. Dirckx, Center for Biofilm Engineering, Montana State University, Bozeman.
11. K.J. Bozic, The increasing number of THA revisions in the United States: Why is it happening? *Orthopedics Today*, 2009.
12. Z. Krishnasami, D. Carlton, L. Bimbo, *et al.*, Management of hemodialysis catheter-related bacteremia with an adjunctive antibiotic lock solution, *Kidney International*, 61(3):1136–1142, Mar 2002.

13. S.O. Trerotola, Hemodialysis catheter placement and management, *Radiology*, 215(3):651–658, Jun 2000.
14. J. Sanders, A. Pithie, P. Ganly, *et al.*, A prospective double-blind randomized trial comparing intraluminal ethanol with heparinized saline for the prevention of catheter-associated bloodstream infection in immunosuppressed haematology patients, *The Journal of Antimicrobial Chemotherapy,* 62(4):809–815, Oct 2008.
15. J.R. Johnson, M.A. Kuskowski, T.J. Wilt, Systematic review: Antimicrobial urinary catheters to prevent catheter-associated urinary tract infection in hospitalized patients, *Annals of Internal Medicine,* 144(2):116–126, Jan 17 2006.
16. D.G. Maki, P.A. Tambyah, Engineering out the risk for infection with urinary catheters, *Emerging Infectious Diseases,* 7(2):342–347, Mar-Apr 2001.
17. J.M. Schierholz, J. Beuth, Implant infections: A haven for opportunistic bacteria, *The Journal of Hospital Infection,* 49(2):87–93, Oct 2001.
18. D. Davies, Understanding biofilm resistance to antibacterial agents, *Nature Reviews. Drug Discovery,* 2(2):114–122, Feb 2003.
19. R.M. Donlan, Biofilms and device-associated infections, *Emerging Infectious Diseases.* 7(2):277–281, Mar-Apr 2001.
20. J. Chastre, J.Y. Fagon, Ventilator-associated pneumonia, *American Journal of Respiratory and Critical Care Medicine,* 165(7):867–903, Apr 1 2002.
21. P.J. Sanderson, Infection in orthopaedic implants, *The Journal of Hospital Infection,* 18 Suppl A:367–375, Jun 1991.
22. L.R. Martinez, G. Han, M. Chacko, *et al.*, Antimicrobial and healing efficacy of sustained release nitric oxide nanoparticles against Staphylococcus aureus skin infection, *The Journal of Investigative Dermatology,* 129(10):2463–2469, Oct 2009.
23. R. Singh, P. Ray, A. Das, M. Sharma, Role of persisters and small-colony variants in antibiotic resistance of planktonic and biofilm-associated Staphylococcus aureus: An in vitro study, *J. Med. Microbiol.,* 58(8):1067–1073, Aug 2009.
24. D.G. Maki, S.M. Stolz, S. Wheeler, L.A. Mermel, Prevention of central venous catheter-related bloodstream infection by use of an antiseptic-impregnated catheter: A randomized, controlled trial, *Annals of Internal Medicine.* 127(4): 257–266, Aug 15 1997.
25. D. Yahav, B. Rozen-Zvi, A. Gafter-Gvili, L. Leibovici, U. Gafter, M. Paul, Antimicrobial lock solutions for the prevention of infections associated with intravascular catheters in patients undergoing hemodialysis: Systematic review and meta-analysis of randomized, controlled trials, *Clinical Infectious Diseases: An Official Publication of the Infectious Diseases Society of America,* 47(1):83–93, Jul 1 2008.
26. S.O. Trerotola, M.S. Johnson, H. Shah, *et al.*, Tunneled hemodialysis catheters: Use of a silver-coated catheter for prevention of infection–a randomized study, *Radiology,* 207(2):491–496, May 1998.
27. C. Logghe, C. Van Ossel, W. D'Hoore, H. Ezzedine, G. Wauters, J.J. Haxhe, Evaluation of chlorhexidine and silver-sulfadiazine impregnated central venous catheters for the prevention of bloodstream infection in leukaemic patients: A randomized controlled trial, *The Journal of Hospital Infection,* 37(2):145–156, Oct 1997.
28. M. Goldberg, R. Langer, X. Jia, Nanostructured materials for applications in drug delivery and tissue engineering, *Journal of Biomaterials Science, Polymer Edition,* 18(3):241–268, 2007.

29. M. Rai, A. Yadav, A. Gade, Silver nanoparticles as a new generation of antimicrobials. *Biotechnology Advances,* 27(1):76–83, Jan-Feb 2009.

30. H.Y. Song, K.K. Ko, L.H. Oh, B.T Lee, Fabrication of silver nanoparticles and their antimicrobial mechanisms, *European Cells and Materials,* 11:58, 2006.

31. H.J. Klasen, A historical review of the use of silver in the treatment of burns: II. Renewed interest for silver, *Burns,* 26(2):131–138, Mar 2000.

32. C. Marambio-Jones, E.M.V. Hoek, A review of the antibacterial effects of silver nanomaterials and potential implications for human health and the environment, *J. Nanopart. Res.,*12(5):1531–1551, Jun 2010.

33. Q.L. Feng, J. Wu, G.Q. Chen, F.Z. Cui, T.N. Kim, J.O. Kim, A mechanistic study of the antibacterial effect of silver ions on Escherichia coli and Staphylococcus aureus, *Journal of Biomedical Materials Research,* 52(4):662–668, Dec 15 2000.

34. R.J. McLean, A.A. Hussain, M. Sayer, P.J. Vincent, D.J. Hughes, T.J. Smith, Antibacterial activity of multilayer silver-copper surface films on catheter material, *Canadian Journal of Microbiology,* 39(9):895–899, Sep 1993.

35. A.M. Mulligan, M. Wilson, J.C. Knowles, The effect of increasing copper content in phosphate-based glasses on biofilms of Streptococcus sanguis, *Biomaterials,* 24(10):1797–1807, May 2003.

36. J.H. Li, R.Y. Hong, M.Y. Li, H.Z. Li, Y. Zheng, J. Ding, Effects of ZnO nanoparticles on the mechanical and antibacterial properties of polyurethane coatings, *Prog. Org. Coat.,*64(4):504–509, Mar 2009.

37. T.P. Martin, S.E. Kooi, S.H. Chang, K.L. Sedransk, K.K. Gleason, Initiated chemical vapor deposition of antimicrobial polymer coatings, *Biomaterials,* 28(6):909–915, Feb 2007.

38. T. Takahashi, Comparative X-ray-photoemission study of monoclinic, trigonal, and amorphous selenium, *Phys. Rev. B.,* 26(10):5963–5964, 1982.

39. P. Cherin, P. Unger, Refinement of crystal-structure of alpha-monoclinic Se. *Acta Crystall. B-Stru.,* B 28:313-&, Jan 151972.

40. O. Foss, V. Janickis, Crystal-structure of gamma-monoclinic selenium. *J. Chem. Soc. Dalton,* (4):624–627, 1980.

41. P. Cherin, P. Unger, Crystal structure of trigonal selenium, *Inorg. Chem.,* 6(8):1589-&, 1967.

42. D.G. Barceloux, Selenium. *J. Toxicol.-Clin. Toxic.,* 37(2):145–172, 1999.

43. L.R. McDowell, *Minerals in Animal and Human Nutrition.* Amsterdam: Elsevier, 2003.

44. M. Navarro-Alarcon, M.C. Lopez-Martinez, Essentiality of selenium in the human body: Relationship with different diseases. *Sci. Total Environ.,* 249(1–3): 347–371, Apr 17 2000.

45. L.C. Clark, K.P. Cantor, W.H. Allaway, Selenium in forage crops and cancer mortality in United-States counties. *Arch. Environ. Health.,* 46(1):37–42, Jan-Feb 1991.

46. G.F. Combs, W.P. Gray, Chemopreventive agents: Selenium. *Pharmacol. Therapeut.,* 79(3):179–192, Sep 1998.

47. J.X. Lu, C. Jiang, M. Kaeck, H. Ganther, C. Ip, H. Thompson, Cellular and metabolic effects of triphenylselenonium chloride in a mammary cell-culture model, *Carcinogenesis,*16(3):513–517, Mar 1995.

48. C. Redman, J.A. Scott, A.T. Baines, *et al.,* Inhibitory effect of selenomethionine on the growth of three selected human tumor cell lines, *Cancer Lett.,* 125(1–2): 103–110, Mar 13 1998.

49. M. Kaeck, J.X. Lu, R. Strange, C. Ip, H.E. Ganther, H.J. Thompson, Differential induction of growth arrest inducible genes by selenium compounds. *Biochem. Pharmacol.*, 53(7):921–926, Apr 4 1997.
50. G.F. Combs, Impact of selenium and cancer-prevention findings on the nutrition-health paradigm. *Nutr. Cancer,* 40(1):6–11, 2001.
51. J.S. Zhang, X.F. Wang, T.W. Xu, Elemental selenium at nano size (Nano-Se) as a potential chemopreventive agent with reduced risk of selenium toxicity: Comparison with Se-methylselenocysteine in mice, *Toxicol. Sci.,* 101(1):22–31, Jan 2008.
52. Z.Y. Jiang, Z.X. Xie, S.Y. Xie, X.H. Zhang, R.B. Huang, L.S. Zheng, High purity trigonal selenium nanorods growth via laser ablation under controlled temperature, *Chem. Phys. Lett.,* 368(3–4):425–429, Jan 17 2003.
53. C.H. An, S.T. Wang, Diameter-selected synthesis of single crystalline trigonal selenium nanowires, *Mater. Chem. Phys.,* 101(2–3):357–361, Feb 15 2007.
54. X.C. Jiang, L. Kemal, A.B. Yu, Silver-induced growth of selenium nanowires in aqueous solution, *Mater. Lett.,* 61(11–12):2584–2588, May 2007.
55. S. Lee, C. Kwon, B. Park, S. Jung. Synthesis of selenium nanowires morphologically directed by Shinorhizobial oligosaccharides, *Carbohyd. Res.,* 344(10): 1230–1234, Jul 6 2009.
56. Y.J. Zhu, X.L. Hu, Preparation of powders of selenium nanorods and nanowires by microwave-polyol method, *Mater. Lett.,* 58(7–8):1234–1236, Mar 2004.
57. E.P. Painter, The chemistry and toxicity of selenium compounds, with special reference to the selenium problem. *Chem. Rev.,* 28(2):179–213, Apr 1941.
58. H.E. Ganther, Selenotrisulfides: Formation by the reaction of thiols with selenious acid, *Biochemistry,* 7(8):2898–2905, Aug 1968.
59. P.J. Hogg, Disulfide bonds as switches for protein function, *Trends Biochem. Sci.,* 28(4):210–214, Apr 2003.
60. I.V. Koval. The chemistry of disulfides, *Russian Chemical Reviews,* 63:735.
61. H.E. Ganther, Reduction of selenotrisulfide derivative of glutathione to a persulfide analog by glutathione reductase. *Biochemistry,* 10(22):4089-&, 1971.
62. P.A. Tran, L. Sarin, R.H. Hurt, T.J. Webster, Differential effects of nanoselenium doping on healthy and cancerous osteoblasts in coculture on titanium. *International Journal of Nanomedicine,* 5:351–358, 2010.
63. J.E. Spallholz, B.J. Shriver, T.W. Reid, Dimethyldiselenide and methylseleninic acid generate superoxide in an in vitro chemiluminescence assay in the presence of glutathione: Implications for the anticarcinogenic activity of L-selenomethionine and L-Se-methylselenocysteine, *Nutr. Cancer,* 40(1):34–41, 2001.
64. J. Yang, K. Huang, S. Qin, X. Wu, Z. Zhao, F. Chen, Antibacterial action of selenium-enriched probiotics against pathogenic Escherichia coli. *Digestive Diseases and Sciences,* 54(2):246–254, Feb 2009.
65. M. Pietka-Ottlik, H. Wojtowicz-Mlochowska, K. Kolodziejczyk, E. Piasecki, J. Mlochowski, New organoselenium compounds active against pathogenic bacteria, fungi and viruses, *Chemical & Pharmaceutical Bulletin,* 56(10): 1423–1427, Oct 2008.
66. P.A. Tran, T.J. Webster, Selenium nanoparticles inhibit Staphylococcus aureus growth. *International Journal of Nanomedicine,* 6:1553–1558, 2011.
67. W.M. Brouwer, R.L.J. Zsom, Polystyrene latex particle surface characteristics, *Colloids Surf.,* 24(2–3):195–208, 1987.

68. J.E. Seebergh and J.C. Berg, Evidence of a hairy layer at the surface of polystyrene latex-particles. *Colloids Surfaces A,* 100:139–153, Jul 25 1995.
69. G.V. Kryukov, S. Castellano, S.V. Novoselov, *et al.*, Characterization of mammalian selenoproteomes, *Science,* 300(5624):1439–1443, May 30 2003.
70. M.P. Rayman, Selenium and human health. *Lancet,* 379(9822):1256–1268, Mar 31 2012.
71. Q. Wang and T.J. Webster, Nanostructured selenium for preventing biofilm formation on polycarbonate medical devices, *Journal of Biomedical Materials Research, Part A,* 100(12):3205–3210, Jun 15 2012.
72. J.S. Garner and M.S. Favero, CDC guideline for handwashing and hospital environmental control–1985, *Infection Control : IC,* 7(4):231–243, Apr 1986.
73. M. McGuckin, Improving handwashing in hospitals: A patient education and empowerment program, *LDI Issue Brief,* 7(3):1–4, Nov 2001.
74. J. Guzewich and M.P. Ross, White paper: Evaluation of risks related to microbiological contamination of ready-to-eat food by food preparation workers and the effectiveness of interventions to minimise those risks. In: Administration FaD, ed. College park (MD): Centre for Food Safety and Applied Nutrition; September 1999.
75. M. Blackmore, The journal of infection control nursing. hand-drying methods. *Nursing Times,* 83(37):71–74, Sep 16–22 1987.
76. J.L. Hattula, P.E. Stevens, A descriptive study of the handwashing environment in a long-term care facility, *Clinical Nursing Research,* 6(4):363–374, Nov 1997.
77. A. Rodriguez, R. Batlle, C. Nerin, The use of natural essential oils as antimicrobial solutions in paper packaging: Part II, *Prog. Org. Coat.,* 60(1):33–38, Aug 2007.
78. H. Yokota, K. Tanabe, M. Sezaki, *et al.*, Arsenic contamination of ground and pond water and water purification system using pond water in Bangladesh, *Eng. Geol.,* 60(1–4):323–331, Jun 2001.
79. W.B. Hu, C. Peng, W.J. Luo, *et al.*, Graphene-based antibacterial paper, *Acs. Nano.,* 4(7):4317–4323, Jul 2010.
80. K. Ghule, A.V. Ghule, B.J. Chen, Y.C. Ling, Preparation and characterization of ZnO nanoparticles coated paper and its antibacterial activity study, *Green Chem.,* 8(12):1034–1041, 2006.
81. T. Xia, M. Kovochich, M. Liong, *et al.*, Comparison of the mechanism of toxicity of zinc oxide and cerium oxide nanoparticles based on dissolution and oxidative stress properties, *Acs. Nano.,* 2(10):2121–2134, Oct 2008.
82. R. Foldbjerg, P. Olesen, M. Hougaard, D.A. Dang, H.J. Hoffmann, H. Autrup, PVP-coated silver nanoparticles and silver ions induce reactive oxygen species, apoptosis and necrosis in THP-1 monocytes. *Toxicol. Lett.,* 190(2):156–162, Oct 28 2009.
83. Q. Wang and T.J. Webster, Short communication: inhibiting biofilm formation on paper towels through the use of selenium nanoparticles coatings, *International Journal of Nanomedicine,* 8:407–411, Jan 23 2013

Hydroxyapatite-Biodegradable Polymer Nanocomposite Microspheres Toward Injectable Cell Scaffold

Syuji Fujii[1,*], Masahiro Okada[2] and Tsutomu Furuzono[3]

[1]Department of Applied Chemistry, Faculty of Engineering, Osaka Institute of Technology, Osaka, Japan
[2]Department of Biomaterials, Osaka Dental University, Osaka, Japan
[3]Department of Biomedical Engineering, School of Biology-Oriented Science and Technology, Kinki University, Wakayama, Japan

Abstract

Hydroxyapatite (HAp)-biodegradable polymer hybrid microspheres have attracted great interest in both academic and industrial areas, because there is a wide range of potential applications especially in the biomedical field. Hybridization of HAp with biodegradable polymer is important for improvement of cell adhesion properties. Usually, hybrid microspheres are fabricated using molecular-level surfactants, which are suspected of causing allergy-like reactions and carcinogenicity. Strategies for the fabrication of HAp-biodegradable polymer hybrid microspheres without the use of such molecular-level surfactants should be developed.

We have developed a facile and versatile "surfactant-free" fabrication method of HAp-biodegradable polymer nanocopmosite microspheres: nanosized HAp particles were employed as a particulate stabilizer in order to prevent flocculation of microspheres as well as to improve cell adhesion properties of the biodegradable polymer. It has been confirmed that the nanocomposite microspheres can work as an effective injectable scaffold, which enhances cell-based therapeutic angiogenesis with bone marrow mononuclear cells.

Keywords: Microspheres, Pickering emulsion, nanocomposite, hydroxyapatite, biodegradable polymer, injectable scaffold

*Corresponding author: s.fujii@chem.oit.ac.jp

9.1   Introduction

There is a growing interest in synthesis of hydroxyapatite (HAp, $Ca_{10}(PO_4)_6(OH)_2$)-synthetic polymer hybrid materials in a form of microsphere, because they have found their applications in the biomedical field [1–3]. HAp is one of the calcium phosphates and the main mineral of bones and teeth in vertebrates, and artificially synthesized HAp has been extensively used in a variety of applications, such as biomaterials in the orthopedic and dental fields, amphoteric ion-exchangers, column packing materials for protein separation, cosmetics, dentifrices, and as catalysts by exploiting their biocompatibility and adsorbability with many compounds [4–6]. HAp exhibits excellent adhesion not only to cells but also to hard and soft tissues [7]. Hybridization of HAp and synthetic polymers is important in order to give the materials high cell adhesion property and desired mechanical property and flexibility, and various approaches have been designed to synthesize the HAp-polymer hybrid microspheres [8–11]. Among the various HAp-synthetic polymer hybrid microspheres, biodegradable polyester-based microspheres are of great importance due to their superiority in biodegradability. Poly(L-lactide) (PLLA), poly(ε-caprolactone) (PCL), poly(L-lactide-*co*-ε-caprolactone) (PLCL) and poly(L-lactide-*co*-glycolide) (PLGA) are biodegradable polyesters, which have already been used as sutures, orthopedic fixation devices, barrier membranes, and drug delivery devices in the medical field [12]. These polyesters are unable to interact specifically with cells due to their relatively high hydrophobicity and lack of functional groups for the attachment of bioactive molecules. In order to improve cell adhesion properties of biodegradable polyesters, the hybridization with HAp has been studied. Kang and coworkers [3] fabricated HAp-coated PLGA microspheres by incubating PLGA seed microspheres in a simulated body fluid and claimed their use as an injectable scaffold for bone regeneration through minimally invasive surgical procedures in orthopedic applications. HAp-coated PLLA microspheres were also prepared by coating PLLA microspheres with HAp nanocrystals via interaction between carboxyl groups on PLLA surfaces and calcium ions on HAp [13]. Lv and coworkers [14] synthesized HAp-PLGA hybrid microspheres, which are suitable for microsphere sintered cell scaffolds, by emulsion solvent evaporation method. Qiu and coworkers [15] prepared HAp nanoparticle/PLLA hybrid microspheres by a solid-in-oil-in-water emulsion solvent evaporation method.

In the abovementioned systems, the biodegradable microspheres were fabricated by an oil-in-water emulsion solvent evaporation method [3, 13–15]: the molecular-level emulsifiers (low-molecular-weight surfactants or polymeric colloidal stabilizers), which are suspected of causing allergy-like reactions and carcinogenicity [16, 17], were usually required to stabilize oil droplets and the microspheres in aqueous media. However,

the application range is limited in some cases, because the functionalities of the microspheres are suppressed by the coating of the microsphere surface with these molecular-level emulsifiers. Strategies for the synthesis of HAp-biodegradable polyester hybrid microspheres without the use of the molecular surfactant or polymeric stabilizer should be developed; however, there are few reports on this research topic [18, 19].

In this chapter, we will describe the fabrication method of HAp-biodegradable polymer nanocomposite microspheres developed in our research group. This method is named the "Pickering emulsion method," in which no molecular-level emulsifier is used and an emulsion stabilized by solid HAp particles is utilized. Here, the HAp particles play a role of an emulsifier, which stabilizes the emulsion as well as the resulting microspheres, and they also form the shell of the fabricated microspheres to improve cell adhesion properties. First, we will explain what the Pickering emulsion is and then show examples of the fabrication of HAp-biodegradable nanocomposite microspheres using the Pickering emulsion method.

9.2   Pickering Emulsion

9.2.1   What is a Pickering Emulsion?

An emulsion stabilized by adsorption of fine solid particles onto an oil/water interface is called a "Pickering emulsion" [20–25]. Fundamental research has been carried out based on physical chemistry and colloid science, and the development of applications in cosmetics, pharmaceuticals and food industries is expected. Several factors can be identified which can control the emulsion stability and the emulsion types [oil-in-water (O/W) type (oil droplets are dispersed in continuous water phase) or water-in-oil (W/O) type (water droplets are dispersed in continuous oil phase)]: type of emulsifier, its concentration, volume ratio of water and oil, temperature, how emulsification energy is added, container wall properties, and addition order of each component [26]. In particular, when the particles are used as the emulsifier, the contact angle (θ, generally measured through the water phase), which indicates the wettability of the particles to oil or water, is an important factor in determining the stability and the type of emulsion. When hydrophilic particles adsorb onto the oil/water interface, more than 50% of the particle surface is exposed to the water phase; thus, θ is less than 90°. In contrast, θ is greater than 90° in the case of hydrophobic particles. When the volume ratio of the water phase and the oil phase is 1:1, hydrophilic particles preferentially stabilize an O/W emulsion, and hydrophobic particles preferentially stabilize a W/O emulsion (Figure 9.1). Thus, the wettability (θ) of particles provides a similar
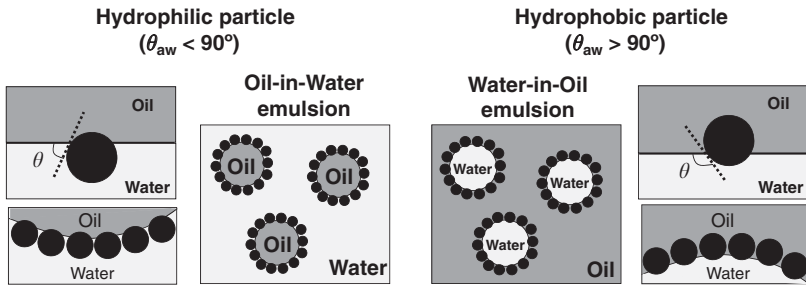
Figure 9.1 Dispersed systems comprising of oil and water stabilized by particles. In mixtures of oil and water, oil-in-water emulsions are formed by using relatively hydrophilic particles and water-in-oil emulsions are formed by using relatively hydrophobic particles.

index to the hydrophile-lipophile balance (HLB) value and the critical packing parameter in an emulsion system stabilized by a molecular-level emulsifier.

The energy change (ΔG) due to the adsorption of spherical solid particles onto the oil/water interface from the phase where the particles are dispersed is expressed by the following equation if the gravity effect can be ignored [27],

$$\Delta G = -\gamma_{ow}\,\pi a^2\,(1 \pm \cos\theta)^2 \tag{9.1}$$

where γ_{ow} is an interfacial tension between oil and water, a is a particle radius, and θ is a contact angle. When the sign inside the parentheses is negative, it represents the case in which the particle adsorption takes place from the water phase onto the oil/water interface. When the sign is positive, it represents the case in which the particle adsorption takes place from the oil phase. From Equation 9.1, we can discern that the larger the particle size and oil-water interfacial tension and the closer the contact angle to 90°, the greater the adsorption energy. For example, if a particle with a radius of 10 nm is adsorbed onto a water-toluene interface (interfacial tension: 36 mN/m) with a contact angle of 90°, the adsorption energy is calculated to be 2750 kT. Since the adsorption energy of a general low-molecular-weight emulsifier is 10–20 kT [28], the adsorption energy of the particulate emulsifier is clearly very high. Thus, once a particle with a suitable wettability is adsorbed onto the interface, desorption from the interface is difficult due to the high adsorption energy. In many cases, the particulate emulsifier densely covers the droplet interface to stabilize the liquid droplets. Because of the above reasons, the stability of a Pickering emulsion against coalescence between liquid droplets is higher than that of an emulsion stabilized with a normal molecular-level emulsifier [22–25].

9.2.2   Pickering Emulsion Stabilized with Nanosized HAp Particles

There has already been active research in Pickering emulsions stabilized with various functional particulate emulsifiers: inorganic fine particles such as silica [29, 30], metals [31], and clays [32, 33], organic fine particles such as polymer particles [34–40], microgels [41–45], and shell crosslinked micelles [46], and more recently, bionanoparticles [47–49]. We have conducted a series of studies on stabilization of emulsion using nanosized HAp particles as a particulate emulsifier [50]. It has been confirmed that both poorly-crystallized HAp nanoparticles prepared by a wet chemical method at room temperature [50–56] and highly-crystallized HAp nanocrystals prepared by calcinations of the HAp nanoparticles at 800°C [57–61] worked as effective particulate emulsifiers under specific conditions as follows.

When an aqueous dispersion of HAp nanoparticles (or nanocrystals) was homogenized with oil [namely, *n*-hexane, *n*-dodecane, methyl myristate, methyl trimethyl acetate, chloroform, toluene, 1-undecanol, or dichloromethane (CH_2Cl_2)] in an equal volume ratio, a stable O/W emulsion was formed only in the methyl myristate or methyl trimethyl acetate system. With the other oils, emulsions were unstable and macro-phase separation into an oil phase and a water phase occurred (Figure 9.2). These results indicate that only oils having an ester group can form stable emulsions. Fourier transform infrared spectroscopy (FT-IR) studies confirmed that there is an interaction between the ester group in methyl myristate or methyl trimethyl acetate molecule and the calcium ion on the HAp surface. It is considered that HAp show moderate wettability to the oil phase through such an interaction; as a result, nanosized HAp particles can be adsorbed to the oil/water interface, leading to stabilization
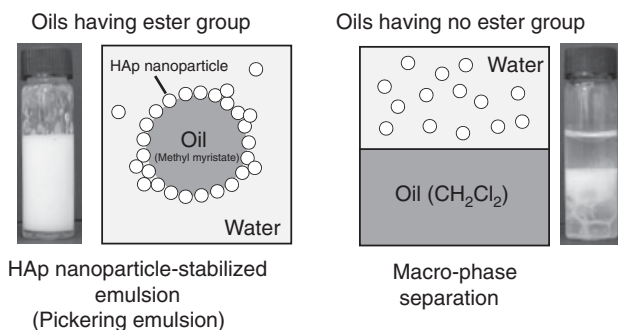
Figure 9.2 Pickering emulsion stabilized using HAp nanoparticles as a particulate emulsifier. Stable emulsions are formed using oils having ester group, and macro-phase separations occur using oils having no ester group.

of the Pickering-type emulsion. The results shown above indicate that the wettability of the particles to the oil phase is an important factor for the formation of a stable emulsion. In addition, it has been clarified that the stabilization of emulsions is possible even using an oil such as CH_2Cl_2, which has no ester groups, by introduction of ester groups into the oil phase by dissolving polymers such as poly(ethylene terephthalate) and poly(methyl methacrylate), which have ester groups on the main/side chain. In this case, the ester groups on polymer chain interact with HAp at the oil/water interface and function as an adsorption promoter (wettability modifier) for nanosized HAp particles to be adsorbed to the oil/water interface.

9.3 Fabrication of HAp-Polymer Nanocomposite Microspheres by Pickering Emulsion Method

As described in Section 9.2.2 above, the HAp nanoparticles (or nanocrystals) cannot effectively function alone as an emulsifier for oils such as CH_2Cl_2, which has no ester groups. However, when a hydrophobic polymer having ester groups is dissolved into the oil phase as an adsorption promoter (wettability modifier), HAp particles can be adsorbed to the oil/water interface and function as an effective particulate emulsifier. Furthermore, evaporation of the organic solvent from the HAp-stabilized polymer solution-in-water emulsion droplets through the aqueous medium can lead to fabrication of HAp-polymer nanocomposite microspheres (Figure 9.3). The nanocomposite microsphere fabrication method has been called the "Pickering emulsion method." The merits of this method are as follows: (1) no molecular-level emulsifier is used; (2) industrial-scale synthesis is possible due to the simple procedure and easy up-scaling; (3) a wide range of polymers can be utilized; and (4) functional materials such as drugs and fluorescent chemicals can be easily introduced into the microspheres.
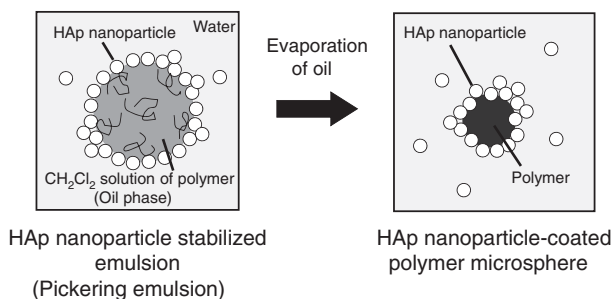
Figure 9.3 Fabrication of nanocomposite microspheres with polymer core-HAp nanoparticle shell morphology by Pickering emulsion method.

9.3.1   Fabrication of HAp-Commodity Polymer Nanocomposite Microspheres

As was described above, a polymer having ester groups functions as an adsorption promoter (wettability modifier) of the HAp nanoparticles (or nanocrystals). A similar function can be expected even for polymers having no ester groups by introducing other functional groups that interact with HAp. An example of such functional groups is the carboxyl group, which is already known to ionically interact with the HAp surface [62]. We have found that even a polymer having no ester groups in main/side chains acts as an adsorption promoter (wettability modifier) for HAp by introducing a carboxyl group only at the polymer chain end. We investigated the effect on the emulsion stability of the polymer chain end groups of polystyrene (PS), which is dissolved in the oil phase [51]. PS having a carboxyl group as a polymer chain end group (PS-COOH) and PS having a methyl group as a chain end group (PS-CH$_3$) were used as samples. They were synthesized by solution polymerization using 4,4′-azobis(cyanovaleric acid) or 2,2′-azobisisobutyronitrile as a free-radical polymerization initiator. When a CH$_2$Cl$_2$ solution of PS-COOH was used, a stable O/W emulsion was formed. This result suggests that adsorption of the HAp nanoparticles onto the oil/water interface was achieved by the interaction of the carboxyl group at the PS chain end and the HAp nanoparticles at oil-water interface. It has been confirmed that the PS-COOH with molecular weight of ranging from 6,700 to 64,500 can lead to formation of spherical emulsion droplets. On the other hand, when a CH$_2$Cl$_2$ solution of PS-CH$_3$ was used as the oil phase and homogenized with an aqueous dispersion of HAp nanoparticles, macro-phase separation of the water phase and oil phase took place or an unstable emulsion was formed. These results indicate that the stability of the emulsion depends on the difference in the polymer chain end group, which is often overlooked compared with the polymer main chain or side chain. These results are crucial for the design of polymers, which can be applied to the Pickering emulsion method [51].

Subsequently, the fabrication of nanocomposite microspheres with PS core/HAp shell morphology was achieved by evaporation of CH$_2$Cl$_2$ from the formed Pickering-type emulsion. The solubility of CH$_2$Cl$_2$ in water is 1.3 g/100 mL (20°C); therefore, CH$_2$Cl$_2$ in oil droplets can gradually evaporate into the gas phase through the continuous water phase. When polymer solutions of the same concentration were used in PS-COOH systems with molecular weights of 26,100 and 64,500, the volume of the oil droplets decreased, accompanied by the evaporation of CH$_2$Cl$_2$, while maintaining their spherical shape. In these systems, spherical microspheres were formed. On the other hand, in the PS-COOH system with the molecular weight of 6,700, the spherical oil droplets were deflated after evaporation of CH$_2$Cl$_2$, and microspheres with concavities were

formed. Scanning electron microscope (SEM) studies confirmed that free HAp nanoparticles that were not adsorbed on the PS microspheres were observed in the molecular weight of 64,500 system, and it was clear that the PS microspheres surface was not completely coated with HAp nanoparticles (Figure 9.4). In the PS molecular weight of 26,100 system, free HAp nanoparticles were present among the PS microspheres, and most microsphere surfaces were completely covered by HAp nanoparticles. On the other hand, few free HAp nanoparticles were observed in
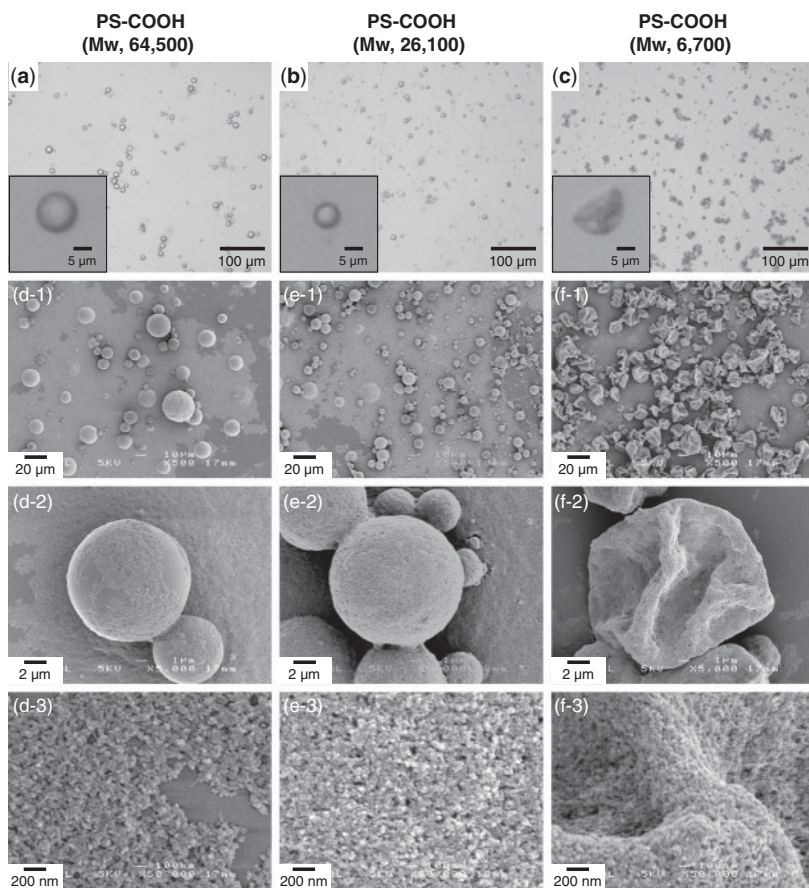
Figure 9.4 (a–c) Optical micrographs and (d–f) SEM photographs of HAp nanoparticle-coated PS microspheres prepared from the emulsions containing (a,d) PS-COOH (Mw, 64,500), (b,e) PS-COOH (Mw, 26,100), and (c,f) PS-COOH (Mw, 6,700), observed at different magnifications. PS-COOH, 1.0 wt% in dichloromethane; HAp nanoparticles, 0.04 wt% in water; oil/water, 1/10 (w/w). Reprinted with permission from [51]. Copyright © 2012 American Chemical Society.

the molecular weight of 6,700 system, and the PS microsphere surfaces were densely coated with the HAp nanoparticles. These results indicated that deformation of droplets/microspheres is influenced by the extent of the interaction between the HAp nanoparticles and polymer at the oil-water interface (Figure 9.5). When weak interactions are involved (in the case of PS-COOH with the molecular weight of 64,500, the number of interaction points between PS-COOH and HAp at oil-water interface is small), nanoparticles can desorb from the interface, and microspheres shrink while maintaining a spherical form due to interfacial tension. In contrast, when strong interactions (in the case of PS-COOH with the molecular weight of 6,700, the number of interaction points is large) prevent nanoparticles from desorbing from the interface, microspheres must
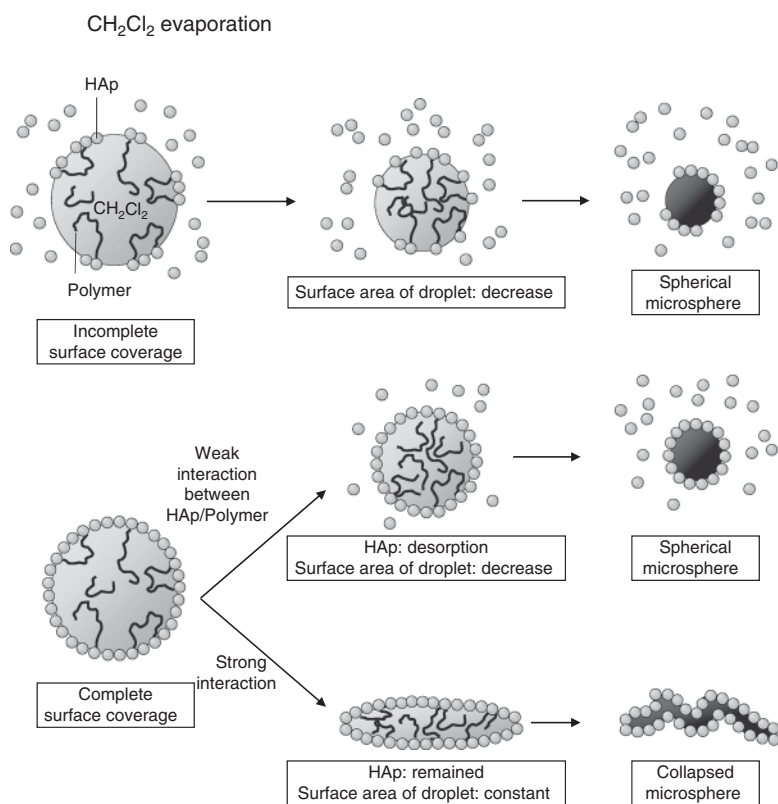
Figure 9.5 Schematic representation of morphological changes of the droplets/ microspheres during dichloromethane evaporation. The strength of the interaction between polymer and HAp is influenced by the polymer structure (end groups and molecular weight) and the polymer concentration. Reprinted with permission from [51]. Copyright © 2012 American Chemical Society.

deflate to maintain the interfacial area. From the above described results, it is clear that morphology control of the formed microspheres is possible by controlling the degree of interaction between the polymer dissolved in the oil phase and the HAp nanoparticles [51]. In addition to the molecular weight of the polymer dissolved in the oil phase, the type of polymer, the chain end structure of the polymer, the evaporation rate of the oil, the homogenization rate during oil evaporation, and the type of oil are factors that can affect the morphology of the nanocomposite microspheres.

9.3.2   Fabrication of HAp-Biodegradable Polymer Nanocomposite Microspheres

The Pickering emulsion method enables the fabrication of nanocomposite microspheres without the use of a molecular-level emulsifier. Thus, we have been studying the synthesis of biodegradable polymer-HAp nanocomposite microspheres by the Pickering emulsion method, targeting the biomedical material field, where the presence of molecular-level emulsifiers is unfavorable because of their toxicity and allergic properties [52–54, 57–61]. As the biodegradable polymer, PLLA, PCL, PLCL, and PLGA, which have been clinically proven to be safe and are in practical use, were selected. These biodegradable polymers have ester groups in the main chain of the molecule and a carboxyl group as the chain end group. Therefore, they can be expected to interact with HAp nanoparticles (or nanocrystals), resulting in the formation of a stable emulsion and the fabrication of nanocomposite microspheres. In fact, FT-IR studies detected the absorption at 1595 cm^{-1} due to the $-COO^-Ca^{2+}$ ionic bond in a mixture of PLLA and HAp nanoparticles, which is formed by the interaction between carboxylate groups (originated from carboxyl end groups) and calcium ions on the HAp nanoparticle surface in addition to the absorption at 1760 cm^{-1}, which was assigned to the carbonyl and carboxyl groups found in PLLA homopolymers (Figure 9.6). For the other biodegradable polymers, similar HAp-polymer interaction was confirmed by FT-IR measurements. Homogenization of CH_2Cl_2 solution of the above described biodegradable polymers with an aqueous dispersion of HAp nanoparticles led to the formation of a stable emulsion in all the systems. In addition, nanocomposite microspheres with biodegradable polymer core/HAp nanoparticles shell morphology were obtained by removing CH_2Cl_2. Optical microscope studies confirmed that the emulsion droplets do not coalesce during the CH_2Cl_2 evaporation process (Figure 9.7). It was also clarified by gas chromatography (GC) measurements that the CH_2Cl_2 concentration decreased from 68,000 ppm to 240 ppm after 6 h from the start of evaporation and reached the GC measurement limit of less than 10 ppm after 13 h. The International Conference on Harmonization of Technical Requirements for Registration of Pharmaceuticals for Human Use (ICH) has classified
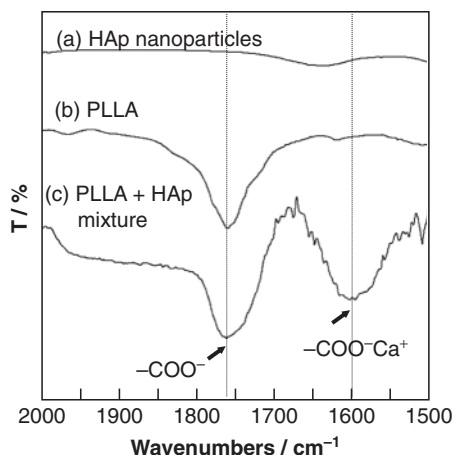
Figure 9.6 FT-IR spectra of (a) pure HAp nanoparticles, (b) PLLA homopolymer and (c) the mixture of PLLA and the HAp nanoparticles. Reprinted with permission from [52]. Copyright © 2009 American Chemical Society.
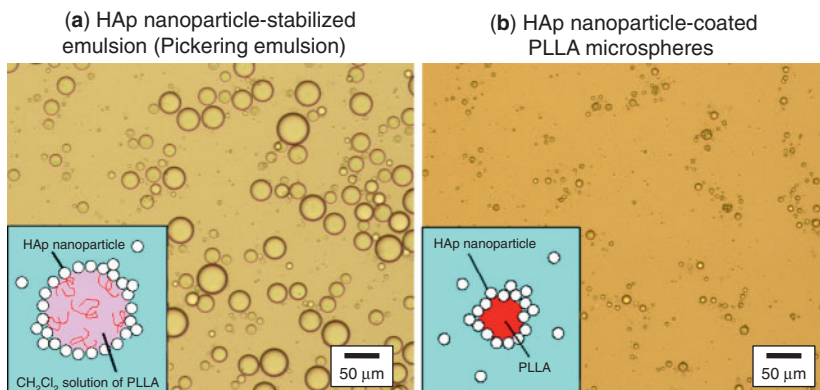
Figure 9.7 Representative optical micrographs of CH_2Cl_2 solution of PLLA-in-water emulsion stabilized with HAp nanoparticles as a particulate emulsifier, before (a) and after (b) evaporation of CH_2Cl_2 from the emulsion. The images were taken at the same area. The HAp-PLLA nanocomposite microspheres were colloidally stable at least for 6 months at 4°C. Reprinted with permission from [52]. Copyright 2009 American Chemical Society.

CH_2Cl_2 as a Class II solvent and described that the concentration limit of 600 ppm in a product can be applicable under the assumption that the product mass of 10 g is administered daily [63]. The residual CH_2Cl_2 amount in the microspheres produced in this study is one order of magnitude lower than that limited in ICH. The surface of the nanocomposite

microspheres was densely coated with the HAp nanoparticles. From the transmission electron microscope (TEM) image of an ultra-thin cross section, it was clarified that poorly-crystalized HAp nanoparticles are present only on the PLLA microsphere surfaces and a shell having a thickness of 40-120 nm (corresponding to the thickness of one to three layers of HAp nanoparticles) is formed. These core-shell nanocomposite microspheres showed dispersion stability in an aqueous medium for more than 1 year of storage at 4°C. Furthermore, it was possible to fabricate core-shell microspheres with a particle size of a few micrometers to a few hundred micrometers by controlling the HAp concentration in aqueous media, the biodegradable polymer concentration in CH_2Cl_2, and the homogenization rate during emulsion preparation. In addition, we succeeded in the fabrication of fluorescent microspheres by the introduction of oil-soluble fluorescent chemicals into the oil phase during the Pickering emulsion formation.

9.3.3 Fabrication of Multihollow HAp-Biodegradable Polymer Nanocomposite Microspheres

Fabrication of nanocomposite microspheres having a multihollow structure is also possible by the Pickering emulsion method, in which the oil is evaporated from a multiple emulsion (Figure 9.8) [55]. In the formation of a multiple emulsion using conventional molecular-level emulsifiers, two or more kinds of emulsifiers having different HLB values are necessary. Likewise, in the case of a Pickering emulsion, two or more kinds of particles having different surface hydrophilicity/hydrophobicity are necessary to obtain multiple emulsions. Binks *et al.* prepared water-in-oil-in-water (W/O/W) type Pickering emulsion using two kinds of silica particles whose surface hydrophilicity/hydrophobicity is controlled by surface
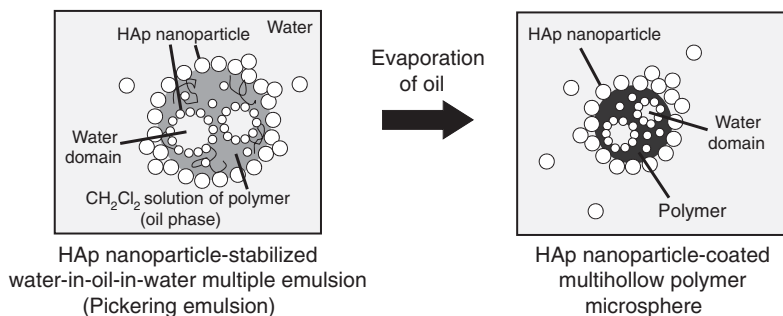
Figure 9.8 Fabrication of multihollow nanocomposite microspheres by evaporation of oil from water-in-oil-in-water Pickering emulsion. Reprinted with permission from [55]. Copyright © 2010 American Chemical Society.

modification agents [64, 65]. In consideration of the microspheres as biomedical materials, it is not favorable to use surface modification agents such as silane coupling agents or long-chain alcohols. Instead, we used a biodegradable polymer, which eventually serves as the base material of the microspheres, as the surface modifier. Hydrophobic HAp nanoparticles were prepared by mixing PLLA and HAp nanoparticles and heating at 200°C, which is higher than the melting point of PLLA. By heating above the melting point, the mobility of polymer increases and the polymer can adhere to the HAp surface. The PLLA-modified HAp nanoparticles have high hydrophobicity and can stabilize a W/O emulsion. The W/O emulsion was subsequently emulsified into an aqueous dispersion of hydrophilic HAp nanoparticles, which have no surface modification, allowing a formation of W/O/W multiphase emulsion (Figure 9.9a). By evaporation of CH_2Cl_2 from the multiple Pickering emulsion, multihollow microspheres carrying inner water domains were fabricated. From the TEM observation of an ultra-thin crosssection of the dried microspheres, it was confirmed that HAp nanoparticles was adsorbed on the inner domain and on the microsphere surfaces (Figs. 9.9b and c). Multihollow HAp nanoparticle-coated PLLA microspheres fabricated from Pickering-type multiple emulsions are expected to be utilized in medical fields, because
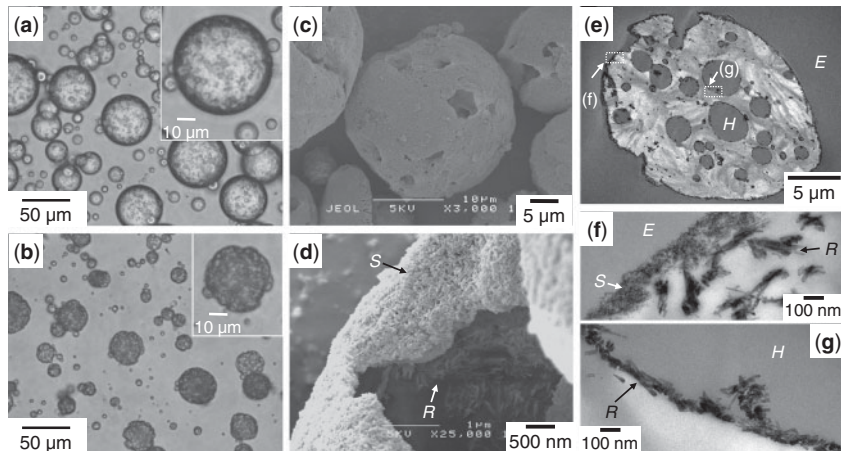
Figure 9.9 (a,b) Optical micrographs of the W/O/W emulsion stabilized with spherical HAp (SHAp) and PLLA-rod-shaped HAp (RHAp) treated at 200°C (a) before and (b) after evaporation of CH_2Cl_2. The insets in the micrographs (a,b) show magnified images. (c,d) SEM images of the multihollow microspheres. The image (d) is a magnified image. (e–g) TEM images of ultra-thin cross sections of the microspheres. The images (f,g) show magnified images of the area shown in the image (e). The symbols E, H, S, and R indicate the exterior of the microsphere (epoxy resin), hollow inside the microsphere, SHAp, and RHAp, respectively. Reprinted with permission from [55]. Copyright © 2010 American Chemical Society.

the surfaces of the microspheres were coated with unmodified and bioactive HAp nanoparticles, and water-soluble drugs can be loaded in the water domains.

9.4 Evaluation of Cell Adhesion Properties of HAp-Biodegradable Polymer Nanocomposite Microspheres

Thanks to excellent cell adhesion properties of HAp [7], the HAp-coated biodegradable polymer microspheres are expected to show improved cell adhesion properties. The cell adhesion properties of PLLA core/HAp shell nanocomposite microspheres were evaluated using L929 mouse fibroblast cells as the model system. As shown in Figure 9.10, it was observed that the cells adhered with stretching their lamellipodia on the surface of the nanocomposite microspheres. When bare PLLA microspheres, where HAp nanoparticles were removed by dissolution from the nanocomposite microspheres, were used in a control experiment, the cells did not stretch lamellipodia, but adhered to the microspheres with small contact area in a nearly spherical shape. The number of the cells adhered on the HAp nanoparticle-coated microspheres was 763 cells/mm^2, which is statistically larger than that on the bare PLLA microspheres (574 cells/mm^2) as shown in Figure 9.11. Results obtained by counting the cells detached from the
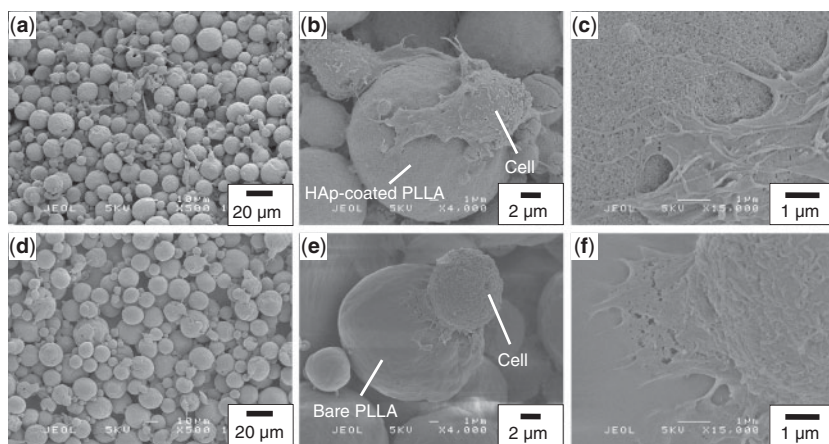
Figure 9.10 SEM images of L929 fibroblast cells adhered on the HAp nanoparticle-coated PLLA microspheres (a–c) and the bare PLLA microspheres (d–f) after incubation at 37°C for 24 h. (b,c) and (e,f) are magnified images of (a) and (d), respectively. Reprinted with permission from [52]. Copyright © 2009 American Chemical Society.
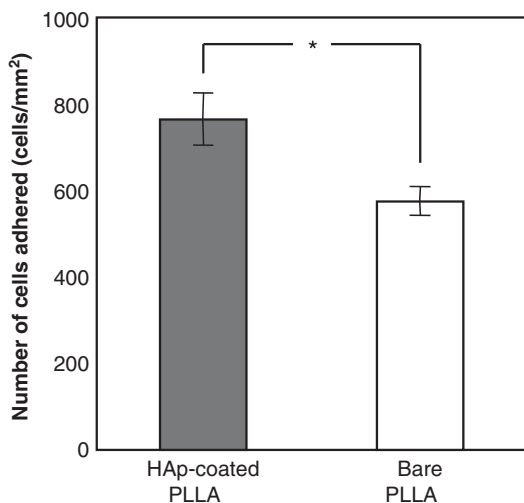
Figure 9.11 The number of cells adhered on each samples after 24-h incubation. The error bar represents standard error (n = 30). *P < 0.05. Reprinted with permission from [52]. Copyright © 2009 American Chemical Society.

sample after trypsin-EDTA treatment using the optical microscope and the Burker-Turk type cell plate also indicated an effectiveness of the HAp nanoparticle coating on the PLLA mircospheres toward cell adhesion; the number of the cells adhered on the HAp nanoparticle-coated microspheres and the bare PLLA microspheres were measured to be 1.5×10^5 and 1.0×10^5 cells/well, respectively (P<0.05; n = 4). It has also been confirmed that the HAp-coated biodegradable microspheres showed an improved cell adhesion property for bone marrow mononuclear cells (BMNCs) which are used for cell-based therapeutic angiogenesis (see Section 9.5).

The cell-microsphere adhesive force was measured with a colloidal probe atomic force microscope, where the nanocomposite microspheres with PLLA core/HAp shell morphology or bare PLLA microspheres were used as the probe. According to the evaluation of the measured force curve, the cell adhesive force increased about 2.8 times thanks to the presence of HAp on the PLLA microsphere surface [56].

9.5 Application of HAp-Biodegradable Polymer Nanocomposite Microspheres as an Injectable Scaffold

It has been confirmed that the HAp nanocrystal-coated biodegradable microspheres can work as an effective injectable scaffold, which enhances

cell-based therapeutic angiogenesis with bone marrow mononuclear cells (BMNCs) [66]. For the angiogenesis experiments, highly-crystallized HAp nanoparticle-coated microspheres were used rather than poorly-crystallized HAp nanoparticles, because the surface stability of the microsphere over 2 weeks (low solubility of HAp component) is important for BMNCs scaffold (Figure 9.12). Various angiogenic growth factors derived from implanted cells are key mediators of therapeutic angiogenesis. However, about 70–90% of the transplanted cells were estimated to disappear from the injection site within 1 week after transplantation [67–69]. Therefore, the efficacy of the cell-based therapeutic angiogenesis could be dependent on the retention, survival, and engraftment of implanted cells in ischemic tissue after implantation. When BMNCs derived from enhanced green fluorescent protein (GFP) transgenic mice were coinjected with the composite microspheres into ischemic muscle, the GFP level in the muscle was approximately 5-fold higher than that in the case of injection of BMNC alone 1 week after injection; whereas GFP levels were not significantly different between the injection of BMNCs alone and or co-injection of BMNC with uncoated PLLA microspheres. These results indicate that the HAp nanocrystals coated on the microspheres promoted BMNC adhesion and retention *in vitro*. Kaplan-Meier analysis demonstrated that co-injection of BMNC with composite microspheres markedly prevented hind limb
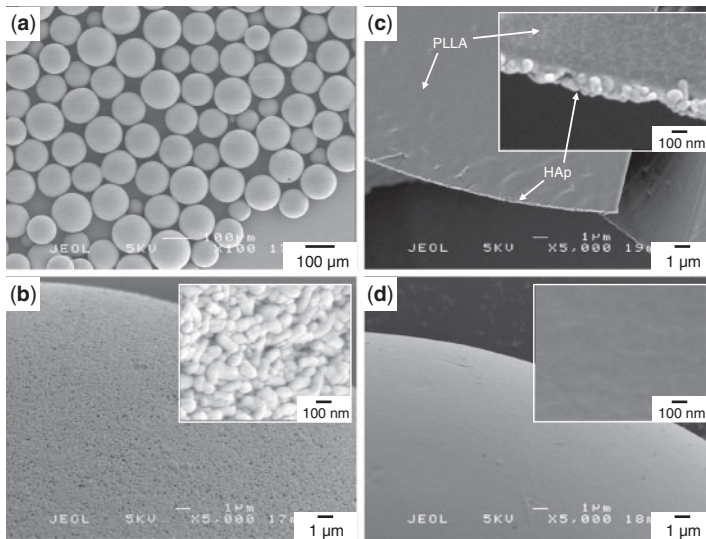
Figure 9.12 SEM photographs of (a–c) HAp nanocrystal-coated and (d) bare PLLA microspheres observed at different magnifications: (a) 100×; (b–d) 5000×(inset) 50,000×. Photograph (c) shows a fractured section of a HAp nanocrystal-coated PLLA microsphere. Reprinted with permission from [13]. Copyright © 2010 Elsevier.

necrosis (P, 0.05 *vs.* BMNC alone or co-injection of BMNC with uncoated microspheres). The co-injection of BMNC with composite microspheres revealed much higher induction of angiogenesis in ischemic tissues and collateral blood flow confirmed by three-dimensional computed tomography angiography than those of BMNC alone or co-injection of BMNC with uncoated microspheres. The enhanced therapeutic angiogenesis and arteriogenesis by co-injection of BMNC with nanocomposite microspheres showed good correlations with increased intramuscular levels of vascular endothelial growth factor and fibroblast growth factor-2. The co-injection of BMNC with composite microspheres also prevented apoptotic cell death of transplanted cells, resulting in prolonged cell retention.

9.6 Degradation Behavior of HAp-Biodegradable Polymer Nanocomposite Microspheres

The HAp nanocrystal-coated PLLA microspheres have been proven to be very effective as an injectable scaffold for cell-based therapeutic angiogenesis. For this purpose, it is ideal that the microspheres retain their spherical biodegradable polymer core/HAp nanocrystals shell morphology until they finish their roles as a scaffold and then are degraded into small fragments/molecules, which can be discharged out of body. Bearing this situation in mind, we felt that it is crucial to evaluate degradability of the HAp nanocrystal-coated biodegradable microspheres. There have been lots of reports on fabrication of biodegradable polymer microspheres, but there is little work on the characterization of their degradation behaviors. This omission is quite surprising, since the biodegradable polymer microspheres are widely used in the medical field.

Based on this situation, *in vitro* degradation behavior of the HAp nanocrystal-coated PLCL microspheres has been studied in buffer solution (PBS) at 37°C in terms of weight, molecular weight, thermal property, and morphological change during an incubation period of up to 48 weeks [61]. It was found that molecular weight decreased rapidly after immersing the microspheres in the PBS at 37°C and, on the other hand, the weight of the microspheres started to decrease after 16 weeks, which was the similar degradation profile with the pristine PLCL bulk sample. This result supports the bulk degradation for the HAp nanocrystal-coated PLCL microspheres. During the degradation, the enthalpy of melting increased progressively, which should be due to the increase of crystallinity because of chain rearrangement of amorphous region induced by water uptake and the preferential degradation of amorphous regions. The HAp nanocrystals detached from the microsphere surface during the degradation, which was confirmed by SEM study. The microspheres were fragile and easy to be broken by external pressure when the molecular weight became at and below 35,000

after 24 weeks incubation period. No/little change in weight of the HAp nanocrystal-coated PLCL microspheres and molecular weight of PLCL and surface morphology was observed after 1 week in PBS at 37°C.

9.7   Conclusions

HAp exhibits excellent biocompatibility with various kinds of cells and tissues, making it an ideal candidate for tissue engineering, orthopedic and dental applications. However, low mechanical strength and low solubility of traditional HAp sintered ceramics generally restricts its use. Therefore the interest is directed to hybridization of HAp with other compounds such as biodegradable polymers. HAp-based nanocomposite microspheres have received much attention as carriers of drugs, proteins and cells because there is a wide ranging choice of polymers, which show different degradation properties. HAp-based nanocomposite microspheres are generally prepared from emulsion droplets (oil-in-water type emulsions for hydrophobic polymers such as biodegradable polyesters, or water-in-oil type ones for water-soluble polymers such as collagen) in which both HAp nanoparticles and polymer are dispersed and dissolved. We described the first use of HAp particles as Pickering-type emulsifiers to fabricate the HAp-polymer nanocomposite microspheres. Neither molecular-level surfactant, polymeric stabilizer nor animal-originated materials such as collagen was used in this method. The surface of the microspheres was covered with HAp particulate emulsifiers, which are expected to have a pristine HAp surface exposed to the continuous aqueous phase, because the particulate emulsifier was used without any surface-active modification and no surface-active molecules were added. Thus, this method is appealing in fields of application where severe restrictions are set for the use of molecular-level surfactants.

From the standpoint of the progress of Pickering emulsions, we have clearly demonstrated that the interactions between polymers dissolved in an oil (dispersed) phase and nanoparticles in an aqueous (continuous) phase at the oil-water interface play important roles in stabilizing Pickering-type emulsions and in controlling the morphology of nanocomposite microspheres. Although this chapter focused on HAp particles as the particulate emulsifier and biodegradable polymers, these novel findings can be extended to other combinations of nanoparticles and polymers.

Acknowledgments

References

1. L. Jongpaiboonkit, T. Franklin-Ford, and W.L. Murphy, *ACS Appl. Mater. Interfaces,* Vol. 1 p. 1504, 2009.
2. E.K. Cushnie, Y.M. Khan, and C.T. Laurencin, *J. Biomed. Mater. Res. Part A,* Vol. 84A, p. 54, 2008.
3. S.-W. Kang, H.S. Yang, S.-W. Seo, D.K. Han, and B.-S. Kim, *J. Biomed. Mater. Res. Part A,* Vol. 85A, p. 747, 2008.
4. J.A.S. Bett, L.G. Christner, and W.K. Hall, *J. Am. Chem. Soc.,* Vol. 89, p. 5535, 1967.
5. P.E. Brown, and B. Constanz, *Hydroxyapatite and Related Materials*, CRC Press, London, 1994
6. J. Norton, K.R. Malik, J.A. Darr, and I. Rehman, *Adv. Appl. Ceram.,* Vol. 105, p. 113, 2006.
7. H. Aoki, *Science and Medical Application of Hydroxyapatite*, Japanese Association of Apatite Science, Tokyo, 1991.
8. H. Tamai, and H. Yasuda, *J. Colloid Interface Sci.,* Vol. 212, p. 585, 1999.
9. S. Schachschal, A. Pich, and H.-J.P. Adler, *Colloid Polym. Sci.,* Vol. 285, p. 1175, 2007.
10. G.S. Sailaja, T.V. Kumary, and H.K. Varma, *Trends Biomater. Artif. Organs,* Vol. 20, p. 3, 2006.
11. A. Ethirajan, U. Ziener, and K. Landfester, *Chem. Mater.,* Vol. 21, p. 2218, 2009.
12. J. Kohn, S. Abramson, and R. Langer, in: B.D. Ratner, A.S. Hoffman, F.J. Schoen, and J.E. Lemons (Eds.), *Biomaterials Science: An Introduction to Materials in Medicine*, 2nd Ed., Elsevier Academic Press, California, p. 115, 2004.
13. M. Okada, and T. Furuzono, *Mater. Sci. Eng.: B,* Vol. 173, p. 199, 2010.
14. Q. Lv, L. Nair, and C.T. Laurencin, *J. Biomed. Mater. Res.,* Vol. 91A, p. 679, 2009.
15. X. Qiu, Y. Han, X. Zhuang, X. Chen, Y. Li, and X. Jing, *J. Nanoparticle Res.,* Vol. 9, p. 901, 2007.
16. J. Wong, A. Brugger, A. Khare, M. Chaubal, P. Papadopoulos, B. Rabinow, J. Kipp, and J. Ning, *Adv. Drug Deliv. Rev.,* 60, 939, 2008.

17. J.W. Fong, French Patent No. 2484281, 1981.
18. F. Nagata, T. Miyajima, and Y. Yokogawa, *Chem. Lett.,* Vol. 32, p. 784, 2003.
19. F. Nagata, T. Miyajima, and Y. Yokogawa, *J. Eur. Ceram. Soc.,* Vol. 26, p. 533, 2006.
20. W. Ramsden, *Proc. R. Soc.,* Vol. 72, p. 156, 1903.
21. S.U. Pickering, *J. Chem.Soc.,* Vol. 91, p. 2001, 1907.
22. B.P. Binks, and T.S. Horozov *"Colloidal Particles at Liquid Interfaces"* Cambridge Univ. Press: Cambridge, 2006.
23. R. Aveyard, B.P. Binks, and J.H. Clint, *Adv. Colloid Interface Sci.,* Vol. 100–102, p. 503, 2003.
24. S. Fujii, and R. Murakami, *Oleoscience,* Vol. 9, p. 511, 2009.
25. S. Fujii, *J. Adh. Soc. Jpn.,* Vol. 47, p. 64, 2007.
26. A. Kitahara, and K. Furusawa, *Chemistry of Dispersion and Emulsion (Bunsan, Nyuka Kei no Kagaku).* 9th ed. Kougakutosho, Ltd, Tokyo, 1995.
27. S. Levine, B.D. Bowen, and S.J. Partridge, *Colloids Surf.,* Vol. 38, p. 325, 1989.
28. R. Aveyard, J.H. Clint, and T.S. Horozov, *Phys. Chem. Chem. Phys.,* Vol. 5, p. 2398, 2003.
29. B.P. Binks, and S.O. Lumsdon, *Phys. Chem. Chem. Phys.,* Vol. 1, p. 3007, 1999.
30. B.P. Binks, and S.O. Lumsdon, *Langmuir,* Vol. 16, p. 2539, 2000.
31. D. Wang, H. Duan, and H. Möhwald, *Soft Mater.,* Vol. 1, p. 412, 2005.
32. S. Cauvin, P.J. Colver, and S.A.F. Bon, *Macromolecules,* Vol. 38, p. 7887, 2005.
33. S.A.F. Bon, and P.J. Colver, *Langmuir,* Vol. 23, p. 8316, 2007.
34. O.D. Velev, K. Furusawa, and K. Nagayama, *Langmuir,* Vol. 12, p. 2374, 1996.
35. A.D. Dinsmore, M.F. Hsu, M.G. Nikolaides, M. Marquez, A. R. Bausch, and D.A. Weitz, *Science,* Vol. 298, p. 1006, 2002.
36. J.I. Amalvy, S.P. Armes, B.P. Binks, J.A. Rodrigues, and G.-F. Unali, *Chem. Commun.,* p. 1826, 2003.
37. S. Fujii, D.P. Randall, and S.P. Armes, *Langmuir,* Vol. 20, 11329, 2004.
38. B.P. Binks, R. Murakami, S.P. Armes, and S. Fujii, *Angew. Chem. Int. Ed.,* Vol. 44, p. 4795, 2005.
39. E.S. Read, S. Fujii, J.I. Amalvy, D.P. Randall, and S.P. Armes, *Langmuir,* Vol. 20, p. 7422, 2004.
40. E.S. Read, S. Fujii, J.I. Amalvy, D.P. Randall, and S.P. Armes, *Langmuir,* Vol. 21, p. 1662, 2005.
41. S. Fujii, E. S. Read, S.P. Armes, and B.P. Binks, *Adv. Mater.,* Vol. 17, p. 1014, 2005.
42. S. Fujii, S.P. Armes, B.P. Binks, and R. Murakami, *Langmuir,* Vol. 22, p. 6818, 2006.
43. B.P. Binks, R. Murakami, S.P. Armes, and S. Fujii, *Langmuir,* Vol. 22, p. 2050, 2006.
44. T. Ngai, S.H. Behrens, and H. Auweter, *Chem. Commun.,* p. 331, 2005.
45. S. Tsuji, and H. Kawaguchi,, *Langmuir,* Vol. 24, p. 3300, 2008.
46. S. Fujii, Y. Cai, J. V. M. Weaver, and S.P. Armes, *J. Am. Chem. Soc.,* Vol. 127, p. 7304, 2005.
47. J.Y. Russell, Y. Lin, A. Böker, L. Su, P. Carl, J. Zettl, K. Sill, R. Tangirala, T. Emrick, K. Littrell, P. Thiyagarajan, D. Cookson, A. Fery, Q. Wang, and T.P. Russell, *Angew. Chem. Int. Ed.,* Vol. 44, p. 2420, 2005.
48. J. He, Z. Niu, R. Tangirala, J.-Y. Wang, X. Wei, G. Kaur, Q. Wang, G. Jutz, A. Böker, B. Lee, S.V. Pingali, P. Thiyagarajan, T. Emrick, and T.P. Russell, *Langmuir,* Vol. 25, p. 4979, 2009.

49. S. Fujii, A. Aichi, M. Muraoka, N. Kishimoto, K. Iwahori, Y. Nakamura, and I. Yamashita, *J. Colloid Interface Sci.,* Vol. 338, p. 222, 2009.
50. S. Fujii, M. Okada, and T. Furuzono, *J. Colloid Interface Sci.* Vol. 315, p. 287, 2007.
51. M. Okada, H. Maeda, S. Fujii, Y. Nakamura, and T. Furuzono, *Langmuir,* Vol. 28, p. 9405, 2012.
52. S. Fujii, M. Okada, H. Sawa, T. Furuzono, and Y. Nakamura, *Langmuir,* Vol. 25, p. 9759, 2009.
53. S. Fujii, M. Okada, T. Nishimura, H. Maeda, T. Sugimoto, H. Hamasaki, T. Furuzono, and Y. Nakamura, *J. Colloid Interface Sci.,* Vol. 374, p. 1, 2012.
54. S. Fujii, M. Okada, T. Nishimura, T. Sugimoto, H. Maeda, H. Hamasaki, T. Furuzono, Y. Nakamura, *Composite Interfaces*, 2013. DOI:10.1080/15685543.2013.762893
55. H. Maeda, M. Okada, S. Fujii, Y. Nakamura, and T. Furuzono, *Langmuir,* Vol. 26, p. 13727, 2010.
56. H. Shinto, T. Hirata, T. Fukasawa, S. Fujii, H. Maeda, M. Okada, Y. Nakamura, and T. Furuzono, *Colloids Surf. B: Biointerfaces*, Vol. 108, p. 8, 2013.
57. M. Okada, S. Fujii, H. Maeda, Y. Nakamura, X. Liu, and T. Furuzono, *Bioceramics*, Vol. 22, p. 623, 2009.
58. X. Liu, M. Okada, H. Maeda, S. Fujii, Y. Nakamura, and T. Furuzono, *Arch. BioCeramics Res.*, Vol. 9, p. 35, 2009.
59. M. Okada, S. Fujii, T. Nishimura, Y. Nakamura, and T. Furuzono, *Appl. Surf. Sci.*, Vol. 262, p. 39, 2012.
60. T. Iwamoto, T. Terada, Y. Kogai, M. Okada, S. Fujii, and T. Furuzono, *Funct. Mater. Lett.*, Vol. 5, p. 1260010–1–6, 2012.
61. S. Fujii, Y. Miyanari, T. Nishimura, Y. Yokoyama, S. Hamasaki, M. Okada, T. Furuzono, S. Matsuda, H. Takamori, and Y. Nakamura, *Polym. Deg. Stab.,* Vol. 98, p. 377, 2013.
62. X. Qiu, L. Chen, J. Hu, J. Sun, Z. Hong, A. Liu, X. Chen, and X. Jing *J. Polym. Sci., Part A; Polym. Chem.*, Vol. 43, p. 5177, 2005.
63. ICH Harmonised Tripartite Guideline. Impurities: Guideline For Residual Solvents Q3C(R3). Parent Guideline Dated 17 July, 1997
64. B.P. Binks, A.K.F. Dyab, and P.D. I.Fletcher, Proceedings of 3rd World Congress on Emulsions, CME, p.1, 2002.
65. K.L. Kilpadi, P.L. Chang, and S.L. Bellis, *J. Biomed. Mater. Res.,* Vol. 57, p. 258, 2001.
66. Y. Mima, S. Fukumoto, H. Koyama, M. Okada, S. Tanaka, T. Tanaka, M. Emoto, T. Furuzono, Y. Nishizawa, and M. Inaba, *PLoS ONE*, Vol. 7, p. e35199, 2012.
67. W. Brenner, A. Aicher, T. Eckey, S. Massoudi, M. Zuhayra, U. Koehl, C. Heeschen, W.U. Kampen, A.M. Zeiher, S. Dimmeler, and E. Henze, *J. Nucl. Med.,* Vol. 45, p. 512, 2004.
68. C. Toma, M.F. Pittenger, K.S. Cahill, B.J. Byrne, and P.D. Kessler, *Circulation*, Vol. 105, p. 93, 2002.
69. T.M. Yau, C. Kim, G. Li, Y. Zhang, R.D. Weisel, and R.K. Li, *Circulation*, Vol. 112: p. I123, 2005.

Biomimetic ECM Scaffolds Prepared from Cultured Cells

Guoping Chen*, Hongxu Lu and Naoki Kawazoe

Tissue Regeneration Materials Unit, International Center for Materials Nanoarchitectonics, National Institute for Materials Science, Ibaraki, Japan

Abstract

Porous scaffolds have been widely used for tissue engineering and regenerative medicine. Biomimetic scaffolds that mimic the extracellular matrix (ECM) micro-environment surrounding cells *in vivo* are desirable to provide appropriate biological cues to control cell functions and guide functional tissue regeneration. ECM scaffolds can be prepared from isolated ECM proteins and decellularized tissues and organs. Recently, cultured cells have been used to create ECM scaffolds. Cells are cultured *in vitro* at controlled conditions to deposit ECM. Cultured cell-derived ECM scaffolds can be obtained after decellularization of the cells/ECM complex. Different cell types can be used for preparation of their respective ECM scaffolds. Cultured cell-derived ECM scaffolds show promotive effects on tissue regeneration. This chapter summarizes the latest achievements of biomimetic ECM scaffolds prepared from cultured cells.

Keywords: ECM, scaffold, porous scaffold, biomimetic scaffold, autologous scaffold, cultured cells, decellularization, template, tissue engineering

10.1 Introduction

Tissue engineering and regenerative medicine has been used to regenerate new tissues and organs to restore or replace lost or malfunctioning tissues and organs [1–3]. Cells isolated from a patient are cultured in biodegradable scaffolds supplemented with growth factors to regenerate functional tissues and organs for transplantation [4–5]. Scaffolds serve as a temporary support for cell adhesion and distribution and provide biological cues to control cell proliferation and differentiation. Scaffolds

---

*Corresponding author: Guoping.Chen@nims.go.jp

should mimic the functional and structural characteristics of the native ECM [6–7]. Native ECM is a complex network composed of collagen, fibronectin and other proteins, all of which are interlaced with proteoglycans [8]. ECM not only serves as a supporting material but also acts to regulate cellular functions, such as cell proliferation, migration and differentiation [9]. Moreover, ECM can modulate the signal transduction activated by various bioactive molecules, such as growth factors and cytokines [10].

Synthetic biodegradable polymers such as polylactide (PLA), polyglycolide (PGA), and poly(lactide-co-glycolide) (PLGA), and natural polymers such as collagen, chondroitin and hyaluronic acid have been frequently used to prepare porous scaffolds [11, 12]. However, synthetic polymers are limited by their biological inertness and the acidic moieties, residual catalysts and microscale particulates that accompany degradation [14, 15]. By using isolated natural polymers, it is difficult to reconstruct a scaffold that has the same composition as that of an *in vivo* ECM because native ECM is composed of many kinds of proteins and has very intricate structures. Although many researchers have been trying to identify the proteins in ECMs *in vivo*, there remain a number of unidentified proteins [15]. Due to these difficulties, acellular matrices have been prepared from decellularization of tissues and oragns and used for tissue engineering. Decellularization of tissues and organs, including small intestinal submucosa, heart valve, blood vessel, skin, nerve, tendon, ligament, urinary bladder, vocal fold, amniotic membrane, heart, liver and lung, have been reported [16–23]. The scaffolds obtained from decellularized tissues and organs offer the advantage of maintaining the structures of their respective tissues and organs. However, they suffer from problems of autologous tissue/organ scarcity, host responses and pathogen transfer when allogenic and xenogenic tissues and organs are used. Use of cultured cells is an alternate way to fabricate ECM scaffolds. ECM scaffolds derived from cultured cells can be prepared from various types of cells by different cell culture methods [24–27]. Cultured cells offer several advantages compared with animal tissues [28]. First, cultured cells can be screened for pathogens and then maintained in a pathogen-free condition for ECM harvesting. Second, cell-derived ECM scaffolds may provide the desired geometry and porosity without the limitation of poor cell penetration that can occur during the repopulating of decellularized native tissues. Third, the use of *in vitro* cultured cells provides the flexibility of mixing ECM samples that have been harvested from different cell types. Furthermore, another important advantage of cell-derived ECM scaffolds is that they can be prepared from autologous cells to generate autologous ECM (aECM) scaffolds because autologous cells can be isolated from patients and then expanded in laboratories. In this chapter, porous ECM scaffolds that are prepared from *in vitro* cultured cells by using removable templates will be the focus [29, 30].

10.2   Cultured Cell-Derived ECM Porous Scaffolds

Preparation method of ECM scaffolds by three-dimensional culture of cells in a selectively removable template is shown in Figure 10.1. Cells are cultured in the template. ECM is secreted by cells and deposited on the template. After cell culture, cellular components are removed by decellularization methods. The template is selectively removed from the ECM. ECM porous scaffolds are obtained after decellularization and template removal.

The method has been used to prepare ECM porous scaffolds by culturing human bone marrow-derived mesenchymal stem cells (MSCs), human dermal fibroblasts and human articular chondrocytes [29]. PLGA knitted mesh is used as a template. MSCs, fibroblasts and chondrocytes are seeded and cultured in the template. The cells adhere, proliferate and secrete ECM in the template. After culture for 5 to 6 days, the cellular components are removed by the decellularization method of freeze-thaw cycling plus the treatment with ammonium hydroxide. The PLGA mesh template is selectively removed by the treatment of immersion in 0.5 M Na_3PO_4 aqueous solution at 37°C for 48 hours. The ECM scaffolds prepared from MSCs, fibroblasts and chondrocytes are referred to as ECM-M, ECM-F and ECM-C, respectively.

The ECM scaffolds have a mesh-like appearance similar to that of the PLGA knitted mesh template. Observation by scanning electron
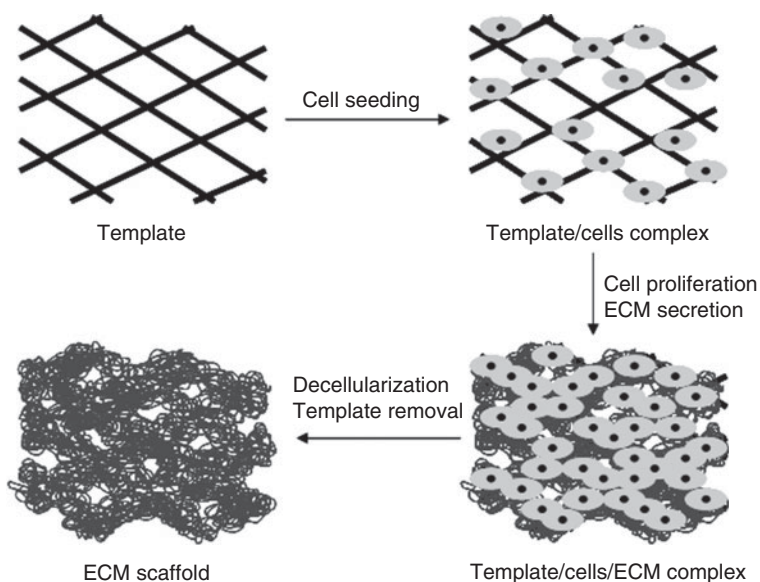
Figure 10.1 Preparation procedure of ECM scaffold from cultured cells.

microscopy (SEM) demonstrates the porous structure of microscale and nanoscale ECM fibers (Figure 10.2). There is no obvious difference among ECM-M, ECM-C and ECM-F scaffolds in terms of morphology. The geometrical properties, porosity, interconnectivity, and nanoscaled fibrous structure are meant to support cell proliferation and differentiation and benefit tissue regeneration [31, 32]. The cell nuclei, cell membrane and F-actin are removed by a decellularization treatment. Removal of PLGA mesh template is confirmed by AIR-FTIR spectra which show the ester carbonyl stretch at 1740 cm^{-1} in the cell-ECM-PLGA complexes disappears in the ECM scaffolds. Examination of the composition of ECM scaffolds shows there is some difference among the compositional biomolecules in ECM-M, ECM-C and ECM-F (Table 10.1). ECM-M consists of type I collagen, type III collagen, fibronectin, vitronectin, laminin, aggrecan, decorin and biglycan. ECM-C consists of type I collagen, type III collagen, fibronectin, vitronectin, laminin, aggrecan, versican, decorin and biglycan. ECM-F consists of type I collagen, type III collagen, fibronectin, vitronectin, laminin, decorin and biglycan. Although primary chondrocytes express type II collagen, the ECM-C does not contain type II collagen because dedifferentiated passage 5 chondrocytes that do not express type II collagen are used to prepare the ECM scaffolds. Therefore, the composition of the ECM scaffolds depends on the cell type and cell phenotype used to prepare the scaffolds.
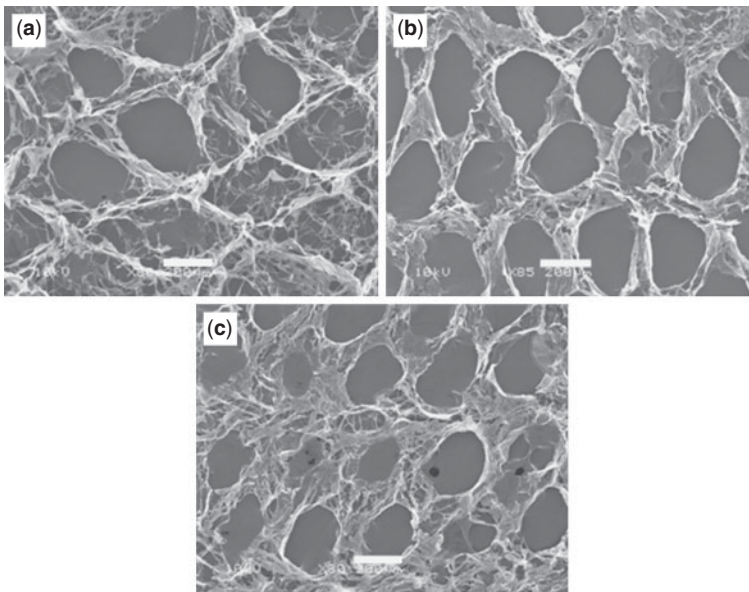
Figure 10.2 SEM image of ECM scaffolds prepared from MSCs (a), chondrocytes (b) and fibroblasts (c). Scale bar = 200 μm.

Table 10.1. Main compositional molecules in ECM scaffolds prepared from MSCs, chondrocytes and fibroblasts

	ECM-M	ECM-C	ECM-F
Type I collagen	+++++	+++++	+++++
Type II collagen	×	×	×
Type III collagen	+	+	++
Fibronectin	++++	++++	++++
Vitronectin	+++	+++	+
Laminin	+	+	++
Aggrecan	+	++	+
Versican	×	+	×
Decorin	+	+	+

"+" indicates detected and "×" indicates not detected

10.3   Autologous ECM Scaffolds

Autologous ECM (aECM) scaffolds should be a safe and reliable biomaterial candidate [33]. The development of aECM scaffolds has been strongly anticipated for use in tissue engineering and regenerative medicine [34, 35]. Use of both autologous cells and autologous scaffolds should eliminate negative host responses and lead to optimal tissue regeneration. However, the availability of autologous sources of donor tissues and organs is highly limited. It has been almost impossible to use such acellular autologous matrices for tissue engineering. The ECM secreted by autologous cells should be a potential alternate to acellular autologous tissues and organs because some autologous cells can be expanded *in vitro* and maintained under a pathogen-free condition.

The above described template method has been used to prepare mouse aECM scaffolds by using mouse fibroblasts. Mouse fibroblasts (mF) are isolated from the biopsies of 6-week-old ICR (Clrj:CD1) mice and expanded *in vitro*. P2 mouse fibroblasts are seeded and cultured in the PGLA mesh template for 10 days. Mouse autologous ECM (aECM-mF) scaffolds are obtained after decellularization and removal of PLGA mesh template. The aECM-mF scaffolds show mesh-like three-dimensional structures and the primary composition is collagen I, collagen III, fibronectin, vitronectin, laminin, decorin and biglycan.

To demonstrate the biocompatibility of the aECM scaffolds, aECM-mF scaffolds are implanted into a subcutaneous pocket of the respective ICR mouse where the fibroblasts are isolated. The host tissue responses to the aECM scaffolds are compared with those to allogeneic ECM scaffolds (ECM scaffolds prepared from allogeneic mouse cells), xenogeneic bovine collagen sponge (BCS) and PLGA mesh. After implantation for one week, the materials are harvested with the surrounding tissues for analysis of inflammatory and immune host responses. Hematoxylin and eosin (HE) staining shows that the host cells have penetrated into the aECM-mF and allogeneic ECM-mF scaffolds. No dense fibrous layers surrounding the implanted materials are observed. However, the BCS and PLGA are wrapped by dense fibrous layers without being remodeled.

Immunocytochemical staining of the 1-week implants shows some neutrophils are observed only in the PLGA, BCS, and allogeneic groups. Among the four implanted materials, the lowest number of macrophages is in the aECM-mF scaffolds. Comparison of percentage of macrophages/ total cells in different groups indicates that the lowest proportion of macrophages is found in the aECM group. The macrophage percentage of the allogeneic group is significantly higher than that of the aECM scaffolds. The macrophage percentages elicited by the BCS and PLGA scaffolds are significantly higher than those elicited by the ECM scaffolds. When biomaterials are implanted, neutrophils and macrophages have been reported to be involved in the inflammatory responses at the implantation site. Neutrophils serve to remove foreign materials and trigger other host responses by secreting factors that summon other immunocytes [36]. And macrophages become activated and act as the main mediators of the host tissue responses. The excretion of soluble mediators by macrophages can influence the behavior of other leukocytes. The absence of neutrophils and lowest macrophage percentage indicate aECM-mF scaffold induces the lowest inflammatory responses. A few MHC class II antigen-presenting cells are observed in the allogeneic ECM-mF and BCS implantation groups. These immunogenic antigen-presenting cells are supposed to exacerbate inflammation and immunological reactions. No T cells are detected in any of the groups after 1-week implantation.

Cytokine profiles, which are the key mediators in the host tissue response, are also investigated. The expressions of genes encoding interleukin-10 (*Il10*), interleukin-2 (*Il2*), interleukin-4 (*Il4*), and tumor necrosis factor- (*Tnf*) in the connective tissues under the 1-week implanted materials are analyzed by real-time RT-PCR. The expression of *Il10* is lower in the aECM and control groups than that in the allogeneic ECM, BSC and PLGA groups. Among the samples, there is no significant difference in the transcription level of *Tnf* although it is lower in the aECM group. No *Il2* and *Il4* gene expressions are detected. These results indicate aECM-mF induce minimal cytokine mediation to modulate the host responses.

All of the results from the host tissue response analyses indicate excellent biocompatibility of the aECM scaffolds, which is essential for ideal tissue engineering scaffolds. Furthermore, the use of autologous serum and serum-free culture is technically possible to reduce the use of animal serum and to minimize the potential side effects induced by exogenous materials [37, 38].

10.4   Application of Cultured Cell-Derived ECM Scaffolds

The ECM scaffolds prepared from cultured cells have been used for tissue engineering of cartilage and dermis [29]. ECM-M and ECM-C were used for the culture of MSCs in chondrogenic induction medium to investigate their effects on cartilage tissue regeneration. MSC are seeded in both ECM-M and ECM-C. The cell seeding efficiency in the ECM-M and ECM-C is $82.1 \pm 4.5\%$ and $81.0 \pm 6.5\%$, respectively. Observation with an optical microscope and a SEM demonstrate that MSCs attach well to the fibers and flakes of the ECM-M and ECM-C scaffolds. However, there is no obvious difference between the ECM-M and ECM-C scaffolds in the cell seeding efficiency, cell distribution and morphology.

The gross appearances of the engineered cartilage after culture for 1, 2 and 4 weeks in the ECM scaffolds are glisteningly white, which is similar to native cartilage. The tissues become larger during the culture in ECM scaffolds. The size of tissues formed in the ECM scaffolds is larger than that of the pellet-cultured MSCs. After 1 week of culture, the MSCs proliferate and secrete new ECM to occupy the spaces in the ECM scaffolds. The cell viability after culture in the scaffolds for 4 weeks is examined by live-dead staining. Green living cells are observed and very few red dead cells are detected. These results indicate that the cells show high viability when being cultured in the ECM scaffolds. The sGAG content and dry weight of the engineered tissues using the ECM scaffolds are higher than those of the tissues constructed by conventional pellet culture. The sGAG content and dry weight increase with the culture time. There is no obvious difference between ECM-M and ECM-C. These results indicate that the ECM scaffolds promote the secretion of ECM.

The chondrogenic differentiation of MSCs is investigated by histological, immunohistochemical and real-time PCR analyses. Toluidine blue staining indicates the typical cartilaginous metachromasia of the engineered tissues. The tissues formed in the ECM scaffolds are more strongly stained than those formed by pellet culture. The cells exhibit a polygonal shape and are surrounded by cartilaginous ECM in ECM-M and ECM-C. Immunohistological staining with antibodies against type II collagen and aggrecan reveals the cartilage-specific ECM composition of the engineered

constructs. These results indicate that the engineered tissues exhibit a cartilage-specific ECM composition.

The expression levels of the genes encoding collagen II (*COL2A1*), aggrecan (*ACAN*) and SOX 9 (*SOX9*) are examined by real-time PCR. The expression levels of these genes are up-regulated when MSCs are cultured in ECM-M and ECM-C in comparison to pellet-cultured MSC. The gene expression levels increase with the culture period. The gene expression results, together with the histological and immunohistochemical staining results, indicate that cartilage-like tissue is engineered when MSC are cultured in the ECM-M and ECM-C scaffolds. ECM-M and ECM-C scaffolds promote chondrogenic differentiation of MSCs. However, the effects of ECM-M and ECM-C on MSCs chondrogenesis are not identical. ECM-M more effectively promotes chondrogenic gene expression relative to ECM-C.

The ECM-F scaffold is used for three-dimensional culture of fibroblasts to regenerate dermal tissue. Human dermal fibroblasts are seeded and cultured in ECM-F. Fibroblasts adhere in ECM-F after a 30 min culture period. The cells distribute into the pores and on the surfaces of the ECM scaffolds. The cell seeding efficiency of fibroblasts in ECM-F is 84.7 ± 8.1%. The ECM molecules in the scaffolds function as adhesion-promoting factors to support cell adhesion. The cells spread on the scaffolds after 3 h of culture. The cells proliferate and produce ECM to cover all of the openings and distribute homogenously after a 4-day culture period.

The viability of the fibroblasts cultured in ECM-F for 12 h, 24 h and 2 weeks is evaluated by calcein-AM/PI double staining. Most of the cells are stained by calcein-AM, and almost no dead cells are detected. And the cells show a typical spindle fibroblastic morphology. These results indicate a high viability of the fibroblasts cultured in the ECM scaffolds. After culture for 2 weeks, the pores in ECM-F are completely filled with ECM and fibroblasts. HE staining of the cultured fibroblast/ECM scaffold implants after 2 weeks of culture indicates that the fibroblasts are distributed throughout the scaffold and form a uniform layer of dermal tissue approximately 150 μm thick. The ECM-F scaffold promote regeneration of dermal tissue.

10.5   Summary

Biomimetic ECM scaffolds can be prepared not only from decellularized tissue and organs, but also from cultured cells. By using a selectively removable template, ECM scaffolds from any cell types can be obtained. The compositions and functions of cultured cell-derived ECM scaffolds are dependent on the type and phenotype of cells used for the preparation of scaffolds. The ECM scaffolds support cell adhesion, proliferation

and tissue regeneration when they are used for three-dimensional culture of MSCs and fibroblasts. The preparation method can be used to culture autologous cells to construct aECM scaffolds. The aECM scaffolds show excellent biocompatibility. By using aECM scaffolds for the culture of autologous cells, "full autologous tissue engineering" will be realized to make the tissue engineered construct more biocompatible with the host. The biomimetic ECM scaffolds derived from cultured cells will be useful for tissue engineering, stem cell research and biomedical applications.

References

1. R. Langer, J.P. Vacanti, *Science* 260:920–6, 1993.
2. L.G. Griffith, G. Naughton, *Science* 295:1009–14, 2002.
3. H. Shin, S. Jo, A.G. Mikos, *Biomaterials* 24:4353e64, 2003.
4. S.J. Hollister, *Nat. Mater.* 4: 518–24, 2005.
5. G.C. Engelmayr Jr., M. Cheng, C.J. Bettinger, J.T. Borenstein, R. Langer, L.E. Freed, *Nat. Mater.* 7:1003–10, 2008.
6. M.P. Lutolf, J.A. Hubbell, *Nat. Biotechnol.* 23:47–55, 2005.
7. D.W. Hutmacher, *Biomaterials* 21:2529–43, 2000.
8. R.I. Manabe, K. Tsutsui, T. Yamada, M. Kimura, I. Nakano, C. Shimono, *et al.*, *Proc. Natl. Acad. Sci. U.S.A.* 105:12849–54, 2008.
9. S.F. Badylak, D.O. Freytes, T.W. Gilbert, *Acta Biomater.,* 5:1–13, 2009.
10. R.O. Hynes, *Science* 326:1216–19, 2009
11. L.S. Nair, C.T. Laurencin, *Prog. Polym. Sci.* 32:762–98, 2007.
12. G. Chen, T. Ushida, T. Tateishi, *Adv. Mater.* 12:455–7, 2000.
13. G. Chan, D.J. Mooney, *Trends Biotechnol.* 26:382–92, 2008.
14. D.F. Williams, *Biomaterials* 29:2941–53, 2008.
15. R. Manabe, K. Tsutsui, T. Yamada, *et al.*, *Proc. Natl. Acad. Sci. U.S.A.* 105: 12849–54, 2008.
16. T. Hoshiba, H.X. Lu, N. Kawazoe, G. Chen, *Expert Opin. Biol. Ther.* 10:1717–28, 2010.
17. R. Chen, H. Ho, Y. Tsai, M. Sheu, *Biomaterials* 25:2679–86, 2004.
18. P.W. Whitlock, T.L. Smith, G.G. Poehling, J.S. Shilt, M. van Dyke, *Biomaterials* 28:4321–29, 2007.
19. F. Bolland, S. Korossis, S. Wilshaw, E. Ingham, J. Fisher, J.N. Kearney, *et al.*, *Biomaterials* 28:1061–70, 2007.
20. H.C. Ott, T.S. Matthiesen, S.K. Goh, L.D. Black, S.M. Kren, T.I. Netoff, *et al.*, *Nat. Med.* 14:213–21, 2008.
21. B.E. Uygun, A. Soto-Gutierrez, H. Yagi, M.L. Izamis, M.A. Guzzardi, C. Shulman, *et al.*, *Nat. Med.* 16:814–20, 2010.
22. H.C. Ott, B. Clippinger, C. Conrad, C. Schuetz, I. Pomerantseva, L. Ikonomou, *et al.*, *Nat. Med.* 16:927–33, 2010.
23. T.H. Petersen, E.A. Calle, L. Zhao, E.J. Lee, L. Gui, M.B. Raredon, *et al.*, *Science* 329:538–41, 2010.
24. H.W. Cheng, Y.K. Tsui, K.M. Cheung, D. Chan, B.P. Chan, *Tissue Eng. C Methods* 15:697–706, 2009.

25. K.H. Choi, B.H. Choi, S.R. Park, B.J. Kim, B.H. Min, *Biomaterials* 31:5355–65, 2010.
26. J. Liao, X. Guo, K.J. Grande-Allen, F.K. Kasper, A.G. Mikos, *Biomaterials* 31:8911–20, 2010.
27. J.C. Wolchok, P.A. Tresco, *Biomaterials* 31: 9595–603, 2010.
28. K. Narayanan, K.J. Leck, S. Gao, A.C.A. Wan, *Biomaterials* 30:4309–17, 2009.
29. H. Lu, T. Hoshiba, N. Kawazoe, I. Koda, M. Song, G. Chen, *Biomaterials* 32:9658–66, 2011.
30. H. Lu, T. Hoshiba, N. Kawazoe, G. Chen, *Biomaterials* 32:2489–99, 2011.
31. G. Chen, T. Ushida, T. Tateishi, *Macromol. Biosci.* 2:67–77, 2002
32. L.A. Smith, P.X. Ma, *Colloids Surf. B Biointerfaces* 39:125–31, 2004.
33. D.J. Cozzolino, M. Cendron, D.P. Devore, P.J. Hoopes, *Neurourol. Urodyn.* 18:487–95, 1999.
34. L.L. Hench, J.M. Polak, *Science* 295:1014–7, 2002.
35. P.M. Taylor, *Philos. Trans. R. Soc. Lond. B* 1313–20, 2007.
36. J.E. Babensee, J.M. Anderson, L.V. McIntire, A.G. Mikos, *Adv. Drug Deliv. Rev.* 33:111–39, 1998.
37. J.E. Ahlfors, K.L. Billiar, *Biomaterials* 28:2183–91, 2007.
38. M.J. Martin, A. Muotri, F. Gage, A. Varki, *Nat. Med.* 11:228–32, 2005.

Design and Synthesis of Photoreactive Polymers for Biomedical Applications

**Ponnurengam Malliappan Sivakumar¹, Di Zhou¹,
Tae Il Son² and Yoshihiro Ito¹,***

*¹Nano Medical Engineering Laboratory, RIKEN Advanced Science Institute,
Saitama, Japan*
*²Department of Biotechnology, Chung-Ang University,
Anseong, Republic of Korea*

Abstract

Photoreactive polymers are useful for biological and medical applications. In this chapter we will describe the preparation of ultraviolet or visible light-curable biological polymer derivatives or synthetic polymers and review our applications for micropatterning surfaces, microarray chips, or biosealants.

Keywords: Photoreactivity, photoimmobilization, photolithography, micropatterning, bio-nonfouling, photocrosslinking, gelatin, polysaccharide, biosealant, and bioadhesive

11.1   Introduction

Various types of photoreactive or photoresponsive polymers have been developed for chemical and medical applications. Here, we discuss some photoreactive biopolymers designed for medical applications. One group comprises ultraviolet (UV) light-reactive biopolymers, including biological macromolecules such as gelatin, hyaluronic acid, chitosan, pullulan, and synthetic polymers such as stimuli-responsive polymers and bio-nonfouling polymers. Another group comprises visible light-reactive polymer systems. The former are utilized for surface micropatterning for cell culture and preparing microarray chips. The latter are used as biosealants or bioadhesives. These are summarized in Figure 11.1.

Corresponding author: y-ito@riken.jp
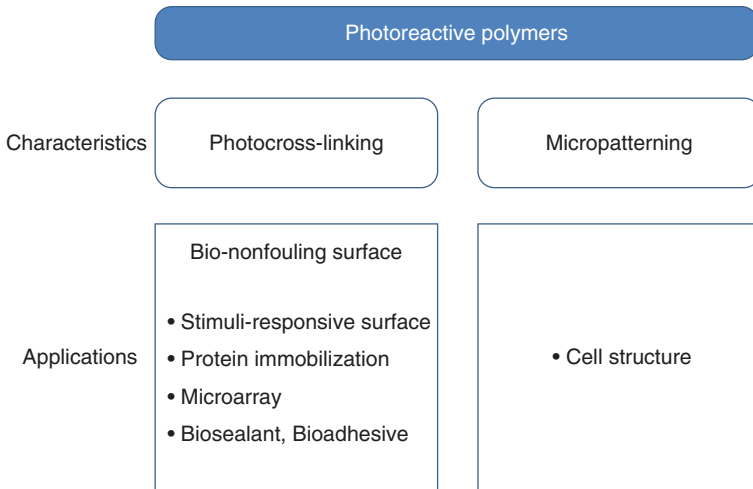
Figure 11.1 Characteristic points and biological and medical applications of photoreactive polymers.
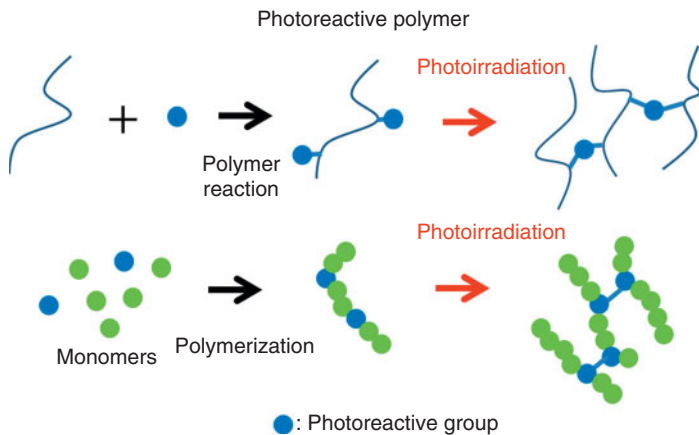
Figure 11.2 Principles of preparing photosensitive crosslinkable biological and synthetic polymers.

Synthesizing procedures are categorized into two groups, as shown in Figure 11.2. One approach is the modification of biological polymers with a photoreactive group, and the other is the production of synthetic polymers by copolymerization with a monomer carrying a photoreactive group.

11.2   UV-Reactive Biological Polymers

Biopolymer derivatives including proteins such as gelatin, and polysaccharides including hyaluronic acid, heparin, chitosan, and pullulan, have

been synthesized by coupling with azidophenyl groups. These are decomposed by UV irradiation, and radical nitrene groups are produced by this decomposition. The nitrene groups contribute to crosslinking of the polymers with each other, and at the same time, they react with other organic materials. Some recent developments have been described by Liu and Yan [1], and the photochemistry is shown in Figure 11.3. The biopolymers can be immobilized on substrata and employed for the immobilization of organic materials including biomolecules such as nucleic acids or proteins. We have utilized the biopolymers for fabrication of a micropatterned cell culture substrate, immobilization of growth factors, and making microarray chips. The surface treatment is very important for biomaterial design.

11.2.1   Gelatin

Collagen, fibronectin, and vitronectin are important adhesion proteins. Gelatin is produced from collagen and is used widely to enhance cell adhesive properties. Matsuda and Sugawara [2] developed a microchemical fixation method using azidophenyl functional groups. Azidophenyl
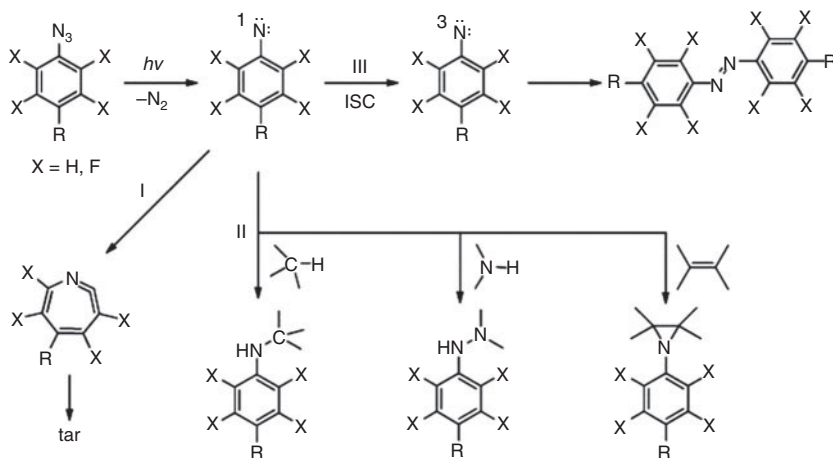
Figure 11.3 Simplified description of azidophenyl photochemistry. Rearrangement of the corresponding seven-membered ketenimine, which reacts with amines to give azepinamines, or produces polymer tars in the absence of the nucleophile (I). CH or NH insertion and C=C addition reactions are the key contributions to the covalent bond formation with the target molecules (II) and relaxation via intersystem crossing to the triplet phenylnitrene, which undergoes H-abstraction reactions to form primarily aniline-type products, or bimolecular reactions to yield the corresponding azo compound (III). hv and ISC mean photoirradiation and intersystem crossing, respectively. Reprinted and adapted with permission from Ref. [1]. Copyright (2010) American Chemical Society.

groups coupled with either proteins or polymer and the azidophenyl group during photolysis produce phenyl nitrene groups, which are responsible for the covalent bond formation that leads to photoimmobilization. They prepared *N*-((4-azidobenzoyl)oxy)succimide-coupled proteins (albumin and gelatin) as shown in Figure 11.4a and synthetic polymers (poly (3-azidostyrene) and poly(*N*,*N*-dimethylacrylamide-co-3-azidostyrene)). Synthesized azidophenyl-coupled proteins were immobilized onto the unmodified polymers. Microchemical immobilization using UV light was characterized by electron spectroscopy for chemical analysis (ESCA), colorimetric immunostaining using antibodies, and atomic force microscopy (AFM). These measurements demonstrated that photoimmobilization is simple for making micropatterns [1].

Similarly, we have synthesized UV-reactive gelatin for covalent photoimmobilization of biological molecules in several ways to induce specific biological responses on material surfaces [3–10]. Photoimmobilization is an effective method for this as it introduces photoreactive groups to the molecules independently of the surface functional groups. For example, the placement of covalently immobilized growth factor proteins by photoirradiation significantly enhanced cell growth when used for culture *in vitro*. Micropattern immobilization of growth factors achieved by photocrosslinking was very effective to confirm this effect because cell growth was observed only on the treated regions. The method for micropatterning using photolithography is illustrated in Figure 11.5a.

Recently, the origin of photoreactive gelatin has been extended from bovine to recombinant human tissues, and its potential for the surface modification of synthetic polymers has been examined using cell culture and tissue engineering [11]. The micropatterning is shown in Figure 11.6. Its effectiveness as a culture substratum was examined by culturing
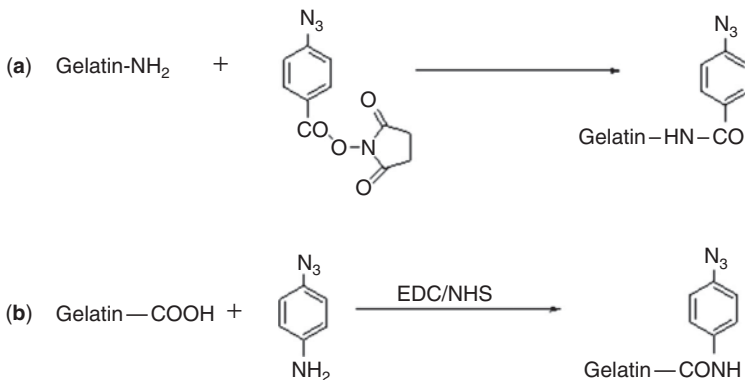
Figure 11.4 Synthesis of azidophenyl gelatin derivatives. EDC/NHS indicates 1-ethyl-3-(3-dimethylaminopropyl)carbodiimide/*N*-hydroxysuccimide.
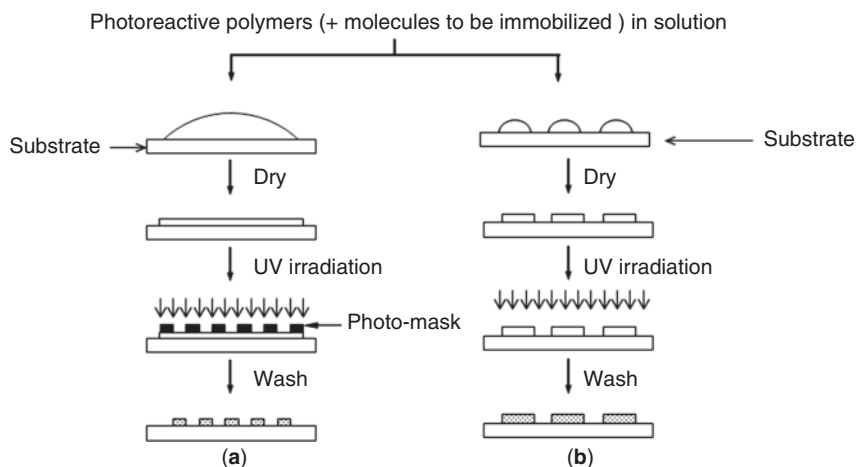
Figure 11.5 Preparative methods using (a) photolithography and (b) microarrays using UV-sensitive crosslinkable macromolecules.
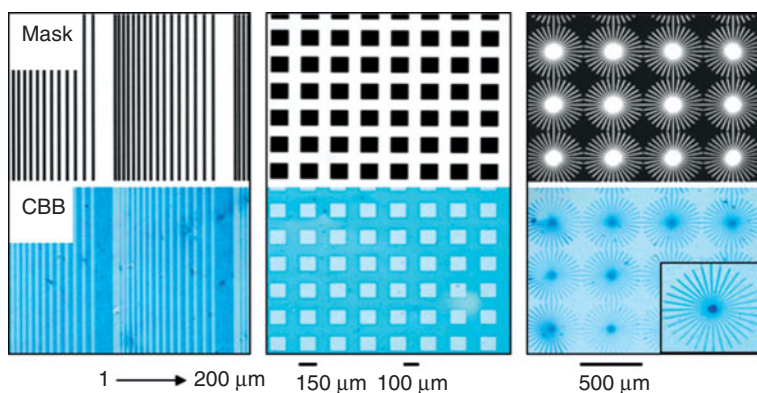
Figure 11.6 Micropattern immobilization of photoreactive human gelatin. Immobilized proteins were stained with Coomassie Brilliant Blue (CBB).

human mesenchymal stem cells, and its applicability was investigated by its capacity to bind to various polymers employed in tissue engineering studies. In addition, its combination with engineered growth factors with a collagen/gelatin affinity was shown to exhibit tissue-repairing activities—such as epidermal cell proliferation, angiogenesis, and endothelialization on and/or around the implanted materials—and was also investigated.

We have immobilized insulin [12–14], epidermal growth factor (EGF) [15–20], nerve growth factor [21], erythropoietin [22], leukemia inhibitory factor [23], and vascular endothelial growth factor [24] using photoreactive

gelatin. In addition to these proteins, basic fibroblast growth factor (bFGF)—used for inducing cell proliferation and secretion of angiogenic factors—together with proteoglycan heparan sulfate was immobilized by Doi *et al.* [25, 26]. They prepared microporous gelatin-treated small-caliber segmented polyurethane grafts for tissue regeneration at both perianastomotic and transmural sites in rat arteries. Impregnated grafts were coated with a mixture of photoreactive gelatin (gelatin with photoreactive benzophenone groups), bFGF, and heparin and photocured with UV irradiation to obtain the coimmobilization of bFGF and heparin. Nonimpregnated control grafts were coated with photoreactive gelatin alone. Both graft types (impregnated and nonimpregnated) were implanted in rat aortas for 4 weeks. Endothelialization in the bFGF/heparin coimmobilized (impregnated) grafts was found to be greater in extent than in the control grafts. Coimmobilization of bFGF/heparin using photoreactive gelatin enhanced neoarterial generation through perianastomotic and transmural tissue ingrowth [25]. Doi *et al.* [26] also prepared polyurethane grafts with controlled micropore diameter and distribution attained using a computer-aided excimer laser ablation technique. The prepared grafts were coated with photoreactive gelatin and fixed photochemically to the polyurethane surfaces using UV. Upon UV irradiation, the photoreactive gelatin bound covalently to the surface and acted like an artificial extracellular matrix. This can help in endothelialization and can be used to immobilize biological molecules that can facilitate tissue growth, such as growth factors. These coatings also increase the biocompatibility of grafts. Thus, a combined excimer laser approach using microporation and photochemical gelatin processing onto surfaces is helpful for enabling transmural tissue growth [26].

On the other hand, Chung *et al.* [27] modified gelatin with 1-(2-carboxyethyl)thymine using carbodiimide as a coupling agent as shown in Figure 11.7a. Upon UV irradiation, photoreactive thyminated gelatin underwent crosslinking. The crosslinking is directly proportional to the degree of derivatization using thymine and UV irradiation time. They also proved that the photoreactive thyminated gelatin can be used for sealant or hemostatic applications in laparoscopy [27].

Nakayama *et al.* [28] developed a photocurable glue with a combination of photoreactive gelatin and poly(ethylene glycol) diacrylate (PEGDA). UV-photocurable agents such as benzophenone and visible light-photocurable agents such as fluorescein, eosin, and Rose Bengal were coupled with gelatin to make photoreactive gelatin. PEGDA molecules of various molecular weights (1,000, 2,100, and 3,900) were used along with photoreactive gelatin at different concentrations to prepare hydrophilic gels with high adhesiveness. This property arose from photocrosslinking and photograft polymerization. These photocurable glues can be used for tissue adhesion in cardiovascular and endoscopic surgery because of their
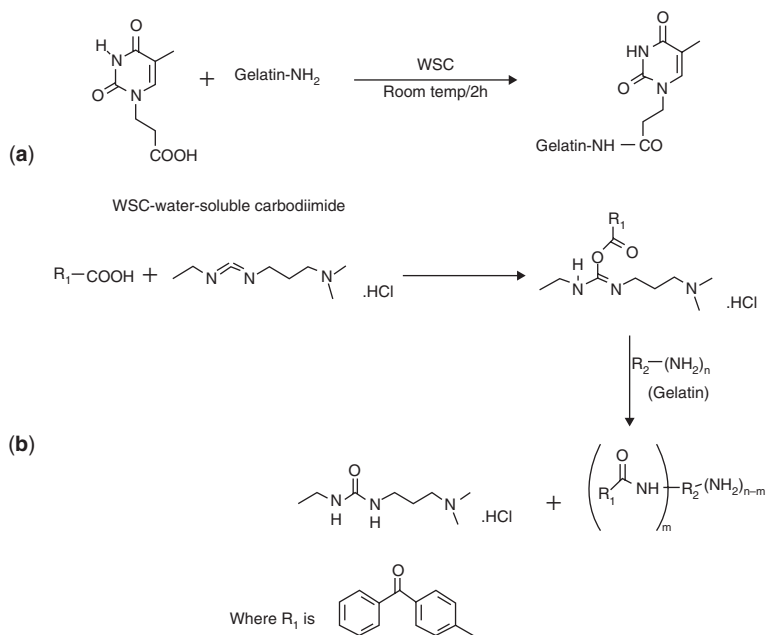
Figure 11.7 Synthetic methods for photoreactive gelatins. Modification with (a) 1-(2-carboxyethyl)thymine and (b) benzophenone.

biodegradability [28]. The scheme for manufacturing benzophenone-derivatized UV-reactive gelatin is shown in Figure 11.7b.

As well as organic or biological surfaces, immobilization of proteins on metal surfaces such as titanium and alloys has become important for medical applications. Mojgan *et al.* [29] immobilized titanium with photoreactive gelatin carrying azidophenyl groups using silane coupling. Weng *et al.* [30] prepared a Ti-O surface engineered with self-assembling 3-aminopropylphosphonic acid (APP), which was further immobilized with azidophenyl gelatin (azidophenyl gelatin was prepared by reacting the carboxyl groups in gelatin to react with 4-azidoaniline, as shown in Figure 11.4b). The APP made an organic bond with the azidophenyl gelatin. The micropattern onto the immobilized surface was made using photomasking against UV irradiation. The micropattern was confirmed by staining with Sirius red and the surface profile was analyzed. The surface was allowed to grow human endothelial EVC304 cells and the cell attachment and growth showed the pattern produced during UV irradiation and photomasking. Thus, an azidophenyl gelatin-modified Ti-O surface can be used for the micropatterning of endothelialization *in vitro* [30]. Recently, photoreactive azidophenyl groups were also introduced to fish gelatin to create an azidophenyl–fish gelatin compound and the curing

ratio was measured using micropatterning on the titanium substrate [31]. The resultant titanium surface was found to be efficient in EGF immobilization and in enhancement of cell growth.

11.2.2   Polysaccharides

11.2.2.1   Hyaluronic Acid

Hyaluronic acid (HA) is a linear polysaccharide of (1-β-4) D-glucuronic acid and (1-β-3) N-acetyl-D-glucosamine. It is an anionic, usually nonsulfated glycosaminoglycan distributed widely throughout connective, epithelial, and neural tissues. Its molecular weight often reaches the millions. One of the chief components of the extracellular matrix, HA contributes significantly to cell proliferation and migration and might also be involved in the progression of some malignant tumors. Artificially sulfated HA was coupled with azidophenyl groups and the UV-reactive hyaluronic acid was employed to construct an antithrombogenic surface [32]. In addition, it is known that the level of HA regulates gene expression, signaling, proliferation, motility, adhesion, metastasis, and morphogenesis of embryonic stem (ES) cells *in vivo*. In humans, the HA content *in vivo* is greatest in undifferentiated ES cells and during early embryogenesis. Therefore, HA is being used widely to culture and propagate stem cells, and the fabrication of biodegradable three-dimensional HA scaffolds enriched with multipotent stem cells seems to be a promising strategy for the repair of irreversibly injured tissues. HA scaffolds support the undifferentiated proliferation of ES cells in the absence of feeder cell layers and retain their ability to differentiate after release from HA hydrogels. Moreover, it is known that the effect of HA on the cellular environment varies according to its molecular weight (MW). For example, it is generally accepted that low-MW HA (LMW-HA) is angiogenic and is involved in tumor metastasis, whereas high-MW HA (HMW-HA) is viscous, nonadherent to cells, and acts as a lubricant. On the other hand, HMW-HA is believed to adhere to cells in a polyvalent manner, leading to the formation of pericellular sheaths that do not facilitate cell–cell and cell–growth factor interactions. LMW-HA interacts with cellular receptors in a monovalent manner and may lead to clustering of cell surface receptors (e.g., CD44) to activate intracellular signaling cascades.

We have prepared photoreactive HMW-HA and LMW-HA, immobilized them onto tissue culture substrates, and compared and contrasted their effects on murine ES cells *in vitro* [33]. We hypothesized that they would affect ES cell behavior differently. We demonstrated the presence and interaction of the HA receptors CD44 and CD168 on these ES cells and examined how these cell receptor–HA interactions determined cell fates *in vitro*.

11.2.2.2 Heparin

Heparin, a highly sulfated glycosaminoglycan, is widely used as an injectable anticoagulant. It has the highest negative charge density of any known biological molecule and has been used to form an inner anticoagulant surface on various experimental and medical devices such as test tubes and renal dialysis machines when coupled with azidoaniline [34–36]. The derivatized heparin was cast onto a film from aqueous solution. After drying, the film was photoirradiated in the presence or absence of a photomask. The subsequent micropatterning was confirmed by staining with a cationic dye. Mouse fibroblast STO and NIH3T3 cells were cultured on the heparin-immobilized film in the presence of bFGF; the growth of cells was enhanced only on the heparin-immobilized regions. This result indicated that micropattern-immobilized heparin activated bFGF for promoting cell growth. In addition, the growth of cells was affected by the surface density of the immobilized heparin. This was regulated by differently sized gaps between 2-μm-wide stripes of the substrate. Although a high-density region with short gaps of immobilized heparin suppressed cell growth in the absence of bFGF, it was enhanced in the presence of bFGF. The dependence of cell growth on the density of immobilized heparin was visualized using this gradient of micropattern immobilization.

11.2.2.3 Chitosan

Chitosan, a deacetylated form of chitin derived from crustacean exoskeletons, is the most abundant biomass on earth, after cellulose. Many studies have revealed its unique biological properties, including wound healing, stimulation of the secretion of fibroblast growth factor, and effects on the restoration of bone tissues. It also displays antibacterial, hemostatic, fungistatic, antitumor, and anticholesteremic activities. Because chitosan is very similar to human tissues when combined with glucosamine, it has been used widely for drug and gene delivery and tissue engineering. Furthermore, the nontoxic nature and antibacterial activity of chitosan make this compound an effective wound-healing agent. It has also been examined for its pharmacological properties including use as an anticoagulant, artificial skin, and medical material because of its cholesterol-lowering effect and antitumor properties. Naturally occurring chitosan is insoluble in water. We have demonstrated the applicability of photocurable chitosan derivatives for medical use [37, 38]. We utilized chitosan with a degree of deacetylation of about 88% from crab shells and prepared low molecular weight chitosan (LMW-CS) as follows. Chitosan was dissolved in acetic acid solution with strong agitation. $NaNO_2$ dissolved in distilled water was added dropwise to the chitosan solution in an ice bath. After stirring for 2 h, the chitosan solution was neutralized with NH_4OH. It is known that nitrous acid decomposition of chitosan results in deamination

of an end unit, forming unstable 2,5-anhydro-D-mannose. Therefore, this unstable end unit was further reduced to stable 2,5-anhydro-D-mannitol by treating with NaBH$_4$. After neutralization, the degraded chitosan was filtered and concentrated by evaporation. Methanol was added to induce precipitation with stirring and stored at 4°C to increase the precipitation yield. After washing, the LMW-CS powders were dissolved in deionized water and subjected to ultrafiltration. Activated 4-azidobenzoic acid was coupled to the LMW-CS, as shown in Figure 11.8a.

To prepare low molecular weight O-carboxymethyl depolymerized chitosan (LMW-O-CMCS), the LMW-CS was dissolved in 60% NaOH solution containing 0.2% dodecyl sodium sulfate and kept on ice for 1 h until frozen. The frozen sample was suspended in isopropanol and mixed with monochloroacetic acid. After the sample had been precipitated with ethanol, the product was vacuum dried at room temperature. Finally, the chitosan derivative was coupled with activated 4-azidobenzoic acid, as shown in Figure 11.8b. Both of the azidophenyl chitosan derivatives were noncytotoxic on the proliferation of mouse embryonic fibroblast 3T3
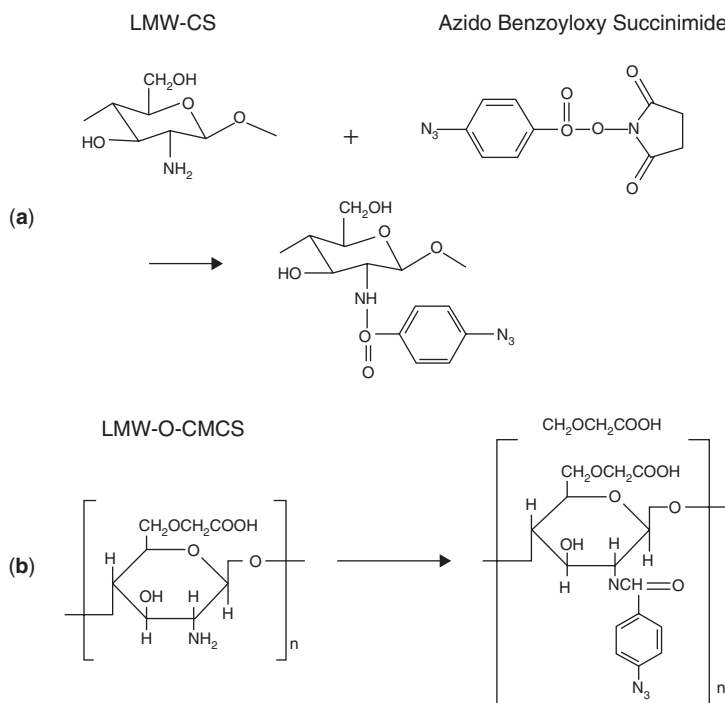
Figure 11.8 Azidophenyl-derivatized (a) low molecular weight chitosan (LMW-CS) and (b) low molecular weight O-carboxymethyl chitosan (LMW-O-CMCS).

cells. The photoreactive LMW-O-CMCS was employed for *in vivo* animal studies as a synthetic anti-adhesive material. Guardix® (hyaluronic acid-carboxymethylcellulose membrane) treated with photoreactive LMW-O-CMCS showed a nondistorted dural contour, but adhesion was more than two-thirds [38]. However, photoreactive LMW-O-CMCS showed no dural adhesion and adequate space in the laminotomy space was sustained [38].

11.2.2.4   Pullulan

Pullulan is a linear homopolysaccharide of glucose that is often described as α-(1-6)-linked maltotriose, secreted primarily by strains of the fungus *Aureobasidium pullulans*. The unique linkage pattern of pullulan endows it with distinctive physical traits, including adhesive properties and the capacity to form fibers, compression moldings, and strong, oxygen-impermeable films. Pullulan and its derivatives have numerous uses in foods, pharmaceuticals, manufacturing, and electronics. UV-reactive pullulan was synthesized by incorporating azidophenyl groups using a conventional coupling between 4-azidobenzoic acid and pullulan in the presence of ethyl(dimethylaminopropyl)carbodiimide/*N*-hydroxysuccimide [39]. The synthesized polymer was photoimmobilized/crosslinked onto polymeric surfaces such as polystyrene, polyethylene, and silane coupled onto glass surfaces using photomasking. The resultant surface has antifouling properties. The micropatterned polymer was employed for culture of RAW264 cells obtained from mouse leukemic monocytes. The immobilized pullulan micropatterns did not allow the cells to adhere, and reduced protein interactions with the surface. Thus, the nonionic and hydrophilic layer produced by photoreactive pullulan upon exposure to an aqueous environment leads to reductions in cell and protein attachment.

11.3   UV-Reactive Synthetic Polymers

11.3.1   Bio-nonfouling Polymers

Bio-nonfouling is important for reducing the nonspecific adsorption of proteins on biomaterial surfaces. To prepare such surfaces, zwitterionic groups such as phosphobetaine, sulfobetaine, and carbobetaine and amphiphilic polymers such as poly(ethylene glycol) (PEG) or poly(vinyl alcohol) have usually been used. We have developed some new photoreactive bio-nonfouling polymers for surface treatment and microarray chip preparation, as described below.

11.3.1.1   Phosphobetaine

2-Methacryloyloxyethyl phosphorylcholine (MPC) polymer is a biomimetic polymer that acts to block thrombogenesis by reducing platelet

adhesion and activation. Because phosphorylcholine is a lipid head found naturally in cell membranes, MPC is considered to reduce interactions with biocomponents such as proteins and cells. The photoreactive polymer is synthesized by coupling 4-azidoaniline with a copolymer containing MPC and methacrylic acid as shown in Figure 11.9 [40, 41]. The synthesized polymer was used for coating onto surfaces such as polyethylene and polypropylene. Micropatterning was carried out using photomasking, and the adhesion of RAW264 cells onto the resultant micropatterned photoreactive phospholipid polymer was investigated. As interactions between the surface and the cells were observed, there was a significant difference between nonimmobilized and immobilized regions. The immobilized region did not show any adherence of cells and form aggregates, but the nonimmobilized region did. In addition, human blood platelets showed reduced adhesion and reduced protein adsorption to the immobilized regions. Hence, this surface modification with a photoreactive phospholipid polymer can be used for biomedical applications that require bio-nonfouling properties.

11.3.1.2 Sulfobetaine

A sulfobetaine group containing a photoreactive polymer was synthesized by copolymerization using 4-azidophenyl methacrylamide and 2-(N-3-sulfopropyl-N, N-dimethyl ammonium)ethyl methacrylate with 2,2'-azobis(isobutyronitrile) (AIBN) as an initiator as shown in Figure 11.10a [42]. The synthesized polymer was coated and photoimmobilized on polymeric surfaces such as polystyrene and polyester by UV irradiation. The immobilization of sulfobetaine onto the coated surface was characterized by Time-of-Flight Secondary Ion Mass Spectrometry (TOF-SIMS) by determining the sulfur content. The surfaces turned hydrophilic, as determined
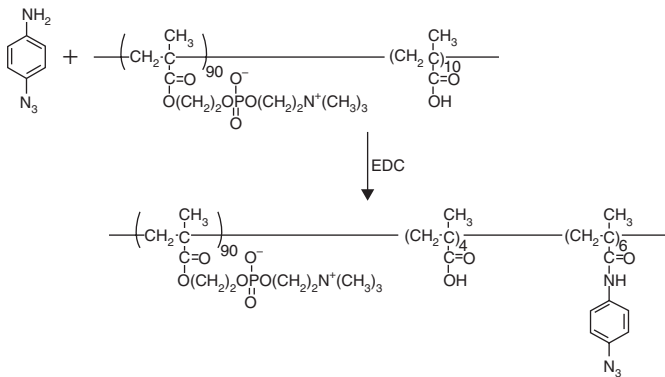
Figure 11.9 Synthesis of a photoreactive phosphobetaine polymer by coupling azidoaniline and a copolymer.
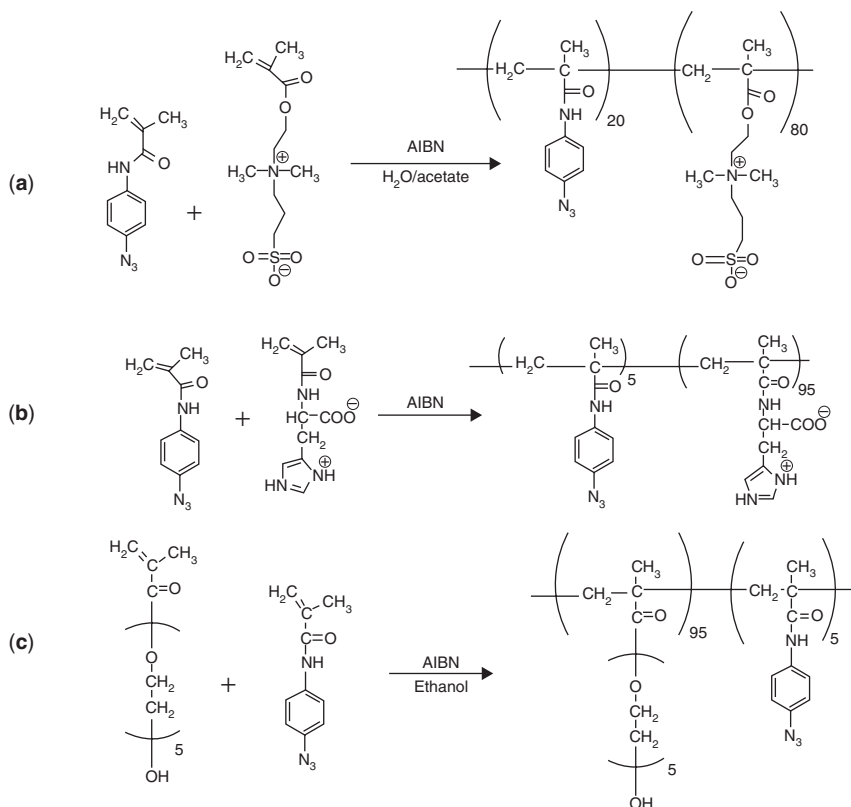
Figure 11.10 Synthesis of photoreactive polymers containing (a) sulfobetamine, (b) carbobetaine, and (c) polyethylene glycol in the side chains. AIBN, azobisisobutylnitrile.

by static contact angle measurements showing that the polar sulfobetaine groups were present on the surface. This zwitterionic group sulfobetaine containing a photoreactive polymer also showed significant reduction in protein and mammalian cell adhesion onto the photoimmobilized surfaces compared with the nonimmobilized surfaces.

11.3.1.3   Carbobetaine

A novel photoreactive polymer with histidine polar groups has been synthesized through the copolymerization of two types of methacrylic acid, one carrying histidine groups and the other carrying azidoaniline groups [43, 44]. Polar histidine groups containing a photoreactive polymer were prepared by reacting two of the methacrylates, namely methacryloyl-L-histidine and 4-azidophenyl methacrylamide carrying histidine and

azidoaniline groups, respectively, as shown in Figure 11.10b. The polymer was photoimmobilized onto polyester disks for surface modification. The effects of this surface modification on the hydrophilic and biofouling properties were investigated. Static contact angle measurements showed that the polymeric surface was modified to be comparatively hydrophilic in the polymer-immobilized region. Micropattern immobilization was carried out with a photolithographic method. AFM measurements showed that the polymer was formed on the disks in response to UV irradiation. Protein adsorption was reduced on the polymer-immobilized regions, and spreading and adhesion of mammalian cells in these regions were reduced compared with the nonimmobilized regions. Thus, this novel histidine-containing polymer was immobilized photoreactively onto a conventional polymer surface and showed reduced interaction with proteins and cells.

11.3.1.4 Amphiphilic Polymers

Polyethylene glycol (PEG) is amphiphilic, and related polymers have nonionic hydrated grafted tails that make them hydrophilic. This prevents biofouling and is helpful in reducing nonspecific protein interactions and ensuring biocompatibility of the biomaterials. We prepared a photoreactive PEG-containing polymer as shown in Figure 11.10c and it was used to make nonadherent or bio-nonfouling surfaces and for microarray applications [45]. PEG-methacrylate was copolymerized with acryloyl-4-azidobenzoic acid in the presence of AIBN as an initiator. The prepared polymer was coated and photoimmobilized onto plastic, glass, and titanium surfaces. The micropatterned surfaces with photoreactive PEG were characterized using TOF-SIMS and AFM analyses, which showed that photoimmobilization had been attained onto the surfaces. Protein adsorption onto the immobilized regions was reduced and COS-7 cells did not adhere to the photoreactive PEG-immobilized regions.

Photoimmobilization using photoreactive non-biofouling polymers has been developed for the preparation of microarray biochips [46–50]. The method is shown in Figure 11.5b. This photoimmobilization method makes it possible to easily covalently immobilize various types of organic molecules and cells on a chip as shown in Figure 11.11. In addition, by using bio-nonfouling polymers as matrixes, it is possible to reduce nonspecific interactions with biological components as shown in Figure 11.12. Various proteins, antibodies, and cells have been microarrayed using this technique and interactions between these proteins, antibodies, and cells have been investigated. Because the immobilization method provided randomly oriented immobilization of proteins including antigens, it is useful to detect polyclonal antibodies as shown in Figure 11.13. This type of microarray biochip will be important for applications such as genomics, proteomics, cellomics, and clinical analyses.
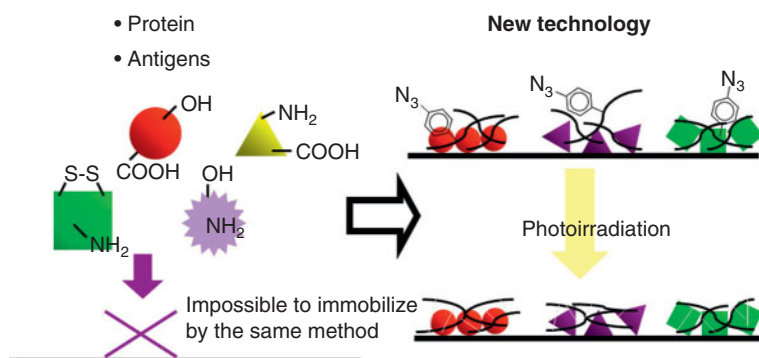
Figure 11.11 Because proteins differ chemically and antigens are heterogeneous, it is difficult to immobilize them all using the same methods (left). The photoimmobilization method was invented ("New Technology") to immobilize various biomolecules covalently, including proteins (right).
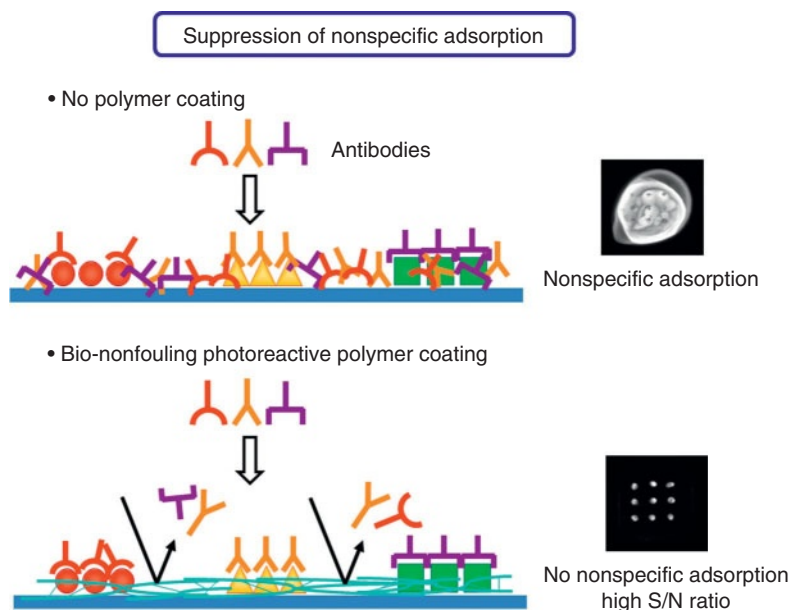
Figure 11.12 There are advantages in using bio-nonfouling polymers for preparing microarrays. These polymers can immobilize organic molecules and inhibit the nonspecific adsorption of proteins including antibodies.
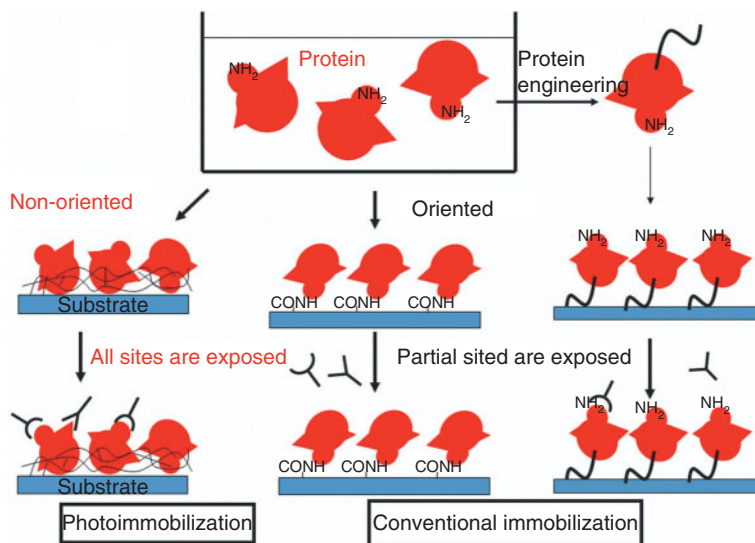
Figure 11.13 Comparison of immobilization methods. Photoimmobilization leads to the random orientation of immobilized molecules, whereas other covalent immobilization methods lead to some orientation because of the uneven distribution of functional groups on the molecules being immobilized. For genetically engineered proteins with adhesive peptide sequences on the end chain, the recognition site is limited to the remaining part of the molecule.

Polyvinyl alcohol derivatives were also prepared by conjugation with azidophenyl groups [51–54]. A novel photoreactive polymer, polyvinyl alcohol modified with azidophenyl groups, was immobilized using micropatterning for cell culture and employed for preparing microarrays. The polymer is soluble in water and is spin-coated onto glass plates. Aqueous solutions of proteins were microspotted onto the coated glass and were fixed by UV irradiation. Subsequently, cell adhesion on the photoimmobilized protein microarray was investigated. Nonspecific adhesion of cells onto the regions not subjected to protein microspotting was reduced in comparison with the previously prepared microarray chip. Adhesion of cells depended on the kind of immobilized proteins and the types of cells. The microarray will be useful for cell diagnosis and for the selection of biomaterials to regulate cell behavior.

11.3.2   Stimuli-Responsive Polymers

We have also synthesized some photoreactive and stimuli-responsive polymers (to pH, temperature, ionic strength, photoirradiation, and redox state) and prepared micropatterned surfaces [55–58]. Among the polymers,

thermoresponsive polymers were employed for investigation on cellular interactions [59–62]. One thermoresponsive copolymer, poly(*N*-isopropylacrylamide-co-acrylic acid), was coupled with azidoaniline. The azidophenyl-derivatized copolymer was grafted in a specific pattern onto a polystyrene matrix by photolithography. The surface micropattern appeared and disappeared interchangeably, as observed under phase-contrast microscopy, by varying the temperature between 10°C and 37°C. The copolymer-grafted polystyrene surface was hydrophobic at 37°C and hydrophilic at 10°C. Albumin and fibronectin adsorption on the matrix was investigated using fluorescence labeling. Fibronectin was adsorbed onto both the grafted and nongrafted regions, while albumin was adsorbed more onto the nongrafted regions than the grafted regions. Protein adsorption did not affect surface wettability. Mouse fibroblast STO cells were cultured on tissue culture plates pattern-grafted with this thermoresponsive copolymer. Fibronectin adsorption enhanced cell spreading, whereas albumin reduced it. When the temperature was lowered, the cells detached selectively from the surface areas grafted with the thermoresponsive copolymer when cultured in serum-free medium; the cells only partially detached from these areas when cultured in serum-containing medium. The effects of serum proteins on cell detachment were similar to that caused by a mixture of albumin and fibronectin. Albumin adsorption did not affect the detachment of cells, whereas fibronectin adsorption inhibited it. These results indicate that a pattern-grafted, thermoresponsive, azidophenyl-derivatized copolymer can effectively facilitate selective cell detachment under conditions such as serum-free culture or following the adsorption of albumin. The pattern-grafting technique will be useful for qualitative microscopic comparison of surfaces prepared differently on single chips under the same conditions.

11.3.3   Other Polymers

A protein microarray, called a "cell chip," was constructed by using a photoreactive poly(acrylic acid) for a cell adhesion assay [63]. Various amounts of albumin or fibronectin were immobilized covalently onto a polystyrene dish using a microspotter with a dip pen. Poly(acrylic acid) carrying azidophenyl groups was synthesized as the photoreactive polymer. An aqueous solution of this polymer (several nanoliters) was cast using the dip pen of the microspotter and dried in air. Subsequently, aqueous solutions of proteins were cast on the same place using the microspotter. After drying, the dish was irradiated with UV light. Finally, the immobilization was confirmed by staining with a dye. The immobilization was stable even after washing with Tween-20 detergent. The protein-immobilized area depended on the manipulation of the microspotter and the size of the dip pen. Subsequently, cell adhesion on the photoimmobilized protein microarray was investigated. The adhesion behavior of cells depended on

the kind of immobilized proteins and the kind of cells. Such protein micro-arrays will be useful for cell diagnosis and for selecting biomaterials to regulate cell behavior.

Photoreactive polyallylamine containing β-galactose moieties in the side chain (LPAN3) was prepared by the reaction of polyallylamine with lacto-bionic acid and azidobenzoic acid [64]. To create micropatterned surfaces, a LPAN3-coated poly(methyl methacrylate) (PMMA) substrate was irradi-ated with a UV lamp under a photomask. The presence of a LPAN3 layer on the substrate was confirmed using ESCA. Micropatterned cell culture was carried out by seeding hepatocytes and/or fibroblasts on the substrate. They adhered only to the LPAN3 and PMMA lanes, respectively. Co-culture on the stripe-patterned substrate was carried out by first seeding hepatocytes and then by seeding fibroblasts. The co-cultured cells produced extracellular matrix molecules such as fibronectin, indicating normal biological activity.

Poly(acrylic acid), polyallylamine, gelatin, and poly(2-methacryloy-loxyethyl phosphorylcholine-co-methacrylic acid) (PMAc50) coupling with azidophenyl groups were photoimmobilized on conventional poly-styrene cell culture dishes [65]. Mouse ES cells were cultured on the immobilized polymer surfaces. Cell morphology, cell growth, staining for alkaline phosphatase, activation of the transcription factor stat3, and expression levels of the octamer-binding protein 3/4 transcription factor and the zinc finger-containing transcription factor were observed. ES cell morphology and growth rate were significantly affected by the polymer surface properties. The ES cells attached to both gelatin and polyallyl-amine surfaces; however, colonies formed on the former but not the latter. In addition, significant enhancement of ES cell growth was observed on the gelatin surface. In contrast, ES cells aggregated to form embryoid bod-ies on the photoimmobilized poly(acrylic acid) surface and the PMAc50 surface, although the cell growth rate was reduced. Significant enhance-ment of aggregation of ES cells onto the PMAc50 surface was observed in terms of morphology and gene expression analyses. Chondrogenic or adi-pogenetic differentiation of mesenchymal stem cells was also investigated on the micropatterned polyelectrolyte surfaces [66, 67].

11.4 Visible Light-Reactive Biopolymer Systems

Irradiation using visible light instead of UV light could bring many advan-tages for biomedical applications. Visible light irradiation has been used to crosslink some synthetic or natural polymers for biomedical purposes. For instance, Johnstone *et al.* [68] defined nontoxic conditions for photoen-capsulating human mesenchymal stem cells (hMSCs) in PEGDA scaffolds using a visible light photoinitiator system composed of eosin Y, trietha-nolamine, and 1-vinyl-2-pyrrolidinone. This produced hydrogel scaffolds

with an increased viability of encapsulated hMSCs and a more tightly crosslinked network in one-third the time taken for UV polymerization with 2-hydroxy-4′-(2-hydroxyethoxy)-2-methylpropiophenone. Younes *et al.* [69] reported a new family of photocrosslinked amorphous poly (diol-tricarballylate) biodegradable elastomeric polyesters. Liquid-to-solid photocuring was carried out by exposing the polymer to visible light in the presence of camphorquinone as a photoinitiator. These new elastomers can be considered as candidates for use in controlled implantable delivery systems of protein drugs and in other biomedical applications. Cui *et al.* [70] reported on the facile preparation of chemically crosslinked alginate microgels in mild conditions by using a reversed microemulsion technique. Sodium alginate was modified by partially grafting phenol groups to the backbone, on the basis of which microgels have been prepared by the irradiation of visible light in the presence of catalyst Ru(II) complex at room temperature. Visible light-induced dextran-methacrylate hydrogels were also prepared using a different photoinitiator and coinitiator to enlarge the applications of this material in the biomedical area (e.g., for eyes or other light-sensitive organs) [71, 72]. Moreover, crosslinking of DNA protein in solution by visible light in the presence of several sensitizers such as methylene blue has also been investigated [73, 74]. Recently, a new biocompatible strategy for photoinduced DNA interstrand crosslinking was reported. Methylene blue-induced $^1O_2$ formation triggers furan oxidation, and the resulting aldehyde then rapidly reacts with complementary adenine or cytosine with formation of stable adducts [75].

We have developed a new visible light-curable polymer system comprising a furan-incorporated biopolymer such as gelatin [76] or chitosan [77, 78] and the dye Rose Bengal with absorbance at a visible light wavelength. When the system is irradiated with visible light, the activated Rose Bengal oxidizes furan groups and the peroxidized furan is decomposed, forming a radical group that crosslinks biopolymers with each other, as shown in Figure 11.14. The reaction occurs in water. Considering that
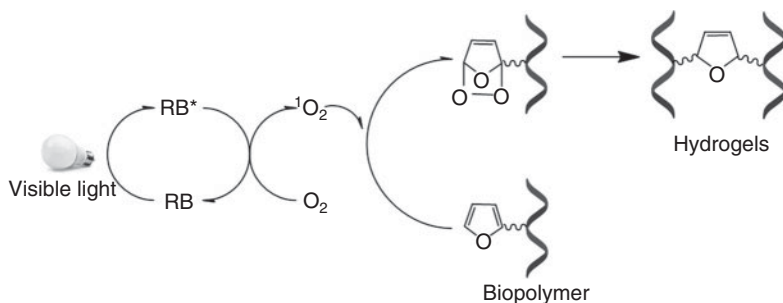
Figure 11.14 Visible light used in crosslinking biopolymer systems. RB indicates Rose Bengal.

visible light is less toxic to tissues than UV light, the system could be applicable directly for clinical therapy.

We have used this system to provide visible light-curable biosealants. The aqueous viscous solution of polymer derivative and dye mixture has been employed as a direct tooth-pulp-capping material in dentistry [76]. In addition, when the biosealant was used to cover a damaged region of skin in a mouse model, it significantly enhanced recovery [77, 78]. Considering these results, this system could be useful as a new type of visible light-induced crosslinked biosealant.

11.4.1   Gelatin

Furfuryl groups have been incorporated into gelatin using furfuryl isocyanate [76]. Subsequently, the modified gelatin was mixed with Rose Bengal in water and irradiated by visible light to form hydrogels. In addition, when the solution was cast on a plate, dried, and photoirradiated in the presence of a photomask, a micropattern was formed that matched that on the photomask. The gelatin-immobilized regions enhanced cell adhesion. It was also confirmed that gelatin incorporating furfuryl and Rose Bengal had no significant toxicity. This modified gelatin has been employed as a direct tooth-pulp-capping material in dentistry.

11.4.2   Chitosan

Chitosan employed for preparing UV-reactive chitosan was also utilized for preparing visible light-curable chitosan. Incorporation of furan groups was performed by furfuryl glycidyl ether or furfuryl isocyanate as shown in Figure 11.15. LMW-CS or LMC-O-CMCS was dissolved in water and pH was adjusted to 11 using NaOH solution at room temperature. Furfuryl glycidyl ether or furfuryl isocyanate dissolved in dimethylsulfoxide was added to the chitosan solution under ice and the solution was heated and stirred. After a suitable reaction time, the solution was neutralized and the modified chitosan was purified by dialysis.

Micropatterning using photomasking was performed to confirm the photoreactivity of a system composed of furfurylated chitosan and Rose Bengal. Micropatterning is useful to check the photoreactivity because it allows light-irradiated surfaces to be compared directly with those not irradiated. The micropattern clearly matched the photomask. This result showed that solidification occurred only on the visible light-irradiated area. The surface wettability of the solidified chitosan was investigated by contact angle measurement, confirming that solidification of chitosan derivatives by visible light irradiation produced a hydrophobic surface.

The furfurylated chitosan derivatives were water soluble, but after crosslinking they became water insoluble. The degree of crosslinking
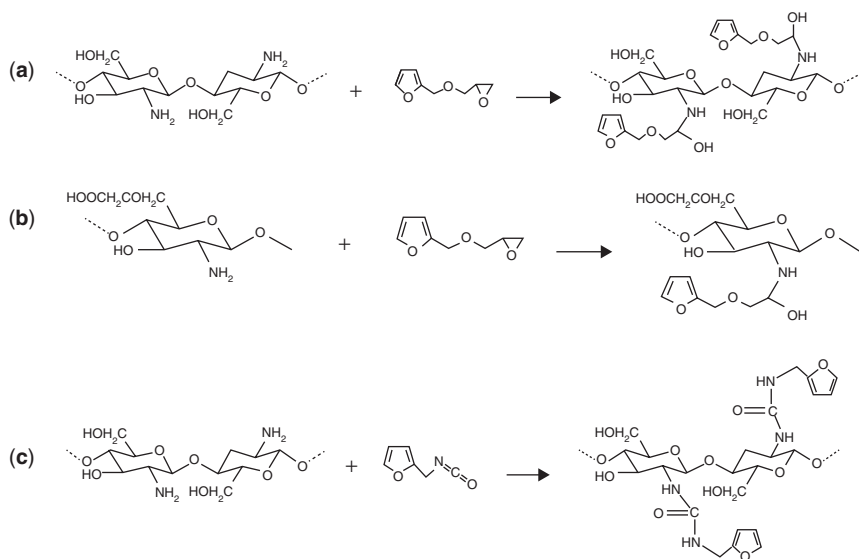
Figure 11.15 Preparation of a visible light-curable (a) furfurylated low molecular weight chitosan and (b) a furfurylated low molecular weight O-carboxymethyl chitosan derivative. (c) Preparation of low molecular weight chitosan introduced with a furfuryl isocyanate derivative.

also increased in proportion to the exposure time to visible light and with higher concentrations. It is important to determine how long the cross-linked gel film can be maintained. A solution of furfurylated chitosan and Rose Bengal was irradiated with visible light for 3 min and kept in phosphate-buffered saline at 37°C, and the crosslinking ratio was mea-sured every 24 h. After 5 days, the amount of remaining film decreased to 60%; it decreased continuously in volume over 1 week and completely dissolved after 2 weeks. Generally, wound healing requires 4–5 days, so the furfurylated chitosan and Rose Bengal system is considered suitable for preventing adhesions in wound treatment.

In vitro cell attachment and viability tests revealed that furfurylated chi-tosan derivatives had no effect on cell behavior, but the photocured mate-rials had a significant inhibitory effect on cell adhesion. These properties might play an important role when they are applied as an anti-adhesive agent or as a wound-dressing material. Because a hydrophobic surface was formed by solidification of furfurylated chitosan systems, interactions between the solidified gel and cells is reduced. An anti-adhesive agent is desirable to act as a kind of barrier for tissues subjected to surgery and helps keep them separate from neighboring tissues. The reduced interac-tion of the visible light-cured chitosan gel with cells is important to reduce side effects when it is used in such applications.

11.5 Conclusions

We have prepared several types of photoreactive biopolymers for surface modification, micropatterning, immobilization of various proteins, and microarray chips. Because photoimmobilization requires no specific functional groups, the technique is applicable for several biological and medical uses.

References

1. L.-H. Liu and M. Yan. Perfluorophenyl azides: New applications in surface functionalization and nanomaterial synthesis. *Acc. Chem. Res.* 43, 1434–1443 (2010).
2. T. Matsuda and T. Sugawara. Photochemical protein fixation on polymer surfaces via derivatized phenyl azido group. *Langmuir* 11, 2272–2276 (1995).
3. Y. Ito. Tissue engineering by immobilized growth factors. *Mater. Sci. Eng.* C6, 267–274 (1998).
4. Y. Ito. Regulation of cell functions by micropattern-immobilized biosignal molecules. *Nanotechnology* 9, 200–204 (1998).
5. Y. Ito, G. Chen and Y. Imanishi. Artificial juxtacrine stimulation for tissue engineering. *J. Biomater. Sci. Polym. Ed.* 9, 879–890 (1998).
6. Y. Ito. Surface micropatterning to regulate cell functions. *Biomaterials* 20, 2333–2342 (1999).
7. Y. Ito. Covalently immobilized biosignal molecule materials for tissue engineering. *Soft Matter* 4, 46–56 (2008).
8. Y. Ito. Growth factors on biomaterial surfaces, in *Biological Interactions on Materials Surfaces: Understanding and Controlling Protein, Cell and Tissue Responses*, D. Puleo and R. Bizios, Eds, pp. 173–197, Springer (2009).
9. B. Joddar and Y. Ito. Biological modifications of materials surfaces with proteins for regenerative medicine. *J. Mater. Chem.* 21, 13737–13755 (2011).
10. Y. Ito. Growth factors and protein modified surfaces and interfaces, in *Comprehensive Biomaterials Vol. 4, Surface Engineering*, P. Ducheyne, K.E. Healy, D.W. Hutmacher, D.W. Grainger, C.J. Kirkpatrick, Eds, pp. 247–279, Elsevier (2011).
11. T. Kitajima, S. Obuse, T. Adachi, M. Tomita and Y. Ito. Recombinant human gelatin substitute with photoreactive properties for cell culture and tissue engineering. *Biotechnol. Bioeng.* 108(10), 2468–2476 (2011).
12. Y. Ito, G. Chen and Y. Imanishi. Photoimmobilization of insulin onto polystyrene dishes for protein-free cell culture. *Biotechnol. Prog.* 12, 700–703 (1996).
13. Y. Ito, S. Kondo, G. Chen and Y. Imanishi. Patterned artificial juxtacrine stimulation of cells by covalently immobilized insulin. *FEBS Lett.* 403, 159–162 (1997).
14. G. Chen, Y. Ito and Y. Imanishi. Regulation of growth and adhesion of cultured cells by insulin conjugated with thermoresponsive polymers. *Biotechnol. Bioeng.* 53, 339–344 (1997).

15. Y. Ito, J.-S. Li, T. Takahashi, Y. Imanishi, Y. Okabayashi, Y. Kido and M. Kasuga. Enhancement of the mitogenic effect by artificial juxtacrine stimulation using immobilized EGF. *J. Biochem.* 121, 514–520 (1997).

16. G. Chen, Y. Ito and Y. Imanishi. Photo-immobilization of epidermal growth factor enhances its mitogenic effect by artificial juxtacrine signalling. *Biochim. Biophys. Acta.* 1358, 200–208 (1997).

17. Y. Ito, G. Chen and Y. Imanishi. Micropatterned immobilization of epidermal growth factor to regulate cell function. *Bioconj. Chem.* 9, 277–282 (1998).

18. G. Chen and Y. Ito. Gradient micropattern immobilization of EGF to investigate the effect of artificial juxtacrine stimulation. *Biomaterials* 22, 2453–2457 (2001).

19. G. Chen, Y. Ito, S. Masuda and R. Sasaki. Growth and secretion of erythropoietin of Chinese hamster ovary cells coexpressing epidermal growth factor receptor and erythropoietin genes: Design of cells for cell culture matrix. *Cytotechnology* 35, 3–8 (2001).

20. Y. Ito, G. Chen, Y. Imanishi, T. Morooka, E. Nishida, Y. Okabayashi and M. Kasuga. Differential control of cellular expression by diffusible and non-diffusible EGF. *J. Biochem.* 129, 733–737 (2001).

21. Y. Ito, Regulation of cellular gene expression by artificial materials immobilized with biosignal molecules. *Jpn. J. Artif. Organs* 27, 541–544 (1998).

22. Y. Ito, H. Hasuda, T. Yamauchi, N. Komatsu and K. Ikebuchi. Immobilization of erythropoietin to culture erythropoietin-dependent human leukemia cell line. *Biomaterials* 25, 2293–2298 (2004).

23. H. Makino, H. Hasuda and Y. Ito. Immobilization of leukemia inhibitory factor (LIF) to culture murine embryonic stem cells. *J. Biosci. Bioeng.* 98, 374–379 (2004).

24. Y. Ito, H. Hasuda, H. Terada and T. Kitajima. Culture of human umbilical vein endothelial cells on immobilized vascular endothelial growth factor. *J. Biomed. Mater. Res.* 74, 659–665 (2005).

25. K. Doi and T. Matsuda. Enhanced vascularization in a microporous polyurethane graft impregnated with basic fibroblast growth factor and heparin. *J. Biomed. Mater. Res.* 34, 361–370 (1997).

26. K. Doi, Y. Nakayama and T. Matsuda. Novel compliant and tissue-permeable microporous polyurethane vascular prosthesis fabricated using an excimer laser ablation technique. *J. Biomed. Mater. Res.* 31, 27–33 (1996).

27. D.J. Chung and T. Matsuda. Gelatin modification with photocuring thymine derivative and its application for hemostatic aid. *J. Ind. Eng. Chem.* 4, 340–344 (1998).

28. Y. Nakayama and T. Matsuda. Photocurable surgical tissue adhesive glues composed of photoreactive gelatin and poly(ethylene glycol) diacrylate. *J. Biomed. Mater. Res. Part A* 48, 511–521 (1999).

29. H. Mojgan, H. Hasuda, M. Sakuragi, Y. Yoshida, K. Suzuki and Y. Ito. Modification of the titan surface with photoreactive gelatin to regulate cell attachment. *J. Biomed. Mater. Res.* 83, 906–914 (2007).

30. Y.J. Weng, J.R. Ren, N. Huang, J. Wang, J.Y. Chen, Y.X. Leng and H.Q. Liu. Surface engineering of Ti–O films by photochemical immobilization of gelatin. *Mater. Sci. Eng. C* 28, 1495–1500 (2008).

31. S.-H. Park, S.-Y. Seo, J.-H. Kang, Y. Ito and T.-I. Son. Preparation of photocured azidophenyl-fish gelatin and its capturing of human epidermal growth factor on titanium plate. *J. Appl. Polym. Sci.*, in press (2012).

32. G. Chen, Y. Ito, Y. Imanishi, A. Magnani, S. Lamponi and R. Barbucci. Photoimmobilization of sulphated hyaluronic acid for antithrombogenicity. *Bioconj. Chem.* 8, 730–734 (1997).

33. B. Joddar, T. Kitajima and Y. Ito. The effects of covalently immobilized hyaluronic acid substrates on the adhesion, expansion and differentiation of embryonic stem cells for in vitro tissue engineering. *Biomaterials* 32, 8404–8415 (2011).

34. Y.S. Park and Y. Ito. Micropattern immobilization of heparin to regulate cell growth with fibroblast growth factor (FGF). *Cytotechnology* 33, 117–122 (2000).

35. Y. Ito, M. Hayashi and Y. Imanishi. Gradient micropattern immobilization of heparin and its interaction with cells. *J. Biochem. Sci., Polym. Ed.* 12, 367–378 (2001).

36. Y. Ito. Micropattern immobilization of polysaccharide. *J. Inorg. Biochem.* 79, 77–81 (2000).

37. H.-N. Na, K.-I. Kim, J.-H. Han, J.-G. Lee, D.-J. Han, Y. Ito, K.-S. Song, E.-C. Jang and T.-I. Son. Synthesis of O-carboxylated low molecular chitosan with azido phenyl group: Its application for adhesion prevention. *Macro. Res.* 18, 1001–1007 (2010).

38. K.-I. Kim, J.-W. Lee, J.-H. Kang, K.-S. Song, E.-C. Jang, Y. Ito and T.-I. Son. Preparation of photo-reactive azidophenyl chitosan derivative for immobilization of growth factors. *J. Appl. Polym. Sci.* 117, 3029–3037 (2010).

39. H. Hasuda, O.H. Kwon, I.-K. Kang and Y. Ito. Synthesis of photoreactive pullulan for surface modification. *Biomaterials* 26, 2401–2406 (2005).

40. T. Konno, H. Hasuda, K. Ishihara and Y. Ito. Photo-immobilization of a phospholipids polymer. *Biomaterials* 26, 1381–1388 (2005).

41. Y. Ito, T. Yamauchi, M. Uchikawa and Y. Ishikawa. Photoimmobilized array of panel cells for assay of antibodies. *Biomaterials* 27, 2502–2506 (2006).

42. M. Sakuragi, S. Tsuzuki, S. Obuse, A. Wada, K. Matoba, I. Kubo and Y. Ito. A photoimmobilizable sulfobetaine-based polymer for a nonbiofouling surface. *Mater. Sci. Eng. C* 30, 316–322 (2010).

43. T. Ishii, A. Wada, S. Tsuzuki, M. Casolaro and Y. Ito. A new nonbiofouling polyzwitterion including L-histidine. *Biomacromolecules* 8, 3340–3344 (2007).

44. M. Sakuragi, S. Tsuzuki, H. Hasuda, A. Wada, K. Matoba, I. Kubo and Y. Ito. Synthesis of a photoimmobilizable histidine polymer for surface modification. *J. Apply. Polym. Sci.* 112, 315–319 (2009).

45. Y. Ito, H. Hasuda, M. Sakuragi and S. Tsuzuki. Surface modification of plastic, glass and titanium by photoimmobilization of polyethylene glycol for antibiofouling. *Acta Biomater.* 3, 1024–1032 (2007).

46. K. Ohyama, K. Omura and Y. Ito. A photo-immobilized allergen microarray for screening of allergen-specific IgE. *Allerg. Int.* 54, 627–631 (2005).

47. Y. Ito. Photoimmobilization for microarrays. *Biotechnol. Prog.* 22(4), 924–932 (2006).

48. T. Matsudaira, S. Tsuzuki, A. Wada, A. Suwa, H. Kohsaka, M. Tomida and Y.Ito. Automated microfluidic assay system for autoantibodies found in autoimmune diseases using a photoimmobilized autoantigen microarray. *Biotechnol. Prog.* 24, 1384–1392 (2008).

49. S. Tsuzuki, A. Wada and Y. Ito. Photo-immobilization of biological components on gold-coated chips for measurements using surface plasmon resonance

(SPR) and a quartz crystal microbalance (QCM). *Biotechnol. Bioeng.* 102, 700–707 (2009).

50. Y. Ito, N. Moritsugu, T. Matsue, K. Mitsukoshi, H. Ayame, N. Ookouchi, H. Hattori, H. Tashiro, S. Sato and M. Ebisawa. An automated multiplex specific IgE assay system using a photoimmobilized microarray. *J. Biotechnol.* 161, 414–421 (2012).

51. Y. Ito, M. Nogawa, M. Takeda and T. Shibuya. Photo-reactive polyvinylalcohol for photo-immobilized microarray. *Biomaterials* 26, 211–216 (2005).

52. W. Song, N. Kawazoe and G. Chen. Dependence of spreading and differentiation of mesenchymal stem cells on micropatterned surface area. *J. Nanomater.* doi (10.1155/2011/265251) (2011).

53. W. Song, H. Lu, N. Kawazoe and G. Chen. Gradient patterning and differentiation of mesenchymal stem cells on micropatterned polymer surface. *J. Bioact. Comp. Polym*. 26, 242–256 (2011).

54. W. Song, H. Lu, N. Kawazoe and G. Chen. Adipogenic differentiation of individual mesenchymal stem cell on different geometric micropatterns. *Langmuir* 27, 6155–6162 (2011).

55. G. Chen, Y. Imanishi and Y. Ito. Photolithographic synthesis of hydrogels. *Macromolecules* 31, 4379–4381 (1998).

56. G. Chen, Y. Imanishi and Y. Ito. pH-sensitive thin hydrogel micro-fabricated by photolithography. Langmuir 14, 6610–6612 (1998).

57. Y. Ito. Photolithographic synthesis of intelligent microgels. *J. Intel. Mater. Sys. Struct*. 10, 541–547 (1999).

58. G. Chen, N. Kawazoe, Y. Fan, Y. Ito and T. Tateishi. Grid pattern of nanothick microgel network. *Langmuir* 23, 5864–5867 (2007).

59. Y. Ito, G. Chen, Y. Guan and Y. Imanishi. Patterned immobilization of thermoresponsive polymer. *Langmuir* 13, 2756–2759 (1997).

60. G. Chen, Y. Imanishi and Y. Ito. Effect of protein and cell behavior on pattern-grafted thermoresponsive polymer. *J. Biomed. Mater. Res.* 42, 38–44 (1998).

61. H. Liu and Y. Ito. Gradient-micropattern-immobilization of a thermo-responsive polymer to investigate its effect on cell behaviors. *J. Biomed. Mater. Res.* 67A, 1424–1429 (2003).

62. H. Liu and Y. Ito. Cell attachment and detachment on micropattern-immobilized poly(N-isopropylacrylamide) with gelatin. *Lab Chip* 2, 175–178 (2002).

63. Y. Ito and M. Nogawa. Preparation of a protein micro-array using a photo-reactive polymer for a cell adhesion assay. *Biomaterials* 24, 3021–3026 (2003).

64. I.K. Kang, G.J. Kim, O.H. Kwon and Y. Ito. Co-culture of hepatocytes and fibroblasts by micro-patterned immobilization of *β*-galactose derivatives. *Biomaterials* 25, 4225–4232 (2004).

65. T. Konno, N. Kawazoe, G. Chen and Y. Ito. Culture of mouse embryonic stem cells on photoimmobilized polymers. *J. Biosci. Bioeng.* 102, 304–310 (2006).

66. L. Guo, N. Kawazoe, Y. Fan, Y. Ito, J. Tanaka, T. Tateishi, X. Zhang and G. Chen. Chondrogenic differentiation of human mesenchymal stem cells on photoreactive polymer-modified surfaces. *Biomaterials* 29, 23–32 (2008).

67. N. Kawazoe, L. Guo, M. J. Wozniak, Y. Imaizumi, T. Tateishi, X. Zhang and G. Chen. Adipogenic differentiation of mesenchymal stem cells on micropatterned polyelectrolyte surfaces. *J. Nanosci. Nanotechnol.* 9, 230–239 (2009).

68. C.S. Bahney, T.J. Lujan, C.W. Hsu, M. Bottlang, J.L. West and B. Johnstone. Visible light photoinitiation of mesenchymal stem cell-laden bioresponsive hydrogels. *Eur. Cells Mater.* 22, 43–55 (2011).

69. M.A. Shaker, J.J.E. Dore and H.M. Younes. Synthesis, characterization and cytocompatibility of a poly(diol-tricarballylate) visible light photo-cross-linked biodegradable elastomer. *J. Biomat. Sci. Polym. Ed.* 21, 507–528 (2010).

70. Y. Yu and S.X. Cui. Facile preparation of chemically cross-linked microgels by irradiation of visible light at room temperature. *Langmuir* 25, 11272–11275 (2009).

71. S.H. Kim and C.C. Chu. Visible light induced dextran-methacrylate hydrogel formation using (–)-riboflavin vitamin B2 as a photoinitiator and L-arginine as a co-initiator. *Fiber Polym.* 10, 14–20 (2009).

72. E.A. Kamoun and H. Menzel. Crosslinking behavior of dextran modified with hydroxyethyl methacrylate upon irradiation with visible light-effect of concentration, coinitiator type and solvent. *J. Appl. Polym. Sci.* 117, 3128–3138 (2010).

73. R. Lalwani, S. Maiti and S. Mukherji. Visible-light induced DNA-protein cross-linking in DNA-histone complex and sarcoma-180 chromatin in the presence of methylene blue. *J. Photoch. Photobio. B* 7, 57–73 (1990).

74. A. Villanueva, M. Canete, C. Trigueros, L. Rodriguez-Borlado and A. Juarranz. Photodynamic induction of DNA-protein cross-linking in solution by several sensitizers and visible light. *Biopolymers* 33, 239–244 (1993).

75. M. Op de Beeck and A. Madder. Sequence specific DNA cross-linking triggered by visible light. *J. Am. Chem. Soc.* 134, 10737–10740 (2012).

76. T.I. Son, M. Sakuragi, S. Takahashi, S. Obuse, J. Kang, M. Fujishiro, H. Matsushita, J. Gong, S. Shimizu, Y. Tajima, Y. Yoshida, K. Suzuki, T. Yamamoto, M. Nakamura and Y. Ito. Visible light-induced cross-linkable gelatin. *Acta Biomat.* 10, 4005–4010 (2010).

77. S.H. Park, S.Y. Seo, H.N. Na, K.I. Kim, J.W. Lee, H.D. Woo, J.H. Lee, H.K. Seok, J.G. Lee, S.I. Chung, K.H. Chung, D.K. Han, Y. Ito, E.C. Jang and T.I. Son. Preparation of a visible light-reactive low molecular-O-carboxymethyl chitosan (LM-O-CMCS) derivative and applicability as an anti-adhesion agent. *Macromol. Res.* 19, 921–927 (2011).

78. S.Y. Seo, S.H. Park, H.J. Lee, H.N. Na, K.I. Kim, J.K. Lee, Y. Ito and T.I. Son. Visible light-induced photocurable (forming a film) low molecular weight chitosan derivatives for biomedical applications: Synthesis, characterization and *in vitro* biocompatibility. *J. Ind. Eng. Chem.* 18, 1258–1262 (2012).

The Emerging Applications of Graphene Oxide and Graphene in Tissue Engineering

Samad Ahadian[1], Murugan Ramalingam[1,2,3] and Ali Khademhosseini[1,4,5,*]

[1]WPI-Advanced Institute for Materials Research, Tohoku University, Sendai, Japan
[2]National Institute of Health and Medical Research U977, Faculty of Dental Surgery, University of Strasbourg, Strasbourg, France
[3]Centre for Stem Cell Research, A unit of Institute for Stem Cell Biology and Regenerative Medicine, Department of Biotechnology (Government of India), Christian Medical College Campus, Vellore, India
[4]Department of Medicine, Center for Biomedical Engineering, Brigham and Women's Hospital, Harvard Medical School, Cambridge, Massachusetts, USA; Harvard–MIT Division of Health Sciences and Technology, Massachusetts Institute of Technology, Cambridge, Massachusetts, USA; Wyss Institute for Biologically Inspired Engineering, Harvard University, Boston, Massachusetts, USA
[5]Department of Maxillofacial Biomedical Engineering and Institute of Oral Biology, School of Dentistry, Kyung Hee University, Seoul, Republic of Korea

Abstract

Scaffolds, growth factors, and cells are the key components of tissue engineering (TE) approaches to tissue repair and regeneration. Scaffolds can be prepared using biocompatible materials with the aim of mimicking the native extracellular matrix (ECM) to provide a suitable microenvironment for the cells to grow. Graphene oxide (GO) and graphene have recently gained much attention as promising TE scaffold materials due to their remarkable characteristics, such as high mechanical properties, unique surface chemistry, high conductivity, and biocompatibility. Physicochemical properties of these materials, including surface functionalization and topography, can be precisely controlled and therefore they can provide a well-designed milieu for various cell and TE applications. Furthermore, GO and graphene could serve as a candidate material to investigate various aspects of

*Corresponding author: alik@rics.bwh.harvard.edu

cell-material interactions. Keeping these points in mind, this chapter describes the design and fabrication of biomimetic GO and graphene materials, their potential applications in cell studies and TE applications, and the potential challenges and future directions for their use.

Keywords: Tissue engineering, stem cells, biomimetic materials, scaffolds, graphene oxide, graphene

12.1 Introduction

Tissue engineering aims to develop tissues *in vitro* that could be used to restore, maintain, or improve the tissue functions. Scaffolds, growth factors, and cells are the key components of tissue engineering that are used to fabricate tissues and organs *in vitro* [1]. Scaffolds aim to mimic and recreate the native ECM to allow the cells to grow *in vitro*. The ECM is composed protein networks that provide mechanical support and biological signals to the cells [2, 3]. Many different natural (e.g., collagen or fibrin) and synthetic (e.g., polycaprolactone (PCL) or polyglycolic acid) materials have been suggested as TE scaffolds, with the material selection depending on the tissue type. However, the creation of an ideal scaffold for a specific cell or tissue type is complicated and is still considered an important topic of research in TE. In particular, surface chemistry and physical structure of scaffolds need to be precisely designed and controlled because they play crucial roles for mediating various cellular behaviors, such as cell adhesion, proliferation, migration, and differentiation. Specific functional groups, such as hydroxyl, carboxyl, and amine groups, even at the molecular level, are important to regulate such behaviors [4]. Therefore, materials with tunable surface chemistry and topography are highly desirable in various cell and TE applications to elucidate and therefore control complex signaling pathways of various cellular behaviors [5–7]. With rapid development on the synthesis and functionalization methods of high quality graphene-based materials, they may be considered as novel and functional materials having great potential applications in cell therapy and TE. Other unique properties of this class of materials are high mechanical properties and conductivity that have made them attractive supplementary materials for the conventional TE scaffolds. Currently used scaffolds have generally low mechanical properties and electrical conductivity that restrict their use for a wide range of applications, in particular for muscle, cardiac, and neural TE. Even though increasing the mechanical properties of scaffolds can be obtained through changing the concentration, chemistry, and molecular weight of scaffolds, these approaches may interfere with the scaffold performance and functionality [8]. Therefore, it is interesting to greatly increase the mechanical properties of scaffolds by adding adequate amount of graphene derivatives while keeping beneficial properties of scaffolds. High conductivity of

graphene can also be used to effectively conduct the electrical current within the scaffold and therefore increase the efficiency of electrical manipulation techniques (e.g., electrical stimulation) of cell and tissue constructs. This property is in particular of great advantage for the electro-active cells, such as muscle [9, 10] and cardiac cells [11, 12], where the electrical stimulation has been used as a valuable tool to fabricate the corresponding engineered tissues. Interestingly, a recent study revealed that various cellular behaviors, such as cell adhesion, proliferation, and differentiation, are influenced by the passive conductivity of scaffolds [13].

Graphene is a thin (single-atom-thick) sheet of hexagonally-bonded carbon atoms forming a two-dimensional (2D) honeycomb lattice structure. Since its exfoliation from graphite in 2004 (see Figure 12.1) [14], graphene has attracted a great deal of attention in the scientific community due to its extraordinary electronic, thermal, mechanical, and optical properties [14–18]. Graphene and its derivatives are a relatively new class of materials for biomedical applications. The first breakthrough work in this area was reported by Liu *et al.*, who used GO (Figure 12.1) as an efficient drug delivery system [19]. Subsequently, an enormous amount of interesting research has been performed to explore the biomedical applications of these functional materials as aforementioned TE scaffolds, antimicrobials [20], drug/gene carriers [21], and biological sensors [22] and detectors [23].

GO and its reduced form have been prepared in freestanding sheets and shown that they have significant antibacterial property [24]. Akhavan *et al.* demonstrated the antibacterial effect of GO and reduced GO as deposited on stainless steel substrates [25]. They used Gram-negative *Escherichia coli* and Gram-positive *Staphylococcus aureus* as bacteria models. It was found that the reduced GO was more toxic to the bacteria than the GO likely due to higher charge transfer of the reduced GO compared to the GO while

Graphite   Oxidation   Graphene Oxide   Dispersion   Exfoliated GO   Reduction   Graphene
                                    (GO)
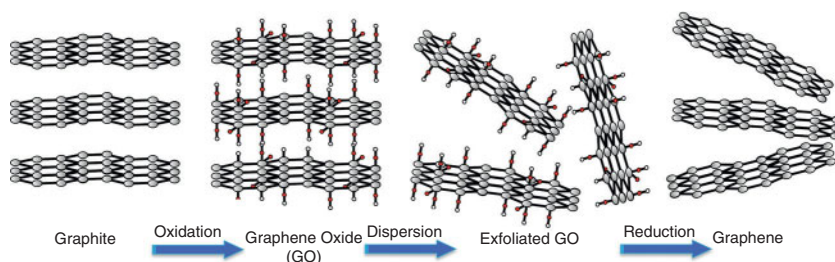
Figure 12.1 Procedure used to fabricate GO and graphene from natural graphite. Graphite is typically oxidized under a harsh acidic environment to obtain GO. GO with oxygen-containing functional groups is then exfoliated into single layers of GO in aqueous solution. GO can then be reduced to obtain graphene. Grey, red, and white circles represent carbon, oxygen, and hydrogen atoms, respectively.

they contacted with the bacteria. Liu *et al.* discovered fascinating antibacterial properties of various graphene derivatives (i.e., graphite, graphite oxide, GO, and reduced GO) toward *Escherichia coli* are regulated through the cell membrane, and oxidative stress similar to that for the carbon nanotubes [26]. Due to low cost and the ability to mass produce graphene-based materials, it is hoped that graphene-based antibacterial products will find wide clinical and environmental applications in the near future.

GO is considered an ideal nanocarrier for drugs/genes due to unique structural and physicochemical properties, such as planar and high surface area, oxygen-containing functional groups, solubility in the physiological conditions, biocompatibility, and capability of carrying drugs/genes through both physisorption and chemical approaches. In particular, -COOH and -OH functional groups of GO facilitate its conjugation with various targets ranging from biomolecules [27], nanoparticles [28], to quantum dots [29]. For instance, nanographene oxide has been demonstrated to efficiently deliver high amounts of gentamicin sulfate (i.e., 2.57 mg/mL) as an antibiotic and water insoluble drug into cells [30]. The drug was bound to the GO nanosheets through the hydrophobic interactions and π-π stacking between the GO and aromatic parts of the drug. This study revealed the potential applications of GO to deliver a whole class of aromatic and water insoluble drugs. The pH-responsive drug release has also been observed using GO sheets [31]. Pan *et al.* also created a thermo-responsive drug delivery system using poly(N-isopropylacrylamide) attached to the graphene sheets [32]. GO derivatives have also shown great promise in gene delivery and therapy [33]. Gene therapy needs a gene vector to avoid the nuclease degradation of DNA and to ensure high transfection efficiency of DNA by cells [34]. A major obstacle in developing the gene therapy approach is in finding safe and highly efficient gene vectors [35]. GO derivatives, such as polyethylenimine-modified GO [21] and chitosan-functionalized GO [36], have shown great potential for efficient gene delivery.

Graphene-based materials have been extensively employed for biosensing and detection [37, 38] mainly based on the following principles: (i) high yield in fluorescence quenching [39], (ii) unique electrical properties [40], (iii) ease of self-assembling with biomolecules [41], (iv) high surface area, and (v) capability to load various biomolecules through physical or chemical bindings [42]. For instance, graphene-based electrochemical devices have been largely used for biomarker detection. These devices rely on the ballistic electron transport properties of graphene that facilitate the electron transfer between the electrode and underlying sample and thus improve the electrochemical feedback. Lin *et al.* fabricated an electrochemical biosensor for ultra-highly sensitive detection of phosphorylated p53 using the GO as a carrier [43]. Application of nanomaterials for biosensing and detection *in vivo* has always been restricted because of their
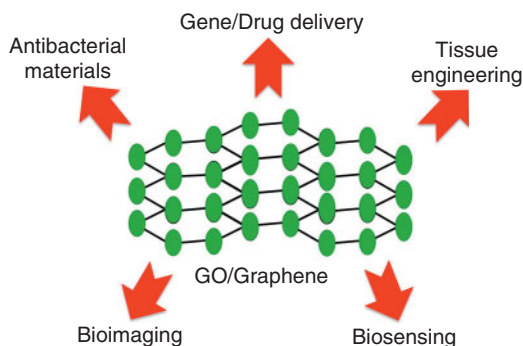
Figure 12.2 Widespread applications of graphene oxide (GO) and graphene in biomedical research. Green circles represent carbon atoms.

low stability and solubility in physiological conditions [44]. However, GO is an exceptional water soluble material with ionizable edges and exhibits high stability in physiological conditions. For example, GO nanosheets with ~100 nm size distribution have been proven to be stable in mammalian cells and mice [45]. Therefore, GO is a robust candidate for biosensing and detection in living systems.

Taken together, it is hoped that graphene and its derivatives provide new horizons for diverse biomedical applications (Figure 12.2) due to their remarkable properties as follows. Graphene features a high surface area (2630 m^2/g), thermal conductivity (~5000 W/m/K), electrical conductivity measured by charge mobility (200,000 cm^2 V^{-1} s^{-1}), and mechanical strength (Young's modulus ~1100 GPa); and GO has the advantages of facile production, low price, and ease of chemical or biological functionalization [33, 38, 46]. Note that economically feasible approaches are now available for the mass production of graphene and its derivatives [47]. These advantages have led to an increase in the investigation and application of these materials.

In this chapter, we will focus on the design strategies and current state of the art of GO and graphene as a new class of biocompatible scaffolds for use in cell and TE applications. Major challenges in this area and future potential routes for the research and development of GO and graphene in TE are also discussed.

12.2 Design and Fabrication of Biomimetic GO/Graphene Materials

Researchers have always taken inspiration from nature for the design of new materials and systems for various biomedical applications.

Biomimetic materials are synthetic biomedical materials, systems, or devices that are designed and engineered based on knowledge gained from biological systems or by mimicking their structure and function. Biomimetic materials can be simpler and can exhibit enhanced performance over conventional materials. Over the previous decades, there has been a great deal of effort to fabricate biomimetic multiscale structures to achieve multifunctional integration within a single material. Within this concept, GO, graphene and their functionalized forms have been used to mimic various natural structures, such as butterfly wings [48], rose petals [49], honeycomb [50], and nacre [51]. Although biomimetic graphene-based materials are of great interest in various biomedical applications, it is rather difficult to design and fabricate these materials. Unlike polymeric materials, which can be shaped into any desired form using conventional fabrication techniques, such as lithography, imprinting or other chemical routes, constructing hierarchical structures using graphene-based sheets is not a straightforward task. Here, irregular stacking and the surface manipulation of graphene sheets are useful approaches to construct various biomimetic micro- and nanostructures. The laser manipulation of GO or graphene films is commonly used to prepare such structures. This technique has several advantages, including its speed, cleanliness, and high efficiency [52]. More importantly, the oxygen content of surfaces as measured by the composition and density of oxygen-containing groups can be easily adjusted by tuning the laser intensity [52]. The biomimetic graphene materials fabricated by this technique are promising scaffolds for TE applications [48]. Yin *et al.* suggested another strategy to fabricate biomimetic graphene-based structures [50]. These authors were inspired by the natural honeycomb and developed a self-assembly method to construct honeycomb-mimetic graphene structures. This fabrication strategy was based on the *breath figure* method, in which the GO is homogenously dispersed in an organic solvent using cationic surfactants. The solution was then cast onto a glass substrate under highly humid airflow (~ 85% humidity). An organized honeycomb appeared following complete evaporation of both water and organic solvents. The humidity is a critical factor controlling the production of honeycomb structures, with a humidity greater than 30% required to form a honeycomb-like structure. These biomimetic structures may provide greater functionality and performance compared to conventional graphene materials.

12.3   Graphene Oxide and its Cell and TE Applications

GO is an intermediate material in the chemical synthesis of graphene, consisting of oxygen-containing chemical groups, such as carboxyls,

epoxides, carbonyls, and hydroxyls, enhancing the solubility compared to neat graphene (Figure 12.1). GO has been used as a supplementary material, acting as a doping agent to enhance the properties of commonly used biomaterials. For instance, adding 1 wt% GO to poly(vinyl alcohol) (PVA) significantly increased the mechanical and thermal properties of pristine PVA due to the high aspect ratio and rigid structure of GO and the strong interaction between GO and PVA [53]. PVA has been deemed a promising biomaterial for TE applications; however, its poor mechanical properties and low water retention have limited its applications. Novel PVA/GO composites have been shown to overcome these obstacles. Following this research direction, Qi *et al.* fabricated and characterized nanofibrous PVA/GO scaffolds [54]. They used the electrospinning method to fabricate the PVA/GO composites. Mouse osteoblasts (MC3T3-E1) were shown to attach to and proliferate on the scaffolds. Electrospinning is a facile, versatile, and inexpensive micro- and nanofabrication technique used in various TE applications in which a melted material is ejected from the tip of an electrically charged syringe called a spinneret and then collected onto a counter electrode, resulting in the formation of micro- and nanofibers of that material. Electrospun fibrous scaffolds can provide a range of mechanical properties that are beneficial for TE applications, such as a high surface-to-volume ratio and high porosity [55]. PVA/GO composites were also achieved using a freeze/thaw method [56]. Adding 0.8 wt% GO to PVA hydrogels led to a significant increase in the mechanical strength of PVA hydrogels compared to the pristine PVA hydrogels. In particular, the tensile and compressive strengths increased by up to 132% and 36%, respectively. Moreover, the PVA/GO composites exhibited good biocompatibility by exposure to osteoblasts. Recently, Li *et al.* fabricated biomimetic nacre-like PVA/GO composite films [57]. Natural nacre has a high toughness despite the fact that it contains brittle and inorganic $CaCO_3$ and soft biopolymers, likely due to the layered arrangement of $CaCO_3$ and soft biopolymers. Li *et al.* [57] aimed to recreate this structure using PVA and GO as components through a solution-casting procedure and post-reduction method. These composites showed remarkable electrical and mechanical properties. The biocompatibility of these materials was also evaluated using human umbilical vein endothelial cells, and no cytotoxicity was observed. The authors recommended the application of this biomimetic material as a TE scaffold, biosensor, and drug delivery vehicle. Yoon *et al.* added GO to poly(D,L-lactic-*co*-glycolic acid) (PLGA), enhancing its thermomechanical properties, such as crystallization temperature and tensile modulus, due to the strong chemical bonding between GO and PLGA [58]. The mechanical properties of alginate fibers can be improved by adding GO [59]. Alginate is a natural polysaccharide material derived from seaweed. Despite widespread biomedical applications of this material, in particular for wound healing, it has low mechanical properties.

Therefore, extensive research has been conducted to improve the mechanical properties of this material. According to He *et al*., adding 4 wt% GO to alginate increased its Young's modulus and maximum tensile strength from 1.9 and 0.32 to 4.3 and 0.62 GPa, respectively, owing to the uniform dispersion of GO within the alginate matrix [59]. The latter composite was obtained using the wet spinning approach and was water soluble and nontoxic to cartilage cells. Another study demonstrated that GO was able to chemically react with the chitosan scaffold [60]. This reaction occurred between the carboxyl groups of GO and the amine groups of chitosan. GO enhanced the biocompatibility and degradation of chitosan scaffolds. Highly porous and interconnected GO/chitosan scaffolds facilitated the adhesion of osteoblast cells and their proliferation within the scaffolds. In addition, the negatively charged carboxyl groups of the GO component were recognized as important for effective cell-scaffold interactions. Chitosan as extracted from the natural chitin is a useful biomaterial to repair chondral and osseous problems. However, a requirement must be met to improve the biological response and mechanical properties of this material for bone TE [61]. The latter study was a successful trial of GO to fulfill this requirement. Wan and Chen [62] reported the successful synthesis of PCL/GO composites, showing that adding 0.3 wt% GO improved the modulus, tensile strength, and energy at breakage of the PCLs by 66%, 95%, and 416%, respectively. In addition, the bioactivity of PCLs during biomineralization was increased due to the presence of GO. Mechanical improvements in PCL/GO composites compared to pristine PCLs were attributed to changes in the morphology of the fibers and the reinforcement of PCL due to the GO component, while the improvement in bioactivity was due to the anionic functional groups of GO, which largely enhanced the nucleation process and therefore the biomineral formation of the composites. The high porosity of the PCL/GO composites (> 94%) is a significant advantage for biomedical applications. While PCL has been approved by the US Food and Drug Administration (FDA) as a biodegradable polymer for particular medical applications (e.g., drug delivery device and suture), its poor mechanical properties have limited its application to hard TE. Researchers hope that PCL/GO biocomposites will find novel applications as tissue scaffolds and biomedical devices, particularly in orthopedics. Taken together, GO demonstrated great influence on the currently used scaffolds to improve their properties, such as cellular responses and mechanical properties. Note that graphene-based materials (e.g., GO and graphene) as the supplementary components for the scaffolds are superior to their CNTs counterparts in terms of cytotoxicity effects. The main reason could be metal catalysts used in the fabrication procedure of CNTs, which can remain inside the nanotubes. Those metals have potential negative effects on the cell survival and growth [63].

GO substrate itself has been shown to exert a significant influence on various cell behaviors, such as cell adhesion, proliferation, and differentiation, likely due to its aromatic structure, which can adsorb natural ECM components, such as fibronectin, laminin, and collagen, through noncovalent interactions [4]. According to our recent study, the degree of reduction of GO appears to be a crucial parameter controlling the production of biocompatible and functional GO films [64]. Here, GO films were thermally reduced at different reduction times. Glass slide substrate was also used as the control sample. Results revealed that moderately reduced GO films for 90 min had the best biological performance as measured by the cell adhesion, proliferation, and differentiation of various cell types, i.e., fibroblast, osteoblast, and muscle myoblast cells [64]. The latter substrate had the highest amount of protein adsorption among films. Another study revealed that osteoblasts showed favorable attachment, viability, and growth on hybrid silicone-GO substrates compared to the neat silicone substrates [65]. The latter effects were attributed to the physico-chemical properties (i.e., hydrophilicity and topography) of the composite substrates due to the presence of the GO component [65].

12.4   Graphene and Its Cell and TE Applications

An early study showed that sheet-like graphene is a biocompatible material as assessed using mouse fibroblast cells (L-929) [66]. Interestingly, the cell proliferation rate for the graphene sheet and the conventional tissue culture dish was almost similar. Biocompatibility is an essential prerequisite for a material to be considered for biomedical applications. Here, graphene solution was prepared so as to reduce the GO with hydrazine. The sheet-like graphene was then fabricated by the filtration of graphene solution through a membrane, followed by air drying and removal from the filter. Recently, Ryoo *et al.* showed that NIH-3T3 fibroblasts could adhere, spread, and grow well on graphene substrates, as demonstrated by the cell proliferation assay, focal adhesion assessment, cell shape analysis, and gene expression analysis of cell adhesion-related genes (i.e., integrin, collagen types I and III, *a*-actin, and focal adhesion kinase) [67]. Interestingly, the gene transfection efficiency of the fibroblast cells grown on the graphene substrates increased to 250% of that of the cells cultured on the conventional cover glasses. Therefore, the graphene substrates can be used for an efficient gene transfection of cells while the cell density is limited. The graphene substrates promoted the neural growth and neurite sprouting of mouse hippocampal cells to a greater degree than the conventional tissue culture polystyrene substrates [68]. Neurites are defined as any projections from the neuron cell body, such as axons or dendrites. Graphene-cell interactions were studied using Western blot analysis,

GAP-43 gene expression, and morphological characterization. GAP-43 is a specific cytoplasmic protein for the neural tissues and is involved in the neurite generation and growth [69]. This protein was significantly up-regulated on the graphene substrates compared to the conventional tissue culture polystyrene substrates. The complex interactions among various stimuli (i.e., mechanical, electrical, and chemical cues) imposed by the graphene substrates made it difficult to determine the origins of the effects of graphene on neural cells. However, the small difference between the average roughness values of the underlying substrates (i.e., graphene and conventional tissue culture substrates) indicated that the effects of graphene are not due to differences in surface roughness. Some graphene composites, such as graphene-heparin/poly-L-lysine, were also used as conductive and biocompatible scaffolds for neural TE. The latter scaffold was fabricated in 2D and 3D structures using layer-by-layer deposition and electrospinning techniques, respectively [70]. Both 2D and 3D scaffolds with tunable conductivity and surface chemistry supported the cellular adhesion and neurite sprouting. Post thermal annealing and hydrodynamic flow procedures were used to obtain uniform coverage area of graphene-heparin/poly-L-lysine on the substrates, and therefore a controlled electrical resistance of scaffolds was obtained. Note that the scaffold capability to transmit applied electrical stimuli is important in the neural TE. A hydrothermal approach was employed to fabricate 3D graphene hydrogels as suitable scaffolds for TE applications [71]. GO was initially used as a building block for the scaffolds, and the lateral size and concentration of GO sheets had significant effects on the hydrogel structure. Reduction of GO through hydrothermal treatment at 180°C for 24 h yielded porous and interconnected graphene hydrogels. MG63 cells were able to proliferate within these scaffolds. Note that biological cells experience a 3D environment *in vivo*. Therefore, there has been a great interest in fabricating 3D scaffold structures resembling the 3D ECM for the cells *in vivo* [72, 73]. Fabrication of 3D scaffolds, consisting of graphene or its derivatives, has been mainly achieved using the aforementioned hydrothermal reduction, filtration, and supramolecular interactions [74]. Ruoff *et al.* recently demonstrated that paper-like GO structures can be formed through the vacuum filtration of dispersed GO sheets [75, 76]. Fabricated GO papers exhibited a superior strength and stiffness and a unique structure where GO sheets were tiled together approximately in a parallel fashion. Reduced GO was also fabricated by the same procedure [66]. Biocompatibility of later structures was confirmed as they were exposed to fibroblast cells. Supramolecular interactions in GO can be controlled to transform them into 3D hydrogels. Here, various gelators, such as metal ions, polymers, and acid, can be used [77]. Since GO consists of various oxygen-contained functional groups, depending on which type of gelator is used, the bonding force of GO is increased or decreased. For example,

acid weakens the electrostatic repulsion force between GO sheets while polymers add hydrogen-bonding sites on the GO sheets and consequently increase the electrostatic interactions between the GO sheets [74].

Stem cells are able to self-renew and differentiate into various cell types. Therefore, they have been extensively used in regenerative medicine to engineer tissues and organs [78]. Both synthetic and natural materials have been employed to transplant stem cells and to differentiate them into specific cell lineages, such as bone, muscle, and neural cells. Physical and chemical properties of used materials are crucial parameters for directing the stem cell fate [79, 80]. Stem cells can be categorized into three main types, consisting of: (i) adult stem cells that can be differentiated into specific cell types, (ii) embryonic stem cells derived from the inner mass of blastocystes, and (iii) induced pluripotent stem cells (iPSCs), a novel stem cell type derived from somatic differentiated cells [81]. Graphene-based materials have shown great promise to direct the fate of stem cells and to elucidate the biological phenomena underlying these pathways. The reason may be the simple physical structure and well-characterized chemical composition of graphene and its derivatives, which allow precise evaluation of stem cells on these substrates. For instance, graphene has been shown to accelerate stem cell differentiation pathways, such as the differentiation of human mesenchymal stem cells (MSCs) along the osteogenic lineage, likely due to the mechanical properties and surface morphology of graphene [82]. Interestingly, graphene-induced differentiation was as effective as growth factor-induced differentiation, the common approach used for stem cells [82]. Note that MSCs derived from the adult bone marrow are able to differentiate into various cell lineages, such as osteoblasts, chondrocytes, and adipocytes. The mechanical properties and topography of scaffolds and some growth factors can induce MSC differentiation toward a specific cell line for biomedical applications. Successful MSCs proliferation and rapid differentiation on the graphene substrates without using specific growth factors hold great promise for bone regeneration therapy using these cells because this approach tackles one of the major challenges in this field, that is the use and precise administration of several growth factors. The latter method has been shown to fail when it comes to the compatibility with implants, cost, and scalability [82]. Lee et al. investigated the origin of favorable MSC growth and differentiation on both GO and graphene substrates [83]. The results showed that MSC differentiation to adipocytes on graphene substrates was largely influenced by the high π-π adsorption and stacking of insulin on these substrates. Insulin is a crucial factor for fatty acid synthesis and was denatured upon adsorption on graphene, while GO interacted with insulin through weak electrostatic bonding and therefore did not significantly interfere with the performance of insulin. Human neural stem cells were also observed to differentiate at a higher rate on graphene substrates than on glass slides
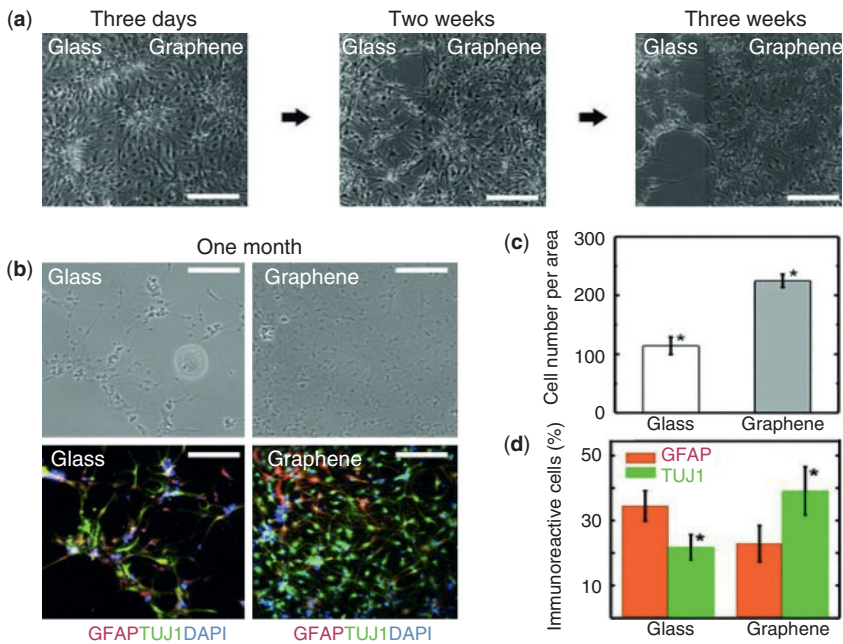
Figure 12.3 Enhanced differentiation of human neural stem cells (hNSCs) on graphene substrates compared to the glass slide (control) substrates. (a) Phase-contrast images of differentiated hNSCs on both graphene and glass slides after three days, two weeks, and three weeks of differentiation. The cells on the glass slide gradually detached from the substrate. (b) Phase-contrast (top row) and fluorescence (bottom row) images of differentiated hNSCs on the graphene and glass substrates after one month of differentiation. Differentiated hNSCs were stained with DAPI (blue), GFAP (red), and TUJ1 (green) to reveal cell nuclei, astroglial cells, and neural cells, respectively. (c) Cell number per area on graphene and glass substrates after one month of differentiation indicating more cells on the graphene than on the glass slide ($p < 0.001$). (d) Immunoreactive glia and neurons stained by GFAP (red) and TUJ1 (green), respectively, on graphene and glass substrates. Note that more glia cells were observed on the glass slides compared to graphene substrates, while more neuron cells were present on the graphene than on the glass substrate ($p < 0.05$). All scale bars are 200 μm. Reproduced with permission from [38].

(Figure 12.3). In addition, stem cells on the graphene substrates differentiated into more neuron cells and less glia cells compared to those on the glass slides. These phenomena were attributed to the strong cell adhesion to graphene, which led to the retention of more cells on graphene than on the glass slide over long culture times [84]. Successful use of human neural stem cells for the neuron generation and brain repair strongly depends on higher differentiation of these cells toward neurons rather

than glia cells. Neural activity of differentiated cells was also recorded through the electrical stimulation of the cells using the graphene as the electrode. Functionalized graphenes have also demonstrated an excellent potential to direct the stem cell fate. For example, fluorinated graphene enhanced the cell attachment, growth, and differentiation of MSCs into neuronal cells through spontaneous cell polarization. This effect was more profound in the presence of neuron-inductive agents (i.e., retinoic acid) [4]. A rapid method based on inkjet printing was also developed to align the MSCs on the graphene substrates. Such cellular alignment promoted the neurogenesis even in the absence of growth factors for the differentiation. Fluorinated graphene was likely used because the presence of fluorine groups in pharmaceuticals improves their metabolic stability and interactions with proteins due to its small size and high electronegativity. Therefore, fluorine is included in approximately 20% of all drugs, such as Prozac, Lexapro, and Lipitor [85]. Graphene was also used to culture and differentiate *i*PSCs [86]. *i*PSCs were first introduced by the Yamanaka group in 2006 [87], and their great promise for regenerative medicine was recognized by the 2012 Nobel Prize in Medicine awarded to Professors Gurdon and Yamanaka. They can be derived from the somatic cells using a cocktail of genes that reprogram the somatic cells into *i*PSCs. This procedure does not require the destruction of embryos and therefore avoids the ethical problems related to embryo destruction. Chen *et al.* [86] demonstrated that mouse *i*PSCs can adhere to and proliferate on GO more rapidly than on graphene and glass slides, most likely due to the oxygen-containing functional groups of the GO, which facilitate cellular adhesion and growth. Graphene was able to maintain *i*PSCs in an undifferentiated state, while GO accelerated *i*PSC differentiation. Finally, both substrates led to *i*PSC differentiation towards the ectodermal and mesodermal lineages. The differences in stem cell behavior on GO and graphene substrates are mainly attributed to the differences in surface chemistry between these two materials. To keep the pluripotency of *i*PSC, they should be cultured on feeder cells, such as mouse embryonic fibroblasts, with suitable soluble factors, such as the leukemia inhibitory factors [88]. Without such supporting materials, *i*PSC are spontaneously differentiated into embryoid bodies followed by the development of various cell types. It is of great interest to control the pluripotency of *i*PSC in the cell therapy and tissue regeneration using simple, cheap, and reproducible procedures and materials, such as graphene substrates. Taken together, GO and graphene are promising materials for studying stem cells and controlling their fate, and represent a facile and inexpensive avenue for stem cell research, as large-scale and high-quality graphene sheets can be fabricated at a low cost [89].

   Although graphene possesses a high electrical conductivity, little work has been conducted to exploit this unique property for TE applications. As an example, Park *et al.* used a graphene substrate as the stimulating

electrode for neural stem cells [84]. They showed that the cells were more electrophysiologically active upon electrical stimulation through the graphene electrodes compared to non-stimulated samples. Another interesting study was performed by Heo *et al.*, who examined the cell-cell interactions by applying a contact-free electrical field stimulation through graphene/ polyethylene terephthalate electrodes [90]. The authors used human neural cells as a model and found that the application of an electric field with this novel stimulator led to an effective cell-cell interaction. As indicated by the authors, the high electrical conductivity of graphene made the electrodes highly sensitive to small changes during the application of the biphasic electrical signals. Therefore, a weak electric field (4.5 mV/mm voltage and 10 s duration over a 32 min period) was sufficient to obtain effective cell-cell communication without damaging the cell membrane. This finding is of great importance for the fabrication of high performance stimulator devices using graphene, which would not be harmful for the human nervous system, consisting of fine and sensitive neural networks. Various cell behaviors, such as cell migration, proliferation, differentiation, and apoptosis can also be regulated by applying electrical fields [91]. Therefore, many research opportunities exist to evaluate cell and tissue responses to direct and alternative electric fields applied through graphene electrodes. Other advantages of these electrodes include their exceptional optical transparency and biocompatibility. In addition, the electronic properties of graphene nanosheets can be precisely controlled [92]. Therefore, they can be adjusted for various cellular interfacing, stimulation regimes, and monitoring applications in both *in vitro* and *in vivo* conditions.

Graphene has also been used as a supplementary material for commonly used biomaterials to enhance their properties. For example, covalently bonded PCL and graphene composites were synthesized and proposed as biocompatible materials for TE applications [93]. The PCL/ graphene composites exhibited better homogeneity compared to the pristine PCL materials. As a result, the tensile strength, Young's modulus, and, more importantly, electrical conductivity of the composites were substantially improved compared to the neat PCLs.

12.5   Conclusions and Future Directions

This chapter has discussed the impact of GO and graphene as a new class of biomimetic materials and their recent cell and TE applications. In addition, it discussed the use of graphene-based materials as biocompatible materials for the adhesion, proliferation, and differentiation of various cell types, such as neurons, osteoblasts, and stem cells. In general, as shown in Table 12.1, these functional materials have been employed in three main categories, namely, as biocompatible cell culture substrates, in stem cell biology and engineering, and in the fabrication of high-performance

Table 12.1 Properties of graphene oxide (GO) and graphene and their current applications in tissue engineering.

Material(s)	Properties	Application(s)	References
GO	Biocompatible, high mechanical (modulus) and electrical properties. Ease of functionalization with various chemical groups	Biocompatible and chemically tunable cell culture substrates/ Elucidation of stem cell biology and fate	[68, 83]
GO/ Graphene	High mechanical properties	Supplementary component for tissue scaffolds	[58, 59]
Graphene	High electrical conductivity	Enhancement of tissue scaffold conductivity	[51, 93]

scaffold composites. The rapid increase in publications on the various biomedical applications of these materials indicates that these materials hold great promise in the near future. While some interesting studies have been performed on various biomedical applications of GO and graphene, particularly in TE, this area of research is still in its infancy. In particular, cell studies on graphene and its derivatives have yet to focus on 2D environment that is far from 3D and physiological conditions. Therefore, rigorous investigations are needed on 3D tissue regeneration using these materials. Such engineered tissue structures could also provide valuable platforms for the drug screening and discovery applications [94].

Obstacles remain before these materials can be widely applied and particularly before they can be clinically applied in TE products. Note that the potential advantages of GO and graphene in molecular imaging [95] could be used to develop noninvasive and real-time imaging and monitoring techniques to trace biomolecules, such as drugs, cells, and engineered tissues, *in vivo*. Therefore, enormous demand exists for *in vivo* applications of graphene derivatives provided that these materials are approved for clinical applications. Important issues for further research include the mechanisms of cellular uptake, cytotoxicity, and the intracellular metabolic effects of GO and graphene, and these issues should be addressed both *in vitro* and *in vivo*. Of particular note is long-term toxicity and non-biodegradability of these materials, which deserve to be critically

investigated. The chemical synthesis, functionalization, and even physical processing of GO and graphene also need to be precisely controlled to obtain functional materials whose size, size distribution, physical morphology, and chemical properties are accurate. The latter parameters have been shown to exert a significant influence on the cytotoxicity and interactions of GO and graphene with living systems. As an example, Akhavan *et al.* recently reported that graphene nanosheets displayed a size-dependent cytotoxicity and genotoxicity upon exposure to human MSCs. These authors synthesized reduced GOs and graphenes with different lateral dimensions ranging from ~11 nm to ~3.8 μm through the reduction of polyethylene glycol-functionalized GO with hydrazine and bovine serum albumin, and observed a direct relationship between the lateral dimension of reduced GO and its cyto- and genotoxicity [96]. *In vitro* toxicity of graphene-based materials is largely related to damage in the cell membrane and oxidative stress. Note that precise control of the GO and graphene patches to obtain well-defined sizes of graphene sheets with specific functional groups is still a major challenge. Such an achievement would definitely help to fabricate more functional graphene-based materials for cell therapy and TE, drug/gene delivery, and biosensing applications.

Micro- and nanofabrication methods provide invaluable tools to create a desired and well-defined microenvironment that presents various substrate characteristics (e.g., topography or roughness) to the cells and enables the study of various cell behaviors [97]. As an example, Wang *et al.* reported the use of inkjet printing technology to create microscale lines of polydimethylsiloxane (PDMS) on fluorinated graphene to obtain aligned MSCs [4]. Here, substrates that controlled the alignment of MSCs increased the differentiation efficiency of the cells toward neuronal cells compared to those with randomly distributed cells. The use of GO and graphene with microfluidic [98] and electrospinning [99] technologies could further reveal the potential advantages of these materials to fabricate 3D and hierarchically organized scaffolds. Note that structurally organized scaffolds play a crucial role in providing suitable cues for the cells to organize themselves at the microscale. Microorganization of cells in 3D is essential to obtain organized and functional tissue constructs mimicking the corresponding tissues *in vivo*. Taken together, further combinations of micro- and nanotechnologies with graphene-based materials may provide an opportunity to create more functional materials for TE applications.

Finally, graphene-based materials can be engineered to obtain biomimetic structures referred to as *biomimetic graphene structures.* For example, graphene-based materials have already been used to mimic butterfly wings [48], rose petals [49], honeycomb [50], and nacre [51]. These structures are of great interest for both fundamental and applied research [52]. The concept of *biomimetic graphene* appears to be based on the following Leonardo da Vinci quotation: "Where nature finishes producing its own

species, man begins, using natural things and with the help of this nature, to create an infinity of species [100]." The ability to fabricate biomimetic graphene structures and the exploration of the potential biomedical applications of these structures, particularly in TE, could lead to the development of novel multifunctional materials and eventually devices with remarkable performance.

Acknowledgement

References

1. R. Langer and J.P. Vacanti, *Science*, Vol. 260, p. 920, 1993.
2. D.E. Discher, P. Janmey, and Y. Wang, *Science*, Vol. 310, p. 1139, 2005.
3. A.J. Engler, S. Sen, H.L. Sweeney, and D.E. Discher, *Cell*, Vol. 126, p. 677, 2006.
4. Y. Wang, W.C. Lee, K.K. Manga, P.K. Ang, J. Lu, Y.P. Liu, C.T. Lim, and K.P. Loh, *Advanced Materials*, Vol. 24, p. 4285, 2012.
5. O.Z. Fisher, A. Khademhosseini, R. Langer, and N.A. Peppas, *Accounts of Chemical Research*, Vol. 43, p. 419, 2009.
6. C. Cha, W.B. Liechty, A. Khademhosseini, and N.A. Peppas, *ACS Nano*, Vol. 6, p. 9353, 2012.
7. I. Wheeldon, A. Farhadi, A.G. Bick, E. Jabbari, and A. Khademhosseini, *Nanotechnology*, Vol. 22, p. 212001, 2011.
8. S.R. Shin, H. Bae, J.M. Cha, J.Y. Mun, Y.-C. Chen, H. Tekin, H. Shin, S. Farshchi, M.R. Dokmeci, S. Tang, and A. Khademhosseini, *ACS Nano*, Vol. 6, p. 362, 2011.
9. S. Ahadian, J. Ramón-Azcón, S. Ostrovidov, G. Camci-Unal, V. Hosseini, H. Kaji, K. Ino, H. Shiku, A. Khademhosseini, and T. Matsue, *Lab on a Chip*, Vol. 12, p. 3491, 2012.
10. S. Ahadian, V. Hosseini, S. Ostrovidov, G. Camci-Unal, S. Chen, H. Kaji, M. Ramalingam, and A. Khademhosseini, *Tissue Engineering Part A*, Vol. 18, p. 2453, 2012.
11. S. Ahadian, J. Ramón-Azcón, S. Ostrovidov, G. Camci-Unal, H. Kaji, K. Ino, H. Shiku, A. Khademhosseini, and T. Matsue, *Biomedical Microdevices*, Vol. 15, p. 109, 2013.
12. A. Khademhosseini, G. Eng, J. Yeh, P. Kucharczyk, R. Langer, G. Vunjak-Novakovic, and M. Radisic, *Biomedical Microdevices*, Vol. 9, p. 149, 2007.
13. G. Cellot, E. Cilia, S. Cipollone, V. Rancic, A. Sucapane, S. Giordani, L. Gambazzi, H. Markram, M. Grandolfo, D. Scaini, F. Gelain, L. Casalis, M. Prato, M. Giugliano, and L. Ballerini, *Nature Nanotechnology*, Vol. 4, p. 126, 2009.
14. K.S. Novoselov, A.K. Geim, S.V. Morozov, D. Jiang, Y. Zhang, S.V. Dubonos, I.V. Grigorieva, and A.A. Firsov, *Science*, Vol. 306, p. 666, 2004.

15. C.N.R. Rao, A.K. Sood, K.S. Subrahmanyam, and A. Govindaraj, *Angewandte Chemie International Edition*, Vol. 48, p. 7752, 2009.
16. A.A. Balandin, S. Ghosh, W. Bao, I. Calizo, D. Teweldebrhan, F. Miao, and C.N. Lau, *Nano Letters*, Vol. 8, p. 902, 2008.
17. S. Latil and L. Henrard, *Physical Review Letters*, Vol. 97, p. 36803, 2006.
18. K. Zhang, L.L. Zhang, X.S. Zhao, and J. Wu, *Chemistry of Materials*, Vol. 22, p. 1392, 2010.
19. Z. Liu, J.T. Robinson, X. Sun, and H. Dai, *Journal of the American Chemical Society*, Vol. 130, p. 10876, 2008.
20. O.N. Ruiz, K.A.S. Fernando, B. Wang, N.A. Brown, P.G. Luo, N.D. McNamara, M. Vangsness, Y.-P. Sun, and C.E. Bunker, *ACS Nano*, Vol. 5, p. 8100, 2011.
21. L. Feng, S. Zhang, and Z. Liu, *Nanoscale*, Vol. 3, p. 1252, 2011.
22. Y. Liu, X. Dong, and P. Chen, *Chemical Society Reviews*, Vol. 41, p. 2283, 2012.
23. K.P. Loh, Q. Bao, G. Eda, and M. Chhowalla, *Nature Chemistry*, Vol. 2, p. 1015, 2010.
24. W. Hu, C. Peng, W. Luo, M. Lv, X. Li, D. Li, Q. Huang, and C. Fan, *ACS Nano*, Vol. 4, p. 4317, 2010.
25. O. Akhavan and E. Ghaderi, *ACS Nano*, Vol. 4, p. 5731, 2010.
26. S. Liu, T.H. Zeng, M. Hofmann, E. Burcombe, J. Wei, R. Jiang, J. Kong, and Y. Chen, *ACS Nano*, Vol. 5, p. 6971, 2011.
27. H. Lei, L. Mi, X. Zhou, J. Chen, J. Hu, S. Guo, and Y. Zhang, *Nanoscale*, Vol. 3, p. 3888, 2011.
28. W. Chen, P. Yi, Y. Zhang, L. Zhang, Z. Deng, and Z. Zhang, *ACS Applied Materials and Interfaces*, Vol. 3, p. 4085, 2011.
29. H. Dong, W. Gao, F. Yan, H. Ji, and H. Ju, *Analytical Chemistry*, Vol. 82, p. 5511, 2010.
30. H. Pandey, V. Parashar, R. Parashar, R. Prakash, P.W. Ramteke, and A.C. Pandey, *Nanoscale*, Vol. 3, p. 4104, 2011.
31. H. Bai, C. Li, X. Wang, and G. Shi, *Chemical Communications*, Vol. 46, p. 2376, 2010.
32. Y. Pan, H. Bao, N.G. Sahoo, T. Wu, and L. Li, *Advanced Functional Materials*, Vol. 21, p. 2754, 2011.
33. H. Shen, Z. Liming, M. Liu, and Z. Zhang, *Theranostics*, Vol. 2, p. 283, 2012.
34. L. Naldini, U. Blömer, P. Gallay, D. Ory, R. Mulligan, F.H. Gage, I.M. Verma, and D. Trono, *Science*, Vol. 272, p. 263, 1996.
35. M.A. Mintzer and E.E. Simanek, *Chemical Reviews*, Vol. 109, p. 259, 2008.
36. H. Bao, Y. Pan, Y. Ping, N.G. Sahoo, T. Wu, L. Li, and L.H. Gan, *Small*, Vol. 7, p. 1569, 2011.
37. Y. Wang, Z. Li, J. Wang, J. Li, and Y. Lin, *Trends in Biotechnology*, Vol. 29, p. 205, 2011.
38. H. Jiang, *Small*, Vol. 7, p. 2413, 2011.
39. H. Chang, L. Tang, Y. Wang, J. Jiang, and J. Li, *Analytical Chemistry*, Vol. 82, p. 2341, 2010.
40. Q. He, H.G. Sudibya, Z. Yin, S. Wu, H. Li, F. Boey, W. Huang, P. Chen, and H. Zhang, *ACS Nano*, Vol. 4, p. 3201, 2010.
41. Q. Zhang, S. Wu, L. Zhang, J. Lu, F. Verproot, Y. Liu, Z. Xing, J. Li, and X.-M. Song, *Biosensors and Bioelectronics*, Vol. 26, p. 2632, 2011.
42. Y. Wan, Y. Wang, J. Wu, and D. Zhang, *Analytical Chemistry*, Vol. 83, p. 648, 2010.

43. D. Du, L. Wang, Y. Shao, J. Wang, M.H. Engelhard, and Y. Lin, *Analytical Chemistry*, Vol. 83, p. 746, 2011.
44. L. Feng, L. Wu, and X. Qu, *Advanced Materials*, Vol. 25, p. 168, 2013.
45. K. Yang, S. Zhang, G. Zhang, X. Sun, S.-T. Lee, and Z. Liu, *Nano Letters*, Vol. 10, p. 3318, 2010.
46. S. Guo and S. Dong, *Chemical Society Reviews*, Vol. 40, p. 2644, 2011.
47. K.S. Novoselov, V.I. Falko, L. Colombo, P.R. Gellert, M.G. Schwab, and K. Kim, *Nature*, Vol. 490, p. 192, 2012.
48. L. Guo, H.-B. Jiang, R.-Q. Shao, Y.-L. Zhang, S.-Y. Xie, J.-N. Wang, X.-B. Li, F. Jiang, Q.-D. Chen, T. Zhang, and H.-B. Sun, *Carbon*, Vol. 50, p. 1667, 2012.
49. J. Rafiee, M.A. Rafiee, Z.-Z. Yu, and N. Koratkar, *Advanced Materials*, Vol. 22, p. 2151, 2010.
50. S. Yin, Y. Zhang, J. Kong, C. Zou, C.M. Li, X. Lu, J. Ma, F.Y.C. Boey, and X. Chen, *ACS Nano*, Vol. 5, p. 3831, 2011.
51. X. Wang, H. Bai, Z. Yao, A. Liu, and G. Shi, *Journal of Materials Chemistry*, Vol. 20, p. 9032, 2010.
52. Y.-L. Zhang, Q.-D. Chen, Z. Jin, E. Kim, H.-B. Sun, *Nanoscale*, Vol. 4, p. 4858, 2012.
53. S. Morimune, T. Nishino, and T. Goto, *Polymer Journal*, Vol. 44, p. 1056, 2012.
54. Y.Y. Qi, Z.X. Tai, D.F. Sun, J.T. Chen, H.B. Ma, X.B. Yan, B. Liu, and Q.J. Xue, *Journal of Applied Polymer Science*, Vol. 127, p. 1885, 2013.
55. R. Murugan and S. Ramakrishna, *Tissue Engineering*, Vol. 12, p. 435, 2006.
56. L. Zhang, Z. Wang, C. Xu, Y. Li, J. Gao, W. Wang, and Y. Liu, *Journal of Materials Chemistry*, Vol. 21, p. 10399, 2011.
57. Y.-Q. Li, T. Yu, T.-Y. Yang, L.-X. Zheng, and K. Liao, *Advanced Materials*, Vol. 24, p. 3426, 2012.
58. O. Yoon, I. Sohn, D. Kim, and N.-E. Lee, *Macromolecular Research*, Vol. 20, p. 789, 2012.
59. Y. He, N. Zhang, Q. Gong, H. Qiu, W. Wang, Y. Liu, and J. Gao, *Carbohydrate Polymers*, Vol. 88, p. 1100, 2012.
60. D. Depan, B. Girase, J.S. Shah, and R.D.K. Misra, *Acta Biomaterialia*, Vol. 7, p. 3432, 2011.
61. B.G. Amsden, A. Sukarto, D.K. Knight, and S.N. Shapka, *Biomacromolecules*, Vol. 8, p. 3758, 2007.
62. C. Wan and B. Chen, *Biomedical Materials*, Vol. 6, p. 55010, 2011.
63. T. Kolodiazhnyi and M. Pumera, *Small*, Vol. 4, p. 1476, 2008.
64. X. Shi, H. Chang, S. Chen, C. Lai, A. Khademhosseini, and H. Wu, *Advanced Functional Materials*, Vol. 22, p. 751, 2012.
65. B. Girase, J.S. Shah, and R.D.K. Misra, *Advanced Engineering Materials*, Vol. 14, p. B101, 2012.
66. H. Chen, M.B. Müller, K.J. Gilmore, G.G. Wallace, and D. Li, *Advanced Materials*, Vol. 20, p. 3557, 2008.
67. S.-R. Ryoo, Y.-K. Kim, M.-H. Kim, and D.-H. Min, *ACS Nano*, Vol. 4, p. 6587, 2010.
68. N. Li, X. Zhang, Q. Song, R. Su, Q. Zhang, T. Kong, L. Liu, G. Jin, M. Tang, and G. Cheng, *Biomaterials*, Vol. 32, p. 9374, 2011.
69. L.I. Benowitz and A. Routtenberg, *Trends in Neurosciences*, Vol. 20, p. 84, 1997.
70. K. Zhou, G.A. Thouas, C.C. Bernard, D.R. Nisbet, D.I. Finkelstein, D. Li, and J.S. Forsythe, *ACS Applied Materials and Interfaces*, Vol. 4, p. 4524, 2012.

71. N.H. Lim, N.M. Huang, S.S. Lim, I. Harrison, and C.H. Chia, *International Journal of Nanomedicine*, Vol. 6, p. 1817, 2011.

72. A. Khademhosseini, R. Langer, J. Borenstein, and J.P. Vacanti, *Proceedings of the National Academy of Sciences of the United States of America*, Vol. 103, p. 2480, 2006.

73. J. Ramón-Azcón, S. Ahadian, R. Obregon, G. Camci-Unal, S. Ostrovidov, V. Hosseini, H. Kaji, K. Ino, H. Shiku, A. Khademhosseini. and T. Matsue, *Lab on a Chip*, Vol. 12, p. 2959, 2012.

74. S.H. Ku, M. Lee, and C.B. Park, *Advanced Healthcare Materials*, Vol. 2, p. 244, 2013.

75. D.A. Dikin, S. Stankovich, E.J. Zimney, R.D. Piner, G.H.B. Dommett, G. Evmenenko, S.T. Nguyen, and R.S. Ruoff, *Nature*, Vol. 448, p. 457, 2007.

76. S. Park, K.-S. Lee, G. Bozoklu, W. Cai, S.T. Nguyen, and R.S. Ruoff, *ACS Nano*, Vol. 2, p. 572, 2008.

77. H. Bai, C. Li, X. Wang, and G. Shi, *Journal of Physical Chemistry C*, Vol. 115, p. 5545, 2011.

78. P. Bianco and P.G. Robey, *Nature*, Vol. 414, p. 118, 2001.

79. F. Edalat, I. Sheu, S. Manoucheri, and A. Khademhosseini, *Current Opinion in Biotechnology*, Vol. 23, p. 820, 2012.

80. F. Edalat, H. Bae, S. Manoucheri, J. Cha, and A. Khademhosseini, *Annals of Biomedical Engineering*, Vol. 40, p. 1301, 2012.

81. S. Martino, F. D'Angelo, I. Armentano, J.M. Kenny, and A. Orlacchio, *Biotechnology Advances*, Vol. 30, p. 338, 2012.

82. T.R. Nayak, H. Andersen, V.S. Makam, C. Khaw, S. Bae, X. Xu, P.-L.R. Ee, J.-H. Ahn, B.H. Hong, G. Pastorin, and B. Özyilmaz, *ACS Nano*, Vol. 5, p. 4670, 2011.

83. W.C. Lee, C.H.Y.X. Lim, H. Shi, L.A.L. Tang, Y. Wang, C.T. Lim, and K.P. Loh, *ACS Nano*, Vol. 5, p. 7334, 2011.

84. S.Y. Park, J. Park, S.H. Sim, M.G. Sung, K.S. Kim, B.H. Hong, and S. Hong, *Advanced Materials*, Vol. 23, p. H263, 2011.

85. K. Müller, C. Faeh, and F. Diederich, *Science*, Vol. 317, p. 1881, 2007.

86. G.-Y. Chen, D.W.-P. Pang, S.-M. Hwang, H.-Y. Tuan, Y.-C. Hu, *Biomaterials*, Vol. 33, p. 418, 2012.

87. K. Takahashi and S. Yamanaka, *Cell*, Vol. 126, p. 663, 2006.

88. H. Niwa, K. Ogawa, D. Shimosato, and K. Adachi, *Nature*, Vol. 460, p. 118, 2009.

89. S. Bae, H. Kim, Y. Lee, X. Xu, J.-S. Park, Y. Zheng, J. Balakrishnan, T. Lei, H.R. Kim, Y.II. Song, Y.-J. Kim, K.S. Kim, B. Özyilmaz, J.-H. Ahn, B.H. Hong, and S. Iijima, *Nature Nanotechnology*, Vol. 5, p. 574, 2010.

90. C. Heo, J. Yoo, S. Lee, A. Jo, S. Jung, H. Yoo, Y.H. Lee, and M. Suh, *Biomaterials*, Vol. 32, p. 19, 2011.

91. M. Hronik-Tupaj and D.L. Kaplan, *Tissue Engineering Part B: Reviews*, Vol. 18, p. 167, 2011.

92. N.A. Kotov, J.O. Winter, I.P. Clements, E. Jan, B.P. Timko, S. Campidelli, S. Pathak, A. Mazzatenta, C.M. Lieber, M. Prato, R.V. Bellamkonda, G.A. Silva, N.W.S. Kam, F. Patolsky, and L. Ballerini, *Advanced Materials*, Vol. 21, p. 1, 2009.

93. B.S. Sayyar, E. Murray, B.C. Thompson, S. Gambhir, D.L. Officer, and G.G. Wallace, *Carbon*, Vol. 52, p. 296, 2013.

94. A.M. Ghaemmaghami, M.J. Hancock, H. Harrington, H. Kaji, and A. Khademhosseini, *Drug Discovery Today*, Vol. 17, p. 173, 2012.

95. Y. Zhang, T.R. Nayak, H. Hong, and W. Cai, *Nanoscale*, Vol. 4, p. 3833, 2012.
96. O. Akhavan, E. Ghaderi, and A. Akhavan, *Biomaterials*, Vol. 33, p. 8017, 2012.
97. A. Khademhosseini, R. Langer, J. Borenstein, and J.P. Vacanti, *Proceedings of the National Academy of Sciences of the United States of America*, Vol. 103, p. 2480, 2006.
98. B. Huang, H. Wu, D. Bhaya, A. Grossman, S. Granier, B.K. Kobilka, and R.N. Zare, *Science*, Vol. 315, p. 81, 2007.
99. O.J. Yoon, C.Y. Jung, I.Y. Sohn, H.J. Kim, B. Hong, M.S. Jhon, and N.-E. Lee, *Compos. Part A: Appl. Sci. Manufacturing*, Vol. 42, p. 1978, 2011.
100. M. Niemeyer, *Angew. Chem. Int. Ed.*, Vol. 40, p. 4128, 2001.

Biomimetic Preparation and Morphology Control of Mesoporous Silica

Qiang Cai* and Ce Peng

Department of Materials Science and Engineering, Tsinghua University, Beijing, China

"The specific goal of moving toward the molecular level understanding of the observed phenomena will be appreciated by readers who wish for a molecular description of biomineralization as well as those who want to learn from nature and adapt the strategies to prepare other inorganic materials and architectures [1]."
— ME. Davis

"The chemists begin with the problem of form as described by structure and then develop the notion of the equilibrium form of crystals and how geomertric shapes are modified in the presence of surface-active molecules [2]"
— S. Mann

Abstract

In this chapter, we have addressed the concepts from biomineralization to biomimic synthesis of mesoporous silica and summarized the recent achievements on its morphologies control of mesoporous silica. The basic concepts such as biomineralization, biomineralization and morphogenesis, biomimic synthesis, and therefrom some derivative concepts such as the self-assembly and morphology formation, etc, have been unfolded in detail. We also have introduced the definition and classification of the mesoporous silica, especially for mesoporous silica nanoparticles (MSN) and its biomedical application. Finally, we made a review of the progresses on the biomimic preparation and morphology control of mesoporous silica, which mainly includes that on general synthesis and the morphology control of mesoporous silica studied by our group in recent years.

Keywords: Biomimetic synthesis, biomineralization, supramolecular self-assembly, coding self-assembly, diatoms, drug-delivery, hierarchical structure, hydrophilic-hydrophobic interaction, MCM-41, SBA-15, mesoporous silica, mesoporous silica

*Corresponding author: caiqiang@mail.tsinghua.edu.cn

nanoparticles, mesoporous vesicles, molecular recognition, morphology control, nanomachines, nanovalves, gatekeeper, stimuli-responsive release

13.1   Introduction

Hybrid material and self-assembly are two important characters in the study of biominerals. The functionality of macroscopic materials is rarely expressed and is embodied simply by pure chemical composition. Many natural biomaterials, such as bone, cartilage, shell and diatom are composites composed of various nanostructured blocks that are made of inorganic crystalline or amorphous materials and organic molecular assemblies [3]. Many past studies have indicated that the organic molecules might control the nanostructure formation of the inorganic materials through molecular recognition.

Besides calcium minerals (e.g., calcium phosphate, calcium carbonate), silica is one of the most important biominerals in nature and earliest forms of biominerals on earth. Silica can be found everywhere, in the biominerals of single-celled algae, bacteria, sponges, protozoa and higher plants *in vivo* [3]. Its ultra-stable amorphous forms provide adjustable mesostructure. Mesoporous silica as well as nano-silica widely exists in plants, sponges and diatoms in the world. Because of its excellent biocompatibity, nontoxicity and non-physiological activity, mesoporous silica is one of the most promising carrier candidates for advanced drug delivery. The biomimetic synthesis of porous silica is usually inspired by biomineralization of sponge or diatom. During the formation process of diatom, a silaffin protein ends with polyamine fragments, works as a functional reaction site, and may affect the pH of the local environment resulting in molecular recognition by weak interaction and enrichment, or even condensation of particular ions of silica precursor [4]. The formation of mesoporous silica adopted a bionic processing self-assembly technique, which originates from the basic principles of biomineralization. In the early stage of the study of mesoporous silica, Stucky [6–8] and Mann [9–10] stated that the synthesis of the mesoporous silica was a typical biomimetic biomineralization, which is in light of the characteristic mesostructure of the biominerals.

13.2   Biomineralization and Biomimic Synthesis

13.2.1   Biomineralization and Morphogenesis

Evolution is a constantly optimized process. After billions of years of biological evolution, both the microstructure and behavior of biological systems of the entire biosphere are gradually self-adaptively optimized, and this optimization is more prominent for biomaterials. It has been proved that biomanufactured materials are superior. Teeth can be biologically manufactured at 37°C, and their strength is even higher than by ceramic

sintering at much higher temperature. From the view of material science, it can be established that the properties of composite material depend not only on its composition, but also its structure, and the special structure of the composite material is the key that gives rise to such an excellent performance. Excellent species as well as biomaterials have been gradually optimized over millions of years of evolution from one generation to the next, and gradually have been selected and cured via the biological interaction among populations and individuals. Therefore, organisms are the most experienced material designers and skillful experts of materials processing.

The synergy between biominerals and organisms enhances the evolution and the performance of the mineral itself unfolds through the new organisms. The intervention of inorganic minerals strengthens some function of the organisms, which extends the biological diversity of evolution. Concretely, the mechanical strength of some part of the organ is increasing so that the organism can survive easily, or the "hard tissue" containing biominerals can protect the nervous system from damage if the organisms are under attack. For example, when calcium phosphate became the main content of bones and teeth, the viability of the species having bones and teeth was improved, and the functionality of the species was enriched. The function can be manifested in different ways in later evolution of the species, and therefore increased in an evolutionary way.
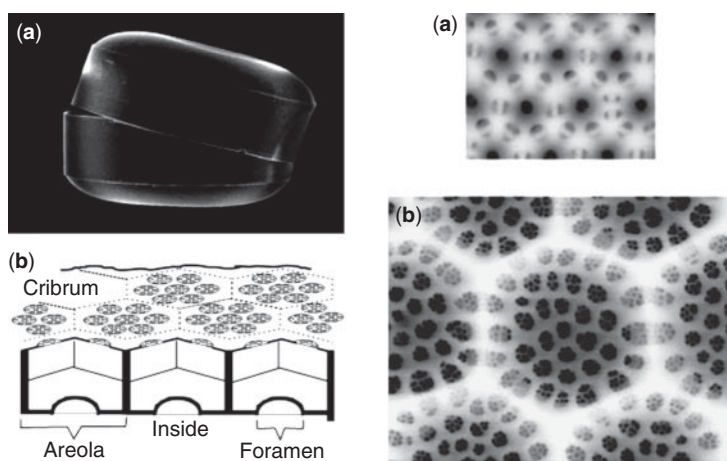
Figure 13.1 Left: the form and microarchitecture of the silicified valve from the diatom genus *Coscinodiscus*. (a) Scanning electron micrograph of a silica shell (*Coscinodiscus* sp.). (b) Diagram of the three-dimensional architecture of the valve. The honeycomb-like chambers are denoted as areolae. The roof on top of each areola is called a cribrum, which contains a regular pattern of larger pores. The siliceous Þne structure within each larger pore of a cribrum is denoted as cribellum. Right: Scanning Electron Microscope (SEM) images of valves from *C. granii* (a) and *C. asteromphalus* (b) and the interpretation of their patterns by the phase separation model. (Reprinted with permission from [11])

Biomineralization is an extremely complex microassembly process in cell modulation [5]. The formation of biominerals is processed by space-time templating of genes, proteins, mesenchymal cells, and further interacting among organic supramolecular and inorganic precursor. This process is the precise control of crystal nucleation and growth on the molecular level. The main feature of the process is that precipitation of inorganic mineral phase is controlled by the interaction of organic functional molecules and inorganic mineral ions at the interface.

The aesthetic morphologies in the natural world have been of great fascination to scientists in various fields. The biominerals often display unusual morphology that are distinct from the inorganic minerals, and the special and unusual morphologies are often targeted and emphasized by scientists who work on biomimetic synthesis. Bio-morphogenesis has been developed in synthesis of inorganic materials with comparable complex forms of biominerals such as diatoms, etc., by a chemistry of constructing inorganic architectures via a biomimetic approach.

Biomineralization is different from general mineralization. In general mineralization, if the solution containing calcium ions and phosphate ion are mixed, the calcium phosphate will precipitate and further convert to thermodynamically stable hydroxyapatite. In mineralization of bone or teeth, calcium or phosphate ions are accumulated near special sites of the matrix proteins in the intracellular or extracellular matrix, in which the calcium phosphate nucleate, then grow together and finally constitute the hard tissue. The reaction site of the matrix protein needs to be pre-self-assembled in order to have mesostructure or hierarchical structure. The self-assembly exists widely in the natural biomineralization.

An example of a study on natural biosilica is shown in Figure 13.2 [4].

13.2.2   Self-Assembly and Biomimic Synthesis

It can be extracted from the study of biomineralization that the most important concepts are molecular recognition and self-assembly. Now self-assembly has become the most important idea and basic principle of basic and even supramolecular chemistry, and can supply the basis of biomimetic synthesis at the microscopic scale.

Whitesides was the first to interpret the concept of self-assembly [12]. He considered that ordered substance itself was formed by the synergistic interaction among its building blocks, and the function of the assemblies as well as the assembly "information" are stored in the assembled fragments. Self-assembly is a fabrication process of molecule assemblies as well as mesostructure. Firstly, it needs construction of the building block, i.e., primitives that are usually molecular assemblies formed by atoms, molecules, supramolecules, as well as uniformed nanoparticles with the determined component. Then the building blocks are assembled to mesoscopic

```
                          MKLTAIFPLLFT      12
     AVGYCAAQSIADLAAANLS                    31
     TEDSKSAQLISADSSDDAS                    50
     DSSVESVDAASSDVSGSSV                    69
     ESVDVSGSSLESVDVSGSS                    88
     LESVDDSSEDSEEEELRIL                   107
R1   SSKKSGSYYSYGTKK                        122
       SGSYSGYSTKKSASRRIL                   140
R2   SSKKSGSYSGYSTKKSGSRRIL                 162
R3   SSKKSGSYSGSKGSKRRIL                    181
R4   SSKKSGSYSGSKGSKRRNL                    200
R5   SSKKSGSYSGSKGSKRRIL                    219
R6   SSKKSGSYSGSKGSKRRNL                    238
R7   SSKKSGSYSGSKGSKRRIL                    257
     SGGLRGSM                               265
```

(d) H_2N–Ser–Ser–Lys–Lys–Ser–Gly–Ser–Tyr–CO_2H n = 5–10

Figure 13.2 Ultrastructure of *C. fusiformis* cell wall analyzed by transmission electron microscopy (TEM). (a) Isolated cell wall. Bar: 2.5 µm. (b and c) Details of a *C. fusiformis* cell in cross section. (b) Lateral region. Each oval-shaped element represents a single silica strip of the cell wall in cross section. (c) Valve region. The ring-like structure and the two oval-shaped elements on either side are silicified cell wall elements. Right of upper figure: Primary structure of sil1p. The signal peptide sequence is shown in italics. Lower left: Structural analysis of modified lysine residues. Proposed schematic structure of the $(m + H)^+ = 573$ ion. The molecule shown below the $(m + H)^+ = 573$ ion represents the decarboxylated derivative that gives rise to ion series 2 (b). Cleavage positions that lead to the observed fragment ions are depicted by rectangular arrows, and the corresponding masses are indicated above the arrow heads. (d) Schematic chemical structure of chymotryptic peptide SSXX'SGSY. Lower right: pH dependence of peptide-induced silica precipitation. The solid line shows the result for silaffin-1A; the dotted line represents the result for synthetic peptide pR5. At each pH value, the amount of respective peptide applied was 28 nmol. (Reprinted with permission from [4])

or macroscopic materials by the interactions among the blocks under appropriate conditions [13]. From the analysis of the biomolecular self-assembly system, it is found that the self-assembly is driven by weak collaborative noncovalent interactions such as multiple hydrogen bonding, hydrophilic hydrophobic interaction, chiral-chiral and donor-acceptor molecular recognition interaction, etc. The product obtained by the weak interaction of chemistry should be thermodynamic metastability. This is mainly due to its correction, transmission and processing on the supramolecular scale, including the information storage of the structural characteristics, as well as the molecular recognition process by specific interaction at the molecular level, which leads to the procedures chemistry. Lehn thinks a future characteristic of supramolecular compound systems is the unity of information

and procedures, mobility and reversibility, composability and diversity of structure [14, 15].

Coding self-assembly is an advanced self-assembly, and thermodynamic self-assembly is a lower one, which can be a simple coding process. The coding self-assembly of protein is composed of manipulation, catalysis of mesoscopic molecules, as well as template effect of the structural protein with conserved sequence. Coding self-assembly also dominates the biomineralization process. That is, (i) the sequence of amino acid residue form the coding of molecular hierarchical structure with biological function; (ii) DNA guide the programmed synthesis of protein sequences in the particular moment, forming the code of a series of processes.

13.3 Mesoporous Silica

13.3.1 Mesoporous Silica: Definition and Classification

Since the discovery of ordered mesoporous silica materials in the 1990s, the synthesis and applications of mesoporous solids have received intensive attention due to their highly ordered structures, larger pore size, high surface area, and potential applications in catalysis [16], biomolecule separations [17], drug-delivery [18–20], fabrication of nanometer functional materials and chromatographic supports, etc. [21–23]. Because of stable mesoporous structure and well-defined surface properties, mesoporous materials seem ideal for encapsulation and release of pharmaceutical drugs, proteins and other biogenic molecules. Since the report by Vallet-Regi *et al.* in 2001 using MCM-41 as a new drug delivery system [24], a lot of studies have been done in this area, developing different types of mesoporous materials with varying porous structure and functionality for sustained drug released and stimuli-responsive release.

A large number of known mesostructure of mesoporous silica such as M41s, SBA-n, etc., and even some of the new structure, have been synthesized, such as a hollow/rattle-type and some more complex forms, which stem from the silica having exceptional plasticity at a mesoscopic scale. For example, M41s, including MCM-41(hexagonal), MCM-48 (cubic) and MCM-50 (lamellar), are a family of a series of orderly mesoporous silica that were invented by Mobil scientists led by Beck *et al.* in 1992 [25, 26]. Several kinds of mesoporous silica are introduced in Table 13.1.

13.3.2 Mesoporous Silica Nanoparticles (MSN)

Nanosized mesoporous materials have always been a goal for material chemists. The application of the MSN is mainly in drug delivery system, controlled release, heterogeneous catalysis, and nanomachines. Among the

Table 13.1 All kinds of mesoporous materials (Reprinted with permission from [18]).

porous structure character	crystalline	highest symmetry space group	typical materials	XRD diffraction peak diffraction conditions
low degree of order	hexagonal		MSU–n HMS, KIT–1	wide 1-2 diffraction peaks
one-dimensional layered (no pore)			MCM–50	$\dfrac{1}{d_{00l}} = \dfrac{l}{a}$; 001, 002, 003, 004…
two-dimensional	hexagonal	p6mm (17) p6m	MCM–41 SBA–3, 15 FSM–16, TMS–1	$\dfrac{1}{d_{hk0}^2} = \dfrac{4}{3}\dfrac{h^2 + hk + k^2}{a^2}$ 100, 110, 200, 210…
(straight channels)	quartet	c2mm (9) cmm	SBA–8 KSW–2	$\dfrac{1}{d_{hk}^2} = \dfrac{h^2}{a^2} + \dfrac{k^2}{b^2}$; 11,20,22,31,40…; h+k=2n
the three-dimensional (cage pore cavities)	hexagonal	P6$_3$/mmc (194)	Cubic the hexagonal	$\dfrac{1}{d^2} = \dfrac{4}{3}\dfrac{h^2 + hk + k^2}{a^2} + \dfrac{l^2}{c^2}$ hhl: l=2n
	cubic	Pm$\bar{3}$n (223)	SBA–1 SBA–6	$\dfrac{1}{d^2} = \dfrac{h^2 + k^2 + l^2}{a^2}$; 110, 200, 210, 211, 220, 310, 222, 320, 321, 400… hhl: l = 2n (first peak 110 has not been observed)

(Continued)

308   Biomimetics

Table 13.1 (Cont.)

porous structure character	crystalline	highest symmetry space group	typical materials	XRD diffraction peak diffraction conditions
three-dimensional cross-channel		Im $\bar{3}$ m (229)	SBA-16	110, 200, 211, 220, 310, 222, 321...h+k+l = 2n
		Fd $\bar{3}$ m (227)	FDU-2	111, 220, 311, 222... H+k=2n, h+l=2n, k+l=2n, 0kl: k+l=4n
		Fm $\bar{3}$ m(225)	FDU-12	111, 200, 220, 311, 222, 400... h+k=2n, h+l=2n, k+l=2n
		Pm $\bar{3}$ m (221)	SBA-11	extinction
	cubic hexagonal	Fm $\bar{3}$ m(225)- P6$_3$/mmc (194)	SBA-2, 7, 12 FDU-1	P6$_3$/mmc (194)
		Im $\bar{3}$ m (229)	SBA-16	110, 200, 211, 220, 310, 222, 321, 400... h+k+l=2n
	cubic	Ia $\bar{3}$ d (230)	MCM-48 FDU-5	211, 220, 321, 400, 420, 332, 422, 431, 440, 532... h+k+l=2n, hhl: 2h+l=4n
		Pn $\bar{3}$ m (224)	HOM-7	110, 111, 200, 211, 220, 221, 310, 311, 222,... 0kl: k+l=2n
	quartet	I4$_1$/a(88)	CMK-1 HUM-1	110, 211, 220...
two-dimensional cross-channel	tripartite (rhombic)	R $\bar{3}$ m(166)	none	101, 102, 003, 110, 201, 202, 104, 113, 211... (hexagonal)

top-ranked materials science research papers indexed in Web of Science, the mesoporous silica nanoparticles (MSN)-based biological applications for controlled release, drug delivery system, as well as 3T3-L1 cells, ranked ninth on the list. By this it can be inferred that the research on MSN now is the *hot* research front in biomaterials and biological pharmacy.

In order to obtain small-sized uniform mesoporous silica, several approaches to synthesize the MSN have been well developed. Lu *et al.* reported a rapid, aerosol-based process for synthesizing solid, well-ordered spherical particles. Their method relied on evaporation-induced interfacial self-assembly, and the obtained mesoporous silica spheres had a diameter of 230 nm [28]. Cai *et al.* were first to introduce a new route to synthesize MCM-41 silica nanospheres ranging from 60 nm to 140 nm in dilute solution, the molar concentration of hexadecyltrimethylammonium bromide (CTAB) was only 5.7 mM [29, 30]. Their method was based on controlling the size of MCM-41 particles by adjusting the length of self-assembled silicates micelles through changing the concentration of surfactant and sodium hydroxide. Afterward, V.S.Y Lin adopted the same method to synthesize mesoporous silica MCM-41 spheres with a diameter of 200 nm, and applied the material for drug delivery system [31–34]. Lin *et al.* reported a method to synthesize dye-functionalized, well-dispersed nanoparticles with a diameter around 110 nm by co-condensation [35]. Lin and coworkers reported a novel method of two-steps reaction, including a prehydrolysis of TEOS and metal alkoxides or salts in acidic solution (pH < 1.0), and fast co-condensation of silica, metal oxides and surfactant in alkaline ammonia solution [36], to prepare alumina-substituted mesoporous silica particles with a size of about 30 ~ 40 nm. In addition, Suzuki *et al.* described their preparation of well-ordered mesostructured particles with a diameter of 20 ~ 50 nm via a two-surfactant system [37].

13.3.3   Biomedical Application of Mesoporous Silica

13.3.3.1   *Biocompatibility Investigation*

Drug delivery systems (DDS) have to deal with the physiological environment when performing their functions during oral intake or implantation. Obviously, the success of mesoporous silica to be a carrier for DDS hinges upon the ability to construct a biocompatible coated environment that allows high loading of drug molecules without any premature release of the cargo before reaching the destination. As outlined below, several features incorporated into such a material make it possible to serve as an efficient DDS. Bioactivity studies on SBA-15, MCM-48 and MCM-41 materials have also been carried out.

The MSN exhibit good biocompatibility and promise excellent potential usage in the field of biomedical and biotechnological applications. The

following points lay out the fundamentals necessary for mesoporous silica to be feasible for drug delivery *in vivo*: a) tunable particle size from 50 to 300 nm allowing a facile endocytosis by living animal and plant cells without any significant cytotoxicity; b) an ordered, uniform and tunable pore size, usually 2 ~ 6 nm, which is very easy to adjust for loading different size drug molecules and control release kinetics; c) a high surface area and a high pore volume, typically over 1000m^2/g and over 0.8 cm^3/g, respectively, implies high potential for drug adsorption; d) a silanol-containing surface that can be functionalized to allow better control over drug loading and release [18–20].

13.3.3.2   Gatekeeper/ Stimuli-Responsive for Controlled Released

Mesoporous silica nanoparticles (MSNP) have been proven to be an extremely effective solid support for controlled drug delivery on account of the fact that their surfaces can be easily functionalized in order to control the nanopore openings. Xiao and coworkers designed pH-responsive carriers in which polycations are grafted to anionic, carboxylic acid modified SBA-15 by ionic interactions [38], poly(N-isopropylacryl amide) (PNIPAm), to produce sponge-like phases [39]. The controlled-release mechanism of the system is based on the reduction of the disulfide linkage between magnetic Fe_3O_4 nanoparticles and the thiol-functionalized silica mesoporous material by reducing agents such as dihydrolipoic acid or dithiothreitol.

Two examples that represent works on MSN-based applications for controlled release are shown in Figure 13.3. Lin *et al.* studied the stimuli-responsive release profiles of vancomycin and adenosine triphosphate
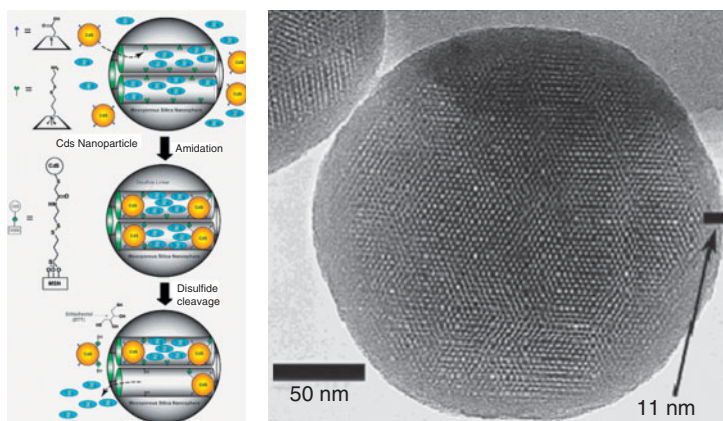
Figure 13.3 Left: Schematic representation of the CdS nanoparticle-capped MSN-based drug/neurotransmitter delivery system. The controlled-release mechanism of the system is based on chemical reduction of the disulfide linkage between the CdS caps and the MSN hosts. Right: TEM image of MSN. (Reprinted with permission from [40])

(ATP)-loaded MSN delivery systems by using disulfide bond-reducing molecules, such as dithiothreitol (DTT) and mercaptoethanol (ME), as release triggers [40]. The biocompatibility and delivery efficiency of the MSN system with neuroglial cells (astrocytes) *in vitro* were demonstrated. In contrast to many current delivery systems, the molecules of interest were encapsulated inside the porous framework of the MSN, not by adsorption or sol-gel types of entrapment, but by capping the openings of the mesoporous channels with size-defined CdS nanoparticles to physically block the drugs/neurotransmitters of certain sizes from leaching out. It can be envisioned that this new MSN system could play a significant role in developing new generations of site-selective, controlled-release
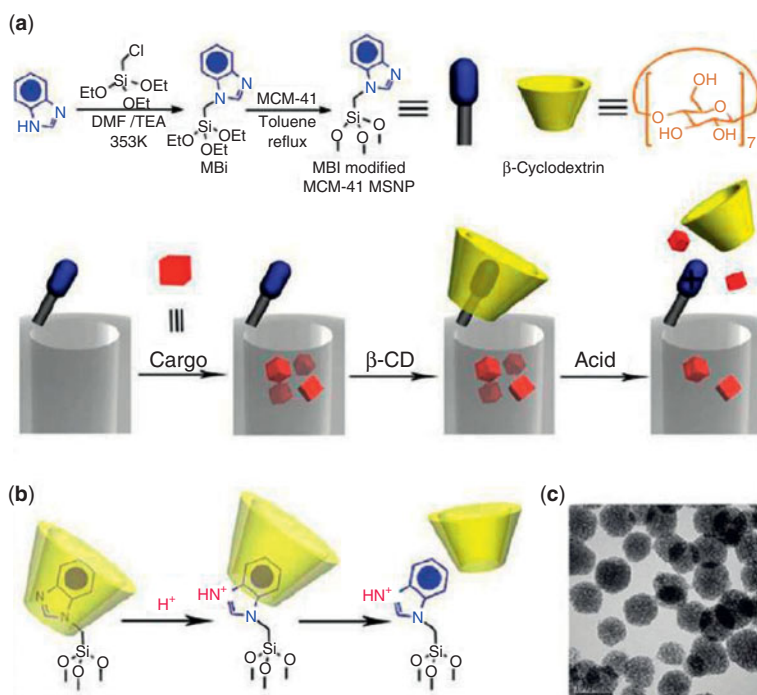
Figure 13.4 A schematic representation of the pH responsive MSNP nanovalve. (a) Synthesis of the stalk, loading of the cargo, capping of the pore, and release of the cap under acidic conditions. Based on our calculations, the maximum number of stalks per nanopore is 6, and the maximum number of fully assembled nanovalves per nanopore is 4. The average nanopore diameter of the MSNP is around 2.2 nm, and the periphery diameter of the secondary side of β-cyclodextrin is ~1.5 nm. Thus, for a cargo with diameter >0.7 nm, a single nanovalve should be adequate to achieve effective pH-modulated release. (b) Details of the protonation of the stalk and release of the β-cyclodextrin. (c) TEM image of capped MSNP. The scale bar is 100 nm. (Reprinted with permission from [41])

delivery nanodevices. In this work, an MSN-based, controlled-release delivery system has been synthesized and characterized using surface-derivatized cadmium sulfide (CdS) nanocrystals as chemically removable caps to encapsulate several pharmaceutical drug molecules and neurotransmitters inside the organically functionalized MSN mesoporous framework.

Zink *et al.* combined mesostructured functional silica with novel supermolecular techniques and have proposed nanomachines based on the MSN by surface modifying, which is hopefully the most important improvement for the future of the nanobiomedical field.[41]. They have described a series of recent mechanized silica nanoparticles, which, under abiotic conditions, are capable of delivering cargo molecules employing a series of nanovalves. The key question for these systems has now become whether they can be adapted for biological use through controlled nanovalve opening in cells. Figure 13.4 shows that they report a novel MSNP delivery system capable of drug delivery based on the function of β-cyclodextrin (β-CD) nanovalves that are responsive to the endosomal acidification conditions in human differentiated myeloid (THP-1) and squamous carcinoma (KB-31) cell lines. Furthermore, they demonstrate how to optimize the surface functionalization of the MSNP so as to provide a platform for the effective and rapid doxorubicin release to the nuclei of KB-31 cells.

13.4 Biomimic Preparation and Morphology Control of Mesoporous Silica

13.4.1 General Synthesis

Of the five elements such as solvent, surfactant, silica source, catalyst and the acid-base properties used in the synthesis of mesoporous silica, surfactant plays an important role. Much of the synthesis of mesoporous silica is based on a surfactant template method that determines templating routes. This is because the surfactant self-assemblies can act as organic supermolecular template similar to that in biomineralization, and the surface can be the reactant site on which the silica precursor can be deposited. The surfactants are usually classified by the head group and charge as: cationic surfactants (the hydrophilic group carries a positive charge, e.g., tetraalkylammonium salts), anionic surfactants (the hydrophilic group carries a negative charge, e.g., sulfates, sulfonates, etc.), and neutral surfactant (nonionic alkyl-poly(ethylene oxide) (PEO) oligomeric surfactants and poly-(alkylene oxide) block copolymers (PO), respectively).

The main formation mechanism has been proposed as liquid-crystal templating (LCT) [42–44], cooperative formation mechanism [24], and the deposition of self-assembled silicate surfactant rod-like micelles [29, 30].

13.4.1.1   MCM-41

A typical synthesis of MCM-41 requires a minimum of four reagents: a solvent (water and/or ethanol), a silica precursor (tetraethyl orthosilicate (TEOS), tetramethyl orthosilicate (TMOS), tetrabutyl orthosilicate (TBOS)), and an ionic (anionic or cationic) or non-charged surfactant, and a catalyst. Depending on the protocol, the reaction could occur in an acidic or basic medium, with different silica/surfactant ratios. The mixture is stirred, aged at room temperature or around 100°C, and placed in a static autoclave for several hours. The surfactant template is removed by calcination. Novel routes have been proposed based either on a nonsurfactant templated method [45, 46] or on a polyelectrolyte/hexadecyltrimethyl -ammonium bromide method [47].

An alternate route [48, 49] involves a microwave treatment of a precursor gel first heated by microwave radiation around 100–150°C followed by conventional heating. The advantages of the microwave-assisted preparation over the conventional hydrothermal method is the significant decrease in reaction time, and a more homogeneous heating which leads to better control of the texture and morphology. However, it has been superseded by faster methods which produce within a few hours the same, if not better, quality materials.

13.4.1.2   SBA-15

Zhao et.al reported the syntheses of well-ordered hexagonal mesoporous silica structures (SBA-15) with tunable large uniform pore sizes (up to ~ 30 nm) which are obtained by use of amphiphilic block copolymers [50, 51] as organic structure-directing agents. In particular, poly(alkylene oxide) triblock copolymers such as poly(ethylene oxide)-poly(ethylene oxide)-poly(ethylene oxide) (PEO-PPO-PEO) are good candidates, because of their mesostructural ordering properties, amphiphilic character, low-cost commercial availability, and biodegradability. Using aqueous acidic conditions (pH ~ 1) and dilute triblock copolymer concentrations, SBA-15 has been synthesized with a highly ordered two-dimensional (2D) hexagonal (p6 mm) mesostructure and thick, uniform silica walls (3 ~ 6nm). The thick silica walls, in particular, are different from thinner-walled MCM-41 structures made with conventional cationic surfactants, and lead to greater hydrothermal stability on the part of SBA-15. The pore size and the thickness of the silica wall can be adjusted by varying the heating temperature (35 ~ 140°C) and time (11 ~ 72 hours) of SBA-15 in the reaction solution.

SBA-15 can be synthesized over a range of reaction mixture compositions and conditions. Use of concentrations of block copolymer higher than 6 wt% yields only silica gel or produces no precipitation of silica, whereas concentrations of copolymer below 0.5 wt% result in only amorphous silica. Preparation of SBA-15 has been achieved with reaction temperatures between 35°C and 80°C. At room temperature, only amorphous

silica powder or poorly ordered products are obtained, whereas higher temperatures (> 80°C) yield silica gel. TEOS, TMOS, and TPOS are suitable sources of silica for the preparation of SBA-15. Hexagonal mesoporous SBA-15 has been formed in acid media (pH < 1) with HCl, HBr, HI, HNO_3, H_2PO_4, or H_3PO_4 acids. At pH values from 2 to 6, above the isoelectric point of silica (pH ~ 2), no precipitation or formation of silica gel occurs. At neutral pH ~ 7, only disordered or amorphous silica is obtained [52–55].

13.4.2 The Preparation and Morphologies Control of Mesoporous Silica

In this section, we will introduce our studies about the morphology control of mesoporous silica. As shown in Figure 13.5, the schematic compass displays our group's research work. The morphology of mesoporous silica can change with the condition of reaction system, such as type of catalysts, solvent, composition ratio, as well as certain factors. The factors could be assistant surfactant, ions and assistant silane. We found that the type of solvent and the total volume of solvent determine the mesoscopic order and the uniformity of the morphologies of the products. This is because the polarity of solvent and the concentration of the surfactant strongly influents the microstructure of the building blocks at the mesoscopic scale, for example, micelles, vesicles, emulsions and so on, but also the reaction rate of hydrolysis as well as condensation from the silicate precursor of silane.

Three systems of solvent will be introduced. They are diluted aqueous system, alcohol-water system, and ether-water system.
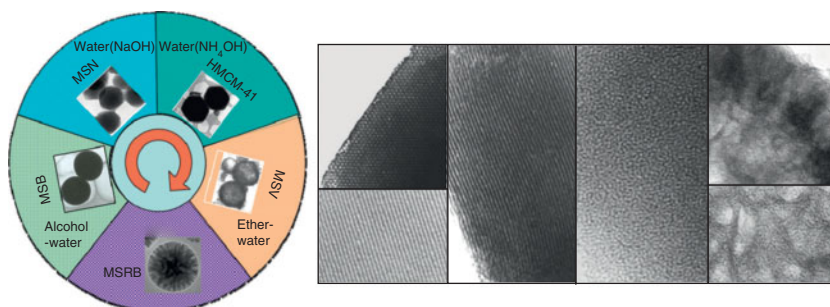
Figure 13.5 Left: the schematic compass. Different typical morphologies in the solvent system. Right: TEM image of the mesoporous silica in the different solvent system. From left to right, MCM-41 single crystal, MCM-41 submicrometer rod, mesoporous silica with worm-like pore structure prepared via alcohol-water solvent system, mesoporous silica with hierarchical pore structure prepared via ether-water solvent system, scale bar, 24 nm.

13.4.2.1   Diluted Aqueous System

In the diluted solution system, MCM-41 silica particles with several morphologies have been controllably synthesized with a basic medium. By changing the reaction factor, such as composition ratio and medium, different morphologies of MCM-41 could be controllably synthesized [29, 30]. They are nanospherical MCM-41 silica with an average size of 100 nm (which is the first synthesis of mesoporous silica nanoparticles), a submicrometer-sized silica rod, 0.3–0.6 μm in diameter and 1 μm in length, and micrometer-sized oblate silica with nominal diameter around 1 μm respectively.

Firstly, the preparation of large MCM-41 single crystals as well as their controllable morphologies has very important meanings not only for their potential applications but also for the exploration of the new morphogenetic mechanism for some special mesoporous crystals.
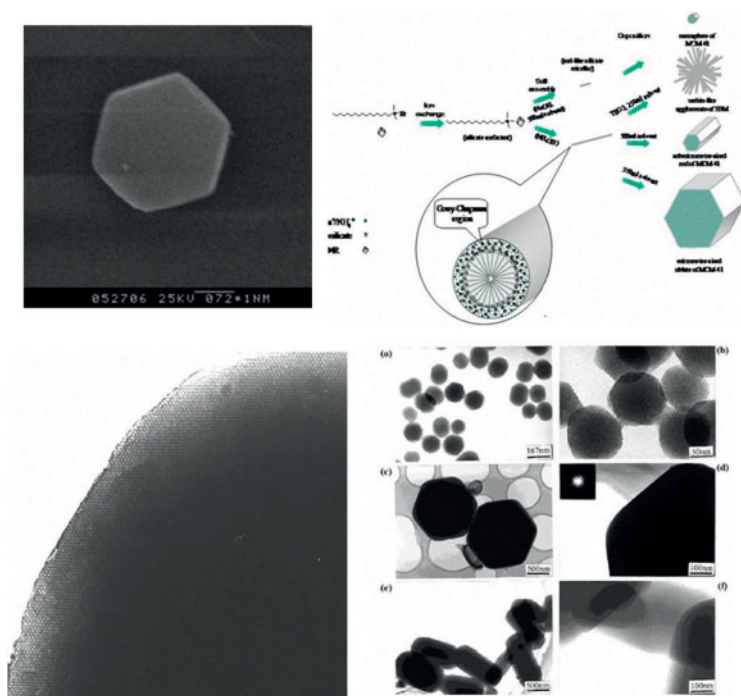
Figure 13.6 Upper left: SEM micrographs of calcined of MCM-41 (scale bar, 3700 nm); right figure, scheme of the morphology control in ammonia medium in extremely diluted system. Lower left: the high resolution TEM image of MCM-41 single crystal. Lower right: TEM image of the calcined materials: (a) nanometer MCM-41 (scale bar, 167 nm); (b) nanometer MCM-41 (scale bar, 50 nm); (c) MCM-41 single crystal (scale bar, 500 nm); (d) MCM-41 single crystal (scale bar, 100 nm); (e) submicrometer rod of MCM-41 (scale bar, 500 nm); (f) submicrometer rod of MCM-41 (scale bar, 100 nm). (Reprinted with permission from [29, 30])

In 1999, we found the optimal composition ratio to synthesize highly ordered MCM-41 in ammonia medium, in which the concentration of CTAB is 4.3 wt% [50, 51]. Recently, the MCM-41 single crystals can grow larger to nearly 10 μm via multiple-growth under the same condition, in extremely diluted ammonia solution. A novel crystal form of hexagonal circular bicone of MCM-41 crystal has been observed, which is the combination form of three hexagonal bipyramid and circular bicone forms [52–55]. In fact, there are still many unknowns about the crystal of MCM-41 and its prior growth habit. For a 2D mesoporous crystal, as a unit of its structure, rod-like micelles make it essentially different from traditional single crystals at the atomic scale of 2D/3D. Especially, certain characteristics of the building blocks are indefinite, for example, the d-spacing of the c-axis of the 2D single crystal is usually uncertain, which makes it possible for a change in crystallography. Generally, the traditional crystallography describes in detail crystal forms as the total 47 geometric forms including hexagonal prism forms, hexagonal bipyramid forms, etc., and combination forms which combine two or more geometric forms. This includes crystals composed of atoms or ions connected by chemical bonds. However, our study indicates that the morphology of a MCM-41 single crystal could be of the combination forms, in which a novel geometric form is different from those described in the traditional crystallography, as illustrated in the scheme of MCM-41 in Figure 13.7.

We also reported preparations of the nanosized mesoporous silica particles with sizes ranging from 10 nm to 60 nm and different pore structures in extremely dilute solutions [56]. By adjusting the concentrations of reactants, we can control the scale of mesoporous silica from 10 nm to 60 nm with different morphologies and pore structures. Compared to traditional methods, surfactant concentrations in our study were extremely low, 0.2 wt% at most. The morphology transformation of samples was observed when altering reactants' concentration, and a mechanism, based on self-assembly of monosilicate combined with surfactant molecular in extremely dilute solution, was proposed to interpret the formation process of nanosized mesoporous materials. It was suggested that the formation of the mesoporous silica nanoparticles could be attributed to the deposition of self-assembled silicate micelles.

The synthesis procedures of the typical preparation of MCM-41 mesoporous silica (MCM-41 MS) nanoparticles were as follows: (1) 3.5 ml of NaOH (2M) and 1 g CTAB were added into a certain volume of deionized water with strong stirring. The reaction temperature was kept about 70°C; (2) when the solution became homogeneous, 5 ml of TEOS was introduced to the resulted solution; (3) 2 h later, the reaction was terminated and the product was filtered and washed with deionized water, then dried at a temperature of about 100°C for 12 h, then calcinated in air for 4 h at 500°C.

In the diluted aqueous system, as shown in Figure 13.8, the different additive factor would lead to special preferred morphology. For example, the nanorod as well as nanofiber of MCM-41 could be synthesized by
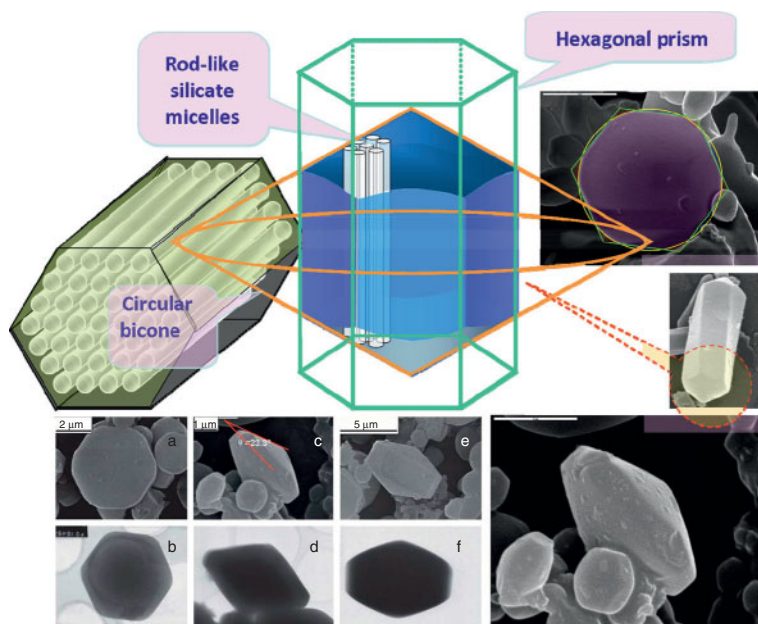
Figure 13.7 Upper left: structural schematic of MCM-41. The middle upper figure: a schematic illustration of MCM-41 single crystal morphology-hexagonal circular bicone-a combination form bounded by circular bicone faces and hexagonal prism faces. Upper right: SEM image of a larger MCM-41 single crystal the hexagonal feature is the view of a single crystal whose c-axis parallels the line of vision. Lower figure: the SEM and TEM images of the as-synthesized samples. (Reprinted with permission from [52–55])

adding Na^+ (sodium ions), K^+ (potassium ion), as well as vulcanization–silane, respectively. We find that if we change the adding factor (usually as certain ions such as Fe^{3+}, K^+, etc.), the morphologies of product can be controllably transformed from the MCM-single crystal to nanorod. And the MCM-41 with different size can be controlled by adjusting the alkalinity of the medium. Moreover, the morphology of the MCM-41 crystal can be controllably modulated through the addition of alkali salts in the synthetic system. Increasing the concentration of KCl can cause the aspect ratio and the conical angle to increase consistently, and the result displays monotonicity with a certain statistical deviation [57, 59].

Novel thiol-functionalized mesoporous silica nanorods or nanofibers can be controllably synthesized by adding of two assistant organoalkoxysilanes: 3-mercaptopropyl trimethoxysilane (MPTMS) and bis[3-(triethoxysilyl) propyl]tetrasulfide (TESPT) through a co-condensation method, in which TEOS were used as silica precursors simultaneously [61, 62]. Results show that the single-axis nanofibers with diameters of about 60–80 nm are obtained. The mesostructure of mesoporous silica nanofiber corresponds
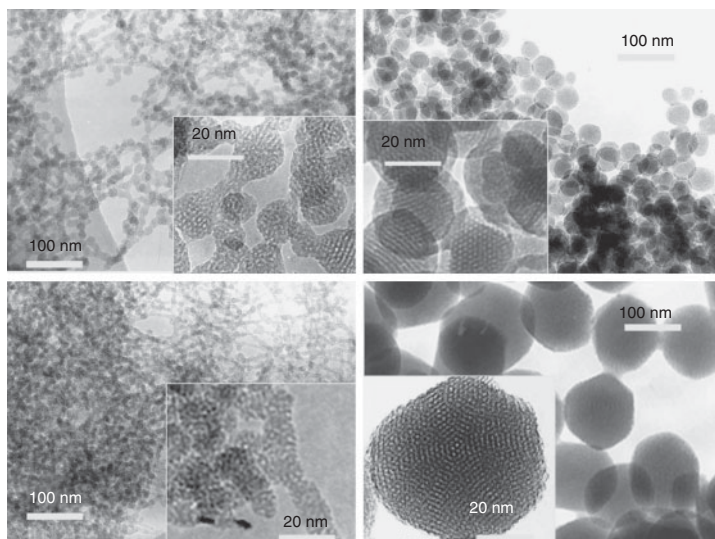
Figure 13.8 TEM images of the nanospherical MCM-41 silica with an average size of about 10 nm, 20 nm, 40 nm, 100 nm was produced through reaction of extremely low surfactant concentrations of CTAB with TEOS in the sodium hydroxide medium at 353 K. insert is the high resolution transmission electron microscopy (HRTEM) image of the sample. (Reprinted with permission from [56])

with that of MCM-41, and periodic mesopores fringes are 120 nm. The BET (Brunauer-Emmett-Teller model) specific surface area and BJH (Barrett-Joyner-Halenda model) pore size of the samples are 784 m^2 g^{-1} and 2.36 nm, respectively.

13.4.2.2   Ether-Water System: Mesoporous Vesicles

An oil-water, two-phase system is introduced in this section, the interface of the ether-water and the microemulsion can be as the template. In ether-water system, a series of vivid morphologies can be obtained, and the key point is using the unstable oil-water interface as the template. Because the ether is an oil phase with low boiling temperature, the interface of ether and water is easy to change. Various morphologies, such as radio-larian-like silica sphere with hollow inner, and so on, have been prepared. A radiolarian-like silica sphere has been prepared in a water-ether binary solvent system. The results indicate its particular morphology and hierarchical structure, i.e., hollow interior and a crust wherein two types of mesopores with radial orientation are located. This silica product embodies a novel morphosynthesis involving unstable water–oil interface [60].

In this system, six kinds of morphologies can be synthesized and have been classified. The TEM images of each kind of morphology can show that they are mesoporous silica vesicles, mesoporous silica particle (including
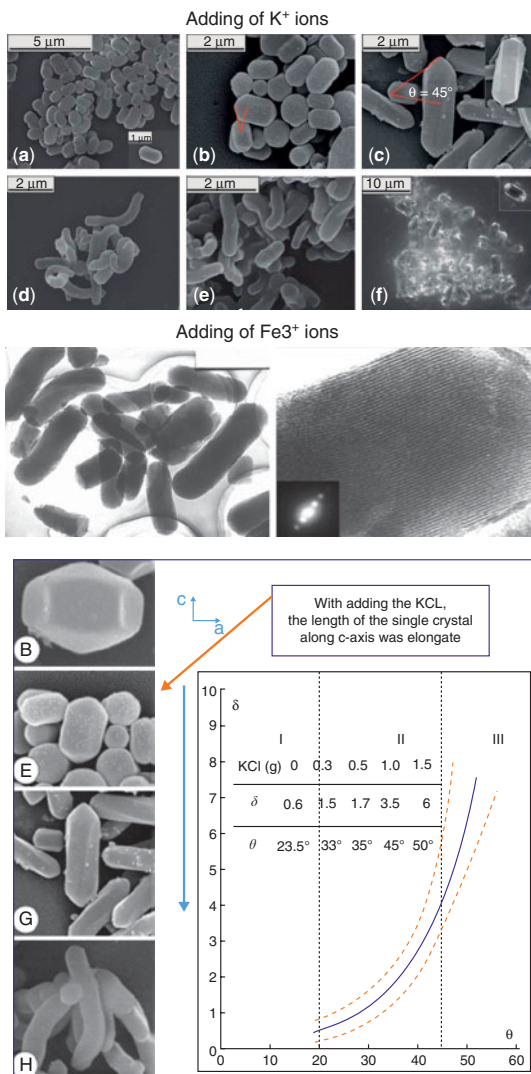
Figure 13.9 Upper left: SEM images of the as-synthesized samples. (a) the sample after adding 0.3 g KCl, (b) the sample after adding 0.5 g KCl, (c) the sample after adding 1.0 g KCl, (d) the sample after adding 1.5 g KCl, (e) the sample after adding 1.0 g NaCl. (f) POM images of the sample after adding 1.0 g KCl. Right figure: high resolution SEM images for MCM-41 single crystal morphology evolution by adding KCl and a conical angle (θ) vs aspect ratio (δ) diagram. By adding the KCl, the length of the single crystal along the c-axis elongated. The trend line (blue line) in the diagram shows the relationship between the conical angle (θ) and the aspect ratio (δ). Note: δ is the average aspect ratio (length/width) of the selected single crystals. θ is the average conical angle of the selected crystal faces except for the sample synthesized by adding 1.5 g of KCl, in which θ is the largest conical angle among all selected crystal faces. (Reprinted with permission from [--]) Lower left: TEM image of the submicrometer-sized rod of MCM-41 after adding 0.2g FeCl$_3$. (Reprinted with permission from [59])
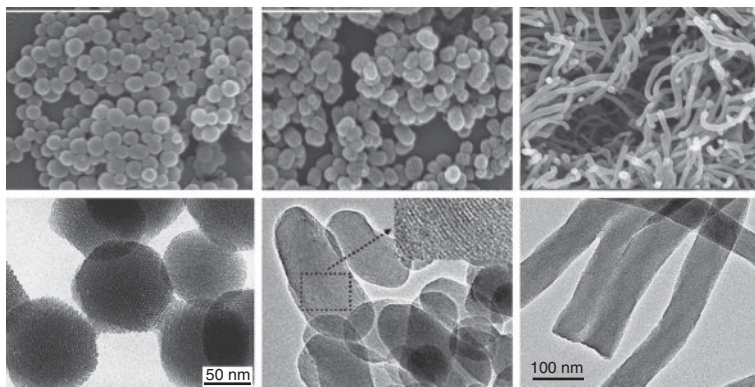
Figure 13.10 Top: SEM images of (a) nanosphere-like, (b) nonorod-like and (c) nanofiber-like morphology of MS. Scale bar: 1μm. Bottom: TEM image of (a) nanosphere-like. Scale bar: 100 nm (b) nonorod-like (inset: magnification image of the selected area) and (c) nanofiber-like. Scale bar: 100 nm. (Reprinted with permission from [61, 62])
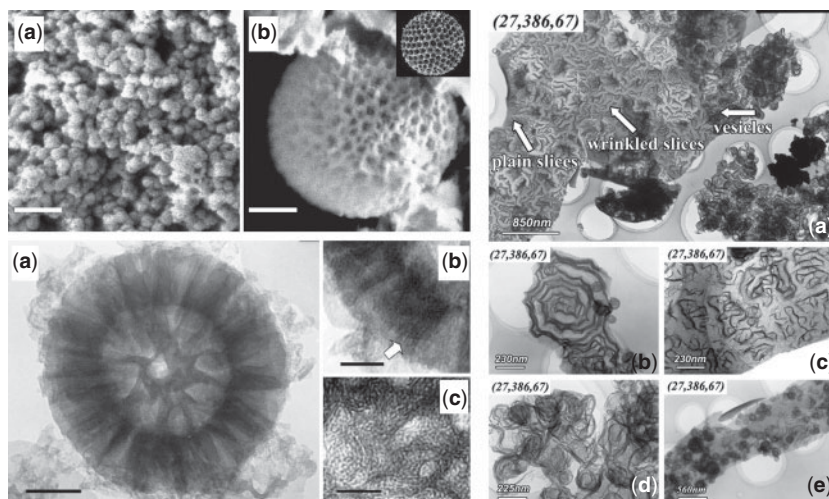
Figure 13.11 Upper left: SEM images of the calcined sample showing the morphology of sphere. (a) Overview morphology of the bulky spherical silica. Scale bar: 2 μm. (b) High magnification SEM image of one sphere exhibiting the radiolarian-like morphology. Scale bar: 290 nm. The inset image shows the silica skeleton of a radiolarian. Lower left: TEM images of the calcined silica sphere. (a) The circle-shaped projection of one sphere. Scale bar: 100 nm. (b) HRTEM reveals that the bundle-like pattern is composed of radial streaks with the oriented periodic distance of 4 nm. Scale bar: 60 nm. (c) The selective district HRTEM on the center of circle-shaped projection of sphere. Scale bar: 60 nm. (Reprinted with permission from [61, 62]) Right figure: overview of so-called "chemical snapshots," revealing the diversity in slices and vesicles (a) and also their intermediate morphologies shown in (b–e), respectively. The applied reaction ratios are shown between the brackets. (Reprinted with permission from [65])

320
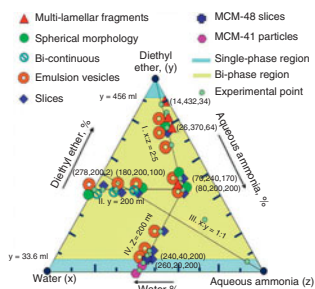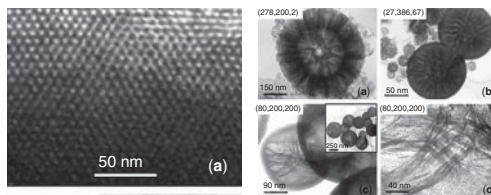
Figure 12.1
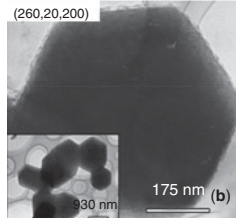
Figure 12.3
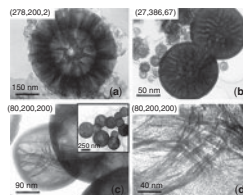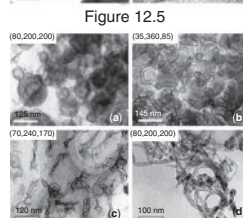
Figure 12.5

Figure 12.6

Figure 12.2
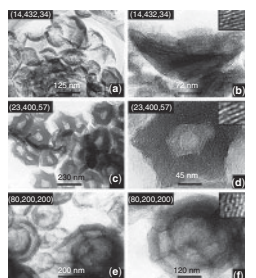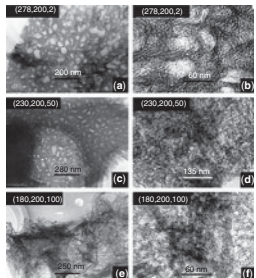
Figure 12.4

Figure 12.7

Figure 13.12 (Figure 12.1) The phase diagram of reaction: products obtained at varying reaction ratios of diethyl ether:water:aqueous ammonia. The points marked in the diagram represent the volumes of H_2O, $C_2H_5OC_2H_5$, $NH_3 \cdot H_2O$ (as x,y, z) of the initial experiments. Five typical structural features of multi-lamellar silica fragments examined by HRTEM formed at the indicated reaction ratios are shown between the brackets. (Figure 12.2) Highly ordered silica slices (MCM-48); (Figure 12.3) Regular particle-like (MCM-41) silicas; (Figure 12.4) multi-lamellar silica fragments; (Figure 12.5) spherical particles; (Figure 12.6) vesicle-like silicas; (Figure 12.7) bi-continuously emulsified silicas. (Reprinted with permission from [65])

MCM-48, or MCM-41), the radiolarian-like silica sphere as well as spherical mesoporous silica with hollow inner, slices, the fragments with lamellar mesostructure, and bicontinuous mesostructure [60].

13.4.2.3   Alcohol-Water System

Monodispersed silica spheres with uniform size are widely applied to fields including catalysts, bioseparation, and drug delivery, as well as high-performance liquid chromatography (HPLC) [66–70]. In 1998 Grün and Unger prepared mesoporous silica spheres based on Stöber's method
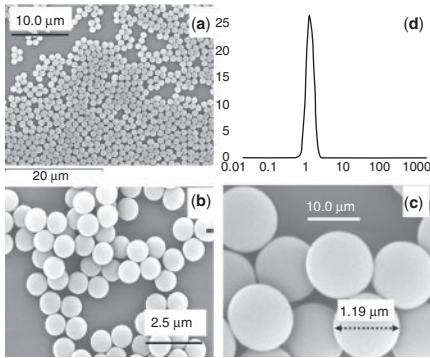
Figure 13.1
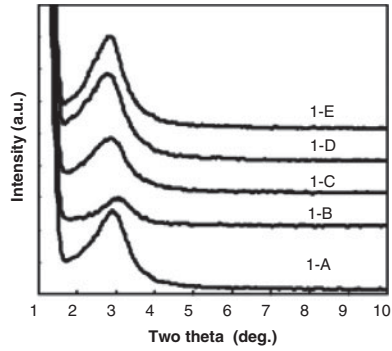
Figure 13.3
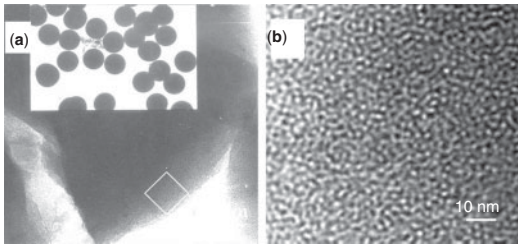
Figure 13.2
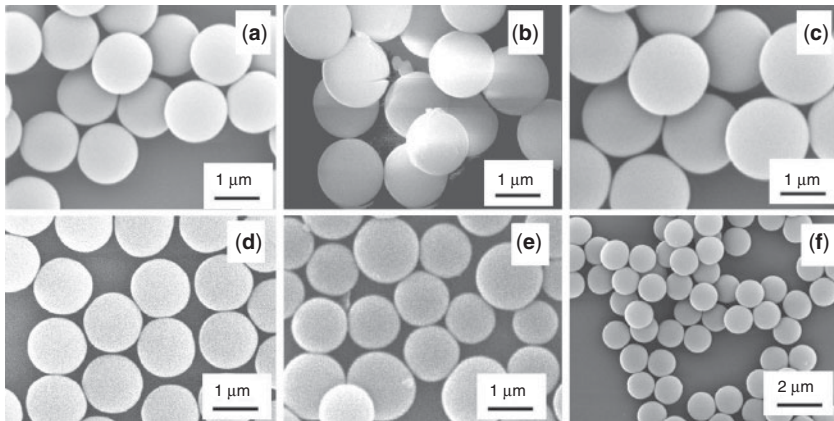
Figure 13.4

Figure 13.13 (Figure 13.1) (a–c) SEM image of sample 1-C with different magnification; (a) low resolution SEM image of sample 1-C, scale bar: 10 µm; (b) the medium magnification SEM images of sample 1-C, scale bar: 2.5 µm; (c) high resolution SEM image of sample 1-C, scale bar: 1.0 µm; the black dotted line ending with arrows shows the MMS diameter of sample 1-C; (d) GMA result of samples 1. (Figure 13.2) TEM images of sample 1-C. The scale bar: (a) 100 nm, (b) 10 nm. (Figure 13.3) X-ray diffraction patterns of MMS of samples. (Figure 13.4) (a~e)
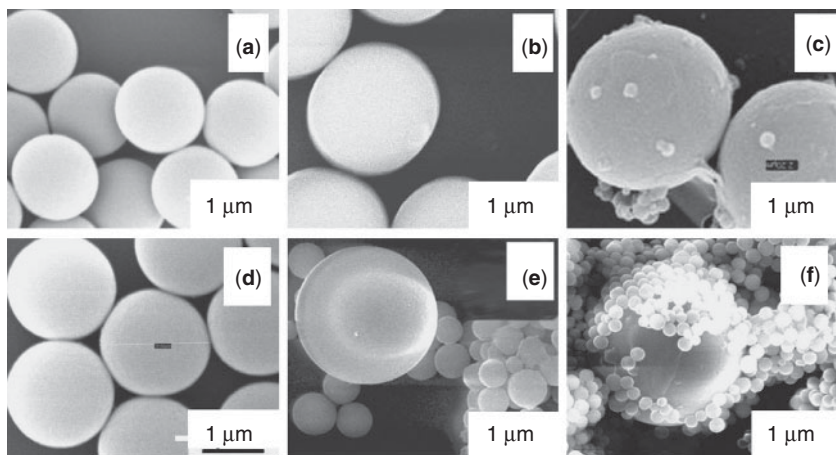
Figure 13.5

Figure 13.13 (Con.) The SEM image of MMS synthesized in which the effect on the morphologies in ternary surfactant system; (a–e) are the SEM images of samples 2-A, 2-B, 2-C, 2-D, 2-E respectively. The scale bar, a–e, 1 μm; (f) is the lower magnification SEM image of sample 2-C, the black: 5 μm. (Figure 13.5) a~f, The SEM image of MMS synthesized in binary surfactant system, in which the effect on the morphologies via changing the proportion of co-solvent is displayed; the scale bar: a–f, 1 μm Right: the plots of the size of the MMS to the co-solvent ratio. The scale bar: a–f, 1 μm. (Reprinted with permission from [73])

by adding alkyltrimethyl-ammonium bromide as templates to control porosity, and the spheres had large specific surface area and an average diameter of nearly 700 nm [71]. Comparatively, Stöber's method in alkaline medium is still a prior choice in the synthesis of the monodispersed and uniform porous spheres, but there are few reports about the study on the synthesis of the porous spheres with diameter above 1.0 μm using this approach. Yano and Fukushima have synthesized the monodispersed mesoporous silica (MMS) sphere with a size of about one micrometer by adding C_nTMACl (C_{18}TMACl, C_{16}TMACl, and C_{14}TMACl) as surfactants and TMOS as silica source in the alkaline medium with methanol and water as co-solvent, and this is already a breakthrough [72].

We will now introduce a one-step preparation of the MMS of silica with a uniform diameter above 1.0 μm by introducing a mixture of cationic surfactant and nonionic surfactant to sol precipitation [73]. The effects on the morphologies of the MMS were investigated by changing the proportion of the surfactant as well as that of the solvent, and the optimal condition for synthesis of the lager MMS in this system was found. A notable feature of the sphere is its large diameter and uniformity. The spheres obtained in CTAB\ dodecylamine (DDA) system have a diameter of nearly 1.20 μm,
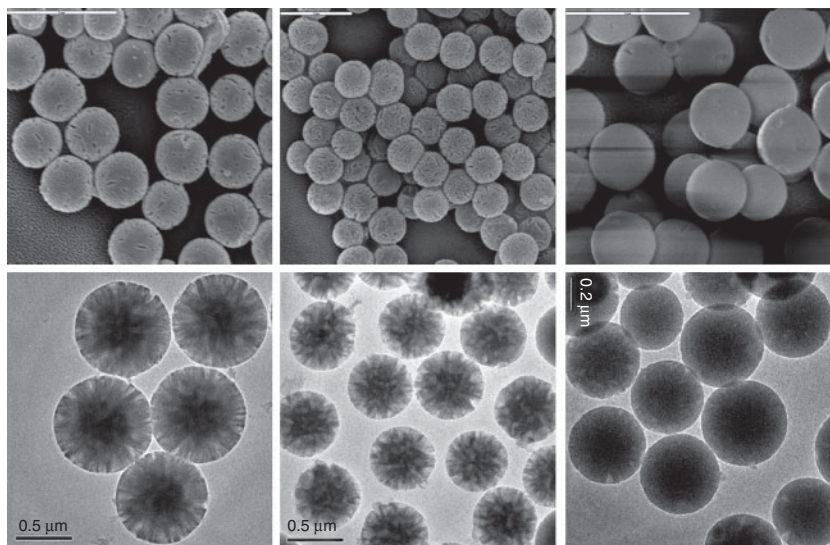
Figure 13.14 The SEM (upper) and TEM (lower) images of uniformed mesoporous silica beads with radical porous structure under water-alcohol-ether ternary system. From left to right, each figure shows the morphologies with different porous structure, which indicates that the ratio of solvent may influence it. (Reprinted with permission from [74])

with a pore size of about 2.0 nm and BET specific surface area around 726m^2/g. These spheres were then used as seeds for one-step growth by a semi-batch process plus surfactants, which could enlarge silica spheres up to 2.0 μm. Furthermore, the effects of initial synthetic condition on the morphology of MMS have been studied. It is found that the combination of surfactant could affect the morphologies of MMS. In binary surfactant system (CTAB+DDA), the diameter of the MMS of silica gradually increases with the increase of the proportion of CTAB/CTAB+DDA while keeping the other reagents constant. The cosolvent proportion also affects the morphologies of MMS of silica. With the increase of isopropanol/H$_2$O, the size of spheres decreases gradually, conglomeration disappears, and the monodispersity of the sphere turns as well, but many silica oligomers appear around large spheres or connect with the spheres.

13.5   Conclusion and Prospective

To sum up, we have addressed concepts from biomineralization to biomimic synthesis of mesoporous silica, and have summarized the recent achievements on its morphological control of mesoporous silica.

Mesoporous silica with its excellent microstructural plasticity could be a promising basic material in the future. Based on the current situation, it can be inferred that the future application of mesoporous silica might focus on drug delivery and control release, nanomachines, as well as hard templates of advanced assembly of nanostructured materials.

For drug delivery, although a lot of work indicates that MSN and mesoporous silica have an excellent biocompatibility and can be a wonderful drug carrier, the biosafety of MSN is an especially big pending problem or obstacle now. Without long-term clinical trial, metabolic pathways *in vivo* of MSN keeps being a serious obstacle for further application at present.

Nanomachines are also exciting, and the most probable exporter of future nanotechnology that set off in the world ten years before. Silicas can be the most suitable materials of the chassis of the nanomachine. In the future development of the nanomachine, mesoporous silica will be the basis of the support, and the supermolecular as well as advanced assembly of the hierarchical structure that is fabricated according to coding self-assembly is another key technique. That is the key point of future nanotechnology, and we need to learn from nature.

References

1. M.E. Davis. *Science* 305, 480 (2004).
2. S. Mann. *Angew. Chem. Int. Ed.* 39, 3392–3406 (2000).
3. S. Mann, J. Webb, R.J.P. Williams. *Biomineralization, Chemical and Biochemical Perspectives*. VCH Verlagsgesellschaft mbH, D-6940 Weinheim (Federal Republic of Germany).
4. N. Kröger, R. Deutzmann, M. Sumper. *Science* 286, 1129–1132 (1999).
5. S. Weiner. *On Biomineralization*. New York Oxford (1989).
6. G.D. Stucky. *Curr. Opin. Solid State Mater.* 1 (3) 425–429 (1996).
7. G.D. Stucky. *Nature* 368, (6469) 317–321 (1994).
8. R.A. van Santen, *et al. Curr. Opin. Solid State Mater.* 8 (2) 111–20 (2004).
9. S. Mann, *et al. Nature* 385 (6615) 420–423 (1997).
10. S. Mann. *Nature* 377 (6547) 320–323 (1995).
11. M. Sumper. *Science* 295, 5564, 2430–2433 (2002).
12. G.M. Whitesides and B. Grzybowski. Self-assembly at all scales. *Science* 295, 2418–2421 (2002).
13. R.C. Merkle. *Nanotechnology* 11, 89–99 (2000).
14. J.M. Lehn. Supramolecular chemistry. *Science* 260 (5115):1762–3 (1993).
15. J.-M. Lehn. *Supramolecular Chemistry*. Wiley-Vch 978-3-527-29311-7 (1995).
16. R. Hoppe, A. Ortlam, J. Rathousky, G. Schulz, E.A. Zukel. *Microporous Mater.* 8, 267–273 (1997).
17. Q.S. Huo, D.I. Margolese, U. Ciesla, D.G. Demuth, P.Y. Feng, T.E. Gier, P. Sieger, A. Firouzi, B.F. Chemlka, F. Schuth, G.D. Stucky. *Chem. Mater.* 6 (8) 1176 (1994).
18. M. Vallet-Regi, A. Rámila, R.P. del Real, J. Pérez-Pariente. *Chem. Mater.* 13, 308 (2001).

19. B. Muñoz, A. Rámila, J. Pérez-Pariente, I. Diaz, M. Vallet-Regi. *Chem. Mater.* 15, 500 (2003).

20. A. Rámila, B. Muñoz, J. Pérez-Pariente, M. Vallet-Regi. *J. Sol. Gel Sci. Technol.* 26, 1199 (2003).

21. M. Grun, A.A. Kurganov, S. Schacht, F. Schüth, K.K. Unger. *J. Chromatogr. A* 740, 1 (1996).

22. Y. Qiao, V.K. Punyamurtula, G.J. Xian, V.M. Karbhari, A. Han. *Appl. Phys. Lett.* 92, 063109 (2008).

23. A. Han, Y. Qiao. *J. Am. Chem. Soc.* 128, 10348 (2006).

24. M. Vallet-Regi, A. Ramila, R.P. del Real. *Chem. Mater.* 13, 308–311 (2001).

25. C.T. Kresge, M.E. Leonowicz, W.J. Roth, J.C. Vartuli, J.S. Beck. *Nature* 359, 710 (1992).

26. J.S. Beck, J.C. Vartuli, W.J. Roch, M.E. Leonowicz, C.T. Kresge, K.D. Schmitt, C.T.-W. Chu, D.H. Olson, E.W. Sheppard, S.B. McCulen, J.B. Higgins, J.L. Dchlenker. *J. Am. Chem. Soc.* 114, 10834 (1992).

27. R.R. Xu. *The Chemistry of Zeolite and Porous Materials* (Chinese Edition) (2004), Beijing, ISBN: 9787030127570.

28. Y.F. Lu, H.Y. Fan, A. Stump, T.L. Ward, T. Rieker, C.J. Brinker. *Nature* 398, 223 (1999).

29. Q. Cai, F.Z. Cui, X.H. Chen, Y. Zhang, Z.S. Luo. *Chem. Lett.* 9, 1044 (2000).

30. Q. Cai, Z.S. Luo, W.Q. Pang, Y.W. Fan, X.H. Chen, F.Z. Cui. *Chem. Mater.* 13, 258 (2001).

31. D.R. Radu, C.Y. Lai, K. Jeftinija, E.W. Rowe, S. Jeftinija, V.S.Y. Lin. *J. Am. Chem. Soc.* 126, 13216 (2004).

32. I. Slowing, B.G. Trewyn, V.S.Y. Lin. *J. Am. Chem. Soc.* 128, 14792 (2006).

33. S. Huh, H.T. Chen, J.W. Wiench, M. Pruski, V.S.Y. Lin. *J. Am. Chem. Soc.* 126, 1010 (2004).

34. D.R. Radu, C.Y. Lai, J.W. Wiench, M. Pruski, V.S.Y. Lin. *J. Am. Chem. Soc.* 126, 1640 (2004).

35. Y.S. Lin, C.P. Tsai, H.Y. Huang, C.T. Kuo, Y. Hung, D.M. Huang, Y.C. Chen, C.Y. Mou. *Chem. Mater.* 17, 4570 (2005).

36. M.C. Chao, H.P. Lin, C.Y. Mou, B.W. Cheng, C.F. Cheng. *Catal. Today* 97, 81 (2004).

37. K. Suzuki, K. Ikari, H. Imai. *J. Am. Chem. Soc.* 126, 462 (2004).

38. J.Y. Zheng, J.B. Pang, K.Y. Qiu, Y. Wei. *Microp. Mesop. Mater.* 49, 189 (2001).

39. J.H. Chang, C.H. Shim, B.J. Kim, Y. Shin, G.J. Exarhos, K.J. Kim. *Adv. Mater.* 17, 634–637 (2005).

40. C.Y. Lai, B.G. Trewyn, D.M. Jeftinija, K. Jeftinija, S.Xu, S. Jeftinija, V.S.Y. Lin. *J. Amer. Chem. Soc.* 125, 4451–4459 (2003).

41. I. Zink. *J. Am. Chem. Soc.* 132, 12690–12697 (2010).

42. J.Y. Ying, C.P. Mehnert, M.S. Wong. *Angew. Chem. Int. Ed.* 38, 56 (1999).

43. N.K. Raman, M.T. Anderson, C.J. Brinker. *Chem. Mater.* 8 1682, (1996).

44. I. Soten, G.A. Ozin. Assembly and mineralization processes in biomineralization. In *Supramolecular Organization and Materials Design*, W. Jones, C.N.R. Rao (Eds.), p. 34, Cambridge University Press, Cambridge (2002).

45. B.J. Pang, K.Y. Qiu, Y. Wei, X.-J. Lei, Z.F. Liu. *Chem. Comm.* 6, 477 (2000).

46. B.J. Pang, K.Y. Qiu, Y. Wei. *Chem. Mater.* 14, 2361 (2001). 8 (1996).

47. C.C. Pantazis, P.N. Trikalitis, P.J. Pomonis, M.J. Hudson. *Microp. Mesop. Mater.* 66, 37 (2003).
48. S.E. Park, D.S. Kim, J.S. Chang, W.Y. Kim. Synthesis of MCM-41 using microwave heating with ethylene glycol. *Catalysis Today* 44(1–4), 301 (1998).
49. C.G. Wu, T. Bein. Microwave synthesis of molecular sieve MCM-41. *Chem. Comm.* 8, 925 (1996).
50. M.J. MacLachlan, N. Coombs, G.A. Ozin. *Nature* 397, 681–684 (1999).
51. J. Lee, S. Yoon, T. Hyeon, S. M. Oh, K. B. Kim. *Chem. Commun.* 1999, 2177–2178.
52. S. A. Bagshaw, E. Prouzet, T.J. Pinnavaia. *Science* 269, 1242 (1995).
53. E. Prouzet, T.J. Pinnavaia. *Angew. Chem. Int. Ed. Engl.* 36, 516 (1997).
54. C.G. Göltner, M. Antonietti. *Adv. Mater.* 9, 431 (1997).
55. M. Antonietti, C. Göltner. *Angew. Chem. Int. Ed. Engl.* 36, 910 (1997).
56. Q. Cai, W.Y. Lin, F.S. Xiao, W.Q. Pang, X.H. Chen, B.S. Zou, *Microp. Mesop. Mater.* 32(1–2), 1–15 (1999).
57. J.J. Qi, B. Qin, J. Liu, Q. Cai. *Cryst. Eng. Comm.* 13, 4666–4675 (2011).
58. Y.T. Shi, H.Y. Cheng, Y. Geng, H.M. Nan, W. Chen, Q. Cai, B.H. Chen, X.D. Sun, Y.W. Yao, H.D. Li. *Mater. Chem. Phys.* 120, 193–198 (2010).
59. J.J. Qi, H.M. Nan, D.Y. Xu, Q. Cai. *Cryst. Growth. Des.* 11, 910–915 (2011).
60. Y. Geng. *Arch. Bioceram. Res.* 5, 306–310 (2005).
61. X. Chen, *Front. Mater. Sci.* 6(3), 278–282 (2012).
62. X. Chen, *Chem. J. Chin. Univ.* 33(8), 1643–1645 (2012).
63. H.X. Lin, K. Cui, Y.W. Yao, Q. Cai, Q.L. Feng, H.D. Li. *Chem. Lett.* 34(7), 918 (2005).
64. K. Cui, Q. Cai, X.H. Chen, Q.L. Feng, H.D. Li. *Microp. Mesop. Mater.* 68 (1–3), 61–64 (2004).
65. Q. Cai, Y. Geng, X. Zhao, K. Cui, Q.Y. Sun, X.H. Chen, Q.L. Feng, H.D. Li, E.G. Vrieling. *Microp. Mesop. Mater.* 108(1–3), 123–135 (2008).
66. C. Boissière, M. Kummel, M. Persin, A. Larbot, and E. Prouzet. *Adv. Funct. Mater.* 11, 129 (2001).
67. K.W. Gallis, J.T. Araujo, K.J. Duff, J.G. Moore, and C.C. Landry. *Adv. Mater.* 11, 1452 (1999).
68. M. Grün, A.A. Kurganov, S. Schacht, F. Schüth, and K.K. Unger. *J. Chromatogr. A* 740, 1 (1996).
69. T. Nassivera, A.G. Eklund, and C.C. Landry. *J. Chromatogr. A* 973, 97 (2002).
70. W. Stöber and A. Fink. *J. Colloid. and Interface Sci.* 26, 62 (1968).
71. M. Grün, K.K. Unger, A. Matsumoto and K. Tsutsumi. *Microp. Mesop. Mater.* 27, 207 (1999).
72. K. Yano, Y. Fukushima. *J. Mater. Chem.* 14, 1579 (2004).
73. J.Q. Qiu, X. Zhao, M.C. Jin, Q. Cai, H.D. Li. *J. Inorg. Mater.* 21 (3), 558–564 (2006).
74. J.J. Qi, Q. Cai, unpublished data.

Biomimetic Materials for Engineering Stem Cells and Tissues

**Kaarunya Sampathkumar[1], Azadeh Seidi[2], Alok Srivastava[1],
T.S. Sampath Kumar[3], Seeram Ramakrishna[4,5] and Murugan Ramalingam[1,6,7,*]**

*[1]Centre for Stem Cell Research (CSCR), (A unit of Institute for Stem
Cell Biology and Regenerative Medicine, Bengaluru) Christian Medical
College Campus, Vellore, India
[2]Technology Center, Okinawa Institute of Science and Technology (OIST),
Onna-son, Okinawa, Japan
[3]Department of Metallurgical and Materials Engineering, Indian Institute of
Technology Madras (IITM), Chennai, India
[4]Center for Nanofibers and Nanotechnology, Faculty of Engineering,
National University of Singapore(NUS), Singapore, Singapore
5Department of Biomedical Engineering, Jinan University,
Guangzhou, China
[6] National Institute of Health and Medical Research UMR977, Faculty of
Dental Surgery, University of Strasbourg, Strasbourg, France
[7]WPI-Advanced Institute for Materials Research (WPI-AIMR),
Tohoku University, Sendai, Japan*

Abstract

The concept of tissue engineering involves the use of cells, scaffolds and other bio-molecular factors for the development of biological tissue alternates for medical needs. Recently, stem cells have been found to be an attractive source for building tissues or organs in the laboratory due their ability to differentiate into tissue-specific lineages. Scaffolds serve as a temporary structural support for the cells to grow in a defined environment and are essential in particular when culturing anchorage-dependent cell lineages. Traditionally, scaffolds for tissue engineering applications were mostly developed from bioinert materials that only provided physical support to the cells. Later, bioactive materials were introduced that stimulated biological processes in addition to serving as a supporting matrix. However, synthetic tissue grafting techniques have not progressed to the level where it

*Corresponding author: rmurug2000@gmail.com

could be used clinically. For example, only a very few tissue engineered products are clinically available since the evolution of tissue engineering. Advances in the development of biomaterials and technology have led to the introduction of new concepts, biomimetics for instance, in tissue engineering approaches in recent days. Biomimetically-developed materials (also called biomimetic materials) could mimic the features of the native extracellular matrix (ECM) suitable for tissue culture, resulting in better cell-material interaction, cell-cell communication and specific tissue organization. Such biomimetic materials can also be used to manipulate the stem cells to control or regulate the cellular functions depending on the needs of the tissue to be engineered. Keeping these points in mind, the main focus of this chapter is to introduce the concept of biomimetic engineering of scaffolds to manipulate stem cells for their use in tissue engineering. The methods of fabrication of biomimetic materials and the surface modification of these materials for better cellular recognition are also discussed.

Keywords: Biomimetic, scaffold, microenvironment, stem cell, tissue engineering

14.1   Introduction

Tissue engineering is an interdisciplinary field of biomedical applied research that involves the combined use of cells and scaffolds, made of biomaterials, to aid in the regeneration of tissues which lack self-regenerating ability, and in the repair of tissues that are severely injured or damaged [1]. The scaffold, by definition, is a temporary supporting structure that helps grow cells and tissues under the laboratory conditions. It is also called synthetic extracellular matrix (ECM) as it plays a key role in supporting the cells to accommodate them. These cells then undergo proliferation, migration, and differentiation in three dimensions in a defined microenvironment, which eventually leads to the formation of a specific tissue with appropriate physiological functions as found in the host tissue. The objective of scaffold design is to create a structure that could mimic the native ECM until cells seeded onto the scaffold and/or those cells derived from the host tissue can synthesize its own matrix proteins. The general properties necessary for the synthetic scaffold include biocompatibility, biodegradability, biointeractiveness and processability. The scaffold should also possess some specific properties depending on the tissue microenvironment it is designed to repair and regenerate. The tissue microenvironment is comprised of a complex mixture of ECM molecules, soluble factors, nonsoluble factors, and other cell types. It is known that the microenvironment of cells is critical for maintaining their normal function. Modulating the cellular microenvironment to regulate cell behavior such as the cell–material interaction is therefore of great importance to enable a defined biological activity.

Extensive research has been directed towards the development of ideal tissue grafts for many tissues such as skin, cartilage, bone, blood vessel,

heart, nerve, liver, etc. But only a few successful tissue grafts have been developed so far for clinical use. For example, Apligraf® was the first tissue engineered skin substitute approved by the US Food and Drug Administration (FDA). Studies on synthetic scaffolds seeded with specialized cells have proved the ability of the scaffold to aid in adhesion, proliferation, migration, orientation and continued functions of the cells [2, 3]. Recently the focus has shifted from using specialized cells to stem cells that have the ability to self-renew indefinitely and differentiate into specialized cells with the right cues [4]. In order to study the behavior of stem cells on synthetic scaffolds and to develop an ideal tissue graft, there still remain many properties of the scaffold that need to be optimized. Hence it is important to engineer the properties of the synthetic scaffold such that it would mimic the native microenvironment of the host tissue that is to be repaired. For example, biomineralization is a biological process that involves the nucleation and growth of minerals within a matrix of bone ECM proteins during bone remodeling [5]. To mimic the process of biomineralization, scaffolds comprised of collagen and hydroxyapatite (HA) have been developed for bone applications [3, 6–8].

The concept of biomimetics to engineer stem cells and tissues would be the convenient way to come up with a successful graft, as it involves simulating their native microenvironment, thereby supporting cellular functions and tissue regeneration. Biomimetics is a bottom-up approach that involves engineering of tissue building blocks, assembling them into complex tissue analogs, and the creation of tissue engineered organs. The purpose of the bottom-up tissue engineering approach is to accurately determine the localization of the biological components of corresponding tissue or organ, and to understand the mechanism of their biological functional process and the complex signaling pathways underlying tissue organization. In this way, it would be possible to engineer the stem cells and tissues to develop a successful tissue graft. Of particular interest, impact of stem cell behaviors such as adhesion, proliferation, migration, and differentiation onto the biomimetically-developed nanofiber scaffolds will be discussed in this chapter in the context of tissue engineering and regeneration. The methods of fabrication of biomimetic materials and the surface modification of these materials for better cellular recognition are also discussed.

14.2   Fabrication of Biomimetic Materials

For stem cells and tissue engineering applications, fabrication of biomimetic materials, in other words the scaffolds, involve the mimicking of native ECM in terms of all structural and functional features that support the cell growth and function. Such biomimetic scaffolds should be porous, possess the required mechanical stability, should be suitably

functionalized and possess a large surface area with structural features as present *in vivo* [9]. Many attempts have been made to fabricate the scaffolds for tissue engineering applications but none fulfill all the requirements of an engineered physiologically functional tissue. Therefore development of biomimetic materials is of great importance. Biomimetic scaffolds can be made up of hydrogels, nanofibers, porous materials, proteins and other biomolecules. Most of the proteins making up the ECM exhibit abundant nanometer-scale structures such as fibrils, ridges, grooves, pillars and pits that are hypothesized to contribute to cell-matrix signaling [10]. Nanotopography is also present in individual ECM molecules, such as collagen molecules, which are approximately 300 nm long and 1.5 nm wide. These molecules can form fibrils that extend for tens of micrometers in length and have diameters between 260 and 410 nm. In order to mimic the native ECM, it is therefore necessary to fabricate nanofiber scaffolds for most of the cell and tissue engineering applications [11]. In the following section, we further focus on biomimetic nanofibers developed through widely used techniques such as electrospinning, electrospray, phase separation and self-assembly.

14.2.1   Electrospinning

Electrospinning is the technique that is practiced most frequently for making nanofiber scaffolds. The basic equipment setup includes a syringe pump, fiber collector, and a high-voltage power system as shown in Figure 14.1. When a polymer solution is forced through a capillary hole, it forms a drop at the needle tip due to surface tension. A high voltage is
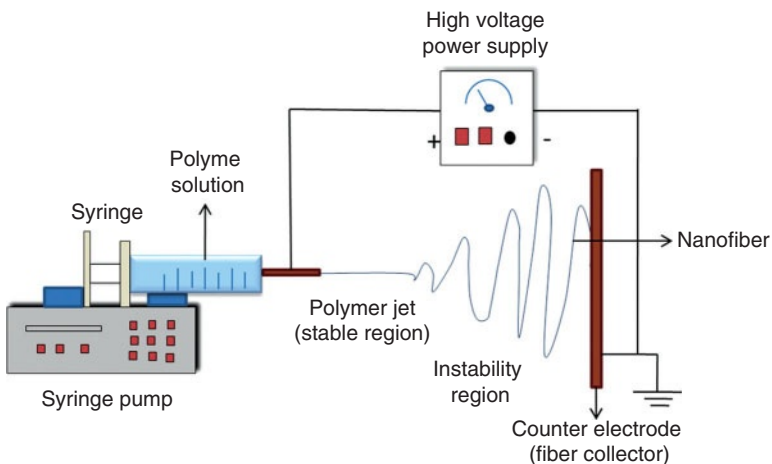
Figure 14.1 Schematic representation of electrospinning setup.

applied between the tip and grounded collector. As voltage is applied, the charges get accumulated on the droplet, which elongates into conical shape called Taylor cone. When the electric field strength overcomes the surface tension of the droplet, a polymeric jet is initiated from the Taylor cone and is accelerated towards the grounded collector. As the jet travels through the air, the solvent evaporates and the polymer jet simultaneously elongates, leading to the deposition of fibers on the collector.

Zhang *et al.* fabricated a method for biomimetic fabrication of HA/chitosan nanocomposites in which the nanocomposite, containing uniformly dispersed HA in chitosan, was electrospun using ultra-high molecular weight poly(ethylene oxide) (UHMWPEO) as an additive. By this method, they obtained biomimetic nanofibers of about 200 nm [3]. Choi *et al.* have fabricated electrospun gelatin nanofibers that were subject to biomimetic mineralization to develop a gelatin/CaP composite nanofibrous scaffold [12]. Gelatin nanofibers containing Ca^{2+} ions showed better adsorption of HA layer than gelatin nanofibers containing PO_4^{3-} ions. The hydroxyapatite layer formed consisted of nanosheets self-assembled to form three-dimensional structures after immersion for 48 hrs in simulated body fluid. The authors concluded that the type of ion included in the gelatin nanofiber strongly influenced the biomimetic mineralization process.

14.2.2   Electrospraying

Electrospraying is a process similar in concept to electrospinning, but the morphology of the polymer scaffold, i.e., droplets or fibers, depends on the parameters during electrospraying such as concentration of the polymer, flow rate of the polymer, the applied voltage and tip to target distance [13]. Hong *et al.* have developed an electrosprayed three-dimensional nanofiber scaffold and tested the same for the culture of human foreskin fibroblast (HFF-1) cells [14]. They demonstrated successful cell attachment and spreading on the scaffold because of the increased pore size of the electrosprayed nanofiber scaffold. Gupta *et al.* have fabricated a nanostructured scaffold by electrospraying of HA nanoparticles on electrospun poly(L-lactic acid)-co-poly(3-capro-lactone)/gelatin nanofibers [15]. Electrospraying of HA imparted surface roughness to the scaffold that enabled the successful adhesion and proliferation of human fetal osteoblast cells (hFOB). As a biomimetic approach to ECM, electrosprayed nano HA on electrospun gelatin scaffolds has also been developed [16]. The scaffold showed better adhesion and proliferation of hFOB and better mineralization. Some works also describe the electrospraying of cells onto electrospun polymer scaffolds to aid in better cellular infiltration of the scaffold [17, 18]. For example, Paletta *et al.* demonstrated the successful proliferation of electrosprayed MG63 cells on electrospun PLLA or PLLA/Col blend scaffolds [18]. Thus electrospraying could be used to fabricate

nanofiber scaffolds or for modification of electrospun nanofiber matrix surface with nanoparticles, as an attempt to mimic the native microenvironment of the tissue being repaired.

14.2.3   Phase Separation

Phase separation is a simple technique for the manufacture of nanofiber scaffolds, which involves various key processing steps such as polymer dissolution followed by simultaneous phase separation and gelation. Finally the solvent is removed and the scaffold is either freeze-dried or the porogens are removed, resulting in porous scaffold as in Figure 14.2. Taboas *et al.* have fabricated biomimetic scaffold with local and global pores using solid free-form fabrication [19]. They have used an image-based design (IBD) method to design the scaffold that mimics the external shape and the internal porous architecture of the bone. They fabricated 8 mm diameter by 8mm height cylindrical molds with interconnected pores. Polylactic acid (PLA) in chloroform was then cast into the mold and solvent was evaporated under atmospheric pressure to create global pores in the scaffold. For a local porous structure, the above process was repeated with sodium chloride as the porogen. In a similar method of fabrication by Hacker *et al.*, porous scaffolds with interconnected pores were fabricated using particulate leaching with paraffin microparticles as the porogens [20]. The method involves the concomitant extraction of the porogen and polymer precipitation in warm n-hexane. These reports, and other studies, indicate that scaffolds that mimic the biological system in terms of porosity can be fabricated using phase separation.

14.2.4   Self-Assembly

The process of self-assembly involves the spontaneous organization of individual components to obtain an ordered structure. These individual components are held by the synergistic interactions of weak noncovalent forces like hydrogen bonding, ionic bonding, hydrophilic, hydrophobic
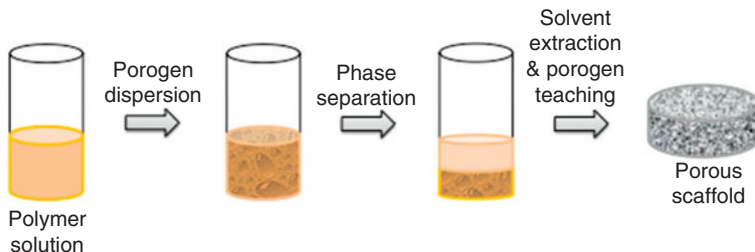
Figure 14.2 Schematic illustration of steps involved in phase separation.

and Van der Waals force interactions. Liao *et al.* demonstrated the self-assembly of calcified collagen to form a nanostructured collagen/HA scaffold [21]. The mineralized layer formed was similar to that on bone, showing potential for the system to help in bone regeneration. Peptide amphiphiles (PA), that consist of a hydrophilic head group and a hydrophobic tail group and readily self-assemble in aqueous solutions in a bottom up manner to form nanofibers, are being studied extensively [22, 23]. Further, ECM peptide sequences have been added to the individual components of PA. The nanofibers hence formed, are ECM-mimic and they guide the adhesion, migration, orientation, proliferation and differentiation of cells onto the nanofibers [24]. Such biomimetic nanofibers have the potential to be used as biomaterial surface coatings [25].

Anderson *et al.* have fabricated PAs that self-assembled into nanofiber matrices with layers stacked one on top of another on glass cover slides [24]. The nanofibers expressed ligands such as RGD, thereby mimicking the native ECM. The biomimetic scaffold was shown to promote osteogenic differentiation of human mesenchymal stem cells (hMSC). Mata *et al.* have demonstrated the successful biomineralization of self-assembled PAs incorporated with phosphoserine. The as formed scaffolds were tested *in vivo* and showed successful nucleation of hydroxyapatite, leading to biomineralization and bone formation [26]. In order to increase the bioactivity of electrospun polycaprolactone (PCL) fibers, Tambralli *et al.* allowed PA with biomimetic cell adhesion ligands to self-assemble on the electrospun PCL matrix [27]. The modified scaffolds have been demonstrated to better enhance adhesion and proliferation of hMSC when compared to unmodified PCL nanofibers.

14.3   Surface Modification

When biomaterials are exposed to biological environments, the ECM proteins interact with them, followed by indirect interaction of cells through the proteins [28]. In contrast, biomimetic materials are designed in such a way that they interact directly with the cells leading to new tissue formation. This is achieved by modification of the biomaterial surface with signaling peptides or peptide sequences that induce cellular responses. The earliest attempts to modify biomaterial surface involved surface modification with ECM proteins such as vitronectin, laminin and fibronectin [29]. The disadvantage of immobilizing proteins to the surface is that they might fold during adsorption and the receptor sites are not available for cell binding. Ranieri *et al.* have fabricated biomaterial surfaces immobilized with peptide sequences such as RGD, YIGSR, IKVAV and REDV, that have shown better cell adhesion [30]. Most of the surface modifications involve the use of a bifunctional crosslinker that utilizes the functional

group on the polymer and the protein for attachment [31]. In an attempt to mimic the adhesive nature of mussel pads, Yang *et al.* developed dopamine-coated polystyrene (PS) or poly(lactic-co-glycolic acid) (PLGA) substrates that could be used to adhere growth factors and peptides suitable for neural stem cell culture [32]. They showed that such biomimetically modified substrates could be used for therapeutic applications of human neural stem cells. Schematic of such a biomimetic surface modification is shown in Figure 14.3. Liu *et al.* have shown that the surface of poly l-lactic acid (PLLA) nanofiber scaffold could be modified with gelatin [33]. The nanofiber scaffold is immersed in solvent along with gelatin. The pores in the scaffold swell in the solvent and these sites are occupied by gelatin. When the PLLA scaffold whose surface is modified with gelatin is immersed in nonsolvent, the pores solidify resulting in entrapment of gelatin. In a radical approach to make the surface of metal implants biomimetic, Ravichandran *et al.* modified the surface of titanium disks using PLGA or PLGA/collagen nanofibers coated with nano-hydroxyapatite (n-HA) as in Figure 14.4 [34]. The surface modification promoted the adhesion, proliferation, migration, orientation, differentiation of hMSC on the scaffold resulting in the biomineralization of the PLGA collagen n-HA scaffold. Their results proved that biomimetic surface modification of Ti
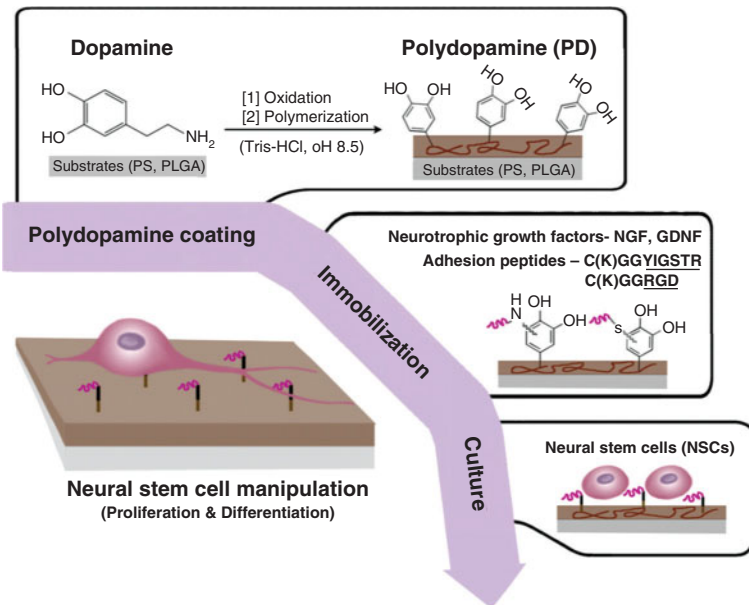
Figure 14.3 Schematic illustration of the polydopamine mediated immobilization of bioactive molecules (ECM-derived adhesion peptides and neurotrophic growth factors). Reprinted with permission from ref. [32]. Copyright (2012) Elsevier [32].
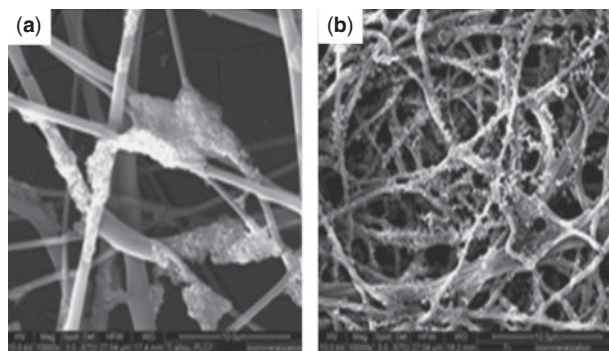
Figure 14.4 Surface Modification of (a) PLGA and (b) PLGA/collagen nanofibers deposited on titanium disks with n-HA. Reprinted with permission from ref. [34],IOP Publishing.

implants imparts osteo integration property to the surface. Thus biomimetic self-assembled scaffolds that are ECM-mimic can be fabricated and the design of building blocks that spontaneously assemble to form biomimetic nanofibers continue to be the key challenge.

14.4 Engineering Stem Cells and Tissues

Having stressed the importance of biomimetic scaffolds to engineer stem cells and tissues in the earlier topics, some of the works aimed at developing such biomimetic scaffolds are discussed further in this section. Reported results reiterate the ability of such biomimetic scaffolds that have resulted in the successful proliferation of tissue specific cells or in the differentiation of stem cells into desired cell types. With the increasing rate of cardiovascular diseases, the serious complications that follow, and the inability of cardiomyocytes to regenerate, there is a demand for a gold standard in the treatment of cardiovascular diseases [35]. Hence the development of biomimetic cardiovascular grafts with functional cardiomyocytes is being studied extensively. This development of a biomimetic scaffold relies on the understanding of the anatomical structure and the biological function of blood vessels [28]. Electrospun polymer nanofibers can be used as heart muscle patches or as blood vessel grafts. Bursac *et al.* have shown that neonatal rat ventricular cells cultured on polymeric scaffolds differentiated into cardiac myocytes after 1 week culture in bioreactors [2]. Cultivation in rotating bioreactors promotes maintenance of cardiac myocyte electrophysiology and molecular properties. In another study, Kofidis *et al.* have shown the uniform distribution and embedding of neonatal rat cardiomyocytes within a three-dimensional collagen matrix. The artificial matrix continued to contract rhythmically for 13 weeks [36]. Zimmermann *et al.*

developed an engineered heart tissue (EHT) which was a highly differentiated and strongly contracting construct of a mixture of type I collagen, other ECM proteins and freshly isolated heart cells. EHT simulated the contractions of heart when tested using a stretching device [37].

In the case of nerve grafts, failure of autologous graft and their inability to bridge gaps greater than 10 mm, calls for the design of biomimetic neural scaffolds to repair damage to the peripheral nervous system. This involves fabricating biomimetic scaffolds that provide biological cues for the specific interactions with neural tissues [38]. Prabhakaran *et al.* fabricated poly(l-lactic acid)-co-poly-(3-caprolactone)/Collagen (PLCL/Coll) nanofiber scaffolds by electrospinning [39]. These scaffolds demonstrated the ability to aid in the differentiation of bone marrow mesenchymal stem cells into neuronal cells when cultured in the presence of neuronal inducing factors like nerve growth factor and epidermal growth factor as in Figure 14.5. The cultured cells showed multipolar elongations similar to neuronal morphology and this was confirmed by immuno-fluorescent microscopy.

Uebersax *et al.* have fabricated silk fibroin scaffold that was designed to guide differentiation of hMSC into trabecular- or cortical-like mineralized networks [40]. Grayson *et al.* showed that fully decellularized bone provided biomimetic topography, composition, and mechanical properties for osteogenic differentiation of hMSC [41]. In another study, as a biomimetic approach to mimic interface tissue, Ramalingam *et al.* developed gradients of amorphous calcium phosphate nanoparticles (nACP) in electrospun PCL nanofibers. The authors cultured osteogenic cells on this scaffold and proved that the gradients in the biomimetic scaffold facilitated the cultured cells to adhere and proliferate as in the biological system [42].

Oliveira *et al.* fabricated hydroxyapatite/chitosan (HA/CS) bilayered scaffolds to study the proliferation of goat marrow stromal cells (GBMCs)
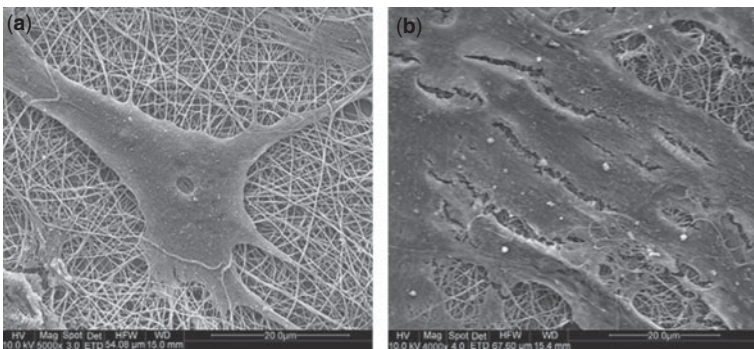
Figure 14.5 SEM images of (a) MSCs induced to neuronal cells, grown using neuronal induction media and (b) undifferentiated MSCs on electrospun PLCL/Coll nanofibers grown using MSC growth media. Reprinted with permission from ref. [39]. Copyright (2009) Elsevier [39].

on the scaffolds [43]. GBMCs adhered, proliferated and showed osteogenic differentiation on the scaffold. This was confirmed after 14 days of culture in osteogenic medium by alkaline phosphatase activity and immunohisto-chemistry assays. The cells differentiated into chondrocytes after 21 days of culture in chondrogenic medium. Their results indicated that bilayered HA/CS scaffolds can be used for repair of osteochondral defects.

Zhang *et al.* cultured human fetal osteoblast cells (hFOB) on electrospun HA/CS nanocomposite scaffold. The cultured cells showed better cell proliferation and mineral deposition than those cells cultured on plain chitosan scaffolds as in Figure 14.6. This is attributed to the osteoconductive
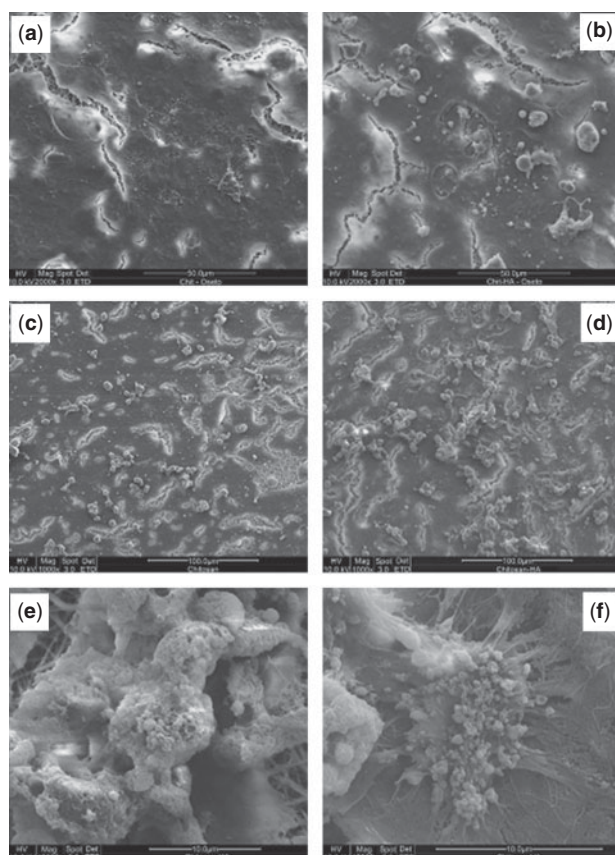
Figure 14.6 Mineral depositions of hFOB on the electrospun nanofibrous scaffolds: CTS, day 10 (a) and day 15 (c); HAp/CTS, day 10 (b) and day 15 (d); apatite-like morphology of deposit at higher magnification (e); visible tiny globular minerals and collagen bundles associated with a single hFOB cell viewed at higher magnification (f). Reprinted with permission from ref. [3]. Copyright (2008) Elsevier.
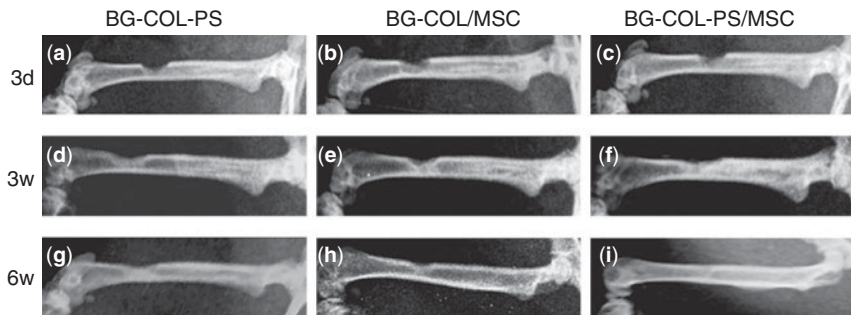
Figure 14.7 X-ray photograph of rat femur defects treated with scaffolds or scaffold/MSC constructs at 3 days, 3 weeks, and 6 weeks post surgery. BG-COL-PS/MSC-treated femurs exhibited the highest degree of healing from week 3 to week 6. Reprinted with permission from ref. [44]. Copyright (2010) Elsevier.
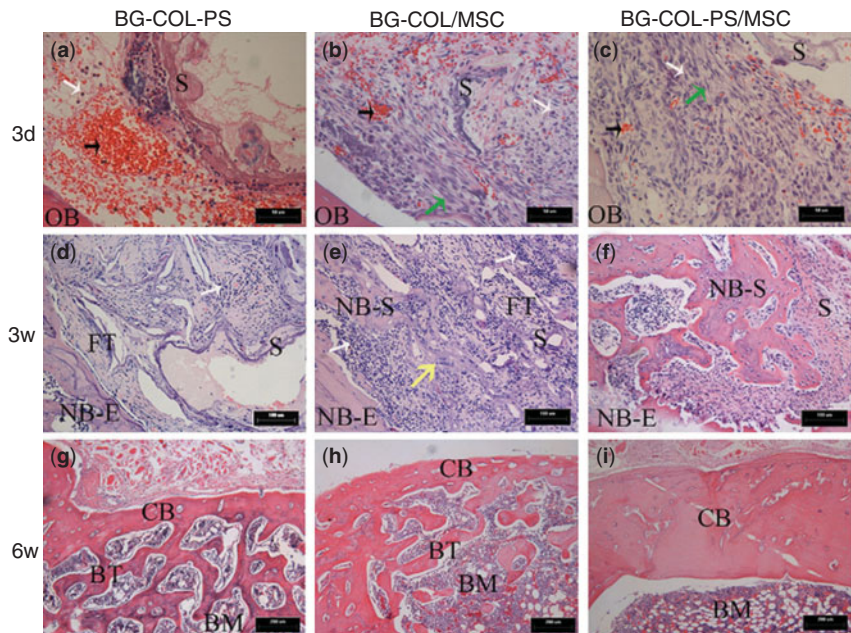
Figure 14.8 Hematoxylin and eosin staining of transverse bone defect sections in different groups at 3 days, 3 weeks, and 6 weeks post-scaffold implantation. Reprinted with permission from [44]. Copyright (2010) Elsevier.

abitilty of HA [3]. Xu *et al.* studied the fate of rat mesenchymal stem cells (rMSCs) seeded on bioglass-collagen-phosphatidylserine (BG-COL-PS) or bioglass-collagen (BG-COL) scaffolds and cultured for 21 days *in vitro*. Their results indicated a higher degree of attachment and osteogenic

differentiation of the rMSCs to the BS-COL-PS scaffolds than those on BG-COL scaffolds. Pure BG-COL-PS scaffolds and BG-COL-PS MSC/ scaffold constructs were implanted in rat femur defects for 6 weeks. The constructs were found to be biocompatible and enhance the neogenic tissue formation process from histological and radiological analysis as in Figures 14.7 and 14.8 [44]. Declercq *et al.* have shown that adipose tissue derived stem cells (ADSC)-laden microcarriers could be used as building blocks (micro tissues) that self-assemble into macro tissues in a bottom-up approach. The cells cultured in these scaffolds were found to successfully undergo osteogenic differentiation making them potential scaffolds for bone grafts that could undergo directed assembling [45].

14.5   Concluding Remarks

Research in the field of biomaterials and tissue engineering over the past two decades has been aimed at developing implantable tissue grafts that help in faster regeneration and repair of damaged tissue. But very few products have been commercialized for human use. The search for a better design of scaffold has led to the idea of copying the design of native tissue. Biomimetic materials are being studied and fabricated extensively to construct tissue-engineering scaffolds that mimic the *in vivo* microenvironment, hence aiding in better integration of scaffold and faster tissue regeneration. The development of these biomimetic materials call for better understanding of the *in vivo* microenvironment along with the biochemical cues that facilitate cell adhesion and proliferation. Studying the behavior of stem cells on such biomimetic scaffolds can help to better understand the structural and biochemical cues involved in their differentiation. But there are many challenges associated with the development of biomimetic scaffolds. The tissue organization *in vivo* is complicated and understanding the composition at the molecular level and replicating it is a challenging task. Even if the composition is mimicked, the method to mimic the biological processes that demarcate the properties of each tissue type remains uncertain. The choice of the right material for biomimetic tissue engineering that supports angiogenesis is another task that requires much attention before developing a biomimetic scaffold. When all these issues are addressed, the challenge still remains for the successful transfer of the graft from the laboratory to clinical use. With the biomimetic approach being the present solution for engineering cells and tissues, we still have a long way to go in fabricating successful biomimetic scaffolds for the repair and regeneration of damaged tissue. Despite these challenges, the biomimetic approach is likely to prove invaluable in the future development of stem cell and tissue engineering.

Acknowledgements

References

1. S. Liao, S. Ramakrishna and M. Ramalingam, Electrospun nanofiber and stem cells in tissue engineering, in M. Ramalingam, Z. Haidar, S. Ramakrishna, H. Kobayashi, Y. Haikel, Eds., *Integrated Biomaterials in Tissue Engineering*, Scrivener Publishing LLC, p. 91–118, 2012.

2. N. Bursac, M. Papadak, J.A. White, S.R. Eisenberg, G. Vunjak-Novakovic, and L.E. Freed, *Tissue Engineering*, Vol. 9, p.1243, 2003.

3. Y. Zhang, J.R. Venugopal, A. El-Turki, S. Ramakrishna and B. Su, *Biomaterials*, Vol. 29, p. 4314, 2008.

4. S. Liao, S. Ramakrishna, and M. Ramalingam, *Journal of Biomaterials and Tissue Engineering*, Vol. 1, p. 111, 2011.

5. R. Murugan, S.S. Liao, S. Ramakrishna, P. Molnar, Z. M. Huang, M. Kotaki, K.P. Rao, and James J. Hickman, Skeletal regenerative nanobiomaterials, in J.D. Santos and N.S. Hussain, Eds., *Biomaterials for Regenerative Medicine*, Trans Tech Publishers, pp. 1–34, 2009.

6. R. Murugan and S. Ramakrishna, Nanoengineered biomimetic bone-building blocks, in G.A. Mansoori, T.F. George, L. Assoufid and G. Zhang, Eds., *Molecular Building Blocks for Nanotechnology*, Springer, pp. 301–352, 2007.

7. Y. Zhang, J.R. Venugopal, S.Y. Wong, L. Xu, B. Su, S. Ramakrishna, and C.T. Lim, *Tissue Engineering Part A*, Vol. 16(6), p.1949, 2010.

8. S. Liao, R. Murugan, C.K. Chan and S. Ramakrishna, *Journal of the Mechanical Behaviour of Biomedical Materials*, Vol. 1(3), p.252, 2008.

9. S.C. Owen and M.S. Shoichet, *Journal of Biomedical Materials Research Part A*, Vol. 94(4), p. 1321, 2010.

10. S. Liao, S. Ramakrishna and M. Ramalingam, Electrospun nanofiber and stem cells in tissue engineering, in M. Ramalingam, Z. Haidar, S. Ramakrishna, H. Kobayashi, Y. Haikel, Eds., *Integrated Biomaterials in Tissue Engineering*, Scrivener Publishing LLC, p. 91–118, 2012.

11. P.X. Ma. *Advanced Drug Delivery Reviews*, Vol. 60(2), p. 184, 2008.

12. M.O. Choi and Y.J. Kim, *International Journal of Biological Macromolecules*, Vol. 50, p. 1188, 2012.

13. S. Tan, X. Huang and B. Wu, *Polymer International*, Vol. 56, p.1330, 2007.

14. J.K. Hong and S.V. Madihally, *Acta Biomaterialia*, Vol. 6(12), p.4734, 2010.

15. D. Gupta, J. Venugopal, S. Mitra, V.R. Giri Dev and S. Ramakrishna. *Biomaterials*, Vol. 30, p. 2085, 2009.

16. L. Francis, J. Venugopal, M.P. Prabhakaran, V. Thavasi, E. Marsano and S. Ramakrishna, *Acta Biomaterialia*, Vol. 6(10), p. 4100, 2010.

17. J.J. Stankus, L. Soletti, K. Fujimoto, Y. Hong, D.A. Vorp and W.R. Wagner, *Biomaterials*, Vol. 28 (17), p. 2738, 2007

18. J.R.J. Paletta, F. Mack, H. Schenderlein, C. Theisen, J. Schmitt, J. H. Wendorff, S. Agarwal, S. Fuchs-Winkelmann and M.D. Schofer, *European Cells and Materials*, Vol. 21, p. 384, 2011.

19. J.M. Taboas, R.D. Maddox, P.H. Krebsbach and S.J. Hollister, *Biomaterials*, Vol. 24, p. 181, 2003.

20. M. Hacker, J. Tessmar, M. Neubauer, A. Blaimer, T. Blunk, A. Gopferich and M.B. Schulz, *Biomaterials*, Vol. 24, p. 4459, 2003.

21. S.S. Liao, F.Z. Cui, W. Zhang and Q.L. Feng, *Journal of Biomedical Materials Research Part B: Applied Biomaterials*, Vol. 69, p. 158, 2004.

22. Y. C. Yu, V. Roontga, V. A Daragan, K. H. Mayo, M. Tirrell and G. B Fields, *Biochemistry*, Vol. 38(5), p. 1659,1999.

23. P. Berndt, G.B. Fields and M. Tirrell, *Journal of the American Chemical Society*, Vol. 117(37), p. 9515, 1995.

24. J.M. Anderson, M. Kushwaha, A. Tambralli, S.L. Bellis, R.P. Camata and H.W. Jun, *Biomacromolecules*, Vol. 10(10), p. 2935, 2009.

25. N.B. Malkar, J.L. Lauer-Fields, D. Juska and G.B. Fields. *Biomacromolecules*, Vol, 4(3), p. 518, 2003.

26. A. Mata, Y. Geng, K. Henrikson, C. Aparicio, S. Stock, R.L. Satcher, and S.I. Stupp. *Biomaterials*, Vol. 31(23), p.6004, 2010.

27. A. Tambralli, B. Blakeney, J. Anderson, M. Kushwaha, A. Andukuri, D. Dean, and H. Jun. *Biofabrication*, Vol. 1(2), p.025001, 2009.

28. H. Shin, S. Jo and A.G. Mikos, *Biomaterials*, Vol. 24, p. 4353, 2003.

29. J.A. Hubbell, S.P. Massia, N.P. Desai and P.D. Drumheller, *Biotechnology*, Vol. 9, p. 568, 1991.

30. J.P. Ranieri, R. Bellamkonda, E.J. Bekos, T.G. Vargo Jr. and J.A.G. Aebischer, *Journal of Biomedical Materials Research*, Vol. 29, p. 779, 1995.

31. A. Rezania, R. Johnson, A.R. Lefkow and K.E. Healy, *Langmuir*, Vol. 15, p. 6931, 1999.

32. K. Yang, J.S. Lee, J. Kim, Y. B. Lee, H. Shin, S.H. Um, J.B. Kim, K.I. Park, H. Lee and S.W. Cho, *Biomaterials*, Vol. 33(29), p. 6952, 2012.

33. X. Liu, Y. Won and P.X. Ma, *Journal of Biomedical Materials Research: Part A*, Vol. 74, p. 84, 2005.

34. R. Ravichandran, C. Ng, S. Liao, D. Pliszka, M. Raghunath, S. Ramakrishna and C.K. Chan, *Biomedical Materials,* Vol. 7, p. 015001, 2012.

35. P.M. Prabhakaran, J. Venugopal, D. Kai and S. Ramakrishna, *Materials Science and Engineering: C*, Vol. 31, p. 503, 2011.

36. T. Kofidis, A. Lenz, J. Boublik, P. Akhyari, B. Wachsmann and K. Mueller-Stahl, *Biomaterials*, Vol. 24, p. 5009, 2003.

37. W. Zimmermann, I. Melnychenko, and T. Eschenhagen, *Biomaterials*, Vol. 25, p. 1639, 2004.

38. M. Borkenhagen, J.F. Clemence, H. Sigrist and P. Aebischer, *Journal of Biomedical Materials Research*, Vol. 40, p. 392, 1999.

39. P.M. Prabhakaran, J.R. Venugopal and S. Ramakrishna, *Biomaterials*, Vol. 30(28), p. 4996, 2009.

40. L. Uebersax, H. Hagenmüller, S. Hofmann, E. Gruenblatt, R. Müller, G. Vunjak-Novakovic, D.L. Kaplan, H.P. Merkle and L. Meinel, *Tissue Engineering*, Vol. 12, p. 3417, 2006.

41. W.L. Grayson, S. Bhumiratana, C. Cannizzaro, G.P. Chao, D. Lennon, A.I. Caplan and G. Vunjak-Novakovic, *Tissue Engineering Part A*, Vol. 14, p. 1809, 2008.

42. M. Ramalingam, M.F. Young, V. Thomas, L. Sun, L.C. Chow, C.K. Tison, K. Chatterjee, W.C. Miles and C.G. Simon Jr., *Journal of Biomaterial Applications*, Vol. 27, p. 695, 2012.

43. J.M. Oliveira, M.T. Rodrigues, S.S. Silva, P.B. Malafaya, M.E. Gomes, C.A. Viegas, I.R. Dias, J.T. Azevedo, J.F. Mano and R.L. Reis, *Biomaterials,* Vol. 27, p. 6123, 2006.

44. C. Xu, P. Su, X. Chen, Y. Meng, W. Yu, A.P. Xiang and Y. Wang, *Biomaterials*, Vol. 32, p. 1051, 2011.

45. A.H. Declercq, T. De Caluwé, O. Krysko, C. Bachert and M.J. Cornelissen, *Biomaterials*, Vol. 34, p. 1004, 2013

Index

Also of Interest

Check out these published and forthcoming related titles from Scrivener Publishing

Encapsulation Nanotechnologies
Edited by Vikas Mittal
Published 2013. ISBN 978-1-118-34455-2

Nanomedicine for Drug Delivery and Therapeutics
Edited by Ajay Kumar Mishra
Published 2013. ISBN 978-1-118-41409-5

Nanomaterials in Drug Delivery, Imaging, and Tissue Engineering
Edited by Ashutosh Tiwari and Atul Tiwari
Published 2013. ISBN 978-1-118-29032-3

Biomedical Materials and Diagnostic Devices Devices
Edited by Ashutosh Tiwari, Murugan Ramalingam, Hisatoshi Kobayashi and Anthony P.F. Turner
Published 2012. ISBN 978-1-118-03014-1

Integrated Biomaterials for Biomedical Technology
Edited by Murugan Ramalingam, Ashutosh Tiwari Seeram Ramakrishna, and Hisatoshi Kobayashi
Published 2012. ISBN 978-1-118-42385-1

Integrated Biomaterials in Tissue Engineering
Edited by Murugan Ramalingam, Ziyad Haidar, Seeram Ramakrishna, Hisatoshi Kobayashi, and Youssef Haikel
Published 2012. ISBN 978-1-118-31198-1

Intelligent Nanomaterials
Processes, Properties, and Applications
Edited by Ashutosh Tiwari Ajay K. Mishra, Hisatoshi Kobayashi and Anthony P.F. Turner
Published 2012. ISBN 978-0-470-93879-9

The Physics of Micropdroplets
Jean Berthier and Kenneth Brakke
Published 2012. ISBN 978-0-470-93880-0

Introduction to Surface Engineering and Functionally Engineered Materials
By Peter Martin
Published 2011. ISBN 978-0-470-63927-6

Handbook of Bioplastics and Biocomposites Engineering Applications.
Edited by Srikanth Pilla
Published 2011. ISBN 978-0-470-62607-8

Biopolymers: Biomedical and Environmental Applications
Edited by Susheel Kalia and Luc Avérous
Published 2011. ISBN 978-0-470-63923-8

Renewable Polymers
Synthesis, Processing, and Technology
Edited by Vikas Mittal
Published 2011. ISBN 978-0-470-93877-5

Miniemulsion Polymerization Technology
Edited by Vikas Mittal
Published 2010. ISBN 978-0-470-62596-5